Vol. 64 January, 1960 No. 1

THE JOURNAL OF PHYSICAL CHEMISTRY

(Registered in U. S. Patent Office)

CONTENTS

NOTES

THE JOURNAL OF PHYSICAL CHEMISTRY

(Registered in U. S. Patent Office)

Published monthly by the American Chemical Society at 20th and Northampton Sts., Easton, Pa.

Second-class mail privileges authorized at Easton, Pa. This publication is authorized to be mailed at the special rates of postage prescribed by Section 131.122.

The *Journal of Physical Chemistry* is devoted to the publication of selected symposia in the broad field of physical chemistry and to other contributed papers.

Manuscripts originating in the British Isles, Europe and Africa should be sent to F. C. Tompkins, The Faraday Society, 6 Gray's Inn Square, London W. C. 1, England.

Manuscripts originating elsewhere should be sent to W. Albert Noyes, Jr., Department of Chemistry, University of Rochester, Rochester 20, N. Y.

Correspondence regarding accepted copy, proofs and reprints should be directed to Assistant Editor, Allen D. Bliss, Department of Chemistry, Simmons College, 300 The Fenway, Boston 15, Mass.

Business Office: Alden H. Emery, Executive Secretary, American Chemical Society, 1155 Sixteenth St., N. W., Washington 6, D. C.

Advertising Office: Reinhold Publishing Corporation, 430 Park Avenue, New York 22, N. Y.

Articles must be submitted in duplicate, typed and double spaced. They should have at the beginning a brief Abstract, in no case exceeding 300 words. Original drawings should accompany the manuscript. Lettering at the sides of graphs (black on white or blue) may be pencilled in and will be typeset. Figures and tables should be held to a minimum consistent with adequate presentation of information. Photographs will not be printed on glossy paper except by special arrangement. All footnotes and references to the literature should be numbered consecutively and placed in the manuscript at the proper places. Initials of authors referred to in citations should be given. Nomenclature should conform to that used in *Chemical Abstracts*, mathematical characters marked for italic, Greek letters carefully made or annotated, and subscripts and superscripts clearly shown. Articles should be written as briefly as possible consistent with clarity and should avoid historical background unnecessary for specialists.

Notes describe fragmentary or incomplete studies but do not otherwise differ fundamentally from articles and are subjected to the same editorial appraisals as are articles. In their preparation particular attention should be paid to brevity and conciseness. Material included in Notes must be definitive and may not be republished subsequently.

Communications to the Editor are designed to afford prompt preliminary publication of observations or discoveries whose value to science is so great that immediate publication is imperative. The appearance of related work from other laboratories is in itself not considered sufficient justification for the publication of a Communication, which must in addition meet special requirements of timeliness and significance. Their total length may in no case exceed 500 words or their equivalent. They differ from Articles and Notes in that their subject matter may be republished.

Symposium papers should be sent in all cases to Secretaries of Divisions sponsoring the symposium, who will be responsible for their transmittal to the Editor. The Secretary of the Division by agreement with the Editor will specify a time after which symposium papers cannot be accepted. The Editor reserves the right to refuse to publish symposium articles, for valid scientific reasons. Each symposium paper may not exceed four printed pages (about sixteen double spaced typewritten pages) in length except by prior arrangement with the Editor.

Remittances and orders for subscriptions and for single copies, notices of changes of address and new professional connections, and claims for missing numbers should be sent to the American Chemical Society, 1155 Sixteenth St., N. W., Washington 6, D. C. Changes of address for the *Journal of Physical Chemistry* must be received on or before the 30th of the preceding month.

Claims for missing numbers will not be allowed (1) if received more than sixty days from date of issue (because of delivery hazards, no claims can be honored from subscribers in Central Europe, Asia, or Pacific Islands other than Hawaii), (2) if loss was due to failure of notice of change of address to be received before the date specified in the preceding paragraph, or (3) if the reason for the claim is "missing from files."

Subscription Rates (1960): members of American Chemical Society, $8.00 for 1 year; to non-members, $16.00 for 1 year. Postage free to countries in the Pan American Union; Canada, $0.40; all other countries, $1.20. Single copies, current volume, $1.35; foreign postage, $0.15; Canadian postage $0.05. Back volumes (Vol. 56–59) $15.00 per volume; (starting with Vol. 60) $18.00 per volume; foreign postage per volume $1.20, Canadian, $0.15; Pan-American Union, $0.25. Single copies: back issues, $1.75, for current year, $1.35; postage, single copies: foreign, $0.15; Canadian, $0.05; Pan American Union, $0.05.

The American Chemical Society and the Editors of the *Journal of Physical Chemistry* assume no responsibility for the statements and opinions advanced by contributors to This Journal.

THE JOURNAL OF PHYSICAL CHEMISTRY

(Registered in U. S. Patent Office) (© Copyright, 1960, by the American Chemical Society)

VOLUME 64 JANUARY 20, 1960 NUMBER 1

STUDIES ON MICELLAR GROWTH IN SURFACTANT SOLUTIONS, WITH AND WITHOUT ADDITIVES

BY ARUN K. BISWAS AND B. K. MUKHERJI

Contribution from the Department of Applied Chemistry, University of Calcutta, Calcutta, India

Received December 30, 1958

A study has been made of micellar formation in ionic surfactant solutions in the presence of sodium chloride and a non-ionic surfactant. Experiments on sodium monolaurin sulfate (SMLS), preparation and properties of which have not been so far reported, reveal that the electrolyte reduces the critical micellar concentration of the surfactant solution. The dye-titration method gives a value of c.m.c. lower than that found by the conductance method; with increased electrolyte concentration, the difference in the two values gradually decreases to a small order. Conductance–concentration curves of ionic detergents with and without non-ionic additive suggest that on addition of non-ionic additive, mixed micelles are formed, in which hydrogen bonds are the main binding factors. While conductance of an anionic detergent solution increases, that of a cationic detergent solution decreases on minute addition of non-ionic detergent; in both the cases, the characteristic bend in the conductance–concentration curve tends to disappear gradually, for which plausible explanations are offered.

Introduction

Surfactant molecules or ions are known to associate to form micelles at a particular concentration known as the critical micellar concentration, or c.m.c. Hartley,[1] McBain and his co-workers[2] and Tartar, *et al.*,[3] have shown that the presence of electrolytes lowers the c.m.c. It has been shown by Williams, *et al.*,[4] that log (c.m.c.) bears a linear relation with log [c + (c.m.c.)] where "c" denotes molarity of added salt and c.m.c. is expressed in moles/liter. Klevens[5] has noted that the dye-titration method gives a lower value for c.m.c. than that obtained by other standard methods. Mukherji and Mysels[6] have shown that log (c.m.c.) *vs.* log [c + (c.m.c.)] plottings in the case of dye-titration and conductimetric experiments give two straight lines which meet and cross each other. The above findings need rechecking and clarification.

Only few available literatures deal with the influence of non-ionic additives to micellar and conductimetric properties of ionic surfactant solutions. Yoda and Meguro[7] showed with sodium dodecyl sulfate that the typical break in the conductance *vs.* concentration curve, which denotes c.m.c., gradually disappears with additions of non-ionic detergents such as polyoxyethylene glycol (PEG) or polyoxyethylene glycoldodecyl alcohol ether (PED). Further work on the above aspects seemed desirable.

Reagents Used. (i) **Sodium Monolaurin Sulfate.**—Purified lauric acid (E. Merck grade lauric acid purified by repeated cryst. from 25% soln. in acetone at −25°; purified product had m.p. 44.1°, sapon. value 279.1, iodine value less than 0.1) was esterified with an equimolar proportion of glycerol; the product obtained was subjected to liquid–liquid extraction in petroleum ether (b.p. 60–80°)–ethyl alcohol system and subsequently crystallized from diethyl ether (m.p. monolaurin 61.9°). (Purity of monolaurin as represented by % α-monoglyceride, determined according to standard method,[8] was 98.5%.) The monolaurin was then sulfated using $ClSO_3H$–NaCl mixture. The sulfate was neutralized with alcoholic NaOH, alcohol was evaporated off and the product crystallized from acetone. (P.C. sulfate ($-SO_3$) gp. as determined by standard method[9] was found to be 21.01.)

(ii).—Lissapol C and LS, used in the experiments, are anionic surfactants manufactured by I.C.I. Ltd., the active ingredients in them being sodium salts of, respectively, cetyl oleyl alcohol sulfate and anisidine sulfate. The com-

(1) G. S. Hartley, *J. Chem. Soc.*, 1968 (1938).

(2) J. W. McBain and A. P. Brady, *J. Am. Chem. Soc.*, **65**, 2072 (1943); J. W. McBain and R. C. Merrill, *Ind. Eng. Chem.*, **34** 915 (1942).

(3) K. A. Wright, A. D. Abbott, V. Sivertz and H. V. Tartar, *J. Am. Chem. Soc.*, **61**, 549 (1939).

(4) R. J. Williams, J. N. Phillips and K. J. Mysels, *Trans. Faraday Soc.*, **51**, 728 (1955).

(5) H. B. Klevens, THIS JOURNAL, **51**, 1143 (1947).

(6) P. Mukherji and K. J. Mysels, *J. Am. Chem. Soc.*, **77**, 2937 (1955).

(7) O. Yoda and K. Meguro, *Nippon Kagaku Zasshi*, **77**, 900, 905 (1956).

(8) W. D. Pohle and V. C. Mehlenbacher, *J. Am. Oil Chemists Soc.*, **27**, 54 (1950).

(9) A.O.C.S. Official and tentative method F2a-44 and 2c-44.

TABLE I

CRITICAL MICELLAR CONCENTRATION (c.m.c.) OF SMLS, WITH OR WITHOUT THE PRESENCE OF NaCl ("*M*" denotes molarity)

Method used	C.M.C. of SMLS: In absence of electrolyte	In presence of NaCl soln. of molarity: 0.004 *M*	0.01 *M*	0.02 *M*	0.03 *M*	0.04 *M*
Conductivity	0.194% (0.0052 *M*)	0.128% (0.0034 *M*)	0.059% (0.0016 *M*)	0.0388% (0.00103 *M*)	0.0227% (0.0006025 *M*)	
Dye titration (0.000125 mole dye/l.)	0.098% (0.0026 *M*)	0.066 (0.00175 *M*)	0.0497% (0.0013 *M*)	0.034% (0.0009 *M*)	0.024% (0.0006300 *M*)	0.017% (0.00045 *M*)

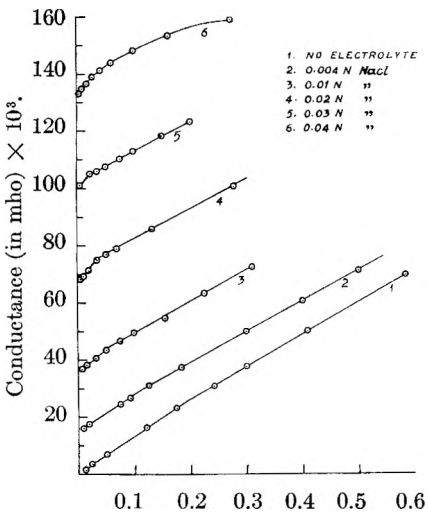

Fig. 1.—Conductance *vs.* concentration of SMLS curves in presence of electrolyte.

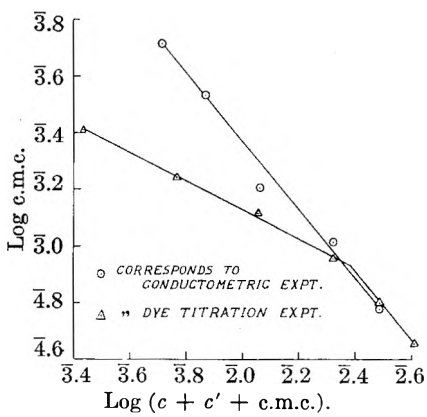

Fig. 2.—Log c.m.c. *vs.* log ($c + c' +$ c.m.c.).

mercial products were purified by refluxing with 95% alcohol, removal of the alcohol-insoluble inorganic electrolytes by filtration, concentration of the alcoholic solution and pouring the residue in dry acetone. Precipitated active ingredients then were filtered, washed in acetone and dried *in vacuo*.

(iii).—Fixanol VR (tetradecylpyridinium bromide) is also an I.C.I. product and was used as such. It contained no inorganic electrolyte, being completely soluble in alcohol and acetone.

(iv).—Lubrol W, fatty alcohol–ethylene oxide condensation product (melting range 43–49°) is also an I.C.I. product. This non-ionic surfactant was found to be completely soluble in alcohol and acetone, and therefore it was taken to be substantially free from any electrolyte. Specific conductances of 0.05, 0.2 and 0.5 p.c. solutions measured at 25 ± 0.1° were only 4.95×10^{-6}, 11.88×10^{-6} and 19.65×10^{-6} mhos, respectively.

(v).—Rhodamine 6G, a cationic dye, was used in the determination of c.m.c. of the anionic detergents.

(vi) C.P. grade NaCl.

Experimental

(i) A self contained conductance meter unit (Leeds and Northrup Co., Philadelphia, model (No. 263941)) having a cell with a constant 0.0396 was used. The conductivity water in all the experiments had sp. conductivity 2.05×10^{-6} ohm^{-1} cm.$^{-1}$. All measurements were made at 25 ± 0.1°. Sets of conductance readings were taken for (1) sodium monolaurin sulfate dissolved in water at various concentrations and also in presence of (2) 0.004 *N* NaCl, (3) 0.01 *N* NaCl, (4) 0.02 *N* NaCl, (5) 0.03 *N* NaCl and (6) 0.04 *N* NaCl solutions, to study the effect of this electrolyte on micellization in the surfactant solution. Points of inflection in the observed conductance values *vs.* concentration curves were taken as c.m.c. Results are given in Table I and Fig. 1.

(ii) C.m.c. of sodium monolaurin sulfate (SMLS) in the presence and absence of electrolytes also was determined by the dye-titration method of Corrin and Harkins[10] and reported in Table I. Five cc. of the detergent solution (concentration at above c.m.c.) were mixed with 5 cc. of 0.01% rhodamine 6G solution in a thin walled vessel. 0.005% rhodamine 6G solution was added gradually from a buret, so that the detergent solution could be diluted progressively, keeping the dye concentration constant (at 0.005%, *i.e.*, 0.000125 mole/l.). The change of color from fluorescent greenish red to non-fluorescent red corresponded to the c.m.c. of the detergent. Experimental accuracy for the determination of c.m.c. by the dye-titration method was of the order of ±2%.

(iii) Effect of increasing concentration of Lubrol W, a "non-ionic," on the conductance and also the nature of conductance *vs.* concentration curves, in the case of Lissapol C, LS and Fixanol VR, were studied. Concentration of Lubrol W, used as additive in different experiments, was 0.05 to 0.5 p.c. which covered the range of c.m.c. of Lubrol W itself (as determined separately from surface tension *vs.* concentration curve).

Results

(1) The points of sharp inflection in the conductance *vs.* concentration curves (Fig. 1) show the c.m.c. values. At higher molar concentration of the electrolyte, angle of inflection is greater and at a concentration of 0.04 *M* NaCl, the inflection assumes the nature of a smooth curve, *i.e.*, it spreads over the whole range of concentration. Obviously, the value of c.m.c., if deduced in such a case, will be doubtful.

(2) Log c.m.c. *vs.* log (c.m.c. $+ c + c'$) curves corresponding to conductivity and dye titration experiments (where c denotes molar concentration of NaCl, *i.e.*, g. ion concentration of the counterion; c' that of rhodamine 6G) are drawn in Fig. 2. These are straight lines converging at a high value of "*c*."

(3) From the conductance *vs.* concentration curves (Figs. 3(i), (ii) and 4) depicting the results of experiments under (iii) above it is obvious that in the case of Lissapol C and LS solutions, conductance increases with addition of non-ionics and

(10) M. L. Corrin and W. D. Harkins, *J. Am. Chem. Soc.*, **69**, 679 (1947).

the inflection gradually tends to disappear. In the case of cationic, Fixanol VR, conductance decreases to a small extent with progressive addition of non-ionics.

Discussion

Increase in concentration of electrolyte (in the case of SMLS) decreases c.m.c. At higher concentration the plotting of conductance *vs.* concentration gives a smooth curve indicating thereby that rate of increase of conductance with increase in concentration does not remain constant above c.m.c. but gradually falls. This indicates increased rate of adsorption of gegenions causing intense micellization.

Present experimental results corroborate previous findings[5,6] that c.m.c. obtained by dye-titration method is lower than the value determined by other methods. It is to be noted that although the gegenion part of the dye is expected to contribute toward lowering the c.m.c., the effect of dye is not merely to supply a few additional gegenions. If it had been so, then log c.m.c. *vs.* log $(c + c' + \text{c.m.c.})$ would give the identical straight line whether c' be positive as in dye titration experiment, or nil as in conductivity experiment. But it will be seen from Fig. 2 that the line obtained from the dye-titration method is different from and its slope less than that in the case of the conductivity experiment. Mukherji, *et al.*,[6] have shown that the above lines meet and cross each other; but in the present set of experiments, it has been observed that though the two curves meet, the extension of the dye-titration line, beyond where it cuts the other, is not linear. Thus, the c.m.c. value obtained by dye-titration experiment at high salt concentration is only slightly greater than the value determined by the other method. A plausible explanation for this would be that as the proportion of dye gegenions in total number of gegenions would diminish with increase in salt concentration, it causes only minor deviation in c.m.c. value.

Figures 3(i), (ii) and 4 show that the breaks in "conductance *vs.* concentration" curves in the case of anionics and cationic occur at higher concentration and tend to disappear gradually with increase in non-ionic concentration, used as additive. This evidently is due to replacement of gegenions by non-ionic molecules, when micellization is less accompanied by the process of adsorption of gegenions resulting in a change in the conductance value. With higher concentration of non-ionic, adsorption of gegenions is possible only at higher concentrations of the detergents supplying greater abundance of gegenions.

Yoda, *et al.*,[7] observed that when non-ionics are added to anionics there occurs an increase in conductance in the micellar zone. In the present series of experiments, conductance has been found to increase in the pre-micellar zone as well. The solvent effect of non-ionic molecules may be one of the contributing factors in the phenomenon,[7] but this would not be expected to increase the conductivity or the slope of the plot in the pre-micellar region except for a possible small contribution due to trace amounts of ionic impurities in the non-ionic. Obviously, the role of non-

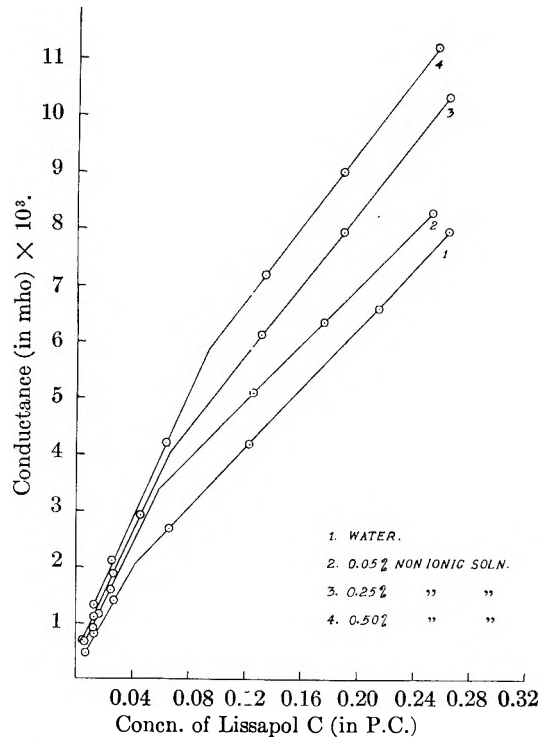

Fig. 3i.—Conductance *vs.* concn. curves for Lissapol C soln. in presence of non-ionic.

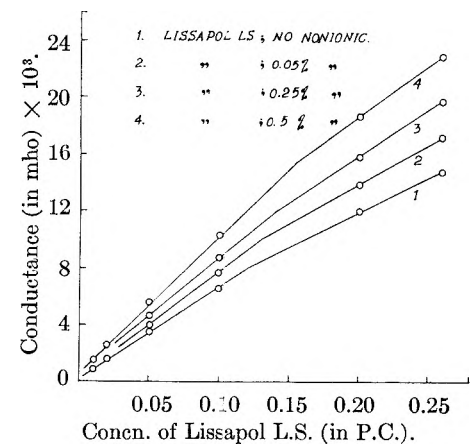

Fig. 3ii.—Conductance *vs.* concentration curves for Lissapo LS soln. in presence of non-ionic.

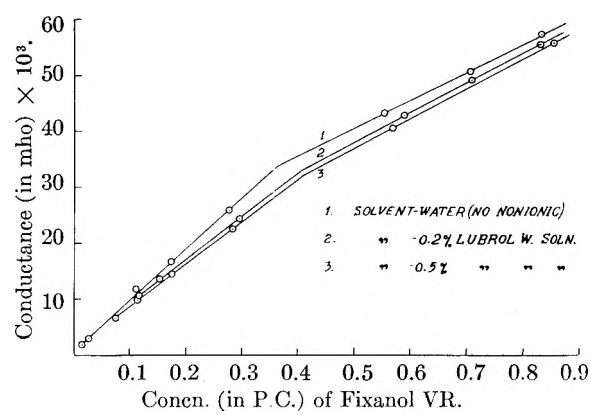

Fig. 4.—Conductance *vs.* concentration curves of Fixanol VR in presence of non-ionic.

ionic is not only to release the Na^+ ions which would increase conductance in the micellar zone but also to form mixed micelle even at a low concentration, as postulated earlier[11-13] resulting in association of the non-polar parts. Such a lamellar mixed micelle would experience a lesser viscous resistance by virtue of its oriented nature and would possess greater ionic mobility and hence greater conductance.[14,15] Once these mixed micelles are formed, this process is apt to survive even at higher concentrations which would explain the cause of rise in conductivity in the micellar zone.

It may be proposed further that the binding factors in the ionic–non-ionic mixed micelle are (i) van der Waals force between the hydrophobic chains in both and (ii) hydrogen bonding between the non-ionic hydroxyl groups and the electronegative atoms in the ionic detergent molecule.[11,12,16] This causes mild association of both the ionic parts of a cationic surfactant molecule with the non-ionic; dissociation of halide ion is diminished if not altogether prevented and, as a result, conductivity decreases to a small extent. Thus, with increase in non-ionic concentration in such solutions, the slope of the conductivity-rise, with increasing concentration of cationic surfactant molecule, in the premicellar zone, gradually decreases, but the corresponding slope in micellar region, where gegenions play their part, remains relatively unaffected. This also results, as in the case of anionic–non-ionic combination, in the tendency toward gradual disappearance of the break in the conductance–concentration curve.

(11) R. Matalon, *J. Colloid Sci.*, **8**, 53 (1953).
(12) M. J. Schick and F. M. Fowkes, THIS JOURNAL, **61**, 1062 (1957).
(13) T. Nakagawa and H. Inoue, *Nippon Kagaku Zasshi*, **78**, 636 (1957).
(14) O. R. Howell and H. G. B. Robinson, *Proc. Roy. Soc. (London)*, **155A**, 386 (1936).
(15) S. L. Gupta, *Sci. and Culture*, **23**, 103 (1957).
(16) L. Osipow, F. D. Snell and J. L. Hickson, *J. Am. Oil Chemists' Soc.*, **35**, 127 (1958).

THE MECHANISM OF OCCLUSION OF HYDROGEN BY PALLADIUM IN CONTACT WITH SULFURIC ACID SOLUTION[1]

BY ROBERT J. FALLON AND GILBERT W. CASTELLAN

Contribution from the Department of Chemistry, The Catholic University of America, Washington 17, D. C.

Received February 13, 1959

The noble potential exhibited by a palladium electrode in hydrogen-stirred sulfuric acid solution has been studied and found to decrease after a period of time, in contradiction to some previous work. The concentration of hydrogen in the metal was found to increase linearly with time. A study of the rates of occlusion as a function of wire size, temperature and partial pressure of hydrogen has led to an elucidation of the over-all mechanism of occlusion. Diffusion of hydrogen in solution is the primary rate-determining process. The contributions of the other steps in the proposed mechanism are discussed. The results of a few experiments indicate that local cell action between platinum and palladium electrodes does not affect the rate of occlusion. Some experiments in sodium sulfate solutions showed that *p*H does not affect the rate. The rate equations show that the rate can be decreased by poisoning the dissociation reaction or by anything that would decrease the stirring at the electrode surface.

Introduction

Aten and Zieren,[2] and Frumkin and Aladjalova[3] have reported a potential difference of zero between a palladium electrode and a Pt/H_2 electrode in the same hydrogen-stirred acid solution, while Hitzler and Knorr,[4] and Stout[5] have reported a potential difference of about 0.050 v., the palladium electrode being more positive (more noble). More recently, Schuldiner, Castellan and Hoare[6] have reported the 0.050 v. potential difference and claim that it is independent of time. They claim that the potential difference eventually will go to zero if impurities are not eliminated carefully or if the palladium electrode is in contact with platinum and the acid solution simultaneously (solution contact). They explain the observation of Aten and Zieren and of Frumkin and Aladjalova by noting that such a solution contact with platinum was present; this solution contact should lead to local cell action with the end result that the potential difference between the palladium and platinum reaches a value of zero.

Schuldiner, Castellan and Hoare also report that a pure palladium electrode after an initial anodic treatment reaches the 0.050 v. potential as the H/Pd atom ratio rises from 0 to 0.03; after reaching these values both the potential and the atom ratio do not vary with time. To explain the sudden halt to the occlusion of hydrogen, they postulate that when the H/Pd ratio reaches the value 0.03 the potential of zero charge of the alloy changes in such a way as to change the sign of the double layer on the palladium surface. This change in the sign of the double layer potential difference produces a reorientation of the water molecules at the surface which could conceivably block further occlusion of hydrogen.

The present work was undertaken as a direct result of the work described above. The outstanding questions concerned the reasons for the sta-

(1) From a dissertation submitted by Robert J. Fallon to the Faculty of the Graduate School of Arts and Science of The Catholic University of America in partial fulfillment of the requirements for the degree of Doctor of Philosophy.
(2) A. N. W. Aten and M. Zieren, *J. Am. Electrochem. Soc.*, **58**, 153 (1930).
(3) A. N. Frumkin and N. Aladjalova, *Acta Physicochem., USSR*, **19**, 1 (1944).
(4) N. Hitzler and G. A. Knorr, *Z. Elektrochem.*, **53**, 233 (1949).
(5) H. P. Stout, *Disc. Faraday Soc.*, **1**, 107 (1947).
(6) S. Schuldiner, G. W. Castellan and J. P. Hoare, *J. Chem. Phys.*, **28**, 16, 20, 22 (1958).

bility of the noble potential with time and the reaction mechanism at the electrode surface by which hydrogen enters the palladium. As the experimental work progressed, the study resolved into a measurement of the rates of occlusion of hydrogen by wires of various diameters at different temperatures and different partial pressures of hydrogen gas.

Experimental

Reagents.—The hydrogen was electrolytic grade and was chemically purified by passage through a train. Two separate purification trains were employed in this work, and a mass spectroscopic analysis of the hydrogen issuing from one train showed only the presence of hydrogen and water vapor (this train had a water saturator in it). The hydrogen–helium mixtures were prepared by The Matheson Company, Inc. The composition of the gas in each of these mixtures was checked by reaction with hot cupric oxide and it fell within the manufacturer's limits of ± 1%. The water used for the preparation of all solutions and for rinsing the cells was triply distilled and was further purified according to the procedure used by Ratchford and Castellan.[7] The palladium wires were obtained from Baker and Company, Inc., and were reported to be 99.8% pure.

Apparatus and Procedure.—All potentials measured were for the cell: $Pt/H_2(p)/H^+(2\ N)/H_2(p)/H\text{-}Pd$. The potential measurements were made with a Leeds and Northrup K-2 potentiometer on one train and with a Leeds and Northrup student-type potentiometer on the other. The total hydrogen content of the wires was measured as a function of time by measuring the resistance of the wires as a function of time. (The resistance of the palladium–hydrogen alloy is essentially a linear function of the H/Pd ratio over the greater part of the concentration range and is independent of the distribution of hydrogen in the wire.[8]) The resistances of the wires were measured with a Mueller thermometer bridge that could be read to 0.0001 Ω. In most cases this accuracy was not necessary and the apparatus was not employed. The contacts to the resistance bridge were made by fastening brass clamps to the large platinum leads (see Fig. 1). To relate the relative resistance of the wires at the different temperatures to the hydrogen content, it was necessary to determine the thermal coefficient of resistance of the alloy at different hydrogen contents. This work will appear elsewhere.[9] The cell was kept in a constant temperature bath regulated to at least ± 0.2°.

Many of our first experiments were done in cells made of glass or of virgin polyethylene. The positive 0.050 v. potential was observed but was not stable. In every case the potential difference went to zero in periods of time varying from a few minutes to several hours. To eliminate the possibility of impurities leaching from the cell walls, Teflon cells of the design shown in Fig. 1 finally were used. The cells were made in three sections. The main body of the cell supported a large platinum gauze electrode. The first top held an inlet tube made by drilling a 0.059″ hole in a 1/8″ piece of Teflon rod. This tube was so situated that the bottom was only a few millimeters from the bottom of the cell. A much smaller piece of platinum gauze attached to the bottom of the inlet tube served as a second reference electrode. The second top held the palladium electrode. The electrodes were made from palladium wires of various sizes welded across two large platinum leads. The platinum leads were covered with polyethylene so that there was no solution contact with platinum. The cells were cleaned in hot nitric acid; occasionally the cells were dismantled and the platinum electrodes flamed.

Using the Teflon cells, many different experimental techniques were employed in the preparation of the Pd wire in the attempt to obtain a stable 0.050 v. potential. It was found that the length of the potential–time plateau was independent of the method of preparing the wire but was dependent on the wire size and the flow rate of the hydrogen

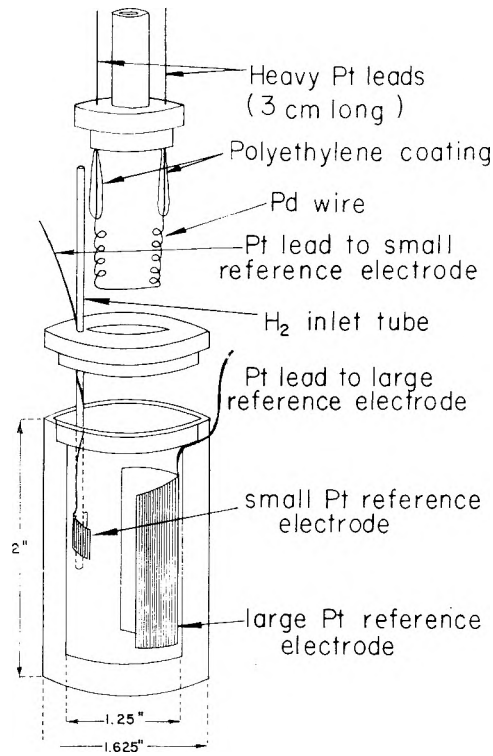

Fig. 1.—Teflon cell.

gas. With these facts in mind we decided to study the open circuit potential–time and concentration–time relationships for wires of different sizes (1, 3, 5, 10 and 15 mil diameter) as a function of temperature and hydrogen pressure.

The cell was filled with 2 N H_2SO_4. The Pd wire was flamed and placed in the cell. Gas flow rates of about 170 ml./min. were used, and the cell was set up so that the hydrogen did not flow directly over the palladium electrode. Runs on the same size wire were carried out in three different cells. At least three runs were carried out with each different set of conditions.

Some experiments were conducted to determine whether the rate of transfer of the hydrogen from the gas phase to the liquid phase was a rate-determining process. In these runs a 15 mil wire was suspended close to a smaller wire (3 or 5 mil) that was being studied.

Results

The results are shown in Table I. $R = d(H/Pd)/dt$. This table lists the average lengths of the wires used as well as the rates of occlusion. The lengths were obtained by taking average values of the initial resistances of all the wires and calculat-

TABLE I

VALUES OF $R \times 10^5$ SEC.$^{-1}$

Flow rate ≈ 170 ml./min.

Press., atm.	Diameter, mils 1	3	5	10	15	Temp., °C.
1	119	21.2	8.57	3.10	1.46	9.8
1	128	22.4	9.35	3.15	1.55	28.6
0.8	101	16.3	8.57	2.67	...	28.6
.6	65.0	11.9	5.83	1.93	...	28.6
.4	43.0	8.27	3.95	1.16	...	28.6
.2	21.3	3.85	1.90	0.506	...	28.6
1	116.5	21.9	8.53	3.30	1.67	49.3
	(runs with 15 mil Pd sink)					
1		19.3	6.90			28.6
	(av. length of wires, cm.)					
	2.38	4.61	6.55	12.18	32.47	

(7) R. J. Ratchford and G. W. Castellan, THIS JOURNAL, **62**, 1123 (1958).

(8) F. Fisher, *Ann. Physik*, **20**, 503 (1906); K. F. Herzfeld and M. G. Mayer, *Z. physik. Chem.*, **26**, 203 (1934).

(9) R. J. Fallon and G. W. Castellan, THIS JOURNAL, **64**, 160 (1960).

ing the lengths from these averages. The total number of experiments collated in Table I is about two hundred.

The reproducibility at this high flow rate was quite good, the average deviation being less than 5%. Figure 2 shows the plot of a typical run on a 15 mil wire. The plots for the other wires were similar to this one.

The rates as a function of the partial pressure of hydrogen for the 1, 3, 5, and 10 mil wires (Table I) are plotted in Fig. 3. The lines drawn through the points were obtained by a least-squares fit in which the points were weighted,[10] because the probable errors in the different points were not equal. These plots definitely demonstrate the linearity of the rate as a function of hydrogen pressure. All these plots show an intercept equal to zero within the experimental accuracy. The values obtained for the open-circuit potential of the saturated α-palladium electrode at the three temperatures agreed very well with the work of Ratchford and Castellan.[7]

Some preliminary experiments in which the flow rate was not controlled carefully showed that solution contact with platinum did not alter the rate of occlusion, although it did alter the potential, as would be expected. In these experiments various sized pieces of platinum foil were clamped to the palladium wires. The rate of occlusion was also measured in 2 N Na_2SO_4 solutions ranging in pH from 2.3 to 10.5. The rate was independent of pH but was less than that in the acid solution. This rate is lower apparently because of the lower solubility of H_2 in the Na_2SO_4 solutions.

Discussion

The linear dependence of the rate on the partial pressure of hydrogen, partial pressure being proportional to concentration according to Henry's law, together with the fact that the potential of the electrode was not dependent on hydrogen pressure excludes diffusion in the wire as a rate-determining process. The fact that the potential was independent of pressure meant that the chemical potential of hydrogen at the electrode surface was also independent of pressure. If diffusion in the metal were rate determining, the chemical potential of hydrogen at the electrode surface would have to vary with pressure to give a pressure-dependent rate. From the dependence of the rate on the partial pressure of hydrogen as well as the results of the earlier work with the sodium sulfate solutions and the platinum contacts, it was concluded that the discharge of hydrogen ions could not be a rate-determining process.

The over-all mechanism for the entrance of hydrogen can be separated into the steps

Process	Reaction	Rate
Solution of gas	$H_2(gas) \rightleftarrows H_2(sol)$	$\frac{dn(sol)}{dt} = (k_0p - k_0'C_b)V_s$
Diffusion in soln.	$H_2(sol) \longrightarrow H_2(sur)$	$^*\frac{dn(sur)}{dt} = \frac{-D_s(C_s - C_b)A_w}{a \ln(1 + \delta/a)}$
Dissociation at the surface	$H_2(sur) \longrightarrow 2H(sur)$	$\frac{dn_H(sur)}{dt} = 2k_1C_sA_w$
Diffusion in the metal	$H(sur) \longrightarrow H(metal)$	$\frac{dn_m}{dt}$ = rapid reaction

$n(sol)$ = total no. moles H_2 in soln.
$n(sur)$ = total no. moles of H_2 at surface of Pd wire
$n_H(sur)$ = total no. moles of hydrogen atoms at surface of Pd wire
$k's$ = rate constants
p = partial pressure of H_2 in atm.
V_s = volume of soln. in the cell (cm.^{3})
a = radius of the wire in cm.
t = time in seconds
C_b = concn. of H_2 in soln (moles/cm.^{3})
C_s = concn. of H_2 at surface of Pd wire (moles/cm.^{3})
A_w = total area of wire (cm.^{2})
D_s = diffusion coefficient for H_2 in soln. (cm.^{2} sec.$^{-1}$)
δ = thickness of diffusion layer at Pd surface in cm.
n_m = total no. of hydrogen atoms in Pd wire
C_b^e = concn. of H_2 in soln. at equilibrium
V_0 = 22414 cm.^{3}
α = Bunsen absorption coefficient for H_2
L = length of Pd wire in cm.
ρ = density of palladium (g./cm.^{3})
M = molecular weight of palladium

* Solution of the diffusion equation for a hollow circular cylinder.

The steady-state conditions are

$$\frac{dn(sol)}{dt} = \frac{dn(sur)}{dt} \quad (1)$$

$$2\frac{dn(sur)}{dt} = \frac{dn_H(sur)}{dt} \quad (2)$$

$$\frac{dn_H(sur)}{dt} = \frac{dn_m}{dt} \quad (3)$$

At equilibrium these two relations hold

$$p = (k_0'C_b^e/k_0) \quad (4)$$

$$p = (V_0/\alpha)C_b^e \quad (5)$$

Solution of the steady-state equations in the light of eq. 4 and 5 yields

$$\frac{dn_m}{dt} = \frac{2k_1A_wk_0V_sp}{(k_0V_sV_0/\alpha)(1 + k_1/k_D) + k_1A_w} \quad (6)$$

where

$$k_D = \frac{D_s}{a \ln(1 + \delta/a)}$$

The total number of moles of hydrogen atoms in the wire, n_m, is related to H/Pd atom ratio of the wire by

$$n_m = \left(\frac{H}{Pd}\right)(\pi a^2L\rho/M) \quad (7)$$

Differentiation of eq. 7 and combination with eq. 6 yields

$$\frac{2M\alpha}{a^2LV_0\pi\rho}\frac{dp}{dR} = \frac{1}{k_DA_w} + \frac{1}{k_1A_w} + \frac{\alpha}{k_0V_sV_0} \quad (8)$$

in which $R = d(H/Pd)/dt$. After evaluating the constants and introducing the expression for k_D one obtains

$$\frac{1}{a^2L} \times \frac{dp}{dR} = \frac{1471}{\alpha D_s}\frac{\log[(a + \delta)/a]}{L} + \frac{0.1789}{k_0V_s} + \frac{4010}{\alpha k_1A_w} \quad (9)$$

The thicknesses of the diffusion layer for the different size wires and at the different temperatures of the experiments were determined by measuring limiting diffusion currents of

(10) H. Margenau and G. M. Murphy, "The Mathematics of Physics and Chemistry," D. Van Nostrand Co., Inc., New York, N. Y., 1943, p. 497.

Cu^{++}. A description of these determinations as well as the values obtained are given in the Appendix.

Using the measured values of δ, the values of $(1/a^2L)(dp/dR)$ as a function of log $[(a + \delta)/a]/L$ were plotted. These are shown in Fig. 4. The line drawn through the points is the best line given by a weighted least-squares treatment.[10]

The values of the diffusion coefficients calculated from these plots are listed in Table II along with some values for hydrogen in pure water and in 1 *N* sulfuric acid obtained from the literature.[11-13] The values derived here are very close to the literature values, which would indicate that the proposed mechanism is essentially correct. An Arrhenius plot of the diffusion coefficients yields an activation energy of about 1.5 kcal., which is the correct order of magnitude for a diffusion process.

TABLE II

DIFFUSION COEFFICIENTS FOR HYDROGEN IN SOLUTION

Solution	Temp., °C.	$D_s \times 10^5$ (cm.^{2} sec.$^{-1}$)	Ref.
2 *N* H_2SO_4	9.8	3.13	Present research
2 *N* H_2SO_4	28.6	3.99	Present research
2 *N* H_2SO_4	49.3	4.07	Present research
Water	18	3.59	11
Water	21	5.2	12
1 *N* H_2SO_4	23	3.83	13

Equation 9 relates the reciprocal of the rate of occlusion to the sum of three terms: a diffusion term, a reaction term (dissociation at the surface) and a solution term. Although it was realized from the plot of Fig. 4 that both the contribution of the solution term and the reaction term was small and the diffusion process was the most important rate-determining step, a check was made on the contribution of the solution term. To do this a length of 15 mil wire was suspended close to a smaller wire to see whether the heavy wire would act as a sink for hydrogen. This experiment was done on a 3 and 5 mil wire; the results are given in Table I. It was noticed that there was a definite decrease in the rate of occlusion, but the inherent errors in the experiments prohibited an exact determination of the contribution of this term. However, it was estimated that this term might contribute as much as 10% to the over-all rate in the case of a 15 mil wire under the conditions of this experiment.

The thickness of the diffusion layer also was measured for the system with the sink to determine whether the stirring was affected by suspending the 15 mil wire near the smaller wire (Appendix). The thickness of the diffusion layer was found to remain the same when the 15 mil wire was introduced. This confirmed the fact that the decreases in the rates were really due to the addition of the sink.

The flow rate of hydrogen can affect the rate of occlusion of hydrogen in two ways. The hydrogen bubbling in the cell stirs the solution, the faster the rate of bubbling the better the stirring. If the solution is not stirred well, the thickness of the diffusion layer will increase and, according to equation 9, the rate of occlusion will decrease. This is the main effect of gas flow rate on the rate of occlusion. The flow rate can also affect the rate of occlusion through the influence of the solution term in eq. 9 (second term on the right side of the equation). The rate of dissolution of molecular hydrogen decreases when the flow rate decreases because of a decrease in the k_0' which depends in a complicated way on the area of the gas bubbles in contact with solution. This will cause the solution term to become larger. Because this term is independent of the wire size while the other terms become smaller

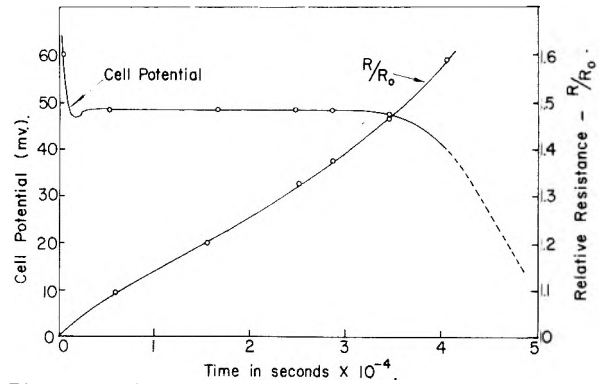

Fig. 2.—Typical variation of relative resistance and potential of palladium wire with time; temp. = 28.6°.

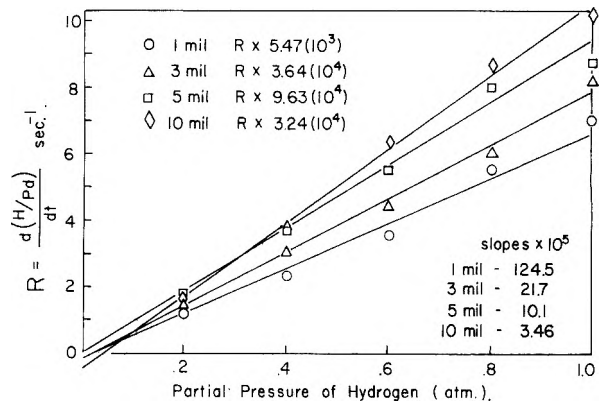

Fig. 3.—Dependence of rate of occlusion on partial pressure of H_2.

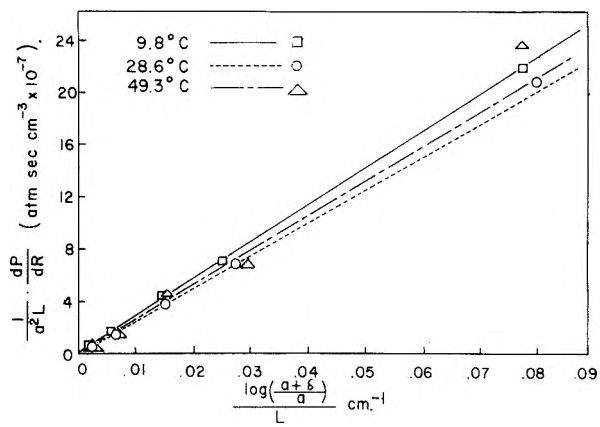

Fig. 4.—Plot to determine diffusion coefficients.

(11) W. Jost, "Diffusion," Academic Press, Inc., New York, N. Y., 1952, p. 475.

(12) "International Critical Tables," Vol. V, McGraw-Hill Book Co., Inc., New York, N. Y., 1929, p. 62.

(13) *C. A.*, **47**, 5768h (1953) (A. E. Aikazyan and A. I. Federova, *Doklady Akad. Nauk, SSSR*, **86**, 1139 (1952)).

for larger wires, it is apparent that this term is more important for larger wires.

Any impurity that would poison the dissociation reaction at the electrode surface would decrease the rate by increasing the value of the third term on the right side of eq. 9. The criterion of purity used by Schuldiner, Castellan and Hoare[7] was that the electrode should exhibit a high pseudo-capacitance on rapid current interruption. Yet they note that a fully charged β-palladium alloy (gas-charged alloy) has a low pseudo-capacitance apparently due to the presence of a passivating film of hydrogen on the surface. Thus it seems that in the case of palladium at least a low pseudo-capacitance may indicate the presence of impurities on the surface or it may mean only that the alloy is saturated with hydrogen.

Some of the work of the previous investigators in this field can be evaluated very nicely in light of these results. One would expect those investigators who used palladized platinum electrodes to obtain a zero potential against a platinum electrode in the same hydrogen-stirred acid solution simply because of the small amount of palladium present in the electrode. In this case a very small amount of hydrogen would transform the palladium into β-palladium and cause the potential to go to zero. The previous explanation proposed by Schuldiner, Castellan and Hoare[7] was that the local cell action set up by the contact of the platinum and palladium charged the palladium with hydrogen. The palladium electrodes with platinum contacts studied in this work indicated, however, that the rate was not increased by platinum contacts.

Schuldiner, Castellan and Hoare[6] reported that a foil of unspecified size maintained the constant positive potential of 0.050 v. for seven days. Their cells were very similar in size to the ones used in this research, but at least in some instances hydrogen was bubbled through the cell only during 8 hr. of the day and therefore the actual stability of the potential can be considered to have lasted only about two days. According to the discussion of the effect of the flow rate on the rate of occlusion given above, it is conceivable that the potential of a foil of suitable size would remain constant over a period of two or three days. This could occur if the flow rate of hydrogen was small enough and if by chance the electrode was placed in such a position in the cell that stirring near the electrode was reduced to a minimum. This report of the stability of the potential is therefore not inconsistent with the mechanism proposed here.

The experiment of Schuldiner, Castellan and Hoare[6] in which they cathodized a β-palladium electrode and noticed that on open-circuit the palladium lost hydrogen to give a 0.050 v. potential was attempted unsuccessfully. In one experiment, a palladium bead electrode was prepared by melting down a wire in an oxygen flame. After cathodization, the potential on open circuit was low, but on standing it rose to the reported 0.050 v. value. This can be explained on the supposition that immediately after cathodization the concentration of hydrogen at the electrode surface is high, while the concentration inside the electrode is low. The hydrogen redistributes itself on standing and the potential rises. This same explanation has been suggested quite recently by Flanagan and Lewis.[14] The rate of occlusion reported by Flanagan and Lewis is much smaller than the rates given here. This may be because their stirring was poor.

A very detailed description of the experimental techniques used here may be found in ref. 15.

Appendix

Measurement of the Thickness of the Nernst Diffusion Layer in Solution.—The thickness of the diffusion layer at the electrode surface was measured by determining the limiting diffusion current of Cu^{++} at the electrode surface. The geometry of the cell and electrode was the same as during an actual run. A 1 N potassium chloride solution was used with varying concentrations of Cu^{++} (10^{-3} to 5×10^{-5} M) and the solution was stirred by bubbling pure helium through the cell instead of hydrogen. The maximum diffusion current can be related to the thickness of the diffusion layer by the equation

$$I = \frac{nFDC}{a \ln [(a + \delta)/a]}$$

where

I = current density, amp./cm.^{2}
n = no. of electrons to discharge one ion
D = diffusion coefficient of the ion in soln., cm.^{2}/sec.
C = concn. of ions in soln. (moles/cm.^{3})

The value of the diffusion coefficient of Cu^{++} was obtained from Kolthoff and Lingane[16] and is equal to 0.72×10^{-5} cm.^{2}/sec. at 25°. The diffusion coefficients for the three temperatures at which these experiments were carried out were calculated using the approximate expression given by Jost[17]

$$D = \frac{kT}{\eta}$$

where

k = constant (dyne deg.$^{-1}$)
T = absolute temperature
η = viscosity of the solvent

The values obtained for the thickness of the diffusion layers are given in Table III. The error

TABLE III

THICKNESS OF THE NERNST DIFFUSION LAYER IN SOLUTION ($\delta \times 10^{+3}$ CM.)

Temp., °C.	Wire diameter, mils 1	3	5	10	15
9.8	0.67	1.16	1.51	2.23	3.11
28.6	.67	1.28	1.57	2.60	3.11
49.3	.61	1.40	1.67	2.76	3.67
	(15 mil sink suspended in soln.)				
28.6		1.16			

in these values estimated from the reproducibility

(14) T. B. Flanagan and F. A. Lewis, *J. Chem. Phys.*, **29**, 1417 (1958).

(15) R. J. Fallon, Diss. The Catholic University of America Press, 1959.

(16) I. M. Kolthoff and J. J. Lingane, "Polarography," Interscience Publishers, Inc., New York, N. Y., 1946.

(17) W. Jost, "Diffusion," Academic Press, Inc., New York, N. Y., 1952, p. 462.

of the current plateaus is about 15%. However, one can see that the thickness does definitely change with wire diameter and that the values do not depend markedly on viscosity or temperature. The points at room temperature are the most reliable since each is the average of about five determinations, while each one at the other temperatures is the average of only two determinations.

Acknowledgment.—The authors wish to express their thanks to Professor Karl F. Herzfeld of the Department of Physics, The Catholic University of America, for very helpful discussions.

TRANSITORY PRODUCTS IN THE GAS PHASE REACTION OF ETHYLENE WITH OZONE

BY ARTHUR E. HEATH, SAMUEL J. BROADWELL, LOWELL G. WAYNE AND PAUL P. MADER

Los Angeles County Air Pollution Control District, Research Division, Los Angeles, Cal.

Received February 23, 1959

In a study of the rates of reactions between ozone and various olefins at low concentrations in air, Cadle and Schadt[1] sought but did not find evidence for the existence of transitory reaction products in the ethylene–ozone system. We have observed such products recently by means of their infrared absorption in a one-meter path. The evidence is definitive for the existence of at least two such substances and one or more others may be involved.

Reactions were carried out in a darkened Vycor cell, one meter long, placed in the beam of a double-monochromator recording spectrophotometer. Partial pressures ranged from 700 to 3500 microatm. for ethylene and from 500 to 1000 microatm. for ozone. Some forty experiments in which the reagents (diluted with oxygen to about one atmosphere) were intimately mixed by simultaneous introduction into the cell through a single stopcock consistently confirmed the order of magnitude of the rate reported by Cadle and Schadt for the disappearance of ethylene. Within five to ten minutes the concentration of ethylene or of ozone became substantially stationary, the other reagent having disappeared from the system. In two tests, spectra recorded within five minutes after mixing showed strong development of a peak at 8.6 μ, which was much reduced in subsequent spectra. Six tests in which the absorption at 8.6 μ was continuously recorded showed that this peak reached a maximum within 30 to 60 seconds after mixing; it then subsided, with a half-time of perhaps five to ten minutes. Formic acid, recognized by its triplet band centered at 9.0 μ, accumulated much more slowly.

When the reactants were introduced into the cell by a technique which avoided rapid mixing, there was strong development of peaks which did not belong to formic acid nor to the compound absorbing at 8.6 μ, which we call Intermediate I. These new peaks subsided after several hours, furnishing clear evidence of the presence of other transitory compounds in the system. In these tests the cell (volume, 1.4 l.) was filled to atmospheric pressure with oxygen containing about 0.1% ozone. A few ml. of ethylene then was injected into the cell by means of a hypodermic needle and syringe through a serological stopper near one end. Under these conditions, reaction rates were limited by diffusion, so that the time available for observing possible transitory products was prolonged; about an hour was required for the substantial disappearance of one reactant.

Figure 1 illustrates changes observed in the spectrum of one diffusion-limited reacting system containing excess ethylene. After two hours in the dark the spectrum (dotted line) showed no traces of

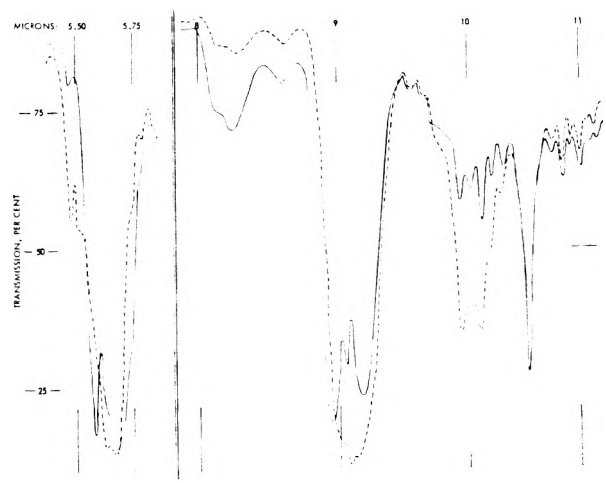

Fig. 1.—Near infrared absorption spectra of reacting system of ethylene and ozone in air, with diffusional mixing. Dotted line shows spectrum after 2 hours; solid line, after 18 hours. Ethylene appears in region 9.9 to 11.2 microns; formic acid at 5.6, 5.7, 8.2 and (triplet) at 9 microns; transitory compounds at 5.5 to 5.7, 9 and 10 microns.

the ozone peaks (9.5 to 9.7 μ), but absorption peaks due to products different from Intermediate I were very prominent at 5.6 to 5.7, 9.0 and 10.0 μ. After 18 hours in the dark, the 10-μ peak had largely subsided, while typical formic acid peaks were well developed at 5.6, 5.7, 8.2 and 9.0 μ. The changes in the interim can only have been caused by the disappearance of one or more transitory products which decompose or react as formic acid accumulates. The absorption at 10 μ is especially intriguing; it has been observed clearly in only three instances, although in several other spectra its presence appears likely.

Comparison of our spectra with published spectra for pure compounds[2-4] reveals that ethylene

(1) R. Cadle and C. Schadt, *J. Am. Chem. Soc.*, **74**, 6002 (1952).

oxide and ethylene ozonide were substantially absent from the reacting mixtures, and that the bands at 8.2, 9.0 and 10.0 μ were not due to formaldehyde, acetaldehyde or acetic acid. Performic acid has main peaks at 9.0 and 5.6 μ[4] and thus seems a likely constituent in the diffusion-limited systems.

It is worth noting that the possible presence of these transitory compounds in smog-laden atmospheres could provide an explanation for discrepancies between chemical[5] and spectroscopic[6] estimates of formic acid concentrations in the atmosphere; that is, one or more of these intermediates might be chemically indistinguishable from formic acid by the usual analyses, while its absorptions would differ from those of formic acid and perhaps obscure them.

This research has been discontinued.

(2) R. H. Pierson, A. N. Fletcher and Et. St. C. Gantz, *Ind. Eng. Chem.*, **28**, 1218 (1956).
(3) D. Garvin and C. Schubert, THIS JOURNAL, **60**, 807 (1956).
(4) P. A. Giguere and A. W. Olmos, *Can. J. Chem.*, **30**, 821 (1952).
(5) P. P. Mader, G. E. Cann and L. Palmer, *Plant Physiology*, **30**, 318 (1955).
(6) W. E. Scott, E. H. Stephens, P. L. Hanst and R. C. Doerr, Paper presented at meeting of American Petroleum Institute's Division of Refining, Philadelphia, Pa., May 14, 1957.

THE THERMODYNAMICS OF DILUTE SOLUTIONS OF $AgNO_3$ AND KCl IN MOLTEN KNO_3 FROM ELECTROMOTIVE FORCE MEASUREMENTS. III. TEMPERATURE VARIATIONS OF THE ACTIVITY COEFFICIENTS

BY J. BRAUNSTEIN[1] AND M. BLANDER

Oak Ridge National Laboratory,[2] P. O. Box Y, Oak Ridge, Tennessee

Received March 26, 1959

The quasi-lattice model of the molten reciprocal salt systems A^+, B^+, C^- and D^- previously proposed[3] leads to the relation for the activity coefficient of the component AD $\gamma_{AD} = [(1 - X)^Z[1 + X/\beta(1 - X)]^{Z-1}]/N_{D^-}$, if A^+ and C^- ions have an extra-coulombic interaction, where Z is the lattice coördination number, $\beta = e^{-\Delta E/RT}$, ΔE is the energy of formation of a mole of A^+–C^- ion pairs and X is the fraction of positions adjacent to A^+ ions occupied by C^- ions and can be calculated in terms of Z, ΔE and the concentrations of the ions. The theory should be valid for low values of N_{Ag^+} and X. Measurements of the activities of $AgNO_3$ were made in the molten salt concentration cell

$$Ag \left| \begin{matrix} KNO_3 \\ AgNO_3 \end{matrix} \right\| \begin{matrix} KNO_3 \\ AgNO_3 \\ KCl \end{matrix} \Bigg| Ag$$

for dilute solutions of Ag^+ and Cl^- ions at 385, 402 and 423°. KCl in solution lowered the activity coefficient of $AgNO_3$, the lowering being larger the larger the concentration of Cl^- ions and the smaller the concentration of Ag^+ ions. A comparison of the experimental data and the theory at low values of N_{Ag^+} ($\lesssim 0.720 \times 10^{-3}$) and X (<0.15) for $Z = 6$ leads to a value of ΔE of $5.6_5 \pm 0.03$ kcal./mole for the temperature range studied here and in paper I of this series (370–436°).[4] The constancy of ΔE shows that the temperature coefficients of the activity coefficients in the range of validity of the theory are correctly predicted. This lends confidence in the usefulness of the quasi-lattice model.

Introduction

A quasi-lattice model of the molten reciprocal salt system A^+, B^+, C^- and D^- has been proposed.[3] In the model, ions of the same charge are the same size and the A^+ and C^- ions have an extra-coulombic interaction. This leads to the relation for the activity coefficient of the component AD, γ_{AD}

$$\gamma_{AD} = \frac{(1 - X)^Z \left(1 + \frac{X}{\beta(1 - X)}\right)^{Z-1}}{N_{n^-}} \qquad [1]$$

where $\gamma_{AD} = a_{AD}/N_{A^+}N_{D^-}$, N_{D^-} is the anion fraction of the D^- ion, Z is the lattice coördination number, $\beta = e^{-\Delta E/RT}$, ΔE is the energy of formation of a mole of $A^+ - C^-$ ion pairs and X is the fraction of anion positions adjacent to an A^+ ion that are occupied by C^- ions. X can be calculated from the distribution function

$$\frac{X}{1 - X} = \left(\frac{N_{C^-} - ZXN_{A^+}}{1 - ZN_{A^+}(1 - X) - N_{C^-}}\right)\beta \qquad [2]$$

The assumptions made in the derivation of equations 1 and 2 limit the range of validity of the theory. Any correlation between positions occupied by different A^+ ions has been neglected. This in effect neglects A^+–C^-–A^+ ion triplets. This neglect is justified at low concentrations of A^+ ions. The assumption also has been made that the energy of interaction of adjacent A^+ and C^- ions is independent of the number of C^- ions already adjacent to the A^+ ion. To the extent that there is a "saturation" effect on the A^+–C^- interaction this assumption will be invalid. Since the number of triplets (C^-–A^+–C^-) increases with the parameter X, deviations from equation 1 due to this effect will increase with increasing X, and the extent of deviation will depend on the extent of the "saturation" effect on A^+–C^- ion interactions. With these restrictions in mind we may test the activity coefficients and their temperature dependence as calculated from the quasi-lattice model by comparison with measured values of the activity coefficients of the component $AgNO_3$ in the system Ag^+, K^+, Cl^-, NO_3^- dilute in Ag^+ and Cl^- ions.

In a previous paper it had been found that for an arbitrarily chosen value of $Z = 6$ at 370 and 436° values of ΔE of 5.6_6 and 5.6_4 kcal./mole, respec-

(1) Summer Research Participant at the Chemistry Division of Oak Ridge National Laboratory, 1958.
(2) Operated for the United States Atomic Energy Commission by the Union Carbide Corporation.
(3) M. Blander, THIS JOURNAL, **63**, 1262 (1959).
(4) M. Blander, F. F. Blankenship and R. F. Newton, *ibid.*, **63**, 1259 (1959).

tively, were found to fit the results at the low concentrations of Ag^+ and Cl^- ions. The purpose of this paper is to test further the apparent constancy of ΔE at several intermediate temperatures. The experimental verification of the apparent constancy of ΔE in this and in other reciprocal salt systems consisting of univalent ions would be empirical evidence for the usefulness of the prediction of the temperature coefficients of the activity coefficients as calculated from measurements at a single temperature by use of equations 1 and 2.

Experimental

Electromotive force measurements were made in the concentration cell

$$\mathrm{Ag}\left|\begin{matrix}\mathrm{KNO_3}\\ \mathrm{AgNO_3}\end{matrix}\right\|\left\|\begin{matrix}\mathrm{KNO_3}\\ \mathrm{AgNO_3}\\ \mathrm{KCl}\end{matrix}\right|\mathrm{Ag}$$

previously described in more detail.[4] Temperatures were measured using a platinum–platinum–10% rhodium thermocouple which was calibrated to ±1° against a similar thermocouple certified by the National Bureau of Standards. The cell assembly was heated in a resistance furnace of 5-inch inside diameter. Separate control by means of autotransformers, of the furnace and of an independent low heat capacity heater set underneath the beaker led to more satisfactory temperature control of the cell than in the assembly previously reported. Periodic checks of freshly prepared and of aged reference half cells (left hand cells) indicated that these half cells were stable within 0.5 mv. for several days. In a given experiment lasting several hours a precision of about 0.2 mv. generally was obtained. This improved precision as compared to previous results was probably due to the improved temperature control.

The experimental procedure for the e.m.f. measurements was to add weighed increments of KCl to the beaker (right hand electrode) which contained an $AgNO_3$–KNO_3 mixture and which was kept at a constant temperature during the course of the experiment. The e.m.f. change with the change of the KCl concentration in solution was measured with a Leeds and Northrup type K2 potentiometer.

Results

Table I lists the experimental results of the change of e.m.f. as a function of the mole ratio of KCl, R_{KCl}, at several fixed mole ratios of $AgNO_3$, R_{AgNO_3}, and at 385, 402 and 423°. The mole ratios of KCl and $AgNO_3$ are defined by

$$R_{KCl} = \frac{n_{KCl}}{n_{KNO_3}} \text{ and}$$

$$R_{AgNO_3} = \frac{n_{AgNO_3}}{n_{KNO_3}}$$

where n_i is the number of moles of the ith component. The ion fractions of Cl^- and Ag^+ are defined by

$$N_{Cl^-} \equiv \frac{n_{Cl^-}}{n_{Cl^-} + n_{NO_3^-}} \text{ and } N_{Ag^+} \equiv \frac{n_{Ag^+}}{n_{Ag^+} + n_{K^+}}$$

and are smaller than the mole ratios R_{KCl} and R_{AgNO_3}, respectively, by the factor $1/(1 + R_{KCl} + R_{AgNO_3})$ which is not very different from unity in dilute solutions.

The interpretation of the data can be made if the liquid junction potential of the cell can be evaluated or estimated. The Nernst equation

$$E = \frac{2.303RT}{F} \log \frac{N_{Ag^+}}{N'_{Ag^+}} \qquad [3]$$

was found to be valid at all temperatures studied, within experimental precision, for the dilute solutions containing no Cl^- ions. This is consistent with the negligible liquid junction potential found

TABLE I

CHANGE OF E.M.F. (VOLTS) OF THE CELL

$$\mathrm{Ag}\left|\begin{matrix}\mathrm{KNO_3}\\ \mathrm{AgNO_3}\end{matrix}\right\|\left\|\begin{matrix}\mathrm{KNO_3}\\ \mathrm{AgNO_3}\\ \mathrm{KCl}\end{matrix}\right\|\mathrm{Ag}$$

WITH THE ADDITION OF KCl TO THE RIGHT HAND HALF CELL

Temperature = 385°

$R_{KCl} \times 10^3$	$-\Delta E$ (v.)	$-\log \gamma_{AgNO_3}$	$R_{KCl} \times 10^3$	$-\Delta E$ (v.)	$-\log \gamma_{AgNO_3}$
$R_{AgNO_3} = 0.279 \times 10^{-3}$			$R_{AgNO_3} = 0.724 \times 10^{-3}$		
0.231	0.0056	0.043	0.248	0.0053	0.041
0.486	.0116	.089	0.590	.0120	.092
1.130	.0255	.195	1.101	.0218	.167
1.761	.0381	.292	1.510	.0295	.226
2.375	.0492	.377	2.129	.0403	.308
2.795	.0566	.434	2.710	.0499	.383
3.300	.0649	.497	3.339	.0599	.459
3.98	.0751	.575	4.215	.0727	.556
$R_{AgNO_3} = 2.20 \times 10^{-3}$			$R_{AgNO_3} = 3.50 \times 10^{-3}$		
0.579	0.0048	0.037	0.267	0.0030	0.023
1.081	.0149	.114	0.869	.0097	.074
1.930	.0270	.207	1.418	.0159	.122
2.615	.0369	.283	1.901	.0215	.165
3.255	.0454	.348			

Temperature = 402°

$R_{KCl} \times 10^3$	$-\Delta E$ (v.)	$-\log \gamma_{AgNO_3}$	$R_{KCl} \times 10^3$	$-\Delta E$ (v.)	$-\log \gamma_{AgNO_3}$
$R_{AgNO_3} = 0.279 \times 10^{-3}$			$R_{AgNO_3} = 2.19 \times 10^{-3}$		
0.086	0.0018	0.013	0.127	0.0016	0.012
0.362	.0076	.057	0.531	.0071	.053
0.701	.0146	.109	1.049	.0139	.104
1.309	.0264	.196	1.445	.0193	.144
2.205	.0426	.317	2.081	.0276	.207
2.860	.0531	.395	2.708	.0357	.267
3.460	.0622	.463	3.333	.0436	.326
4.11	.0716	.533	3.930	.0512	.384
4.82	.0810	.603			
			$R_{AgNO_3} = 3.50 \times 10^{-3}$		
			0.414	0.0056	0.042
			1.119	.0130	.097
			1.851	.0212	.159
			2.510	.0280	.210
			3.138	.0351	.263
			4.028	.0460	.325

Temperature = 423°

$R_{KCl} \times 10^3$	$-\Delta E$ (v.)	$-\log \gamma_{AgNO_3}$	$R_{KCl} \times 10^3$	$-\Delta E$ (v.)	$-\log \gamma_{AgNO_3}$
$R_{AgNO_3} = 0.278 \times 10^{-3}$			$R_{AgNO_3} = 0.718 \times 10^{-3}$		
0.168	0.0034	0.025	0.088	0.0019	0.013
0.627	.0121	.088	0.562	.0104	.075
1.239	.0230	.167	1.083	.0194	.140
1.700	.0311	.225	1.634	.0287	.208
2.340	.0415	.301	2.28	.0389	.281
3.330	.0564	.409	3.11	.0514	.372
3.828	.0634	.459	3.89	.0623	.451
4.355	.0706	.511	4.65	.0728	.527
			5.35	.0811	.588
$R_{AgNO_3} = 2.19 \times 10^{-3}$			$R_{AgNO_3} = 3.50 \times 10^{-3}$		
0.435	0.0058	0.042	0.303	0.0042	0.030
1.060	.0137	.099	0.916	.0105	.077
1.835	.0235	.170	1.735	.0191	.138
2.271	.0288	.209			
2.761	.0347	.252			
3.448	.0431	.312			
4.030	.0500	.362			
4.950	.0608	.431			

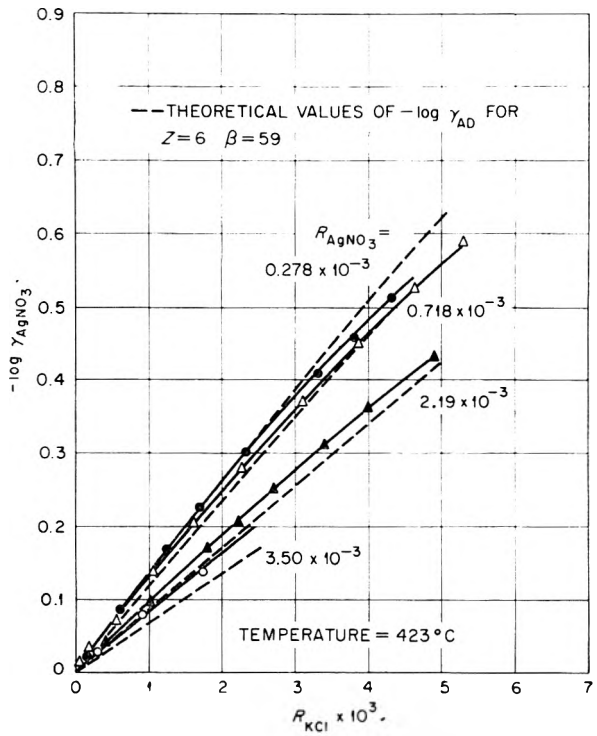

Fig. 1.—Comparison of the values of $-\log \gamma_{AgNO_3}$ measured at 423° to the values calculated from the quasi-lattice model for $Z = 6$ and $\beta = 59$.

in the $AgNO_3$–$NaNO_3$ system[5] over a much wider range of concentrations. The liquid junction potential due to Cl^- ions is estimated as less than 0.6 mv. in the concentration range studied.[6] A detailed experimental study of the transference numbers of Ag^+ and Cl^- ions would decrease the uncertainty in the liquid junction potential, an uncertainty which is somewhat larger than the experimental precision at the higher concentrations studied. If a standard state is chosen such that the activity coefficient of the component $AgNO_3$ is unity at infinite dilution of all solutes in KNO_3, then the activity coefficients of $AgNO_3$ in KNO_3 with no KCl added are unity in the range of concentrations studied. Within the uncertainty of the liquid junction potential, the e.m.f. change upon addition of KCl is then

$$\Delta E = \frac{2.303RT}{F} \log \gamma_{AgNO_3} \qquad [4]$$

Values of $-\log \gamma_{AgNO_3}$ are listed in Table I. Figure 1 is a plot of $-\log \gamma_{AgNO_3}$ as a function of the mole ratios R_{AgNO_3} and R_{KCl} at 423°. The activity coefficients decrease with increasing concentrations of KCl, the decrease being greater, the lower the value of R_{AgNO_3}. The deviations from ideality are more negative and exhibit a stronger dependence on R_{AgNO_3} the lower the temperature. This is consistent with previously reported observations[4] on this system.

Comparison of the Results with the Quasi-lattice Theory.—The dashed lines of Fig. 1 are a plot of $-\log \gamma_{AD}$ *versus* N_{C^-} at several values of N_{A^+} for $Z = 6$ and $\beta = 59$. The value of β was chosen by comparison of the theoretical calculations obtained by using equations 1 and 2, with the experimental results at 423° for $R_{AgNO_3} = 0.000279$ and $R_{KCl} < 0.0032$. The value of Z was chosen arbitrarily as being reasonable. The calculated values of $-\log \gamma_{AD}$ were relatively insensitive to different values of Z at constant values of $Z(\beta - 1)$.

Qualitatively, the theoretical and experimental results are strikingly similar. The theoretical values of γ_{AD} correspond satisfactorily with the experimental values of γ_{AgNO_3} at the low concentrations of A^+ ($N_{A^+} < 0.000720$) and at low values of X ($X < 0.15$). At higher values of N_{A^+} the calculated values of $-\log \gamma_{AD}$ are lower than the experimental values of $-\log \gamma_{AgNO_3}$. As has been discussed, this probably is due to the approximation implicit in the theory which in effect leads to the neglect of A^+–C^-–A^+ ion triplets. This approximation leads to too great a dependence of $-\log \gamma_{AD}$ on N_{A^+} at a fixed value of N_{C^-}. At high values of X and low values of N_{A^+} the experimental values of $-\log \gamma_{AgNO_3}$ are lower than the calculated values of $-\log \gamma_{AD}$. This difference may be due to the neglect of a "saturation" effect on the A^+–C^- ion interaction as discussed in the Introduction.[8]

In column 2 of Table II are listed the values of β which led to a fit of the experimental and theoretical values of the activity coefficients at several temperatures and at values of $N_{A^+} = 0.00028$. Column 3 lists ΔE, the values of the energy of formation of a mole of A^+–C^- ion pairs, calculated from β. Column 4 lists the concentration of C^- ions at which $X = 0.15$ when $N_{A^+} = 0.28 \times 10^{-3}$. These values of N_{C^-}, with $N_{A^+} = 0.00028$ were the highest concentrations to which the theory was applied in calculating β.

TABLE II

DERIVED PARAMETERS FOR A COÖRDINATION NUMBER OF 6

Temp. (°K.)	β ($Z = 6$)	ΔE (kcal./mole)	N_{C^-}
709[3]	55	-5.6_4	0.0035
696	59	-5.6_3	.0032
675	67	-5.6_4	.0029
658	77	-5.6_8	.0026
643[3]	84	-5.6_6	.0024

The constancy of the derived values of ΔE over the range of temperatures for which measurements have been made leads to confidence in the usefulness of the proposed theory. Other reasonable choices of the parameter Z lead to values of ΔE as constant as those in Table II. For a choice of

(5) R. W. Laity, *J. Am. Chem. Soc.*, **79**, 1849 (1957).

(6) The effect of the Cl^- ion is dependent on the mobilities of the Cl^- and NO_3^- ion relative to the K^+ ions in solutions dilute in Ag^+ ion. Making the very reasonable assumption that the mobility m_{Cl^-} of Cl^- ions lies in the very broad range $0 < m_{Cl^-} < 2m_{NO_3^-}$ then $|t_{Cl^-}| < (N_{Cl^-}/(1 - N_{Cl^-}))$ and the liquid junction potential probably is less than (RTN_{Cl^-}/F) or about 0.6 mv. at the highest concentrations studied.[7] The actual value of the liquid junction potential is probably a fraction of this. This low value is a consequence of the fact that most of the current is carried by the solvent KNO_3.

(7) G. N. Lewis and M. Randall, "Thermodynamics," McGraw-Hill Book Co., 1923, p. 337.

(8) It should be made clear that the lattice model approximation takes into account only nearest neighbor interactions. Although the authors believe that these are the predominant interactions in this system, longer range interactions and effects of different ionic sizes or shapes cannot be distinguished from the "saturation" effect.

$Z = 4$, $\Delta E = 6.1_8$ and for $Z = 5$, $\Delta E = 5.8_8$. Within the range of validity of the theory, a single parameter will lead to a correct prediction of the deviations from ideality at all temperatures.

Acknowledgments.—The authors wish to express appreciation to Drs. R. F. Newton and F. F. Blankenship of this Laboratory and to Prof. G. Scatchard for many fruitful discussions, to Richard Mashburn for the numerical calculations and to W. R. Grimes for encouragement in this work.

THE EFFECT OF SURFACE ACTIVE AGENTS ON CRYSTAL GROWTH RATE AND CRYSTAL HABIT

BY A. S. MICHAELS AND A. R. COLVILLE, JR.

Department of Chemical Engineering, Massachusetts Institute of Technology, Cambridge, Massachusetts

Received April 25, 1959

The growth of adipic acid crystals from aqueous solution in the temperature range 25–45° was studied under controlled supersaturation conditions, both in the presence and absence of low concentrations of an anionic and cationic surface active agent. Microscopic measurements of the crystals permitted calculation of the individual rates of growth of the (001), (010) and (110) faces. Facial growth rates could be correlated satisfactorily with supersaturation by two dimensional nucleation theory. Low (50 p.p.m.) concentrations of surfactant caused substantial reductions in facial growth rates. The anionic agent caused much greater reduction in growth rate of the (010) and (110) faces than of the (001) face and the cationic agent had the opposite effect. Surfactant effects appear to be related to the hydroxyl-densities on the crystal face. The influence of surfactants on the facial growth rates of large adipic acid crystals is significantly less than on those of small ones, suggesting that growth at dislocations predominates on large crystals and is less sensitive to surfactant-interference than growth from two-dimensional nuclei.

Introduction

An understanding of the mechanism of growth of crystals and of the influence of environmental factors upon growth kinetics and crystal shape or habit, is of great importance in many fields such as chemicals processing, metallurgy, ceramics and biochemistry. The effect of impurities or trace-additives on crystal growth-kinetics and crystal habit has long been observed, but quantitative studies, wherein the effects of additives upon the specific growth rates of individual crystal faces are described, are rather scarce.

Fysh[1] has reported that the habit of adipic acid crystals grown from aqueous solution can be modified in different ways by additions of anionic or cationic surfactants. He postulated that adsorption of the additives took place preferentially on certain faces of the crystal, presumably due to the differing carboxylic natures of the different faces. Adipic acid therefore appeared to be a desirable candidate for further study. Two pure, well-characterized surface active agents were examined as additives to this system, *viz.*, sodium dodecylbenzene sulfonate (SDBS) and trimethyldodecylammonium chloride (TMDAC).

Adipic acid normally crystallizes as flat, slightly-elongated, hexagonal, monoclinic plates from aqueous solution, as shown in Fig. 1. From X-ray diffraction studies,[2] it has been established that the predominant face of these plates is the (001) face, the elongated side faces are (010) faces, and the end faces are (110) faces. The linear, six-carbon, dicarboxylic acid molecules are aligned end-to-end in parallel array in the crystal, with their long axes parallel to the (010) face so that the (001) face is made up entirely of carboxyl groups, while the (010) and (110) faces contain both carboxylic and hydrocarbon portions of the molecule. The angle formed by the (001) and (010) faces is 42.9°. (Unit cell dimensions: a 10.07 Å., b = 5.16 Å., c = 10.03 Å., β = 137.1°. The cell contains two molecules.[2])

From these crystallographic parameters, it is possible to determine all the crystal dimensions and facial areas by measurement of any three characteristic linear dimensions. The three dimensions selected in this work were the length of the (001) face (designated L), the width of the (001) face (designated W), and the thickness of the plate normal to the (001) face (designated C'). For brevity, the (110), (010) and (001) faces are henceforth referred to as the A-, B- and C-faces, respectively. By way of example, the total areas of the A-, B- and C-faces are related to the dimensions L, W and C′, by the equations

$$A_A = 2.52WC' \quad (1)$$

$$A_B = 2.94C'(L - 0.51W) \quad (2)$$

$$A_C = 2.02W(L - 0.258W) \quad (3)$$

In a similar fashion, the rates of change of facial area, or specific rates of growth on individual faces, can be calculated in terms of the rates of change of L, W and/or C'. Alternately, measurement of the mass (or volume) of a crystal, and of the two dimensional ratios L/C' and W/C', permit the same calculations to be made.

In essence, the growth rate and growth habit of adipic acid crystals, and the influence of surfactants thereon, were studied by cooling agitated saturated aqueous solutions of the acid at various rates, both in the presence and absence of a known quantity of seed crystals. By measuring the mass-yield of crystals, the mean crystal size, and the mean dimension of the crystals, and by employing the geometric relations described above, it was possible to calculate the absolute or relative rates of growth of the three primary crystal faces and

(1) D. Fysh, private communication cited in "Surface Activity," J. L. Moilliet and B. Collie, editors, D. Van Nostrand Co., Inc., New York, N. Y., 1951, p. 144.

(2) R. W. Morrison and A. R. Robertson, *J. Chem. Soc.*, 987 (1949).

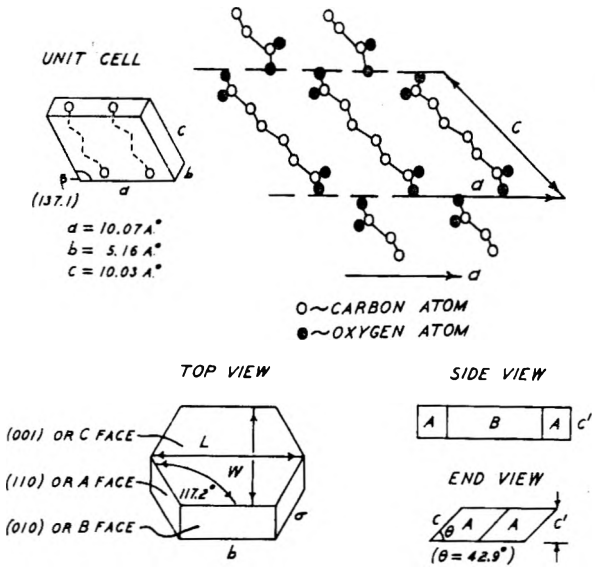

Fig. 1.—Molecular structure and habit of adipic acid crystals grown from aqueous solution.

thereby to correlate the growth data with environmental variables such as supersaturation level and surfactant concentration.

Materials and Apparatus

Materials used in this study were as follows.

Crystalline adipic acid [$(CH_2)_4(COOH)_2$], of purity greater than 99.6%, was provided by the Chemstrand Corporation; m.p. 151 ± 0.5° density (20°/4°) 1.366 g./cc. Solubility–temperature dependency in water determined in this study agrees within limits of experimental error with that reported by Davies and Griffiths.[3]

Sodium tetrapropyl(dodecyl)benzene sulfonate, anhydrous, was provided by the Monsanto Chemical Company, reported to be free of sodium sulfate, and to contain less than 0.1% unsulfonated hydrocarbon. It was prepared as stock solution in distilled water, containing 1.0 g./l. SDBS.

Trimethyldodecylammonium chloride, crystalline, provided by Armour Research Division. Prepared as stock solution containing 0.96 g./l. TMDAC.

Distilled water was used throughout.

The crystallization vessel consisted of a 500-ml. three-necked distilling flask, immersed in a constant temperature water-bath regulated to ±0.1°. The flask was provided with a variable-speed stirring apparatus (0–500 r.p.m.), and a precision thermometer (range 0–55°) readable to ±0.05°. The stirrer used was made of glass, as other materials such as Teflon or stainless steel were found to cause heterogeneous nucleation to take place.

Procedure

A. Concurrent Nucleation-and-Growth Measurements.—A saturated water solution of adipic acid was prepared by equilibration with excess solid at a specified temperature (usually 45°). A measured volume of surfactant solution (0–20 ml.) was placed in the crystallizer and the water-bath temperature was set to some desired value below the saturation temperature of the stock adipic acid solution. Enough of this stock solution (maintained at about 10° above its saturation temperature), then was measured out and placed in the crystallizer to bring the total volume of solution to 400 ml. Agitation was begun and the temperature of the solution was followed as it cooled toward the bath temperature. Timing was begun when the flask contents reached their saturation temperature; the time of appearance of turbidity, and the corresponding solution temperature, was measured. The crystal slurry was allowed to remain at the bath temperature long enough to establish saturation equilibrium (about 30 min.); the flask contents then were removed, the suspended crystals were separated from the mother liquor by vacuum filtration through a fritted glass funnel, and dried in a warm oven.

The dry crystals were sized and counted by passing them through a series of sieves with U.S. Standard mesh sizes 30, 40, 60, 80, 100, and the amount retained on each sieve was determined gravimetrically. The number of crystals on each sieve was calculated by assuming that the crystals were spheres whose diameter was equal to the mean mesh opening. In those cases where the habit modification was extreme the size distribution was obtained approximately by microscopic examination.

After sizing and counting, the crystals were examined under a 40 × microscope. From each sample, about four or five well-formed crystals were selected and each was mounted on the drawn tip of a glass rod by means of a small bead of canada balsam. By rotating the crystal in the objective plane of a 20 × projection microscope, its image dimensions could be measured by means of a micrometer scale traced on the image plane at the same magnification. The length, width and thickness of the prisms were thus measured, the ratios (L/W) and (C'/W) were calculated, and averaged to obtain suitable mean habit-parameters for each crystal batch. On the whole, well-formed crystals represented a significant fraction of the total crystal yield (about 50%), and shape variations from one crystal to another were small, so that the average shape data are believed to be reasonably representative of the entire crystal batch.

B. Growth from Seeds.—The growth of seed crystals was followed by first nucleating and growing crystals as just described, without surfactant present. After reaching saturation equilibrium at the bath temperature, instead of separating all the crystals from the mother liquor, only a small sample was taken for analysis. Then, surfactant was added and the flask contents cooled slowly to room temperature. The rate of cooling was increased in each succeeding run until further nucleation took place in the crystallizer, as determined by comparing the number of crystals present at the beginning and at the end of the run. These crystals were, as above, separated from the mother liquor by vacuum filtration, dried, sieved and examined microscopically.

Results

A. Nucleation-and-Growth Experiments.—Since the size-distribution of the crystals produced in these experiments was found to be very narrow, a suitable average crystal mass could be determined with reasonable accuracy. On dividing the total crystal yield by the weight of the "average" crystal so determined, it was found that, irrespective of the cooling rate (which was varied from about 0.02 to 7.5 deg./min.) or ultimate extent of cooling (varied from 1.8 to 25°), the total *number* of crystals formed per unit volume of solution was essentially constant. From this, it was deduced that onset of turbidity in the system corresponded to a concentration of suspended solid which was essentially constant for all runs; this concentration was subsequently established to be about 0.13 g./100 ml. of solution, and represented between 3 and 20% of the ultimate crystal yield, depending upon the extent of cooling.

Granting that nucleation occurs in the very earliest stages of the cooling process near the cold wall of the crystallizer, the average mass rate of growth up to appearance of turbidity can be represented by the ratio of the weight of crystals formed at turbidity divided by the time interval (designated θ_T) between initial saturation and onset of turbidity. If it is further assumed that the shape of the final crystals produced in this fashion is the same as that of the crystals throughout their growth, it then becomes possible to calculate the average specific growth rates for the individual crystal faces.

(3) M. Davies and D. M. L. Griffiths, *Trans. Faraday Soc.*, **49**, 405 (1953).

In all runs, the total concentration of adipic acid in solution (about 6.5 g./100 ml.) far exceeded the quantity of adipic acid which had precipitated when turbidity developed. Hence, the ratio of the initial solution concentration to the saturation concentration corresponding to the temperature at which turbidity appeared was very nearly equal to the supersaturation ratio at turbidity. Since the crystallizer wall-temperature is close to the bath temperature throughout the cooling process, the supersaturation ratio at turbidity is believed to be a good approximation to the average supersaturation to onset of turbidity. Hence, from the "apparent supersaturation ratio at turbidity," designated S_T, and the average growth-rate in the time θ_T, it is possible to relate growth rate to supersaturation level in the presence or absence of surfactants.

The growth rate on each face of an adipic acid crystal was found to increase with increasing supersaturation, very rapidly at low supersaturations and more slowly as the supersaturation increased. The shape of the crystals formed changed from a thick, elongated hexagonal plate at low supersaturations to a thinner more regular hexagonal plate at higher supersaturations.

The presence of even a low concentration of surfactant during growth caused a decrease in the growth rate on the faces. At a concentration of fifty parts per million (0.137 mmole/l.), SDBS was three times more effective in reducing the growth rates on the A and B faces than on the C face, causing the plates to become thicker. Higher concentrations of this surfactant caused extreme habit modification, the crystals becoming long thin rods or needles. TMDAC, on the other hand, at a concentration of 96 r.p.m. (0.364 mmole/l.) was twice as effective in hindering growth on the C face as in hindering growth on the A and B faces, causing the plates to become thinner. Higher concentrations of this surfactant also caused extreme habit modification, the crystals becoming very thin plates or flakes.

B. Growth from Seeds Experiments.—At the higher concentrations of the surfactants, it was found that the number of crystals formed per unit volume of solution was far greater than normal and the habit modifications were so extreme that serious crystal-breakage occurred during even mild agitation. It was thus impossible to determine the actual crystal shape and to relate conditions at the onset of turbidity to those observed at lower surfactant concentrations. For this reason, it was decided to study the effect of higher surfactant concentrations by (1) forming normal seed-crystals of adipic acid by nucleation and growth without additive, and then (2) adding surfactant and continuing growth by continued cooling, measuring changes in crystal habit.

In these experiments, no attempt was made to measure supersaturation levels during growth. Instead, a slurry of a known number of seed crystals in a given volume of saturated solution (containing varying concentrations of surfactant) was allowed to cool at progressively increasing rates until secondary homogeneous nucleation occurred, as evidenced

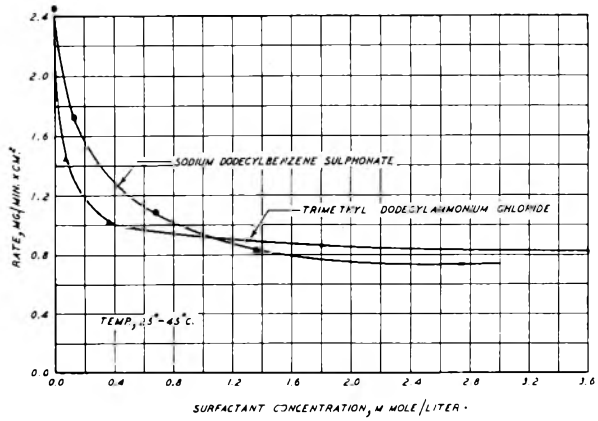

Fig. 2.—Effect of surfactant concentration on average specific growth rate on A (_10) and B (010) faces of adipic acid seed crystals.

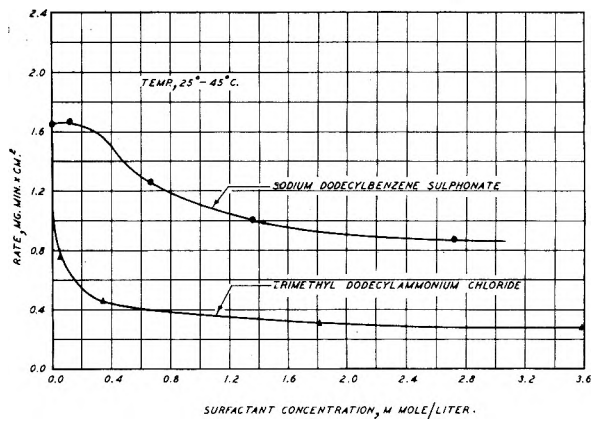

Fig. 3.—Effect of surfactant concentration on specific growth rate on C (001) face of adipic acid seed crystals.

by the formation of more product crystals than seeds. The critical cooling rate above which secondary nucleation occurred could thus be determined. Since the supersaturation was low in these experiments, the cooling rate could be converted into precipitation rate from the solubility–temperature relation. As this critical precipitation rate corresponds to the maximum growth rate on the seed crystals at a supersaturation just short of that for homogeneous nucleation, it was thus possible to determine the extent to which the surfactants altered the over-all growth rate on the seeds at constant supersaturation and, from microscopic measurements, to determine the effect of the additives on the relative rates of growth of the individual crystal faces. Because of the rather minor influence on crystal habit of variations in growth rate of the A-face relative to the B-face it was found convenient (and no less informative) to treat the A and B faces as a single "AB" face, and to measure the growth on the C-face relative to the average growth on this "AB" surface. Results of these experiments are shown in Fig. 2 and 3. It was found that the growth rate on a face first decreased rapidly with increasing surfactant concentration and then became nearly constant at higher concentrations. As observed in the nucleation-and-growth experiments, the anionic surfactant (SDBS) suppressed growth more on the A- and B-faces

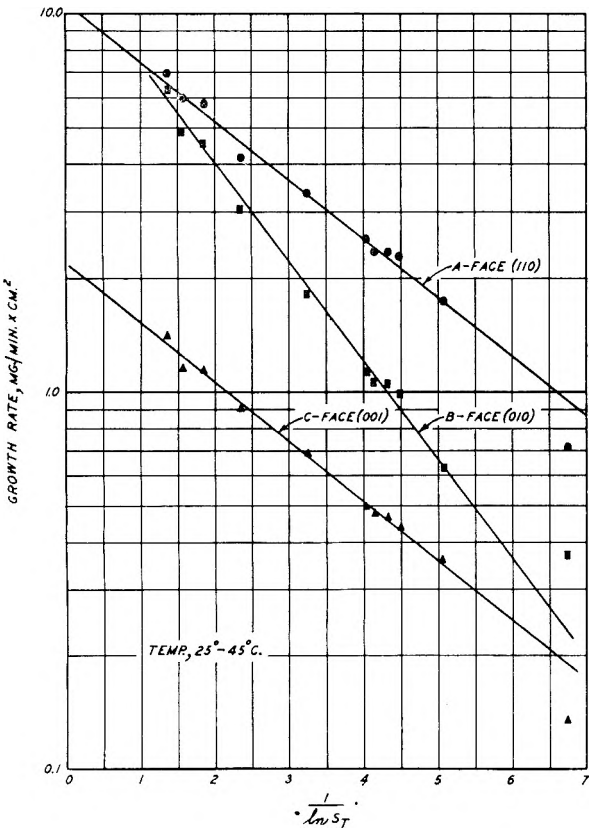

Fig. 4.—Specific growth rates of the faces of adipic acid crystals as a function of supersaturation (no additives).

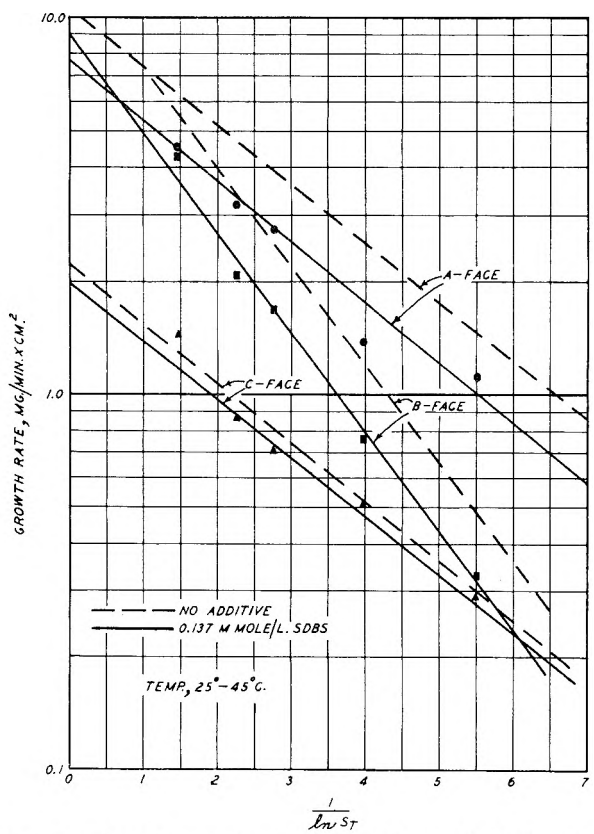

Fig. 5.—Specific growth rates of the faces of adipic acid crystals as a function of supersaturation (SDBS present).

than on the C-face of the crystal, while the cationic agent (TMDAC) had the opposite effect.

Discussion of Results

A. Nucleation-and-Growth Experiments.—The data indicate a rapid increase in growth rate with supersaturation at low supersaturations, suggesting that an activated process at the crystal surface is the growth-controlling mechanism. One tenable hypothesis of crystal growth, proposed by Koessel and Stranski, and further developed by Brandes and others,[4,5] is that the rate of deposition of material on a crystal face is controlled by the frequency of two-dimensional nucleation on the face. Thermodynamic analysis based on this assumption leads to the rate expression

$$R = Ke^{-\beta/\ln S} \qquad (4)$$

where

R = growth rate of a face, mg./min. cm.²
S = supersaturation ratio in solution
β = a constant, dependent on the absolute temp. and the edge-free-energy of the two dimensional seed (dimensionless)
K = proportionality constant (units of R)

Figures 4 to 6 indicate that the results of this study (at low concentration of surfactants or in their absence) can be correlated quite accurately by equation 4. Deviations are apparent at supersaturations close to unity. In this region, however, a small error in S produces a large error in $(1/\ln S)$, and the "apparent supersaturation at turbidity" is known to be higher than actual supersaturation, so that the observed deviations might be anticipated.

Values of β and K, determined from Fig. 4 to 6, are given in Table I. According to two-dimensional nucleation theory, the quantity β is determined by the contribution, to the edge-free-energy of the "seed," of a single molecule. If it is assumed that a seed consists of an array of $n \times n$ molecules, the following relation applies

$$\beta_k = \left(\frac{a_j\sigma_j + a_i\sigma_i}{kT}\right)^2 \qquad (5)$$

where

β_k = (β) value for the k-face
a_i, a_j = area occupied by a molecule in the i- and j-faces
σ_i, σ_j = free surface energy of the i- and j-faces

TABLE I

RATE CONSTANTS FOR ADIPIC ACID CRYSTALLIZATION DERIVED FROM EQUATION 4 AND FIGURES 4 TO 6

Additive	A (110) Face β	A (110) Face Ka	B (010) Face β	B (010) Face Ka	C (001) Face β	C (001) Face Ka
None	0.35	1.05	0.60	1.35	0.39	0.22
0.137 mmole/l. SDBS	.37	0.76	.63	0.90	.38	.20
0.364 mmole/l. TMDAC	.36	.96	.61	1.15	.39	.15

[a] Mg./min. cm.²

On the C (001)-face of an adipic acid crystal, a seed will consist of a bundle of molecules whose edges are probably comprised of A (110) and/or B (010) faces; by making orthogonal projections

(4) H. Brandes, *Z. physik. Chem.*, **126**, 196 (1927).

(5) A. V. Shubnikov, editor, "Growth of Crystals," Reports of the First Conference on Crystal Growth, U.S.S.R., March 5–10, 1956.

of the unit cell, the average area occupied by a molecule in these faces can be estimated to be about 45 Å.^{2}. On the A-face, a seed is bounded by B- and C-faces, and on the B-face, by A- and C-faces; the area occupied by a molecule in a C-face is only about 26 Å.^{2}. From these figures, and equation 5, it becomes possible to estimate the free surface energies of the three crystal faces; the quantities so calculated are

$$\sigma_A = 3.8 \text{ erg/cm.}^2$$
$$\sigma_B = 1.8 \text{ erg/cm.}^2$$
$$\sigma_C = 5.8 \text{ erg/cm.}^2$$

Considering only the relative magnitudes of these free energies (the absolute quantities seem far smaller than would be expected for the free energy of a crystal–solution interface), it is seen that the free surface energy increases in the order B-face < A-face < C-face. It is considered significant that, according to the unit cell dimensions, the area–density of hydrogen-bonding OH-groups on the three faces increases in exactly the same order: *i.e.*, 1.92, 2.31 and 3.85 hydroxyls per 100 Å.^{2} on the B, A and C faces, respectively.

Thermodynamic considerations would lead to the prediction that the C (001) face, being the one of highest free surface energy, would be the most rapidly growing whereas, in point of fact, it is the slowest growing face. The explanation for this anomaly lies, it is believed, in the fact that the (001) face contains a high area–density of hydroxyl groups and is therefore highly adsorptive for water molecules. In order for nucleation to occur on a C-face in aqueous solution, it is necessary that an area of the surface be denuded of adsorbed water molecules and a suitably large number of adipic acid molecules cluster on that denuded area. This is quite clearly a less probable occurrence than a mere clustering of a critical number of acid molecules on a "clean" crystal face. The probability of finding a suitably large water-free area on a face at any instant is reflected in the magnitude of the K-value for that face; it is provocative to note that the "K" values for the three faces decrease in the order B-face > A-face > C-face, which is precisely the order of increasing OH-density and thus expected water adsorptivity. (Further support to this argument is provided by the observation that adipic acid crystals grown from the vapor phase or from non-polar solvents assume the form of needles with dominant (010) faces; this is, of course, the habit with minimum free surface energy.) It can be argued that growth on the C-face (and to a lesser degree, on the A- and B-faces) is retarded by surface-ionization of carboxyl groups and development of electrostatic repulsive forces excluding adipic acid from the resultant double layer; clearly, however, this process must be secondary to water adsorption. Determination of the specific role of the double layer in this process will necessitate a study of the effect of pH and indifferent electrolyte concentration on adipic acid crystal growth from aqueous solution.

Since neither the anionic nor cationic surfactant appears to alter the (β) values for the three crystal faces implies that the surfactants do not alter the free energy of two-dimensional nucleation, and

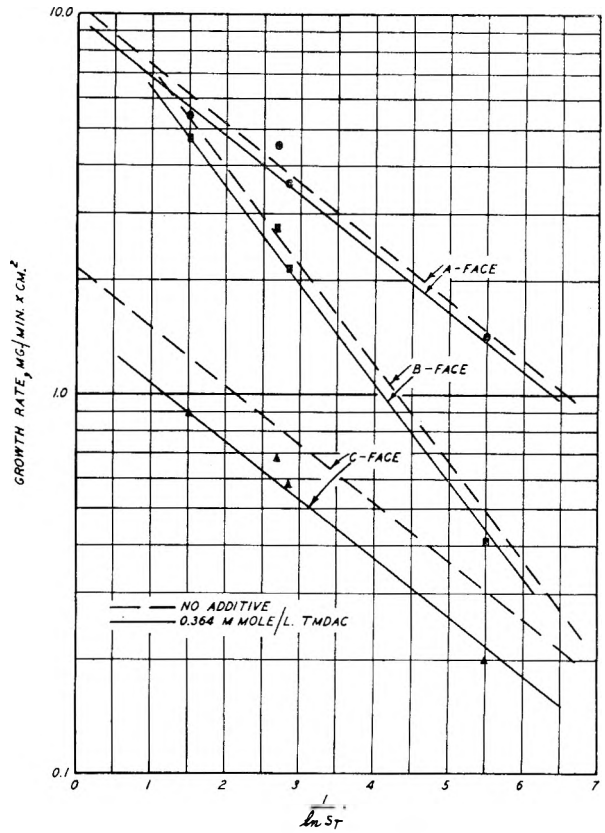

Fig. 6.—Specific growth rates of the faces of adipic acid crystals as a function of supersaturation (TMDAC present).

hence do not participate in the nucleation process, both additives reduce the (K) values, which suggests that they reduce the frequency of nucleation on a face. Possibly the surfactants adsorb on the different faces, thereby blocking a fraction of the facial area to attachment of nuclei. If this picture is correct, then there should be a correlation between the degree of retardation of growth on a face by a surfactant and its level of adsorption on that face.

Table II gives the fractional reduction in growth rate constants (K-values) of the A, B and C faces of adipic acid crystals caused by low concentrations of sodium dodecylbenzene sulfonate and trimethyldodecylammonium chloride. It would normally be expected that an amphipathic molecule would be adsorbed from aqueous solution preferentially to interfaces of low polarity or cohesive energy density. Since the most polar constituent of the adipic acid molecule is the carboxylic (OH) group, it should follow that greatest adsorption (from water) should occur on the crystal face with lowest hydroxyl density. With (SDBS), the percentage reduction in growth rate increases in the order C face < A face < B face, which is precisely the order of decreasing hydroxyl density. Exactly the opposite trend is observed with TMDAC; since the fatty quaternary ammonium ion carries a charge opposite to that of adipate ions undoubtedly present in the crystal lattice-face, an increase in adsorption of the cationic surfactant with increasing hydroxyl-density on a face might be anticipated. In short, the data of Table II appear to

support an adsorption-mechanism of growth-retardation; furthermore, they suggest that SDBS is adsorbed "tail-first" on the faces, while TMDAC is ionically adsorbed "head-first" and confirm the speculations of Fysh.[1]

TABLE II

RETARDATION OF SPECIFIC GROWTH RATE CONSTANTS BY SURFACTANTS

Additive and concn.	% Reduction in (K) A (110) Face	B (010) Face	C (001) Face
SDBS—0.137 mmole/l.	27.7	33.4	9.1
TMDAC—0.364 mmole/l.	9.5	14.8	31.8

B. Growth-from-Seeds Experiments.—The results of these experiments (Figs. 2 and 3) are qualitatively consistent with those discussed above, in that they show that the anionic surfactant exerts a far greater retarding effect on growth of the A- and B-faces than on growth of the C-face, and conversely for the cationic additive. As concentration of either surfactant is increased, relative differences in facial growth rates become less marked, whence it is evident that the greatest habit-changes are likely to occur at rather low surfactant concentrations.

The shape of the growth rate–surfactant concentration plots strongly suggested a self-limiting adsorption mechanism of growth-retardation and an effort was made to correlate the data in these terms. If it is assumed (a) that the fractional rate-reduction caused by the surfactant is proportional to the fraction of the face covered by adsorbed surfactant, and (b) that surfactant adsorption can be represented by a simple Langmiuir isotherm,[6] the growth rate of a face then can be expressed as a simple function of the surfactant concentration in solution as

$$R = R_0\left[1 - \frac{K^* b C_a}{1 + bC_a}\right] \qquad (6)$$

where

R = growth rate with surfactant
R_0 = growth rate without surfactant
K^* = fraction of surface covered when the surface is "saturated" with surfactant
C_a = surfactant concn. in bulk soln.
b = Langmuir isotherm constant

It is found that the data of Fig. 2 and 3 can, within the limits of experimental accuracy, be represented by such a correlation; the corresponding values of the constants K^* and b are given in Table III.

TABLE III

ADSORPTION AND GROWTH-INHIBITION CONSTANTS FOR SURFACTANTS ON ADIPIC ACID CRYSTALS

Surfactant	Av. value for A- and B-faces K^*	b	C-face K^*	b
SDBS	0.73	4.9	0.73	0.72
TMDAC	0.67	21.4	0.83	25.5

The constant K^* is, in effect, a measure of the saturation capacity of a face for the surfactant. For SDBS, the K^* values are the same for both the C-face and the "AB"-face, an observation consistent with the presumption of physical adsorption made earlier. For TMDAC, the K^* value for the C-face is significantly greater than that for the "AB"-face, as might be expected for ionic absorption. Also, the b-values are indicative of adsorption intensity or bond-strength, and it will be noted that these values are much higher for TMDAC than for SDBS; this, too, lends further support to the hypothesis of chemisorption of the former compound and physical adsorption of the latter.

Some rather important disparities between the nucleation-growth and seed-growth results merit comment. First, in the latter experiments, the growth rate of the C-face in the absence of the additives (1.65 mg./min. cm.^{2}) was substantially higher than the highest value observed in the nucleation–growth runs. Secondly, at low concentrations, the cationic surfactant had a much greater effect on the growth rate of macroscopic seed crystals than on the growth rate of nuclei. Thirdly, at high surfactant concentrations, the effect of both additives on the relative rates of growth of the individual faces was orders of magnitude greater during growth from nuclei than during growth upon seeds.

These disparities, can, it is believed, be qualitatively reconciled by recognizing that crystal growth can proceed by at least one mechanism other than two-dimensional nucleation—namely, by propagation from dislocations.[7,8] The probability that a dislocation will develop in a growing crystal face will increase with the length of time a crystal has been growing; in other words, larger crystals are likely to contain more dislocations than smaller ones, and large-area faces, more than small-area ones. Since growth from a dislocation is a process of lower activation energy than nucleation, the observed higher growth-rate on the predominant (001) face of a large adipic acid crystal relative to a small one might be expected. Furthermore, since a dislocation on a crystal face is normally self-perpetuating, mere contamination of parts of the crystal face by surfactant adsorption would be expected to be far less likely to impede growth of the face than would such adsorption on a "perfect" face where two-dimensional nucleation was the sole growth-initiating mechanism; hence, the much greater effect of surfactants upon growth of extremely small crystals relative to large ones. The peculiar enhanced activity of the quaternary surfactant upon the A- and B-faces of large crystals cannot be so readily explained; it is, however, possible that dislocations on the (010) and (110) faces of adipic acid crystals exhibit a specific adsorptive affinity for the fatty quaternary ion, whereupon such dislocations are inactivated for continued growth.

Several conclusions may be drawn from this investigation.

(1) The growth rates of the individual faces of adipic acid crystals deposited from water can

(6) Maximum surfactant concentrations studied were far below the reported c.m.c.'s of these compounds.

(7) W. K. Burton .N. Cabrera and F. C. Frank, *Disc. Faraday Soc.*, No. 5 (1949).

(8) W. K. Burton, N. Cabrera and F. C. Frank, *Nature*, **163**, 398 (1949).

be conveniently correlated with supersaturation level in terms of nucleation theory.

(2) The growth rates of the normal faces of the adipic acid crystal increases in the order (110) > (010) > (001). Rate constants correlate with hydroxyl-densities on the faces.

(3) Addition of trace-quantities (50–100 p.p.m.) of an anionic (SDBS) or cationic (TMDAC) surfactant causes reduction of the growth rate of all faces; SDBS retards growth on the (110) and (010) faces more than on the (001) face, thus favoring formation of prismatic or needle crystals, while TMDAC has the opposite effect, favoring growth of micaceous flakes.

(4) Surfactants appear to function as growth retarders by adsorbing on a crystal face and reducing the area on which nucleation can occur. With relatively large crystals, the influence of surfactants on growth can be correlated satisfactorily in terms of a Langmuir adsorption isotherm.

(5) Anionic surfactants such as SDBS appear to be physically adsorbed on the faces of the adipic acid crystal, while cationics such as TMDAC appear to be chemisorbed.

(6) Surfactants, in general, exhibit a far greater retarding influence on growth of very small crystals than on growth of large ones. It is deduced that growth from dislocations is less sensitive to interference by adsorbed contaminants than is growth by two-dimensional nucleation.

Acknowledgment.—The authors wish to express their gratitude to the Monsanto Chemical Company and to the G. L. Cabot Solar Energy Research Project, whose financial support (through Fellowship-aid to the junior author) made this study possible. Thanks are also extended to Mr. A. S. Kiziroglou, who performed the microscopic studies, and to Dr. R. D. Swisher of Monsanto, who so kindly provided the surfactant samples.

PROBABILITY MODEL THEORY OF CHAIN-END ACTIVATED POLYMER DEGRADATION. III. STATISTICAL KINETICS OF THE DEGRADATION OF POLYMETHYL METHACRYLATE[1]

BY MANFRED GORDON

Contribution from the Arthur D. Little Research Institute, Inveresk, Midlothian, Scotland

Received May 6, 1959

In this paper it is shown that exact analytical solutions can be obtained, in accordance with a proper statistical theory, for the kinetics of degradation of polymethyl methacrylate. The chemical model employed is that suggested by Brockhaus and Jenckel, which is a development of earlier findings by Grassie and Melville. In particular, the "spectrum" of chain-ends comprises three varieties: double-bonded ends, single-bonded ends without catalyst fragments and single-bonded ends with catalyst fragments. Of these the first is most reactive to zip-initiation during degradation, the second are much less reactive and the third are unreactive. The proportions of the three end-groups vary during the degradation reaction in accordance with statistical theory. The theory is based on published work by the author, and by Gordon and Shenton (*J. Polymer Sci.*, **38**, 157, 179 (1959)) on the use of probability models in degradation studies. Exact allowance is made in the theory for the initial distribution of polymer chain lengths, for the variation of the zip-length distribution as a function of reaction progress and for the effect of the radical disproportionation reaction. Up to 50% conversion, the solutions give almost quantitative agreement with the measurements by Brockhaus and Jenckel of the rate and double-bond content as a function of conversion, over the whole molecular weight range available. At higher conversions, the agreement is qualitative, and systematic deviations are attributable to minor side reactions. The agreement is somewhat better if it is assumed that the monomeric radicals are lost by evaporation, than if these radicals are imagined to participate in the general disproportionation reaction of the pool of radicals. The simpler rate theory by Brockhaus and Jenckel is shown to be the limiting case of the present theory for very long initial polymer chains. The model theory is applied to the temperature effect on degradation. The data of Brockhaus and Jenckel at 300° agree well with those of Madorsky at 240–270°. These results differ from those of Cowley and Melville at much lower temperature (192.5°), in that the termination step shows practically no activation energy (absence of gel effect). Arrhenius plots show that the unimolecular initiation at double-bonded ends has an activation energy of 29.6 ± 4.4 kcal./mole and a frequency factor of $10^{9.0 \pm 1.5}$ sec.$^{-1}$.

Introduction

Using ideas expounded in three previous papers,[2–4] exact solutions are here obtained for a number of variants of a kinetic model designed to fit chain-end activated depolymerization. The chemical situation treated applies to the thermal degradation of polymethyl methacrylate *in vacuo*. Data on this reaction were obtained at 220° by Grassie and Melville[5] and (in fair general agreement) more recently at 240–270° by Madorsky[6] and at 300° by Brockhaus and Jenckel.[7] The improved model solutions here derived will be successfully fitted to the results obtained by the latter two teams. Comparison of the rate curves by Madorsky and by Brockhaus and Jenckel with that found by Cowley and Melville[8] for the photodegradation of similar polymer *in vacuo* at a much lower temperature (192.5°) shows that the latter conforms to the same general pattern. Curves consisting of two straight lines meeting at a kink fit all the data for the rate of monomer loss as a function of the residual weight (Fig. 2, 6). Cowley and Melville proved that the termination reaction

(1) For parts I and II see references 3 and 4.

(2) M. Gordon, *Trans. Faraday Soc.*, **53**, 1662 (1957).

(3) M. Gordon and L. R. Shenton, *J. Polymer Sci.*, **38**, 157 (1959).

(4) M. Gordon and L. R. Shenton, *ibid.*, **38**, 179 (1959).

(5) N. Grassie and H. W. Melville, *Proc. Roy. Soc. (London)*, **A199**, 14, 24 (1949).

(6) S. L. Madorsky, *J. Polymer Sci.*, **11**, 491 (1953).

(7) A. Brockhaus and E. Jenckel, *Makromol. Chem.*, **18/19**, 262 (1956).

(8) P. R. E. J. Cowley and H. W. Melville, *Proc. Roy. Soc. (London)*, **A210**, 461 (1951).

was bimolecular, since the intensity exponent was found to be $^1/_2$ within experimental error. It will be shown in the discussion of Fig. 9 that the gel effect observed by Cowley and Melville at low temperatures does not operate at the higher temperatures used in the experiments of the other workers. The present work does not propose any changes in the chemical picture of the reaction as deduced by previous workers but is intended merely to eliminate all those approximations made in the kinetic theory which significantly affect the solutions. By way of introduction, the situation regarding these approximations in previous theories is now outlined in relation to the present work.

(1) End-group spectrum: the previous workers deduced that benzoyl peroxide catalyzed polymethyl methacrylate had a "spectrum" of three kinds of end-groups. Of these two were reactive in the initiation of zips during degradation, but their reactivities were widely different. Brockhaus and Jenckel proposed a theory which takes into account the initial end-group spectrum and that part of its variation with reaction progress which is due to the difference in reactivity just mentioned. However, they approximated by ignoring the effects of the disproportionation of radicals on the end-group spectrum (*i.e.*, through the re-formation of single-bonded and double-bonded end units). The elegant kinetic theories of degradation by Simha do not so far[9] take into account the effects of an end-group spectrum.

(2) The statistical effects due to the initial distribution of the polymer chains[2-4] are here taken into exact account (*cf.* Simha),[9] as are the effects of the zip-length distribution. Simha has criticised Brockhaus and Jenckel's theory because it does not treat these statistical effects, but it is here shown (see Appendix) that their solution to the rate problem applies exactly in the limiting case of sufficiently long zips (*i.e.*, when the mean zip length is much larger than the mean chain length). The reason is that in this limiting case the statistical effects become negligible. The present work also allows for the important variation of the zip-length distribution with reaction progress.

(3) Significant differences in the solutions are here obtained for the first time as a result of making different assumptions concerning the fate of the monomer radicals. The best fit of Brockhaus and Jenckel's data is achieved if these radicals are postulated to escape from the polymer by evaporation, which is in fact the postulate to which previous workers have inclined.

List of Symbols

b	reciprocal mean zip-length
$b(0)$	initial value of b
C	concn. of polymer radicals
c	concn. of monomeric radicals with catalyst fragment
DP	degree of polymerization ($= I$)
DP_n	mean degree of polymerization
DP_w	weight av. degree of polymerization
E	rate of evaporation of radicals with catalyst fragment (mole g.$^{-1}$ sec.$^{-1}$)
E_i	activation energy of initiation at double-bonded chain end
E_p	activation energy of depropagation
E_t	activation energy of disproportionation
F	$k_i'/(k_i'' - k_i')$
f	fraction of reactive chain ends which have double bonds
$f(0)$	initial value of f
$f(I)$	chain length distribution function
I	polymer chain length ($=$ DP)
k_i	initiation constant (sec.$^{-1}$)
k_i'	initiation constant for single-bonded chain end (sec.$^{-1}$)
k_i''	initiation constant for double-bonded chain end (sec.$^{-1}$)
k_p	depropagation constant (sec.$^{-1}$)
k_t'	disproportionation constant (g. mole^{-1} sec.$^{-1}$)
K	$k_p k_i^{1/2} M_0^{1/2}/k_t'^{1/2}$ (sec.$^{-1}$)
K'	$4k_t'(k_i'' - k_i')/M_0 k_p^2$
M	relative mass of polymer $m/m(0)$
M_∞	asymptotic value of M as $t \rightarrow \infty$
M_∞''	intercept of initial line of (dM/dt)–M plot on M-axis
M_0	mol. wt. of monomer ($=$ 100 for methyl methacrylate)
m	absolute mass of polymer
$m(0)$	initial absolute mass of polymer
n	no. of polymer chains
q	reciprocal mean polymer chain length ($= 1/DP_n$)
R	$(d \ln M/dt)/(d \ln M/dt)_0$
r	ratio $b(0)/q$ of mean chain length to initial mean zip length
T	absolute temperature
$\mathfrak{T}$	see eq. (48)
t	time
X_i	frequency factor for initiation at double-bonded chain end (sec.$^{-1}$)
X_p	frequency factor for depropagation (sec.$^{-1}$)
X_t	frequency factor for disproportionation (g. mole^{-1} sec.$^{-1}$)

Description of Model.—We assume that benzoyl peroxide catalyzed polymethyl methacrylate consists of an equimolar mixture of two chain distributions, which differ only in the nature of their end groups. Thus one-half of the chains have the structure

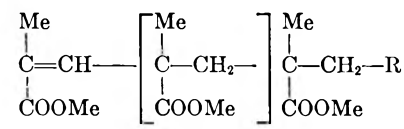

(1)

I-2

and the other half have the structure

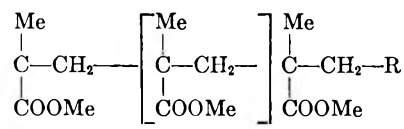

(2)

I-2

The single and double-bonded end groups on the left of the two chains arise in equal numbers from radical disproportionation in the termination reaction during polymerization. The groups denoted by R are an unspecified mixture of phenyl and phenylcarboxy radicals which have served for chain initiation in the polymerization process. The distribution of the chain length I, arising from the variable subscript in (1) and (2), is the same exponential distribution for both kinds of chain

$$f(I) = q \exp(-qI) \qquad (3)$$

where q is the reciprocal mean (number average) DP.

The models considered for the depolymerization of the above polymer involve initiation, depropagation and termination steps. Transfer, in particular transfer to polymer, is considered to play at most a minor part in the kinetics and is

(9) R. Simha, *Trans. Faraday Soc.*, **54**, 1345 (1958).

neglected. Initiation is taken to involve only the terminal units of a chain, and the ends carrying the catalyst fragment R are taken to be completely unreactive in the initiation process, which is thus confined to the particular links shown schematically elongated (to the left of the bracket of chains (1) and (2) above). Following Simha's picture for the initiation step, we shall describe this step merely as an activated homolytic scission of these bonds holding the terminal units. The initiation step thus produces in each case a chain radical and a monomeric radical, the latter comprising a double or a single "backbone" bond according to the kind of end-group involved in initiation. Grassie and Melville[5] and Brockhaus and Jenckel[7] have produced evidence for the fact that the double-bonded end units are much more easily split off to initiate depropagation than the single-bonded end units, and we shall accordingly introduce independent rate constants of initiation for the two kinds of ends. The rapid depropagation or "zipping" reaction, initiated as just described, consists of a succession of steps in which the chain radical loses its terminal unit in the form of a stable methyl methacrylate monomer molecule to leave behind a chain radical reduced in length by the loss of this one unit

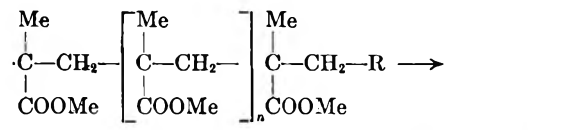

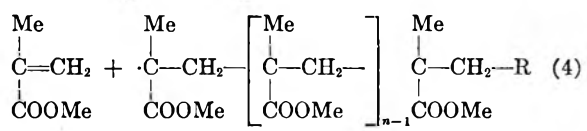

The bimolecular radical termination step is identical with the disproportionation reaction occurring in the polymerization reaction of methyl methacrylate at lower temperatures and produces two stable chains such as (1) and (2) from two radical-bearing chains.

Exhaustive and Non-exhaustive Zips.—We define by these two terms the two kinds of zip that can occur, *viz.*, respectively, the zips which terminate by disproportionation before the zipping process has reached the stable end of the chain, and those zips which degrade the affected chain completely. There are two kinds of monomer radicals: one kind arising at the beginning of *any* zip, having a single or double backbone bond but bearing no catalyst fragment; and another kind arising at the end of exhaustive zips only, having a single bond and carrying a catalyst fragment R.

Fate of Monomer Radicals.—In a *small* polymer sample, monomer radicals will rapidly reach the surface by diffusion, where they will be lost and later suffer dimerization in the liquid air trap of the vacuum system. (At very low temperatures, radical combination takes place rather than disproportionation.) Bywater[10] calculated that diffusion of monomer radicals was fast enough for them to be lost in this way under the conditions of his degradation experiments on emulsion-polymerized polymethyl methacrylate. If the specimen used for degradation experiments were sufficiently *bulky*, then the monomer radicals would have time to partake in the radical disproportionation reaction. We consider two cases.

(a) **Monomer Radical Evaporation.**—*I.e.*, all the monomer radicals, both with and without catalyst fragments, are immediately lost from the system by distilling out.

(b) **Monomer Radical Disproportionation.**—All the monomer radicals carrying catalyst fragments partake in the radical disproportionation reaction (each with a partner radical which may be of any size and with the same rate constant of disproportionation as the rest of the pool of radicals). The monomer radicals without catalyst fragment are still taken to be immediately lost by distilling out of the system. This is partly justified because they are physically smaller and because this scheme also fits exactly the case where initiation does not produce monomeric radicals. Moreover, if the monomer radicals without catalyst fragments are allowed to join the pool of disproportionating radicals, only *trivial* changes result. Let the monomer radicals without catalyst fragments still be denoted by c, and C embrace all other radicals. Then C in (10) has to be replaced by $(C - c)/2$, and k_i by $2k_i$ in (8) and (16) only. As a result, K becomes $K/2^{1/2}$ in the solutions (17), (19) and (21), and K' becomes $2K'$ in the solutions (27), (29) and (36).

An approximation has been involved in all previous treatments, according to which the *weight loss* by the escape of the monomer radicals produced by initiation of zips was not accounted for exactly as due, but by merely counting the mean zip to be increased by one unit in length. Simha[9] has shown that this approximation is really negligible in effect, and we continue to use it.

We abolish, however, the approximation made earlier[2] that the concentration of monomer radicals is sufficiently small for the termination reaction between two monomeric radicals to be neglected. Denoting the concentration of polymeric radicals by C and of monomeric ones by c, this approximation involved the neglect of the term c^2 with respect to Cc. As was stated,[2] within this approximation, the solutions for the cases of monomer radical evaporation and monomer radical disproportionation are identical. When the approximation is abolished, the solutions are still identical in the limiting cases when the mean zip length is much longer or much shorter than the mean polymer chain length, as will be shown below. However, the data by Brockhaus and Jenckel happen to cover the intermediate range where zip length and chain length are comparable, and the exact treatment then leads to small but significant differences (Fig. 1-3).

The model theory is now developed by first restating the exact (steady-state) solutions, rightly qualified as "intermediate solutions" by Simha.[9] They have the disadvantage of involving not only the relative mass of polymer M remaining at time t, the reciprocal mean chain length q at time t, but also the time derivatives of these two quantities. These intermediate solutions are capable of being checked against experimental data, and

(10) S. Bywater, THIS JOURNAL, 57, 879 (1953).

they have the great advantage of being independent of the form of the polymer chain length distribution at any time. Moreover, for the present case of the exponential distribution (3), the intermediate solutions immediately become final solutions in virtue of the invariant property,[2-4] which preserves this distribution throughout the course of chain-end activated degradation. Thus we may substitute in the intermediate solution

$$q = q(0),\ dq/dt = 0 \qquad (5)$$

and integrate with respect to time to remove the term in dM/dt. The intermediate and final solutions are obtained first for the case in which double-bonded and single-bonded end units are initiated at the same rate with one constant k_i (and as always the catalyst-fragment bearing ends are unreactive). Subsequently we have only to substitute a new composite initiation constant

$$k_i \longrightarrow k_i''f + k_i'(1 - f) \qquad (6)$$

where k_i'' is the initiation constant of a double-bonded end unit, and k_i' that of a single-bonded one. Without loss of generality, we shall assume

$$k_i'' > k_i' \qquad (7)$$

Of course, f denotes the fraction of double-bonded end units, and $(1 - f)$ the fraction of single-bonded ones at any time. A new variable f having been introduced, we need another equation to eliminate it. A differential equation to eliminate f is written down by considering the rate at which double-bonded and single-bonded end units are consumed (by initiation) and re-formed (by disproportionation), and the new general solution is obtained by integration.

Intermediate and Final Solutions in More Exact Form: Half of Chain Ends Equally Reactive, Other Half Unreactive to Initiation; Second-order Termination.—We re-write the equations obtained in the first paper[2] in identical notation but eliminating the assumption that $c << C$. As discussed above, the equations split up into two cases, according to whether the monomer radicals left over from fully depropagated chains suffer

Disproportionation		Evaporation	
$k_iMq/M_0 = k_t'M\,(C + c)^2$ (eq. 14, 15, ref. 2)	(8)	$k_iMq/M_0 = k_t'MC^2 + E$	(9)
$dM/dt = -k_pM_0MC$	(10)	$dM/dt = -k_pM_0MC$ (eq. 3, ref. 2)	(11)
$k_t'Mc(C + c) = -[M(dq/dt) + q(dM/dt)]/M_0$ (*cf.* eq. 8b, ref. 2)	(12)	$E = -[M(dq/dt) + q(dM/dt)]/M_0$ (*cf.* eq. 8b, ref. 2)	(13)
$b = k_t'(C + c)/k_p$	(14)	$b = k_t'C/k_p$	(15)
$K = k_pk_i^{1/2}M_0^{1/2}/k_t'^{1/2}$ (eq. 10, ref. 2)	(16)	$K = k_pk_i^{1/2}M_0^{1/2}/k_t'^{1/2}$ (eq. 10, ref. 2)	(16)

The fractional weight $m/m(0)$ of polymer remaining undegraded is throughout denoted by M. The molecular weight of the repeat unit is designated by M_0, which is 100 for polymethyl methacrylate.

The (steady-state) rate of evaporation of the monomer radicals left over is denoted by E. The reciprocal mean zip length b of all non-exhaustive zips is given, according to (14) and (15), as the ratio of the rate of disproportionation of polymer radicals to their rate of depropagation.

The intermediate solutions are obtained by eliminating C and c.

$$\text{(Disprop.)}\quad \frac{dM}{dt} = -\frac{K(k_iq + (dq/dt))}{Kq + k_iq^{1/2}}M \qquad (17)$$

$$\text{(Evap.)}\quad \frac{dM}{dt} = -\frac{K^2q}{2k_i}\left[\sqrt{1 + \frac{4k_i}{K^2q}\left(k_i + \frac{d(\ln q)}{dt}\right)} - 1\right]M \quad \text{(eq. 9, ref. 2)} \qquad (18)$$

In addition we may eliminate C and c from (14) and (15)

$$\text{(Disprop.)}\quad b = k_iq^{1/2}/K \qquad (19)$$

$$\text{(Evap.)}\quad b = \left[\sqrt{1 + \frac{4k_i}{K^2q}\left(k_i + \frac{d(\ln q)}{dt}\right)} - 1\right]q/2 \qquad (20)$$

By means of eq. 5 we obtain the final solutions from (17) and (18), *viz.*, the first-order rate laws (which can immediately be integrated if required)

$$\text{(Disprop.)}\quad \frac{dM}{dt} = -\frac{Kk_iq^{1/2}}{Kq^{1/2} + k_i}M \qquad (21)$$

$$\text{(Evap.)}\quad \frac{dM}{dt} = -\frac{K^2q}{2k_i}\left[\sqrt{1 + \frac{4k_i^2}{K^2q}} - 1\right]M \quad \text{(eq. 9b, 11, ref. 2)} \qquad (22)$$

The last two equations are asymptotically equal for large and small q, as is visible in Fig. 1. This reproduces Fig. 2 of the first paper[2] but incorporates the additional graph C corresponding to the new rate law 21, for monomer radical disproportionation. The differences between this and graph B for monomer radical evaporation are seen to be small but significant in the central parts of the graph where chain length and zip length are comparable. The reciprocal mean length of exhaustive zips is found from (20) by means of substituting from eq. 5

$$\text{(Evap.)}\quad b = \left[\sqrt{1 + \frac{4k_i^2}{K^2q}} - 1\right]q/2 \qquad (23)$$

while (19) stands without further treatment. It has been shown from the probability model theory that the rate of mass loss can be expressed in terms of k_i, q and b alone. The appropriate equation, derived previously, must of course fit both the monomer radical disproportionation and evaporation cases, and it is obtained by eliminating K either between (19) and (21) or between (22) and (23)

$$dM/dt = -k_iMq/(q + b) \quad \text{(eq. 54, ref. 3)} \qquad (24)$$

The factor 2 previously[3] included on the right was due to the earlier assumption of two active chain-ends per chain.

Final Solutions for the Model with an End-group Spectrum; Radical Termination by Dispropor-

tionation.—According to the plan of action described, we now effect the substitution (6) in the solutions (19–24) just obtained. For this purpose K must be split up into its constituent constants (eq. 16) because k_i is also amongst these and must be substituted by $k_i''f + k'(1 - f)$ wherever it occurs. The resulting expressions can, however, be simplified by introducing the new dimensionless constants

$$K' = 4k_t'(k_i'' - k_i')/M_0k_p^2 \; (= k_t'(k_i'' - k_i')/25k_p^2) \tag{25}$$

and

$$F = k_i'/(k_i'' - k_i') \tag{26}$$

Thus with the use of (6), (16), (25) and (26), equations 21 and 22 for the rate of mass loss become

$$\frac{dM}{dt} = -\frac{(k_i'' - k_i')(f + F)}{1 + \frac{1}{2}\sqrt{\frac{K'(f + F)}{q}}} M \tag{27}$$

(Disprop.)

$$\frac{dM}{dt} = -\frac{2(k_i'' - k_i')q}{K'}\left[\sqrt{1 + \frac{K'(f + F)}{q}} - 1\right] M \tag{28}$$

(Evap.)

and equations 19 and 23 for the reciprocal mean zip-length become

$$b = \frac{1}{2}\sqrt{K'q(f + F)} \tag{29}$$

(Disprop.)

$$b = \frac{q}{2}\left[\sqrt{1 + \frac{K'(f + F)}{q}} - 1\right] \tag{30}$$

(Evap.)

The equation 24 which is common to both the disproportionation and evaporation schemes, becomes

$$dM/dt = -(k_i''f + k_i'(1 - f))Mq/(q + b) \tag{31}$$

in virtue of (6). The exact differential equation which is required to eliminate f from the solutions 27 to 30 will be shown to be

$$\frac{d(fM)}{dt} = -\frac{M}{q + b}\left(k_i''fq + \frac{1}{2}k_i''fb - \frac{1}{2}k_i'(1 - f)b\right) \tag{32}$$

The chains carrying double-bonded end units, and those carrying single-bonded ones, severally obey the invariant distribution (3) throughout the course of the degradation reaction. Therefore the relative mass M remains proportional to the total number n of chains present, and M may be replaced by n in all the equations where it has occurred from (21) onwards. Equation 32 is best derived in the form

$$\frac{d(fn)}{dt} = -\frac{n}{q + b}\left(k_i''fq + \frac{1}{2}k_i''fb - \frac{1}{2}k_i'(1 - f)b\right) \tag{33}$$

which governs the rate of decay of the number fn of those chains which carry double-bonded end units. For comparison we similarly rewrite (24) in the form

$$dn/dt = -k_inq/(q + b) \tag{34}$$

Since non-exhaustive zips do not change the numbers of polymer chains present, $-dn/dt$ in (34) represents exactly the rate at which exhaustive zips occur in an exponentially distributed population of n chains, when each chain bears only one reactive end with initiation constant k_i. The total rate at which exhaustive and non-exhaustive zips occur in such a population is k_in, and therefore the rate of occurrence of non-exhaustive zips is $k_i \cdot nb/(q+b)$.

The population of chains in our model comprises various subclasses, *e.g.*, double-bonded chains, single-bonded chains, chains in the process of undergoing a non-exhaustive zip, or chains under-

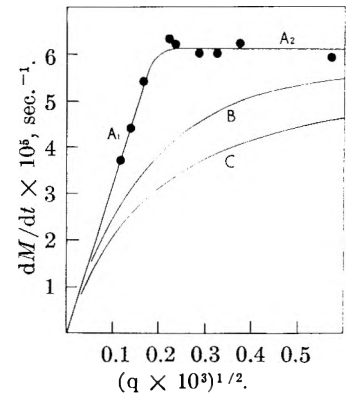

Fig. 1.—Initial rates at 220° for polymethyl methacrylate[11] as function of $q^{1/2}$ according to Grassie. The points fit the asymptotes A_1 and A_2, but not the actual solutions B (eq. 22, evaporation) or C (eq. 21, disproportionation).

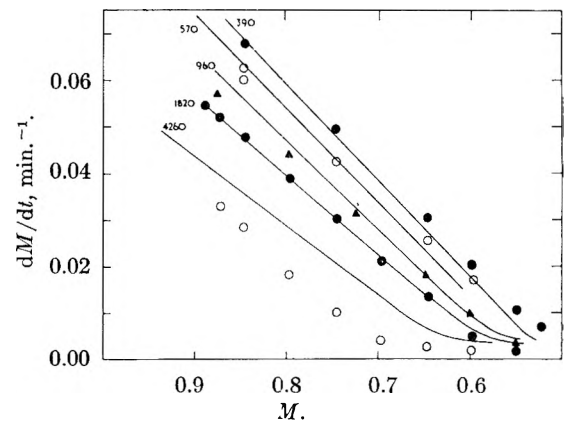

Fig. 2.—Approximate optimum fit of Brockhaus and Jenckel's data[7] of rate *versus* conversion at 300° for polymethyl methacrylate. Monomer radicals are assumed to *disproportionate* (eq. 27, 36). The curves are labelled with the weight average DP (= $2/q$) of the polymer.

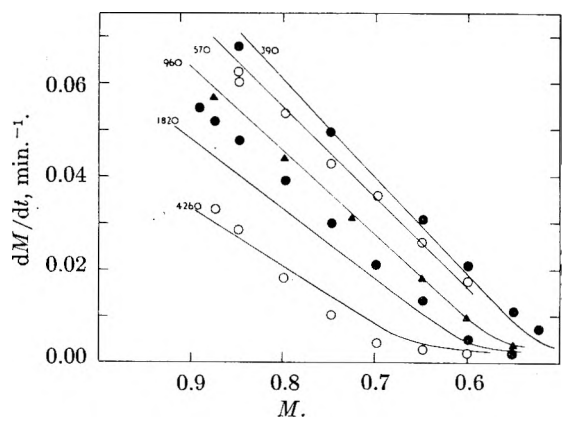

Fig. 3.—Approximately optimum fit of the data in Fig. 2, calculated from eq. 28, 37 for *evaporation* of monomer radicals.

going their final, exhaustive zip, etc. Each such class of chains is distributed according to eq. 3, *i.e.*, as the population as a whole. This follows because of the normal assumption that initiation, propagation and termination constants (and therefore b) are independent of the length of the polymer chain whose fate is under discussion. Applying the expressions obtained in the last paragraph to various such subclasses in the model, we prove eq. 33: The model comprises at time t a total of n chains, of which a fraction f bear double-bonded end units. Therefore, the left side of (33) denoted the net rate of change in the number of double-bond ended chains. The right side sums three terms which contribute to this net change

$-k_i''nfq/(b+q)$ = rate at which double-bond ended chains are lost by exhaustive zips

$-k_i''nfb/2(q+b)$ = rate at which double-bond ended chains are lost by non-exhaustive zips which result in stabilization of the chain-end as a single-bonded unit by disproportionation (*i.e.*, with probability $1/2$)

$+k_i'n(1-f)b/2(q+b)$ = by symmetry, rate of gain of double-bond ended chains by stabilization after non-exhaustive zips initiated at a single-bonded end unit

Integrated solutions for f and M as functions of time can be obtained from either (27), (29) and (32) for monomer radical disproportionation, or from (28), (30) and (32) for monomer radical evaporation. Equation 31 is consistent with both schemes; it gives no new information but is used for convenience of manipulation. Thus eliminating t between (31) and (32), one finds

$$+\frac{df}{d(\ln M)} = \frac{k_i''fq + \frac{1}{2}k_i''fb - \frac{1}{2}k_i'(1-f)b}{(k_i''f + k_i'(1-f))q} \quad (35)$$

Substituting for b from (29) or (30), eliminating k_i'' and k_i' by means of (26), separating the variables, and integrating, yields

$$\ln M = \int_{f(0)}^{f} \frac{(x+F)dx}{x(1-x) + \frac{1}{4}(K'(x+F)/q)^{1/2}[(2F+1)x - F]}$$

(Disprop.) (36)

$$\ln M = \int_{f(0)}^{f} \frac{(x+F)\,dx}{x(1-x) + \frac{1}{4}\{(1+(K'(x+F)/q))^{1/2} - 1\}[(2F+1)x - F]} \quad (37)$$

(Evap.)

In accordance with our model, the initial value $f(0)$ will be taken to be $1/2$. Having thus obtained M as a function of f, the time can be evaluated as an explicit function of either of these quantities from (27) or (28). In fact, the quadratures in (36) and (37) can be evaluated in terms of elementary functions. In this way we shall derive in the Appendix the complete solution of the model system for all the limiting cases of interest. For the most general case, however, it is preferable to carry out the quadratures numerically (using Simpson's rule) and this was then done below to obtain the fitting of the experimental data by Brockhaus and Jenckel in Fig. 2 and 3.

It is apparent that the two systems of solutions, *viz.*, (27), (36) for monomer radical disproportionation and (28), (37) for monomer radical evaporation agree asymptotically for sufficiently large or sufficiently small reciprocal mean chain length q. The general features of the solutions can be discussed by reference to the traditional plot of rate of monomer loss against conversion (Fig. 2, 3). It is recalled that provided all the chain ends have equal initiation constants, such a plot is linear under many sets of reasonable assumptions, especially irrespective of the nature or reaction order of the termination step.[2] This linearity betokens the kinetic first-order character of the rate of monomer loss and has been observed experimentally using numerous polymers.[2] Detailed examination of the solutions just obtained for the more elaborate model, involving two different initiation constants and radical disproportionation, reveals that the corresponding plots generally fall into two regions of almost exact linearity (first-order monomer loss), joined together by a transition region which features as a sharp kink in the plot (Fig. 3, bottom plot, and Fig. 6). Figures 2 and 3 present the (approximately) best fits obtainable, respectively, from the solution for monomer radical disproportionation (eq. 27, 36) and evaporation (eq. 28, 37) to the data in Fig. 8 of the paper by Brockhaus and Jenckel.[7] These fittings were obtained by calculating first M as a function of f (eq. 36 or 37) and then dM/dt as a function of M (eq. 27 or 28).

The graphs are labeled with the values of the initial weight average used. The number average is calculated from the viscometric DP_w measurements of these authors by assuming that

$$DP_n = 0.5DP_w \quad (38)$$

This theoretical relationship for an exponential chain population is borne out by direct osmometric measurements by the same authors only at the highest DP studied, while at the lowest molecular weights the relation 38 is in error by 40 to 50%. In these circumstances the viscometric DP_w would be regarded as more reliable than the osmometric DP_n, and trials showed that the optimum fit in Figs. 2 and 3 would be seriously impaired if it were based on the osmometric *in lieu* of the viscometric DP.

To simplify the diagrams, the data referring to two separate runs ($0.5DP_w$ = 260 and 310), which gave almost identical rates of monomer loss over the whole range of conversion, were fitted to a single curve calculated for DP_n = 285. The fitting of all the five plots in each figure depends on the choice (Table I) of three parameters: K', k_i'' and k_i' (and hence F (eq. 26) in (27), (36) or (28), (37)). Of these three, K' figures only as a multiplier of $1/q$ (= DP_n) and thus exerts its influence on the placing of the plots, *i.e.*, suitable adjustments of K' will transform any one plot into any of the others. The kinks occur generally in the region where f and F are approximately equal. In each run f is initially $f(0) = 0.5$ and falls monotonically (Fig. 4) during the run to a small asymptotic value

($f(\infty)$ in Table I). The adjustment of k_i'' affects mainly the slope of the initial, linear plots of dM/dt against M, while F governs the final slopes of these graphs after they have passed their central kink. As regards these final linear portions of the plots, converging on the point $M = 0$, $dM/dt = 0$, the experimental results were shown by their authors[7] on a separate plot on a much larger scale (their Fig. 9). The corresponding plots calculated from the model solutions and using the same parameters as for the Figs. 2 and 3 do show qualitatively the correct shapes, *i.e.*, straight lines converging on the same point. However, their slopes ($-d \ln M/dt$) are too small compared with the experimental lines, as is set out in Table I. The discrepancies between the experimental and calculated final slopes, range from a factor of about 3 at low DP_n to about a factor 15 at high DP_n. These discrepancies could be reduced quite appreciably by lowering the value of k_i' chosen, without affecting the fit in Fig. 2 and 3. However, further adjustments of this kind are not worthwhile. The model used leads to the result of eq. 5, *i.e.*, constancy of the DP_n with conversion. This is very reasonably obeyed for the conversions covered by Fig. 3 and 4 but breaks down in practice at higher conversions, especially at high initial DP_n. This quantitative failure of the model at high conversion has been tentatively attributed[4] to some small superposed scission reaction, which for some reason becomes more important at high conversion.

TABLE I

PARAMETERS USED IN (AND DEDUCED FROM) FIGS. 2 AND 3

A. Parameters used

Monomer radicals	k_i' (min.$^{-1}$)	k_i'' (min.$^{-1}$)	$F = k_i'/(k_i'' - k_i')$	K'	$f(0)$
Disproportionate	0.0070	0.2870	0.025	0.00805	0.5
Evaporate	0.0056	0.2856	0.020	0.0235	0.5

B. Parameters deduced

Run at DP_n	Monomer radicals	$f(\infty)$ Eq. 36, 37 ($M \to 0$)	$-(d \ln M/dt)_{t\to\infty}$ min.$^{-1}$, Eq. 27, 28	$-(d \ln M/dt)_{t\to\infty}$ min.$^{-1}$ Exptl.
2130	Disproportionate	0.00372	0.0060	0.0015
	Evaporate	.00201	.0058	
910	Disproportionate	.00249	.0063	.0014
	Evaporate	.000968	.0062	
285	Disproportionate	.00145	.0066	.00063
	Evaporate	.00032	.0064	
195	Disproportionate	.00120	.0067	.00043
	Evaporate	.000222	.0063	

The scheme based on monomer radical evaporation (Fig. 2) gives a better fit of the data than the scheme for monomer radicals participating in disproportionation (Fig. 3), and this in agreement with views of workers in this field. The two schemes do not differ at all in their abilities to fit individual curves of dM/dt *versus* M, since both solutions range over curves of practically identical shapes, but they do differ somewhat in the parametric dependence of these curves on the mean DP

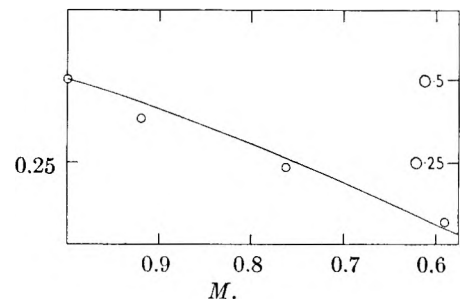

Fig. 4.—Fitting of Brockhaus and Jenckel's data[7] for the fraction f of double-bonded reactive ends as a function of conversion for polymethyl methacrylate of $DP_w = 805$. The curve is calculated from eq. 37 without adjustment of parameters (*i.e.*, using the parameters deduced from Fig. 3 and shown in Table I).

(or its reciprocal q) within the experimental range. (These differences regarding the effect of q were already apparent in Fig. 1, which was based on the simpler scheme involving a single initiation constant.) Thus in Fig. 2 the position of the experimental results accords well with the calculated curves over the whole of the 11-fold molecular weight range studied. The curve at $DP_w = 1820$ has suffered a systematic displacement from the experimental data, which could be wholly accounted for if the measured DP_w was a little too high. The theoretical explanation of the effect of molecular weight on the rate of degradation, inherent in Fig. 2, is a considerable advance on the fitting based on the cruder model of earlier data (Fig. 1). Concerning the detailed shapes of the curves in Fig. 2, the theory and measurements show that the kinks occur near $M = 0.5$ at low DP_n but gradually move to the left and downward as the DP_n increased above the mean zip length, and the quantitative agreement achieved in this respect leaves little doubt as to the essential correctness of the assumptions made in the kinetic scheme.

It would clearly be useful to clinch the proof of the degradation mechanism by showing that the concentration of double-bonded ends during the reaction decreases in accordance with the values of f calculated from the solution of eq. 37. Fortunately this is possible, because Brockhaus and Jenckel applied their elegant oxidation technique for estimating double-bonded end-groups to their polymers at various stages of degradation. The results (in their Fig. 13) are not very extensive nor can they be expected to be extremely accurate. Their most reliable plot, referring to $DP_n = 402.5$, is shown in Fig. 4 against the theoretical curve obtained from eq. 37. Since K' and F are already known from the curve-fitting process in Fig. 2, there are no parameters involved in the very reasonable fitting of Fig. 4. The scale factor along the f-axis is fixed by the requirement to make the measured unsaturation of undegraded polymer ($M = 1$) correspond to $f(0) = 1/2$. Similar plots for the unsaturation measurements at other DP values would reveal no *systematic* deviations from the theory, and the assumptions of the kinetic scheme (for monomer radical evaporation) are considered to have been proved for conversions in the range from $M = 1$ to $M \simeq 0.5$.

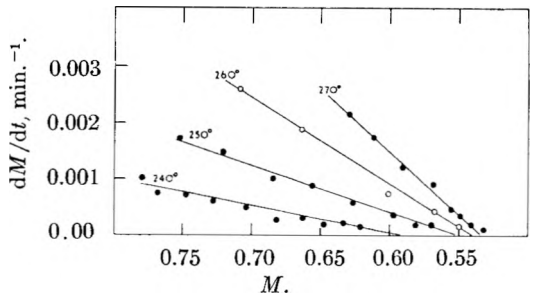

Fig. 5.—Determination of intercepts M_∞'' on the conversion axis from Madorsky's rate data[6] at the four temperatures shown.

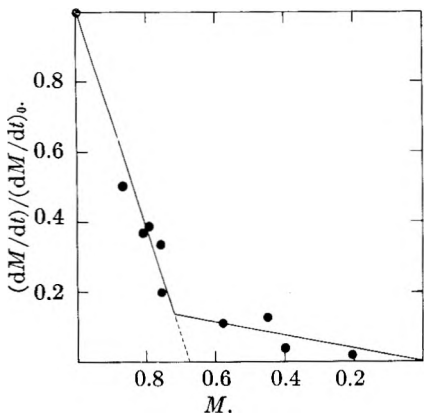

Fig. 6.—Determination of intercept M_∞'' on the conversion axis from Cowley and Melville's rate data[8] for photodepolymerization at 192.5°.

Discussion of the Kinetic Zip-lengths

The mean zip-length $1/b$ can be computed from the model at various stages of the reaction, using eq. 29 and 30. The fraction f of the reactive chain ends which consist of double-bonded ends falls markedly (Fig. 4) during the experimental range of the degradation reaction in Fig. 2 and 3. This causes marked falls in the radical concentration and marked rises in the mean zip length. At a point in the region where the rate curves of Fig. 2 and 3 have their kinks, we have f equal to F. Table II compares initial zip lengths (*i.e.*, $f(0) = 0.5$) with those prevailing at $f = F$, while the value of the constant F is always that listed in Table I.

TABLE II

MEAN CHAIN-LENGTHS AND ZIP-LENGTHS FOR BROCKHAUS AND JENCKEL'S DATA

Run at DP_n ($=1/q$)	Monomer radicals	Initial zip-length $1/b(0)$	$b(0)/q = r$	Zip-length $1/b$ when $f = F$	b/q
2130	Disproportionate	1410	1.51	4580	0.47
	Evaporate	1010	2.11	5810	.37
910	Disproportionate	930	0.98	3000	.30
	Evaporate	730	1.25	5030	.18
285	Disproportionate	520	0.55	1680	.17
	Evaporate	510	.56	4520	.063
195	Disproportionate	430	.45	1390	.14
	Evaporate	465	.42	4430	.044

Thus our model reveals that changes in zip-length of up to 10-fold can occur over the experimental range covered by Brockhaus and Jenckel's data. All previous theories have used models based on a mean zip-length independent of reaction progress. Our last paper[4] showed that this provides a good approximation when all the reactive chain ends are equally reactive, though it would obviously be quite inappropriate here. In particular, Brockhaus and Jenckel themselves interpreted their data on a model in which neither the initial chains nor the zips were distributed in size. The zip-lengths they deduced are intermediate between our *initial* values for disproportionation and evaporation of monomer radicals, respectively, at any given DP_n. It should be noted that our treatment solves quantitatively the problem which arises[8,11] when treating the intensity exponent in photo-polymerization. There, one requires to know the fraction of all the zips which are exhaustive, and we have shown above that this is given by $q/(b+q)$.

The Effects of Temperature.—Before developing the model treatment of the energetics of depolymerization of polymethyl methacrylate, we note that the relevant solutions of this paper are functions only of the *ratio* of the mean chain-length to the mean zip-length but do not otherwise depend on q, on k_p or on k_t'. We shall denote the initial value of the ratio just mentioned by

$$r = b(0)/q \qquad (39)$$

The effect of temperature on depolymerization rate was studied by Madorsky[6] using a commercial sample of benzoyl peroxide catalyzed polymer. The molecular weight is stated to have been 150,000, without any reference to the method of averaging adopted. The results harmonize very well with Brockhaus and Jenckel's if we assume that in fact the weight average was 150,000 (*i.e.*, $DP_w = 1500$, $DP_n = 750$), and the Arrhenius plots (Fig. 8 and 9) have been drawn on this assumption. If the number average molecular weight were taken to be 150,000, both Arrhenius plots would be somewhat impaired, since Madorsky's points would be moved downwards in Fig. 8 and upwards in Fig. 9, in each case by an amount $\frac{1}{2} \log 2 = 0.15$. The present theory permits the drawing of two Arrhenius plots (Fig. 8, 9) in place of the conventional one for over-all initial rates. The new plots refer to $k_p/k_t'^{1/2}$ and to K' (which is proportional to $(k_i'^{1/2} k_t'^{1/2}/k_p)^2$ by eq. 25). The cruder analysis of previous models equated the activation energy corresponding to the over-all initial rate to $\frac{1}{2}E_i + E_p - \frac{1}{2}E_t$ and this turns out to be exact within experimental error as a result of our analysis, without adding any new information. The Arrhenius parameters deduced from the plots (Fig. 8,9) are collected in Table III, together with rough estimates of the probable errors.

The plot (Fig. 8) of $\log K'$ against $1/T$ uses the value of $K' = 0.0235$ obtained in Table I from fitting all Brockhaus and Jenckel's rate curves at 300°K. (Fig. 3). The remaining four values at different temperatures are deduced from Madorsky's data.[9] To this end, the intercepts M_∞'' on the M-axis of his experimental linear portions of the rate plots in Fig. 5 are used, these being comparable to the initial linear portions of the curves in Fig. 3. Since $F \ll 1$ (Table I), eq. 37 shows that this inter-

cept is a function of K'/q. This in turn can be expressed as a function of r, by solving eq. 30

$$K'/q = 4r(r + 1)/(f(0) + F) \qquad (40)$$

Putting $f(0) = {}^1/_2$ as throughout, and neglecting F in comparison, yields

$$K'/q = 8r(r + 1) \qquad (41)$$

The functional relation between the intercept M_∞'' and r was found numerically from eq. 37 (and using (41)). A smooth graph was obtained (Fig. 7) by plotting $\log 2(1 - M_\infty'')/(M_\infty'' - 0.5)$ against $1 - \log r$. The form of this interpolation formula ensures (eq. 62) that for large r the plot becomes linear; and over the required range (Fig. 7) curvature is not serious. The plot was used to convert the experimental intercepts in Fig. 5 to theoretical r values recorded in Table IV. Hence ${}^1/_2 \log K'$ was computed by eq. 41 at various temperatures (Table IV) and plotted in the Arrhenius plot (Fig. 8). The scatter of the points in relation to the scale of the plot is not too serious. Turning to the Arrhenius plot (Fig. 9) for $\log k_p^2/k_t'$, we first show how this expression can be computed from the experimental data. Thus, by again neglecting F with respect to f, it is seen from eq. 25, 28 and 30, that

$$k_p^2/k_t' = -(dM/dt)_0/100rq \qquad (42)$$

The initial rates listed in Table IV were taken from the sources listed, except that in the case of 300° the value of k_p^2/k_t' was calculated from the parameters used in Table I (using eq. 25), so that this value again receives its support from the whole of Brockhaus and Jenckel's data for different molecular weights. In addition, Fig. 9 shows one point for the rate curve (Fig. 6) obtained at 192.5° by Cowley and Melville[8] for the photo-catalyzed degradation of benzoyl peroxide catalyzed polymethyl methacrylate. The reason for the much larger value of k_p^2/k_t' at this lower temperature is well understood and is due to the diffusion control of the termination constant (gel effect) in the very viscous polymer. Cowley and Melville were able

TABLE III

ACTIVATION ENERGIES E AND FREQUENCY FACTORS X FROM ARRHENIUS PLOTS (FIGS. 8, 9)

Fig.	Analysis of slope	Analysis of intercept (in sec.$^{-1}$)
8	${}^1/_2E_i - E_p + {}^1/_2E_t = -4.2 \pm 2.0$	${}^1/_2 \log X_i - \log X_p + {}^1/_2 \log X_t = 1.8 \pm 0.7$
9	$E_p - {}^1/_2E_t = 19.0 \pm 0.8$	$\log X_p - {}^1/_2 \log X_t = 6.3 \pm 0.3$

to prove this directly by the low value of k_t' and by its high activation energy (about 20 kcal./mole). In the higher temperature range covered by Madorsky's and Brockhaus and Jenckel's data, analysis of the slope of the line in Fig. 9 shows that k_t' has practically no activation energy as is consistent with the absence of the gel effect. Thus E_p is known to be about 18.5 by adding[8] the heat (13.5 kcal./mole) of polymerization to the activation energy (about 5 kcal./mole) of the propagation step in the polymerization reaction, which represents the formal reversal of the propagation step in depolymerization. Again, E_t should equal the activation energy (about[12] 1 kcal./mole)

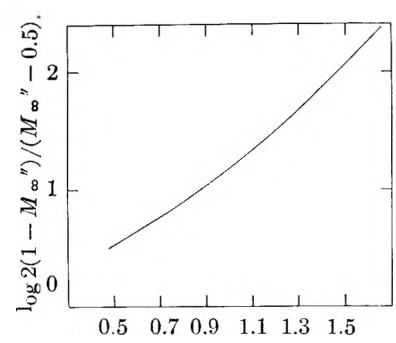

Fig. 7.—Interpolation graph to convert the intercepts M_∞'' of the last two figures to r-values.

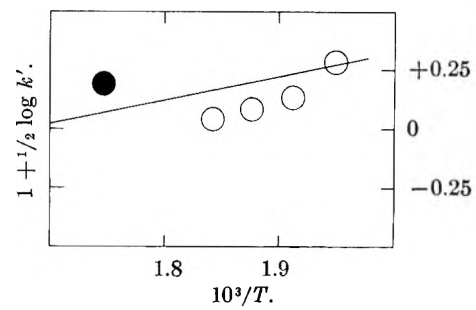

Fig. 8.—Arrhenius plot for $(k_i''k_t')^{1/2}/k_p$ (*cf.* Table IV): ○, data of Madorsky[6]; ●, data of Brockhaus and Jenckel.[7]

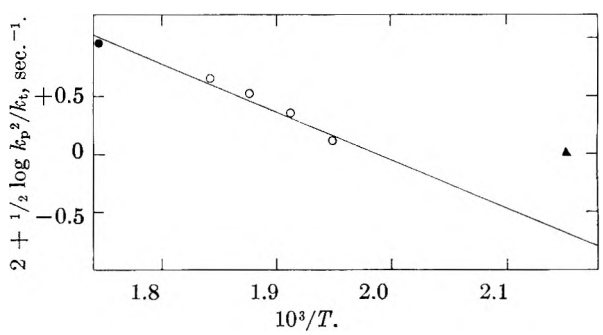

Fig. 9.—Arrhenius plot for $k_p/k_t^{1/2}$ (*cf.* Table IV): ●, Brockhaus and Jenckel; ○, Madorsky; ▲, Cowley and Melville, displacement from line due to gel effect.

of the termination step in the polymerization reaction measured in absence of the gel effect. The value of $E_p - {}^1/_2E_t = 18$ kcal./mole thus predicted agrees very acceptably with that of 19.0 found in Table III. The Arrhenius parameters of the unimolecular initiation of zips at a double-bonded chain end (1) can be found from Table III without additional assumptions, *viz.*, $E_i = 29.6 \pm 4.4$ and $\log X_i = 9.0 \pm 1.5$. For an ordinary homolytic scission of the bond drawn schematically lengthened in (1) a higher value of E_i would be expected, and $\log X_i$ would be about 13. Therefore, the real process is energetically easier and configurationally more difficult than such a scission, perhaps because of an intramolecularly cyclic transition state.

Appendix

In this appendix we list integrated solutions for the limiting cases $b/q >> 1$ and $b/q << 1$, which are equally valid for disproportionation or evaporation of radicals. We also list such solutions for the limiting cases $k_i' = k_i'' = k_i$ (say), and $k_i' =$

TABLE IV

DATA USED FOR ARRHENIUS PLOTS (FIG. 8, 9)

Temp. °C.	Ref.	Intercept M_∞''	r = Chain-length / Zip-length	DP_n (= $1/q$)	$1 + {}^1/_2 \log K'$ (Table I or eq. 41)	$\left(\frac{dM}{dt}\right)_0 \times 10^5$ sec.$^{-1}$	$2 + {}^1/_2 \log \frac{k_p^2}{k_t'}$ (sec.$^{-1}$) (eq. 25 and Table I or eq. 42)
300	7	...	...	..	0.185	...	0.955
270	6	0.533	0.684	750	.0448	18.3	.651
260	6	.541	.785	750	.0875	11.5	.520
250	6	.551	.912	750	.1348	6.25	.355
240	6	.590	1.413	750	.2802	3.33	.114
192.5	8	.675	2.92	1250	....	2.38	.005

0, in forms which are exact for monomer radical disproportionation and approximate for monomer radical evaporation.

The Case $b/q >> 1$ (Long Chains and Short Zips).—For any given set of values of k_i'' and k_i', the case $b/q>>1$ will be realized if the initial value $b(0)/q = r$ is sufficiently large. By putting $b/q>>1$ in (27) and (29)—or in (28) and (30)—one obtains

$$\frac{d \ln M}{dt} = -\frac{k_i'' - k_i'}{r}\sqrt{(f + F)(f(0) + F)} \quad (43)$$

The relative rate R is therefore given by

$$R = \frac{d \ln M/dt}{(d \ln M/dt)_0} = \sqrt{(f + F)/(f(0) + F)} \quad (44)$$

Again neglecting q with respect to b, eq. 35 reduces to

$$\frac{df}{d \ln M} = \frac{r((1 + 2F)f - F)}{\sqrt{(f + F)(f(0) + F)}} \quad (45)$$

By multiplying eq. 43 and 45 together, and integrating, the fraction f of double-bonded ends is seen to decay exponentially with time to its asymptotic value $k_i'/(k_i' + k_i'')$, thus

$$= \left[\left(f(0) - \frac{k_i'}{k_i' + k_i''}\right)\exp - \frac{k_i' + k_i''}{2}t\right] + \frac{k_i'}{k_i' + k_i''} \quad (46)$$

Inserting this in (43) to eliminate f and integrating yields M as a function of t, and hence R as a function of t (eq. 44). Quoting the latter solution first

$$R = \left[\left((1 - \mathfrak{T}^2)\exp\left(-\frac{k_i' + k_i''}{2}t\right)\right) + \mathfrak{T}^2\right]^{1/2} \quad (47)$$

where we define

$$\mathfrak{T} = \left[\frac{2k_i''F}{(k_i' + k_i'')(f(0) + F)}\right]^{1/2} \quad (48)$$

For the usual case $f(0) = 0.5$, and $\mathfrak{T}$ reduces to the ratio of the geometric to the arithmetic mean of k_i'' and k_i'.

The solution for M is most simply quoted as a function of R, thus

$$\ln M = \frac{2(f(0) + F)}{r(1 + 2F)}\left\{R - 1 - \frac{\mathfrak{T}}{2}\ln\frac{(R + \mathfrak{T})(1 - \mathfrak{T})}{(R - \mathfrak{T})(1 + \mathfrak{T})}\right\} \quad (49)$$

The Case $b/q << 1$ (Short Chains and Long Zips).—This case will be realized whenever r is sufficiently small. By neglecting b with respect to q in (35), we obtain

$$\frac{df}{d \ln M} = \frac{f(1 - f)}{f + F} \quad (50)$$

and similarly we obtain from (27) and (29) (or from (28) and (30))

$$\frac{d \ln M}{dt} = -(k_i'' - k_i')[f + F] \quad (51)$$

The solution of the last two equations is given by

$$f = \frac{f(0)\exp -(k_i'' - k_i')t}{f(0) + [1 - f(0)]\exp -(k_i'' - k_i')t} \quad (52)$$

and

$$M = [1 - f(0)]\exp(-k_i't) + f(0)\exp(-k_i''t) \quad (53)$$

Equation 50 is exactly Brockhaus and Jenckel's equation 5, because the neglect of all the statistical effects in their treatment is asymptotically justified as $b/q<<1$. However, Table II shows that for their data b/q is sometimes *more* than unity, so that the solutions of this paragraph are poor approximations for such data.

The Case $k_i' = k_i'' = k_i$.—As regards the rate behavior, this case obviously reduces to eq. 24, *i.e.*, it is equivalent to the case without a spectrum of end-groups (*cf.* eq. 6). However, we can obtain the solution for the fraction f of double-bonded ends as a function of time, by the substitution $k_i' = k_i'' = k_i$ in (35)

$$\frac{df}{d \ln M} = b(f - 0.5)/q \quad (54)$$

Moreover, eq. 25 shows that $K' = 0$, and accordingly eq. 29 or 30 yields $b = b(0)$; it is, of course, physically obvious that the mean zip-length remains invariant throughout the reaction under discussion. Thus (54) can immediately be integrated to give f as a function of M

$$f - 0.5 = (f(0) - 0.5)M^r \quad (55)$$

This solution meets the obvious expectation that f remains equal to 0.5, provided it has this value initially and otherwise approaches this value in the course of the degradation reaction (*i.e.*, with decreasing M).

The Case $k_i' = 0$ and Disproportionation of Monomer Radicals.—Here (35) reduces to

$$\frac{df}{d \ln M} = \frac{b}{2q} + 1 - f \quad (56)$$

With the help of (29), this becomes

$$\frac{df}{d \ln M} = \frac{r}{2}(f/f(0))^{1/2} + 1 - f \quad (57)$$

Again with the aid of (29), (27) becomes

$$-\frac{d \ln M}{dt} = \frac{k_i''f(f(0))^{1/2}}{(f(0))^{1/2} + rf^{1/2}} \quad (58)$$

Although t can be found from the last two equations as explicit functions of M and f in closed form, we content ourselves with the integration of (57)

$$\ln M = \ln \frac{f(0)^{1/2}(2 - 2f(0) + r)}{2f(0)(1 - f) + rf} + \frac{r}{(16f(0) + r^2)^{1/2}} \ln \frac{((16f(0) + r^2)^{1/2} + 4f^{1/2}f(0)^{1/2} - r)((16f(0) + r^2)^{1/2} - 4f(0) + r)}{((16f(0) + r^2)^{1/2} - 4f^{1/2}f(0)^{1/2} - r)((16f(0) + r^2)^{1/2} + 4f(0) - r)} \quad (59)$$

From the last two equations, by using f as a parameter, the rate dM/dt can be found as a function of conversion.

The most interesting case arises for $r>>1$, *i.e.*, short zips occurring in long chains. We obtain the following solutions, now valid for both monomer radical disproportionation and evaporation, by making the appropriate approximations in equations 57 and 58. The same solutions naturally result by putting $k_i' = 0$, which also implies that $F = 0$ (by eq. 26), in equations 46 and 43

$$r >> 1 \begin{cases} f = f(0)\exp(-k_i''t/2) & (60) \\ k_i' = 0 \quad \ln M = 2f(0)(\exp(-k_i''t/4) - 1)/r & (61) \end{cases}$$

The last equation implies that the polymer never degrades completely, but asymptotically approaches a fractional weight of

$$M_\infty = \exp(-2f(0)/r) \simeq 1 - [2f(0)/r] \quad (62)$$

While equation 60 shows that the fraction f of double-bonded ends decays with first-order kinetics, the mass decay implied by (61) obeys a remarkable law, probably new to chemical kinetics. Here ln M instead of M decays exponentially with time, *i.e.*, the process behaves like a first-order reaction in which the rate "constant" itself decreases with time according to first-order kinetics. Nevertheless, the plot according to (61) of dM/dt against M would still be practically a straight line (joining the points $M = 1$, $dM/dt = (dM/dt)_0$ and $M = \exp(-2f(0)/r)$, $dM/dt = 0$.)[11,12]

(11) N. Grassie, "Chemistry of High Polymer Degradation Processes," Butterworths, London, 1956, p. 45.

(12) M. H. Mackay and H. W. Melville, *Trans. Faraday Soc.*, **45**, 323 (1949).

ION-EXCHANGE PROPERTIES OF KAOLINITE SLURRIES[1]

By Murry A. Tamers[2a] and Henry C. Thomas[2b]

Contribution from the Department of Chemistry, Yale University

Received May 13, 1959

The ion-exchange properties of kaolinite have been studied by use of isotopic exchange reactions on continuously stirred slurries of the material in a fluidized bed type of arrangement. The results show that the cation and anion exchange capacities of the clay vary with the concentration and type of electrolyte used. An isotherm is presented which illustrates the specificity of kaolinite for cesium over sodium exchange. The slow attainment of ion-exchange capacity equilibrium and other unusual properties are explained by the changing state of aggregation of the clay particles. Flocculation removes both anion and cation exchange sites from availability and thus reduces the observed ion-exchange capacity in the more dilute solutions.

In earlier work[3] we have been concerned with the ion-exchange behavior of clay minerals in which lattice replacements produce the sites against which the ions are held. In such minerals the composition of the silicate "backbone" is correspondingly complex, as in the minerals montmorillonite and attapulgite. Kaolinite, however, is a very nearly pure aluminosilicate. Its relatively stable 1–1 structure favors the survival of crystals, large for clay minerals, which expose a relatively small surface. The cation exchange capacity of kaolinite is a factor of fifty or a hundred lower than that of montmorillonite. It is not far from equal to the anion-exchange capacity and is certainly not primarily due to substitutions in the lattice. Perhaps the principal result of the present work is a demonstration of conditions under which there are relations between the amounts of anion and cation sorbed on kaolin.

The low values of the exchange capacities of kaolinite make entirely impractical the technique of the "equilibrium column" for investigating these quantities. Batch equilibrations in the study of ion-exchange equilibria are quite successful with materials of high capacity which are easily separated from the solutions by simple drainage or centrifugation. However, errors increase rapidly as capacity decreases; and with kaolin, which forms difficultly dispersible masses on centrifugation, the batch method is quite unsatisfactory. Either of these methods must necessarily give results obscured by the uncertain state of aggregation of the clay. We have therefore turned to a method of the "fluidized bed" in which we measure the effluent composition of solutions passing through a continuously stirred suspension of the clay mineral. It was found possible to maintain the clay in a constant or only slowly varying state of aggregation and so to study rapid ion-exchange effects as very slow changes in aggregation took place.

Experimental

The apparatus finally adopted consisted of cylindrical Pyrex reaction vessels two inches in diameter and having hold-up volumes of approximately one hundred ml. The reactors have short necks about one-half inch in diameter. The solution enters the bottom of a vessel through a one-way glass ball valve, passes a magnetic stirrer and is mixed with the suspension of clay. The stirring speed and the rate of flow of the solution are adjusted to maintain the level of the suspension not far below the neck of the container. The

(1) Contribution No. 1581 from the Sterling Chemistry Laboratory of Yale University, based on the dissertation submitted to the Faculty of the Graduate School by Murry A. Tamers in partial fulfillment of the requirements for the degree of Doctor of Philosophy.

(2) (a) Department of Chemistry, University of Texas, Austin, Texas. (b) Department of Chemistry, University of North Carolina, Chapel Hill, North Carolina.

(3) C. N. Merriam and H. C. Thomas, *J. Chem. Phys.*, **24**, 993 (1956).

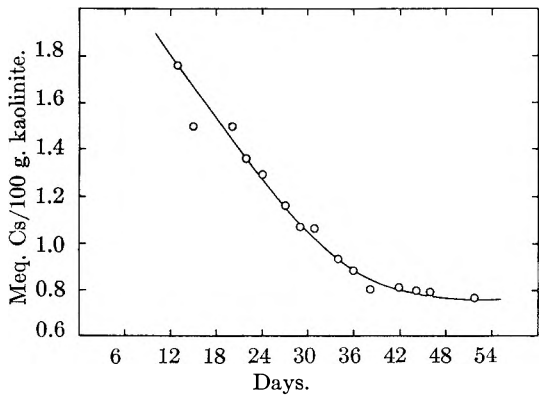

Fig. 1.—Approach to cation-exchange capacity equilibrium of an agitated kaolinite suspension in 0.0005 N CsCl.

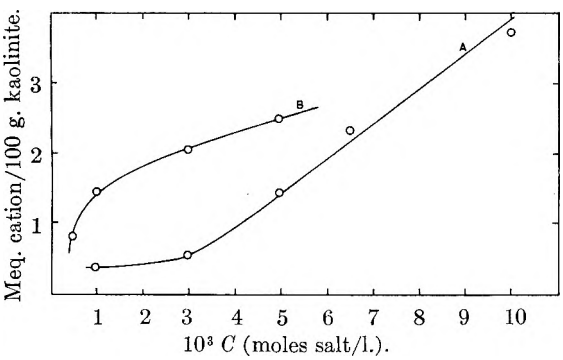

Fig. 2.—Dependence of the cation-exchange capacity of kaolinite suspensions on the concentration of the equilibrating solution: curve A, NaCl; curve B, CsCl.

solution passes out through a compact glass wool filter filling the neck of the vessel. It is possible with this equipment to maintain a relatively sharp slurry level, the clay settling against the flow of the solution. A small amount of kaolinite gradually collects in the filter and increasingly obstructs the flow of the solution. From time to time this obstruction is washed out by a brief forced backward flow of the eluate. In this operation the ball valve maintains the slurry in the reactor; the liquid level momentarily rises in a small air reservoir provided at the top of the vessel. On return to normal operation the liquid content of the apparatus returns to its original volume (to ± 0.1%), a necessity in the treatment of the results.

By a sufficiently long preliminary elution, the clay in the reaction vessel is brought to ionic equilibrium with the flowing solution. This equilibrium is studied by measurements of the distribution of isotopic (radioactive) tracers between solution and clay.

If we suppose that isotopic exchange between the solution and the suspended solid is rapid, *i.e.*, complete in a time short compared to the residence time of the solution in the reaction vessels, then for a solution carrying tracer into an initially full reaction vessel at chemical equilibrium we have

$$-\log(1 - \theta/\theta_0) = 2.30V/(V_h - Q/c)$$

In this equation θ/θ_0 is the ratio of effluent to input counting rate when a volume V of effluent has been passed in; V_h is the hold-up volume of the reaction vessel; Q the number of milliequivalents of exchange capacity associated with the clay in the vessel, and c is the concentration of the solution. The value of V_h was determined by weighing after the reaction vessel had been filled to marks on the inlet and outlet tubes. Evidently for small values of Q and relatively high values of c, errors in the determinations of V_h have significant effects on the determination of Q. Many of these isotopic elutions were carried out and the activity of the effluents followed up to θ/θ_0 as high as 0.85. Plots of $-\log(1 - \theta/\theta_0)$ *vs.* V give excellent straight lines. Such results cannot, however, be taken as proof that we actually have an equilibrium single stage reactor. V_h generally was higher than Q/c: V_h was always near 100 ml. and Q/c varied widely according to the conditions of the experiment, from about 30 ml. to 90 ml. Thus only large deviations in the measured values of Q from final equilibrium values would manifest themselves as changes in the slopes of these lines. Actually values of Q were not determined from slopes of these lines; rather the contents of the reaction vessel were brought to the desired composition by passing 2 liters of labeled solution over the clay during a period of about 8 hr. and the total retention, $V_h + Q/c$, of the reaction vessel then determined after a similar elution of the tracer with 2 liters of untraced solution and by a measurement of the activity of the entire eluate. In all cases approximately twenty times the equivalent volume of the reactor was passed before making measurements, and the clay was treated with at least 10 liters of solution of the same concentration before the actual runs were started. Ideally the exchanges should have been within 0.1% of completion. In an experiment designed to confirm this point, a sample was equilibrated with a total of 4 liters of 0.001 N Cs(137)Cl. The isotopic exchange was carried out with 1.8 liters 0.001 N CsCl. The eluate showed an activity corresponding to 2.6 meq. Cs/100 g. clay. An additional 2 liters of 0.001 N CsCl was passed, and after evaporation to small volume, an activity corresponding to 0.008 meq./100 g. was found. The clay then was boiled for 2 hr. with 0.05 N CsCl. The activity found in this solution corresponded to less than 0.001 meq./100 g. clay. It seems safe to suppose that these elutions actually went to within 0.4% of completion.

Standard counting procedures with glass jacketed solution counters were employed, all significant corrections being applied. The isotopes used were Cl^{36}, Na^{22} and Cs^{137}. In the case of the cesium tracer the Geiger tubes were filled and allowed to stand for 20 minutes before counting to ensure radioactive equilibrium with Ba^{137m}. The Cl^{36} as obtained was of high specific activity but contained some inactive chloride, corrections for which were made in preparing the solutions.

Kaolinite from the Lamar Pit, Bath, South Carolina,[4] was used in all the work. The clay was prepared merely by grinding to pass a 100 mesh screen and drying at room temperature under reduced pressure. This particularly pure clay mineral has been characterized by the American Petroleum Institute under Research Project No. 49 and denoted as Sample 5.

Undoubtedly the principal error in these experiments stems from the necessity of subtracting the relatively large hold-up volume of the reaction vessel from the total retention. The effects of errors in counting and in measuring V_h depend on the conditions of the experiments and amount to 5–10% in Q. All other errors are negligible by comparison.

Cation- and Anion-exchange Capacities of Kaolinite.—The most significant advantage of the method of investigation just described is exhibited in the direct confirmation that with kaolinite the approach to true chemical equilibrium with a solution is very slow. We have shown that isotopic equilibration between a solution and a suspension of the clay (in its "momentary" state) is relatively rapid. When, however, a sample of the clay is maintained in a nearly steady state of suspension in a given solution over a long period and intermittently subjected to isotopic exchange, the result illustrated in Fig. 1 is obtained. Here it is seen that the cesium content of the clay, continuously in contact with a 0.0005 N solution of CsCl, steadily decreases over a period of nearly two months and finally approaches a constant value for a given state of suspension in the solution. In Fig. 2 are given the final equilibrium values, based on two months suspension with intermittent elutions, of the total cation capacity of kaolinite in solutions of cesium chloride and of sodium chloride of different concentrations. It appears that there are relations between the cation capacities and the concentrations of the ions in solution, different for the two ions.

In these experiments the anion capacities were likewise measured. The ion capacities for a particular sample were measured within two days of each other by making three isotopic exchanges, one with the radioactive cation, one with radioactive chloride, the third again with traced cation. In this short time the total exchange capacities changed but little, and we assume that we get nearly corresponding values of the two capacities. In the case of the experiments with

(4) From Ward's Natural Science Establishment, Rochester, New York.

sodium solutions, curve A in Fig. 3, five out of six of the experiments were done at true equilibrium, as evidenced by unchanging exchange capacity. In the following we shall refer to this condition as one of "capacity equilibrium." The single point lying off the curve was determined before capacity equilibrium had been reached. Curve B in Fig. 3 gives the results with solutions of cesium chloride, the points marked by flagged symbols referring to capacity equilibrium. For the cesium solution the data suggest that the relation between anion and cation content is independent of the degree of approach to full equilibrium. In the sodium solutions it appears that this may not be true. The point, however, cannot be considered as established by these data.

Cesium–Sodium Exchange Isotherms.—Several series of experiments were made to investigate the nature of the cation-exchange isotherms for cesium and sodium, the procedure being essentially the same as that outlined above. The clay suspension was eluted with a mixed solution of the desired compositions to bring it into ionic equilibrium with this solution. In each series of compositions the total concentration was maintained constant (0.001, 0.002, 0.003 *N*). In the series at concentration 0.002 *N* the clay was also in capacity equilibrium. The composition of the clay was determined by isotopic exchange with cesium, followed by isotopic exchange with sodium. The procedure thus measured both composition and total cation capacity. In some cases the results were checked by a repetition of the cesium exchange. In most of these cases very little change in cesium content was found, and these checks were not carried out in the series at capacity equilibrium. Although the results of all these experiments show qualitatively the high selectivity of the clay for cesium, especially at low cesium content, only in the case done at total capacity equilibrium is there discernible a smooth relation between the total cation capacity and the cesium content of the clay. This relation is shown as curve A in Fig. 4; the single point which lies well off the curve belongs to the only experiment in this series in which the clay was not at capacity equilibrium. Curve B in Fig. 4 gives the exchange isotherm for this case. The isotherms for those series not at capacity equilibrium lie close to curve B, Fig. 4; their quantitative meaning is, however, obscured by the lack of full equilibrium, and we omit the results.

Discussion

The unusual ion-exchange properties of kaolinite can be explained on the supposition that the exchange behavior depends upon the degree of flocculation of the clay. According to van Olphen[5] the edges of the crystallites of kaolin are positively charged and open three-dimensional networks are formed when these sites are associated with negative sites on other particles. Schofield and Samson[6] advance this idea by suggesting that the flocculation is due to association between positive edges and negative cleavage faces. These authors go further and suggest that the edge-to-face flocculation occurs only in dilute solutions, that the effect of higher concentrations of electrolyte is to decrease this type of flocculation, and, with some electrolytes, to produce another type of aggregation in which the crystallites are associated face-to-face.

Our results are in complete qualitative agreement with these ideas. The slow approach to capacity equilibrium, Fig. 1, is easily understandable in terms of a slow adjustment in the degree of flocculation. The increase in cation capacity with concentration, Fig. 2, corresponds to a decrease in degree of flocculation in which a larger proportion of the sites are made available to exchange. Furthermore, since cesium is selectively sorbed in preference to sodium the cesium capacity increases

(5) H. van Olphen, *Disc. Faraday Soc.*, **11**, 82 (1951).
(6) R. K. Schofield and H. R. Samson, *ibid.*, **18**, 135 (1954).

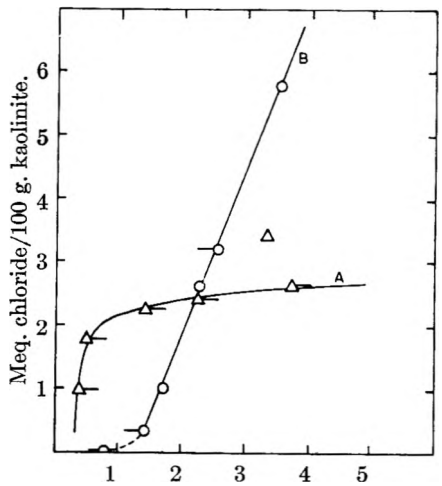

Fig. 3.—Relations between cation- and anion-exchange capacity of kaolinite in suspension: curve A, NaCl; curve B, CsCl.

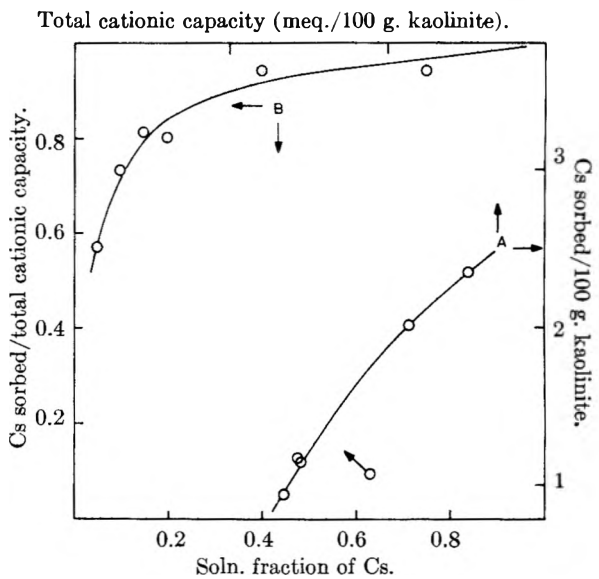

Fig. 4.—Exchange sorption Cs–Na on kaolinite: curve A, Cs content *vs.* total cation-exchange capacity; curve B, Cs–Na exchange isotherm.

more rapidly with concentration. (An analogous effect is observed in precipitation titrations.) Additional confirmation of this interpretation is found in the character of the relations between cation and anion capacity, Fig. 3. The capacities rise together, corresponding to a simultaneous release by deflocculation of positive and negative sites. The fact that neither with cesium nor with sodium is a simple 1–1 relation obtained requires further explanation. The linear relation obtained for cesium would indeed be the result of the deflocculation of edge-to-face aggregates if some chloride ion sorbed on the edges were effectively shielded from the solution in the aggregate. The splitting of such a combination would then increase the anion capacity both by making more sites available and by offering more anions for exchange. We have only to suppose that a constant proportion of the anions is thus shielded in

the aggregate to obtain the observed relation. In the case of the sodium chloride solutions the situation is not so simple; at least two types of shielding would be necessary to explain the results. Some independent evidence for such an explanation is to be found in the work of Schofield and Samson[7] who found viscosities of kaolinite suspensions in sodium chloride solution lower than those for potassium chloride, the effect being very large indeed. This may be interpreted to mean that a large part of the flocculation in NaCl is face-to-face even at the low concentrations measured (less than 0.01 *M*), while the greater viscosity of the KCl suspensions is due to the bulky edge-to-face aggregates. We may certainly suppose that cesium behaves like potassium, so that the more complex relation between anion and cation uptake in sodium solutions parallels the viscous behavior.

THE QUANTUM MECHANICAL CORRECTION FOR THE HIGH TEMPERATURE VAN DER WAALS INTERACTION OF LIGHT GASES AND SURFACES. A NEW METHOD OF DETERMINING SURFACE AREA

BY MARK P. FREEMAN[1]

Contribution from the Department of Chemistry, University of California, Berkeley, California

Received May 15, 1959

An experiment is reported in which the exact magnitude of the effect of negative discrete energy levels in the potential energy well for gas–surface interaction is determined. The experiment involves the surface interaction of two kinds of gas molecules differing only in mass (H_2 and D_2 with about 1700 m.^{2} of a low ash charcoal surface) and the interpretation of the data with the high temperature equation of state for gas–surface interaction as properly modified for an "almost classical" quantum mechanical assembly. Quantitative agreement of certain independently obtained parameters indicates that the quantum mechanical equation of state for these light gases is at least as good as the classical equation has been for interpreting data for the heavier gases. Unexpected verification of the 9-3 potential model is apparently found and a new unambiguously defined surface area is discussed.

Introduction

The theory of the high temperature interaction[2] of gases and solids seems to be surprisingly well supported by experiment. That is, it has been found possible to derive an equation of state for the interaction of gas and surface (after the manner in which one derives the virial equation of state in gas–gas interaction) assuming spherical gas systems (molecules or atoms) and a uniform structureless surface. This equation has been successful in reconciling theory and experiment to within the experimental error for a large number of assemblies, including some that depart rather far from the model.[3] At the same time, it is true that the detailed description obtained for the theoretical gas–surface behavior is remarkably indifferent to the exact shape of the assumed potential model, especially the repulsive portion. Furthermore, although the treatment yields a capacity factor As_0 (the product of the area A and a collision parameter), there has been no way consistent within the model of obtaining the area. Again, although something can be inferred about the nature of the surface from the classical interpretation, the amount of information one obtains is relatively small. Finally, a very deep potential energy well exists between the individual gas systems and the surface. The very depth of the well ensures a spacing of energy levels that might very well cause a light molecule to interact peculiarly even at high temperatures which would complicate the interpretation of the parameters obtained by fitting the data to the classical model. That this could be so becomes apparent when one realizes that most of the time that a gas system is interacting with a surface it will simply be oscillating back and forth in the potential well as it travels over the surface. If the gas system is light, only certain amplitudes of this oscillation will be allowed and this could clearly affect the gas-containing capacity of the surface.

This quantum effect was first considered by DeMarcus, *et al.*,[4] who developed the quantum mechanical configuration integral for the 9-3 potential model and fitted some data of Steele and Halsey[5] for helium interacting with carbon black to their model. Unfortunately, the temperature dependence for the quantum mechanical configuration integral is not different enough from that for the classical integral to distinguish the better fit by curve fitting. Furthermore, although their theory claimed that a large difference in surface capacity should exist at any temperature for He interpreted classically or quantum mechanically, when they used the respective parameters As_0 together with s_0 obtained through use of the Kirkwood–Mueller formula[2] to get the area, they found a difference in surface areas of only 5%. It is clear now that this was because of a cancellation of effects, but it was primarily this fact that first directed the attention of the present author toward exploring this quantum effect.

An examination of the equations obtained by DeMarcus, *et al.*, showed that one should be able to obtain some or all of the following advantages

(1) American Cyanamid Company, Research Division, Stamford, Connecticut.

(2) For summary of references see: M. P. Freeman, THIS JOURNAL, 62, 723, 729 (1958).

(3) J. F. Hanlan and M. P. Freeman, *Can. J. Chem.*, **37**, 1575 (1959).

(4) W. C. DeMarcus, E. H. Hopper and A. M. Allen, A.E.C. Bulletin K-1222 (1955).

(5) W. A. Steele and G. D. Halsey, Jr., *J. Chem. Phys.*, **22**, 979 (1954).

by simply investigating the behavioral difference of two isotopically substituted gas systems:

(1) The order of magnitude of the mass-dependent discrepancy (the difference in the amount of each gas taken up by the surface) should be an exacting test of the physical picture used in deriving the equation of state.

(2) The consistency of the fit for two types of gas systems differing only in mass as well as the fit for their discrepancy is an independent test of the potential model, particularly the repulsive portion (for the zero point energy is determined by curvature at the bottom of the well, which in turn depends mostly on the repulsive portion).

(3) If all goes well in the curve fitting in (2), one will be left with three parameters which may be combined with fundamental constants to yield an unambiguously defined surface area independent of any information from outside the model.

(4) If any quantum effect shows up, it probably would represent the highest temperature phenomenon for which a measurable quantum mechanical effect arising from purely physical forces had been observed, and as such is of interest as a curiosity.

These advantages and the ready availability of such suitable isotopic pairs as H_2, D_2 and He^3, He^4 made this experiment especially attractive. Because of limitations in time and apparatus available, only the former isotopic pair was investigated and on a single surface.

Theory

Derivation.—If N systems (atoms or molecules) of a gas are admitted into a vessel at temperature T, containing a solid of area A in which the gas is assumed insoluble, the equilibrium pressure is given by[2]

$$\frac{P}{NkT} = \frac{1}{V_a} = \frac{1}{V+B} - \frac{NC}{(V+B)^3} \qquad (1)$$

where V is the geometric volume (the volume excluded by the solid and enclosed by the vessel) and k is the Boltzmann constant. The temperature behavior of C is known[2] once it has been determined at one temperature, and so one need only make a pressure dependent plot at one temperature to calculate the value of $V + B$ at any other temperature at which he has measured the "apparent volume," V_a, at pressure P. $V + B$ is, of course, just equal to V_a^0, the apparent volume extrapolated to zero pressure. V may be determined directly and in fact may be defined[2] as the apparent volume for He at room temperature, so that one may define the more theoretically interesting "excess volume" V_{ex}

$$V_{ex} = V_a^0 - V = B \qquad (2)$$

B may be simply related to the molecular configuration integral. For a spherical system interacting with a structureless uniform surface this is, in the classical case

$$B_c = \int_v [\exp(-\phi_{1s}/kT) - 1]\,dv_1$$

where dv_1 is the differential volume element in configuration space. Here ϕ_{1s} is the potential function operating between a gas system and the surface.

In this theoretical treatment for the quantum effect it is necessary that the potential function ϕ must everywhere have finite and continuous first derivatives. For this reason DeMarcus, *et al.*, departed from the hard-sphere-repulsion inverse-cube-attraction model introduced by Halsey and used an inverse ninth power law. Subsequent authors[2,6] have adopted this model because of its more realistic functional behavior, even though the high temperature interaction theory is not sufficiently sensitive to the repulsive potential function to discriminate conclusively by goodness of fit. The quantum effect, however, depends mainly on the curvature at the bottom of the well, which in turn is chiefly determined by the repulsive potential, so that now the choice of this function could be very important. The exact form of the potential used here is

$$\phi_{1s} = \frac{-3\sqrt{3}}{2}\epsilon^*\left[\left(\frac{s_0}{s}\right)^9 - \left(\frac{s_0}{s}\right)^3\right] \qquad (4)$$

where ϵ^* is the depth of the potential energy well and s_0 is the distance of zero net gas surface interaction. When fitting experimental results to reduced values of the integral B_c, the parameters that emerge are the reduced energy ϵ^*/k and the product of area and characteristic distance s_0, As_0. Although s_0 can be given crudely by the Kirkwood–Mueller formula, there is no way that an area can be determined within the classical model.

Hirschfelder, *et al.*,[7] consider at some length the proposition that it is only necessary to substitute the Slater sum over states

$$\mathcal{W} = N!\left(\frac{h^2}{2\pi mkT}\right)^{\frac{3}{2}N}\sum_\rho \psi_\rho^* \exp\{-\mathcal{H}/kT\}\,\psi_\rho \qquad (5)$$

(exp $\{-\mathcal{H}/kT\}$ defined as $\sum_j \frac{(-\mathcal{H}/kT)^j}{j!}$ where $\mathcal{H}$ is the quantum mechanical Hamiltonian operator for n particles and the Ψ_ρ are a complete orthonormal set of wave functions)[8] for the Boltzmann factor in any molecular configuration integral to make the expression quantum statistically valid. Kirkwood[9] in turn has shown that the Slater sum for an almost classical assembly (an assembly at temperatures where the behavior is nearly classical) is given correct to terms in h^4 (neglecting symmetry effects) by

$$\mathcal{W} = W\left\{1 - \frac{\hbar^2}{12m(kT)^2}\sum_j\left[\nabla_j^2\phi_1 - \frac{1}{2kT}(\nabla_j\phi_1)^2\right]\right\} \qquad (6)$$

where W is the Boltzmann factor

$$W = \exp\{-\phi_{1s}/kT\} \qquad (7)$$

$\hbar$ is Planck's constant over 2π and m is the molecular mass. The summation index j in equation 6 is over all 3 N coördinates of configuration space. But for each molecule the only force acting is that normal to the surface so that the factor B becomes

(6) R. S. Hansen, THIS JOURNAL, **63**, 743 (1959).

(7) J. O. Hirschfelder, C. F. Curtiss and R. B. Bird, "Molecular Theory of Gases and Liquids," John Wiley and Sons, Inc., New York, N. Y., 1954, p. 401.

(8) J. O. Hirschfelder, *et al.*, ref. 7, p. 396.

(9) J. G. Kirkwood, *Phys. Rev.*, **44**, 31 (1933).

$$B = B_c - \frac{\hbar^2 A}{12m(kT)^2}\int_{s=0}^{\infty} e^{-\phi_1/kT}\left[\frac{\partial^2\phi_1}{\partial s_1^2} - \frac{1}{2kT}\left(\frac{\partial\phi_1}{\partial s_1}\right)^2\right]ds_1 \quad (8)$$

This expression can be simplified further through integration by parts (dropping the subscript)

$$-\frac{1}{2kT}\int_{s=0}^{\infty} e^{-\phi/kT}\left(\frac{\partial\phi}{\partial s}\right)^2 ds = \frac{1}{2}e^{-\phi/kT}\left(\frac{\partial\phi}{\partial s}\right)\Big|_0^{\infty} - \frac{1}{2}\int_0^{\infty} e^{-\phi/kT}\frac{\partial^2\phi}{\partial s^2}\,ds \quad (9)$$

But the integrated term on the right vanishes at both limits so that (8) finally becomes (expressing the mass m in atomic mass units)

$$B = B_c - \frac{As_0\alpha}{m}\frac{I}{T^2} \quad (10)$$

where

$$\alpha = \frac{\hbar^2(\epsilon^*/k)\eta}{24s_0^2 k} \quad (11)$$

$$I = (\epsilon^*)^{-1}\int_0^{\infty} e^{-\phi/kT}\left(\frac{\partial^2\phi}{\partial\sigma^2}\right)d\sigma \quad (12)$$

$\sigma = s/s_0$ is the reduced gas–solid separation and η is Avogadro's number.

Values of the reduced integrals I and B_c/As_0 evaluated for the 9-3 model as tabulated by DeMarcus, *et al.*,[4] are reproduced in the Appendix. These integrals also have been evaluated analytically through a summation technique by Hansen,[6] who has given them, to a high degree of accuracy, as simple empirical functions of ϵ^*/kT over the entire range of interest.

Interpretation of Data.—Identifying B with V_{ex}, it is now clear from equation 10 that if one were to measure V_{ex} at a given temperature for two assemblies identical in everything but the mass of the gas systems, the difference would be (where super I denotes the lighter)

$$\Delta V_{ex} = V_{ex}^{II} - V_{ex}^{I} = V_a^{0II} - V_a^{0I} = As_0\alpha\left(\frac{1}{m_I} - \frac{1}{m_{II}}\right)\frac{I}{T^2} \quad (13)$$

or

$$\ln\left\{\frac{\frac{m_I m_{II}}{m_{II} - m_I}\Delta V_{ex}T^2}{As_0\alpha}\right\} = \ln I \quad (14)$$

Clearly, one need only fit data of $\ln([(m_{II} - m_I)/m_I m_{II}]\Delta V_{ex}T^2)$ to the theoretical curve of $\ln I$ *vs.* ϵ^*/kT to evaluate the parameter ϵ^*/k and the group $As_0\alpha$. This is necessarily a very sensitive test of the potential model and so the nature of the fit is of great interest. Having evaluated ϵ^*/k in this manner, one may return to equation 10 to see that if data for one of the isotopes of the form $\ln(V_{ex} + (As_0\alpha/m)(I/T_2))$ is adjusted to the theoretical curve of $\ln B_c/As_0$ *vs.* ϵ^*/kT by adjusting As_0, then one obtains this parameter as well. Using the definition of α (equation 11), one of the more interesting aspects of the quantum mechanical fit emerges

$$A = \left[\frac{24k(As_0)(As_0\alpha)}{\hbar^2(\epsilon^*/k)\eta}\right]^{1/2} \quad (15)$$

That is, one has a uniquely defined area that emerges unambiguously from a single model with no assumptions external to the model.

There are two independent checks on the validity of the gas–surface interaction model. First, if one has a detailed picture of the excess volume discrepancy for the two gases as a function of temperature, the goodness of the fit to the calculated model should be a very rigorous test of the model and the way most likely to reveal the applicability of the repulsive potential. Secondly, the fit of $\ln(V_{ex} + (As_0\alpha I/mT^2)$ to the $\ln B_c/As_0$ *vs.* ϵ^*/kT curve should yield the same value of As_0 for both isotopes and the fit should be perfect. Were all of these conditions to be perfectly met, the potential model in question could be considered unimpeachable.

It is, perhaps, not immediately obvious what effect the presence of discrete negative energy levels will have on the detailed picture of gas–surface interaction. The Slater sum in the quantum case is the analog[8] of the Boltzmann factor in the classical and represents the probability of finding a gas system a given distance from the surface. If one plots these two measures of statistical probability as a function of separation from the surface for hydrogen at 100°K., he will find (for the 9-3 potential model) that for both cases the majority of gas systems lie between 1.1 and 1.4 times the gas–surface collision parameter s_0 from the surface. The most probable separation is about 1.2 for the classical case and about 1.21 for the quantum case. The quantum distribution tends to run a little wider near the bottom, but this tendency to increase the total statistical mechanical probability is much more than compensated by a 10% decrease in peak height for the Slater sum. This, of course, is consistent with the observation that with all else the same, heavier molecules are taken up more readily by the surface than light molecules. An alternate way to describe this effect is to say that the zero point energy level puts a "false bottom" in the potential energy well; the lighter the molecule the shallower the well. This simple interpretation is given some credibility by the fact that when the Slater sum is plotted as a function of separation from the surface, the curve is shaped very much like that for the Boltzmann factor for a somewhat shallower well.

Experimental

Apparatus.—The apparatus consisted of a conventional gas transfer apparatus connected to a 10 kg. thermostated copper block containing the adsorbent. The sensing element for temperature control (± 0.01°) was a thermistor seated firmly in the block and electrically situated in the bridge circuit of a proportional amplifier whose a.c. output passed through the main block heater. The temperature was maintained by a balance between heat lost by radiation through a hard vacuum (10^{-6} mm.) to a surrounding stainless steel test-tube immersed in liquid nitrogen and the heat input of the block and subsidiary heater. Temperature of the block was determined by a completely recessed platinum resistance thermometer read with a Mueller bridge. The block heater and thermal sensing devices were installed in the upper portion of the two-part block and access to the block cavity was gained through a spring loaded ball-vee joint near the bottom. The portion of the block below this vacuum tight joint was kept at the same temperature as the remainder by an auxiliary heater and a differential thermocouple. The stem (the tube through which gas is admitted to the block) was about 1 mm. in inside diameter and made of stainless steel as was the shield which coaxially surrounded the stem and the sensitive wires running to the block. The shield was equipped

with appropriate thermocouples and heaters to ensure rapid duplication of stem conditions.

The pressure of gas in the gas buret was indicated by a free leg manometer while the equilibrium pressure of gas over the solid was determined by a constant volume manometer. All variable manometer legs (back lighted with horizontally focussed and polarized light) were mounted in a block where they could be read to the nearest 0.01 mm. by a suitably calibrated cathetometer (made by Griffin and George, Ltd.).

The apparatus as described was originally designed for another purpose and, although quite versatile, could not be controlled below 180°K. because of large thermal leaks. Unfortunately, it turned out that the most interesting temperature region for this effect is below 180°. One additional low temperature point was obtained, however, by shunting the block to the test-tube by a mixture of acetone and ethanol and using liquid oxygen as coolant. After the block had cooled down, the test-tube was continually pumped on to duplicate as nearly as possible the high temperature stem conditions.

Materials.—Adsorbent for this experiment (designated SU-60) was obtained from R. Nelson Smith of Pomona College, Claremont, California, and was a low ash sugar charcoal of nominal B.E.T. area, 1000 m.²/g. This was contained in a screen-stoppered brass cartridge inserted in the block cavity. Cartridge size determined the amount of adsorbent used (1.6979 g.).

The helium and hydrogen used were the reagent grade gases of the Air Reduction Company. The deuterium was obtained in a metal cylinder from the Stuart Oxygen Company. Local gas-spectrometric analysis revealed the helium to be contaminated to 0.08 mole% with nitrogen and carbon dioxide while nitrogen was the principal contaminant in the other reagent gases (0.19 mole% for H_2 and 0.15 mole% for D_2). The deuterium also contained 0.96 atom % hydrogen.

Procedure.—The block and adsorbent were outgassed by removing the external fittings of the block and illuminating it directly with a 250 watt heat lamp which raised its temperature to the steady-state value of about 105°. Initial outgassing after exposure of the adsorbent to air involved pumping on the solid at this temperature for about three days, whereas outgassing between runs with hydrogen or helium was done overnight.

The method of operation requires a knowledge of the apparent volume of the block cavity with adsorbent as determined by the ideal gas law. Room temperature, the equilibrium pressure and the known emergent volume from the thermostat (taken to be 9.90 cm.³) permitted the apparent volume to be corrected for the emergent dead space, while the empty block was employed over the accessible temperature range (−90 to 100°) as a gas thermometer to get the correction to apparent volume of the stem as a function of temperature. This function was extrapolated a long way to provide this correction at the one available cold temperature (about −182°) but fortunately at this temperature the stem holdup was inconsequential anyway. It was found that all errors combine to give a probable error of 0.04 cm.³ over the entire range in determining the apparent volume of the empty block. Most of this uncertainty probably comes from the stem. The geometric volume, also important to this experiment, is defined as the "helium apparent volume" at room temperature and was actually determined with He at 309.53°K.

The apparent volume determined at each temperature was extrapolated to zero pressure by determining C in equation 1 for H_2 at 199.6° K. and then using this value in the hard sphere repulsive model[2] to get C for the other points. Rather than risk too long an extrapolation of the third-order interaction model, the low temperature data were taken as a function of pressure for each gas and extrapolated to zero pressure through use of equation 1. Finally, it was assumed that the impurities in the hydrogen and deuterium would be quantitatively removed by the solid and so the apparent volumes were corrected for this factor.

Data.—Eight data points were taken for hydrogen and six for deuterium. Seven points for hydrogen and five for deuterium were taken in the temperature range 188 to 243°K. One of the deuterium points was discarded on a statistical argument. In addition, one more point for each gas was taken at about 91.2°K.

As an aid to objective curve fitting, all of the fitting reported in this paper was done to a high degree of accuracy by a computer. When the entire temperature range is considered, there seems to be a slight departure from model which is as yet unexplained. That is, the root mean square deviation of the best fit of the data to the model runs to about 3% of the measured excess volume (defined in equation 2). If the measured geometric volume is increased by 2%, the r.m.s. deviation drops to 1% and is completely random. However, it is hard to believe that the error in geometric volume could be so great and so it was deemed best not to tamper with the data. It should be noted that the discrepancy in apparent volumes (equation 13), the most important quantity, is independent of which geometric volume is chosen.

Experimental Results

The data are given in Table I. A graphical representation would reveal that the mass-caused discrepancy in the apparent volumes for hydrogen and deuterium is about 250 cm.³ at 91.2°K. and has vanished completely at 225°. This high temperature disappearance of this discrepancy at first made it appear that there were no observable quantum discrepancies because of an unexpected difference in this quantum effect and that for the virial coefficients in the virial equation of state. If the parameters for the potential energy model are evaluated with the classical model from the low temperature behavior of the gaseous virial coefficients, one apparently finds[10] that the collision parameter σ is just the same for two gases differing only in molecular mass, although the heavier gas exhibits a deeper potential energy well. When investigating gas–surface interaction behavior in the same way, however, one finds that although the heavier gas still exhibits a deeper potential energy well, it also exhibits a smaller collision parameter s_0 which in this case is also proportional to the capacity factor As_0. Thus, the cancellation of effects and the premature disappearance of the discrepancy.

TABLE I

RAW DATA (APPARENT VOLUME) AT ZERO PRESSURE

	V_a(cm.³)[a]	$10^3/T$
Hydrogen	1584.3	10.961
	46.83	5.010
	46.45	4.943
	45.99	4.875
	44.76	4.652
	43.80	4.458
	42.82	4.238
	42.31	4.116
Deuterium	1830.9	10.967
	49.56	5.328
	45.88	4.843
	44.55	4.604
	43.91	4.488

[a] Measured geometric volume = 37.602 cm.³.

The parameters evaluated by the various fittings of the data are given in Table II. When an attempt is made to fit the classical model to the data, one finds that D_2 exhibits a potential energy well 48.5 cal. per mole deeper than that for H_2 and that this is somewhat counteracted by a capacity factor 12% smaller. The third entries in the table are ϵ^*/kT and $As_0\alpha$ obtained by fitting the interpolated volume discrepancy of the two gases to the model

(10) J. O. Hirschfelder, *et al.*, ref. 7, The Appendix.

(equation 14). Unfortunately, the size of the temperature gap precludes making any deduction about the potential model from the good fit obtained. Note that the apparent impossibility has occurred that deuterium (interpreted classically) has a deeper apparent well than the "true" potential energy function. This probably results partly from the fact that the paucity of data in the gap prevents a perfect fit of the discrepancy and partly from the poorly understood interrelationship of classically interpreted parameters, As_0 and ϵ^*/k.

TABLE II

	ϵ^*/k	As_0	$As_0\alpha$
	Classical fit; raw data		
H_2	938.9	0.264	
D_2	963.3	0.237	
	Quantum fit; apparent volume, discrepancy		
	960	...	62.2
	Fit of quantum corrected data at $\epsilon^*/k = 960$		
H_2	960	0.256	..
D_2	960	0.252	..
	Best fit of quantum corrected data ($\epsilon^*/k = 960$)		
H_2	974.1	0.240	..
D_2	979.9	0.226	..

If one uses the value of ϵ^*/k obtained from fitting the discrepancy and adjusts the "quantum corrected data," of the form ln $(V_{ex} + As_0\alpha I/mT_2)$, to the reduced plot of ln B_c/As_0 *vs.* ϵ^*/kT to evaluate the parameters As_0, he obtains the values of As_0 given next in Table II. The fact that both isotopes fit with the same value of As_0 (to within 1.6%) is highly satisfactory confirmation of the potential model. If, as a measure of goodness of fit one makes the best fit of these "corrected" data to the theoretical curve, he obtains the final entries in Table II: namely, the curve fittings seek a somewhat higher value of the energy and develop a discrepancy of about 11.5 cal. mole^{-1} in the energy and a 7% discrepancy in the capacity factor. This small inconsistency evidently results from a slight departure from the model but it is impossible to say without further data on other systems whether it is significant or is merely an artifact. It is possible, for example, that small heterogeneities in the surface could prevent a completely consistent fit regardless of the potential model used.

Returning to the consistent quantum mechanical fit to the data represented by the third, fourth and fifth entries in Table II, one may use equation 15 to get the unambiguously defined area for the interaction of gas and surface. The value as obtained is just 530 square meters per gram of solid. This in turn implies an s_0 value of 2.8 Å. There seems to be no method of comparable rigor for checking either number, but both seem very reasonable from an intuitive standpoint. It is not at all unreasonable that the B.E.T. method should over-estimate the area of such a porous solid by a factor of two and in fact one almost expects it. Secondly, if one averages the non-bonding thickness of a graphite plane[11] and the van der Waals collision diameter of the hydrogen molecule[11] he gets 3.1 Å., which is within 10% of the value obtained here. If, on the other hand, the Kirkwood–Mueller formula is employed as described elsewhere[2] to get an independent estimate of this distance, one gets 2.5 to 2.7 Å. (depending on the density used). One would expect this distance to be at least a little less than the non-bonding distance because of the magnitude of the interaction energy, and so to the best of present knowledge one could not improve on this estimated distance. This would seem to be an unexpected but very good independent verification of the 9-3 potential energy model.

Separations.—Since there is a difference of 16% in the amount of H_2 and D_2 taken up by the surface at liquid oxygen temperatures, one might suppose that this could somehow be used to separate the isotopes. This is in fact the case. It has been shown elsewhere[3] that the parameters B of this theory relate simply (in the limit of zero pressure) to the excess retention volume concept of gas adsorption chromatography. This means that if H_2 and D_2 could be passed through a column containing 1.7 grams of SU-60 charcoal at liquid oxygen temperature and a flow rate of 70 ml. of eluent per minute one would get 3.5 minutes difference in time of emergence. For a mixture of, say, HD and D_2, one might expect nearly two minutes. Just such a separation was found recently by T. Kwan and his co-workers for the isotopic pair HD and D_2 using Linde molecular sieve number five at liquid *air* temperatures.[12]

Conclusion.—It is apparent that the physical picture employed in interpreting gas–surface interaction is just as successful for the "almost classical" quantum mechanical interpretation as it is for the classical. As the calculated quantum effect is critically dependent on the curvature at the bottom of the potential energy well and this curvature in turn is critically dependent on the nature of the repulsive potential, it is remarkable that the agreement is so very good for the 9–3 potential model which was chosen in an essentially arbitrary manner.

Work remaining to be done in investigating this phenomenon involves accumulating considerably more data for this assembly and others and interpreting them for several different potential energy models. In addition to the two principal tests for a potential model: (1) the consistency of the parameters derived from the discrepancy fit and the quantum corrected excess volume fits and (2) the goodness of fit in both cases, one may possibly infer something from the magnitude of the s_0 parameter. Furthermore, if more than one isotope pair can be run on the same solid, the consistency of resultant areas serves as a check.

Finally, because of the direct applicability of these equilibrium measurements to the techniques of gas adsorption chromatography, the effect is one of considerable potential utility.

Acknowledgment.—The author especially wants to acknowledge the help and encouragement of Pro-

(11) L. Pauling, "The Nature of the Chemical Bond," 2nd edition, Cornell University Press, Ithaca, N. Y., 1948, p. 192.

(12) S. Ohkoshi, Y. Fuguto and T. Kwan, *Bul. Chem. Soc. Jap.*, **31**, 770 (1958); S. Ohkoshi, S. Tenma, Y. Fuguto and T. Kwan, *ibid.*, **31**, 772, 773 (1958).

fessor K. S. Pitzer in this undertaking. He further wishes to express his gratitude for stimulating conversations with Drs. Berni Alder and William E. Donath; the help of Professor M. C. DeMarcus who suggested the simplifying relationship 9; the mass spectrometric analyses run by Mr. Amos Newton of the University of California Radiation Laboratory in Berkeley; the assistance of that laboratory in procuring He^3 (which he was unable to use); and the gratuitous time given him on the IBM 701 computer sponsored jointly by the IBM Corporation, the Regents of this University, and the National Science Foundation.

APPENDIX

TABLE OF VALUES OF REDUCED INTEGRALS
(reproduced from a more extensive table in ref. 4)

ϵ^*/kT	$Bc/A\beta_0$	I
10.00	4452.8900	78239.1
9.50	2789.2800	48778.7
9.00	1751.1400	30460.1
8.50	1102.2400	19055.7
8.00	695.7870	11945.2
7.50	440.6520	7505.44
7.00	280.0840	4728.56
6.50	178.7210	2988.34
6.00	114.514	1895.55
5.50	73.6704	1207.66
5.00	47.5335	773.565
4.50	30.7764	498.824
4.00	19.9047	324.411
3.50	12.8029	213.356
$3.33^1/_3$	11.0226	186.126
2.50	4.9813	97.260
2.00	2.8550	68.649
1.428	1.2173	49.479
1.00	0.3562	42.580

A CONDUCTIMETRIC STUDY OF DILUTE SOLUTIONS OF MAGNESIUM AND CADMIUM CHLORIDES IN ETHANOL FROM −70 TO 20°

BY MICHAEL GOLBEN AND LYLE R. DAWSON

Contribution from the Department of Chemistry, University of Kentucky, Lexington, Kentucky

Received June 1, 1959

The conductances of dilute solutions of magnesium and calcium chlorides in ethanol have been measured over the temperature range −70 to 20°. In the most dilute range, magnesium chloride dissociates as a bi-univalent electrolyte, and cadmium chloride as a uni-univalent electrolyte. A mass law expression for the second dissociation of a weak bi-univalent electrolyte, corrected for interionic effects and based on the assumption that the first dissociation is complete in sufficiently dilute solution, was used to interpret the data for magnesium chloride. The Shedlovsky method for uni-univalent electrolytes was applied to the data for cadmium chloride. The limiting conductances, classical ionization functions and thermodynamic dissociation constants of these salts have been determined at each temperature interval studied.

A literature survey revealed a lack of conductance data for solutions of bi-univalent or uni-bivalent electrolytes in ethanol over a range of temperatures. This type of study of non-aqueous solutions is particularly valuable in extending the knowledge of the behavior of unsymmetrical electrolytes in solvents having relatively low dielectric constants.

A conductimetric study of solutions of magnesium halides in ethanol at 20° has been reported earlier.[1] In the present paper similar data are given for solutions of magnesium and cadmium chlorides in ethanol over the temperature range −70 to 20°. The plotted data for magnesium chloride at 20° have been included, even though previously reported, in order to permit convenient comparisons.

The treatment of data for non-aqueous solutions of multi-dissociated salts is hampered greatly by lack of transference data. It seemed that the use of estimated values of transference numbers was justified, since the error of estimation and its effect on the final results probably was smaller than the experimental error.

Experimental

The methods of purification of the salts and of ethanol, the method of analysis and the general procedure and apparatus used were described in a previous paper.[1]

(1) L. R. Dawson and M. Golben, *J. Am. Chem. Soc.*, **74**, 4134 (1952).

At all temperatures lower than 20°, an acetone–methanol bath was used. The essential features of the temperature control described earlier[1] were retained; a bimetallic thermoregulator was substituted for the mercury regulator, and the coolant consisted of powdered Dry Ice in a large Pyrex test-tube immersed in the bath. Control was better than ± 0.1° at other than −60° or −70°.

The cell constant of the unplatinized cell at 20° was 0.075-224. The cell constant at different temperatures was computed in the following manner: given the inside surface area of one electrode (A), the distance between the electrodes (d), and the cell constant (K), at 20°, an arbitrary constant (c) was computed from the relationship

$$c(d/A) = K \qquad (1)$$

Knowing the linear coefficients of expansion of Pyrex glass and platinum and the dimensions of the cell, these factors were applied in calculating new values of d and A at different temperatures, remembering that contraction of the glass brings the electrodes together while contraction of the platinum moves them apart. Substituting the value of d/A at a new temperature in equation 1 and inserting the value of c determined the value of K at that temperature. The average change in cell constant per degree was calculated to be 0.00033%.

Though solution conductivity was quite low at low temperatures, pure solvent conductivity was low also (in some cases nearly zero); thus measurements could be made in very dilute solutions.

Results and Treatment of Data

The data for magnesium and cadmium salts were mutually supporting, thus facilitating the calculation of ion mobilities and the estimation of transference numbers. Cadmium chloride showed

a typical uni-univalent dissociation even in the lowest practicable concentration range, while magnesium chloride showed double dissociation. Conductance data for magnesium chloride, together with supplementary information from the literature, yielded the chloride ion limiting conductances at various temperatures; this permitted calculation of ratios of the limiting ion conductances of $CdCl^+$ to Cl^-, from which the ratios for the conductance of $MgCl^+$ to Cl^- were taken, making the assumption that the complex ions $CdCl^+$ and $MgCl^+$ are about the same size.

The best mass law expression was found first for each electrolyte. The correction for interionic effects for solutions of magnesium chloride was made as before[1]; in the case of cadmium chloride, which dissociated as a uni-univalent salt, the Shedlovsky method[2] was used. Plots of the corrected mass law expressions permitted evaluations, after reiterated calculations, of the limiting equivalent conductance (Λ_0), thermodynamic dissociation constant (K) and degree of dissociation at various concentrations (γ).

Calculations for magnesium chloride at 20, 0, −20 and −40° were made using the method and equations previously developed[1]

$$F\Lambda^* = \Lambda_0 - (1.5/K\Lambda_0)cf_{Mg^{++}}[(F\Lambda^*)^2 - 0.1111\Lambda_0^2] \quad (2)$$

$$\Lambda^* = 1/3\Lambda_0(1 + 2\gamma') \quad (3)$$

$$t^1/_{2Mg^{++}} = 0.6667 - 0.1315\,(\Lambda_0/\sigma) \quad (4)$$

Where

Λ_0	=	limiting equivalent conductance
γ'	=	apparent degree of dissociation
K	=	thermodynamic dissociation constant
c	=	normality
$f_{Mg^{++}}$	=	Debye–Hückel activity coefficient for the Mg^{++} ion
F	=	Shedlovsky function[2] ($F = 1 + Z + \ldots$)
$t^1/_{2Mg^{++}}$	=	limiting transference number for the Mg^{++} ion
σ	=	$28.94/(DT)\eta$, where D, T and η are dielectric constant, absolute temp., and viscosity of the solvent, respectively.

This equation is derived from the mass law equation, given below, expressing relationships under the assumption that the first dissociation is complete (K' = classical ionization function)

$$\Lambda' = \Lambda_0' - (1/K'\Lambda_0')c\Lambda'(\Lambda' + \Lambda_0') \quad (5)$$

Various numerical constants for ethanol at different temperatures are summarized in Table I.

TABLE I

NUMERICAL CONSTANTS FOR ETHANOL

Temp., °C.	Density[3]	Viscosity (poise)[4]	Dielectric constants[5]
25	0.78506	0.01078	24.3
20	.78934	.01186	25.0
0	.80625	.01778	28.2
−20	.82327	.02838	31.9
−40	.84051	.04700	36.0
−60	.85780	.08712	40.7
−70	.86660	.1247	43.2

The transference numbers, listed in Table II, were calculated from values of $\Lambda°m$ for cadmium chloride and λ for the chloride ion (from data for magnesium chloride).

TABLE II

ESTIMATED TRANSFERENCE NUMBERS FOR MAGNESIUM CHLORIDE AND CALCIUM CHLORIDE IN ETHANOL

Temp., °C.	$MgCl_2$		$CdCl_2$	
	$t^1/_{2\ Mg^{++}}$	$t^0_{Cl^-}$	$t^1/_{2\ Cd^{++}}$	$t^0_{Cl^-}$
25	0.474	0.526		
20	.466	.534	0.327	0.676
0	.444	.556	.299	.701
−20	.447	.553	.217	.783
−40	.455	.545	.170	.830
−60	.469	.531		
−70	.471	.529	.274	.726

The dissociation of cadmium chloride in ethanol is assumed to reach only the first stage in the measurable concentration range

$$CdCl_2 \rightleftarrows CdCl^+ + Cl^- \quad (6)$$

Under this assumption, a reasonable value of 32.75 was obtained for the limiting molar conductance of $CdCl_2$. If double dissociation had been assumed, the limiting equivalent conductance could have been 16.38—far too low to be reasonable. Furthermore, upon assuming a single dissociation, the mass law plot showed straight lines without the inflection observed for the magnesium halides (under the same assumption).

The Shedlovsky method[2] for weak uni-univalent electrolytes was applied, using an equivalent form of his equation

$$1/F\Lambda_m = 1/\Lambda^0_m + (1/K\Lambda^0{}_m^2)(M\Lambda_m f_\pm{}^2 F) \quad (7)$$

where $f_\pm$ = mean activity coefficient of Cl^- and $CdCl^-$ ions.

The mass law equation for uni-univalent electrolytes is

$$1/\Lambda = 1/\Lambda^0_m + (1/K'\Lambda^0{}_m^2)(M\Lambda_m) \quad (8)$$

In the above method a preliminary value of Λ^0_m was obtained by an extrapolation of the mass law plot. This was substituted in equation 7, plotting $1/F\Lambda_m$ against $M\Lambda_m f_\pm{}^2 F$ and extrapolating by the method of least squares to obtain the intercept $1/\Lambda^0_m$, and thus Λ^0_m. The computations were repeated until Λ^0_m remained the same.

Kohlrausch plots for magnesium and cadmium (as a uni-univalent electrolyte) chlorides are shown in Fig. 1 and 2. Plots of $F\Lambda^*$ as a function of $cf_{Mg^{++}}[(F\Lambda^*)^2 - 0.1111\Lambda_0^2]$ for magnesium chloride and of $1/F\Lambda_m$ as a function of $[M\Lambda_m f_\pm{}^2 F]$ for cadmium chloride may be found in Fig. 3 and 4.

Though magnesium and cadmium chlorides are both weak electrolytes in ethanol, the former dissociates far more readily than the latter (the Kohlrausch plots for cadmium chloride showed no linearity and could not be extrapolated). This difference may be ascribed to the smaller crystal ionic radius of magnesium, resulting in greater charge density per unit surface area, thus stronger solvation and tendency to exist as an ion. Though

(2) T. Shedlovsky, *J. Franklin Inst.*, **225**, 739 (1938).

(3) For 25 and 20°, data of Osborne, McKelvy and Bearee were used (*Bur. Standards Bull.*, **9**, 327 (1913)). For 0° and below, Timmerman's formula was used ("International Critical Tables," Vol. III, McGraw–Hill Book Co., New York, N. Y., 1930, p. 27).

(4) For 25° from Barak and Hartley (*Z. physik. Chem.*, **A165**, 272 (1933)). For 20°, original data. For 0° and below, from graph of data of Mitsukuri and Tonomura ("Landolt–Börnstein Physikalische-Chemische Tabellen," 2nd suppl., pt. 1, p. 98).

(5) G. Akerlof, *J. Am. Chem. Soc.*, **54**, 4125 (1932).

not exhibited by cadmium chloride, there is a tendency for some cadmium salts to form complex ions in ethanol as shown by conductance data for cadmium iodide not included in this paper.

The Kohlrausch plots for magnesium chloride can be extrapolated at all temperatures, but the values for Λ_0 thus obtained are not valid except at very low temperatures (-60 and $-70°$) because of the large discrepancy between actual and theoretical slopes even at the lowest practicable concentrations. Values of Λ_0 as obtained from the Kohlrausch plots, from plots of equation 2 and from mass law plots of equation 5, as well as the thermodynamic dissociation constants, the actual and theoretical (Onsager) slopes, and the ionization functions are collected in Table III.

TABLE III

SUMMARY OF DATA FOR SOLUTIONS OF MAGNESIUM CHLORIDE IN ETHANOL FROM -70 TO 20°

Temp., °C.	Λ^0 $\Lambda - \sqrt{C}$	Λ^0 (eq. 5)	Λ^0 (eq. 2)	Actual slope	Theor. slope	K' $\times 10^4$	K $\times 10^4$
20	43.45	41.08	41.70	−1510	−271.7	1.709	1.619
0	31.43	29.45	30.02	− 975.5	−178.4	2.386	2.115
−20	18.81	17.83	18.34	− 413.4	−104.8	4.530	3.990
−40	10.83	10.22	10.58	− 204.2	− 59.9	6.837	6.000
−60	4.87	...	...	− 49.0	− 30.8	...	...
−70	3.23	...	...	− 30.9	− 20.9	...	...

It is apparent that there is considerable divergence between the actual and theoretical slopes, decreasing with lower temperatures. The percentage decrease between the correct value of Λ_0 as obtained by a plot of equation 2 and Λ_0 as obtained by the Kohlrausch plot becomes smaller at lower temperatures. At -60 and $-70°$ the actual and theoretical slopes are sufficiently close so that extrapolation of the Kohlrausch plots yields values of Λ_0 which probably are correct within experimental error. The increase in the dissociation constant with decrease in temperature, the increase in degree of dissociation for comparable concentrations and an increase in the percentage correction of Λ_0 as obtained by equation 5, all indicate that magnesium chloride in ethanol becomes a stronger electrolyte as temperature is lowered. Evidently this effect is attributable to the increased dielectric constant of the solvent at lower temperatures.

In making computations for plotting equation 2, it was found that the difference between Λ and Λ^* decreased with lower temperature, becoming negligible at $-40°$. This effect is due probably to the gradual disappearance of the intermediate ion, $MgCl^+$, and is another indication of more complete dissociation at lower temperatures. The actual condition becomes more nearly that implied in the Onsager equation for ternary dissociation into the two types of ions, Mg^{++} and Cl^-. The dissociation constant K remained reasonably constant over the dilute range at all temperatures, while K' increased with concentration, usually by 30% or more. As noted previously,[1] this type of result substantiates equation 2 and the assumptions under which it was derived.

In Table II it is shown that the calculated transference number of the magnesium ion reaches a minimum at 0°. According to equation 4, the transference number of the cation depends upon

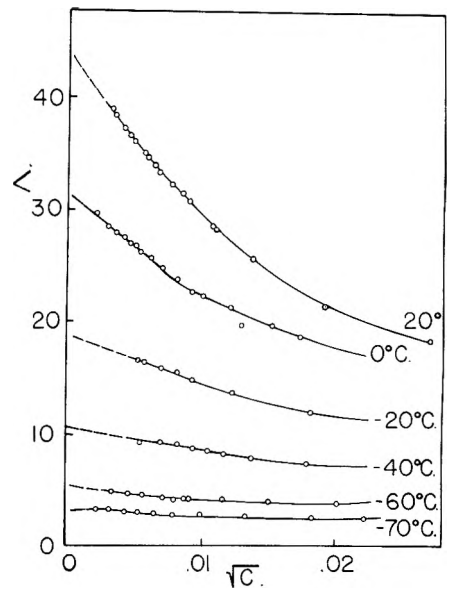

Fig. 1.—Equivalent conductance of $MgCl_2$ at 20, 0, -20, -40, -60 and $-70°$, as a function of the square root of the concentration.

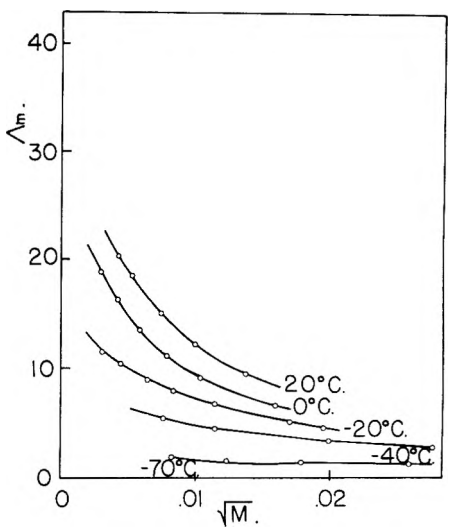

Fig. 2.—Molar conductance of $CdCl_2$ at 20, 0, -20, -40 and $-70°$ as a function of the square root of concentration.

the ratio Λ_0/σ, and decreases as this ratio increases. Substituting the expression for σ into equation 4, it turns out that $t_\pm^0$ is inversely proportional to the quantity $\Lambda_0(DT)^{1/2}\eta$ as temperature varies. Of the four variables involved, Λ_0 decreases, while D and η increase as temperature T is lowered. The effect of D and η is predominant at 0° and above, while the change in Λ_0 and T is predominant below 0°. Consideration of the change with temperature of the Walden rule "constant," $\Lambda_0\eta$, as shown in Table IV for both salts, reveals a maximum in this quantity at 0°, again indicating that change in η predominates at 0° and above, while change in Λ_0 predominates below 0°.

An equation similar to (4) can be derived for the cationic transference number of a uni-univalent salt. Assuming that such a relationship holds true for cadmium chloride as a uni-univalent salt,

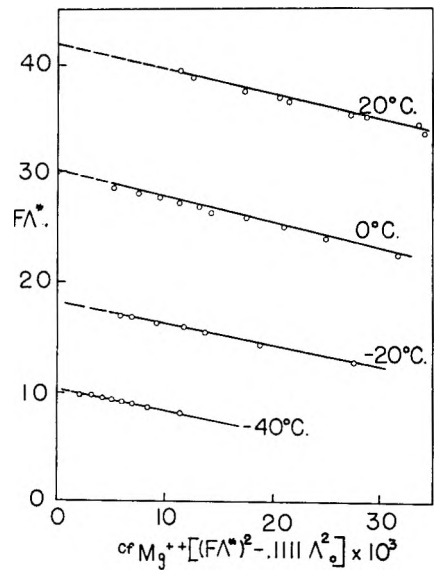

Fig. 3.—Shedlovsky plot for the second ionization of $MgCl_2$ in ethanol at 20, 0, −20 and −40°.

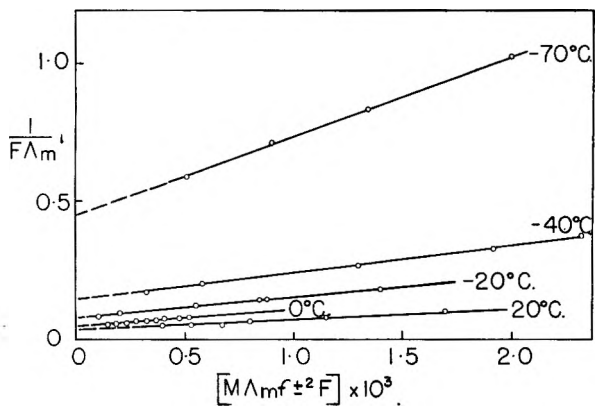

Fig. 4.—Shedlovsky plot for $CdCl_2$ as a uni-univalent salt at 20, 0, −20, −40 and −70°.

the estimated transference number of the ion $CdCl^+$, over a range of temperatures, as shown in Table II, provides evidence that the effect of the increase in D and η is greater than the effect of a decrease in Λ_0 and T, even at −40°. Since D, η and T are the same for cadmium chloride as for magnesium chloride, it might be said that the effect of a decrease in Λ_0 is greater for magnesium chloride as a bi-univalent electrolyte than for cadmium chloride as a uni-univalent electrolyte.

Table V contains a summary of the results calculated from the data for solutions of cadmium chloride.

TABLE IV

WALDEN RULE CONSTANTS FOR SOLUTIONS OF $MgCl_2$ AND $CdCl_2$ IN ETHANOL AT SEVERAL TEMPERATURES

Temp., °C.	$\Lambda_0\eta$ for $MgCl_2$[a]	$\Lambda^0_m\eta$ for $CdCl_2$[b]
20	0.494	0.388
0	.534	.424
−20	.520	.369
−40	.497	.326
−60	.424	...
−70	.402	.293

[a] As bi-univalent electrolyte. [b] As uni-univalent electrolyte.

TABLE V

SUMMARY OF DATA FOR SOLUTIONS OF $CdCl_2$ IN ETHANOL FROM −70 TO 20°

Temp., °C.	Λ^0_m eq. 8	Λ^0_m eq. 7	$K' \times 10^5$	$K \times 10^5$
20	32.07	32.75	2.397	2.222
0	23.58	23.82	2.740	2.640
−20	12.90	13.03	7.817	7.501
−40	6.73	6.94	23.19	21.28
−70	2.22	2.35	57.89	50.20

It is apparent from a comparison of Tables III and V that the proportionate increase in the dissociation constant as temperature is lowered is much greater for cadmium chloride as a uni-univalent electrolyte than for the second dissociation of magnesium chloride. For cadmium chloride, K increases from 2.35×10^{-5} at 20° to 50.2×10^{-5} at −70°. But at −70° cadmium chloride in ethanol is still too weak an electrolyte to show any evidence of a second dissociation at dilutions within the experimental range. The values of Λ^0_m as obtained by means of the mass law (equation 8) and by Shedlovsky's method (equation 7) are reasonably close. With weak electrolytes the mass law yields a fair approximation of Λ^0_m because of the partial cancellation of errors resulting from neglecting the effect of change in concentration on ion mobility and activity coefficient. However, the "classical ionization function," K', differs from the dissociation constant K and shows a drift with change in concentration. Since the major correction applied to K' to obtain K is the square of the mean activity coefficient, the constancy of K represents correspondence with the Debye–Hückel theory.

The approach used herein which produces convincing evidence of the distinctly different modes of dissociation of magnesium and cadmium chlorides in ethanol may be generally useful for multivalent electrolytes in non-aqueous solvents.

THE DECARBOXYLATION OF MALONIC ACID IN ACID MEDIA

BY LOUIS WATTS CLARK*

Contribution from the Department of Chemistry, Saint Bonaventure University, Saint Bonaventure, New York

Received June 8, 1959

Kinetic data are reported on the decarboxylation of malonic acid in propionic acid, butyric acid, β-mercaptopropionic acid and monochloroacetic acid. The constants of the Eyring equation are evaluated. The inductive effect of the methyl group substituted in place of a hydrogen on to the propionic acid molecule results in a lowering of $\Delta H^{\ddagger}$ on passing from propionic acid to butyric acid. In monochloroacetic acid ΔH^{*} of the reaction is lower than it is in propionic acid. This is attributed to an increase in electron density on the hydroxyl oxygen atom due to a +E effect of the halogen. The data for β-mercaptopropionic acid indicate that the electrophilic carbonyl carbon atom of malonic acid probably coördinates with an unshared pair of electrons on the S atom of the sulfhydro group and not on the O atom of the hydroxyl group. Steric effects are manifested by changes in ΔS^{*} for the reaction between the different liquids.

Kinetic studies on the decarboxylation of malonic acid in various liquids[1] have established the essential validity of the mechanism of the reaction proposed by Fraenkel and co-workers,[2] namely, the formation, prior to cleavage, of a transition complex involving coördination of the electrophilic carbonyl carbon atom of the un-ionized malonic acid with an unshared pair of electrons on the nucleophilic atom of the solvent molecule.

The tendency possessed by malonic acid to coordinate with an unshared pair of electrons and subsequently to split into acetic acid and carbon dioxide affords a convenient means of deducing the characteristics of the transition complex on the basis of the absolute reaction rate theory and obtaining thereby an insight into the electron structures of polar liquids in general. The method has been applied successfully, up to the present time, to the study of 34 non-aqueous solvents, comprising representatives of 9 homologous groups, namely, aromatic amines, alicyclic amines, aromatic nitro compounds, ethers, esters, phenols, thiophenols, sulfoxides and polyhydric alcohols.[1]

The present paper describes the results of kinetic studies carried out in this Laboratory on the decarboxylation of malonic acid in four monocarboxylic acids, namely, propionic acid, *n*-butyric acid, monochloroacetic acid and β-mercaptopropionic acid.

Experimental

Reagents: (1) Reagent Grade malonic acid, 100.0% assay, was used in this investigation. (2) Solvents: (a) the propionic acid, *n*-butyric acid and monochloroacetic acids used in this research were Reagent Grade chemicals. Each sample of each liquid was fractionally distilled at atmospheric pressure into the reaction flask immediately before the beginning of each experiment. (b) The β-mercaptopropionic acid used in these experiments was obtained from Evans Chemetics Inc., 250 E. 43rd St., N. Y., N. Y. Its physical characteristics were: m.p. 16.8°; b.p. 110.5–111.5° at 15 mm.; sp. gr. 21/4, 1.218; assay, 99.6%. Samples of this liquid were taken directly from the container without any further purification.

Apparatus and Technique.—The details of the apparatus and technique have been described previously.[1b] In these experiments a sample of malonic acid weighing 0.1857 g. (corresponding to 40 ml. of CO_2 at STP on complete reaction) was weighed into a fragile glass capsule weighing approximately 0.1 g. blown from 6 mm. soft-glass tubing. A weighed quantity of solvent (saturated with dry CO_2 gas) was placed in the 100-ml., 3-neck, standard-taper flask immersed in the oil-bath. The temperature of the thermostat controlled oil-bath (maintained to within ±0.05°) was determined using a thermometer graduated in tenths of a degree and calibrated by the U.S. Bureau of Standards.

Results

Decarboxylation experiments were carried out in each solvent at three or four different temperatures over a 10–20° temperature range, two or three experiments being performed at each temperature in each solvent. In every experiment the plot of $\log (a - x)$ *vs.* t (where a is the maximum theoretical volume of CO_2 evolved, and x the volume evolved at time t) yielded a straight line. The reaction was generally carried out in approximately 50 ml. of solvent. However, as in the case of previous studies conducted in various types of solvents,[1] variation in the ratio of solvent to solute had no appreciable effect upon the rate of reaction.

The average values of the apparent first-order rate constants for the reaction in the four acids at the various temperatures studied, obtained from the slopes of the experimental logarithmic plots, are listed in Table I. The parameters of the Eyring equation are shown in Table II. Data for the decarboxylation of malonic acid in aniline and in thiophenol are included for comparison.

TABLE I

APPARENT FIRST-ORDER RATE CONSTANTS FOR THE DECARBOXYLATION OF MALONIC ACID IN SEVERAL LIQUIDS

Solvent	Temp. (°C. cor.)	No. of runs	$k \times 10^4$ (sec.$^{-1}$)
Propionic acid	128.05	3	0.928 ± 0.05[a]
	133.77	2	1.74 ± .07
	138.44	3	2.82 ± .06
n-Butyric acid	138.04	2	2.08 ± .05
	144.22	3	3.84 ± .04
	149.20	3	6.15 ± .06
	156.72	2	12.20 ± .03
Monochloroacetic acid	139.70	2	1.42 ± .06
	150.15	3	3.71 ± .05
	154.65	3	5.61 ± .04
	159.35	2	9.80 ± .03
β-Mercaptopropionic acid	141.94	3	3.76 ± .03
	148.96	3	7.05 ± .05
	156.66	2	13.77 ± .07
	158.15	2	15.15 ± .04

[a] Average deviation.

* Department of Chemistry, St. Mary of the Plains College, Dodge City, Kansas.

(1) (a) L. W. Clark, THIS JOURNAL, **60**, 825 (1956); (b) **60**, 1150 (1956); (c) **60**, 1340 (1956); (d) **60**, 1583 (1956); (e) **61**, 1009 (1957); (f) **61**, 1575 (1957); (g) **62**, 79 (1958); (h) **62**, 368 (1958); (i) **62**, 500 (1958); (j) **62**, 1478 (1958).

(2) G. Fraenkel, R. L. Belford and P. E. Yankwich, *J. Am. Chem. Soc.*, **76**, 15 (1954).

TABLE II

KINETIC DATA FOR THE DECARBOXYLATION OF MALONIC ACID IN SEVERAL LIQUIDS

	Solvent	ΔH^* (kcal.)	ΔS^* (e.u.)	$\Delta F^*_{140°}$ (kcal.)	$k_{140°} \times 10^4$ (sec.$^{-1}$)
(1)	Propionic acid	33.6	+6.1	31.1	3.4
(2)	*n*-Butyric acid	32.3	+2.5	31.3	2.5
(3)	Monochloroacetic acid	31.7	−0.07	31.7	1.5
(4)	β-Mercaptopropionic acid	30.3	−1.9	31.3	3.1
(5)	Aniline[1g]	26.9	−4.5	29.0	50.0
(6)	Thiophenol[1i]	34.3	+6.9	31.5	1.9

Discussion of Results

The hydroxyl oxygen atom of the monocarboxylic acids may act as a Lewis base, donating an unshared pair of electrons to an electrophilic agent.[3] In the decarboxylation of malonic acid in these media the transition complex is evidently formed by the coördination of the electrophilic carbonyl carbon atom of the malonic acid with one of the unshared pair of electrons on the hydroxyl oxygen atom of the solvent molecule. An increase in the effective negative charge on the nucleophilic atom of the solvent molecule increases the attraction between the reactants and results in a lowering of ΔH.[4] Aniline is generally regarded as a weak base, propionic acid as a weak acid. Nevertheless these polar liquids are both amphiprotic, acting either as a Lewis acid or Lewis base depending upon the nature of the second reactant. In this sense, therefore, propionic acid is evidently a weaker "base" than aniline. The decrease in ΔH^* from 33.6 kcal. for the reaction in propionic acid to 26.9 kcal. for the reaction in aniline is in harmony with this difference in relative basicities (compare lines 1 and 5 of Table II).

Since the ethyl group exerts a larger +I effect than does the methyl group it would be expected that the effective negative charge on the hydroxyl oxygen atom or butyric acid would be slightly larger than that in the case of propionic acid. The lowering of ΔH^* from 33.6 kcal. for the reaction in propionic acid to 32.3 kcal. for the reaction in *n*-butyric acid (see lines 1 and 2 of Table II) supports this expectation. The decrease in ΔS^* from +6.1 e.u. in propionic acid to +2.5 e.u. in *n*-butyric acid is evidence of the greater steric effect of the larger molecule.

The mechanism of the decarboxylation of the trichloroacetate ion in polar media has been shown to be analogous to that of malonic acid.[5] In studies on the decarboxylation of the trichloroacetate ion in acid media[6] it was demonstrated that the halogen atom in monochloroacetic acid exerts a pronounced −I effect, strongly reducing the electron density on the hydroxyl oxygen atom, resulting in an increase in ΔH^* for the reaction from 35.5 kcal. in acetic acid to 48.9 kcal. in monochloroacetic acid. The halogens are potentially capable of exerting either a −I effect or a +E effect. In the case of the trichloroacetate ion, the negative charge on the resonating carboxylate group probably acts effectively to repel the mobile electrons on the monochloroacetic acid molecule so as totally to prevent the +E effect from operating. The −I effect represents a permanent state of the molecule, whereas the +E effect is temporary, and comes into play at the precise moment of reaction on the demands of the reagent.[7]

In the case of the decomposition of the unionized, neutral malonic acid molecule, which, in this case, is the entity involved in the coördination with the nucleophilic atom of the solvent molecule prior to cleavage, there is nothing to prevent the +E effect from operating. It would be expected, therefore, that for the decomposition of malonic acid in monochloroacetic acid, the halogen would not be halted in its tendency to release electrons to the reactive center at the precise moment of reaction on the demands of the reagent—in other words, for this reaction, a +E effect should operate, producing an increase in the electron density on the hydroxyl oxygen atom, and result in a lowering of ΔH^*. Comparison of lines 1 and 3 of Table II reveals that the result anticipated is, in fact, actually obtained. On going from propionic acid to monochloroacetic acid ΔH^* decreases from 33.6 to 31.7 kcal. Here, obviously, we are dealing with a +E effect which makes the monochloroacetic acid a stronger base than propionic acid—but only, of course, at the moment of reaction.

An interesting question arises in the case of the reaction in β-mercaptopropionic acid. In previous studies on the decarboxylation of malonic acid in thiophenol[1i] it was established that the electrophilic carbonyl carbon atom of malonic acid coördinated with one of the unshared pairs of electrons on the sulfur atom. Since it is possible for malonic acid to coördinate with the oxygen of the hydroxyl group as well as with the sulfur of the sulfhydro group the question is: with which atom will it coördinate? Some insight into this puzzle may be gained by considering lines 2, 4 and 6 of Table II. Since sulfur has the same electronegativity as carbon,[8] the effective negative charge on the hydroxyl oxygen atom of β-mercaptopropionic acid should be approximately the same as that in the case of *n*-butyric acid. Therefore, if the malonic acid attacked the hydroxyl oxygen atom of β-mercaptopropionic acid, ΔH^* for the reaction would be expected to be approximately the same as that for *n*-butyric acid. Instead, however, we find that ΔH^* is 2.0 kcal. lower for the reaction in β-mercaptopropionic acid than for that in *n*-butyric acid. In β-mercaptopropionic acid the sulfhydro group is linked to a carboxyethyl group, which would not be expected to have any very appreciable negative inductive effect, inasmuch as the carboxy group is separated from

(3) L. F. Fieser and M. Fieser, "Introduction to Organic Chemistry," D. C. Heath and Co., Boston, Mass., 1957, p. 138.

(4) K. J. Laidler, "Chemical Kinetics," McGraw-Hill Book Co., Inc., New York, N. Y., 1950, p. 138.

(5) L. W. Clark, THIS JOURNAL, **63**, 99 (1959).

(6) L. W. Clark, *ibid.*, **63**, 1760 (1959).

(7) A. E. Remick, "Electronic Interpretations of Organic Chemistry," 2nd Ed., John Wiley and Sons, Inc., N. Y., N. Y., 1949, p. 225.

(8) L. Pauling, "College Chemistry," W. H. Freeman and Company, San Francisco, Cal., 1955, p. 236.

the sulfur atom by two methylene groups. In thiophenol, however, the sulfhydro group is linked directly to the phenyl group which exerts a very strong $-I$ effect. The decrease of 4.0 kcal. for the reaction on going from thiophenol to β-mercaptopropionic acid is in harmony with this large difference in the relative electron withdrawing tendencies of the phenyl group and the carboxyethyl group. Another argument which might be adduced for the choice by the malonic acid of the electrons on the sulfur atom rather than those on the oxygen atom is the fact that monocarboxylic acids are stronger acids, and therefore weaker bases, than thiols. The electrophilic agent will tend to combine with the stronger nucleophilic agent—in this case the sulfur atom.

H-bonding and therefore association cannot take place between molecules of thiophenol, whereas in the monocarboxylic acids H-bonding leads to dimerization. This increase in complexity of the molecule, leading to increased steric hindrance, is revealed by the decrease in ΔS^* of nearly 9 e.u. on going from thiophenol to β-mercaptopropionic acid. Further investigation of this reaction is contemplated.

Acknowledgments.—This research was supported in part by the National Science Foundation, Washington, D. C.

RECIPROCATION OF ELECTROSTATIC AND ELECTROMAGNETIC FORCES IN LIGAND FIELD THEORY[1,2]

BY ANDREW D. LIEHR

Bell Telephone Laboratories, Incorporated, Murray Hill, New Jersey

Received June 9, 1959

If ionic spin-orbital forces are weak, electronic motions in inorganic complexes are governed primarily by the electrostatic coercions of the surrounding ligands, whilst the presence of feeble coulombic directives, but robust spin-orbit correlations, dictates electronic trajectories which are only slightly modified over those characteristic of the free ion. Electronic itineraries of both types have been exhaustively discussed, in the past thirty years, within the framework of the Bethe–Kramers–Van Vleck theory of crystalline fields. However, the rather more esoteric situation in which the spin-orbital and addend field potentials are of comparable magnitude does not seem to have received as thorough a consideration. In this report an account will be given of the optical and magnetic properties expected of d^n, (n = 1,9), molecular systems, in several geometries, which exhibit equi-energetic spin-orbital and augend field interactions, and will be applied, where observational data is extant, to the transition metal complexes of the second and third group. An experimental prospectus s outlined in the hope that such will stimulate future research into this somewhat neglected domain.

Introduction

The renascent exploitation of the Bethe–Kramers–Van Vleck theory of ligand (crystalline) fields in spectro- and magneto-chemical investigations of inorganic systems has led, of late, to an enhanced appreciation of the puissance of symmetry considerations in the resolution of complex electronic problems.[3] Indeed, the explicatory success of this theory may be traced directly to its maximal utilization of molecular regularity.[4] It has not, however, been widely appreciated that such geometrical regularity also imposes quite stringent correlations upon the orbital and spin segments of the electronic charge density distribution.[5,6] This circumstance has prevailed since current, as well as past, applications of the crystalline field theory have dealt with either of two limiting behaviors: (1) the electronic motions are governed predominantly by the electrostatic (coulombic) forces of the ligand field—the electromagnetic subjection of spin and orbital magnetic moments (spin-orbit coupling) acts solely as a minor irritant to these movements; (2) the electronic spatial excursions are preponderantly guided by spin and orbital magnetic coercions—the coulombic constraints serve only as a small directive inducement on their regional jaunts. For interpretive investigations of the spectral and magnetic properties of the iron group (the $3d^n$ elements), approximation (1) is normally sufficient (note through reference 5); while for the lanthanide ($4f^n$) and actinide ($5f^n$) groupings, description (2) is usually completely adequate (but see ref. 7 and 8).

Yet for similar researches on the palladium ($4d^n$) and platinum ($5d^n$) group metals, these viewpoints are woefully deficient.[9–11] In these

(1) The Editors after careful consideration have decided to accept this manuscript in its present form. The scientific work is not questioned seriously by the referees. The style of writing differs from that customarily employed in scientific articles. To the extent that this style makes difficult the understanding of much of this article the author disagrees. On the other hand it seems best to publish this article as desired by the author.—Ed.

(2) Presented at the Symposium on Molecular Structure and Spectroscopy, Columbus, Ohio, June 15–19, 1959.

(3) Recent reviews of this theory have been given by the following authors: (a) W. E. Moffitt and C. J. Ballhausen, *Ann. Rev. Phys. Chem.*, **7**, 107 (1956); (b) J. S. Griffith and L. E. Orgel, *Quart. Rev.*, **11**, 381 (1957); (c) M. H. L. Pryce, *Nuovo Cimento, Suppl.* 3 [10], **6**, 817 (1957); (d) H. Hartmann, *Z. Elektrochem.*, **61**, 908 (1957); (e) W. A. Runciman, *Repts. Prog. Phys.*, **21**, 30 (1958).

(4) J. H. Van Vleck, *J. Chem. Phys.*, **3**, 803, 807 (1935).

(5) A. D. Liehr and C. J. Ballhausen, *Ann. Phys.* [*N.Y.*], **6**, 134 (1959).

(6) C. J. Ballhausen and A. D. Liehr, *Mol. Phys.*, **2**, 123 (1959).

(7) G. L. Goodman, *ibid.*, in press.

(8) G. L. Goodman and M. Fred, *J. Chem. Phys.*, **30**, 849 (1959).

(9) The secular determinants given in ref. 5, which are common to all the kd^n, (k = 3, 4, 5), configurations illustrate this point quite clearly, as the systems kd^n, (k = 4, 5), are characterized by the stipulation $\lambda \approx Dq$ (n.b., ref. 10 and 11 in this regard).

(10) W. E. Moffitt, G. L. Goodman, M. Fred and B. Weinstock *Mol. Phys.*, **2**, 109 (1959).

(11) G. L. Goodman, *J. Chem. Phys.*, in press; Doctoral dissertation, Harvard, 1959.

latter systems the electrostatic and electromagnetic forces present continuously reciprocate in their prescriptive action upon the itinerant electrons: the electrostatic coercions are dominant in the vicinity of the ligands, and the electromagnetic compulsions paramount in the neighborhood of the metal ion nucleus. The resultant circuit traversed by the negative particles is thus compromissary in nature. The specific compromise struck rests, of course, upon the relative importance of these two rival propensities. In this article we shall derive "exact" energy expressions[12] for a single kd, (k = 3, 4, 5), electron or positron[13] driven, alternately, by equally robust electrostatic and electromagnetic forces. We shall also formulate a crude, but instructive, approximational program which should be useful in the delineation of configurations kd^n, when n is larger than unity. Some indicative applications will be discussed and especially close attention will be focused upon the characterization of the recently recorded hexafluorides of tungsten and molybdenum.[14]

Theory

Equations of Motion.—The possible dynamical trajectories which an electron may pursue are selected, according to Schrödinger, from amongst the well-behaved solutions of the differential (eigenvalue) equation

$$\mathcal{H}\Psi = E\Psi \qquad (1)$$

where

$$\mathcal{H} = -\frac{\hbar^2}{2m}\nabla^2 - \frac{\hbar^4}{8m^3c^2}\nabla^4 + \xi(r)\,\vec{l}\cdot\vec{s} + U(r) + V_{\text{C.F.}}(r, \theta, \varphi) \qquad (2)$$

The initial quaternary of terms in the Hamiltonian, $\mathcal{H}$ represents the orthodox hydrogenic Hamiltonian operator, with relativity correction[15]; the remaining expression, $V_{\text{C.F.}}$, particularizes the nonsphericity of the attendant potential field of the encompassing ligands. At present there exist two analytical modes which may be employed to determine the permissible electronic treks—the weak and strong field formalisms. It is the former that will be pondered first.

Weak Field Portrait–Wave Functions.—In the event the ligand (crystalline) field $V_{\text{C.F.}}$ vanishes, the solutions of equation 1 are expressible in the form[15]

$$|j,m> = \sum_{ml.\ m_s} |l,m_l>\,|s,m_s><s,l;\ m_l m_s|j,m> \qquad (3)$$

where $|l,m_l>$ and $|s,m_s>$ are the usual orbital (Condon and Shortley[13c] phases) and spin wave functions, respectively, and $|j,m>$ is the requisite state function with total angular momentum $\vec{j} = \vec{s} + \vec{l}$.[16] The numerical coefficients which relate the $\{s,l,m_s,m_l\}$ basis to that of $\{s,l,j,m\}$ are as given in Table I[3] of Condon and Shortley.[16] Hence, as j is here permitted but two values, 5/2 and 3/2, we may write the free ion functions as

$$\left|\tfrac{5}{2}, m\right> = \sqrt{\frac{5+2m}{10}}\left|2,m-\tfrac{1}{2}\right>\left|\tfrac{1}{2},\tfrac{1}{2}\right> + \sqrt{\frac{5-2m}{10}}\left|2,m+\tfrac{1}{2}\right>\left|\tfrac{1}{2},-\tfrac{1}{2}\right>$$

$$\left|\tfrac{3}{2}, m\right> = \sqrt{\frac{5-2m}{10}}\left|2,m-\tfrac{1}{2}\right>\left|\tfrac{1}{2},\tfrac{1}{2}\right> - \sqrt{\frac{5+2m}{10}}\left|2,m+\tfrac{1}{2}\right>\left|\tfrac{1}{2},-\tfrac{1}{2}\right> \qquad (4)$$

Now Bethe[17] has shown that a reduction in eurythmy from that characteristic of the sphere requires additional specifications of the wave functions Ψ. It is relatively easy to visualize how this happens. For globular symmetry, an angular rotation α about the z-axis multiplies the state vector by a phase factor $e^{im\alpha}$. As the magnitude of α may be chosen arbitrarily, the half-integer m serves to uniquely differentiate transformational properties, and hence to isolate the functions themselves,[18] for each given energy state. However, upon descent to cubic eurythmy, only those values of α which are multiples of $\pi/2$ may be selected, and it is thus impossible to segregate states whose m values differ by an adjunctive multiple of four. For example, the functions $|5/2,5/2>$ and $|5/2, -3/2>$ do not portray distinct states in fields of cubic (or lower) symmetry.[19]

In crystalline fields, $V_{\text{C.F.}}$, of eurythmy lower than spherical, an electronic state is specified by (1) the value of m modulo the order of the axis of maximum rotational symmetry[20] and (2) the number of orthogonal states to which it is symmetrically congruent (the degeneracy factor). Hence if the potential $V_{\text{C.F.}}$ is of cubic constitution, the wave functions defined in equation 1 must be recatagorized into three new subclasses itemized by the quantum numbers $\{\gamma, s, l, j, m\}$, where γ is the symmetry specification, and takes on the species cognomina γ_6, γ_7 and γ_8.[17,20,21] The analogous generic symbols, γ_i^Y, for quadrate (Y = Q) and trigonal (Y = T) potentials are (γ_6^Q,γ_7^Q) and ($\gamma_4^T,\gamma_5^T,\gamma_6^T$), respectively.[17,20,21]

The application of suitable coördinate trans-

(12) By "exact" we but wish to imply that no simplifications other than the inherent basal suppositions of ligand field theory have been invoked.

(13) It may be shown that the collective motions of nine kd, (k = 3, 4, 5), electrons is dynamically equivalent to that of a single positron. An extended discussion of this theorem may be found in (a) J. H. Van Vleck, *Phys. Rev.*, **41**, 208 (1932); (b) G. J. Kynch, *Trans. Faraday Soc.*, **33**, 1402 (1937); (c) E. U. Condon and G. H. Shortley, "The Theory of Atomic Spectra," Cambridge Univ. Press, London and New York, 1953, Chapter XII.

(14) (a) G. B. Hargreaves and R. D. Peacock, *J. Chem. Soc.*, 4212 (1957); (b) 3776 (1958).

(15) Ref. 13c, Chapter V.

(16) The choice of phase which corresponds to the canonical ordering or angular momenta, $\vec{j} = \vec{s} + \vec{l}$, is discussed on pages 123 and 270, ref. 13c.

(17) H. A. Bethe, *Ann. Physik*, [5] **3**, 133 (1929).

(18) As such symmetry operations leave the Hamiltonian $\mathcal{H}$ invariant, an eigenstate is individualized by both its energy and transfigurational behavior.

(19) This follows as the interaction matrix element $<5/2, 5/2|\mathcal{H}|5/2, -3/2<$ no longer vanishes for symmetry reasons. To see this we need only remark that a rotation of the original coördinate axes implies that this matrix element equals $e^{4i\alpha}$ times itself. As α may only assume values which are integral multiples of $\pi/2$, this requirement is now identically fulfilled.

(20) (a) K. H. Hellwege, *Ann. Physik*, [6] **4**, 95 (1948), *et seq.*; (b) E. Fick, *Z. Physik.*, **147**, 307 (1957); (c) E. Fick and G. Joos, "Kristallspektren," Handbuck der Physik, Band XXVIII, Spektroskopie II, Springer, Berlin, 1957.

(21) W. Opechowski, *Physica*, **7**, 552 (1940).

formation operators[22] leads to the desired wave functions tabulated below

(a) Cubic (Γ_7, Γ_8) and Quadrate (Γ_8^Q, Γ_7^Q) Functions[23-26]

$$\Gamma_{7a}(^2D_{5/2}) = \Gamma_{7a}^{Q(1)}(^2D_{5/2}) = +\sqrt{\frac{1}{6}}\left|\frac{5}{2}, -\frac{5}{2}\right\rangle - \sqrt{\frac{5}{6}}\left|\frac{5}{2}, \frac{3}{2}\right\rangle$$

$$\Gamma_{8a}(^2D_{5/2}) = \Gamma_{7a}^{Q(2)}(^2D_{5/2}) = \sqrt{\frac{1}{6}}\left|\frac{5}{2}, \frac{3}{2}\right\rangle + \sqrt{\frac{5}{6}}\left|\frac{5}{2}, -\frac{5}{2}\right\rangle$$

$$\Gamma_{8c}(^2D_{5/2}) = \Gamma_{8a}^{Q}(^2D_{5/2}) = \left|\frac{5}{2}, -\frac{1}{2}\right\rangle$$

$$\Gamma_{8a}(^2D_{3/2}) = \Gamma_{7a}^{Q}(^2D_{3/2}) = \left|\frac{3}{2}, \frac{3}{2}\right\rangle$$

$$\Gamma_{8c}(^2D_{3/2}) = \Gamma_{8a}^{Q}(^2D_{3/2}) = \left|\frac{3}{2}, -\frac{1}{2}\right\rangle \qquad (5)$$

(b) Cubic ($\bar{\Gamma}_7$, $\bar{\Gamma}_8$) and Trigonal (Γ_4^T, Γ_5^T, Γ_6^T) Functions[26-29]

$$\bar{\Gamma}_{7a}(^2D_{5/2}) = \Gamma_{6a}^{T(1)}(^2D_{5/2}) = \frac{2}{3}\left|\frac{5}{2}, \frac{5}{2}\right\rangle - \frac{\sqrt{5}}{3}\left|\frac{5}{2}, -\frac{1}{2}\right\rangle$$

$$\bar{\Gamma}_{8a}(^2D_{5/2}) = \Gamma_{6a}^{T(2)}(^2D_{5/2}) = -\frac{\sqrt{5}}{3}\left|\frac{5}{2}, \frac{5}{2}\right\rangle - \frac{2}{3}\left|\frac{5}{2}, -\frac{1}{2}\right\rangle$$

$$\bar{\Gamma}_{8c}(^2D_{5/2}) = \Gamma_5^T(^2D_{3/2}) = \frac{e^{-3i/4\,[\pi+\beta]}}{\sqrt{2}}\left\{\left|\frac{5}{2}, -\frac{3}{2}\right\rangle + i\left|\frac{5}{2}, \frac{3}{2}\right\rangle\right\}$$

$$\bar{\Gamma}_{8d}(^2D_{5/2}) = \Gamma_4^T(^2D_{5/2}) = \frac{e^{+3i/4\,[\pi+\beta]}}{\sqrt{2}}\left\{\left|\frac{5}{2}, -\frac{3}{2}\right\rangle - i\left|\frac{5}{2}, \frac{3}{2}\right\rangle\right\}$$

$$\bar{\Gamma}_{8a}(^2D_{3/2}) = \Gamma_{6a}^{T}(^2D_{3/2}) = \left|\frac{3}{2}, -\frac{1}{2}\right\rangle$$

$$\bar{\Gamma}_{8c}(^2D_{3/2}) = \Gamma_5^T(^2D_{3/2}) = \frac{e^{+3i/4\,[\pi+\beta]}}{\sqrt{2}}\left\{\left|\frac{3}{2}, -\frac{3}{2}\right\rangle - i\left|\frac{3}{2}, \frac{3}{2}\right\rangle\right\}$$

$$\bar{\Gamma}_{8d}(^2D_{3/2}) = \Gamma_4^T(^2D_{3/2}) = \frac{e^{-3i/4\,[\pi+\beta]}}{\sqrt{2}}\left\{\left|\frac{3}{2}, -\frac{3}{2}\right\rangle + i\left|\frac{3}{2}, \frac{3}{2}\right\rangle\right\} \qquad (6)$$

(22) Our coördinate transfigurations are defined as *replacement*, not transference, operations. *E.g.*, the counterclockwise rotation about the z-axis by $\pi/2$ *replaces* x by $-y$, y by x, and z by z. With this definition of coördinate changes, the spin functions transform as given by H. Goldstein, "Classical Mechanics," Addison-Wesley, Cambridge, 1951, page 116. The orbital function alterations are readily determined from their cartesian representations. In reading Hellwege's paper[20a] please note the alternate choice of cartesian coordinate transformations and Eulerian angle designations.

(23) We have oriented the cubic and quadrate functions by their behavior under a $\pi/2$ rotation ($\mathcal{C}_4$) about the fourfold z-axis, and under a reflection (σ) in the x–z-plane. We have elected to classify our symmetry cliques in the ensuing manner

$$\mathcal{C}_4\gamma_{7(b)}^{a} = -e^{\mp\pi i/4}\,\gamma_{7(a)}^{b};\quad \sigma\gamma_{7(a)}^{b} = \pm\gamma_{7(b)}^{a};\quad \gamma_{7(b)}^{Q} = \gamma_{7(a)}^{a}$$
$$\mathcal{C}_4\gamma_{8(b)}^{a} = -e^{\mp\pi i/4}\,\gamma_{8(a)}^{b};\quad \sigma\gamma_{8(b)}^{a} = \pm\gamma_{8(a)}^{b};\quad \gamma_{8(b)}^{Q} = \gamma_{8(a)}^{a}$$
$$\mathcal{C}_4\gamma_{8(d)}^{c} = +e^{\mp\pi i/4}\,\gamma_{8(c)}^{d};\quad \sigma\gamma_{8(d)}^{c} = \pm\gamma_{8(c)}^{d};\quad \gamma_{6(b)}^{Q} = \gamma_{8(d)}^{c}$$

One must carefully note that the inclusion of spin function variations (see footnote 22) implies that the identity transformation is a rotation by 4π. Therefore, the operators $\mathcal{C}_4$ and σ obey the relations $\sigma^2 = \mathcal{C}_4^4 = -1$. As a matter of definition, we have taken our spin functions to be *even* under inversion (i) in the origin. Hence, we have that the reflection $\sigma(x - z)$ is mathematically equivalent to a rotation by $\pi(\mathcal{C}_2)$ about the y-axis.

(24) The explicit form of the γ_{7a} expression may be determined by the application of a counterclockwise $2\pi/3$ rotation ($\mathcal{C}_3$), about the (1, 1, 1) direction, to a linear combination of functions, with arbitrary coefficients, which have the required demeanor under $\mathcal{C}_4$. The restriction that only those functions whose $\mathcal{C}_4$ deportment introduces a multiplicative factor $-e^{\mp\pi i/4}$ may appear amongst the gyrated functions serves to fix the numerical value of these coefficients. The appositive γ_{8a} form is then simply the orthonormal complement of γ_{7a}. As a $^2D_{5/2}$ term gives rise to a single set of γ_7 and γ_8 functions,[17,20,21] this completes the "double group" codification of the atomic $^2D_{5/2}$ state. The second γ_{8a} composite is uniquely begotten by the atomic $^2D_{3/2}$ level, as this level contains no redundant m values. To generate the b and d wave function components from those of a and c, listed in the text, we require the formula

$$\sigma\,|j, m> = (-1)^{j+m-1}\,|j, -m>,\ (j = 0, 1/2, 1, \ldots).$$

(25) By definition, the tetragonal group is that particular subgroup of the cubic group which is generated by the operators $\mathcal{C}_4(z)$, $\sigma(x$-$z)$, and i (inversion). Hence, the above constituted cubic functional vectors (footnotes 23 and 24) are also quadrate basis vectors.

(26) We shall use a capital gamma to designate over-all symmetry specification and a lower case gamma to denote a single electron symmetry state.

(27) The atomic wave functions $|j, m>$ have been azimuthally quantized about the (1, 1, 1) direction (the z'-axis), rather than around the (0, 0, 1) position (the z-axis), as before (ref. 22). Hence, the cubic and trigonal functions tabulated above are implicitly oriented as succeeds ($\sigma' \equiv \sigma(x' - z')$)

$$\mathcal{C}_3\bar{\gamma}_{7(b)}^{a} = e^{\mp\pi i/3}\,\bar{\gamma}_{7(b)}^{a};\quad \sigma'\bar{\gamma}_{7(b)}^{a} = \pm\,\bar{\gamma}_{7(a)}^{b};\quad \gamma_{6(b)}^{T} = \bar{\gamma}_{7(b)}^{a}$$
$$\mathcal{C}_3\bar{\gamma}_{8(b)}^{a} = e^{\mp\pi i/3}\,\bar{\gamma}_{8(b)}^{a};\quad \sigma'\bar{\gamma}_{8(b)}^{a} = \pm\,\bar{\gamma}_{8(a)}^{b};\quad \gamma_{6(a)}^{T} = \bar{\gamma}_{8(b)}^{a}$$
$$\mathcal{C}_3\bar{\gamma}_{8(d)}^{c} = -\,\bar{\gamma}_{8(c)}^{d};\qquad \sigma'\bar{\gamma}_{3(d)}^{c} = \mp\,i\bar{\gamma}_{8(c)}^{d};\quad \gamma_{(b)}^{T} = \bar{\gamma}_{8(a)}^{d}$$

(28) The procedure utilized to derive these functional forms differs from that outlined in ref. 24 merely in the replacement of $\mathcal{C}_4(z)$ by $\mathcal{C}_3(z')$ and $\sigma(x - z)$ by $\sigma(x' - z')$. By ref. 27 the operator σ' induces the same change in our new trigonally oriented functions $|j, m>$ as σ did in the old tetragonally oriented functions $|j, m>$. The (x', y', z') coördinate system is related to the (x, y, z) plan by means of the orthonormal transformation, A, where A is defined by the equation

$$\begin{bmatrix} z \\ y \\ x \end{bmatrix} = \begin{bmatrix} \sqrt{\frac{1}{3}} & 0 & \sqrt{\frac{2}{3}} \\ \sqrt{\frac{1}{3}} & -\sqrt{\frac{1}{2}} & -\sqrt{\frac{1}{6}} \\ \sqrt{\frac{1}{3}} & +\sqrt{\frac{1}{2}} & -\sqrt{\frac{1}{6}} \end{bmatrix}\begin{bmatrix} z' \\ y' \\ x' \end{bmatrix}$$

Alterations in the state vectors under $\mathcal{C}_4$ are most easily computed in the cartesian (x', y', z') representation of the basis functions $|j, m>$. In this picture the effect of $\mathcal{C}_4$ is ascertained from the relations

$$\mathcal{C}'_4\begin{bmatrix} z' \\ y' \\ x' \end{bmatrix} = \tilde{A}\mathcal{C}_4 A\begin{bmatrix} z' \\ y' \\ x' \end{bmatrix};\quad \mathcal{C}_4 = \begin{bmatrix} 1 & 0 & 0 \\ 0 & 0 & 1 \\ 0 & -1 & 0 \end{bmatrix}\ \text{(by ref. 22)}$$

To fix the needful Eulerian angles, we simply identify the matrix $\tilde{A}\mathcal{C}_4 A$ with the Eulerian matrix of Goldstein (page 109).[22] The gyrated spin functions may then be singularized by the substitution of the angular values into the spinor array of Goldstein (page 116)[22]

$$\mathcal{C}_4'\begin{bmatrix} \left|\frac{1}{2}, \frac{1}{2}\right\rangle \\ \left|\frac{1}{2}, -\frac{1}{2}\right\rangle \end{bmatrix} = \begin{bmatrix} \sqrt{\frac{2}{3}}\,e^{\pi i/6} & i\sqrt{\frac{1}{3}} \\ i\sqrt{\frac{1}{3}} & \sqrt{\frac{2}{3}}\,e^{-\pi i/6} \end{bmatrix}\begin{bmatrix} \left|\frac{1}{2}, \frac{1}{2}\right\rangle \\ \left|\frac{1}{2}, -\frac{1}{2}\right\rangle \end{bmatrix}$$

(29) The comments in ref. 25 apply equally well here once the word trigonal is substituted for tetragonal and quadrate, and the operators $\mathcal{C}_4(z)$ and $\sigma(x - z)$ are supplanted by $\mathcal{C}_3(z')$ and $\sigma(x' - z')$. Mark well the appearance of the phase factors exp $[\pm 3i/4(\pi + \beta)]$. These have been inserted into the $\bar{\Gamma}_{8c,\,d}$ basis vector definitions to retain the identity of the *cubic* Hamiltonian matrix in both its quadrate and trigonal manifestations. The angle β which equates the off-diagonal matrix element of $\mathcal{H}(\Gamma_8)$ in these two equivalent cubic representations is, as may be surmised, the tetrahedral angle ($\cos\beta = -1/3$, $\sin\beta = 2/3\sqrt{2}$).

Weak Field Portrait—Energy Values.—The fabrication of the cubic, quadrate and trigonal secular determinants proceeds along familiar paths. A few words might be said, however, as to the structure of the ligand potential matrix elements in the quadrate and trigonal limits. In complete generality, we may take the quadrate (V_Q) and

trigonal (V_T) potentials to be the resultant of a cubic (V_C) and an axial field[30,31]

$$V_{Q,T} = V_C + V_\infty^T$$

$$V_C = \sum_i D\left(x^4 + y_i^4 + z_i^4 - \frac{3}{5}r_i^4\right)$$

$$V_\infty = \sum_i \{B_2(3\bar{z}_i^2 - r_i^2) + B_4(35\bar{z}_i^4 - 30r_i^2\bar{z}_i^2 + 3r_i^4)\} \tag{7}$$

where the collective symbol $\bar{z}$ denotes z(for V_∞^Q) and z'(for V_∞^T), respectively. The cubic portion of these expressions is known to require two quantities for its total specification: the field strength D and the average quartic radial displacement,[32] $\langle r_i^4 \rangle$.[33] To date no universaly accepted notation has been adopted for the axial fragment of the ligand potential. We shall espouse the Moffitt and Ballhausen[3a,34] labels for tetragonal addend arrangements and extend their notions to also embrace trigonal ligand dispositions. Hence,

(b) Trigonal Orientation

$$\langle 2, \pm 2|\, V\, |\pm 2, 2\rangle = -\frac{2}{3}Dq + 2D\sigma - D\tau$$

$$\langle 2, \pm 1|\, V\, |\pm 1, 2\rangle = \frac{8}{3}Dq - D\sigma + 4D\tau$$

$$\langle 2, 0|\, V\, |0, 2\rangle = -4Dq - 2D\sigma - 6D\tau$$

$$\langle 2, \pm 2|\, V\, |\mp 1, 2\rangle = \langle 2, \mp 1|\, V\, |\pm 2, 2\rangle = \pm\frac{10}{3}\sqrt{2}\,Dq \tag{9}$$

With these preliminaries dispatched, the appropriate weak field secular determinants may be readily set into print[36]:

(a) Cubic Fields

$$\begin{vmatrix} {}^2D_{5/2} \\ \lambda - 4Dq - E \\ (\Gamma_7) \end{vmatrix} = 0; \quad \begin{vmatrix} {}^2D_{5/2} & {}^2D_{3/2} \\ \lambda + 2Dq - E & -2\sqrt{6}Dq \\ (\Gamma_8) & -\frac{3}{2}\lambda - E \end{vmatrix} = 0 \tag{10}$$

(b) Quadrate Fields

$$\begin{vmatrix} \Gamma_8({}^2D_{5/2}) & \Gamma_8({}^2D_{3/2}) \\ \lambda + 2Dq - \frac{8}{5}Ds - 2Dt - E & -2\sqrt{6}\,Dq + \frac{\sqrt{6}}{5}[Ds + 10Dt] \\ (\Gamma_8^Q) & -\frac{3}{2}\lambda - \frac{7}{5}Ds - E \end{vmatrix} = 0$$

$$\begin{vmatrix} \Gamma_7({}^2D_{5/2}) & \Gamma_8({}^2D_{5/2}) & \Gamma_8({}^2D_{3/2}) \\ \lambda - 4Dq + \frac{7}{3}Dt - E & \frac{2\sqrt{5}}{15}[3Ds - 5Dt] & \frac{2}{5}\sqrt{\frac{5}{6}}[3Ds - 5Dt] \\ & \lambda + 2Dq + \frac{1}{15}[24Ds - 5Dt] - E & -2\sqrt{6}\,Dq - \frac{\sqrt{6}}{15}[3Ds - 5Dt] \\ (\Gamma_7^Q) & & -\frac{3}{2}\lambda + \frac{7}{5}Ds - E \end{vmatrix} = 0 \tag{11}$$

(c) Trigonal Fields[29,37]

$$\begin{vmatrix} \Gamma_8({}^2D_{5/2}) & \Gamma_8({}^2D_{3/2}) \\ \lambda + 2Dq - \frac{2}{5}D\sigma + 3D\tau - E & -2\sqrt{6}\,Dq + \frac{2}{5}e^{3i/2[\pi+\beta]}[3D\sigma - 5D\tau] \\ (\Gamma_4^T, \Gamma_5^T) & -\frac{3}{2}\lambda + \frac{7}{5}D\sigma - E \end{vmatrix} = 0$$

$$\begin{vmatrix} \Gamma_7({}^2D_{5/2}) & \Gamma_8({}^2D_{5/2}) & \Gamma_8({}^2D_{3/2}) \\ \lambda - 4Dq - \frac{14}{9}D\tau & -2\sqrt{5}\left[\frac{2}{5}D\sigma + \frac{1}{9}D\tau\right] & -\sqrt{30}\left[\frac{1}{15}D\sigma + \frac{2}{3}D\tau\right] \\ & \lambda + 2Dq + \frac{2}{5}D\sigma - \frac{13}{9}D\tau - E & -2\sqrt{6}\,Dq - 2\sqrt{6}\left[\frac{1}{15}D\sigma + \frac{2}{3}D\tau\right] \\ (\Gamma_6^T) & & -\frac{3}{2}\lambda - \frac{7}{5}D\sigma - E \end{vmatrix} = 0 \tag{12}$$

we coalesce the parametric products $-2/7\ B_2\langle r_i^2\rangle$ and $-8/21\ B_4\langle r_i^4\rangle$ into the *single indivisible* quadrate emblems Ds and Dt, respectively, and designate the analogous indissoluble trigonal aggregates by $D\sigma$ and $D\tau$.[35] The non-vanishing matrix elements essential for the delineation of the augend potential energy may thus be written

(a) Quadrate Orientation

$$\langle 2, \pm 2|\, V\, |\pm 2, 2\rangle = Dq + 2Ds - Dt$$
$$\langle 2, \pm 1|\, V\, |\pm 1, 2\rangle = -4Dq - Ds + 4Dt$$
$$\langle 2, 0|\, V\, |0, 2\rangle = 6Dq - 2Ds - 6Dt$$
$$\langle 2, \pm 2|\, V\, |\mp 2, 2\rangle = 5Dq \tag{8}$$

(30) In quadrate (θ, ω) or trigonal (θ', φ') spherical coördinates, the cubic potential has the alternant forms (Condon and Shortley phases)[13c]

$$V_C = \frac{4\sqrt{\pi}}{15}D\sum_i \left\{ Y_4^0(\theta_i, \varphi_i) + \sqrt{\frac{5}{14}}[Y_4^4(\theta_i, \varphi_i) + Y_4^{-4}(\theta_i, \varphi_i)] \right\} r_i^4$$

$$V_C = -\frac{8\sqrt{\pi}}{45}D\sum_i \left\{ Y_4^0(\theta_i', \varphi_i') + \sqrt{\frac{10}{7}}[Y_4^3(\theta_i', \varphi_i') - Y_4^{-3}(\theta_i', \varphi_i')] \right\} r$$

(31) The axial field may also be written in terms of normalized tesseral harmonics [($\bar{\theta}$, $\bar{\varphi}$) = (θ, φ) or (θ', φ')]

$$V_\infty = \sum_i \left\{ \frac{4}{5}\sqrt{5\pi}B_2 r_i^2 Y_2^0(\bar{\theta}_i, \bar{\varphi}_i) + \frac{16}{3}\sqrt{\pi}B_4 r_i^4 Y_4^0(\bar{\theta}_i, \bar{\varphi}_i) \right\}$$

(32) More usually the parameter q equal to $2/105\langle r_i^4\rangle$ is employed.

(33) If a radial potential of greater flexibility is utilized, say by equating $R_4(r_i)$ to $4/15\sqrt{\pi}Dr_i^4$, in equation 7 and in ref. 30, the historical product of the two *separate* parameters D and q is yet retained in the portraiture of the cubic field, but henceforth labors as a *single* parameter Dq whose value assesses the numerical magnitude of the matrix element, $\langle 2, \pm 2|V_C|2, \pm 2\rangle$, *i.e.*, of the radial average $\langle R_4(r_i)\rangle/14\sqrt{\pi}$.

(34) C. J. Ballhausen and W. E. Moffitt, *J. Inorg. & Nuclear Chem.*, **3**, 178 (1956).

(35) In terms of the more pliant centric forms $R_2(r_i)$ and $R_4'(r_i)$, where $R_2(r_i)$ and $R_4'(r_i)$ are proxies for $4/5\sqrt{5\pi}B_2r_i^2$ and $16/3\sqrt{\pi}B_4r_i^4$ in equation 7 and ref. 31, the parameters $D\omega$, (ω = s, t, σ, τ), assume the guise

Strong Field Picture—Wave Functions.—Whenever the spin-orbit energy is subservient to the crystalline energy $V_{C.F.}$, the Hamiltonian matrix may be diagonalized, by suitable linear combinations of the free ion orbital functions, $|l,m_l>$.[38] As demonstrated by Bethe,[17] such linear combinations of atomic functions no longer are degenerate in energy if the Hamiltonian $\mathcal{H}$, describes a cubic conformation, but are segregated by the supplementary quantum ciphers t_{2g} and e_g.[39] The sums of state vectors, $|l,m_l>$, which adorn themselves with the cubic appellations t_{2g} and e_g, may be discerned by their transformative demeanor. We shall here catalogue these series for future reference

(a) Cubic Functions with Tetragonal Orientation[40]

$$^2T_{2g}:\ t_{2ga}\zeta(m_s) = d_{xy}\zeta(m_s) = \frac{1}{i\sqrt{2}}\{|2,+2> - |2,-2>\}\left|\frac{1}{2}, m_s\right>$$

$$t_{2g\binom{b}{c}}\zeta(m_s) = d\pi_{\pm}\zeta(m_s) = \mp|2,\pm1>\left|\frac{1}{2}, m_s\right>$$

$$^2E_g:\quad e_{ga}\zeta(m_s) = d_{z^2}\zeta(m_s) = |2,0>\left|\frac{1}{2}, m_s\right>$$

$$e_{gb}\zeta(m_s) = d_{x^2-y^2}\zeta(m_s) = \frac{1}{\sqrt{2}}\{|2,+2> + |2,-2>\}\left|\frac{1}{2}, m_s\right> \quad (13)$$

(b) Cubic Functions with Trigonal Orientation[41]

$$^2T_{2g}:\ t_{2ga}\zeta'(m_s) = d_{z'^2}\zeta'(m_s) = |2,0>\left|\frac{1}{2}, m'_s\right>$$

$$t_{2g\binom{b}{c}}\zeta'(m_s) = \left\{\sqrt{\tfrac{1}{3}}\,d\pi'_{\pm} - \sqrt{\tfrac{2}{3}}\,d\delta'_{\mp}\right\}\zeta'(m_s),\qquad d\delta'_{\pm} \equiv |2,\pm2>$$

$$^2E_g:\ e_{g\binom{a}{b}}\zeta'(m_s) = \left\{\sqrt{\tfrac{2}{3}}\,d\pi'_{\pm} + \sqrt{\tfrac{1}{3}}\,d\delta'_{\mp}\right\}\zeta'(m_s) \quad (14)$$

The relevant wave functions which convert decently under coördinate permutations are uncovered by means parallel to those already discussed.[22–29] We shall hence be content to summarily record our results

(a) Cubic (Γ_7, Γ_8) and Quadrate (Γ_6^Q, Γ_7^Q) Functions[25,26,40,42]

$$\Gamma_{7a}(^2T_{2g}) = \Gamma_{7a}^{Q(1)}(^2T_{2g}) = \frac{-i}{\sqrt{3}}\left\{d_{xy}\zeta\left(-\tfrac{1}{2}\right) + i\sqrt{2}\,d\pi_+\zeta\left(\tfrac{1}{2}\right)\right\}$$

$$\Gamma_{8a}(^2T_{2g}) = \Gamma_{7a}^{Q(2)}(^2T'_{2g}) = \frac{-i}{\sqrt{3}}\left\{\sqrt{2}\,d_{xy}\zeta\left(-\tfrac{1}{2}\right) - id\pi_+\zeta\left(\tfrac{1}{2}\right)\right\}$$

$$\Gamma_{8c}(^2T_{2g}) = \Gamma_{6a}^{Q}(^2T_{2g}) = d\pi_-\zeta\left(\tfrac{1}{2}\right)$$

$$\Gamma_{8a}(^2E_g) = \Gamma_{7a}^{Q}(^2E_g) = d_{x^2-y^2}\zeta\left(-\tfrac{1}{2}\right)$$

$$\Gamma_{8c}(^2E_g) = \Gamma_{6a}^{Q}(^2E_g) = d_{z^2}\zeta\left(-\tfrac{1}{2}\right) \quad (15)$$

(b) Cubic ($\bar\Gamma_7$, $\bar\Gamma_8$) and Trigonal (Γ_4^T, Γ_5^T, Γ_6^T) Functions[26,29,41,43]

$$\bar\Gamma_{7a}(^2T_{2g}) = \Gamma_{6a}^{T(1)}(^2T_{2g}) = -\sqrt{\tfrac{1}{3}}\,d_{z'^2}\zeta'\left(-\tfrac{1}{2}\right) - \sqrt{\tfrac{2}{3}}\left\{\sqrt{\tfrac{1}{3}}\,d\pi'_- - \sqrt{\tfrac{2}{3}}\,d\delta'_+\right\}\zeta'\left(\tfrac{1}{2}\right)$$

$$\bar\Gamma_{8a}(^2T_{2g}) = \Gamma_{6a}^{T(2)}(^2T_{2g}) = \sqrt{\tfrac{2}{3}}\,d_{z'^2}\zeta'\left(-\tfrac{1}{2}\right) - \sqrt{\tfrac{1}{3}}\left\{\sqrt{\tfrac{1}{3}}\,d\pi'_- - \sqrt{\tfrac{2}{3}}\,d\delta'_+\right\}\zeta'\left(\tfrac{1}{2}\right)$$

$$\bar\Gamma_{8c}(^2T_{2g}) = \Gamma_5^T(^2T_{2g}) = \frac{e^{-i\beta/4}}{\sqrt{2}}\left\{\left[\sqrt{\tfrac{1}{3}}\,d\pi'_+ - \sqrt{\tfrac{2}{3}}\,d\delta'_-\right]\zeta'\left(\tfrac{1}{2}\right) + i\left[\sqrt{\tfrac{1}{3}}\,d\pi'_- - \sqrt{\tfrac{2}{3}}\,d\delta'_+\right]\zeta'\left(-\tfrac{1}{2}\right)\right\}$$

$$\bar\Gamma_{8d}(^2T_{2g}) = \Gamma_4^T(^2T_{2g}) = \frac{e^{+i\beta/4}}{\sqrt{2}}\left\{\left[\sqrt{\tfrac{1}{3}}\,d\pi'_+ - \sqrt{\tfrac{2}{3}}\,d\delta'_-\right]\zeta'\left(\tfrac{1}{2}\right) - i\left[\sqrt{\tfrac{1}{3}}\,d\pi'_- - \sqrt{\tfrac{2}{3}}\,d\delta'_+\right]\zeta'\left(-\tfrac{1}{2}\right)\right\}$$

$$\bar\Gamma_{8a}(^2E_g) = \Gamma_{6a}^T(^2E_g) = \left\{\sqrt{\tfrac{2}{3}}\,d\pi'_- + \sqrt{\tfrac{1}{3}}\,d\delta'_+\right\}\zeta'\left(\tfrac{1}{2}\right)$$

$$\bar\Gamma_{8c}(^2E_g) = \Gamma_5^T(^2E_g) = \frac{e^{+i\beta/4}}{\sqrt{2}}\left\{\left[\sqrt{\tfrac{2}{3}}\,d\pi'_+ + \sqrt{\tfrac{1}{3}}\,d\delta'_-\right]\zeta'\left(\tfrac{1}{2}\right) + i\left[\sqrt{\tfrac{2}{3}}\,d\pi'_- + \sqrt{\tfrac{1}{3}}\,d\delta'_+\right]\zeta'\left(-\tfrac{1}{2}\right)\right\}$$

$$\bar\Gamma_{8d}(^2E_g) = \Gamma_4^T(^2E_g) = \frac{e^{-i\beta/4}}{\sqrt{2}}\left\{\left[\sqrt{\tfrac{2}{3}}\,d\pi'_+ + \sqrt{\tfrac{1}{3}}\,d\delta'_-\right]\zeta'\left(\tfrac{1}{2}\right) - i\left[\sqrt{\tfrac{2}{3}}\,d\pi'_- + \sqrt{\tfrac{1}{3}}\,d\delta'_+\right]\zeta'\left(-\tfrac{1}{2}\right)\right\} \quad (16)$$

$$D\mu = -<2,\pm1|\,V_{\sigma\sigma}^{(2)}\,|\pm1,2> = -\frac{1}{14}\sqrt{\frac{5}{\pi}}<R_2(r_i)>,\ (\mu = s,\sigma)$$

$$D\nu = -<2,\pm2|\,V_{\sigma\sigma}^{(4)}\,|\pm2,2> = -\frac{1}{14\sqrt{\pi}}<R'_4(r_i)>,\ (\nu = t,\tau)$$

(36) The spin-orbit energy of the weak field picture is trivial to evaluate. Simple vector model arguments relate $\vec{l}\cdot\vec{s}$ to the number $1/2[j(j+1) - 27/4]$. The radial mean, $<\xi(r_i)>$, of the spin-orbit potential $\xi(r_i)$ has been typified as λ (it is called ζ_d in ref. 10 and 11).

(37) In the absence of magnetic flux, the operator, $\mathcal{K}$, which reverses the direction of all angular momenta vectors,[20b,c] commutes with the Hamiltonian, $\mathcal{H}$. Hence, wave functions which permute under the application of $\mathcal{K}$ are representable by identical matrices. As $\mathcal{K}\Gamma_{8\binom{c}{d}}$ equals $i\Gamma_{8\binom{d}{c}}$, equation 6 predicts the coincidence of the Γ_4 and Γ_5 secular determinants.

(38) The Hamiltonian, in this case, may be regarded as spin independent.

(39) To avoid the creation of added turmoil, we shall employ Mulliken's (*Phys. Rev.*, **43**, 279 (1932)) notation for ordinary quantum states and reserve the Bethe symbolism for double group quantum configurations. Bethe calls the t_{2g} and e_g coteries γ_5 and γ_3, each.

(40) The tetragonal, or fourfold, axis is taken to be the z-axis, as before (ref. 22–25). Spin functions have been displayed both as $\zeta(m_s)$ and $|1/2, m_s>$, as aesthetic principles demanded.

(41) The prime mark indicates quantization of angular momenta along the (1, 1, 1) direction, *i.e.*, along the z'-axis (ref. 27–29).

(42) The phase factor i ensures the reality of the quadrate secular determinants.

(43) Pursuant to our previous convention,[22] the counterclockwise rotation by $2\pi/3(C_3)$ about the (1, 1, 1) direction (the z'-axis) *replaces* x' by $x'\cos 2\pi/3 - y'\sin 2\pi/3$, y' by $x'\sin 2\pi/3 + y'\cos 2\pi/3$ and z' by z. The occurrence of the phase angle β is as rationalized in ref. 29.

Strong Field Picture—Energy Values.—In accordance with our prior specialization of the ligand field, the parameters Dq and λ suffice to detail cubic domains while two added measures $D\mu$, ($\mu = s, \sigma$), and $D\nu$, ($\nu = t, \tau$), are demanded for realms of tetragonal or trigonal disposition. Equations 8 and 9, when subjoined to 13–16, allow the necessary crystalline matrix elements to be expressed in terms of these quantities, and, hence, permit the analysis of the eigenvalue problem.

In the subsequent lines are collected those strong field determinental forms from which the needed energy distribution is issuant[44]

(a) Cubic Fields

$$\begin{vmatrix} {}^2T_{2g} \\ \lambda - 4Dq - E \\ (\Gamma_7) \end{vmatrix} = 0, \quad \begin{vmatrix} {}^2T_{2g} & {}^2E_g \\ -\frac{\lambda}{2} - 4Dq - E & \sqrt{\frac{3}{2}}\lambda \\ (\Gamma_8) & 6Dq - E \end{vmatrix} = 0 \tag{17}$$

(b) Quadrate Fields

$$\begin{vmatrix} \Gamma_8({}^2T_{2g}) & \Gamma_8({}^2E_g) \\ -\frac{\lambda}{2} - 4Dq - Ds + 4Dt - E & \sqrt{\frac{3}{2}}\lambda \\ (\Gamma_6^Q) & 6Dq - 2Ds - 6Dt - E \end{vmatrix} = 0$$

$$\begin{vmatrix} \Gamma_7({}^2T_{2g}) & \Gamma_8({}^2T_{2g}) & \Gamma_8({}^2E_g) \\ \lambda - 4Dq + \frac{7}{3}Dt - E & \frac{\sqrt{2}}{3}(3Ds - 5Dt) & 0 \\ & -\frac{\lambda}{2} - 4Ds + D_s + \frac{2}{3}Dt - E & \sqrt{\frac{3}{2}}\lambda \\ (\Gamma_7^Q) & & 6Dq + 2Ds - Dt - E \end{vmatrix} = 0 \tag{18}$$

(c) Trigonal Fields[37,43]

$$\begin{vmatrix} \Gamma_8({}^2T_{2g}) & \Gamma_8({}^2E_g) \\ -\frac{\lambda}{2} - 4Dq + D\sigma + \frac{2}{3}D\tau - E & \sqrt{\frac{3}{2}}\lambda - \frac{\sqrt{2}}{3}e^{i\beta/2}[3D\sigma - 5D\tau] \\ (\Gamma_4^T, \Gamma_5^T) & 6Dq + \frac{7}{3}D\tau - E \end{vmatrix} = 0$$

$$\begin{vmatrix} \Gamma_7({}^2T_{2g}) & \Gamma_8({}^2T_{2g}) & \Gamma_8({}^2E_g) \\ \lambda - 4Dq - \frac{14}{9}D\tau - E & \frac{\sqrt{2}}{9}[9D\sigma + 20D\tau] & \frac{2}{3}\sqrt{\frac{1}{3}}[3D\sigma - 5D\tau] \\ & -\frac{\lambda}{2} - 4Dq - \frac{1}{9}[9D\sigma + 34D\tau] - E & \sqrt{\frac{3}{2}}\lambda + \frac{1}{3}\sqrt{\frac{2}{3}}[3D\sigma - 5D\tau] \\ (\Gamma_6^T) & & 6Dq + \frac{7}{3}D\tau - E \end{vmatrix} = 0 \tag{19}$$

Weak Field—Strong Field Conjunctive Relations.—As precisely the self-same ten orthonormal basis functions have been utilized in the formulation of the weak and strong field "exact" energy expressions,[12] these expressions can differ only superficially. The confluence of the two descriptive processes is promptly established when the separate basis vectors are expanded, the one in terms of the other. The conjugative algebra is thus found to be as displayed

(a) Quadrate Orientation[23,25,26]

$$\Gamma_7: \ {}^2D_{5/2}\left|\left|{}^2T_{2g}\right|_{+1}\right|; \quad \Gamma_8: \begin{matrix} {}^2D_{5/2} \\ {}^2D_{3/2} \end{matrix}\begin{vmatrix} {}^2T_{2g} & {}^2E_g \\ \sqrt{\frac{2}{5}} & \sqrt{\frac{3}{5}} \\ \sqrt{\frac{3}{5}} & -\sqrt{\frac{2}{5}} \end{vmatrix} \tag{20}$$

(b) Trigonal Orientation[26,27,29]

$$\bar{\Gamma}_7: \ {}^2D_{5/2}\left|\left|{}^2T_{2g}\right|_{+1}\right|;$$

$$\bar{\Gamma}_8: \begin{matrix} {}^2D_{5/2} \\ {}^2D_{3/2} \end{matrix}\begin{vmatrix} {}^2T_{2g} & {}^2E_g \\ -\sqrt{\frac{2}{5}} & -\sqrt{\frac{3}{5}} \\ -\sqrt{\frac{3}{5}} & +\sqrt{\frac{2}{5}} \end{vmatrix} \times e^{i\epsilon}, \quad \begin{bmatrix} \bar{\Gamma}_{8(\frac{a}{b})}: & \epsilon = 0 \\ \bar{\Gamma}_{8(\frac{c}{d})}: & \epsilon = \mp\frac{3\pi}{4} \end{bmatrix} \tag{21}$$

If the transformation matrices exhibited overhead are depicted as $T(\Gamma_j)$, the relationship which conjoins the weak and strong field Hamiltonian arrays, $\mathcal{H}_W$ and $\mathcal{H}_S$, is well illustrated by the exemplary formula

$$\mathcal{H}_S = \tilde{T}(\Gamma_j)\mathcal{H}_W T(\Gamma_j)^* \tag{22}$$

Applications

Optical Spectra.—The sparsity of spectral data for the second and third transition group, d^n, ($n = 1, 9$), complexes precludes the numerical usage of the derived secular equations.[45,46] How-

(44) The spin-orbit members of these matrix arrays can be compiled, without stress or strain, by use of Condon and Shortley's[13c] equation 7[33]. Please keep in mind, though, that Condon and Shortley introduce the factor *minus one* into all orbital functions, $|l, m_l>$, whenever m_l is both *odd* and *positive*.

(45) The detailed experimental characterization of the newly made neutral (octahedral) hexafluorides of rhenium, osmium, iridium and platinum has stimulated theoretical investigations somewhat similar to our own. The numerical accord of theory and experiment for these compounds is excellent.[10,11]

(46) These equations are, of course, equally applicable to first transition group, d^n, ($n = 1, 9$), molecular clusters. Indeed, many authors have developed theoretical expressions, of some resemblance to several given here, for usage in the delineation of such complexes: (a) O. M. Jordahl, *Phys. Rev.*, **45**, 87 (1934); (b) A. Siegert, *Physica*, **3**, 85 (1936); (c) J. H. Van Vleck, *J. Chem. Phys.*, **7**, 61 (1939); (d) D. Polder, *Physica*, **9**, 709 (1942); (e) A. Abragam and M. H. L. Pryce, *Proc. Roy. Soc. (London)*, **206A**, 164 (1951); (f) F. E. Ilse and H. Hartmann, *Z. physik. Chem.*, **197**, 239 (1951); (g) C. J. Ballhausen, *Dan. Mat. Fys. Med.*, **29**, No. 4 (1954); (h) L. E. Orgel, *J. Chem. Phys.*, **23**, 1004 (1955); (i) G. Felsenfeld, *Proc. Roy. Soc. (London)*, **236A**, 506 (1956); (j) R. L. Belford, M. Calvin and G. Belford, *J. Chem. Phys.*, **26**, 1165 (1957). Watchful inspection of these alternant formulations will, however, reveal significant differences.

ever, it is to be anticipated that such will not always be so, and, hence, several phrases in the way of an experimental prospectus should not be inappropriate. The avenues of greatest promise lie in divers directions: (a) optical studies of the recently prepared hexafluorides of Mo(V) and W (V); [14] (b) spectroscopic particularization of the oxy salts of Mo(V) and W(V)[47]; (c) spectral characterization of solid solutions of Ag(II), Au(II), Zr(III), Hf(III), Nb(IV), and Ta(IV)[48,49]; (d) careful low temperature observation of light absorption in tetra- and hexa-coördinated Cu(II) systems.[50]

For future reference, the solutions of the cubic secular equations will be presented. If one defines the angle η such that $-\sqrt{6}\,\lambda\cot\eta$ is equal to $^1/_2\lambda + 10Dq$,[51] the eigenvalues and functions can be written in the succinct form (lower root: $\pi > \eta > 0$; upper root: $2\pi > \eta > \pi$)

$$E(\Gamma_7) = \lambda - 4Dq$$

$$E(\Gamma_8) = -\frac{1}{2}\lambda - 4Dq - \frac{\sqrt{6}}{2}\lambda\cot\frac{\eta}{2} \qquad (23)$$

$$\psi(\Gamma_7) = \Gamma_7(^2T_{2g})$$

$$\psi(\Gamma_8) = \sin\frac{\eta}{2}\,\Gamma_8(^2T_{2g}) - \cos\frac{\eta}{2}\,\Gamma_8(^2E_g) \qquad (24)$$

The choice of equi-valued amplitudes for λ and Dq requires η to be 166°52′6.8″ (lower root) or 346°52′6.8″ (upper root). The exemplary selection[52] of 3000 cm.$^{-1}$ for Dq predicts absorption bands at 4923 cm.$^{-1}$ and 32346 cm.$^{-1}$. Without advance knowledge of the pertinent tetragonal or trigonal field strengths, little can be said concerning spectral features expected of quadrate and trigonal environs.

At this juncture it seems apropos to mention an approximational scheme which is applicable to the many electron problem. It is simply this. One assigns each electron to either one of the four γ_8, two γ_7, or four γ_8^* orbitals. The state of lowest energy is obtained by a sequential assignment. For example, the ground state of the mono-negative rhenium hexafluoride ion would be described as γ_8^2, which procreates the terms Γ_j, (j = 1, 3, 5). The first excited state would then correspond to $\gamma_8^1\gamma_7^1$, which begets the levels Γ_j, (j = 3, 4, 5); the second to γ_7^2, which produces the state Γ_1; the third to $\gamma_8^1\gamma_8^{*1}$, which sires the components Γ_j, (j = 1, 2, 3 (once); and 4, 5(twice)), etc.[53] A synthesis, in this manner, of the multielectron terms from the single particle spin-orbit functions, with the concomitant neglect of electron coulombic repulsions, is the direct analog of the composition of term values, from the j-j coupling view, in atomic spectroscopy.[54,55] As in the appositive atomic situation, a first approximation to the true energetics is then determined by the perturbative addition of the electron–electron electrostatic repulsions. A calculation along these lines has recently been utilized in the elucidation of the neutral hexafluorides of the platinum group.[10,11]

Magnetic Properties.—Remarks as to the handiness of germane magnetic facts strongly parallel those made in antecedent paragraphs concerned with spectroscopic conduct. Generally speaking, magnetic demeanor is more greatly influenced by environmental vagaries than optical deportment, as the former is dependent upon the detailed visitatorial schedule of the transient electrons. Several sentences might, however, be profitably devoted to contemplation of the magnetism of the newly recorded mono-negative hexafluorides of tungsten and molybdenum.[14]

It is apparent from equation 24 that values of Dq and λ in the proximity of 3000 cm.$^{-1}$ more than suffice to ensure the validity of Van Vleck's "high frequency" magnetic susceptibility separation.[56] Consequently, the paramagnetic susceptibility[57] may be written as

$$\chi_p = \frac{N}{3kT}\left\{\frac{3}{4}\sum_{s=a}^{d}|\langle s|\mu_z|s\rangle|^2 + 3kT\alpha\right\} \qquad (25)$$

where $|s\rangle$ symbolizes the Γ_{8s} wave function, μ_z the z-component of the magnetic dipole moment operator, $L_z + 2S_z$, and α the temperature independent paramagnetism. If μ^2 denotes the square of the magnetic dipole moment, the *effective* magnetic dipole moment is defined by[58]

$$\mu_{eff} = \sqrt{\frac{3kT\chi_p}{N}} = \sqrt{\mu^2 + 3kT\alpha} \qquad (26)$$

$$\mu^2 = \frac{3}{4}\sum_{s=a}^{d}|\langle s|\mu_z|s\rangle|^2 \qquad (27)$$

(47) C. K. Jørgensen, *Acta Chem. Scand.*, **11**, 73 (1957).

(48) F. J. Morin (private communication) will attempt to prepare and individualize solid solutions of this type.

(49) With respect to Au(II), the use of these secular equations might resolve questions as to its existence in mixtures of Au(I) and Au(III) in solution (R. L. Rich and H. Taube, THIS JOURNAL, **58**, 6 (1954)), as Au(I) should show no d^n transitions and Au(III) should exhibit spectral features in accord with the d^8 secular equations of ref. 5.

(50) Fused salt spectral observations should also furnish helpful data.

(51) This means of simplification of the resultant eigenvalue and eigenfunction expressions is due to Moffitt, Goodman, Fred and Weinstock.[10]

(52) The Dq option of 3000 cm.$^{-1}$ is peculiar to neutral rhenium hexafluoride.[10,11]

(53) The "exact" term values for this ion may be procured by the substitution of the appropriate numerical magnitudes for the sundry parameters which appear in the energy determinants of ref. 5.

(54) Ref. 13c, Chapter X.

(55) In this framework, we should assign the weak absorption at ~32,000 cm.$^{-1}$, which is characteristic of the dinegative platinum group hexafluorides [M. A. Hepworth, P. L. Robinson and G. J. Westland, *J. Chem. Soc.*, 611 (1958); A. G. Turner, Jr., and A. F. Clifford, *Nature*, **182**, 1369 (1958)] as $\gamma_8(\text{or }\gamma_7) \rightarrow \gamma_8^*$. The high intensity band at ~50,000 cm.$^{-1}$ is most probably due to charge transfer. Readers interested in the basal properties of further palladium and platinum group complexes are urged to peruse the following papers: M. A. Hepworth, P. L. Robinson and G. J. Westland, *J. Chem. Soc.*, 4269 (1954); R. D. Peacock, *ibid.*, 1291 (1956); 467 (1957); C. K. Jørgensen, *Acta Chem. Scand.*, **9**, 710 (1955); **11**, 151 (1957); 166 (1957); H. Hartmann and C. Buschbeck, *Z. physik. Chem.* (*Frankfurt*) [*N.F.*], **11**, 120 (1957); H. Hartmann and H. J. Schmidt, *ibid.*, 234 (1957). The review article by C. K. Jørgensen (Reports to the X'th Solvay Council, Bruxelles, May, 1956) contains an exhaustive tabulation of pat spectral data.

(56) J. H. Van Vleck, "The Theory of Electric and Magnetic Susceptibilities," Oxford Univ. Press, London and New York, N. Y., 1932, Chapter VII.

(57) The susceptibilities of certain diamagnetic palladium group metals have been surveyed by J. D. Dunitz and L. E. Orgel, *J. Chem. Soc.*, 2594 (1953); J. S. Griffith and L. E. Orgel, *Trans. Faraday Soc.*, **53**, 601 (1957); C. J. Ballhausen and R. W. Asmussen, *Acta Chem. Scand.*, **11**, 479 (1957).

(58) In equation 28 terms between the two different Γ_8 states have been dropped.

$$\alpha \approx \frac{2}{4} \sum_s \frac{|\langle \Gamma_{8s}|\mu_z|\Gamma_{7s}\rangle|^2}{h\nu_1} \qquad (28)$$

And direct computation with equations 24 and 27 reveals that[59,60]

$$\mu^2 + \frac{1}{4}(1 + \cos\eta)(19 - 13\cos\eta - 4\sqrt{6}\sin\eta) \qquad (29)$$

The omission of contributions from the $\Gamma_8(^2E_g)$ fraction of the ground charge density distribution yields an $\alpha \sim 2\beta^2/h\nu_1$.[61] With the previously enumerated values of η and $h\nu_1$, we find that μ_{eff} equals $\sim(0.20 + 0.08 \times 10^{-2}T)^{1/2}$.

If sufficiently potent tetragonal fields are extant, the orbital momentum will be partially quenched and the spin moment will be proportionately released from its stagnant orbital union. This situation finds mathematical confirmation from equation 18's disclosure that a mixture of the $\gamma_7^{Q(1)}(^2T_{2g})$ and $\gamma_7^{Q(2)}(^2T_{2g})$ habitats will subsume a position of minimum energy. The resultant magnetic moment μ of such an abode, $\sin\xi\gamma_7^{Q(1)} + \cos\xi\gamma_7^{Q(2)}$, is expressible as $\sqrt{3}\,|\mu_z|$ or, equivalently, $\sqrt{3}\,|\sin^2\xi - \sqrt{2}\sin 2\xi|$. The specific magnitude of ξ is determinable only if the structure of the quadrate potential is known. A simple estimate of 15° predicts a magnetic moment of 1.11; the larger value of 1.58 is obtained if ξ reaches 45°.

Without resolved spectral lineaments, it is premature to individualize theoretically the mononegative hexafluoride ions of molybdenum and tungsten. Several anticipatory remarks might perhaps be helpful to future workers, although the antiferromagnetic proclivity of the crystalline materials gives a tenuous air to all pronouncements.

The Curie–Weiss behavior and the large attendant permanent moment of the molybdenum salts most probably implies a tetragonal (or trigonal) stabilization of an orbital quenched state, as a sizeable Curie constant is incompatible with a truly cubic site. Contrariwise, the small effective moment and complex susceptibility deportment of the tungsten salts indicates but minor deviations from (octahedral) regularity. The magnetism should therefore be explicable on the basis of equation 20, plus a suitable thermal element, either linear (equations 26 and 28) or transcendental (Kotani[61]).[62,63]

Conclusion

To close this study of conflictive electronic propensities, a few comments anticipative of future trends will be put forth. First, it is expected that solids built of octa- and dodeca-(cubically) coördinated palladium and platinum group ions will be found. These systems will be described by Dq values which are $-{}^8/_9$ and $-{}^1/_2$, severally, times that of their octahedral counterparts (recall[46g] that for tetrahedral coördination this multiplicand is $-{}^4/_9$). Naturally the spin-orbit coupling parameter, λ, and the ligand field constant, Dq, will concurrently assume appropriate positive or negative values accordingly as there are one or nine d electrons present.[13]

It is proper to point out that questions of inherent configurational instability have been suppressed. Consideration of such complications is beyond the compass of this work: it should be mentioned that Goodman[64] is at present investigating problems of this sort. But note that in complexes with more than one electron, but less than nine, orbital degeneracy does *not* perforce imply instability. An excellent example of this nature is already visible in the first transition series—tetrahedral divalent nickel complexes, by virtue of their moderate spin-orbit correlations, do *not* exist in a degenerate ground state.[5] Hence, these compounds may exhibit, at most, pseudo Jahn–Teller forces.[65]

The predicted admixture of the antibonding e_g orbitals to the σ-non-bonding t_{2g} orbitals may be

(59) This particular structure of μ^2 is due to Moffitt, Goodman, Fred and Weinstock.[10]

(60) The corresponding expression in the weak field formalism may be reckoned from the identity of $\langle s|\mu_z|s\rangle^2$ with

$$\left[\frac{11}{6}g_{5/2}\sin^2\omega - \frac{3}{2}g_{3/2}\cos^2\omega - \frac{\sqrt{6}}{15}\sin 2\omega\right]^2,$$

$(s = a, b)$, and $\left[\frac{1}{2}g_{5/2}\sin^2\omega + \frac{1}{2}g_{3/2}\cos^2\omega - \frac{\sqrt{6}}{5}\sin 2\omega\right]^2$, $(s = c, d)$;

where the angle ω is deduced from the relation $\psi(\Gamma_8) = \sin\omega\Gamma_8(^2D_{5/2}) + \cos\omega\Gamma_8(^2D_{3/2})$. The choice of $\sim$3000 cm.$^{-1}$ for Dq and λ fixes ω at $\sim$33°. All essential matrix elements may be extracted from Condon and Shortley,[13c] Chapter III, pages 48–49 and 63–67. (The symbol g_j, $j = {}^5/_2, {}^3/_2$, represents the appropriate *atomic* g-factors.)

(61) If this same charge density function is also eliminated in the calculation of the ground state magnetic self-interaction terms, the magnetic secular determinant becomes $(s = a, b)$

$$\begin{vmatrix} & \Gamma_{8s} & \Gamma_{7s} \\ -\frac{\lambda}{2} - E & & -\sqrt{2}\,\beta H_z \\ -\sqrt{2}\,\beta H_z & \lambda \pm \beta H_z - E & \end{vmatrix} = 0$$

The plus sign holds when s equals a. The solution of this determinental equation by means of second-order perturbation theory, and the subsequent use of equation 4, ref. 56, produces Kotani's (*J. Phys. Soc.* (*Japan*), **4**, 293 (1949)) susceptibility expression. Upon expedient disregard of all exponential factors, the constant α will emerge from the Kotani susceptibility.

(62) Other discussions, not previously cited, which take cognizance of the interplay of the crystalline and spin-orbital forces may be found in papers by B. Bleaney (*Proc. Phys. Soc.*, **63A**, 407 (1950)); H. Kamimura (*Proc. Phys. Soc.* (*Japan*), **11**, 1171 (1956)); Y. Tanabe and H. Kamimura (*ibid.*, **13**, 394 (1958)); J. S. Griffith (*Trans. Faraday Soc.*, **54**, 1109 (1958)); and B. N. Figgis, (*Nature*, **182**, 1568 (1958)). Of course, the fundamental contributions of A. Abragam and M. H. L. Pryce (*Proc. Roy. Soc.* (*London*), **205A**, 135 (1951), *et sqq.*) must not be overlooked.

(63) Examinations of paramagnetic resonance phenomena in palladium and platinum group metals are not numerous. Apt references are: (a) S. Ramasesham and G. Suryan, *Phys. Rev.*, **84**, 593 (1951); (b) K. D. Bowers, *Proc. Phys. Soc.*, **66A**, 666 (1953); (c) J. H. Griffiths, J. Owen and I. M. Ward, *Proc. Roy. Soc.* (*London*), **219A**, 526 (1953); (d) K. W. H. Stevens, *ibid.*, 542 (1953); (e) J. H. E. Griffiths and J. Owen, *Proc. Roy. Soc.* (*London*), **226A**, 96 (1954); (f) H. M. Gijsman, H. J. Gerritsen and J. Van Den Handel, *Physica*, **20**, 15 (1954). Excellent surveys of both the resonant and static magnetism of these metals are given in the books by D. J. E. Ingram ("Spectroscopy at Radio and Microwave Frequencies," Butterworths, London, 1955) and P. W. Selwood ("Magnetochemistry," Interscience Publishers, Inc., New York and London, Second Edition, 1955).

(64) G. L. Goodman (private communication). A preliminary peek into this matter has been reported by W. E. Moffitt and W. R. Thorson, *Phys. Rev.*, **108**, 1251 (1957).

(65) A. D. Liehr, *Ann. Phys.* [*N. Y.*], **1**, 221 (1957). A similar conclusion may be drawn for tetrahedral cupric complexes, all of which possess Jahn-Teller resistant Γ_7 ground states (H. A. Jahn, *Proc. Roy. Soc.* (*London*), **164A**, 117 (1938)); see eqn. 10 or 17 (Note that such complexes should exhibit an infrared transition ($\Gamma_7 \rightarrow \Gamma_8$) at $\sim$1350 cm.$^{-1}$ ($Dq = -\lambda = 1000$ cm.$^{-1}$)).

experimentally verified by means of nuclear magnetic resonance techniques. The procedure to be followed is that of Shulman and Jaccarino[66] who show that the magnitude of the paramagnetic shift in the fluorine (or any other ligand with nonzero nuclear spin, for that matter) resonant frequency is directly related to the presence of unpaired electrons in antibonding trajectories.

Lastly, some thought must be given as to the validity of the crystalline field approach to complexes of the highly electropositive metallic ions situated in the fifth and sixth rows of the periodic table. A moments reflection will reveal that no approximation is actually entailed in the introduction of the parameter, Dq, for this parameter serves only to assess the *symmetry induced* separation of the t_{2g} and e_g spatial orbitals.[67] It thus symbolizes a known sum of interaction integrals. All approximations derive from semi-empirical specifications of this sum.[68] Entirely analogous arguments may be advanced for the tetragonal and trigonal measures $D\mu$, ($\mu = s, \sigma$) and $D\nu$, ($\nu = t, \tau$).[69]

A restriction must, however, be introduced to procure the spin-orbit matrix. This circumstance springs from the presence of a cross integral between the t_{2g} and e_g classes.[70] Theoretically two spin-orbit constants, $\lambda(t_{2g})$ and $\lambda(t_{2g}, e_g)$, should be employed, but simplicity dictates outlaw such finicking requirements. It is therefore perceived that loss in generality of the "exact" addend field approach[12] issues from the suppression of a second spin-orbital parameter[71]; for the clarification of some physical phenomena, this may not be a trivial defect.

NOTE ADDED IN PROOF.—Recent experiments of F. J. Morin on oxides of the second and third group transition elements indicate that these are *metallic* in nature. Therefore, Morin suspects there will also be Pauli type (metallic) paramagnetic contributions to the observed susceptibilities (see C. Kittel, "Introduction to Solid State Physics," John Wiley and Sons, Inc., New York, N. Y., Second Edition, pp. 259–262 (1956)). [A general discussion of metallic behavior in the first transition series oxides is given in F. J. Morin, *Bell Syst. Tech. J.*, **37**, 1047 (1958), and F. J. Morin, Chapter 14, "Semiconductors," A. C. S. Monograph No. 140, Editor N. B. Hannay, Reinhold Publishing Corporation, New York, N. Y., 1959.]

Acknowledgments.—The author is extremely grateful to Gordon L. Goodman for making available to him, in advance of publication, preprints of his discourses on similar topics. This thoughtfulness on Dr. Goodman's part has saved the author a considerable amount of futile effort and rescued his readers from dull redundancy. The present article has also benefited from several illuminating discussions with Dr. Goodman.

It is also a great pleasure to acknowledge fruitful conversations with Frank J. Morin, Robert G. Shulman and James C. Phillips. Through Dr. Phillips' kind consideration the author was privileged to read a prepublication draft of his important manuscript.

(66) R. G. Shulman and V. Jaccarino, *Phys. Rev.*, **108**, 1219 (1957). R. G. Shulman (private communication) plans to look at the fluorine resonance in molybdenum and tungsten hexafluorides.

(67) If one measures all energies from the mean of the t_{2g} and e_g orbital energies, $1/5[3E(t_{2g}) + 2E(e_g)]$, and calls the energy difference, $E(e_g) - E(t_{2g})$, $10Dq$, one readily infers both the strong and weak field cubic matrix elements. To see this one need note that when the null value, $3\bar{E}(t_{2g}) + 2\bar{E}(e_g)$, is combined with the energy separation $10Dq$, one obtains the magnitudes of the apposite strong field matrix elements, $\langle t_{2g}|V|t_{2g}\rangle$ and $\langle e_g|V|e_g\rangle$, as $-4Dq$ and $6Dq$, each. Similarly, the equality of $1/\sqrt{2}[e_{gb} \pm it_{2ga}]$ and $|2, \pm 2\rangle$, etc., permits the deduction of the needed weak field matrix components.

(68) In an important paper, soon to be published, J. C. Phillips [*J. Phys. Chem. Sols.*, in press] has shown, without resort to a full scale molecular orbital treatment (*vide, e.g.*, Y. Tanabe and S. Sugano, *J. Phys. Soc. (Japan)*, **11**, 864 (1956)), that the simple point charge model[17] has good theoretical justification. This article thus eliminates the extremely disconcerting result of W. H. Kleiner (*J. Chem. Phys.*, **20**, 1784 (1952)).

(69) These arguments involve the specification of separations, internal to the e_g and t_{2g} states, in terms of linear combinations of the axial measures.

(70) An equivalent complication occurring in atomic spectroscopy is discussed in Condon and Shortley,[13c] p. 376–377.

(71) Naturally, there are always present inaccuracies due to the complete disregard of configurational interaction of $t_2^n e_g^m$ states with terms of disparate origin.

THE REACTION OF FERRIC ION WITH ACETOIN (3-HYDROXY-2-BUTANONE) IN AQUEOUS SOLUTION

BY J. K. THOMAS, G. TRUDEL AND S. BYWATER

National Research Council, Applied Chemistry Division, Ottawa, Canada

Received June 16, 1959

The reaction between ferric ion and acetoin (3-hydroxy-2-butanone) has been studied in aqueous perchloric acid solution. It was found that two moles of ferric ion is required to oxidize 1 mole of acetoin. At low ferric ion concentrations the reaction is first order in acetoin and ferric ion. The variation in rate with pH is interpreted in terms of differing reactivities of the various hydrolysis products of ferric ion.

Introduction

The standard method for the analysis of acetoin consists of oxidizing it with ferric chloride. In this reaction biacetyl is formed quantitatively and can be estimated as the nickel glyoxime complex.[1] The present investigation was undertaken in order to elucidate the mechanism of this ferric ion reduction. Preliminary results were obtained using ferric sulfate solutions in dilute sulfuric acid, but all the quantitative experiments were carried out using ferric perchlorate–perchloric acid mixtures at low pH's since the preliminary experiments showed that the reaction rate is strongly dependent on the ferric ion species existing in the solution. The

(1) L. C. E. Kniphorst and C. I. Kruisheer, *Z. Untersuch. Lebensm.*, **73**, 1 (1937).

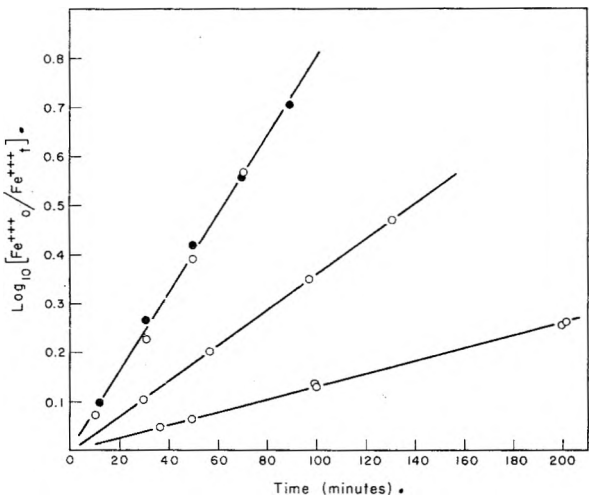

Fig. 1.—First-order plots of ferric ion disappearance: open circles: $[Fe^{3+}] = 2 \times 10^{-4} M$; [acetoin], 0.136, 0.34 and 0.68 M; $[H^+] = 0.99 M$; $\mu = 0.99$. Closed circles: $[Fe^{3+}] = 2 \times 10^{-3} M$; [acetoin] = 0.68 M; $\mu = 1.02$.

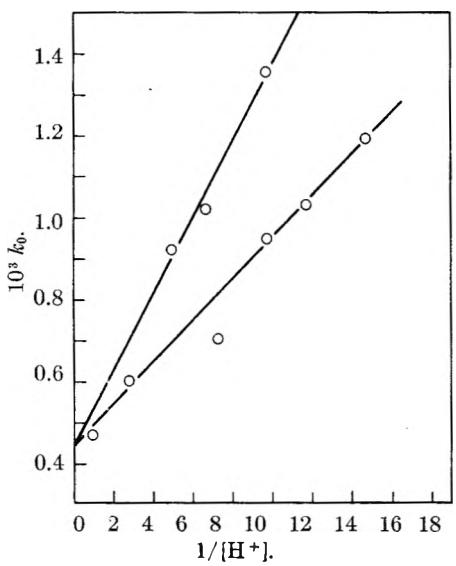

Fig. 2.—Variation of rate constant with $1/[H^+]$: upper line, $\mu = 0.20$; lower line, $\mu = 0.99$.

use of perchlorates greatly reduces the number of complex ferric ions in solution.

Experimental

Perchloric acid and ferric perchlorate were obtained from G. F. Smith Co. and used as received. Sodium perchlorate was obtained by neutralizing C.P. grade sodium bicarbonate with the perchloric acid. Acetoin (Eastman, practical grade) was obtained in the crystalline dimeric form. It was repeatedly extracted with acetone and then dried in a vacuum desiccator. The dimeric form of acetoin has been shown by Dirscherl and Braun[2] to be simply a hydrogen bonded structure which should be broken down completely into the monomeric form in aqueous solutions. The reaction was carried out in a nitrogen atmosphere in a double flask where the reagents could be degassed separately. Reaction was started by tipping the double flask and mixing the contents. Samples were blown out through a side arm by nitrogen pressure when required and analyzed for ferric ion using the ammonium thiocyanate method. Optical densities were measured at 475 mμ using a Beckman DU spectrophotometer, the method being standardized using stock solutions of known concentration analyzed gravimetrically. The reaction cell was maintained at 40 ± 0.05° for all measurements except those involving the temperature coefficient of the reaction. The ionic strength of the solutions was maintained at 0.99 unless otherwise stated by substituting sodium perchlorate for perchloric acid where necessary.

(2) W. Dirscherl and E. Braun, *Ber.*, **63**, 416 (1930).

Results

The rate of reduction of ferric ion was measured as a function of ferric ion concentration, acetoin concentration, pH, ionic strength and temperature. The initial ferric ion concentrations normally used were $2 \times 10^{-4} M$ and $2 \times 10^{-3} M$, and in order to obtain conveniently measurable rates acetoin concentrations 0.1 to 0.7 M were necessary. Under these conditions the acetoin is in large excess and its concentration will remain virtually constant during an experiment. The yield of biacetyl in the reaction was measured using the weak biacetyl absorption band at 405 mμ. While it is extremely difficult to analyze accurately for trace amounts of biacetyl in a large excess of acetoin, the measurements established that 0.5 ±0.05 mole of biacetyl was formed per mole of ferric ion reduced.

It is known that even in ferric perchlorate solutions, complex ions exist in aqueous solution except at very low pH and, since each ionic species in solution could be expected to react with acetoin at a different rate, the initial experiments were carried out in 0.99 N $HClO_4$ where the extent of ferric ion hydrolysis is small. Figure 1 shows first-order plots of ferric ion disappearance at various acetoin concentrations. The results indicate that the reaction is first order in ferric ion and of order 1.1 with respect to acetoin. Further experiments were carried out at acetoin concentrations of 0.68 M in order to avoid the small error introduced by the order in acetoin differing slightly from unity.

Figure 2 shows the effect of increasing the pH of the solution, whilst maintaining the ionic strength constant at 0.99 at an initial iron concentration of 2×10^{-4} molar. It is clear that the reaction rate increases under these conditions. A similar effect is produced when the ionic strength is reduced to 0.20. Since the observed rates closely approximate the relation

$$-\frac{d[Fe^{3+}]}{dt} = k_0[Fe^{3+}{}_{total}]\,[CH_3COCHOHCH_3] \quad (a)$$

the results are plotted in terms of observed second-order rate constants (k_0). Similar experiments carried out at an initial ferric ion concentration of $2 \times 10^{-3} M$ showed that the reaction ceases to be first order with respect to ferric ion at hydrogen ion concentrations less than about 0.3 M, first-order plots being curved over their whole length with initial slopes considerably less than those observed at $2 \times 10^{-4} M$ iron but approaching these slopes as the total ferric ion concentration drops. The order of the reaction with respect to acetoin, however, remains close to unity (1.0).

The experiments at 0.99 N acid were repeated at temperatures between 25 and 50° giving an apparent activation energy for the reaction of 24.7 kcal. per mole and an A factor of 3.6×10^{13} (l. mole^{-1}sec.$^{-1}$).

Discussion

The data reported are consistent with the following reaction scheme at very high acid con-

centrations

$$Fe^{3+}_{aq.} + CH_3COCHOHCH_3 \xrightarrow{k_1} Fe^{2+}_{aq.} + H^+ + CH_3C\dot{O}(OH)CH_3 \quad (1)$$

$$Fe^{3+}_{aq.} + CH_3C\dot{O}(OH)CH_3 \xrightarrow{k_2} Fe^{2+}_{aq.} + CH_3COCOCH_3 + H^+ \quad (2)$$

where the first step would be expected to be slow and rate controlling. This reaction scheme is similar to other electron transfer mechanisms suggested by Bawn[3] and Baxendale[4] for the oxidation of various compounds with cobaltic and ferric salts. The presence of radicals was demonstrated by adding about 1% of methyl methacrylate to the system when a voluminous precipitate of polymer was obtained. The reaction was also partially suppressed under the experimental conditions by the presence of oxygen, low and erratic rates of reaction being obtained, presumably due to peroxy radicals being formed. The scheme requires that two moles of ferric ion be reduced per mole of acetoin oxidized as observed. The reaction rate would be of the form given by equation (a) with $k_0 = 2k_1$ and first order with respect to total ferric ion and acetoin. The observed results indicate that the order with respect to acetoin is slightly greater than unity, to an extent which should be outside the limits of experimental error. The deviation may be a medium effect due to the large concentrations of acetoin used. Complications due to radical recombination or the presence in solution of acetoin dimers would tend to reduce the observed order below unity and, hence, could not account for the observations. The reaction has been written involving the removal of the tertiary hydrogen atom from acetoin, since experiments with 3-methyl-3-hydroxy-2-butanone showed that this compound is inactive toward ferric ion.

The experiments require that k_0 should be a function of pH and ionic strength, a variation which can be explained by the progressive hydrolysis of ferric ion which is known[5-8] to occur at higher pH's.

$$Fe^{3+}_{aq.} + H_2O \underset{}{\overset{K_1}{\rightleftharpoons}} FeOH^{2+} + H^+$$

$$2FeOH^{2+} \overset{K_2}{\rightleftharpoons} Fe_2(OH)_2^{4+}$$

$$Fe^{3+}_{aq.} + 2H_2O \overset{K_3}{\rightleftharpoons} Fe(OH)_2^+ + 2H^+$$

In the pH range studied, and at an initial iron concentration of 2×10^{-4} M only the first hydrolysis product is present in appreciable quantities.[2-4] Neglecting all species except Fe^{3+} aq. and $FeOH^{2+}$, the apparent variation in k_0 with ionic strength and pH can be explained by assuming that the species $FeOH^{2+}$ reacts much faster with acetoin than Fe^{3+} aq.

$$FeOH^{2+} + CH_3COCHOHCH_3 \xrightarrow{k_3} Fe^{2+} + H_2O + CH_3C\dot{O}(OH)CH_3$$

The total reaction rate would then be given by the expression

$$-\frac{d[Fe_t^{3+}]}{dt} = 2\left\{k_1 + \frac{k_3K_1}{[H^+]}\right\}[Fe_t^{3+}][\text{acetoin}] \quad (b)$$

where $[Fe_t^{3+}]$ is the total ferric ion concentration, under conditions where $K_1/[H^+]$ is small compared with unity, which should be true in these experiments. Hence plots of observed rate constant k_0 against $1/[H^+]$ would be expected to be linear in conformity with the observed results. As a check on this reaction scheme, it is possible to calculate the ratio of K_1 values at ionic strengths of 0.99 and 0.20 from the ratio of the slopes of the k_0 *vs.* $1/[H^+]$ plots. The observed value of the ratio is 1.8. This is to be compared with a ratio of 1.5 as determined by extrapolation of the spectroscopically obtained K_1 data of Milburn[9] to a temperature of 40°. The agreement must be considered satisfactory particularly since k_1 and k_3 themselves will be slightly dependent on ionic strength. If the value of K_1 at 40° and $\mu = 1$ is taken as 3.5×10^{-3} as obtained from Milburn's data and k_1 is taken as 2.25×10^{-4} l. mole^{-1}sec.$^{-1}$ from the extrapolated data of Fig. 2, then k_3 is 7.1×10^{-3} l. mole^{-1}sec.$^{-1}$; the first hydrolysis product is thus considerably more reactive toward acetoin.

The results at an initial total ferric ion concentration of 2×10^{-3} M and less than 0.3 N acid could be explained qualitatively if an increasingly large fraction of ferric ion was present as $Fe_2(OH)_2^{4+}$ at higher iron concentrations and this was supposed to be inactive in the reaction. The presence of dimeric species would produce deviations from first-order behavior since the percentage of iron present in this form is proportional to the square of the total iron concentration. Quantitatively, however, the equilibrium constant for the dimerization would have to be several powers of ten larger than the accepted range of values obtained by spectroscopic or magnetic means in order to reduce the concentration of active ferric species to the extent required by these experiments. The effect, however, appears to be connected with the presence of dimeric ferric species since the departures from pseudo first-order behavior are dependent only on the ratio of the total iron concentration to the hydrogen ion concentration. Thus low initial rates are observed even with 2×10^{-4} M iron concentrations if the acid concentration is below 0.03 N and at an initial ferric ion concentration of 10^{-2} M the curves are abnormal even with 1.0 N acid.

An alternative explanation of the pH dependence of the reaction in terms of varying concentrations of ionized species of acetoin with changes in hydrogen ion concentration cannot be excluded.[3,4] However, the fact that the rate constant change with ionic strength is in agreement with the known change in equilibrium constant for the formation of the first hydrolysis product of ferric ion under these conditions, makes the alternative explanation more reasonable.

(3) C. E. H. Bawn and A. G. White, *J. Chem. Soc.*, 339, 343 (1951).

(4) J. H. Baxendale, The Chemical Society, London, Special Publications No. 1, 40 (1954).

(5) R. M. Milburn and W. C. Vosburgh, *J. Am. Chem. Soc.*, **77**, 1352 (1955).

(6) L. N. Mulay and P. W. Selwood, *ibid.*, **77**, 2693 (1955).

(7) A. R. Olsen and T. R. Simonson, *J. Chem. Phys.*, **17**, 1322 (1949).

(8) B. O. A. Hedstrom, *Arkiv Kemi*, **6**, 1 (1953).

(9) R. M. Milburn, *J. Am. Chem. Soc.*, **79**, 537 (1957).

It has been assumed that the ferric species present at high perchloric acid concentrations is simply hydrated ferric ion. Sykes[10] has suggested that the perchlorate anion complexes appreciably with ferric ion, although his results are not in agreement with those of Sutton.[11] It must, therefore, be borne in mind that the reaction at very high acid concentrations may be due to the ion $FeClO_4^{2+}$ and not to hydrated ferric ion.

(10) K. W. Sykes, The Chemical Society, London, Special Publication No. 1, 64 (1954).

(11) J. Sutton, *Nature*, **169**, 71 (1952).

SELECTIVE ADSORPTION STUDIES BY RADIO TRACER TECHNIQUE: SELECTIVE ADSORPTION OF LABELED ALKALI *p*-DODECYLBENZENE SULFONATE S^{35} OR LABELED POTASSIUM HEXADECANOATE C^{14} AT THE AIR–SOLUTION INTERFACE OF AQUEOUS SOLUTIONS OF SURFACTANT MIXTURE

BY KŌZŌ SHINODA AND KAZUYOSHI MASHIO

Department of Chemistry, Faculty of Engineering, Yokohama National University, Minamiku, Yokohama, Japan

Received June 17, 1959

Well drained foams generated from aqueous solution of surfactant mixture were collapsed and collected in a small vessel. The concentration of surfactant of collapsed foams was determined with a micro-balance and that of labeled surfactant was determined from the measurements of the ratio of the counts of dried samples of collected foams and of original solution in the same geometry using G–M counter. Therefore, there are no disturbances in counting from geometry, self-adsorption, back-scattering, etc., in the present study. Selective adsorptivity of highly surface active substances at the air–solution interface of aqueous solutions of surfactant mixtures has been determined from these data. Selective adsorptivities of alkali *p*-dodecylbenzene sulfonate to sodium dodecyl sulfate, potassium dodecanoate and potassium tetradecanoate were 35–50, 180–280 and 5–6, and that of potassium hexadecanoate to potassium dodecanoate and potassium tetradecanoate were 50–66 and 5–8, respectively. These values allow an analysis of the actions of surfactant mixture, and an understanding of the effect of small amount of certain impurities. The concentration of collapsed foam was six times more concentrated in the case of aqueous solution of sodium dodecyl sulfate. The concentration of radioactive sodium *p*-dodecylbenzene sulfonate in collapsed foams was about 125–155 times larger than in the original solution in the case of mixture with sodium dodecyl sulfate.

Introduction

Selective adsorption phenomena have been recognized in solutions composed of surfactant mixture or solution which contains highly surface active impurities,[1–5] such as, long chain alcohols or higher homologs. The determination of selective adsorptivity is very important in order to understand the action of surfactants mixture and to clarify the effect of highly surface active impurities. However, the determination of the concentration and composition of small amount of surfactant mixture is very difficult without the aid of the radio tracer technique. So far as we know there is no report which determined the selective adsorptivity of one surfactant to the other. The use of radioactive surfactant is particularly valuable in the determination of the selective adsorptivity in the solution of surfactant mixture and in the detection of the concentration or the elimination of highly surface active substances by foam fractionation. In the present investigation, the selective adsorptivity was determined from the measurements of (1) the ratio of counts from the dried samples of collapsed foams to those from solution and (2) the concentration of collapsed foams.

Experimental

Materials.—Radioactive labeled palmitic acid 1-C^{14} was obtained from the Daiichi Pure Chemicals Company, Ltd., whose specific activity was 600 mc./mole. This compound was synthesized using very pure tetradecanoic acid.

Radioactive labeled sodium *p*-dodecylbenzene sulfonate S^{35} whose specific activity was 660 mc./mole was synthesized in an amount of 135 mg. from purified dodecylbenzene (b.p. 164–167° at 9 mm.) and radioactive sulfuric acid at the Radio Isotope Laboratory of the Daiichi Pure Chemicals Company, Ltd. The S^{35} was obtained as carrier free sulfuric acid through the Rikagaku-Kenkyusho (The Institute of Physical and Chemical Research).

Sodium dodecyl sulfate was obtained by neutralization of dodecylsulfuric acid with sodium hydroxide which was prepared by sulfation of very pure dodecanol with sulfuric anhydride. This was further purified by repeated recrystallization from water and extraction of dodecanol by ethyl ether.

Fatty acid soaps were prepared by neutralizing a known quantity of carbonate-free potassium hydroxide solution with respective fatty acids which were obtained from the Nihon Yushi Company, Ltd. The c.m.c. values of these soap solutions were in excellent agreement with accepted values, and melting points were all sharp and exact indicating the purity of these fatty aicds.[6]

Procedures.—Aqueous solutions of surfactant mixture were prepared by dissolving known amounts of radioactive and radioinactive surfactants accurately weighed on a micro-balance. About 100–170 cc. of solution of known concentration and composition was introduced into an apparatus shown in Fig. 1. The apparatus was kept in an air thermostat and the experiment was carried out at constant temperature. The bubbles were generated by the action of a circulating pump. The size and the number of bubbles generated per minute were controlled by changing the position of a vibrator and the frequency of the intermittence of the current. Air was passed through a soda lime absorbent at the beginning of the experiment to eliminate errors which might be caused by carbon dioxide in the air.

Bubbles attained adsorption equilibrium while they moved from one end to the other end of the nearly horizontal

(1) G. Aniansson, THIS JOURNAL, **55**, 1286 (1951).

(2) G. Nilsson and O. Lamm, *Acta Chem. Scand.*, **6**, 1175 (1952).

(3) G. Nilsson, THIS JOURNAL, **61**, 1135 (1957).

(4) L. Shedlovsky and J. Ross, *J. Colloid Sci.*, **4**, 25 (1949).

(5) A. Wilson, M. B. Epstein and J. Ross, *ibid.*, **12**, 345 (1957).

(6) K. Shinoda, THIS JOURNAL, **58**, 1136 (1954).

glass tube of about 90 cm. in length. The foams were well drained while they gradually moved upwards through a glass tube of about 30–130 cm. length. Depending on the stability of the foams the length of the draining tube was adjusted. This glass tube was inclined to facilitate drainage of the foams. The well drained foams were collapsed while they expanded or contracted at the end of the tube and collected in the small collector. In the case of very stable foams, the collector was cooled to about 0° to collapse the foams. In this case a correction due to the condensation of water vapor was necessary to determine the concentration of foams.

Fixed volumes of original solution and of collapsed foams were taken with micro (overflow type) pipet and transferred to sample plates which were coated with silicone oil to prevent wetting. The solutions were placed on the sample plate in position equidistant from the center of the plate. When the count of the dried sample of the solution is not large (strong) enough, equal volumes of solution were poured into the four positions. Accordingly, the geometry of samples is equivalent. The solution was dried with infrared ray lamp. All the radio counts from sulfur 35 were, of course, corrected for decay. Finally, the concentration of the solution of collapsed bubbles was determined by weighing. Selective adsorptivity was determined using these values. The procedures of the calculation are described in the next section.

Results

Selective adsorptivity at air–solution interface in aqueous solution of surfactant mixtures was determined from the combinations of sodium *p*-dodecylbenzene sulfonate S^{35}–sodium dodecyl sulfate, potassium *p*-dodecylbenzene sulfonate S^{35}–potassium dodecanoate, potassium *p*-dodecylbenzene sulfonate S^{35}–potassium tetradecanoate, potassium hexadecanoate 1-C^{14}–Potassium dodecanoate and potassium hexadecanoate 1-C^{14}–potassium tetradecanoate.

The concentration of collapsed foams and the ratio of the radioactivity from the same volume of collapsed foams to that from solution were determined. The results are summarized in Tables I, II, III, IV and V.

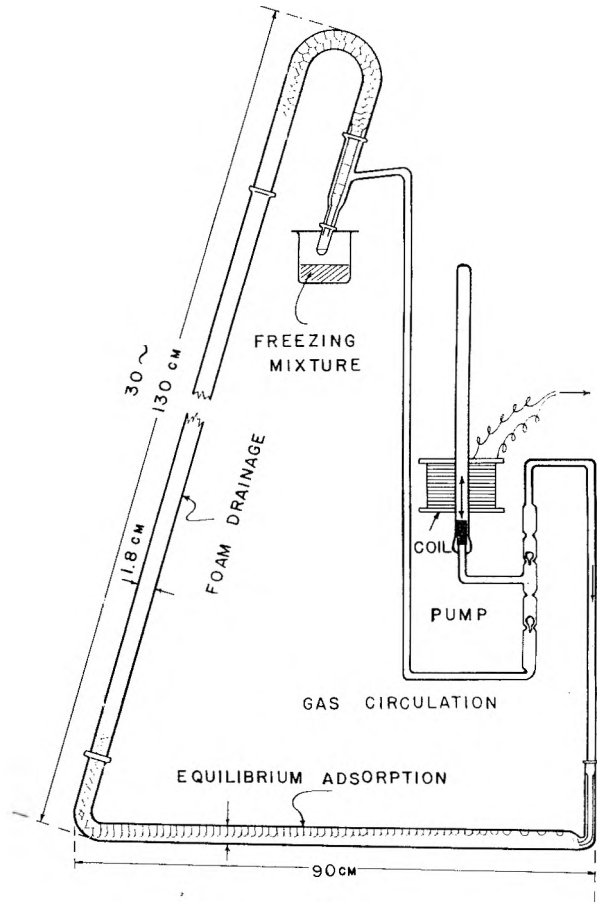

Fig. 1.—Apparatus of selective adsorption, foam drainage and/or foam fractionation.

TABLE I

SELECTIVE ADSORPTION AT AIR–SOLUTION INTERFACE IN AQUEOUS SOLUTION OF MIXTURE OF SODIUM *p*-DODECYLBENZENE SULFONATE S^{35} AND SODIUM DODECYL SULFATE AT 25°

		1	2	3	4	5
1	Counts (bulk)	57.0	48.0	40.3	28.4	16.0
2	X_{bulk}	0.0112	0.0095	0.0080	0.0056	0.0032
3	Concn. (soln.)	0.205	0.205	0.204	0.204	0.203
4	Counts (foams)	7039	6698	6377	4370	2339
5	Concn. (foams)	1.33	1.23	1.11	1.22	1.27
6	Ratio of concn.	6.49	6.00	5.44	5.98	6.26
7	Ratio of counts	123	140	158	154	146
8	X_{ads}	0.265	0.278	0.299	0.179	0.091
9	Selective adsorptivity	32	40	53	39	31

TABLE II

SELECTIVE ADSORPTION AT AIR–SOLUTION INTERFACE IN AQUEOUS SOLUTION OF POTASSIUM *p*-DODECYLBENZENE SULFONATE S^{35} AND POTASSIUM DODECANOATE MIXTURE AT 18°

		1	2	3	4
1	Counts (bulk)	95.1	89.7	80.5	74.6
2	X_{bulk}	0.0116	0.0110	0.00986	0.00913
3	Concn. (soln.)	0.524	0.523	0.522	0.522
4	Counts (foams)	4133	5128	3981	5409
5	Concn. (foams)	1.01	1.12	1.04	1.19
6	Ratio of concn.	1.927	2.145	1.988	2.291
7	Ratio of counts	43.5	57.2	49.4	72.5
8	X_{ads}	0.737	0.754	0.649	0.690
9	Selective adsorptivity	239	275	186	241

TABLE III

SELECTIVE ADSORPTION AT AIR-SOLUTION INTERFACE IN AQUEOUS SOLUTION OF POTASSIUM *p*-DODECYLBENZENE SULFONATE S^{35} AND POTASSIUM TETRADECANOATE MIXTURE AT 25°

		1	2	3	4
1	Counts (bulk)	64.3	62.2	60.0	58.3
2	X_{bulk}	0.0270	0.0261	0.0252	0.0245
3	Concn. (soln.)	0.141	0.141	0.140	0.140
4	Counts (foams)	550.8	525.3	391.8	415.5
5	Concn. (foams)	0.355	0.333	0.312	0.339
6	Ratio of concn.	2.52	2.36	2.23	2.42
7	Ratio of counts	8.6	8.4	6.5	7.1
8	X_{ads}	0.141	0.150	0.118	0.110
9	Selective adsorptivity	5.9	6.6	5.2	4.9

In the course of bubbles generation, the radioactivity in solution decreased appreciably, because the labeled surfactant had higher adsorptivity than radioinactive one and removed more rapidly in the foam. The logarithmic averages of the counts (c.p.m.) of dried samples of fixed volumes of the solutions at the beginning and at the end of respective experiments are shown in the 1st line. All the radio counts are the average values obtained from two or three individual samples. As the con-

TABLE IV

SELECTIVE ADSORPTION AT AIR–SOLUTION INTERFACE IN AQUEOUS SOLUTION OF POTASSIUM HEXADECANOATE AND POTASSIUM DODECANOATE MIXTURE AT 18°

		1	2	3	4	5
1	Counts (bulk)	215.2	195.0	178.2	162.5	147.0
2	X_{bulk}	0.0124	0.0113	0.0103	0.0094	0.0085
3	Concn. (soln.)	0.523	0.522	0.522	0.521	0.521
4	Counts (foams)	5534	7842	5505	5551	6198
5	Concn. (foams)	0.944	1.150	0.971	0.983	1.220
6	Ratio of concn.	1.81	2.20	1.86	1.89	2.34
7	Ratio of counts	25.7	40.2	30.9	34.2	42.2
8	X_{ads}	0.422	0.403	0.393	0.386	0.278
9	Selective adsorptivity	58	59	62	66	45

TABLE V

SELECTIVE ADSORPTION AT AIR–SOLUTION INTERFACE IN AQUEOUS SOLUTION OF POTASSIUM HEXADECANOATE 1-C^{14} AND POTASSIUM TETRADECANOATE MIXTURE AT 25°

		1	2	3	4
1	Counts (bulk)	102.2	97.4	94.8	91.3
2	X_{bulk}	0.0998	0.0955	0.0933	0.0900
3	Concn. (soln.)	0.145	0.144	0.143	0.143
4	Counts (foams)	1324	1354	1083	1162
5	Concn. (foams)	0.531	0.649	0.556	0.573
6	Ratio of concn.	3.66	4.51	3.89	4.01
7	Ratio of counts	13.0	13.9	11.4	12.7
8	X_{ads}	0.473	0.365	0.348	0.364
9	Selective adsorptivity	8.1	5.5	5.2	6.4

centration and the composition of the original solution were known, the mole fractions of radioactive surfactant in respective solutions are calculated from the radioactivity change and shown in the 2nd line. The total concentrations of surfactant in weight per cent. are also shown in 3rd line. The radio counts of dried samples of fixed volume of collapsed foams are shown in the 4th line. Assuming the interior of foams have the same composition with solution and neglecting the volume of adsorbed molecule, all the calculations were carried out. The concentrations of collapsed foams are shown in the 5th line. The ratio of the concentration of foams and of solution is shown in the 6th line. The ratio of radio counts from the same volumes of collapsed foams and bulk solution is shown in the 7th line. Assuming the weight ratio is equal to the mole ratio, the mole fraction of highly surface active species in the adsorbed layer was calculated using the ratio of counts from the same amount of surfactants (zeroth approximation). This gives the average molecular weight of the adsorbed layer. Considering the change in average molecular weight, the mole fraction of highly surface active substance in the adsorbed layer is calculated (First approximation). By the same procedure, we may obtain the accurate mole ratio. The mole fraction of radioactive surfactants, shown in the 8th line is calculated using the values in lines 1, 2, 4 and 5. Finally, the selective adsorptivity shown in the 9th line is calculated from the ratio of mole ratios in adsorbed and in bulk phase,

$$\alpha = \frac{X_{ads}}{1 - X_{ads}} \times \frac{1 - X_{bulk}}{X_{bulk}}$$

where X_{ads} and X_{bulk} are given in lines 8 and 2. It is assumed that the difference in atomic weight between radioactive and radioinactive atoms had no effect on adsorption.

The averages of the selective adsorptivity data in respective combinations of surfactant mixture are summarized in Table VI.

TABLE VI[a]

Surfactant 1	Surfactant 2	Selective adsorptivity of 1 to 2	Temp., °C.	State of soln.
$R_{12}C_6H_4SO_3^*Na$	$R_{12}OSO_3Na$	35~50	25	Homogeneous
$R_{12}C_6H_4SO_3^*K$	$R_{11}COOK$	180~280	18	Homogeneous
$R_{12}C_6H_4SO_3^*K$	$R_{13}COOK$	5~6	25	Heterogeneous
R_{15}^*COOK	$R_{11}COOK$	50~66	18	Homogeneous
R_{15}^*COOK	$R_{13}COOK$	5~8	25	Heterogeneous

[a] * Stands for radioactive atoms.

Discussion

Selective adsorption were already detected qualitatively by some authors using radio tracer technique.[1–3] These experiments, however, do not give selective adsorptivity. In the present paper, selective adsorptivity was determined for the first time measuring the mole fraction of a selected surfactant in an adsorbed layer.

The distinctive features of this experiment as a radio tracer method are (1) many serious errors which usually arise in the determination of counts, such as, differences in geometry, back-scattering, self-adsorption, efficiency of G–M counter, etc. are eliminated and (2) specific activity, which has usually to be large for the study of surface phenomena, may in these experiments be very small and still yield accurate results.

The concentrations of solutions examined were all close to, or slightly less than, the c.m.c. values of respective surfactants solution. The c.m.c. values of surfactant mixtures were estimated with high accuracy using the theoretical equation obtained before.[7] The foams are stable in this concentration region and the mole ratio of monodispersed surfactants is very close to the stoichiometric mole ratio, *i.e.*, there is no shift in mole ratio of monodispersed surfactants due to the micelle formation. Above the c.m.c. the apparent selective adsorptivity decreases as the highly surface active substance preferentially adsorbs in the micelles. The mole ratio of radioactive surfactant to radioinactive one in monodispersed state decreases. The solution was heterogeneous in the case of potassium tetradecanoate solution. Therefore, the results do not correspond to the selective adsorptivity found in the homogeneous solution.

Concentration of collapsed foams was about six times that of the original solution in the case of sodium *p*-dodecylbenzene sulfonate and sodium dodecyl sulfate mixture. If a c.m.c. value of a mixture were small, and therefore the solution were dilute, the ratio of the concentration of collapsed foams to original solution might increase much more. The ratio of radio counts of collapsed foams to solution was about 125–155 in this system. This result suggests an effective way of elimination or concentration of highly surface active substances by foam fractionation.

(7) K. Shinoda, THIS JOURNAL, **58**, 541 (1954).

If the mole fraction in bulk changes, the ratio of the mole fractions of adsorbed to dispersed molecules changes, but the ratio of mole ratios remains unchanged. Therefore, selective adsorptivity defined in this paper is a constant value over all mole fraction ranges for respective combinations of surfactants. The isotherms for preferential adsorption from binary liquid mixtures was discussed recently by Klinkenberg on the basis of the concept of a constant relative adsorbability (selective adsorptivity).[8] The concept and derivations are quite similar.

From the experiment on the mixture of potassium hexadecanoate and potassium dodecanoate, it is concluded that the selective adsorptivity of hexadecanoate to dodecanoate is about 60, *i.e.*, selective adsorptivity increases about 2.75 per methylene group. From the experiment on the mixture of sodium *p*-dodecylbenzene sulfonate and sodium dodecyl sulfate, it is concluded that the selective adsorptivity of benzene ring attached between hydrocarbon chain and polar group is about 55, considering the ratio of c.m.c. values of sulfate and sulfonate. A benzene ring, therefore, corresponds to about 3.5–4 methylene groups in its contribution to adsorptivity. The results obtained in the present study are also applicable to the selective adsorption at liquid–liquid or solid–liquid interface.

(8) A. Klinkenberg, *Rec. trav. chim.*, **78**, 83 (1959).

Acknowledgments.—We wish to thank the Ministry of Education for the support to the "Collective Study of Radioactive Surfactant and Radioactive Dye" and the Daiichi Pharmaceutical Company, Ltd. for the synthesis of Radioactive Surfactants.

PROTON RESONANCE SHIFTS IN NITRIC ACID SOLUTIONS OF ALUMINUM NITRATE[1]

BY ROBERT C. AXTMANN,[2] WOODFIN E. SHULER AND BRUCE B. MURRAY

Savannah River Laboratory, E. I. du Pont de Nemours and Company, Aiken, South Carolina

Received June 22, 1959

Proton magnetic resonance spectra were used to measure the dissociation of nitric acid between 25 and 80° in solutions that were 0 to 1.5 molar in aluminum nitrate. In every case studied, the salt repressed the dissociation of the acid markedly. At temperatures above room temperature, the salt was even more effective at diminishing the dissociation of the acid. The results at room temperature agree fairly well with a simple theory that combines a common ion effect due to the added nitrate ion and the assumption that water bound in the hydrated aluminum ion is unavailable for reaction with molecular nitric acid.

Introduction

Although many different techniques have been applied to the measurement of the dissociation of strong acids,[3,4] until recently Raman spectroscopy has furnished the most satisfactory data. In 1953, however, Gutowsky and Saika[5] demonstrated that a nuclear magnetic resonance (n.m.r.) technique might also be applied to the same problem. Hood, Redlich and Reilly[6] repeated some of Gutowsky and Saika's measurements with better apparatus, corrected their data for changes in the bulk magnetic susceptibility of the samples and obtained results that are in fair agreement with the earlier Raman data.

The variation with temperature of the dissociation of nitric acid has been studied with the Raman method by Rao[7] and by Young and Krawetz.[8] Most recently Happe and Whittaker[9] made a few measurements of the temperature coefficient of the proton n.m.r. shift in HNO_3–H_2O solutions, but the studies were confined to extremely concentrated (>94%) solutions and covered a limited temperature range.

In this work, the n.m.r. method for determining the dissociation of nitric acid was extended to a system in which an additional solute was present.

Experimental

The n.m.r. measurements were made with a Varian Associates V-4300B high resolution spectrometer in conjunction with a 12-inch electromagnet system. The chemical shifts relative to pure water, $\delta = [(H_{ref} - H)/H_{ref}] \times 10^6$, were measured at 40.0 megacycles in a field that was stabilized by a Varian Model VK-3506 super stabilizer. The samples were rotated in precision coaxial glass tubing[10] with the water reference in the annular space. The theory of measurements with this sample arrangement has been given by Zimmerman and Foster.[11] The field was swept with a linear sawtooth sweeping potential and the data were recorded on a Sanborn 151 recorder that was calibrated at the time of each measurement with the sideband technique. In every case the chemical shifts were reproducible to ±0.01 and in many cases to ±0.005.

A novel method was used to measure the chemical shifts of solutions of lithium salts which were only slightly shifted from water. Absolute ethyl alcohol was placed in the inner Wilmad tube and the unknown in the outer tube. A slow scan (*ca.* 10 c.p.s./min.) of the magnetic field was then made across the triplet arising from the proton in the O–H group of the alcohol. The aqueous signal showed up between two branches of the triplet and had an amplitude comparable to that of the triplet. The recorder chart paper was then

(1) The information contained in this article was developed during the course of work under contract AT(07-2)-1 with the U. S. Atomic Energy Commission.

(2) Department of Chemical Engineering, Princeton University, Princeton, N. J.

(3) O. Redlich and G. C. Hood, *Disc. Faraday Soc.*, **24**, 87 (1957).

(4) O. Redlich, *Chem. Revs.*, **39**, 333 (1946).

(5) H. Gutowsky and A. Saika, *J. Chem. Phys.*, **21**, 1688 (1953).

(6) G. C. Hood, O. Redlich and C. A. Reilly, *ibid.*, **22**, 2067 (1954).

(7) N. R. Rao, *Indian J. of Phys.*, **17**, 295 (1943).

(8) T. F. Young and A. A. Krawetz, Abstracts of papers given at the Meeting of the American Chemical Society (Miami, Florida, April 7–12, 1957).

(9) J. A. Happe and A. G. Whittaker, *J. Chem. Phys.*, **30**, 417 (1959).

(10) Wilmad Glass Co., Landisville, N. J.

(11) J. R. Zimmerman and M. R. Foster, THIS JOURNAL, **61**, 282 (1957).

calibrated from an earlier measurement of the separation of triplet, 4.94 ± 0.1 c.p.s. Chemical shifts from water of 0.01–0.1 could be measured easily with a precision of 0.002 (0.1 c.p.s. at 40 Mc.) The technique was combined with the sideband technique to measure separations greater than 6 c.p.s. The temperature of the sample was carefully controlled in these experiments. For experiments in which such control is not feasible, a standard with a smaller temperature coefficient than that of the OH proton from ethyl alcohol would be preferable.

The temperature studies were performed with commercial apparatus[12] similar to the equipment described by Shoolery and Roberts.[13] Temperatures were measured with a copper–constantan thermocouple located at the n.m.r. probe insert. Temperatures at the sample itself were then determined to ±2° from a curve derived from calibration data of an earlier experiment. In all of the studies the temperature of the sample and of the water reference differed by no more than a few tenths of a degree centigrade.

Reagent grade aluminum nitrate was used to prepare solutions that were approximately two molar in aluminum. These solutions were standardized gravimetrically by ignition to aluminum oxide. C.P. concentrated nitric acid was standardized by density and by titration with standard base. Samples containing both nitric acid and aluminum nitrate were prepared by diluting mixtures of the standard solutions.

The magnetic susceptibilities of the nitric acid solutions that contained salts were determined by the Gouy method. An attempt to duplicate the n.m.r. measurements of the magnetic susceptibility of pure nitric acid solutions reported by Hood, *et al.*,[6] was unsuccessful. Values for the volume magnetic susceptibility were then computed from Pacault and Chedin's careful measurements with a modified Faraday apparatus.[14] Densities of the salt solutions were determined with a Westphal balance.

Treatment of Data

Since their original paper,[6] Hood, *et al.*, have published n.m.r. data on the dissociation of several strong acids.[15–17] The theory of the measurements and the assumptions involved are discussed in detail in that series of papers. Briefly, for the case of nitric acid more dilute than 18 M, it is assumed that (1) the only proton-containing species are H_2O, $H_3{}^+O$, and the monohydrate of nitric acid, $HNO_3 \cdot H_2O$, (2) each of these species has a characteristic n.m.r. shift and (3) the total n.m.r. shift exhibited by a solution is the sum of the individual shifts multiplied by their respective mole fractions.

In this work the assumption of the additivity of chemical shifts is extended to include the proton shift due to the hydrated aluminum ion. The effect of hydrated cations on the proton resonance in aqueous solution has been studied by Shoolery and Alder[18] and by Axtmann[19] who found that cations shift the resonance to lower fields. The shifts are linear with concentration in dilute (<2 M) solutions and are ascribed[18] to attraction of the electrons of the hydrogen atom by the cation. The predominant effect of anions is a shift in the opposite direction resulting from the depolymerization of the water. This latter effect is normally overcome by the cationic effect whenever the cation is at all strongly hydrated. The extent of the cationic shift in a number of nitrates has been related to the degree of hydrolysis experienced by the hydrated cation.[19]

The observed chemical shift must be corrected, then, for the presence of the aluminum nitrate as well as the difference between the magnetic susceptibility of the sample and the reference.[6,11] The corrected chemical shift δ_{cor} is

$$\delta_{cor} = \delta + g - h \qquad (1)$$

where δ is the experimental chemical shift for the protons in the sample relative to water, g is the magnetic shielding correction given by

$$g = 2.6\,(K \times 10^6 + 0.718) \qquad (2)$$

K is the volume magnetic susceptibility of the sample, and

$$h = \delta_{an} M \qquad (3)$$

where δ_{an} is the molar shift of aluminum nitrate, corrected for magnetic susceptibility and M is the molarity of the salt.

The molar shift for aluminum nitrate δ_{an} was determined from chemical shift and magnetic susceptibility measurements on a series of 0.5 M HNO_3 solutions containing 0 to 2 M aluminum nitrate. The shift was found to vary linearly with salt concentration in this range except at the lowest acid and salt concentrations. At low concentrations (<0.5 M) hydrolysis of the hydrated aluminum ions according to

$$Al(H_2O)_6{}^{+++} + H_2O \longrightarrow H_3{}^+O + Al(H_2O)_5(OH)^{++} \qquad (4)$$

and

$$Al(H_2O)_5(OH)^{++} + H_2O \longrightarrow H_3{}^+O + Al(H_2O)_4(OH)_2{}^+ \qquad (5)$$

presumably introduces additional proton-containing species whose shifts differ from that of the normal hexahydrated aluminum ion. Four different solutions gave a value of $\delta_{an} = 0.615 \pm 0.013$ mole^{-1} which agrees well with published data.[18,19] There was some evidence of a decrease in δ_{an} with increasing acid concentration, which might be expected from the saturation effect observed with various salt solutions.[18] The effect was not investigated here, however, since errors in h become progressively less important as acid concentration increases.

The degree of dissociation α is

$$\alpha = \frac{1}{\delta_1 - \delta_2}\left[\frac{\delta_{cor}}{p} - \delta_2\right] \qquad (6)$$

where p is the stoichiometric mole fraction of $H_3{}^+O$ given by

$$p = 3x/2 - x \qquad (7)$$

with x the mole fraction of acid. In the computations of p and x, only the hydrogen-containing species are considered. The constants δ_1 and δ_2 have the same value in aluminum nitrate solutions as in nitric acid solutions with no salts, since δ_1 and δ_2 represent the chemical shifts for pure $H_3{}^+O$ and $HNO_3 \cdot H_2O$.[6]

In the case of dilute acid solutions, small errors in the determination of the density of the solutions

(12) Varian Associates, Palo Alto, California.

(13) J. N. Shoolery and J. D. Roberts, *Rev. Sci. Instr.*, **28**, 61 (1957).

(14) A. Pacault and J. Chedin, *Bull. soc. chim. France*, **17**, 766 (1950).

(15) G. C. Hood, O. Redlich and C. A. Reilly, *J. Chem. Phys.*, **23**, 2229 (1955).

(16) G. C. Hood and C. A. Reilly, *ibid.*, **27**, 1126 (1957); **28**, 329 (1958).

(17) G. C. Hood, A. C. Jones and C. A. Reilly, THIS JOURNAL, **63**, 101 (1959).

(18) J. N. Shoolery and B. J. Alder, *J. Chem. Phys.*, **23**, 805 (1955).

(19) R. C. Axtmann, *ibid.*, **30**, 341 (1959).

are reflected in large errors in the quantity p of equation 6. This, in turn, leads to large errors in α. In addition, when insufficient acid is present to suppress the reactions 4 and 5, hydrolysis products accumulate whose shifts are neither known nor accounted for in the analysis. For these reasons no data are reported for solutions that were less than one molar in acid. A few solutions that were more dilute were studied but the data gave unreasonably low value of α.

Results and Discussion

I. Room Temperature Studies.—Chemical shift data and α values were determined at room temperature (24–26°) for four series of solutions that were 0, 0.525, 1.05 and 1.50 molar in aluminum nitrate and contained various concentrations of nitric acid. A number of the solutions with the highest ionic concentrations were supersaturated but the n.m.r. measurements were made before any crystallization took place.

For the pure nitric acid solutions, the agreement with the earlier α values of Hood, *et al.*,[6] is excellent if the same magnetic susceptibility corrections are used for both sets of data. Values for $\delta_1 = 11.73$ and $\delta_2 = 4.27$, computed from the data reported here, differ by less than 1% from Hood's although the precision of individual measurements in the present work was undoubtedly greater due to the use of precision glass tubing for the sample vials.

The data are plotted in Fig. 1 which clearly shows reduced dissociation of nitric acid in the presence of aluminum nitrate. The addition of 1.5 M $Al(NO_3)_3$ to 6 M HNO_3, for example, almost halves the concentration of hydronium ion.

In the absence of a quantitative theory for strong solutions of electrolytes, it is possible to gain some understanding of the data plotted in Fig. 1 through consideration of the mass action law. If the reaction

$$HNO_3 + H_2O \rightleftarrows H_3{}^+O + NO_3{}^- \qquad (8)$$

is used as a description of the dissociation of nitric acid in solutions more dilute than 18 M, then a stoichiometric equilibrium constant K_s may be defined

$$K_s = \frac{\alpha^2[HNO_3]}{(1-\alpha)[H_2O]} \qquad (9)$$

where the brackets signify stoichiometric concentrations in moles per liter. K_s, which may be evaluated from the n.m.r. measurements of α, decreases fairly rapidly with increasing acid concentration. If it is assumed that: (1) K_s does not vary with *salt* concentration, and (2) highly hydrated ions, such as Al^{+++}, effectively remove some water from the scene and force reaction 8 to the left, then α's for aluminum nitrate solutions of nitric acid may be computed on the basis of the common ion effect of the added nitrate, an effective hydration number n for the aluminum ion and experimental values for the degree of dissociation of pure nitric acid. If α' represents the degree of dissociation computed in the fashion just described, then

$$\alpha' \frac{(\alpha'[HNO_3] + 3[Al(NO_3)_3])}{(1-\alpha')([H_2O] - n[Al(NO_3)_3])} = K_s \qquad (10)$$

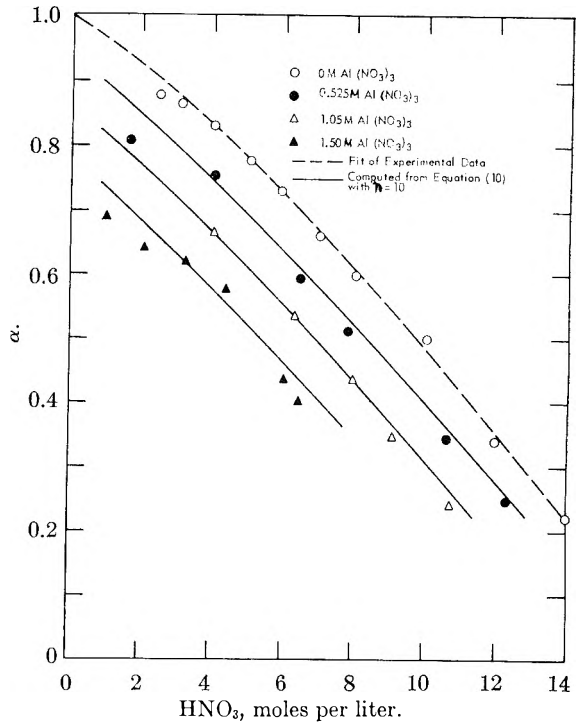

Fig. 1.—Dissociation of nitric acid in aluminum nitrate solutions.

The choice of a proper hydration number n is difficult. Experimental evidence supports a formulation of $Al(H_2O)_6{}^{+++}$, corresponding to a single layer of water molecules around each cation, not only in crystals but in solution.[19] N.m.r. data from proton line widths[18] and relaxation time measurements[20] suggest an exchange time for water in the innermost hydration sphere of 6–8 millisec. The exchange time of the protons in reaction 8, on the other hand is $\leqq 10^{-4}$ seconds.[5,18] As far as the n.m.r. measurements are concerned, then, n is at least six. Broersma infers from his relaxation time data that there is a second and perhaps a third hydration shell around the aluminum ion in concentrated solutions.[20] In these outer shells, undoubtedly the bonding is weaker and the lifetimes shorter, approaching those of reaction 8. The "effective" hydration number is, in any case, greater than six. The assignment of $n = 10$ would be equivalent to the claim that the loose bonding of the 20–40 water molecules in the outer hydration shells is equivalent to the tight bonding of four water molecules in the innermost shell.

The curves on Fig. 1 for the solutions containing aluminum nitrate were computed from equation 10, with $n = 10$. The agreement with the experimental data is certainly satisfactory considering the roughness of the model that has been used.

An experiment was performed to corroborate the hypothesis that the repression of the dissociation of nitric acid by aluminum nitrate is due to a common ion effect and to the tying up of water molecules by the hydrated cations. In this experiment, α was measured in a 6 M HNO_3 solution that contained additional nitrate ion accompanied by a cation that is less hydrated than Al^{+++}, and

(20) S. Broersma, *J. Chem. Phys.*, **27**, 481 (1957).

in a second 6 M HNO_3 solution that contained a salt with neither a common ion nor a highly hydrated cation. Two-molar solutions of lithium chloride and lithium nitrate were chosen because Shoolery and Alder's table of molar shifts[18] predicts that the shift caused by the salts themselves—the h term in equation 1—is relatively small. The larger portion of any observed change in the shift, therefore, should be due to an alteration in the dissociation of the acid. The actual value of h for the two 6 M HNO_3 solutions of lithium salts was determined from chemical shift and magnetic susceptibility measurements on solutions that contained no acid.

The data presented in Table I show the common ion effect clearly since α for the $LiNO_3$–HNO_3 solution is significantly less than that for the LiCl–HNO_3 solution.

TABLE I

PROTON SHIFTS OF LITHIUM SALT AND NITRIC ACID SOLUTIONS AT 22–23°

Solution	δ	g	h	δ_{calc}	p	α
6 M HNO_3	1.768	0.075	...	1.843	0.188	0.74
6 M HNO_3 + 2 M LiCl	1.818	.029	−0.018	1.865	.1995	.68
6 M HNO_3 + 2M $LiNO_3$	1.693	.094	−0.089	1.876	.205	.65
2 M LiCl	0.037	− .055	...	−0.018	...	..
2 M $LiNO_3$	−0.092	.003	...	−0.089	...	..

The substantial decrease in α for the LiCl–HNO_3 solution compared with the pure 6 M HNO_3 solution is a little surprising but can be attributed, at least partially, to the hydration of the lithium ion. Because of its low formal charge but comparable size, the lithium ion is clearly not as highly hydrated as the aluminum ion. Nonetheless there is some hydration in Li^+, amounting to several times that of the other alkali metal ions, as shown by the transference experiments of Washburn and Millard.[21]

A comparison of the lithium salt results with those for the aluminum nitrate solutions shows qualitative agreement with the postulated mechanism for repression of the dissociation. From Fig. 1, a solution that is 6 molar in HNO_3 and 0.67 molar in $Al(NO_3)_3$ would have $\alpha \cong 0.62$. Such a solution would contain the same amount of added nitrate ion as the $LiNO_3$–HNO_3 solution which gave $\alpha = 0.65$. Although there is twice as much Li^+ in the latter solution as Al^{+++} in the 0.67 M $Al(NO_3)_3$ solution, apparently the Li^+ is not hydrated enough to reduce the dissociation to the extent that the lesser amount of Al^{+++} would. A more quantitative comparison would not seem rewarding because of the uncertainty in the hydration numbers of the two cations involved.

II. Studies above Room Temperature. A. HNO_3 Solutions.—Chemical shifts from water were measured for four different nitric acid solutions in the temperature range 40–80°. Although the molarities of the solutions decrease somewhat with temperature, the stoichiometric mole fraction p defined by equation 7 remains constant thus simplifying the analysis of the data. The constants δ_1 and δ_2 of equation 6 were determined graphically at 40, 60 and 80° from the present data plus Happe and Whittaker's determination of the shift for pure (24 M) nitric acid.[9]

The results, given in Table II, show little change in α with temperature in this range for the two more dilute solutions. The 8.17 M and 15.95 M solution showed decreased dissociation on heating in qualitative agreement with the earlier Raman results.[7,8]

TABLE II

PROTON SHIFTS OF NITRIC ACID SOLUTIONS AT 40–80°

HNO_3, moles/l.[a]	δ	g	p	α
I. T = 40°; δ_1 = 11.77; δ_2 = 4.17				
2.02	0.605	0.034	0.0572	0.921
4.10	1.188	.065	.1218	.805
8.17	2.240	.133	.273	.595
15.95	3.490	.338	.780	.097
II. T = 60°; δ_1 = 11.90; δ_2 = 4.11				
2.02	0.613	0.039	0.0572	0.936
4.10	1.200	.070	.1218	.811
8.17	2.213	.143	.273	.580
15.95	3.418	.354	.780	.094
III. T = 80°; δ_1 = 12.20; δ_2 = 4.06				
2.02	0.623	0.039	0.0572	0.923
4.10	1.220	.073	.1218	.806
8.17	2.170	.153	.273	.547
15.95	3.363	.364	.780	.088

[a] All solutions were made up at 23–24° to the molarities shown.

B. $d\delta_{an}/dT$.—Before the effect of temperature on $HNO_3 \cdot Al(NO_3)_3$ solutions could be determined, it was necessary to measure the temperature coefficient of the molar shift of aluminum nitrate. A solution that was 1.05 M $Al(NO_3)_3$ and 1.0 M HNO_3 was used for the measurement. The coefficient is constant in the interval 25–90° and equal to $+2.46 \times 10^{-3}$/mole deg., corrected for changes in magnetic susceptibility and density. The fact that the coefficient is positive may be explained in terms of Shoolery and Alder's interpretation of shifts in aqueous solutions. In either salt solution or pure water, a rise in temperature causes depolymerization, *i.e.*, rupture of hydrogen bonds, which results in the shifting of the proton signal to higher fields. Since, in the present case, the shift measured is that between water and the aqueous solution, the fact that the shift increases with increasing temperature indicates that the pure water signal moves toward higher field strength at a more rapid rate than does the signal from the salt solution. This result is reasonable since the n.m.r. shift is a colligative property and there are fewer hydrogen bonds initially present in the salt solution due to the depolymerizing action of the salt.

C. $HNO_3 \cdot Al(NO_3)_3$ Solutions.—When approximately one mole per liter of aluminum nitrate was added to nitric acid solutions of intermediate strength, heating decreased the dissociation of the acid markedly. Table III contains data for two 1.05 M $Al(NO_3)_3$ solutions that were 3.95 and 6.32 M HNO_3, respectively. These data show that the addition of the salt causes about a 10–20% reduction in hydrogen ion concentration when the solutions are heated from 40 to 80°. On the other

(21) E. W. Washburn and E. B. Millard, *J. Am. Chem. Soc.*, **37**, 694 (1915).

hand, 3.95 *M* HNO_3 with no added salt is not appreciably affected by temperature as shown in Table III.

An interpretation of these latter studies is not as readily derived from the mass action law as one was in the case of the studies at room temperature. It might even be reasonable to expect that nitric acid in aluminum nitrate solution would dissociate *more* at higher temperatures since the outer hydration shells of the aluminum ions should be less stable and thus would make additional water available to drive reaction 8 to the right.

Unfortunately there does not seem to be a ready explanation for the experimental fact that the dissociation of the acid diminishes with temperature in the presence of the aluminum salt. For the solutions studied here, however, the effect is not a particularly large one.

TABLE III

PROTON SHIFTS OF $HNO_3 \cdot H_2O \cdot Al(NO_3)_3$ SOLUTIONS AT 23–80°

T, °C.,[b]	δ	g	h	p	α
	I. 1.05 *M* $Al(NO_3)_3$, 3.95 *M* HNO_3[a]				
23	1.805	0.021	0.626	0.1278	0.665
40	1.835	.029	.680	.1278	.670
60	1.864	.036	.727	.1278	.651
80	1.878	.042	.773	.1278	.603
	II. 1.05 *M* $Al(NO_3)_3$, 6.32 *M* HNO_3[a]				
23	2.388	0.070	0.626	0.2200	0.532
40	2.351	.081	.654	.2199	.516
60	2.344	.091	.709	.2199	.480
80	2.333	.096	.709	.2199	.420

[a] Solutions were made up at 23–24° to the molarities shown. [b] Values for δ_1 and δ_2 are given for each temperature in Table II.

Acknowledgment.—This problem was originally suggested by Dr. C. S. Schlea. The work benefited from a number of helpful discussions between the authors and Drs. D. G. Karraker and C. H. Ice. Dr. Karraker was also kind enough to read and criticize the manuscript. Mr. E. F. Furr and Mr. J. W. Crooks determined the solution densities. Mrs. Patricia Rice measured the magnetic susceptibilities.

THE HEATS OF HYDROLYSIS OF DIBORANE AND BORON TRICHLORIDE[1]

BY STUART R. GUNN AND LEROY G. GREEN

Lawrence Radiation Laboratory, University of California, Livermore, California

Received June 25, 1959

The heats of hydrolysis of B_2H_6 and BCl_3 have been remeasured to determine the consistency of the heats of formation of the two compounds and to improve the derived values of the heats of formation of boric acid and boric oxide. Measured values are: $B_2H_6(g) + 2006H_2O(l) = 2(H_3BO_3 \cdot 1000H_2O) + 6H_2(g)$, $\Delta H = -112.22 \pm 0.10$ kcal. mole^{-1}; $BCl_3(l) + 2403H_2O(l) = (H_3BO_3 + 3HCl) \cdot 2400H_2O$, $\Delta H = -68.68 \pm 0.06$. Derived values for the heat of formation of $H_3BO_3 \cdot 1000H_2O$ (from amorphous boron) from the two reactions are -257.70 ± 0.28 and -257.06 ± 0.33, respectively. The standard heat of formation of B_2O_3 (from crystalline boron) is estimated to be -305.50 ± 0.45.

Because of the difficulty of measuring the heat of combustion of boron directly, the best value of the heat of formation of boric oxide is obtained from its heat of solution to form aqueous boric acid. The heat of formation of this solution may be derived by two routes: (1) the heat of pyrolysis of diborane to its elements[2] combined with the heat of hydrolysis of diborane[3] and (2) the direct heat of formation of boron trichloride[4] combined with the heat of hydrolysis of boron trichloride.[5] The values of the heat of formation of aqueous boric acid derived by the two routes are in good agreement. However, since all four measurements are fairly difficult and have rather large estimated uncertainties, it seemed desirable to remeasure both heats of hydrolysis with greater precision and in the same calorimeter in order to check the consistency of the heats of formation of diborane and boron trichloride, and to secure a better estimate of the reliability of the heats of formation of boric acid and boric oxide, which are fundamental to the thermochemistry of most boron compounds.

Experimental

The calorimeter was of the sealed rocking-bomb type previously described.[6] It is excellently adapted to the performance of such violent hydrolytic reactions as these because there is no possibility of escape of reactants or products and because all parts of the bomb are continually washed down by the solution following the reaction, thus ensuring chemical and thermal equilibrium within and between the phases. The bomb, laboratory designation ID, was similar to 1A[6] but was fabricated of coinage gold. The only other materials in contact with the solution were tantalum, Pyrex and neoprene. Operating procedures and auxiliary equipment were essentially as described,[6] electrical standards were compared with others certified by the N.B.S. The defined thermochemical calorie, 4.1840 absolute joules, is used throughout. All reactions were performed at 25.00 ± 0.03°. The internal volume of the bomb was 650 ml.; about 375 ml. of water was used for all runs.

The diborane sample bulbs ranged from 50 to 65 ml. internal volume. They were made from 100-ml. round-bottom centrifuge tubes with a thin-walled enlargement blown out at the bottom and drawn down near the middle and attached to a small tube for filling and sealing off. A blank experiment with one of these bulbs filled with water and 400 ml. of water in the bomb showed the breaking process to evolve 0.05 ± 0.05 cal. The boron trichloride sample

(1) This work was performed under the auspices of the U. S. Atomic Energy Commission. Contract No. W-7405-eng-68.

(2) E. J. Prosen, W. H. Johnson and F. Y. Pergiel, *J. Research Natl. Bur. Standards*, **61**, 247 (1958).

(3) E. J. Prosen, W. H. Johnson and F. Y. Pergiel, *ibid.*, **62**, 43 (1959).

(4) W. H. Johnson, R. G. Miller and E. J. Prosen, *ibid.*, **62**, 213 (1959).

(5) H. A. Skinner and N. B. Smith, *Trans. Faraday Soc.*, **49**, 601 (1953).

(6) S. R. Gunn, *Rev. Sci. Instr.*, **29**, 377 (1958).

bulbs were blown on 9-mm. Pyrex tubing and had internal volumes of about 4 ml.

A gas measuring system consisting of water-jacketed burets calibrated gravimetrically with mercury, a Toepler pump, a manometer and a cathetometer was used to measure the diborane samples and the hydrogen produced. The system was checked by dissolving weighed pieces of high-purity magnesium in acid; the average volume of hydrogen found was 100.00% of the theoretical, the average deviation being 0.05%. Gas imperfection corrections were applied, the data of MacWood and Paridon[7] being used for diborane. The water in the bomb was deaerated before each run by successive stirring and pumping to eliminate any possibility of reaction with oxygen, to permit determination of the volume of hydrogen produced in the case of the diborane runs and to permit detection of unreactive impurity gases in the case of the BCl_3 runs.

The solutions produced by the reactions were titrated for boric acid, and also hydrochloric acid from the boron trichloride runs. Most of the required sodium hydroxide was added as a weighed aliquot of solution standardized by weight against NBS benzoic acid. End-points were detected with a *p*H meter and mannitol was used in the boric acid titrations.

Three preparations of diborane were used. The first was prepared by reaction of sodium borohydride with concentrated sulfuric acid using a polyglycol wetting agent. It was purified by repeated fractional condensation using traps at −160 and −196°. The vapor pressure was 224 mm. in a carbon disulfide slush bath (literature, 224 ± 2 mm. at −112.1°).[8] Duplicate mass spectral analyses on two different spectrometers suggested, after subtraction of background effects, the presence of about 0.6 mole % carbon dioxide. The second and third preparations were performed by reaction of boron trifluoride ethyl etherate with potassium borohydride in a polyether medium. The second was purified by the same procedure as the first; it approached the same constant vapor pressure much more rapidly with successive passes. The third was purified by fractional distillation at one-atmosphere pressure using a Podbielniak column. Following the diborane there appeared a small amount of a slightly higher boiling fraction which was apparently ethane; it is probable that this was the major impurity in the second preparation.

The diborane sample bulbs were mounted on the vacuum line, flamed, and then pretreated with diborane to eliminate moisture. Samples of diborane measured in the gas buret were then condensed in the bulbs with a liquid nitrogen bath and the tubes were sealed off while the bulb was immersed in the liquid nitrogen. It is possible, however, that some heat radiated to the sample might have permitted a small amount to volatilize and escape. To prevent decomposition of the diborane the bulbs were stored in liquid nitrogen until mounted in the calorimeter four to six hours before reaction.

Boron trichloride was purified by shaking with mercury and then by repeated fractional vaporization and condensation using a grease-free vacuum line equipped with mercury float valves. All seven samples listed below were from the same middle cut. The first two samples were distilled from the beginning of this batch, the next three near the middle and the last two from the very end. The front end and bulk of the material showed a vapor pressure of 477 mm. at 0° and had been so through several passes; the last sample was about 3 mm. lower.

Results

The kinetics of the diborane hydrolysis were moderately rapid and quite reproducible, 90% of the temperature rise occurring in two minutes. Results of the measurements are given in Table I.

Several corrections must be applied to the calorimetric observations to derive ΔH^0 for the reaction. These may be considered with the following steps in the bomb process and conversion to standard conditions.

(7) G. E. MacWood and L. J. Paridon, American Chemical Society, San Francisco, 1958.

(8) J. T. Clarke, E. B. Rifkin and H. L. Johnston, *J. Am. Chem. Soc.*, **75**, 781 (1953).

TABLE I

HEAT OF REACTION OF B_2H_6 WITH H_2O

Run	Prepn.	Sample, mmole	q, cal.	H_2, % theo.	H_3BO_3, % theo.	$-\Delta H$, kcal./mole
1	A	3.9469	452.86	(99.48)	99.63	112.30
2	A	4.0532	464.80	99.52	99.65	112.20
3	A	4.0071	459.33	99.48	99.55	112.20
4	A	3.9946	458.10	99.43	99.57	112.30
5	B	3.9878	452.44	98.48	98.55	112.17
6	B	3.9665	449.71	98.42	98.44	112.17
7	C	4.0265	463.19	99.83	100.67	112.19
8	C	4.0219	462.48	99.78	99.91	112.21
9	C	4.0280	463.24	99.82	99.95	112.17
10	C	4.0106	461.31	99.74	99.93	112.29
					Av.	112.22

(1) The bulb is broken and the diborane expands into the free space. $\Delta H = 0$.

(2) Water vaporizes to fill the increased vapor volume; 0.0134 cal. per ml. of bulb volume are absorbed. This correction, about 0.8 cal., has been included in the values of q in Table I.

(3) The reaction proceeds at constant volume. From the solubility data of Seidell[9] and the ratio of the gas or liquid volumes it may be calculated that 2.56% of the hydrogen will remain in solution at equilibrium; hence, the reaction is

$$B_2H_6(g) + 6H_2O(l) \longrightarrow 2H_3BO_3(aq) + 5.846H_2(g) + 0.154H_2(aq) \quad (1)$$

To convert the measured ΔE to ΔH, $\Delta nRT = 2.871$ kcal. mole^{-1} is added.

(4) The dissolved hydrogen is removed from the solution. Calculating the heat of solution from Seidell's data to be −1.06 kcal. mole^{-1}, then 0.163 kcal. mole^{-1} are absorbed in this process and ΔH is 0.163 kcal. mole^{-1} less negative.

(5) Water is removed from the solution to change the concentration from $H_3BO_3 \cdot 2600H_2O$ to $H_3BO_3 \cdot 1000H_2O$. The latter concentration has been adopted as the reference state for aqueous boric acid by the NBS workers and the same convention will be followed here. The heat of dilution data of Smisko and Mason[10] indicate a negligible heat effect. The values given in the last column of Table I are then for the reaction

$$B_2H_6(g) + 2006H_2O \longrightarrow 2(H_3BO_3 \cdot 1000H_2O) + 6H_2(g) \quad (2)$$

The amount of reaction is based solely on the hydrogen volume measurement; since the results show no trend with apparent purity it is evident that the impurities have a negligible thermal effect, and all values are weighted equally in the average.

The boric acid titrations given in the last column of Table II are calculated with respect to the sample volume measurement. While they are rather consistently about 0.1% higher than the hydrogen determination, the agreement is felt to be very adequate in view of the difficulty of titrating boric acid in dilute solutions.

One possible source or error would be non-

(9) A. Seidell and W. F. Linke, "Solubilities of Inorganic and Metal-organic Compounds," 4th Ed., Vol. 1, The American Chemical Society, 1958.

(10) J. Smisko and L. S. Mason, *J. Am. Chem. Soc.*, **72**, 3679 (1950).

equilibrium distribution of hydrogen between the liquid and gas phases at the end of the reaction period. This affects the ΔnRT and the heat of solution of hydrogen corrections in opposite directions; the true value of ΔH, if the solution contained twice the calculated amount of hydrogen, would be 0.07 kcal. mole^{-1} less negative and, if it contained half the calculated amount, 0.04 more negative. However, experience with recovery of hydrogen from the bomb solution by rocking and pumping indicates that in the ten-minute reaction period, equilibration should be nearly complete. It is believed that in view of this and other uncertainties, limits of error for ΔH should be set at ± 0.10 kcal. mole^{-1} although the standard deviation is much smaller.

Prosen, Johnson and Pergiel[3] have given a value of −111.46 ± 0.54 for reaction 2; the two determinations disagree by only slightly more than the sum of the estimated uncertainties.

The boron trichloride hydrolysis was essentially instantaneous. Results of the measurements are given in Table II.

TABLE II

HEAT OF REACTION OF BCl_3 WITH H_2O

Run	Sample, mmole	q, cal.	HCl, % theo.	H_3BO_3, % theo.	$-\Delta H$, kcal./mole
1	9.0153	618.95	99.82	98.80	68.66
2	8.9666	615.42	99.78	100.16	68.64
3	8.2568	567.15	99.99	100.20	68.68
4	8.5516	587.66	99.93	100.23	68.72
5	8.6691	595.68	99.91	100.21	68.71
6	8.3083	570.42	99.89	100.06	68.65
7	8.6829	596.62	99.91	100.05	68.71
				Av.	68.68

The values of q include corrections for the heat of vaporization of the gaseous portion of the BCl_3 in the sample bulb, using the value 5.60 kcal. mole^{-1} for the heat of vaporization.[4] The values of ΔH tabulated are for the reaction

$$BCl_3(l) + 2403H_2O \longrightarrow (H_3BO_3 + 3HCl)\cdot 2400H_2O \quad (3)$$

Small corrections have been applied for the heats of dilution of HCl from the actual concentration to that given; actual mole ratios of H_2O to BCl_3 ranged from 2290 to 2570.

Determination of the amount of reaction was based solely on the weight of the sample, corrected to vacuo and using a molecular weight of 117.19. In view of the difficulties of washing out the bomb thoroughly and of titrating boric acid in very dilute solutions, the agreement of the HCl and H_3BO_3 determinations is felt to be adequate. Only negligible traces of gas were found in the bomb after the runs by pumping through a trap at −78°. Two of the possible impurities, hydrogen chloride and phosgene, would introduce little error since they give, on a weight basis, about the same heat of reaction with water. An uncertainty of ± 0.06 kcal. mole^{-1} will be assigned.

Skinner and Smith[5] obtained a value of −69.2 kcal. mole^{-1} for the heat of hydrolysis of BCl_3 at a mole ratio of about 5000. Corrected to the concentrations of reaction 3, this corresponds to −69.15, some 0.5 kcal. mole^{-1} more negative than the present result.

Two measurements were made of the heat of the reaction

$$H_3BO_3\cdot 2100H_2O + 3(HCl\cdot 100H_2O) \longrightarrow (H_3BO_3 + 3HCl)\cdot 2400H_2O \quad (4)$$

using a diborane-type bulb to contain the HCl. Values obtained for ΔH_4 were −534 and −543 cal. mole^{-1}. For the reaction

$$3(HCl\cdot 100H_2O) + 2100H_2O \longrightarrow 3(HCl\cdot 800H_2O) \quad (5)$$

the data of the NBS[11] and Harned and Owen[12] give −567 and −558, respectively; thus the enthalpy of the hydrochloric acid is only slightly affected by the presence of the boric acid.

Subtracting reaction 4 from reaction 3 and again neglecting the heat of dilution of boric acid, one obtains $\Delta H_6 = -68.14$ for the reaction

$$BCl_3(l) + 1303H_2O \longrightarrow H_3BO_3\cdot 1000H_2O + 3(HCl\cdot 100H_2O) \quad (6)$$

Discussion

The heat of formation of boric acid, referred to amorphous boron may now be calculated from reactions 2 and 6 using the following auxiliary data:

$$B_{(amorph)} + \frac{3}{2}H_2(g) + \frac{3}{2}O_2(g) + 1000H_2O(l) \longrightarrow H_3BO_3\cdot 1000H_2O \quad (7)$$

$$2B_{(amorph)} + 3H_2(g) \longrightarrow B_2H_6(g);\ \Delta H_8 = +6.73 \pm 0.52 \text{ kcal./mole}^2 \quad (8)$$

$$H_2(g) + \frac{1}{2}O_2(g) \longrightarrow H_2O(l);\ \Delta H_9 = -68.317 \text{ kcal./mole}^{11} \quad (9)$$

$$B(amorph) + \frac{3}{2}Cl_2(g) \longrightarrow BCl_3(g);\ \Delta H_{10} = -97.51 + 0.32 \text{ kcal./mole}^4 \quad (10)$$

$$BCl_3(l) \longrightarrow BCl_3(g);\ \Delta H^0 = +5.60 \text{ kcal./mole}^4 \quad (11)$$

$$\frac{1}{2}H_2(g) + \frac{1}{2}Cl_2(g) + 100H_2O(l) \longrightarrow HCl\cdot 100H_2O;\ \Delta H = -39.713 \text{ kcal./mole}^{11} \quad (12)$$

$$\Delta H_7 = \frac{1}{2}\Delta H_2 + \frac{1}{2}\Delta H_8 + 3\Delta H_9 = -257.70 \pm 0.28 \text{ kcal./mole}$$

$$\Delta H_7 = \Delta H_6 + 3\Delta H_9 + \Delta H_{10} - \Delta H_{11} - 3\Delta H_{12} = -257.06 \pm 0.33$$

Thus, the values of heat of formation of aqueous boric acid derived by the two routes disagree by approximately the sum of the limits imposed by the uncertainties in the heats of formation of B_2H_6 and BCl_3. We shall select a value of −257.40 ± 0.20 kcal. mole^{-1} for ΔH_7 and, using the data selected by Prosen, *et al.*,[3] from the literature for the heats of transition of boron and boric oxide and the heat of solution of amorphous boric oxide, calculate the standard heat of formation of boric oxide

$$2B(c) + \frac{3}{2}O_2(g) \longrightarrow B_2O_3(s);\ \Delta H_{13}^0 = -305.50 + 0.45 \text{ kcal./mole} \quad (13)$$

(11) F. D. Rossini, *et al.*, Circular of the National Bureau of Standards, No. 500, 1952.

(12) H. S. Harned and B. B. Owen, "The Physical Chemistry of Electrolytic Solutions," 3rd Ed., Reinhold Publ. Corp., New York, N. Y., 1958, pp. 707, 708.

MISCIBILITY OF LIQUID METALS WITH SALTS. IV. THE SODIUM–SODIUM HALIDE SYSTEMS AT HIGH TEMPERATURES[1]

BY M. A. BREDIG AND H. R. BRONSTEIN

Chemistry Division, Oak Ridge National Laboratory, Oak Ridge, Tennessee

Received June 29, 1959

The use of thermal analysis and of equilibration with a new method of sampling yielded improved data for consolute temperatures and compositions as well as for the solubilities of the metal in the molten salts in the lower temperature range. The consolute compositions of 28 mole % Na (at 1180°), 50 (1080°), 52 (1026°) and 59 (1033°) for the NaF–Na, NaCl–Na, NaBr–Na and NaI–Na systems, respectively, reflect the influence of the relative sizes of the metal and halide constituent on the symmetry of the phase diagrams. The depression of the melting point of the salt represented by the monotectic temperature and composition of the salt-rich phase corresponds to a positive deviation from Raoult's law similar to the one observed in the KX–K systems. A similar tentative interpretation, namely, the association of the metal to diatomic molecules, is proposed.

Introduction

Liquid–liquid phase equilibria in the binary systems composed of an alkali metal with each of its halides have been found to lead at moderately high temperatures to complete miscibility, *i.e.*, miscibility in all proportions, of the metal with the salt.[2–4] While in the potassium and cesium systems the temperatures of complete miscibility were experimentally accessible, this was not the case, at the time of the first report,[2] for the NaX–Na systems for which approximate critical solution, or consolute, temperatures were instead only *estimated* by extrapolation. The results of an extension of the actual measurements to the higher temperature range and, in addition, several significant refinements of the data at the lower temperatures are discussed in the following.

Experimental

The original method[2] of determining the phase equilibria by equilibration and sampling at the test temperature, had, in the case of the salt-rich phase, left uncertainties about completeness in the removal of the metal phase therefrom before sampling. This is particularly true at higher temperature and metal concentration, where differences in the physical properties of the two phases to be separated become smaller. For this reason, the method of thermal analysis was substituted and proved successful in the determination of the KX–K equilibria (X = F, Cl, Br and I).[4] A modification required for a similar application of thermal analysis to the high temperature phase equilibria of the NaX–Na systems was the provision of an inert atmosphere of increased pressure around the capsules containing the sample in order to balance the pressure exerted on the capsule walls by the volatile sodium metal. This was achieved by mounting the capsules on a frame inside a tank made of Inconel and pressurized with up to 100 lb. per square inch of pure argon gas.

The remainder of the procedure was similar to that described for the KX–K systems.[4] However, the capsules were not evacuated but filled with argon and were welded shut with a flat top rather than a crimped end. The materials were similar to those employed in the earlier report. Two to four cooling curves were obtained for each composition, with variations in the positions of the thermal halts usually less than 2°.

The method of thermal analysis fails in the lower temperature range because the mutual miscibility of the two components increases too slowly with temperature to yield a detectable thermal effect on cooling. In this range, a redetermination of the solubility of the metal in the molten salt was carried out by the method of equilibration and sampling described previously in connection with the electrical conductance measurements.[5] In this method, an error of the older method[2] is avoided, which was introduced by the presence of metal phase in the salt sampling chamber during the equilibration period prior to sampling and by the apparently inevitable retention of liquid metal therein, possibly in the form of a thin ring around the bottom of the chamber.

Results and Discussion

Results obtained both by thermal analysis and by the new equilibration-and-sampling technique are given in Table I. Figure 1 shows the phase equilibria in diagrammatic form but, for the sake of clarity, does not show all experimental points. A comparison of Fig. 1b of this paper with Fig. 2 and 3 of ref. 2 shows that the earlier results for the solubility of sodium metal in molten sodium chloride were distorted by what is now believed to have been incomplete removal, before sampling, of the metal-rich phase from the salt-rich phase. It must now be assumed that the long periods of equilibration with continuous violent motion applied then were excessive and probably led to an undesirable breakup, if not colloidal dispersion, of the liquids. This must have caused portions of the metal-rich phase to cling to the walls of that part of the equilibration capsule used subsequently for sampling the salt-rich phase (see Figs. 1a and 1b of ref. 2). Among the earlier equilibration tests, one had been carried out without shaking at 950° for a heating period of ten hours and with the salt prefused first in the bottom of the capsule before adding sodium metal; a value of 7.5 mole % Na had been obtained, which was then erroneously considered too low and not published. Actually, this type of test in which metal phase never entered the sampling chamber gave a result in good agreement with the new equilibrium curve.

On the other hand, incomplete phase separation, *i.e.*, failure to remove all of the metal phase from the salt sampling chamber, after continuous shaking must have also produced the earlier faulty results on the salt side of the fluoride system (Fig. 3, ref. 2). (These earlier fluoride data had to be rejected

(1) This paper is based on work performed for the U. S. Atomic Energy Commission at the Oak Ridge National Laboratory, operated by the Union Carbide Corporation, Oak Ridge, Tennessee. It was presented in part at the 132nd Semiannual Meeting of the American Chemical Society, New York City, September, 1957.

(2) M. A. Bredig, J. W. Johnson and Wm. T. Smith, Jr., *J. Am. Chem. Soc.*, **77**, 307 (1955).

(3) M. A. Bredig, H. R. Bonstein and Wm. T. Smith, Jr., *ibid.*, **77**, 1454 (1955).

(4) J. W. Johnson and M. A. Bredig, THIS JOURNAL, **62**, 604 (1958).

(5) H. R. Bronstein and M. A. Bredig, *J. Am. Chem. Soc.*, **80**, 2077 (1958).

TABLE I

EQUILIBRIUM PHASE COMPOSITIONS IN THE SODIUM METAL–HALIDE SYSTEMS[a]

Sodium–sodium fluoride			Sodium–sodium chloride			Sodium–sodium bromide			Sodium–sodium iodide		
Na, mole %	Two-liquids temp., °C.	Monotectic, °C.	Na, mole %	Two-liquids temp., °C.	Monotectic, °C.	Na, mole %	Two-liquids temp., °C.	Monotectic, °C.	Na, mole %	Two-liquids temp., °C.	Monotectic, °C.
Salt-rich phase			Salt-rich phase			Salt-rich phase			Salt-rich phase		
10.0	1126	989	2.93	844	[b]	4.12	797	[b]	1.85	661	[b]
19.0	1175	990	3.10	845	[b]	4.97	808	[b]	2.02	678	[b]
			3.16	854	[b]	8.92	897	[b]	2.15	702	[b]
Metal-rich phase			3.24	869	[b]	9.10	896	[b]	2.35	696	[b]
			3.84	891	[b]	15.4	948	[a]	2.38	704	[b]
33.5	1176	..	3.87	895	[b]	48.5	1032	743[f]	2.47	705	[b]
50.0	1156	986	3.97	880	[b]	48.8	1013	730[f]	3.22	727	[b]
60.5	1130	987	4.25	895	[b]	49.0	1018	732[f]	6.08	797	[b]
60.8	1130	988	7.55	948	[c]				6.32	803	[b]
67.0	1107	987	14.2	1009	796.5	Metal-rich phase			12.15	897	[b]
78.4	1030	986	25.0	1054	795.0				29.0	990	648
90	932 (solid	..	35.0	1068	...	74.5	1004	730[f]	32.0	998	652
	NaF precip.)		50.0	1079	795.5	75.0	1000	731[f]	48.0	1031	637[f]
			Metal-rich phase						Metal-rich phase		
			75.0	1055	794.6				74.5	1011	653
			90.0	946 + 960[d]	792.0						

[a] Comprises new results from both equilibration-and-sampling tests (marked *b*) and cooling curves (not marked, or marked *f*). For the solubilities of the salts in the liquid metal, see also ref. 2. [b] Equilibration-and-sampling tests by new method described in ref. 4. [c] Equilibration for 10 hours in (ref. 2)-type capsule, without shaking and with prefusing of salt preventing presence of metal phase in sampling chamber. [d] One of these two halts may be due to precipitation of traces of solid oxide. [e] Fifteen minutes equilibration in old style (ref. 2) capsule. [f] Cause for low monotectic temperature (*cf.* Table II) may be some slight oxide contamination. Effect on liquid miscibility believed to be minor.

(*dotted* line, Fig. 3, ref. 2) also on theoretical grounds, as an extrapolation of the solubility curve cannot possibly intersect the temperature axis, but must approach it asymptotically: ($ds/dT = s(\Delta H/RT^2)$; $ds/dT \rightarrow 0$ as $s \rightarrow 0$). In Fig. 1a the new Na–NaF phase diagram is compared with those of K–KF and Cs–CsF. Conclusions regarding the obvious trend in the degree of miscibility[3] are not altered by the new shape of the Na–NaF diagram.

The bromide and iodide systems were very much less affected by this difficulty (compare Fig. 1c and 1d of this paper with Fig. 3 of ref. 2). Here, different from the fluoride and chloride systems, the larger differences in specific gravity of the two liquid phases and possibly more favorable conditions of surface tension led to essentially complete phase separation even after prolonged shaking. In the present work, periods of equilibration with agitation as short as a few minutes were found ample. The results obtained for the salt-rich solutions with bromide and iodide by thermal analysis at temperatures above 950° merge rather smoothly with most of those obtained below this temperature by equilibration and sampling in the earlier work.

For the metal-rich solutions of all four systems, the earlier solubility values also fit well the new values at higher temperatures from cooling curves. However, there is a slight discrepancy between the thermal analysis and the equilibration tests for the solubility of sodium fluoride in the metal phase. The slightly low NaF solubility values from the earlier equilibration experiments[2] (crosses on the right side of Fig. 1a) are believed to have been caused by distillation, during the cooling period, of a small amount of alkali metal from the main portion of the mixture into the relatively large, vapor-filled space of the capsule, followed by condensation and reflux into the small side chamber containing the sample of the metal-rich phase (Fig. 1c, ref. 2).

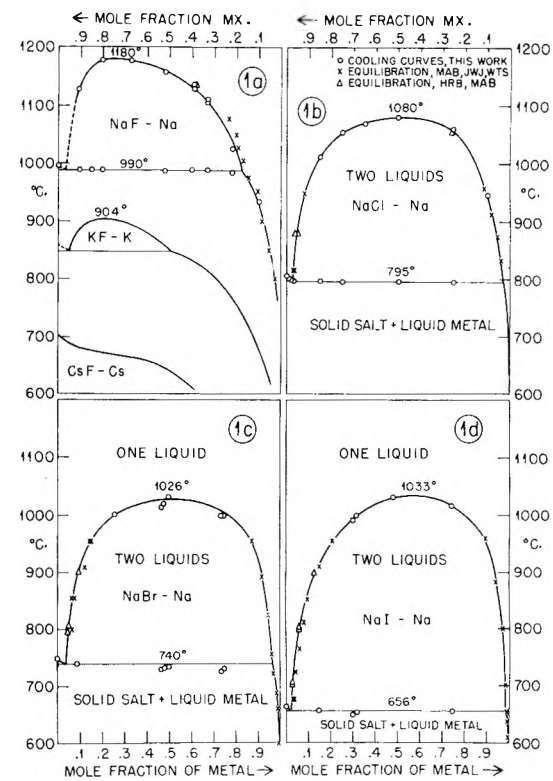

Fig. 1.—Phase equilibria in the sodium metal–halide systems. In 1a, KF–K and CsF–Cs from ref. 4 and 3, respectively, included for comparison with the new Na–NaF diagram. (For additional experimental points see Table I and Fig. 2.)

In the present work, a special point was made of

TABLE II

SUMMARY OF PRINCIPAL DATA FOR SODIUM–SODIUM HALIDE SYSTEMS

		Systems of Na with			
		NaF	NaCl	NaBr	NaI
Consolute: Temp., °C.		1180	1080	1026	1033
Consolute: Comp. mole % Na		28	50	52	59
T_m = m.p. pure salt, °C.		995[a]	800[b]	747[a]	660.1[c]
ΔH_f = heat of fusion (salt), calcd.		8030[d]	6850[e]	6240[e]	5620[e]
Monotectic: Comp. of salt-rich liquid phase	T_{mon}, °C.	990[a]	795.3[b]	740[a]	656.7[c]
	X_{solute} (calcd.)[f]	0.012	0.014	0.020	0.011
	X_{Na} (anal.)	.....	.021	.029	.016
	α (approx.)[g]	.....	.3	.4	.4

[a] Ref. 2. [b] J. W. Johnson and M. A. Bredig, 1956, unpublished. [c] A. Dworkin and M. A. Bredig, calorimetric measurements to be published. [d] C. J. O'Brien and K. K. Kelley, *J. Am. Chem. Soc.*, **79**, 5616 (1957). [e] K. K. Kelley, U. S. Bureau of Mines Bull. 476,166, 1949. [f] Ideal (Raoult's law) mole fraction of solute: X_{solute} (calcd.) = $(\Delta H_f/R) \times (T_m - T_{mon})/T_m T_{mon}$. [g] Estimate of degree of dissociation of Na_2 molecules

$$\alpha = \frac{2X_{solute}\,(calcd.)}{X_{Na}\,(anal.)} - 1$$

where X_{solute} (calcd.) = total moles (Na + Na_2) after dissociation of Na_2, and $\frac{1}{2}X_{Na}$ (anal.) = moles of Na_2 before dissociation, both per one mole of metal–salt mixture.

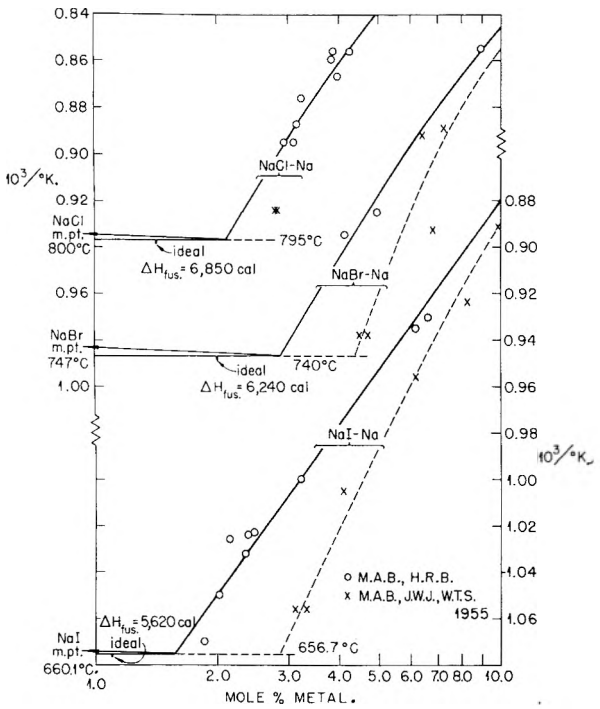

Fig. 2.—Derivation of monotectic liquid salt-rich phase composition from intersection of solubility curves with monotectic horizontals. Comparison with "ideal" composition (positive deviation from Raoult's law). Dotted lines and crosses from earlier publication (ref. 2), when faulty sampling technique was used. Open circles are new data obtained with the sampling method of ref. 4.

ascertaining once more the occurrence of strong positive deviation from Raoult's law for the salt component through determination of the depression of its melting point. This deviation, interpreted[4,5] as being due to the formation of diatomic metal molecules, Na_2 or K_2, represented the principal basis for explaining the initial decline—with increasing metal concentration—of the equivalent conductance of the dissolved sodium metal.[5] The lowering of the melting temperatures of sodium chloride and iodide, previously given as 9 and 5° at monotectic compositions of 2.4 and 2.9 mole % Na, respectively, was now found to be in error due to a slight contamination of the salt–metal mixtures with oxide. According to the new measurements on the NaCl–Na system (J. W. Johnson, 1956), the true monotectic horizontal lies only 4.7 ± 0.2° below the melting point of the pure salt. For NaI–Na, the figure is 3.4°. Also, the metal concentration in the monotectic salt-rich phase as determined by the intersection of the monotectic horizontal with the curve for the solubility of the metal in the salt was found, in the recent work, to be lower (Fig. 2, smooth lines) than originally reported on the basis of equilibration capsule tests[2] (Fig. 2, dotted lines). The new values are based on solubility data obtained by sampling during the conductance measurements[5] and by some additional tests in which the same improved method of sampling was used.

Table II and Fig. 2 give a comparison of the experimental compositions of the monotectic, liquid salt phases with compositions calculated from the (approximate) equation

$$X_{solute}\,(calc.) = \frac{\Delta H_{fusion}}{RT^2} \times \Delta T$$

where ΔT is the difference between the melting point of the pure salt and the monotectic temperature. ΔT and ΔH_{fusion} are believed to have been determined with a precision of approximately 10 and 2%, respectively. The ratio X_{metal} (anal.): X_{metal} (calc.) is seen to be greater than unity, approximately 1.4, corresponding to positive deviation from Raoult's law for the salt component. This fact is here again, as in the KX–K systems, tentatively interpreted to indicate association of the solute, the metal, to diatomic molecules, Na_2. The degree of association is expressed in Table II as α, degree of dissociation of the Na_2 molecules, the latter amounting to approximately 0.3 to 0.4 in the monotectic salt-rich liquid.

If in the phase diagrams of Fig. 1 lines are drawn representing the mean compositions of the two coexisting liquid phases—and corresponding somewhat to the "rectilinear diameters" in density *vs.* temperature plots of one-component systems—these "diameters", although slightly curved rather than straight, lead to the consolute compositions

59, 52, 50 and 28 mole % Na for the iodide, bromide, chloride and fluoride systems at the consolute temperatures 1033, 1026, 1080 and 1180°, respectively. These critical compositions show at a glance the trend in the symmetry of the two-liquid-phase coexistence areas from one in the iodide system favoring miscibility in the salt phase to one in the fluoride system favoring it very much in the metal phase.

This distinct trend naturally is related to the relative sizes of the atoms and ions of the two components: In the fluoride system, the most asymmetric of the four, the metal has by far the larger molar volume, V_{Na} = 33 cm.^{3}, than the salt with V_{NaF} = 22 cm.^{3}. The reverse is true for the iodide system, V_{NaI} = 55 cm.^{3}, the chloride and bromide being intermediate (V_{NaCl} = 38 cm.^{3}, V_{NaBr} = 45 cm.^{3}). Plots of temperature *vs.* volume fraction instead of mole fraction yield more symmetrical diagrams for the fluoride and iodide systems. Similar relationships were reported for the potassium systems.[4] In evaluating the significance of these observations, it must be remembered, however, that molar volume is only one of several variables affecting the forces determining the degree of mixing of different kinds of molecules. Qualitatively, however, the influence of the volume ratio upon the symmetry of the liquid–liquid phase equilibria is undeniably an important one.[6]

Acknowledgment.—Considerable assistance of J. E. Sutherland in the experimental work, as well as helpful discussions with Professor William T. Smith, Jr., Chemistry Department, University of Tennessee and with J. W. Johnson, a former associate, are gratefully acknowledged.

(6) *Cf. e.g.*, J. H. Hildebrand and R. L. Scott, "The Solubility of Non-Electrolytes," Third Edition, Reinhold Publ. Corp., New York, N. Y., 1950.

A PHYSICO-CHEMICAL STUDY OF THE SYSTEM DIPHENYLMETHANE–DIPHENYL ETHER[1]

BY ROBERT H. DETTRE[2]

Contribution from the Department of Chemistry, The Johns Hopkins University, Baltimore, Maryland

Received June 29, 1959

Freezing point, density, viscosity and refractive index values are reported for the system diphenylmethane–diphenyl ether over the entire range of composition. Activity coefficients, volume changes on mixing and excess free energies of mixing have been calculated. The volumes of mixing are compared with those calculated from the excess free energies of mixing. The experimental fluidities are compared with those obtained from various theoretical considerations. The results show that the system exhibits a slight negative deviation from ideal behavior.

This system is one in which the two components are very similar in molecular size and geometry. Their freezing points are within 1.7° and their boiling points are within 6.5° of each other; their heats of vaporization are within 150 cal./mole. The system does not form solid solutions and the solid–liquid equilibrium diagram is a simple eutectic.[3] It was considered of interest to study this system to determine the direction and magnitude of deviations from ideal behavior.

Experimental

Materials.—The method of purification and purity of the diphenylmethane and diphenyl ether have been discussed in a previous publication.[4]

The water used for calibration in density and viscosity determinations had been recently distilled; it was free of dissolved gases.

Apparatus and Procedure.—With the freezing point apparatus and methods previously described,[4] the results listed in Table I were obtained.

The density and viscosity measurements were made in a constant temperature bath controlled at 24.9 ± 0.05°.

TABLE I

FREEZING POINTS OF DIPHENYLMETHANE (1) AND DIPHENYL ETHER (2) SOLUTIONS

x_2	F.p., °C.	Method[a]	x_2	F.p., °C.	Method[a]
0.0000	25.248 ± 0.002	A	0.5110	−1.18 ± 0.01	C
.0042	25.086 ± .002	A	.5442	1.30 ± .02	B
.0217	24.396 ± .005	A	.6016	5.37 ± .01	B
.0514	23.218 ± .005	A	.6525	8.68 ± .01	B
.1059	20.95 ± .01	A	.7008	11.76 ± .01	B
.1531	18.87 ± .01	A	.8014	17.36 ± .01	B
.2078	16.35 ± .01	A	.8617	20.44 ± .01	A
.3068	11.44 ± .01	B	.8870	21.66 ± .01	B
.3534	8.86 ± .01	B	.8915	21.91 ± .01	A
.4038	5.80 ± .01	B	.9493	24.620 ± .005	A
.4432	3.39 ± .01	B	.9749	25.791 ± .002	A
			1.0000	26.897 ± .002	A

[a] A, extrapolation of the equilibrium portion of the cooling curve[5] and correction for undercooling[6]; B, constant temperature differential freezing points extrapolated to zero cooling rate[4]; C, eutectic point, a constant maximum in the cooling curve; concentration obtained by extrapolation of points on both sides of the eutectic point.

Densities were determined using a 25-ml. Gay-Lussac specific gravity bottle. Measurements were made on solutions which had been freshly prepared by direct weighing into glass stoppered flasks. Weighings were made using calibrated weights; all weights were corrected to vacuum.

Several Ostwald–Cannon–Fenske viscometers were used in the viscosity determinations. Three to five efflux times were taken on each solution with agreement to 0.1 second.

(1) Taken in part from a dissertation submitted in partial fulfillment of the requirements for the degree of Doctor of Philosophy at The Johns Hopkins University. This research was supported in part by the United States Air Force Office of Scientific Research of the Air Research and Development Command under contract No. AF 18(600)-765. Grateful acknowledgment is made of fellowships from the Procter and Gamble Company and the Kennecott Copper Corporation.

(2) Organic Chemicals Department, E. I. du Pont de Nemours and Company, Inc., Wilmington, Delaware.

(3) A. Lüttringhaus, *Ann.*, **528**, 223 (1937).

(4) R. H. Dettre and D. H. Andrews, THIS JOURNAL, **62**, 559 (1958).

(5) W. J. Taylor and F. D. Rossini, *J. Research Natl. Bur. Standards*, **32**, 197 (1944).

(6) B. J. Mair, A. R. Glassgow and F. D. Rossini, *ibid.*, **26**, 591 (1941).

The efflux times were between 170 and 230 seconds. The volume of liquid used for each measurement was 10 ml. At least two viscometers were used at each concentration in order to check results; agreement was within 0.002 centipoise. The viscosities listed in Table II were obtained from the relative (to water) values using 0.8958 centipoise as the viscosity of water.

TABLE II

DENSITY, VOLUME OF MIXING AND VISCOSITY OF DIPHENYLMETHANE (1) AND DIPHENYL ETHER (2) SOLUTIONS AT 25°

x_2	Density, d^{25}_4, g./ml.	ΔV^M, ml./mole	Viscosity η, cp.
0.0000	1.0021[a]	0	2.797
.2070	1.0159	−0.039	2.987
.4186	1.0301	− .033	3.178
.5057	1.0362	− .051	3.258
.6129	1.0436	− .055	3.348
.6974	1.0493	− .022	3.414
.8001	1.0566	− .028	3.496
1.0000	1.0707[b]	0	3.642

[a] Previously reported values for the density of diphenylmethane are d^{25}_4 1.0019[7] and 1.0024.[9] [b] Previously reported values for the density of diphenyl ether are d^{25}_4 1.0704[8] and 1.0706.[10]

Refractive index was measured at 24 ± 0.1° with an Abbe refractometer.

Both diphenylmethane and diphenyl ether, whose freezing points are above 25°, remained in the undercooled state long enough to carry out the above measurements on them.

Calculated Properties.—The activity coefficient of the component that freezes out was calculated at each measured freezing point using the equation

$$\frac{d \ln a_i}{dT} = \frac{\Delta H_i^f}{RT^2} \quad (1)$$

where a_i is the activity of component i and is equal to the product of the activity coefficient γ_i, and the mole fraction x_i. The heat of fusion ΔH_i^f is expressed as a function of temperature using the Kirchhoff equation

$$\left(\frac{\partial \Delta H_i^f}{\partial T}\right)_p = \Delta C_{pi} \quad (2)$$

where ΔC_{pi}, the difference in heat capacity between solid and liquid phases, is also expressed as a function of temperature. The heat capacity and heat of fusion used for diphenyl ether are

$$\Delta H^f = 4114.7 \text{ cal./mole}^{11}$$

C_p(solid) = $(-4.596 + 0.1889T)$ cal./deg. mole (from −3° to m.p.)[11]

C_p(liquid) = $(31.949 + 0.1072T)$ cal./deg. mole (from m.p. to 100°)[11]

The corresponding values for diphenylmethane are

$$\Delta H^f = 4601.6 \text{ cal./mole}^{13}$$

C_p(solid) = $(47.06 - 0.2340T + 0.000904T^2)$ cal./deg. mole (from −10° to m.p.)[12,13]

C_p(liquid) = $(33.46 + 0.1054T)$ cal./deg. mole (from m.p. to 40°)[13]

The activity coefficients were corrected to 25° in the following manner. Assuming ideal entropy of mixing

$$\overline{\Delta H_i^M} = \overline{\Delta F_i^E} = RT \ln \gamma_i \quad (3)$$

where $\overline{\Delta H_M^j}$ is the partial molar heat of mixing and $\overline{\Delta F_i^E}$ is the partial molar excess free energy of mixing of component i. $\overline{\Delta H_i^M}$ was then used to correct the activity coefficient to 25° using the equation

$$\frac{d \ln \gamma_i}{dT} = -\frac{\overline{\Delta H_i^M}}{RT^2} \quad (4)$$

The maximum correction in γ_i (occurring at the eutectic point) is less than 0.1%. Over the range $x_2 = 1$ to 0.5110, values for γ_1 were obtained from those of γ_2 and over the range $x_2 = 0.5110$ to 0, γ_2 values were obtained from those of γ_1 by graphical integration of the Gibbs–Duhem equation.

The excess free energy of mixing ΔF^E was calculated using the equation

$$\Delta F^E = RT \sum_i x_i \ln \gamma_i \quad (5)$$

The volume change on mixing ΔV^M was calculated using the density data.

The estimated uncertainties in the various properties of the system are: 5% for ΔF^E, approximately 0.1% for γ_i, ±0.01 ml./mole for ΔV^M, ± 0.00007 g./ml. for d^{25}_4, ± 0.00008 mole fraction for x_i, ± 0.01 centipoise for η and ±0.0001 for $n^{24}D$.

Results

The following equation[14] was obtained from a least squares fit of the values of ΔV^M listed in Table II.

$$\Delta V^M = -x_1 x_2[0.186 + 0.053(x_1 - x_2)] \quad (6)$$

The standard deviation of the experimental values from those of equation 6 is ± 0.011 ml./mole. Multiplication of equation 6 by $n_1 + n_2$, the total number of moles, and partial differentiation of the right-hand side of the resulting expression with respect to the number of moles of each component will give the partial molar volume changes

$$\overline{\Delta V_1^M} = \bar{V}_1 - V_1^0 = -0.343x_2^2 + 0.210x_2^3 \quad (7)$$

$$\overline{\Delta V_2^M} = \bar{V}_2 - V_2^0 = -0.028x_1^2 - 0.210x_1^3 \quad (8)$$

where V_1^0 and V_2^0 are the molar volumes of the pure components and $\bar{V}_1$ and $\bar{V}_2$ are their partial molar volumes.

The activity coefficients listed in Table III are smoothed values obtained from the best curves through plots of γ_i against composition. These values were used to calculate the excess free energies of mixing given in Table III. The following equation fits these values to within the estimated uncertainty in ΔF^E

$$\Delta F^E = -x_1 x_2[30.3 + 3.7(x_1 - x_2) + 3.6(x_1 - x_2)^2] \quad (9)$$

It has been shown that if the entropy of mixing is ideal[15,16]

$$\overline{\Delta V_i^M} = \beta_0 \overline{\Delta F_i^E} \quad (10)$$

where β_0 is the volume fraction average of the coefficient of compressibility. For non-polar liquids[17]

$$\beta \cong \frac{\alpha T}{\delta^2} \quad (11)$$

where α is the coefficient of thermal expansion and δ is the solubility parameter.[18] The coefficients

(7) R. R. Dreisbach, "Physical Properties of Chemical Compounds," Advances in Chemistry Series, No. 15, American Chemical Society, Washington, D. C., 1955, p. 518.

(8) Ref. 7, p. 521.

(9) A. Riedinger, *Physik. Z.*, **39**, 380 (1938).

(10) J. Kendall and A. H. Wright, *J. Am. Chem. Soc.*, **42**, 1778 (1920).

(11) G. F. Furukawa, D. C. Ginnings, R. E. McCoskey and R. A Nelson, *J. Research Natl. Bur. Standards*, **46**, 195 (1951).

(12) H. M. Huffman, G. S. Parks and A. C. Daniels, *J. Am. Chem. Soc.*, **52**, 1547 (1930).

(13) L. J. Todd, R. H. Dettre and D. H. Andrews (to be published).

(14) The form of the equation is due to G. Scatchard, *Chem. Revs.*, **44**, 7 (1949).

(15) G. Scatchard, *Trans. Faraday Soc.*, **33**, 160 (1937).

(16) J. H. Hildebrand and R. L. Scott, "The Solubility of Nonelectrolytes," Reinhold Publ. Corp., New York, N. Y., 1950, p. 141.

(17) Ref. 16, p. 429.

(18) Ref. 16, p. 129.

TABLE III

THERMODYNAMIC PROPERTIES OF DIPHENYLMETHANE (1) AND DIPHENYL ETHER (2) SYSTEM AT 25°

x_2	γ_1	γ_2	ΔF^E, cal./mole
0.0000	1.0000	....	0
.0500	0.9998	0.9460	−1.77
.1000	.9991	9530	−3.34
.1500	.9982	9596	−4.59
.2000	.9970	9657	−5.56
.2500	.9958	.9712	−6.24
.3000	.9941	.9761	−6.73
.3500	.9921	.9806	−7.12
.4000	.9898	.9845	−7.36
.4500	.9873	.9876	−7.48
.5000	.9845	.9902	−7.57
.5500	.9816	.9922	−7.47
.6000	.9789	.9940	−7.18
.6500	.9762	.9954	−6.78
.7000	.9735	.9964	−6.25
.7500	.9710	.9974	−5.54
.8000	.9685	.9982	−4.67
.8500	.9661	.9989	−3.65
.9000	.9636	.9994	−2.50
.9500	.9611	.9998	−1.31
1.0000	....	1.0000	0

of thermal expansion obtained from the change in density with temperature are

$\alpha_1^{25} = 7.98 \times 10^{-4}$ deg.$^{-1}$ for diphenylmethane[7]
$\alpha_2^{25} = 8.13 \times 10^{-4}$ deg.$^{-1}$ for diphenyl ether[8]

The solubility parameters as calculated from the heats of vaporization at 25°[7,8] are

$\delta_1^{25} = 9.573$ cal.$^{1/2}$/ml.$^{1/2}$
$\delta_2^{25} = 9.851$ cal.$^{1/2}$/ml.$^{1/2}$

It is apparent from the above values that $\beta_1 = \beta_2 = \beta_0$ is a good approximation. Using 0.00255 ml./cal. for β_0 in equation 10 gives at $x = 0.5$ a value for ΔV^M of −0.02 ml./mole. ΔV^M from equation 6 is −0.046 ml./mole at $x = 0.5$.

The observed fluidity ϕ of the solution was compared with that calculated for "ideal" behavior from[19]

$$\phi = x_1\phi_1 + x_2\phi_2 \qquad (12)$$

and from[10,20]

$$\log \phi = x_1 \log \phi_1 + x_2 \log \phi_2 \qquad (13)$$

where ϕ_1 and ϕ_2 are the fluidities of the pure components. The mixture exhibits slight negative deviations with respect to both of these equations. The difference between observed and calculated values at $x = 0.5$ is 2.8% using equation 12 and 1.8% using equation 13. Using the following formula[21]

$$\log \phi = x_1 \log \phi_1 + x_2 \log \phi_2 + \frac{\Delta F^E}{(2.303)(2.45)RT} \qquad (14)$$

and values for ΔF^E from Table II, the calculated fluidity is greater than the observed by 1.2% at $x = 0.5$. The viscosities η of the mixtures were found to obey an equation proposed by Ishikawa[22]

$$\frac{x_1}{x_2}\frac{\eta - \eta_1}{\eta_2 - \eta} = K \qquad (15)$$

where η_1, and η_2 are the viscosities of the pure components and the constant K is equal to 1.16 ± 0.03.

The fluidity calculated using the equation[23]

$$\eta^{1/3} = x_1\eta_1^{1/3} + x_2\eta_2^{1/3} \qquad (16)$$

is greater than the observed by 1.5% at $x = 0.5$ and a formula proposed by Lima[24] gives a fluidity greater than the observed by 8% at $x = 0.5$.

Refractive index values for the system at 24° are given in Table IV. A linear relationship between mole fraction and refractive index is observed. Molar refractions for pure components and mixtures were calculated.[25,26] Molar refraction is also a linear function of x_i. For example, at $x_2 = 0.5057$ the molar refraction $R_{1,2}$ as calculated from the refractive index of the mixture, is 54.08 ml. and that calculated from a linear combination of the molar refractions of the pure components ($R_1 = 55.45$ ml.; $R_2 = 52.77$ ml.) is 54.09 ml.

TABLE IV

REFRACTIVE INDEX OF DIPHENYLMETHANE (1) AND DIPHENYL ETHER (2) SOLUTIONS AT 24°

x_2	Refractive index, $n^{24}D$	x_2	Refractive index, $n^{24}D$
0.0000	1.5751	0.6508	1.5775
.3068	1.5762	0.8617	1.5781
.4432	1.5767	1.0000	1.5787
.5461	1.5771		

Discussion

The negative deviation from ideal behavior is presumably due to hydrogen bond formation. Since the deviation is small, the extent of the interaction should be small. By fitting the activity coefficients to an equation proposed by Mastrangelo,[27] one can conveniently obtain an estimate of the equilibrium constant ($K = a_{1,2}/a_1a_2$) for hydrogen bonding. A functionality f equal to 1.0 (corresponding to one interaction site per molecule)[27] was obtained and the following equations were found to give the best fit to the observed values

$$\gamma_1 = 0.9563 + 0.0720a_1 - 0.0283a_1^2 \qquad (17)$$
$$\gamma_2 = 0.9465 + 0.1111a_2 - 0.0576a_2^2 \qquad (18)$$

A comparison between these values and those observed is given in Table V. The equilibrium constant calculated[27] from equation 17 is 0.042 and from equation 18 it is 0.058.

(19) E. C. Bingham, *Am. Chem. J.*, **35**, 195 (1906).

(20) (a) J. Kendall, *Medd. Vetenskapsakad. Nobelinst.*, **2**, 1 (1913); (b) J. Kendall and K. P. Monroe, *J. Am. Chem. Soc.*, **39**, 1787 (1917).

(21) (a) R. E. Powell, W. E. Roseveare and H. Eyring, *Ind. Eng. Chem.*, **33**, 430 (1941); (b) W. E. Roseveare, R. E. Powell and H. Eyring, *J. App. Phys.*, **12**, 669 (1941); (c) S. Glasstone, K. J. Laidler and H. Eyring, "The Theory of Rate Processes," McGraw-Hill Book Co., New York, N. Y., 1941, p. 514.

(22) (a) T. Ishikawa, *Bull. Chem. Soc. Japan*, **31**, 791 (1958); (b) **4**, 5 (1929); (c) **5**, 47 (1930).

(23) J. Kendall and K. P. Monroe, *J. Am. Chem. Soc.*, **43**, 115 (1921).

(24) (a) F. W. Lima, *J. Chem. Phys.*, **19**, 137 (1951); (b) THIS JOURNAL, **56**, 1052 (1952).

(25) See "Physical Methods of Organic Chemistry," A. Weissberger (ed.), Vol. I, Part II, Interscience Publishers, Inc., New York N. Y., 1949, p. 1170.

(26) In these calculations the density of each mixture was corrected to 24° by assuming that its temperature coefficient of density is the same as those of the pure components. The coefficients for the pure components are almost identical (see ref. 7 and 8).

(27) S. V. R. Mastrangelo, THIS JOURNAL, **63**, 608 (1959).

TABLE V

COMPARISON OF ACTIVITY COEFFICIENTS IN DIPHENYLMETHANE–DIPHENYL ETHER

	γ_1(Diphenylmethane)				γ_2(Diphenyl ether)			
x_2	Obsd.	Eq. 17	Eq. 19	Eq. 21	Obsd.	Eq. 18	Eq. 20	Eq. 22
0.0000	1.0000	1.0000	1.0000	1.0000	(0.9382)	(0.9465)	(0.9511)	(0.9380)
.1000	0.9991	0.9982	0.9995	0.9991	.9530	.9564	.9597	.9541
.2000	.9970	.9957	.9981	.9968	.9657	.9657	.9677	.9668
.3000	.9941	.9929	.9956	.9935	.9761	.9741	.9749	.9767
.4000	.9898	.9890	.9921	.9894	.9845	.9812	.9813	.9842
.5000	.9845	.9849	.9875	.9848	.9902	.9873	.9869	.9899
.6000	.9789	.9802	.9819	.9798	.9940	.9922	.9915	.9940
.7000	.9735	.9749	.9752	.9746	.9964	.9965	.9951	.9969
.8000	.9685	.9692	.9674	.9693	.9982	.9985	.9978	.9987
.9000	.9636	.9630	.9585	.9639	.9994	.9998	.9994	.9997
1.0000	(.9585)	(.9563)	(.9484)	(.9585)	1.0000	1.0000	1.0000	1.0000

If hydrogen bonding between unlike molecules were the only interaction taking place, then, since $f = 1$, equations 17 and 18 would be symmetrical. The asymmetry indicated by equations 17 and 18 is also present in the partial molar volume changes given by equations 7 and 8 and is similar to that of the system chloroform–actone[28] where diphenylmethane is analogous to chloroform and diphenyl ether is analogous to acetone.

The equations proposed by Hildebrand for regular solutions permit asymmetry.[29] For this system the equations are

$$\log \gamma_1 = -0.0230_1 \left[\frac{x_2}{1.056_2 x_1 + x_2}\right]^2 \quad (19)$$

$$\log \gamma_2 = -0.0218_9 \left[\frac{1.056_2 x_1}{1.056_2 x_1 + x_2}\right]^2 \quad (20)$$

where $V_1/V_2 = 0.0230_1/0.0218_9$. In Table V the activity coefficients calculated from equations 19 and 20 are compared with the observed values.

The best agreement is obtained by assuming a greater "effective" volume q_2 for diphenyl ether than for diphenylmethane.[30] The above equations then become

$$\log \gamma_1 = -0.0184_0 \left[\frac{1.510_3 x_2}{x_1 + 1.510_3 x_2}\right]^2 \quad (21)$$

$$\log \gamma_2 = -0.0278_0 \left[\frac{x_1}{x_1 + 1.510_3 x_2}\right]^2 \quad (22)$$

where $q_2/q_1 = 0.0278_0/0.0184_0$. A comparison with the observed values is given in Table V. The physical meaning of the above assumption concerning "effective" volumes is not clear.[30]

The observed asymmetry is in the direction that one would expect if diphenyl ether were more self-associated than diphenylmethane. This seems reasonable since diphenyl ether has a larger liquid density and a higher viscosity (see Table II) while both molecules have similar molecular geometry.

Acknowledgments.—Grateful acknowledgment is made to Dr. Daniel R. Stull of the Dow Chemical Company and Mr. Delmo P. Enagonio of the National Bureau of Standards for providing the materials used for the measurements and to Professor Donald H. Andrews for his helpful suggestions.

(28) J. Zawidski, *Z. physik. Chem.*, **35**, 129 (1908).

(29) Ref. 16, p. 180.

(30) Ref. 16, p. 181.

THE MAGNETIC RESONANCE PROPERTIES OF SOME SANDWICH COMPOUNDS

BY RICHARD E. ROBERTSON[1] AND HARDEN M. MCCONNELL[2]

Gates and Crellin Laboratories of Chemistry,[3] California Institute of Technology, Pasadena, California

Received July 1, 1959

In developing a theory of the magnetic resonance properties of the sandwich molecules and ions containing the transition metals titanium to nickel, the ionic model is treated first. This leads to a conservation of orbital angular momentum about the symmetry axis. With the exception of $Ti(cp)_2$ and $Mn(cp)_2$, the observed magnetic susceptibility data indicate that the metal orbitals beyond argon form a group of three close, low-lying, 3d-type orbitals, with the others considerably higher; and electrons are added to the three lower orbitals according to Hund's rule. A general "covalent" model is also considered. While with this model orbital angular momentum about the symmetry axis is not conserved, it need not be zero. Again, the three low-lying orbital scheme is retained: the former high-lying $3d_{\pm 1}$ orbitals are now replaced by the $3d_{\pm 1}'$* antibonding orbitals. With the two models of bonding there are obtained expressions in first order for the g-factors and zero-field splittings of the sandwich compounds. Because of the uncertainties involved with the models, these parameters are somewhat indefinite; but the basis is set for interpretation as more experimental results become available. Hyperfine structure is commented upon briefly, again as the ground work for later experimental results.

Introduction

Magnetic resonance properties are intimately related to the electronic structure of molecules. We are restricting our attention to the sandwich molecules and ions of the transition metals titanium to nickel. Therefore, to pursue the calculation of the magnetic resonance properties it is important to study first the electronic structure. Many workers have studied the electronic structure of the sandwich molecules (the bis-cyclopentadiene metal

(1) General Electric Charitable and Educational Fund Fellow, 1958–1959.

(2) Alfred P. Sloan Fellow.

(3) Contribution No. 2477.

and dibenzene metal molecules)[4-8] from the ionic models of Liehr and Ballhausen[5] and Matsen[6] to the covalent models of Ruch[7] and Dunitz and Orgel.[8] We shall begin our discussion of the electronic structure with the ionic model for the dicyclopentadienyl molecules. This serves as an introduction to the covalent model. The discussion of the electronic structure, although somewhat qualitative, is used in obtaining expressions for the magnetic resonance properties.

The calculation of the magnetic resonance properties is based on the work of Abragam and Pryce.[9] While these authors used the atomic states (total L and S) of the ions as the basis functions, we shall use basis functions which are products or sums of products of one-electron orbitals. This is just the difference between weak and strong ligand field theory.

Electronic Structure

Ionic Model.—Before proceeding to the more general electronic structure of the sandwich molecules, the covalent model, we shall consider the purely ionic model. However, the present section is not applicable to the dibenzene compounds, for these molecules can in no sense be considered as ionic. For convenience in the following, we shall write "cp" for the cyclopentadienide ion.

The ligand field potential acting on the metal ion is $K(r', \theta', \phi')$. The first-order energy change and hence the splitting is obtained from

$$W' = \langle \xi' | K | \xi'' \rangle \qquad (1)$$

where $|\xi'>$ and $|\xi''>$ represent the manifold of 3d, 4s and 4p orbitals. Because of the particular symmetry of the ligand field, it is convenient to write $K(r', \theta', \phi')$ as an expansion of spherical harmonics (Y_{lm}), each multiplied by a radial function of the form $r_<^{\,l}/r_>^{\,l+1}$, where $r_<$ and $r_>$ are, respectively, the lesser and greater of the distances from the origin to the field and ligand points. Since K represents the ligand field, it must have the symmetry of the ligand field. Therefore, only spherical harmonics with l even will occur in the expansion of K because the molecule will have either a center of inversion (if the cp rings are staggered) or a plane of symmetry parallel to the rings (if the cp rings are eclipsed). Also, K must have the same rotational symmetry as the ligand field. Thus, m must be zero or a multiple of five. Although K is an expansion in an infinite set of spherical harmonics, equation 1 vanishes for $l > 4$ because of the limited set of orbitals under consideration. This leads to result

$$\langle \xi' | [l_z, K] | \xi'' \rangle = 0 \qquad (2)$$

This means that our limited set of orbitals "see" only a cylindrical potential and, hence, the orbital angular momentum about the symmetry axis is a good quantum number in this approximation.

Having discussed the general form of K, it is convenient to replace the actual ligands by a simple distribution of charge. We could replace each carbon atom by a point charge; however, because of the cylindrical symmetry seen by our set of orbitals, we shall replace the cp rings by circular line charges each of charge $-q$. K then is given by

$$K(r', \theta', \phi') = -2q \left\{ 2\sqrt{\pi}\,\frac{1}{r_>}\,Y_{0,0}(\theta', \phi') + \sqrt{\frac{\pi}{5}}\,\frac{r_<^{\,2}}{r_>^{\,3}}\left(1 - \frac{3}{2}\gamma^2\right) Y_{2,0}(\theta', \phi') + \frac{\sqrt{\pi}}{12}\,(8 - 40\gamma^2 + 35\gamma^4)\,\frac{r_<^{\,4}}{r_>^{\,5}}\,Y_{4,0}(\theta', \phi') \right\} \qquad (3)$$

where

$$\gamma = \sqrt{1 - \cos^2\theta_0} \qquad (4)$$

$$= 0.851 b/r_0 \qquad (5)$$

θ_0 is the angle between the symmetry axis and one line charge, b is the C–C bond distance in the cyclopentadienide ring and r_0 is the distance from the origin to the line charge. Equation 5 results from our setting the radius of the circular line charge equal to the distance from the center of the cyclopentadienide ring to a carbon atom.

Because of the explicit dependence of equation 3 on γ, we have calculated the splitting of the 3d orbitals for various values of this parameter. To make the calculation systematic, we have chosen to keep the radius of the ring charge constant (b = 1.41 Å.) and vary r_0 by moving the rings closer to the metal ion. These results are shown in Fig. 1. We have calculated these results using the 3d radial function for Mn^{+2} given by Hartree.[10] The

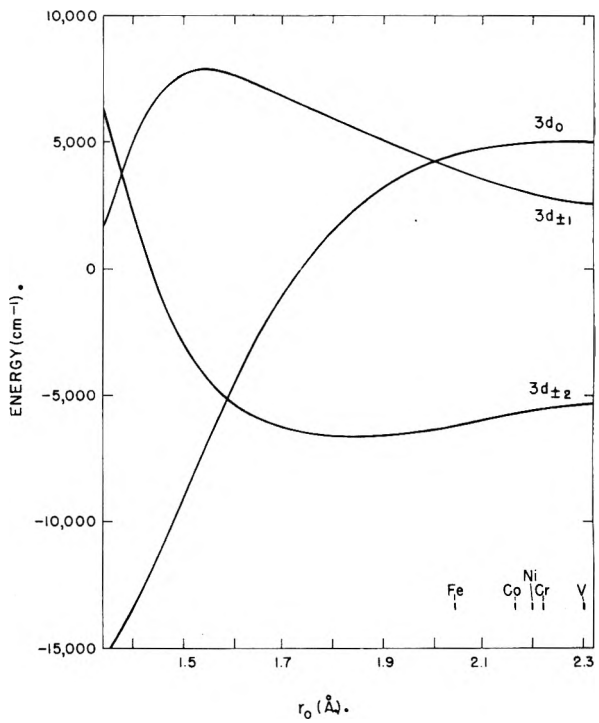

Fig. 1.—Splitting of the 3d-orbitals under K. The energy units are for unit charge $-e$ on each ring. r_0 is the distance between the charge rings and the metal atom; and the lines marked V, Cr, Fe, Co and Ni represent taking the charge ring at the carbon–metal distance for the respective molecules.

(4) W. Moffitt, *J. Am. Chem. Soc.*, **76**, 3386 (1954).
(5) A. D. Liehr and C. J. Ballhausen, *Acta Chem. Scand.*, **11**, 207 (1957).
(6) F. A. Matsen, *J. Am. Chem. Soc.*, **81**, 2023 (1959).
(7) E. Ruch, *Rec. trav. chim.*, **75**, 638 (1956).
(8) J. D. Dunitz and L. E. Orgel, *J. Chem. Phys.*, **23**, 954 (1955).
(9) A. Abragam and M. H. L. Pryce, *Proc. Roy. Soc.* (*London*), **A205**, 135 (1950).
(10) D. R. Hartree, "The Calculation of Atomic Structures," John Wiley and Sons, Inc., New York, N. Y., 1957, pp. 166–173.

energy units of Fig. 1 are based on letting $|q| = |e|$, the electronic charge. The orbitals are denoted by the subscript which is the orbital angular momentum about the symmetry axis in terms of $\hbar$. The carbon–metal distances for $V(cp)_2$, $Cr(cp)_2$, $Fe(cp)_2$, $Co(cp)_2$ and $Ni(cp)_2$ are also shown in Fig. 1. However, because the π-electrons of the aromatic rings are distributed in regions closer than the carbon–metal distance to the metal ion, it may be better to evaluate the 3d-orbital splitting of these molecules with r_0 between 1.5 and 1.7 Å. This corresponds to taking the ring charges about 0.8 Å. closer than the aromatic groups to the metal ion. Although we have calculated only the splitting of the 3d orbitals, it should be pointed out that K mixes the 4s and $3d_0$ orbitals. These are the only orbitals that mix under K. This will then lower the energy of the $(3d_0 - 4s)$ mixed orbital.

From these considerations, we shall assume that the $3d_0$ and $3d_{\pm 2}$ orbitals lie close together while the $3d_{\pm 1}$ orbitals are considerably higher in energy. We shall now proceed to show that this assumption is borne out by the observed magnetic susceptibilities.

The experimental values of the magnetic susceptibility can be expressed in terms of effective magnetic moments by the relation

$$\mu = [3kT\chi/N]^{1/2}\beta \qquad (6)$$

In equation 6 χ is the magnetic susceptibility corrected for the diamagnetism of the ligands, k is the Boltzmann constant, T is the absolute temperature, N is Avogadro's number and β is the Bohr magneton. The effective magnetic moments for the sandwich compounds are given in Table I.

TABLE I

EXPERIMENTALLY MEASURED MAGNETIC MOMENTS OF THE SANDWICH COMPOUNDS

Compd.[i]	No. of d-elect.	μ expt. (β)	μ spin only (β)
$Ti(cp)_2^{++}$	0	0[a]	0
$Ti(cp)_2^{+}$	1	2.29 ± 0.05[b]	1.73
$V(cp)_2^{++}$	1	1.90 ± 0.05[b]	1.73
$Ti(cp)_2$	2	0[c]	0
$V(cp)_2^{+}$	2	2.86 ± 0.06[b]	2.83
$V(cp)_2$	3	3.84 ± 0.04[d]	3.87
$Cr(cp)_2^{+}$	3	3.73 ± 0.08[e]	3.87
$Cr(cp)_2$	4	3.20 ± 0.16[f]	2.83
$V(bz)_2$	5	1.68 ± 0.08[g]	1.73
$Cr(bz)_2^{+}$	5	1.71[h]	1.73
$Mn(cp)_2$	5	5.71 ± 0.29[i]	5.91
$Fe(cp)_2^{+}$	5	2.34 ± 0.12	1.73
$Cr(bz)_2$	6	0[e]	0
$Fe(cp)_2$	6	0[f]	0
$Co(cp)_2^{+}$	6	0[f]	0
$Co(cp)_2$	7	1.76 ± 0.07[f]	1.73
$Ni(cp)_2^{+}$	7	1.82 ± 0.09[f]	1.73
$Ni(cp)_2$	8	2.86 ± 0.11[f]	2.83

[a] G. Wilkinson and J. M. Birmingham, *J. Am. Chem. Soc.*, 76, 4281 (1954). [b] G. Wilkinson, P. L. Pauson, J. M. Birmingham and F. A. Cotton, *ibid.*, 75, 1011 (1953). [c] A. K. Fischer and G. Wilkinson, *J. Inorg. & Nuclear Chem.*, 2, 149 (1956). [d] E. O. Fischer and W. Hafner, *Z. Naturforsch.*, 9b, 503 (1954). [e] E. O. Fischer and U. Piesberger, *ibid.*, 11b, 758 (1956). [f] F. Engelmann, *ibid.*, 8b, 775 (1953). [g] E. O. Fischer, G. Joos and W. Meer, *ibid.*, 13b, 456 (1958). [h] E. O. Fischer and W. Hafner, *ibid.*, 10b, 665 (1955). [i] E. O. Fischer and H. Leipfinger, *ibid.*, 10b, 353 (1955); $Mn(cp)_2$ was diluted with $Mg(cp)_2$. [j] cp = cyclopentadiene negative ion, bz = benzene.

For the cp sandwich molecules and ions we can discern a general orbit arrangement from Table I: three d-orbitals lie considerably below the other two d-orbitals (we are neglecting the 4s- and 4p-orbitals for the moment, although the 4p-orbitals are presumably considerably higher than the d-orbitals) and electrons are added to the three low-lying d-orbitals according to Hund's rule of maximum multiplicity. There are two exceptions to this general pattern, however. Ti^{+2} has only two d-electrons but it is diamagnetic. This might arise from the interaction with neighboring molecules in the crystal which quenches the spin; although, it may arise from the d_0-orbital being considerably below the $d_{\pm 2}$-orbital. $Mn(cp)_2$ has five unpaired electrons instead of only one. This must arise from the especially great stability of the ^6S state of free Mn^{+2}.

Except for $Ti(cp)_2$, the sandwich ion with two d-electrons has two unpaired electrons, while the compounds with three d-electrons have three unpaired electrons. Except for $Mn(cp)_2$ the cp sandwich molecules with ν d-electrons ($\nu = 4, 5, 6$) have $(6 - \nu)$ unpaired electrons. These latter are $Cr(cp)_2$, $Fe(cp)_2^+$, $Fe(cp)_2$ and $Co(cp)_2^+$. Then the molecules $Co(cp)_2$ and $Ni(cp)_2^+$ with seven d-electrons have only one unpaired electron.

The three low-lying orbitals are not pure 3d-orbitals. One of them is some combination of $3d_0$ and 4s orbitals. The other orbital formed from the $3d_0$ and 4s orbitals must be considerably above the three low-lying orbitals.

We wish to emphasize the closeness of the $3d_0$ and $3d_{\pm 2}$ energy levels and hence the Hund's rule addition of electrons to these orbitals. This is in contrast to Matsen's[6] work where he took the $3d_0$ orbital to be considerably below the other orbitals, although this work parallels the work of Liehr and Ballhausen.[5]

Covalent Model.—In this section we shall discuss the covalent model of the sandwich compounds. This model is a better representation of the sandwich molecules, except $Mn(cp)_2$, which is known to be ionic,[11] than the ionic model considered in the last section. For the covalent model, we shall use molecular orbital theory. The molecular orbitals can be obtained simply in a representation which is diagonal with respect to l_z, the operator for orbital angular momentum about the symmetry axis. This representation lends itself quite nicely to the calculation of the magnetic resonance properties to be considered later.

We shall first form molecular-type orbitals for the aromatic system alone and then combine these with the orbitals of the metal ion to obtain the desired orbitals. For cyclopentadienyl, using the five $2p_z$ orbitals, we get the symmetry orbitals

$$a_1 = \nu_0'\{p_{z1} + p_{z2} + p_{z3} + p_{z4} + p_{z5}\}$$
$$e^m = \nu_m'\{p_{z1} + \omega^m p_{z2} + \omega^{2m} p_{z3} + \omega^{3m} p_{z4} + \omega^{4m} p_{z5}\}$$
$$m = \pm 1, \pm 2 \qquad (7)$$

where $\omega = \exp(i\,2\pi/5)$, the ν's are normalizing factors and the subscripts of p_z number the carbon at-

(11) G. Wilkinson, F. A. Cotton and J. M. Birmingham, *J. Inorg. & Nuclear Chem.*, 2, 195 (1956).

oms around the ring. We have generated these orbitals by using the fivefold rotation operator C_5. Similarly, for benzene we obtain the orbitals

$$\begin{aligned} a_1 &= \nu_0''\{p_{z1} + p_{z2} + p_{z3} + p_{z4} + p_{z5} + p_{z6}\} \\ e^m &= \nu_m''\{p_{z1} + \omega^m p_{z2} + \omega^{2m} p_{z3} + \omega^{3m} p_{z4} + \\ &\qquad \omega^{4m} p_{z5} + \omega^{5m} p_{z6}\} \\ &\qquad m = \pm 1, \pm 2 \qquad (8) \\ b_1 &= \nu_3''\{p_{z1} - p_{z2} + p_{z3} - p_{z4} + p_{z5} - p_{z6}\} \end{aligned}$$

where for benzene $\omega = \exp(i\ 2\ \pi/6)$. The calculated energy for these molecular orbitals is shown in Table II.

TABLE II

AROMATIC MOLECULAR ORBITAL ENERGIES

Cyclopentadienyl		Benzene	
Mol. orb.	Energy	Mol. orb.	Energy
a_1	$Q + 2\beta$	a_1	$Q + 2\beta$
e^{+1}, e^{-1}	$Q + 2\beta \cos\left(\frac{2\pi}{5}\right)$	e^{+1}, e^{-1}	$Q + \beta$
e^{+2}, e^{-2}	$Q - 2\beta \cos\left(\frac{2\pi}{5}\right)$	e^{+2}, e^{-2}	$Q - \beta$
		b_1	$Q - 2\beta$

Q is a constant and β, which is negative, is the usual resonance integral. We can now combine these molecular-type orbitals for the individual aromatic rings into a set of molecular-type orbitals for the aromatic system. We shall assume that the molecule has a center of inversion. We combine each orbital of one ring with the corresponding orbital of the other ring to form two other orbitals which are symmetrical and antisymmetrical with respect to inversion. We shall denote these by the subscripts g and u, respectively. To a first approximation, the g and u aromatic orbitals having the same rotational symmetry remain degenerate.

We now have to combine these aromatic orbitals with the orbitals of the metal ion. Since s- and d-orbitals are symmetrical with respect to inversion, they will combine with g aromatic orbitals, while p-orbitals being antisymmetrical will combine with the u-orbitals. Also, the e^m-aromatic orbitals have been formed so that they have the same rotational symmetry as metal orbitals with the component of orbital angular momentum about the symmetry axis m. We thus obtain the molecular orbitals for the sandwich molecule

$$\begin{aligned} d'_0 &= \nu_0(d_0 + \gamma s + \delta a_{1g}) \\ d'_{\pm 1} &= \nu_1(d_{\pm 1} + \epsilon e_g^{\pm 1}) \\ d'_{\pm 2} &= \nu_2(d_{\pm 2} + \kappa e_g^{\pm 2}) \\ s' &= \nu_3(s + \zeta d_0 + \eta a_{1g}) \qquad (9) \\ a'_{1u} &= \nu_4(a_{1u} + \iota p_0) \\ \bar{e}_u^{\pm 1} &= \nu_5(e_u^{\pm 1} + \lambda p_{\pm 1}) \\ a'_{1g} &= \nu_6(a_{1g} + \mu d_0 + \xi s) \end{aligned}$$

where the ν's are normalizing factors. Except for d'_0 and s', we have defined here only the bonding orbitals: there is an analogous set of antibonding orbitals.

From Table II for the dicyclopentadienyl system, the ground state configuration is $(a_{1g})^2(a_{1u})^2(e_g^{\pm 1}e_u^{\pm 1})^6$ and for dibenzene $(a_{1g})^2(a_{1u})^2(e_g^{\pm 1})^4(e_u^{\pm 1})^4$. Let us now consider the bonding between a metal ion with two electrons beyond argon (*e. g.*, Ti^{+2}) and the dicyclopentadienyl system. Which of the metal orbitals is to be used in bonding will depend on (a) the overlap with the aromatic rings and (b) promotional energy involved in rearranging the electrons in the metal ion and the dicyclopentadienyl system. The overlap between metal and π-orbitals has been calculated by Dunitz and Orgel for ferrocene[5] and is shown in Table III.

TABLE III

OVERLAP BETWEEN METAL AND π-ORBITALS IN FERROCENE

$S(a_{1g}, 3d_0)$	0.01
$S(e_g^{\pm 1}, 3d_{\pm 1})$	.37
$S(e_g^{\pm 2}, 3d_{\pm 2})$	.29
$S(a_{1g}, 4s)$	.50

It appears that the configuration $(a'_{1g})^2(a'_{1u})^2(\bar{e}_u^{\pm 1})^4(d'_{\pm 1})^4$ would be more important than the configuration $(a'_{1g})^2(a'_{1u})^2(\bar{e}_u^{\pm 1})^4(d'_{\pm 2})^4$: first, because $S(e_g^{\pm 1}, d_{\pm 1}) > S(e_g^{\pm 2}, d_{\pm 2})$, and secondly, because the $d'_{\pm 2}$ molecular orbitals are presumably higher energetically than $d'_{\pm 1}$ molecular orbitals. Moffitt[1] has estimated that the $e_g^{\pm 1}$ orbitals of the dicyclopentadienyl system have about the same energy as the $3d_{\pm 1}$ orbitals of iron while the $e_g^{\pm 2}$ orbitals lie considerably above the $d_{\pm 2}$ orbitals. Thus, the $d'_{\pm 1}$ orbitals are almost completely covalent and probably lie below the $d'_{\pm 2}$ molecular orbitals. Then, the orbitals used beyond $Ti(cp)_2^{++}$ will be low-lying d'_0 and $d'_{\pm 2}$ orbitals, the $d'^*_{\pm 1}$ antibonding orbitals, and the s' antibonding orbitals. This also explains how an ionic model gave useful results: the higher $3d_{\pm 1}$ orbitals are now replaced by the $d'^*_{\pm 1}$ antibonding orbitals.

In the dibenzene metal compounds, there may be only one low-lying magnetic orbital, the d'_0-orbital, because from Table I the observed value of the magnetic moment is the same as the spin only value. The use of the $d'_{\pm 2}$-orbitals is of great importance to the stability of the dibenzene molecules as follows from the electroneutrality principle.[12] Charge transferred to the metal atom through the a'_{1g}, a'_{1u}, $\bar{e}_u^{\pm 1}$ and $d'_{\pm 1}$ orbitals is balanced by the charge transferred to the aromatic groups through the $d'_{\pm 2}$ orbitals.

In dealing with the ionic model, we noted that within a limited set of orbitals l_z was conserved. Although with the covalent model l_z is not conserved, the expectation value of l_z is not necessarily zero. This follows from the fact that $(e_g^{+1}|l_z|e_g^{+1})$ is not necessarily zero so we can write

$$(d'_{+1}|l_z|d'_{+1}) = k\hbar \qquad (10)$$

and similar equations for the other orbitals. Here k is less than one, being an orbital angular momentum reduction factor.

Magnetic Resonance Properties

The basis of the electron magnetic resonance experiment is the spin Hamiltonian

$$\begin{aligned} \mathcal{H} &= |\beta|[g_x H_x S_x + g_y H_y S_y + g_z H_z S_z] + \\ &\quad D[S_z^2 - {}^1/_3 S(S+1)] + E(S_x^2 - S_y^2) + \\ &\quad AS_zI_z + BS_xI_x + CS_yI_y \qquad (11) \end{aligned}$$

or with an axis of symmetry

$$\begin{aligned} \mathcal{H} &= |\beta|\ [g_\parallel H_z S_z + g_\perp(H_x S_x + H_y S_y)] - D[S_z^2 - \\ &\quad 1/3S(S+1)] + AS_zI_z + B(S_xI_x + S_yI_y) \qquad (12) \end{aligned}$$

Our concern will be in finding theoretical expressions for the parameters. We shall first treat the

(12) L. Pauling, "Nature of the Chemical Bond," Cornell University Press, Ithaca, New York, 1948, p. 257.

fine structure which involves the g's, D and E and then briefly treat the hyperfine structure later.

Fine Structure.—The g-factors depend upon spin–orbit interaction while the zero-field splitting depends upon both spin–orbit interactions and spin–spin dipole interaction. As the spin–spin dipole interaction is difficult to treat and is small compared with the spin–orbit interaction, we shall say little more about it. It is convenient to treat the ground states of the sandwich molecules as a product or sum of products of one-electron orbitals. Also, we have previously found Hund's rule of maximum multiplicity to hold often within a limited set of orbitals. Then, with these conditions, the g-factors and zero-field splitting are given by

$$g_\mu = 2[1 - (\zeta\Lambda_\mu/2S)],\ \mu = x, y, z \qquad (13)$$
$$D = -(\zeta/2S)^2[\Lambda_z - 1/2(\Lambda_x + \Lambda_y)] \qquad (14)$$
$$E = -1/2(\zeta/2S)^2(\Lambda_x - \Lambda_y) \qquad (15)$$

where S is the total spin, ζ is the one-electron spin–orbit coupling coefficient, and

$$\Lambda_\mu = \sum_{n\neq 0} \sum_i \frac{\langle 0|l_\mu(i)|n\rangle\langle n|l_\mu(i)|0\rangle}{E_n - E_0} \qquad (16)$$

In equation 16 $|0>$ denotes the orbital ground state and $|n>$ the excited orbital state and the operators are summed over the electrons i.

Several comments need be made about these equations. First, they have been diagonalized. This is based on the assumption that any distortion in the molecule will be small. Secondly, these formulas are good only to second order. If the orbital ground state is nearly degenerate, as may be true for several of the sandwich molecules, a better approach is to treat the spin–orbit interaction with a secular equation. However, with the many unknowns concerning the orbitals and their energy, this is not warranted at present.

We shall proceed to enumerate the expressions for the fine structure parameters, assuming the orbital ground state to be non-degenerate; though it may be nearly degenerate, in which case we obtain only a first approximation. To avoid degeneracy, we have at times invoked a distortion. The distortion splits the degeneracy and mixes the orbitals. We have taken the y-axis along the direction of the distortion and the z-axis along the symmetry axis of the molecule. We shall comment briefly on the result of an orbitally degenerate ground state later.

One or Five d-Electrons, the Benzene Compounds, $Ti(C_5H_5)_2^+$, $V(C_5H_5)_2^{++}$ and $Fe(C_5H_5)_2^+$.—With benzene as the ligands, it appears from Table I that the sub-configuration $(d'_{\pm 2})^4(d'_0)$ lies considerably below $(d'_{\pm 2})^3(d'_0)^2$ because the observed magnetic moments are essentially the same as the spin only values. The possible reason for this has been discussed previously. The g-factor is expected to be near 2.00. The g-factor for Cr-$(C_6H_6)_2^+$ has been found to be 1.99.[13–15]

We shall consider $Fe(cp)_2^+$ to have one hole rather than five electrons. The two types of energy level arrangements we shall consider are represented by (I) and (II) for one electron or one hole.

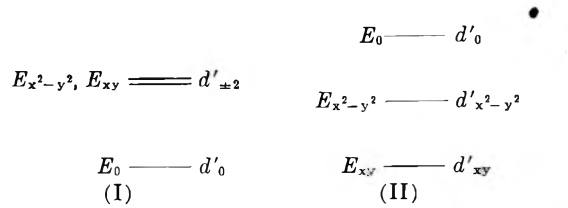

Since d'_0 and $d'_{\pm 2}$ orbitals are not mixed in first order, the orbital arrangement (I) leads to $g \approx 2.00$. If the molecule is distorted slightly, the degenerate $d'_{\pm 2}$-orbitals are split into the corresponding real orbitals, which yield the g-factors for an orbital arrangement analogous to (I).

$$g_x = 2 - 2\zeta\left[\frac{|a|^2}{E_{xy} - E_0} + \frac{|b|^2}{E_{x^2-y^2} - E_0}\right]$$
$$g_y = 2 - 2\zeta\left[\frac{|c|^2}{E_{xy} - E_0} + \frac{|e|^2}{E_{x^2-y^2} - E_0}\right] \qquad (17)$$
$$g_z = 2 - 2\zeta\frac{|f|^2}{E_{xy} - E_0}$$

The orbital arrangement (II) gives

$$g_x = 2 - 2\zeta\frac{|a|^2}{E_0 - E_{xy}}$$
$$g_y = 2 - 2\zeta\left[\frac{|g|^2}{E_{x^2-y^2} - E_{xy}} + \frac{|c|^2}{E_0 - E_{xy}}\right] \qquad (18)$$
$$g_z = 2 - 2\zeta\left[\frac{|k|^2}{E_{x^2-y^2} - E_{xy}} + \frac{|f|^2}{E_0 - E_{xy}}\right]$$

ζ is positive for $Ti(cp)_2^+$ and $V(cp)_2^{++}$ but is negative for $Fe(cp)_2^+$ because of replacing the five electrons by one hole in the latter. For equations 17 and 18, we have let

$$a = (d'_0|l_x|d'_{xy})$$
$$b = (d'_0|l_x|d'_{x^2-y^2})$$
$$c = (d'_0|l_y|d'_{xy})$$
$$e = (d'_0|l_y|d'_{x^2-y^2}) \qquad (19)$$
$$f = (d'_0|l_z|d'_{xy})$$
$$g = (d'_{xy}|l_y|d'_{x^2-y^2})$$
$$k = (d'_{xy}|l_z|d'_{x^2-y^2})$$

While the matrix elements a, b, c, e, f, and g will be small, k will be of the order of one. Thus, the g-factor given by equation 17 will deviate only slightly from 2.0.

Two or Four d-Electrons ($S = 1$), $V(C_5H_5)_2^+$ and $Cr(C_5H_5)_2$.—Again, replacing electrons by holes, we shall represent the four electrons of $Cr(cp)_2$ by two holes. Thus, ζ for $Cr(cp)_2$ will be negative. We shall consider the two types of orbital energy diagrams (III) and (IV).

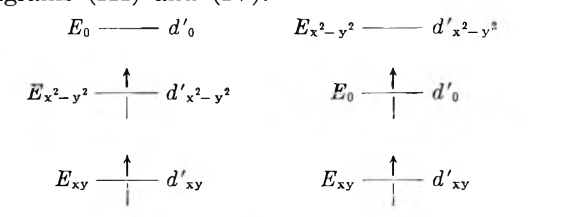

The energy level arrangement (III) leads to

$$g_x = 2 - \zeta\left[\frac{|a|^2}{E_0 - E_{xy}} + \frac{|b|^2}{E_0 - E_{x^2-y^2}}\right]$$
$$g_y = 2 - \zeta\left[\frac{|c|^2}{E_0 - E_{xy}} + \frac{|e|^2}{E_0 - E_{x^2-y^2}}\right] \qquad (20)$$
$$g_z = 2 - \zeta\frac{|f|^2}{E_0 - E_{xy}}$$

(13) R. D. Feltham, P. Sogo and M. Calvin, *J. Chem. Phys.*, **26**, 1354 (1957).

(14) B. Elschner and S. Herzog, *Z. Naturforsch.*, **12a**, 860 (1957).

(15) Tsuetkov, Voevodsky, Rozuvaev, Sorokin and Domrachev, *Doklady Akad. Nauk S.S.S.R.*, **115**, 118 (1957).

while (IV) gives

$$g_x = 2 - \zeta \frac{|b|^2}{E_{x^2-y^2} - E_0}$$
$$g_y = 2 - \zeta \left[\frac{|g|^2}{E_{x^2-y^2} - E_{xy}} + \frac{|e|^2}{E_{x^2-y^2} - E_0} \right] \quad (21)$$
$$g_z = 2 - \zeta \frac{|k|^2}{E_{x^2-y^2} - E_{xy}}$$

where we have used the matrix elements defined by equation 19. Using equations 13–16 the zero-field splitting is given by

$$D = (1/4)\,\zeta[g_z - 1/2(g_x + g_y)] \quad (22)$$
$$E = (1/8)\,\zeta(g_x - g_y) \quad (23)$$

Three d-Electrons ($S = 3/2$), $V(C_5H_5)_2$ and $Cr(C_5H_5)_2^+$.—According to the approximation used thus far, in this case each of the low-lying orbitals would have one electron and the g-factor would be precisely the free spin value. To obtain a g-factor differing from the free spin value requires consideration of the more highly excited orbitals. In view of this, we shall consider a ground state that reflects electron correlation, which has been neglected thus far. The orbital ground state for the three unpaired electrons is

$$|o\rangle = \{ad_{+2}d_0d_{-2} + bd_{+1}d_0d_{-1}\} \quad (24)$$

with the excited states

$$\begin{aligned} |1a\rangle &= \{cd_{+2}d_0d_{-1} + ed_{+2}d_{+1}d_{-2}\} \\ |-1a\rangle &= \{cd_{+1}d_0d_{-2} + ed_{+2}d_{-1}d_{-2}\} \\ |1b\rangle &= \{cd_{+2}d_{+1}d_{-2} - ed_{+2}d_0d_{-1}\} \\ |-1b\rangle &= \{cd_{+2}d_{-1}d_{-2} - ed_{+1}d_0d_{-2}\} \end{aligned} \quad (25)$$

This leads to

$$g_{\parallel} = 2.00 \quad (26)$$

$$g_{\perp} = 2 - (4\zeta/3)\left\{ \frac{[a(c + \sqrt{3/2}e) + bc]^2}{E_{\pm 1a} - E_0} + \frac{[a(e - \sqrt{3/2}c) + be]^2}{E_{\pm 1b} - E_0} \right\} \quad (27)$$

and the zero-field splitting

$$D = (\zeta/3)^2\left\{ \frac{[a(c + \sqrt{3/2}e) + bc]^2}{E_{\pm 1a} - E_0} + \frac{[a(e - \sqrt{3/2}c) + be]^2}{E_{\pm 1b} - E_0} \right\} \quad (28)$$

The observed g-factor for $V(cp)_2$ is 2.00 in solution.[16] Recent measurements[17] of D for diluted crystalline $V(cp)_2$ show it to be fairly large ($\sim$40 kMc.). Such a large zero-field splitting is understandable, for a small difference between $g_{\parallel}$ and $g_{\perp}$ can lead to a large value of D because ζ is large.

Five Unpaired Electrons, $Mn(C_5H_5)_2$.—The ground state of Mn^{+2} in $Mn(cp)_2$ is the ^6S term. Since spin–orbit interaction does not affect the ^6S term, the g-factor is expected to be near 2.00—the observed values are between 1.99 and 2.01.[18] The calculation of the zero-field splitting is different for Mn^{+2} than we have considered previously. Neither spin–orbit interaction alone nor the ligand field alone gives rise to a zero-field splitting, but the combined effects of the two do by consideration of the excited states of the ion.[19]

The lowest order term that does not vanish is the fourth order correction

$$W^{(4)} = \frac{\langle {}^6S|W_{s-0}|{}^4P\rangle\langle {}^4P|K|{}^4D\rangle\langle {}^4D|K|{}^4P\rangle\langle {}^4P|W_{s-0}|{}^6S\rangle}{(E^4_P - E^6_S)^2(E^4_D - E^6_S)} \quad (29)$$

where W_{s-0} is the spin–orbit interaction. It is the $Y_{2,0}(\vartheta', \phi')$ term in K, V_2, which produces the splitting. Letting $V_2 \approx 5\cdot10^3$ cm.$^{-1}$, $\zeta \approx 300$ cm.$^{-1}$, and $(E_{^4P} - E_{^6S}) \approx (E_{^4D} - E_{^6S}) \approx \Delta E \approx 3\cdot10^4$ cm.$^{-1}$

$$D \sim \frac{V_2^2\zeta^2}{(\Delta E)^3} \sim 0.1 \text{ cm.}^{-1} \quad (30)$$

Besides the spin–orbit contribution to the zero-field splitting, there is the magnetic dipole interaction between electron spins. In Mn^{+2} the spin–spin interaction deforms the otherwise spherical symmetry of the ion producing elliptical symmetry. Thus, the combined effects of the spin-spin interaction and the axial field produce a zero-field splitting[20]

$$D \sim \frac{\beta^2\langle r^{-3}\rangle K}{\Delta E} \sim 0.1 \text{ cm.}^{-1} \quad (31)$$

In equation 31 ΔE is the energy difference between the $3d^4\,4s\,{}^6D$ and the $3d^5\,{}^6S$ states and K represents a matrix element of the form $\langle 3d|K|4s\rangle$. Since the zero-field splitting term D in equation 30 usually enters with the opposite sign from D in equation 31,[20] the zero-field splitting will probably be of the order of 0.01 cm.$^{-1}$.

Seven d-Electrons ($S = 1/2$), $Co(C_5H_5)_2$ and $Ni(C_5H_5)_2^+$.—With ferrocene the three low-lying orbitals are filled with six electrons. The seventh electron can either be placed in the 4s′ orbital, giving $g = 2.0$, or into one of the d'^*_{xz} or d'^*_{yz} strongly antibonding orbitals. In this latter case we cannot use equations 13 and 16 to compute the g-factor because this does not correspond to Hund's rule of maximum multiplicity in the manifold of d-orbitals. Since there is only one electron in either the d'^*_{xz} or d'^*_{yz} orbitals, we take ζ positive and mix these orbitals with l_z. This yields $g_{\parallel} < 2$. l_x and l_y mix d'^*_{xz}, say, with the d'_0, $d'_{x^2-y^2}$ and d'_{xy} orbitals (which are filled so ζ is taken to be negative), which yields $g_{\perp} > 2$. Since the energy difference between d'^*_{xz} and the d'_0, $d'_{x^2-y^2}$, and d'_{xy} orbitals is probably considerably greater than that between d'^*_{xz} and d'^*_{yz}, the over-all g-factor may be less than 2 for this case.

Eight d-Electrons ($S = 1$), $Ni(C_5H_5)_2$.—We shall first consider the situation where all eight electrons are in d-type orbitals. As with $V(cp)_2$ and $Cr(cp)_2^+$, we shall acknowledge correlation. Replacing the eight electrons by two holes, the ground state has the form

$$|0\rangle = \{ad_{+1}d_{-1} + bd_{+2}d_{-2}\} \quad (32)$$

with excited states

$$\begin{aligned} |1a\rangle &= \{cd_{+1}d_0 + ed_{+2}d_{-1}\} \\ |-1a\rangle &= \{cd_0d_{-1} + ed_{+1}d_{-2}\} \\ |1b\rangle &= \{cd_{+2}d_{-1} - ed_{+1}d_0\} \\ |-1b\rangle &= \{cd_{+1}d_{-2} - ed_0d_{-1}\} \end{aligned} \quad (33)$$

(16) H. M. McConnell, W. W. Porterfield and R. E. Robertson, *J. Chem. Phys.*, **30**, 442 (1959).

(17) W. W. Porterfield and H. Dearman (private communication).

(18) J. Voitländer and E. Schimitschek, *Z. Electrochem.*, **61**, 941 (1957).

(19) J. H. Van Vleck and W. G. Penney, *Phil. Mag.*, **17**, 961 (1934).

(20) M. H. L. Pryce, *Suppl. Nuovo Cimento*, **6**, 817 (1957).

This gives

$$g_{\parallel} = 2.00 \tag{34}$$

$$g_{\perp} = 2 + 2|\zeta| \left\{ \frac{(ac\sqrt{3/2} + eb)^2}{E_{\pm 1a} - E_0} + \frac{(ae\sqrt{3/2} - bc)^2}{E_{\pm 1b} - E_0} \right\} \tag{35}$$

with the zero-field splitting parameter

$$D = (\zeta^2/2) \left\{ \frac{(ac\sqrt{3/2} + eb)^2}{E_{\pm 1a} - E_0} + \frac{(ae\sqrt{3/2} - bc)^2}{E_{\pm 1b} - E_0} \right\} \tag{36}$$

These equations, when multiplied by a suitable reduction factor, correspond to putting the two unpaired electrons into the $d'^{*}_{\pm 1}$ antibonding orbitals.

On the other hand, the two unpaired electrons may go into 4p-type orbitals. Because of the small spin–orbit coupling coefficient for the 4p-type orbitals, the g-factor would be nearly 2.0—possibly a little less. Finally, one electron might go into the 4s′ orbital and the other into a d'^{*}_{xz} or d'^{*}_{yz} antibonding orbital. This last case corresponds to $Ni(cp)_2^+$ and $Co(cp)_2$ as regards g-factor.

Although we have disregarded the spin–spin contribution to the zero-field splitting in most of our work, it gets progressively larger in proceeding from Ti^{+2} to Ni^{+2},[21] and thus may be important in $Ni(cp)_2$. Also, it may well enter with the opposite sign of D obtained from spin–orbit interaction.

Before leaving this fine structure discussion, we shall consider the situation where the orbital ground state is exactly degenerate. The orbital degeneracy is then assumed to be split by spin–orbit interaction to the extent that the Jahn–Teller effect is inoperative. In this situation the g-factor is

$$g_{\parallel} = \langle l_z + 2s_z \rangle / \langle s_z \rangle \tag{37}$$

$$g_{\perp} = 0 \tag{38}$$

so the over-all g-factor is

$$g = g_{\parallel}/\sqrt{3} \tag{39}$$

By calculating the g's in equation 39 for the different states into which the orbital degeneracy is split and averaging over the temperature distribution, a g-factor is obtained which can be compared with the observed magnetic moments in Table I. It is found that if the magnetic moments in Table I are assumed correct that this degenerate situation could only occur in $Fe(cp)_2^+$.

Hyperfine Structure

Hyperfine structure which is the nuclear magnetic effect on the paramagnetic moment of the molecule is derived from two types of interactions.[8] The dipolar interaction between the nuclei and the paramagnetic moment leads to an anisotropic hyperfine structure, while the Fermi contact interaction is isotropic. The nuclei of interest are the protons of the aromatic groups and the central metal atoms. The group of metal atoms can be narrowed even more because only V, Co and Mn combine large natural abundances with large nuclear magnetic moments.

The hyperfine spin-Hamiltonian for the central metal atom is

$$W_{hfs} = (8\pi\gamma\hbar|\beta|/S) \left\langle \sum_i \delta(\mathbf{r}(i)) s_z(i) \right\rangle_{m_s = S} \mathbf{S}\cdot\mathbf{I} + (P/2S) \sum_{\mu = x,y,z} \left\{ \sum_i \langle 3(r_\mu'^2(i)/r^2) - 1 \rangle_{\theta i', \phi i'} - 2\zeta\Lambda_\mu \right\} S_\mu I_\mu \tag{40}$$

where we have diagonalized the dyadic in the braces. This equation neglects the second order term arising from the combined effects of electron-spin nuclear-spin dipolar and spin–orbit interaction.[8] In equation 40

$$P = 2\beta|\gamma\hbar\overline{r^{-3}} \tag{41}$$

and $\langle 3(r_\mu'^2(i)/r^2) - 1 \rangle_{\theta i', \phi i'}$ represents the angular integration of the ith one-electron orbital of the ground state. We shall not proceed any further, however, with the second or anisotropic term in equation 40 but shall concentrate on the Fermi contact term, which is often far more important. This latter causes a splitting that depends on the s-orbital spin density, which in turn arises in two ways. There can be a positive s-orbital spin density from the unpaired electrons having a certain probability of being in the 4s orbital. Also, there can be a negative spin density resulting from the slight exchange polarization of the electron spins in the 1s, 2s, and 3s orbitals due to the paramagnetism of the ion.[22,23]

For an electron in an s-orbital the hyperfine splitting can be obtained from the semi-empirical equation due to Goudsmit.[24] If the unpaired electron in $Co(cp)_2$ goes into the 4s′ orbital rather than into the $3d'^{*}_{xz}$ or $3d'^{*}_{yz}$ antibonding orbitals, we expect a large hyperfine splitting, possibly as large as ~4800 Mc., as would be expected for an electron in the 4s orbital of Co^{+2}. Also, as mentioned before, the 4s orbital can mix with the $3d_0$ orbital under the ligand field. This will contribute to the hyperfine splitting in $V(cp)_2$. Therefore, when due care is taken in correcting for the exchange polarization of the 1s, 2s and 3s electron spins, the amount of mixing of the 4s and $3d_0$ orbitals in $V(cp)_2$ can be calculated from the hyperfine splitting.

By an exchange polarization of the electron spins in the 1, 2 and 3s-orbitals we mean that the electron with spin α is in a slightly different orbital than the corresponding electron with spin β. This is a result of the fact that when the ion has a net spin α, say, there is an exchange integral between this unpaired electron and the electrons with spin α in the 1s, 2s and 3s orbitals, but none between the unpaired electron and the electrons with spin β.[22] The values of the isotropic hyperfine constant a for V^{+2}, Mn^{+2} and Co^{+2} obtained experimentally from a number of ionic molecules are given in Table IV.[25] These values appear to arise from exchange polarization.

TABLE IV

ISOTROPIC HYPERFINE CONSTANTS

Ion	a (Mc.)
V^{+2}	−264
Mn^{+2}	−273
Co^{+2}	−210

The observed hyperfine splitting in $V(cp)_2$[16] of only 77 Mc. in solution can be understood by assuming that there is about 341 Mc./4600 Mc. or

(21) M. H. L. Pryce, *Phys. Rev.*, **80**, 1107 (1950).

(22) V. Heine, *ibid.*, **107**, 1002 (1957).

(23) J. H. Wood and G. W. Pratt, *ibid.*, **107**, 995 (1957).

(24) S. Goudsmit, *ibid.*, **43**, 636 (1933).

(25) A. Abragam, J. Horowitz and M. H. L. Pryce, *Proc. Roy. Soc. (London)*, **A230**, 169 (1955).

about 7.4% 4s-orbital mixed with the $3d_0$ orbital because

$$+341 \text{ Mc.} - 264 \text{ Mc.} = +77 \text{ Mc.} \quad (42)$$

However, it is possible that the splitting is -77 Mc., meaning $187/4600 = 4.1\%$ 4s-orbital is mixed with the $3d_0$ orbital.

For the proton hyperfine structure, we shall again limit ourselves to the isotropic term. The Fermi contact term can act in two ways. First, there is the direct overlap of the metal orbital containing the unpaired electron with the proton. This effect will be small when the metal orbital is made orthogonal to the 1s orbitals (strictly the C–H bond orbitals of the hydrogen atoms as required by the Pauli principle.[26,27] Secondly, there is the indirect contribution which acts through the carbon atoms. This has been considered by McConnell and Chesnut,[28] who give the formula

$$a_N \approx -|Q|\rho_N \text{ gauss} \quad (43)$$

where a_N is the proton hyperfine splitting, ρ_N is the unpaired electron density at the adjacent carbon atom (in a p-orbital) and Q is a constant with the nominal values 22.5. This latter is presumably the principal source of hyperfine splitting in $Cr(C_6H_6)_2^+$ and related benzenoid molecules which have been found to have $|a_N| = 3.5$ gauss.[13-15]

(26) P. O. Lowdin, *J. Chem. Phys.*, **18**, 365 (1950).
(27) W. E. Blumberg and T. P. Das, *ibid.*, **30**, 251 (1959).
(28) H. M. McConnell and D. B. Chesnut, *ibid.*, **28**, 107 (1958).

DYNAMIC STRUCTURE IN DETERGENT FOAMS[1]

BY G. F. DASHER AND A. J. MABIS

The Procter and Gamble Company, Miami Valley Laboratories, Cincinnati 31, Ohio

Received April 16, 1959

Measurements of the quantity of surface active material adsorbed at an air–water boundary, when coupled with analysis of the X-ray diffraction patterns obtained from that same surface, give strong evidence that a hydrous gel structure makes up the surface film in a soap or detergent foam. Detailed data are given for the system sodium alkyl sulfate and fatty alcohol in water solution, and a tentative model for the gel structure is proposed. In systems where the surface active materials are readily dispersible in water, there appears to be no close packing of hydrocarbon chains. It would seem that close packing of hydrocarbon chains in a surface film is a special case, associated only with very insoluble monolayers spread carefully on the surface of the water.

Introduction

At present the generally accepted picture of the surface of a soap or detergent solution involves an oriented monolayer. This layer is usually thought to be of the type demonstrated by Langmuir,[2] as present in carefully spread films of fatty acids on aqueous surfaces. The hydrocarbon chains are pictured as being oriented toward the gas phase with the polar ends oriented toward the water layer. However, there are certain experimental facts which do not appear to be in accord with this picture.

High surface viscosity and a marked elasticity of the film have long been observed in foaming systems. Adsorption measurements have shown that the fatty chains are not sufficiently adsorbed to give a close packed structure if oriented vertically. It is well known that the presence of a soap or detergent film does little or nothing to retard evaporation of water. Only when a film such as that of a fatty alcohol is present, *under a spreading pressure*, do we see appreciable reduction in water evaporation rates. The marked slowing of a torsional disk when oscillating in some surface films is well known. All are familiar with the ability of a bubble to be grossly deformed without rupture. Such high viscosity and elasticity would seem to be phenomena associated with larger scale structures. These observations seem to exclude the existence of simple monolayers and suggest that water, perhaps partly bound in some fashion, might contribute to a fairly extensive structure in a foaming system. There seems to be insufficient organic material to explain the cited phenomena. There have been previous suggestions that water may be involved with the organic material in the interfacial region of soap films.

Schulman and Teorell[3] and also Crisp[4] showed that a thick layer of subphase accompanies the transfer of what has been called a monolayer. This was again reported by Blank and LaMer[5] who showed that monolayer transfer drags a very much thicker layer of subphase with it even against a counter hydrostatic flow of the subphase.

It has also been suggested by many authors that the interface *per se* may exert an orienting effect over considerable distances. These distances are considerably larger than can be accounted for by London–van der Waals type forces. Henniker[6] has compiled an excellent review of the experimental evidence for the existence of long range forces at interfaces. These forces are said to be induced by molecular orientation at phase boundaries. The review covers work done up to 1947. Derjaguin's[7] work showing condensation on smooth surfaces to give thick layers at pressures just short of saturation should also be cited when one discusses the occur-

(1) Presented in part before the Colloid Division of the 135th National Meeting of the American Chemical Society, Boston, Massachusetts, April 10, 1959.
(2) I. Langmuir, *J. Am. Chem. Soc.*, **39**, 1848 (1917).
(3) J. H. Schulman and T. Teorell, *Trans. Faraday Soc.*, **34**, 1337 (1938).
(4) D. J. Crisp, *ibid.*, **42**, 619 (1946).
(5) M. Blank and V. K. LaMer, THIS JOURNAL, **61**, 1611 (1957).
(6) J. C. Henniker, *Rev. Modern Phys.*, **21**, 223 (1949).
(7) B. V. Derjaguin and V. M. Zorin, "Proc. Sec. Intl. Cong. on Surface Activity," Vol. II, Academic Press, Inc., New York, N. Y., 1957, p. 145.

rence of multimolecular structures at interfaces. His evidence suggests that some force causes condensation of the liquid at a distance beyond that which can be attributed to the force field of the adsorbent. With the thought that larger scale ordered structures might be present in surface films, X-ray diffraction techniques were applied to the detergent foam system. The X-ray scattering results reported in this paper cast considerable doubt on the validity of the oriented monolayer concept of structure at soap or detergent solution boundaries.

I. Composition of the Surface Film

Organic Content of the Surface Layer.—Before discussing the results of the X-ray diffraction studies it is useful to review what is known of the composition of the surface layer. Considerable data are available on adsorption of detergent molecules at the air–water interface. The most recent work on the system described here is that of Nilson.[8] This investigator used tritium tagging to determine the surface concentration of sodium dodecyl sulfate and sodium tetradecyl sulfate separately as well as mixed, and also in the presence of dodecanol and tetradecanol. Unpublished studies in these laboratories using the technique of foam fractionation, in one case with chemical analyses and in the other with radiotracer counting, concur with Nilson in showing that the adsorbed layer in these systems contains about 5×10^{-10} mole of organic material per cm.^{2}. From these data, it is apparent that not enough material is present to form a close packed monolayer. 5×10^{-10} mole cm.$^{-2}$ corresponds to about 34 Å.^{2} per organic molecule. It is known, however, that these alkyl sulfate–fatty alcohol films are highly viscous. Each of these studies also shows concentration of the fatty alcohol in the surface layer in amounts greater than that observed for the alkyl sulfate. In the system described, over the concentration range studied, about twice as much fatty alcohol as alkyl sulfate was found to be present in the surface.

Water Content of the Surface Layer.—There has been no previous attempt to measure the water content of the surface layer of a detergent solution. However, the presence of sufficient structure in the foam to give a diffraction pattern permits an approach to this problem. A foam was generated from a solution containing 0.1% fatty alcohol[9] sulfate and 0.04% fatty aclohol[9] in distilled water. This solution in bulk does not show a diffraction pattern under the conditions which were used to obtain the diffraction pattern from the foam. The diffraction pattern obtained from the foam of the dilute detergent solution was compared to those which result from the direct irradiation of several concentrated systems of known composition. Solutions having the same organic composition as that experimentally found to be present in the adsorbed surface layer but with different water contents were used in this study. A constant ratio of 2 parts of a fatty alcohol to 1 part of the corresponding alkyl sulfate was maintained while the water content was varied over the range from 45% water to 95% water.

The diffraction pattern on the detergent foam was obtained by aspirating a column of foam through a thin walled capillary placed in the X-ray beam. Filtered copper K_α radiation was used. The sample to film distance was 10 cm. The pattern obtained in this manner is a "powder" pattern because the individual air bubbles act as the powder grains. The diffraction pattern is presented as a densitometer tracing in Fig. 1. The diffraction patterns of the various bulk systems were obtained on an XRD-3 (Gen. Elec. Co.) diffractometer. The moisture content was maintained by sealing a thin plastic film, transparent to X-radiation in this range of scattering angle, across the face of the sample holder. Results are presented as the diffractometer tracings in Fig. 1.

It would appear from matching the relative intensities of the peaks at 2, 6 and 8° 2θ in these diffraction patterns that the water content of the *scattering structure* in the detergent film is between 80 and 85%. As stated above, the composition of the surface film has been shown to have alcohol/sulfate in the ratio of 2/1. A bulk composition having this ratio of alcohol to sulfate and a water content of 85% has the same X-ray diffraction pattern as the column of foam formed from the very dilute solution referred to previously. Therefore, it would seem that structure responsible for the diffraction pattern in this freshly formed foam is roughly 12% fatty alcohol, 6% alkyl sulfate and 82% water.

II. Study of Orientation and Structure of Detergent Films by X-Ray Diffraction Techniques

Introduction.—The previous section has discussed the probable composition of the scattering structure in the surface layer in a detergent solution as determined by adsorption measurements and X-ray diffraction technique. The next step in the study was an attempt to get an estimate of the orientation and structural details in this layer.

By making use of the diffractometer with single films or lamellae of detergent solution, one gains several advantages over the bubble system. The systems are oriented. Only spacings in the structure oriented perpendicularly to the film surface are observed. Better resolution is possible by using collimated slits ranging from 0.1 to 1°. The smaller slit gives a collimated beam, the larger slit a divergent one. High intensity of scattering is possible since a large amount of sample is irradiated. Changes in scattering pattern can be compared with film thickness as judged by interference colors. The effect of time on the scattering pattern of a single film can be determined.

Experimental Arrangement.—A schematic diagram of the experimental arrangement is shown in Fig. 2.

In order to maintain the film, it is necessary to keep it in a humid atmosphere. The cylinder shown in the schematic serves this purpose. Films are formed by dipping an aluminum holder into a dilute detergent solution.[10] In these studies,

(8) G. Nilson, THIS JOURNAL, **61**, 1135 (1957).

(9) The fatty chain composition was 67% C_{12} and 33% C_{14}.

the concentration of the solution varied between the critical micelle concentration and 0.01 molar.

The composite diffraction pattern of an alkyl sulfate–fatty alcohol–water film is shown in Fig. 3. This diffractometer tracing is a composite of several tracings on separate films. Different collimating slit sizes and amplification settings are needed to record the intensity of scattering as a function of scattering angle over the range involved. The range of scattering angles studied is from 0.1° 2θ upward. This means that any repeat unit of structure less than 1000 Å. may be expected to show a scattering peak within this range. For instrumental reasons, the diffraction of films was studied in two parts. They were the range from 0.1 to 1° 2θ and the range from 1° 2θ upwards. This corresponds to lattice spacings from 1000 to 80 Å. and to lattice spacings from 80 Å. downward with the radiation used here.

Possible Causes of Scattering Maxima.—A number of possibilities were considered as the source of the observed scattering maxima.

Reflection Interference Maxima.—Interference maxima may be produced by reflection of X-rays from top and bottom of thin layers. Kiessig,[11] among others, has described this situation for metals. However, most of the data herein reported, and in addition some from metals,[12] occur at angles too large for total reflection of X-rays. It was also observed that the position of the observed maxima did not move to smaller angles with increasing thickness of evaporated gold films. Furthermore, the various maxima for detergent films are present while the film is several thousand Å. thick, as judged by optical interference colors. Reflection interference maxima are, therefore, discarded as a possibility.

Double Bragg Diffraction.—Particularly in the case of metal data, double Bragg diffraction from adjacent crystallites needs to be considered. However, a look at the possible positions calculated from the structures of several of the metals involved shows that no double diffraction lines should occur below about 4° 2θ. Furthermore, doubly diffracted lines should have an asymmetric shape, sharp on the low angle side. Such was not usually observed. Hence this possibility is eliminated.

Reflection Grating.—It has been suggested that an ordered surface structure might act like a reflection grating, giving rise to reflection maxima. However, the observed maxima are at angles too large for reflection, as mentioned above, and fantastically large grating dimensions would be necessary to give maxima in the angular ranges observed.

Reflection Trap.—Parratt[13] suggested that a particular electron density distribution near the surface of a metal might produce a reflection "trap" leading to a maximum at low angles.

(10) The details of the experimental techniques, as well as the X-ray diffraction implications of this work, will be discussed in a forthcoming publication.

(11) H. Kiessig, *Ann. Physik*, **10**, 769 (1931).

(12) In the process of choosing the best interpretation for the observed phenomena, considerable data were gathered on evaporated metal films and polished metal surfaces.

(13) L. G. Parratt, *Phys. Rev.*, **95**, 359 (1954).

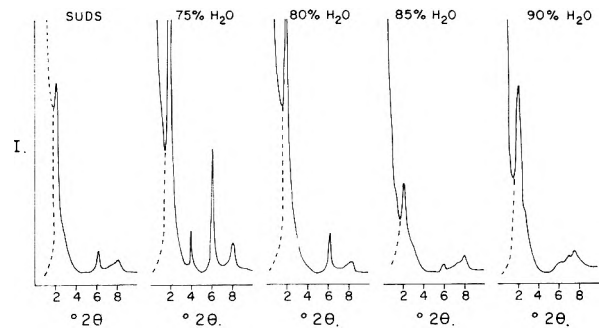

Fig. 1.—Low angle diffraction patterns for sodium alkyl sulfate, fatty alcohol and water systems (foam and bulk solutions).

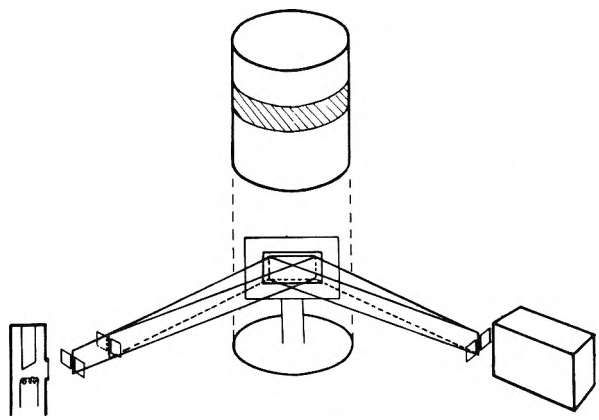

Fig. 2.—Schematic diffractometer arrangement for detergent film measurements.

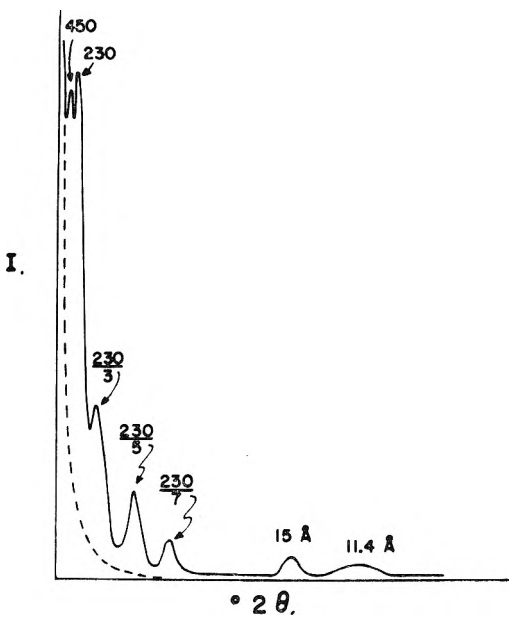

Fig. 3.—Composite diffraction pattern for a detergent film.

However, he did not observe such a maximum for 2000 Å. thick evaporated Cu. Only one maximum was predicted, whereas the aqueous films examined give a number of maxima. It does not seem likely that this possibility exists for the aqueous systems.

Interparticle Scattering.—Dynamic scattering from particles is suggested, particularly for the detergent films, in view of the usual micelle situation

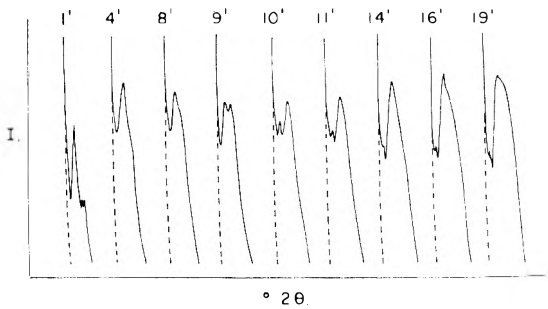

Fig. 4.—Change of diffraction pattern with film age.

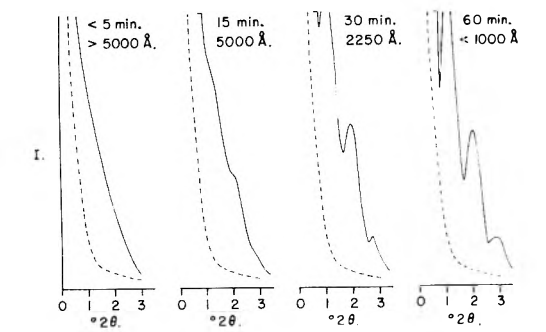

Fig. 5.—Changing diffraction pattern with film thickness and age.

which is supposed to exist in dilute solutions. Interparticle scattering, however, from randomly oriented particles does not seem a likely explanation for the following reasons: (1) the independent variation of the intensity of some of the observed lines, particularly the first at 0.2° 2θ and the second at 0.4° 2θ. (2) The observed maxima are sharper than those calculated for interparticle scattering from spheres, cylinders or ellipsoids.[14] (3) The intensities of successive observed maxima do not drop as fast as predicted for interparticle scattering. (4) The various maxima occur at positions that are in much better agreement with prediction when considered as orders of a Bragg diffraction rather than as interparticle scattering maxima. (5) The scattering lattice appears to be 3-dimensional (see below).

Ordinary Bragg Diffraction.—One is left with Bragg diffraction as the most likely explanation for the observed data. There is another piece of evidence which strongly supports this position. The shape of the reciprocal lattice in the region of the scattering maxima was investigated for both polished metals and detergent films. This was done by varying the specimen to X-ray source angle (angle of incidence) while keeping the detector fixed at an angle corresponding to the observed maximum. It was possible to do this by mounting the specimen on the G. E. Single Crystal Orienter. It was found that the intensity distribution in reciprocal space was very sharp, indicating that a 3-dimensional lattice exists in the scattering structure. The possibility may exist that scattering from highly oriented particles could also show this behavior in reciprocal space.

A change in radiation from filtered CuKα to filtered CrKα showed that the observed maxima for polished metals and for detergent films changed diffraction angle as predicted from the Bragg equation.

Results.—The following discussion is based on considering the scattering maxima as originating from a three-dimensional lattice. Choice of this interpretation is based on the considerations outlined above. If the observed scattering results from highly oriented particles, the dimensions used for lattice parameters will be slightly different.

Diffraction Spacings Larger Than 80 Å.—Diffraction patterns in detergent films in the Bragg angle range below 1° 2θ (80 Å. with Cu Kα radiation) are shown in Fig. 4. The sequence of changes shown was obtained on the same detergent film. Scanning speed was 1°/minute. Thus each tracing required one minute from start to finish. The sequence shown best illustrates the changing pattern in the diffracting film.

It is evident that a fairly sharply defined long range scattering structure exists in a detergent film and that this structure *is dynamic*. There is a fairly stable scattering line at a spacing corresponding to a lattice dimension in the range of 450 Å. using Bragg theory. The other scattering line is at a somewhat larger Bragg angle corresponding to a lattice dimension of about 230 Å. The intensity of the 230 Å. line increases with time (the film is aging and thinning) while that of the 450 Å. line decreases. This behavior could be caused by a major change in the symmetry of the developing structure which changes the relative intensities of odd and even orders of a diffraction line. It could be that the 230 Å. line is not a higher order of the 450 Å. line, but the changes in intensity are related to changes in particle orientation in the surface film. As developed below, this latter explanation is preferred.

Spacings somewhat larger and smaller than this one at 450 Å. are observed in other detergent systems. Different spacings are also observed under different conditions of film formation. It does not seem likely that the absolute value of these spacings is invariant. It seems more likely that the actual values observed will be found to vary with the conditions and compositions under examination. In the film shown here, the very long 450 Å. spacing remained nearly fixed throughout the life of the film. On some occasions the spacing represented by this peak docs not remain fixed but instead grows larger with time. This growth in long spacing dimension causes the peak to disappear into the main beam.

Diffraction Spacings Smaller Than 80 Å.—At higher scattering angles, some minutes are required for the structure to become sufficiently ordered to give reasonably sharp diffraction lines as indicated by the relatively slow development of the 230 Å. spacing (Fig. 4).

The changing diffraction patterns obtained from a single film as it changes thickness and grows older are shown in Fig. 5. The lines increase in sharpness as the system becomes more ordered. Film thickness was measured optically (development of interference colors in white light).

(14) A. G. Malmon, *Acta Cryst.*, **10**, 630 (1957).

Detergent Film Diffraction Compared to that of Crystalline Solids.—The intensity of scattering and the sharpness of the scattering peak in these films is surprising. To orient the reader, Fig. 6 shows the diffraction patterns of coconut soap and sodium chloride. Both solid coconut soap and NaCl are considered to be quite highly crystalline. These diffraction patterns were obtained with exactly the same geometry and instrumental settings as those used in obtaining the tracing shown in Fig. 5. The degree of crystallinity as judged by line sharpness and the amount of crystallinity as judged by line intensity are of the same order of magnitude in the detergent films as in these crystalline solids.

Review.—To review these diffraction data, a series of clearly defined intensity peaks are observed in a detergent film. Apparently within the detergent film a well oriented scattering structure exists. As the film thins and grows older, this structure becomes increasingly well ordered. The increased sharpness of the diffraction lines may indicate an increase in the size of the scattering particle, *i.e.*, line narrowing as the crystals grow larger. It may also indicate that a higher degree of order develops within the unit cell. Until the diffraction theory describing the functional relation of scattering intensity with scattering angle has been worked out for structures of this order of magnitude containing a subcell structure, one cannot choose between these alternatives. Such calculations are beyond the scope of this paper.

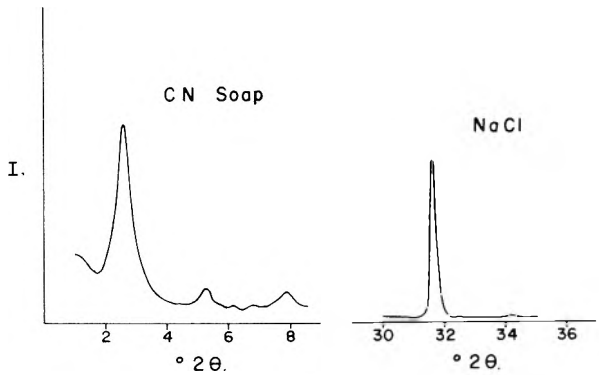

Fig. 6.—Diffractometer tracing of crystalline materials.

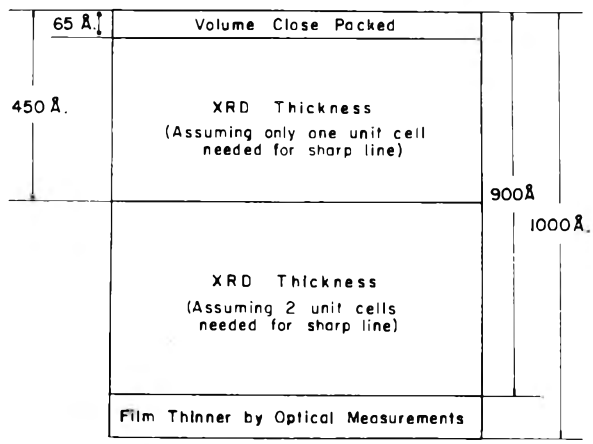

Fig. 7.—Possible range of film thickness.

Discussion

Structure of Film at the Detergent Solution–Air Interface.—It is informative to see what structural information can be deduced from these data. It is most convenient to do this in two parts. First the long range structure thought to be responsible for film properties will be discussed. Then evidence for assigning a structure to the individual unit cells making up the long range structure will be presented.

Long Range Structure.—The probable composition of the surface film was discussed above. This composition was estimated by a combination of surface adsorption measurements with the matching of X-ray diffraction patterns from foams and bulk solutions. For the purpose of this discussion the assumption was made that the bulk system which gave a diffraction pattern matching that observed in the foam was the same composition as the scattering structure in the foam. The scattering portion of the film was thus estimated to be 12% lauryl alcohol, 6% coconut alkyl sulfate and 82% water. Knowing the respective densities and the amount present in a unit area of surface, it is possible to calculate the thickness that this amount of material would occupy.

When such a calculation is made we find that this quantity of matter would occupy 65×10^{-8} cm.^{3} which is equivalent to a layer 1 cm.^{2} in area and 65 Å. thick. However, it is clear that a spacing of approximately 450 Å. is present in the film. From the geometry of the X-ray beam and the sample position in the diffractometer, this unit cell dimension must be oriented perpendicularly to the surface of the film. Assuming a homogeneous distribution of these structural units, the matter responsible for the diffraction pattern can occupy no more than (65/450) or about 15% of the film volume. It is also possible, though not as likely from film thickness considerations, that at least two unit cells must be stacked perpendicularly to the surface in order to observe such high scattering intensity. If this is the case, the scattering matter can only occupy (65/900) or 7.5% of the film volume.

These calculations and the experimental bases for the limitations which have been presented are illustrated in Fig. 7.

The X-ray diffraction data would indicate that each surface layer of the film has an initial thickness of at least 450 Å. When the film thins with age to be less than 1000 Å. by optical measurements, the surface layers must have come in contact with each other. The film would then appear to be a continuous structure. The organic portion of this structure can be no more than 3% (15% × 18%) solids by weight. Because of the high viscosity of this surface film, it seems reasonable to assign a gel-like structure to the detergent film. The X-ray scattering material would thus be the framework of this gel.

Postulated Shape for the Scattering Particle.—To go further with this attempt at determination of film structure, an assumption must be introduced as to the form assumed by these scattering particles. The repeat distances corresponding to the 450 and 230 Å. scattering peaks are present in the

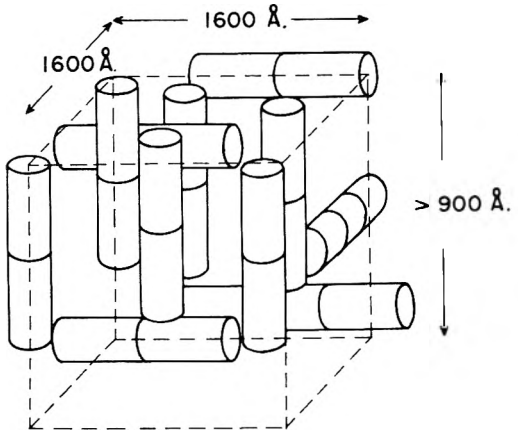

Fig. 8.—Tentative structure for a nascent detergent film.

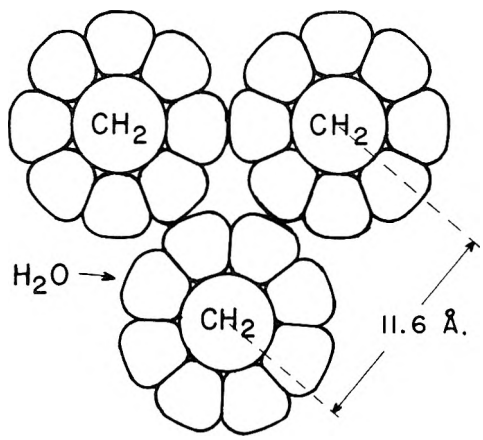

Fig. 9.—Tentative cross-sectional packing in "unit cell."

film. It seems most reasonable to associate these distances with actual dimensions of the unit cell responsible for X-ray scattering. As only two dimensions have been observed, it is *assumed* that these unit cells are cylinders, about 450 Å. in length and 230 Å. in diameter. The disc shape 450 Å. in diameter and 230 Å. high fits the X-ray data equally well. The term unit cell is not correct in the strictest sense. It is not possible to build up a continuous structure by translating a unit cell of cylindrical or disc shape in three dimensions. However, there is the experimental fact that these spacings of 450 and 230 Å. are part of a 3-dimensional lattice. Optical techniques have shown that there is no room for more than one or at most two of these 450 Å. spacings perpendicular to the film. These spacings are clearly dimensions of the structural unit. Hence the term unit cell is used from this point (for lack of a better term) to describe the basic structural unit of the gel. Perhaps the development of the diffraction theory for structures of this magnitude (particularly when they include a substructure) will clarify this point.

From the dimensions assigned these cylinders one can compute the volume occupied by each. Then knowing the total volume occupied by the cylinders one can compute the number present in a cm.^{2} of surface. The computation shown below gives a figure of 3×10^{10} cylinders in each cm.^{2} of surface. Thus in a film only 900–1000 Å. thick there would thus be 6×10^{10} cylinders.

Vol. of scattering structure/cm.^{2} of surface $= 65 \times 10^{-8}$ cm.^{3} (composition known by adsorption + X-ray measurements, vol. computed from density of components)

Vol. of cylinder $= \pi \times (115)^2 \times 10^{-16} \times 450 \times 10^{-8} = 2 \times 10^{-17}$ cm.^{3}

$$\text{Number of cylinders on one surface/cm.}^2 = \frac{65 \times 10^{-8}}{2 \times 10^{-17}} = 3 \times 10^{10}$$

It is interesting to note that cylinders packed as edges of a box, 900 Å. deep with sides of 1600 Å. will satisfy this density requirement.

Possible Arrangement of "Unit Cells."—Initially we suppose that the film might appear as shown in Fig. 8. Our X-ray data do not require that the cylinders lying in the surface be uniformly spaced. It is only necessary that they lie in the plane of the surface. By the same token these data do require that many cylinders be oriented perpendicular to the surface. This is required by the observed changes in intensity of scattering in these two peaks with time as shown in Fig. 4.

Initially, most of the cylinders appear to be perpendicular to the surface. With time there appears to be a gradual increase in the proportion of particles lying in the surface or parallel to it. However, even at the time the film breaks the diffraction line showing presence of cylinders with their long dimension perpendicular to the surface is still observed. Of course, there are undoubtedly other arrangements which would fit the experimental data as well. However, this arrangement satisfies the *diffraction pattern* and the *quantity of organic material* known to be present in the surface.

Structure of the Individual "Unit Cell."—From chemical composition of the scattering structure it can be calculated that approximately 5 molecules of water are associated with each CH_2 group in the organic molecule. An alternate method for calculation of individual cell structure can be based on the assignment of the X-ray long spacings at 450 and 230 Å. to unit cell dimensions. This makes possible a direct calculation of the number of water molecules associated with each hydrocarbon chain. Three assumptions are required for this calculation. (1) The organic chains extend the length of the unit cell. (2) The organic chains are symmetrically located throughout the unit cell. (3) The cross sectional area of the hydrocarbon chain is 20 Å.^{2} and that of water is 10 Å.^{2}. If this composition of matter were symmetrically packed together, it would have a configuration similar to that shown in Fig. 9. Notice that the distance between CH_2 chains, packed in this fashion, is 11.6 Å.

A fairly broad peak is observed at a spacing corresponding to 11.2–11.8 Å. in the diffraction pattern of the film and the freshly generated foam. This peak is broader than those associated with the unit cell dimensions. It thus does not appear to be related to them.

The complete diffraction pattern as shown in Fig. 3 can be summarized as follows. The lines at 450 and 230 Å. appear associated with the dimensions of unit cells making up the gel frame-

TABLE I

RELATIVE AREAS OF WATER TO CH_2 GROUP IN "UNIT CELL" CROSS SECTION

Cross section of unit cell = $\pi \times (115)^2 = 40{,}000$ Å.^{2}

CH_2 contribution $\approx 20\% = 8000$ Å.^{2}

H_2O contribution $\approx 80\% = 32{,}000$ Å.^{2}

Area/CH_2 = 20 Å.^{2} No. of CH_2 chains = $\frac{8000}{20} = 400$

Area/H_2O = 10 Å.^{2} No. of H_2O = $\frac{32{,}000}{10} = 3200$

Ratio of H_2O:CH_2 = 3200/400 = 8:1

work of the film. The sharp, progressively less intense peaks at 80, 45 and 33 Å. appear to be the third, fifth and seventh orders of the 230 Å. line. A more detailed development of a model must, therefore, satisfy the condition that even orders of the 230 Å. spacing are very weak or missing. The line at 11.4 Å. appears best explained when both intensity and line width are considered, as the average distance separating CH_2 chains in the unit cell. In addition there is a relatively sharp line at a spacing corresponding to 16 Å. The intensity of this line also is such that it does not appear to belong to the 230 Å. series. This spacing may be related to the chain length of the individual detergent or alkanol molecules present in those cylinders aligned perpendicular to the plane of the film.

Speculations.—It is tempting to speculate that the size of the unit cell is a function of temperature. As was stated above, on some occasions the very long spacing, *ca.* 450 Å. initially, increased as the film aged. This occurred when the enclosure surrounding the film was relatively low in humidity so that evaporative cooling was pronounced.

As precise temperature and humidity control become available for the diffractometer, the influence of these variables will be studied. Qualitative experiments indicate that increased temperature decreases the length of the unit cell. This is expected as the cohesive forces operative in the film appear to be almost solely those between ordered water molecules. Perhaps the "iceberg" structure of Frank and Evans[15] or the different type of water around proteins referred to by Klotz[16] are also involved here.

Nuclear magnetic resonance measurements also support the idea that water is an integral part of the film structure. A bulk sample having the same diffraction pattern and the chemical composition as the "unit cells" described earlier shows the water proton line width to be 4–8 times that of liquid water. This indicates experimentally that the water present here has a markedly greater viscosity than that of liquid water.

Also the work of Sasaki, Okuyama and Saito[17] show that the ultraviolet absorption spectra of *trans*-azobenzene, when present in micelles with sodium dodecyl sulfate, appears to be in an aqueous media rather than a hydrocarbon one. These experimental data were also observed by Riegelman, *et al.*[18]

Conclusions

The combination of surface adsorption measurements and X-ray diffraction data on foams and films requires a new and different picture of the structure of a foam.

The hypothesis that water makes up an integral portion of the unit cell is substantiated by nuclear magnetic resonance measurements in addition to the adsorption and diffraction data.

In systems where the surface active material is soluble, the data demonstrate that water makes up a principal portion of the surface film (at least 97% by weight). Ordered water is probably almost solely responsible for both cohesion within the "unit cell" as well as binding between "unit cells." Close packing of hydrocarbon chains in surface films would seem to be a special case associated only with very insoluble monolayers spread carefully on the surface of water. The more general case would seem to involve water, oriented in an ice-like configuration, acting as *the linkage* between solute molecules or particles. The extensive structural distances which we have observed in such diverse systems as films from ovalbumin solutions, gelled dispersions of amorphous silica particles and films from soap or detergent solutions would seem to require such a postulate.

Acknowledgments.—The authors wish to recognize the invaluable aid of Mr. R. H. Lindahl in carrying out the precise scattering intensity measurements which made this work possible. We would also like to acknowledge many helpful discussions of these data with Dr. W. L. Courchene of these Laboratories, Professor Peter Debye of Cornell University and Professor P. M. Harris of Ohio State University.

(15) H. S. Frank and M. W. Evans, *J. Chem. Phys.*, **13**, 507 (1945).

(16) I. M. Klotz, *Science*, **128**, 815 (1958).

(17) H. Sasaki, H. Okuyama and S. Saito, *Bull. Chem. Soc. Japan*, **29**, 752 (1956).

(18) S. Riegelman, N. A. Allawala, M. K. Hrenoff and L. A. Strait, *J. Colloid Sci.*, **13**, 208 (1958).

THE TEMPERATURE–INTERFACIAL TENSION STUDIES OF SOME HALO-ALKYLBENZENES WITH WATER

BY JOSEPH J. JASPER AND HELEN R. SEITZ

Contribution from the Department of Chemistry, Wayne State University, Detroit, Michigan

Received July 8, 1959

This paper involves the study of the thermodynamic properties of the interfacial region between water and five halo-alkylbenzenes. The interfacial tensions were measured over a temperature range of 60° and the method of least squares was applied to formulate empirical equations relating these variables. These equations enabled the calculation of the entropy, enthalpy and latent heat for unit area of interface. The calculated values of these properties, together with the interfacial tensions and densities of the mutually saturated liquids, are presented in tables as functions of the temperature.

The interfacial tensions of a relatively large number of organic liquids with water have been reported in the literature but generally such data involved a single temperature. This is inadequate for a complete picture of the interfacial region especially since the approach to the critical solution temperature is generally attended by a marked expansion of the transition phase. Likewise there is little evidence of any systematic study and correlation of interfacial tension data with molecular properties of the organic liquids involved.

In view of the present knowledge of solutions and of the laws which govern solubility, it appears obvious that the magnitude of the interfacial tension is the resultant of the determined by the forces which make the interface possible. These forces in turn are determined by certain molecular properties of the liquids between which the interface is formed, and if their nature and exact contribution is established, it appears quite possible that the interfacial tension could be evaluated from these properties.

The procedure followed in this Laboratory is to determine how substituted groups in a given homologous series influence the interfacial tension with an arbitrarily chosen reference liquid. For comparisons such a liquid should have a minimum of intermolecular interaction with the organic liquids, therefore, water was chosen for this purpose. It was assumed, therefore, that any alteration in the binary composition of the interface with temperature is due to change in solubility alone.

The proposed series of interfacial tension studies is designed to determine how groups of varying electronegativity, when substituted in a given compound to form an homologous series, influence the interfacial tension against water. Previous studies involved the halogenated benzenes,[1] the halogenated toluenes[2] and some alkyl benzenes.[3] The present paper reports the results of the study of five halo-alkylbenzenes over the temperature range 20 to 80°. The interfacial tension data were applied to calculate the temperature variation of some thermodynamic properties of the interfacial region.

Experimental

Purification of the Compounds.—The best grades of 2-chloro-ethylbenzene, 2-bromoethylbenzene, 2-iodo-ethylbenzene, 3-chloro-propylbenzene and 3-bromo-propylbenzene were obtained from Eastman Organic Chemicals Industries and further purified by vacuum fractionation. To accomplish this a 15 inch column was employed which was packed with single-turn glass helices and which was equipped with a total reflux variable take-off head. In each case the middle third was retained for use in the experimental operations which followed. The refractive indexes of the purified compounds agreed with the authoritative literature values to the third and fourth place of decimals.

Determination of the Densities.—It was important that the densities of the mutually saturated liquids be measured accurately, so great care was exercised in this phase of the investigation. The densities and interfacial tensions were measured simultaneously and for the former a modified form of the "type D" pycnometer described by Bauer[4] was used. Three pycnometers, each of which had a volume of 20 ml., were constructed as nearly identical as possible in dimensions and shape. These were calibrated and two reserved for the respective liquids. The third was used as a counterpoise. The organic liquids and water were saturated with each other by shaking quantities of each together and then allowing the two layers to remain in contact at least 24 hr. before use. The liquids were introduced into the pycnometers by means of a 30-ml. glass hypodermic syringe equipped with a 12-cm., 20-gauge, stainless steel needle which could be inserted the full length of the capillary necks of the pycnometers. A constant volume of liquid was maintained in the pycnometer by adding or withdrawing small quantities during the temperature variation of the experiments. The densities of the two mutually saturated liquids are shown in Table I and these represent the average of four independent determinations. A constant temperature was maintained during the various measurements with the aid of a specially designed glass-wool insulated water-bath. The bath container was equipped with heat resistant plate glass windows and a cover of one-inch fiber board. Four thermoregulators were used at respective instrument settings of 20, 40, 60 and 80°, and these were used interchangeably, to facilitate the checking of data at precisely the same temperature previously used. To ensure conditions of true equilibrium for these measurements, readings were made both from the side of increasing and of decreasing temperature. The thermoregulator system was sensitive enough to maintain a temperature constant to 0.002° in the range 20–40° and to 0.004° up to 80°. The actual temperatures were read from NBS certified thermometers which had two-degree ranges and 0.01° scale divisions.

Determination of the Interfacial Tensions.—A modification of the drop-weight apparatus of Harkins and Brown[5] was used in measuring the interfacial tensions. Drop volumes instead of drop weights were measured because of the greater experimental difficulties attending the latter. A detailed description of the apparatus assembly, and the exact procedure, have been described in a previous paper.[1] A series of interchangeable tips, having radii varying from 0.0785 to 0.2850 cm., and a selection of measuring pipets of different volumes, permitted measurement of the various liquids over the range of densities.

Preliminary experiments proved that the aqueous phase wet the flat surface of the tip and spread on it much more readily than the organic phase; hence the former was selected as the liquid of which the drops formed. Since the aqueous

(1) J. J. Jasper and T. D. Wood, THIS JOURNAL, **59**, 541 (1955).
(2) J. J. Jasper and Helen R. Seitz, *ibid.*, **62**, 1331 (1958).
(3) J. J. Jasper and Helen R. Seitz, *ibid.*, **63**, 1429 (1959).
(4) N. Bauer in "Physical Methods of Organic Chemistry," Vol. I, Interscience Publishers, Inc., New York, N. Y., 1945, p. 79.
(5) W. D. Harkins and F. E. Brown, *J. Am. Chem. Soc.*, **41**, 499 (1919).

TABLE I

THE DENSITIES OF THE MUTUALLY SATURATED LIQUID COMPOUNDS

Compound	Temp., °C.	Density, g./ml. Aq. phase	Org. phase
2-Chloro-ethylbenzene	20	0.9961	1.0689
	40	.9900	1.0500
	60	.9808	1.0310
	80	.9701	1.0134
2-Bromo-ethylbenzene	20	.9960	1.3640
	40	.9901	1.3413
	60	.9811	1.3176
	80	.9701	1.2959
2-Iodo-ethylbenzene	20	.9959	1.6285
	40	.9899	1.6026
	60	.9810	1.5769
	80	.9700	1.5514
3-Chloro-propylbenzene	20	.9960	1.0445
	40	.9899	1.0269
	60	.9812	1.0094
	80	.9700	0.9914
3-Bromo-propylbenzene	20	.9960	1.3088
	40	.9899	1.2874
	60	.9809	1.2657
	80	.9700	1.2441

phase was in every case the less dense, it was necessary to arrange the tip in such a position that the drops could form vertically upward, subsequently becoming detached and passing through the more dense organic phase to coalesce into a homogeneous layer at the top. The choice of pipet and tip for delivery of the drops depended upon the density differential. For the chloroethylbenzene the pipet and tip selected delivered 22 to 33 drops; for the bromo-ethylbenzene 62 to 75 drops, for iodo-ethylbenzene, 145 to 155 drops; for chloro-propylbenzene 10 to 25 drops; and for bromo-propylbenzene, 50 to 60 drops. Twenty-four hours were required to make the measurements for each compound, and each measurement was repeated four times.

Results and Discussion

The equation used for calculating the interfacial tension values was that employed by Harkins and Cheng[6] as

$$\gamma_i = vg(d_o - d_w)/2\pi rF$$

where γ_i is the interfacial tension in ergs per cm.^{2}, v the drop volume in ml., d_o the density of the organic phase, d_w the density of the aqueous phase, g the gravitational factor, r the radius of the tip in cm., and F the Harkins and Brown[5] correction factor.

To calculate the magnitude of the entropy of the interface s the latent heat l, and the enthalpy h, the two-dimensional form of the Clapeyron equation was used.[7] Each of these thermodynamic properties refer to unit area of the interface measured under isobaric and isothermal conditions. These, together with the interfacial tension values, are presented in Table II. With the aid of least squares empirical equations were formulated which relates the interfacial tension to the centigrade temperature. These were used to calculate the values of the interfacial tensions for the temperature given in the table. The equations are

(6) W. D. Harkins and Y. C. Cheng, *J. Am. Chem. Soc.*, **43**, 35 (1921).

(7) W. D. Harkins, "The Physical Chemistry of Surface Films," Reinhold Publ. Corp., New York, N. Y., 1952, p. 6–8.

2-Chloro-ethylbenzene:

$$\gamma_i = 33.592 - 0.03397t - 0.000364t^2$$

2-Bromo-ethylbenzene:

$$\gamma_i = 28.452 + 0.05237t - 0.000597t^2$$

2-Iodo-ethylbenzene:

$$\gamma_i = 38.817 + 0.02997t - 0.001484t^2$$

3-Chloro-propylbenzene:

$$\gamma_i = 31.361 + 0.06898t - 0.001350t^2$$

3-Bromo-propylbenzene:

$$\gamma_i = 27.768 + 0.08636t - 0.000874t^2$$

The form of the empirical equations suggests that the corresponding functions are concave toward the temperature axis; a phenomenon which has been observed in all interfacial tension studies made in this Laboratory. The interfacial tensions of the two chlorides and the iodide are monotonically decreasing functions but those of the two bromides pass through a rather flat maximum. It is to be noted that the interfacial tensions of the two chlorides resemble each other, and this is also true for the two bromides. Studies of several alkyl benzenes[3] proved that the interfacial tension increased with increasing molecular weights of the organic compounds over the same temperature range employed in the present study, but this is not true for the present series of compounds. In some manner, not immediately obvious, substitution of bromine and chlorine into the alkyl group

TABLE II

INTERFACIAL TENSIONS, ENTROPIES, LATENT HEATS AND ENTHALPIES OF THE INTERFACES

Compound	Temp., °C.	γ_i	s	l	h
2-Chloro-ethyl-benzene	20	32.77 ± 0.07	0.0485	14.22	46.99
	40	31.65 ± .02	.0630	19.73	51.38
	60	30.25 ± .02	.0776	25.85	56.10
	80	28.55 ± .05	.0921	32.54	61.09
2-Bromo-ethyl-benzene	20	29.26 ± .06	− .0285	−8.36	20.90
	40	29.59 ± .13	− .0047	−1.47	28.12
	60	29.45 ± .08	.0192	6.40	35.85
	80	28.82 ± .07	.0431	15.22	44.04
2-Iodo-ethyl-benzene	20	38.82 ± .03	.0294	8.62	47.44
	40	37.64 ± .11	.0888	27.81	65.45
	60	35.27 ± .05	.1481	49.34	84.61
	80	31.72 ± .06	.2075	73.28	105.00
3-Chloro-propyl-benzene	20	32.20 ± .06	− .0150	−4.40	27.80
	40	31.96 ± .04	.0390	12.21	44.17
	60	30.64 ± .11	.0930	30.98	61.62
	80	28.24 ± .42	.1469	51.89	80.13
3-Bromo-propyl-benzene	20	29.15 ± .02	− .0514	−15.07	14.08
	40	29.82 ± .23	− .0165	−5.17	24.65
	60	29.80 ± .15	.0185	6.16	35.96
	80	29.08 ± .07	.0535	18.89	47.97

which is attached to the benzene has the effect of lowering the interfacial tension. This effect is greatest for the bromine substituted compound. Since the magnitude of the interfacial tension is determined by the degree of dissimilarity between the molecular species of the contiguous phases, one must conclude that the bromine-substituted compounds not only attract water more strongly than do the others, but must have a thicker transition phase. Increasing temperature expands this transition phase but little in the case of the bromides; somewhat more for the chlorides; and considerably for the one iodide studied. It is also observed from plots that the temperature *vs.*

interfacial tension curve for the iodide is almost linear above 40°. This seems to imply that the solubility of this compound in water, which must be small according to the large interfacial tension values, increases but little with the temperature. Accordingly its transition phase with water must be small in thickness.

From reference to Table II, it is seen that the entropies, latent heats and enthalpies of the various interfaces all increase with the temperature. Plots of these intensive interfacial properties as functions of the temperature show that these relations are linear but very definitely not parallel. A comparison of the temperature rate of increase of the entropies of the interfaces of *n*-ethylbenzene and *n*-propylbenzene with the corresponding halogen substituted compounds of the present series, shows that, with the exception of the chloroethylbenzene, the entropies of the latter not only increase more rapidly but to a greater extent. This seems surprising in view of the expected restriction in the intra-molecular activity suggested by Adam[8] due to the addition of the relatively heavy halogen atoms on the alkyl chain.

(8) N. K. Adam, in "The Physics and Chemistry of Surfaces," Oxford Univ. Press, 1941, p. 67.

VAPOR PRESSURES OF $FeCl_2$, $FeBr_2$ AND FeI_2 BY THE TORSION EFFUSION METHOD

BY R. J. SIME AND N. W. GREGORY

Contribution from the Department of Chemistry at the University of Washington, Seattle, Washington

Received July 9, 1959

Total vapor pressures developed over solid $FeCl_2$, $FeBr_2$ and FeI_2, respectively, have been measured between 400 and 470° by the torsion effusion method. Results are discussed in relation to other published information concerning the vaporization of these substances.

A study of the vapor pressure of iron(II) bromide (350 to 900°), using effusion, transpiration and diaphragm gage techniques, has been reported previously from this Laboratory.[1] Effusion pressures, measured near 400° in the conventional manner, were found to be about 30% lower than transpiration pressures when monomeric $FeBr_2$ was assumed to be the principal vapor phase molecular species; this assumption was suggested by comparison of transpiration and diaphragm gage data near the melting point (690°). In the present work additional information on the vapor pressure of $FeBr_2$ and new data for $FeCl_2$ and FeI_2 have been obtained using a torsion effusion apparatus. In this method knowledge of the molecular weight of the effusing vapor is not required for evaluation of the total pressure within the effusion cell.

Very recently, a mass spectrometric analysis of the vapor species in equilibrium with $FeBr_2$[2] and with $FeCl_2$[3] has been published by Porter and Schoonmaker. Their findings confirm that the major vaporizing species for $FeBr_2$ (and also $FeCl_2$) in the effusion temperature range is the monomeric form but indicate that the dimer becomes increasingly important at higher temperatures.

Experimental Part

The torsion effusion method[4] has been actively used by a number of investigators in recent years.[5] A brief description of our apparatus follows. Two holes of nearly equal area were symmetrically placed *ca.* 1.5 cm. from the axis of suspension on opposite sides of a quartz effusion cell (5 cm. long and 1.5 cm. o.d.). Holes were blown in thinned sections of the quartz wall. Two independent cells, attached to tungsten wires *ca.* 55 cm. long, were used; cell 1, hole areas 1.95×10^{-2} and 1.725×10^{-2} cm.^{2}, to a 2 mil. wire, torsion constant 1.820 dyne cm. radian^{-1}, and cell 2, hole areas 2.60×10^{-3} and 3.72×10^{-3} cm.^{2}, to a 1 mil wire, 0.1004 dyne cm. radian^{-1}. At the bottom of each wire the cell assembly was attached by a clamp to which was bolted a small aluminum disk. To measure the torsion constant of the wires, rings of known moments of inertia were placed on this disk and the entire assembly treated as a torsion pendulum system. A rigid tungsten wire, to which was attached a mirror and an aluminum vane ($10 \times 1 \times 0.01$ (cm.) which, through interaction with a magnet, aided in damping oscillations), connected the aluminum disk to a quartz rod attached to the cell.

The cell was heated by directing radiation from three 500 watt projection bulbs onto a blackened copper cylinder, 6 cm. o.d., 7 cm. high, with walls 0.1 cm. thick. The top of the cylinder was a split disk which could be closed around the support rod of the cell after the latter was lowered inside. The projection bulbs were mounted so as to place their filaments at the foci of eliptical reflectors, major axis 8 in., semi-major axis 6.5 in., placed at 120° intervals around the furnace.[6] A dummy cell was placed in the jacket as close as possible to the suspended cell. The dummy was supported by three thermocouples (placed at the center and each end); the temperature indicated by these couples was assumed to represent the temperature of the torsion cell. Thermocouple leads were brought out of the vacuum system through Stupakoff seals at the bottom of the apparatus.

The entire assembly was surrounded by a 10 cm. o.d. Pyrex tube and could be dismantled *via* an "O" ring seal. The pressure within the tube, monitored continuously with an ionization gage, was kept below 10^{-5} mm. The angle of twist was measured with a conventional telescope and scale assembly. Scale deflections were read within 0.05 cm., corresponding to an uncertainty of the torque angle of 5×10^{-4} radian.

Although the wire characteristics were determined by a pendulum treatment, the entire assembly was finally calibrated to remove uncertainties associated with slight irregu-

(1) R. O. MacLaren and N. W. Gregory, THIS JOURNAL, **59**, 184 (1955).

(2) R. F. Porter and R. C. Schoonmaker, *ibid.*, **63**, 626 (1959).

(3) R. C. Schoonmaker and R. F. Porter, *J. Chem. Phys.*, **29**, 116 (1958).

(4) Introduced by M. Volmer, *Z. physik. Chem., Bodenstein Festband*, 836 (1931).

(5) See for example: (a) R. F. Barrow, D. G. Dosworth, A. R. Downie, E. A. N. S. Jeffries, A. C. P. Pugh, F. J. Smith and J. M. Swinstead, *Trans. Faraday Soc.*, **51**, 1354 (1955); (b) R. D. Freeman and A. W. Searcy, *J. Chem. Phys.*, **22**, 762 (1954); (c) M. D. Scheer, THIS JOURNAL, **61**, 1184 (1957).

(6) L. R. Weisberg and G. R. Gunther-Mohr, *Rev. Sci. Instr.*, **26**, 896 (1955).

larities in the holes and their placement in the cells. Zinc was found a convenient calibrating substance[5a]; its vapor pressure is known with good accuracy[7] and the effusion temperature range is reasonably close to that of interest for the iron halides. The calibration provides an apparatus constant which relates the pressure to the torque angle, $P = k\theta$; $k_1 = 0.0323 \pm 0.0013$, $k_2 = 0.0129 \pm 0.0006$.

$FeBr_2$ and FeI_2 were prepared (by others in this Laboratory)[8] by direct reaction of reagent grade iron with reagent grade (ACS) samples of the respective halogens at elevated temperatures. The iron content indicated a purity of better than 96% for FeI_2 and 99% for $FeBr_2$. $FeCl_2$ was prepared by dehydration of $FeCl_2 \cdot 4H_2O$ (J. T. Bakers Analyzed, 99.9) *in vacuo*, initially at *ca.* 120° and finally by resubliming the anhydrous $FeCl_2$ at *ca.* 500°. All samples were purified by vacuum resublimation; material was introduced into the torsion cell through a small filling tube attached to the bottom; this tube was sealed off quickly and subsquent evacuation of the apparatus accomplished within a very few minutes to minimize hydrolysis of the samples, exposed to the atmosphere only through the pinholes. Hydration of $FeCl_2$ and $FeBr_2$[9] is easily reversed *in vacuo* (presumably also the iodide, although the system FeI_2–H_2O has not been studied in detail) without appreciable oxidation. In the previous work with $FeBr_2$[1] no evidence was observed to indicate a dependence of the vapor pressure on the presence of small amounts of oxide; a similar behavior has been assumed for $FeCl_2$ and FeI_2.

As the temperature of the samples was raised, degassing was followed by observing the angular deflection of the cell. Vapor pressures were calculated from the minimum torsion deflection reached at a given temperature on heating, or from the deflection observed as the sample was cooled in steps after being held at the highest experimental temperature for 1 to 2 hr. The vapor pressures obtained were the same with both procedures; the latter method was faster and hence more convenient.

Results and Discussion

Results are shown graphically in Figs. 1, 2 and 3.[10] Lines based on points obtained with cell 2 alone, may be represented by equations of the form $\log P_{mm.} = -AT^{-1} + B$. Values of A and B, and associated thermodynamic properties, if the vaporization process is assumed to be of the simple form $FeX_2(s) \rightarrow FeX_2(g)$, are summarized below (temperature range 670–740°K.). A comparative plot of sigma functions ($-R \ln P - 8 \ln T$), where ΔC_p (sublimation) has been estimated from the behavior

TABLE I

	A	B	ΔH^0, kcal. mole^{-1}	ΔS^0, cal. mole^{-1} deg.$^{-1}$ (std. state 1 atm.)
$FeCl_2$	9890	11.10	45.3 ± 2	37.6
$FeBr_2$	10220	11.95	46.7 ± 2	41.5
FeI_2	960	11.82	(44.7 ± 4)	(40.9)

of similar halides[11,12] as −8 cal. mole^{-1} deg.$^{-1}$, is shown in Fig. 4. The relative volatilities are as expected for solids in which the bonding is largely ionic. Bond energies of the vapor molecules have been estimated from the extrapolated heat of sublimation and other relevant data at 298°K.

$$2(Fe\text{–}X) = -\Delta H^0(\text{sub. } FeX_2) - \Delta H^0(\text{form. } FeX_2(s))^{14} + \Delta H^0(\text{sub. Fe})^{14} + \Delta H^0(\text{diss. } X_2)^{13}$$

giving values of Fe–X of 94.7, 81.5 and (66.2) kcal. for the chloride, bromide and iodide, respectively.

In Fig. 1 data from cells 1 and 2 are seen to be in close agreement for $FeCl_2$, indicating that the con-

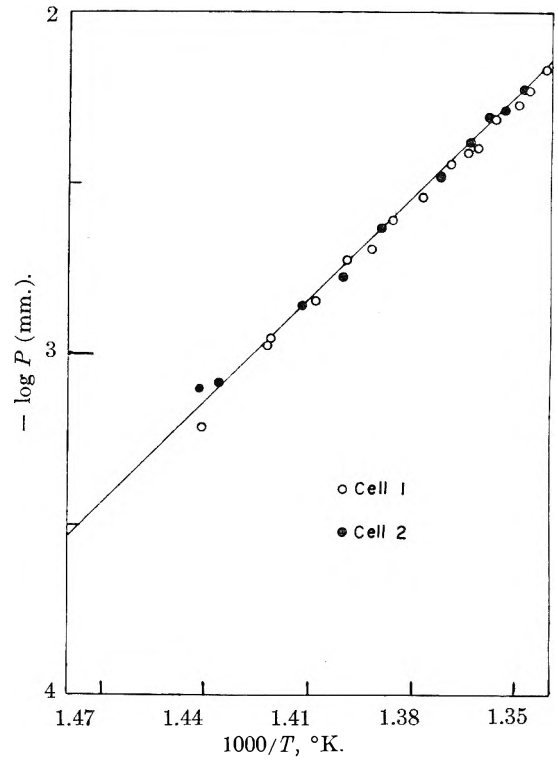

Fig. 1.—Vapor pressure of iron(II) chloride.

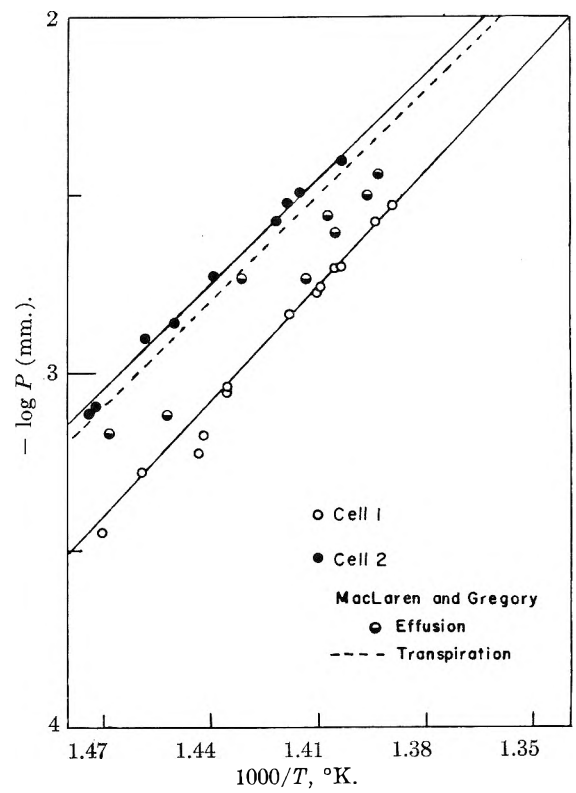

Fig. 2.—Vapor pressure iron(II) bromide.

(7) K. K. Kelly, Bureau of Mines Bulletin 383 (1935).
(8) L. E. Wilson and H. E. O'Neal, private communication.
(9) N. W. Gregory, THIS JOURNAL, **61**, 369 (1957).
(10) For detailed tables see the Doctoral Thesis of R. J. Sime, University of Washington, Seattle, Washington, 1959.
(11) H. A. Doerner, Bureau of Mines Bulletin 577, 1937.
(12) T. L. Allen, *J. Am. Chem. Soc.*, **78**, 5476 (1956).
(13) NBS Circ. 500: "Selected Values of Chemical Thermodynamic Properties," U. S. Govt. Pr. Office, Washington, D. C., 1950.
(14) T. L. Cottrell, "The Strengths of Chemical Bonds," Academic Press, Inc., New York, N. Y., 1954, Chapters 2 and 8.

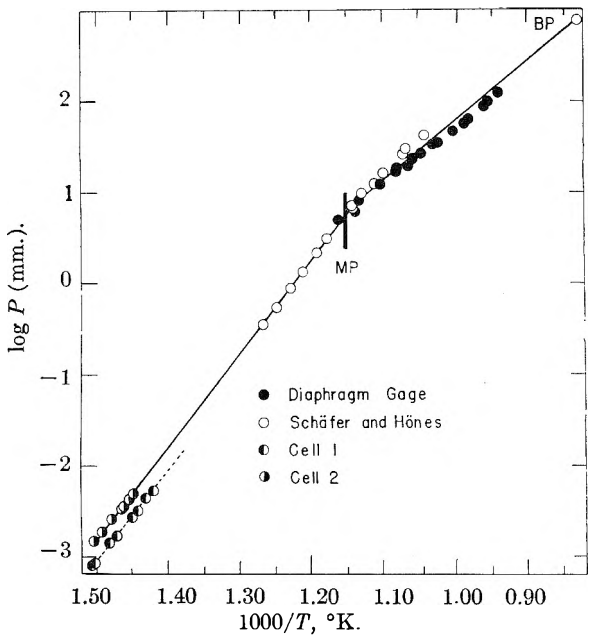

Fig. 3.—Vapor pressure iron(II) iodide.

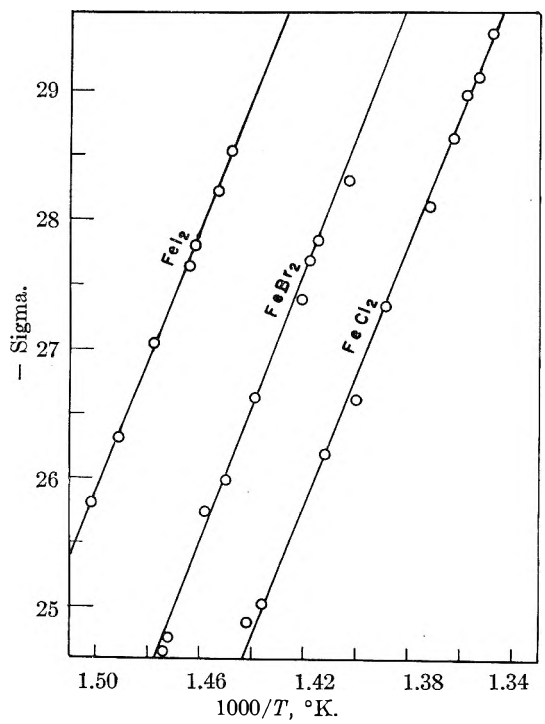

Fig. 4.—Ferrous halide sigma functions for vaporization.

densation coefficient is sufficiently large, >0.05, that steady-state pressures in both cells are virtually equilibrium values. Schoonmaker and Porter[3] measured the vapor pressure of $FeCl_2$ by conventional effusion at two temperatures to assist them in estimating the entropy of vaporization. Their values straddle the line in Fig. 1 and hence are in general agreement with our findings. The heat of sublimation indicated by our work is within experimental uncertainty of that obtained from the mass spectrographic study (44 ± 3).[3]

Figures 2 and 3 show a marked dependence of torsion effusion pressures for $FeBr_2$ and FeI_2 on the effusion hole area, somewhat surprising in view of the behavior of $FeCl_2$. The $FeBr_2$ pressure dependence on hole area appears somewhat greater than observed in the conventional effusion measurements,[1] shown in Fig. 2 as intermediate points. The different geometrical relation of the effusion orifices to cell body in the torsion arrangement may be responsible for the difference.

Cell 2 pressures (smaller orifices) are in substantial agreement with the earlier transpiration measurements[1] (dotted line, Fig. 2) for $FeBr_2$. Hence we suggest these values should be taken as the correct vapor pressure of $FeBr_2$ in this temperature range. The earlier effusion results are presumed to be low because of the accommodation coefficient effect; the difference is not appreciably beyond experimental error when data from the smallest orifices are compared. The agreement of the torsion effusion and transpiration data provides further evidence that the monomer is the principal vaporizing species at these low temperatures. Heats of sublimation from all determinations agree within experimental error.

From their mass spectrographic study, Schoonmaker and Porter[2] conclude that the pressure of Fe_2Br_4 is *ca.* 4% of that of $FeBr_2$ at 665°K. Using their heats of sublimation together with a vapor pressure based on a mean of the earlier effusion pressures reported from this Laboratory,[1] they estimate that the equilibrium vapor contains from 30–70% dimer at the melting point, 964°K. If this calculation is repeated using the slightly higher vapor pressure at 665°K. indicated in Fig. 2, the amount of dimer expected at 964°K. (in the equilibrium vapor) lies between 23 and 50%. The lower value is more nearly compatible with the comparative vapor pressures observed in transpiration and diaphragm gage studies, although it is still higher than the estimate (less than 15%) based on these data alone.

Schäfer and Hönes[15] have made an extensive study of the iron–iodine system, including transpiration measurements of the vapor pressure of FeI_2 in the vicinity of its melting point (594°) and a measurement of the temperature at which the liquid boils under an external pressure of one atmosphere (935°). Our torsion effusion results, the transpiration measurements of Schäfer and Hönes and total pressures above solid and liquid FeI_2 measured in this work in a quartz diaphragm gage study are shown together in Fig. 3. The effusion data from cell 2 are seen to be in good agreement with an extrapolation of the results of Schäfer and Hönes; they have assumed the major vaporizing species to be monomeric FeI_2. The total pressures measured by torsion effusion in our work give some support for this assumption. The straight line consistent with both sets of data for the vaporization of the solid may be represented by the equation $\log P_{mm.}\ (FeI_2)_g = 10270T^{-1} + 12.60$, corresponding to values of $\Delta H^0 = 47.0$ kcal. and $\Delta S^0 = 44.4$ e.u. Pressures obtained with cell 1 (larger orifices) are markedly lower than cell 2, as

(15) H. Schäfer and W. J. Hönes, *Z. anorg. allgem. Chem.*, **288**, 62 (1956).

observed with $FeBr_2$, suggesting a small accommodation coefficient for FeI_2.

Schäfer and Hönes state that FeI_2 is not very stable, liberating iodine at high temperatures by decomposition. We have also observed liberation of iodine in experiments in which a *ca.* 0.2-g. sample of FeI_2 was resublimed in several steps in a quartz tube (sample sublimed from a zone between 550 and 600° to the cool portion of the tube adjacent to the furnace) under continuous evacuation. The amount of iodine collected (in an adjacent trap) during the sublimation was less than 10% of the original sample; no visible residue in the portion of the tube remaining in the hot zone could be seen. Since the major portion of the sample sublimed without change, it has been assumed that the contribution of iodine to the total pressure measured in the effusion study can be neglected. This assumption is also suggested by the agreement of our measured pressures with those expected by an extrapolation of the data of Schäfer and Hönes.

Very recent work by Schoonmaker, Friedman and Porter[16] indicates, by mass spectrometric analysis, that a small amount of Fe_2I_4 is present in the equilibrium vapor of FeI_2 in the effusion range; the concentration of the dimer increases at higher temperatures (*ca.* 50% near the boiling point). The existence of appreciable amounts of dimer at high temperatures offers a possible explanation for the observation (Fig. 3) that transpiration data of Schäfer and Hönes, in which only monomer was assumed, lie appreciably above the total pressures measured in this Laboratory at the highest temperatures of their measurements. Their values are also high compared with the temperature at which they observed the total pressure above liquid FeI_2 to be one atmosphere. At these high temperatures the iodine dissociation pressure may also make an appreciable contribution; vapor pressure data above the melting point cannot be interpreted with certainty at this time.

Acknowledgment.—The work was supported by a grant from the National Science Foundation.

(16) R. C. Schoonmaker, A. H. Friedman and R. F. Porter, private communication, publication forthcoming.

THE EXTRACTION OF IRON(III) FROM ACID PERCHLORATE SOLUTIONS BY DI-(2-ETHYLHEXYL)-PHOSPHORIC ACID IN *n*-OCTANE

BY C. F. BAES, JR., AND H. T. BAKER[1]

Contribution from the Oak Ridge National Laboratory, Oak Ridge, Tennessee, Operated by Union Carbide Corporation for the U. S. Atomic Energy Commission and Texas Woman's University, Denton, Texas

Received July 10, 1959

The distribution of iron(III) between acidic aqueous perchlorate solutions and solutions of di-(2-ethylhexyl)-phosphoric acid [$(RO)_2PO_2H$, DPA] in *n*-octane has been examined as a function of various extraction variables at constant aqueous ionic strength. The organic solutions involved have been investigated by means of isopiestic molecular weight determinations and viscosity measurements. The distribution behavior at low iron levels (iron:DPA <0.1) is consistent with the formation of the extraction complex, FeX_6H_3, in which X denotes the anion $(RO)_2PO_2^-$. However, the DPA concentration dependence of extraction indicates partial trimerization of (dimeric) DPA in octane, $3(HX)_2 \rightleftarrows 2(HX)_3$, with an equilibrium constant of *ca.* 10 M^{-1}. The results at high iron levels suggest the formation of two additional iron:DPA complexes, $[Fe_3X_8ClO_4 \cdot \sim 5H_2O]_n$ ($n \sim 4$) and $Fe_5X_8ClO_4(OH)_6 \cdot \sim 7H_2O$.

Introduction

Dialkylphosphoric acids ($(RO)_2PO_2H$), as well as other organophosphorus compounds, have been used as solvent extraction reagents for a large number of aqueous cations. Much of this work has been cited by Blake, *et al.*,[2,3] and Peppard, *et al.*[4] Both conclude that the dialkylphosphoric acids extract cations in low concentration by the cation-exchange reaction

$$M^{+z}(a) + z(HX)_2(o) \rightleftarrows M(X_2H)_z(o) + zH^+(a) \quad (1)$$

in which X denotes the anion $(RO)_2PO_2^-$. That the extractant is present in non-polar solvents as a dimer has been shown by Peppard, *et al.*,[5] Baes, *et al.*,[6] and Dyrssen.[7] As metal concentrations in the organic phase are increased, it is found in many cases that additional extraction complexes are formed which involve M:X ratios greater than 1:2*z*. However, detailed study of these higher complexes has been carried out only in the case of uranyl ion,[6] where it was found that increasingly long chain polymers of the type $HX_2UO_2X_2 \ldots UO_2X_2H$ are formed.

One purpose of the present detailed investigation of iron(III) extraction by di-(2-ethylhexyl)-phosphoric acid, DPA, has been to characterize the higher complexes of a trivalent cation. Another has been to verify the predicted extraction reaction at low iron concentrations

$$Fe^{+++}(a) + 3(HX)_2(o) \rightleftarrows FeX_6H_3(o) + 3H^+(a) \quad (2)$$

Previous limited results[1] indicated a second power rather than third power dependence of iron(III)

(1) Summer research participant with the Oak Ridge National Laboratory, 1958, sponsored by the Oak Ridge Institute of Nuclear Studies. Chemistry Department, Texas Woman's University, Denton, Texas.

(2) C. A. Blake, Jr., C. F. Baes, Jr., K. B. Brown, C. F. Coleman and J. C. White, "International Conference on the Peaceful Uses of Atomic Energy," Geneva, 1958, p. 1550.

(3) C. A. Blake, Jr., C. F. Baes, Jr., and K. B. Brown, *Ind. Eng. Chem.*, **50**, 1763 (1958).

(4) D. F. Peppard, G. W. Mason, W. J. Driscoll and R. J. Sironen, *J. Inorg. Nucl. Chem.*, **7**, 276 (1958).

(5) D. F. Peppard, J. R. Ferraro and G. W. Mason, *ibid.*, **7**, 231 (1958).

(6) C. F. Baes, Jr., R. A. Zingaro and C. F. Coleman, THIS JOURNAL **62**, 129 (1958).

(7) D. Dyrssen, *Acta Chem. Scand.*, **11**, 1771 (1957).

extraction on DPA concentration and so the tentative suggestion was made that $FeOH(X_2H)_2$ is formed rather than FeX_6H_3. This unexpected behavior requires confirmation because the data were not only limited but also were of doubtful accuracy owing to the relatively slow iron(III) extraction rate.

As in the previous investigation of DPA-uranyl ion extraction[6] acidic perchlorate aqueous solutions of ionic strength 2 *M* have been used, and the extraction measurements have been supplemented by isopiestic measurements on the organic phase. Octane has been used as the solvent rather than hexane (previously used) because its lower volatility was an advantage in the volumetric work and in the isopiestic measurements.

Isopiestic measurements of DPA–octane solutions have been reported previously.[8] While they indicate the expected dimerization, the observed isopiestic ratios show up to 10% deviation from ideal solution behavior of the dimer indicating possible further association of DPA.

Experimental

Reagents.—The DPA used was purified by the procedure previously described,[9] yielding a reagent which, by potentiometric titration was 99.5% dioctylphosphoric acid containing <0.1% monooctylphosphoric acid. The principal impurities were probably 2-ethylhexanol and the trioctylphosphate ester which in such small amounts are not expected to appreciably influence the extraction results. It has been reported that the presence of straight chain alkyl groups in a dialkylphosphoric acid results in precipitation of extracted iron(III).[2] With the present reagent no such precipitation was noted even in nearly saturated iron(III)–DPA solutions which had stood for months. In addition, unlike the uranium(VI) extraction system previously studied,[6] there was no evidence of decomposition in iron(III)–DPA solutions. The octane used as the solvent was Phillips Petroleum Co. Pure Grade (99 mole % minimum).

The iron-59 tracer[10] (a 45.1 day γ-emitter) was received as ferric chloride (*ca.* 0.01 *M*) in hydrochloric acid solution, 0.5–1 ml. (*ca.* 0.5–1 millicurie) at a time. It was purified[11] by adjusting the hydrochloric acid concentration to 9 *M* and passing the solution through a small column of Dowex-1 anion-exchange resin. After washing with several column volumes of 9 *M* HCl, the iron(III) was eluted with 0.5 *M* HCl, and this solution was evaporated nearly to dryness. Perchloric acid was added, the sample was evaporated to fuming and then diluted to 100 ml. with water. These stock solutions (giving several million counts/min./ml.) were analyzed for iron(III) by a colorimetric thiocyanate method[12] and for acid by titration with standard base.

Tracer-free iron(III) perchlorate stock solutions were prepared by fuming ferric nitrate solution several times with perchloric acid and then diluting to volume. The iron(III) concentration was determined by the volumetric dichromate method.[13] The excess perchloric acid was determined by titration with standard base and correction for the precipitation of the iron as ferric hydroxide. Sodium perchlorate stock solutions were made by careful neutralization of perchloric acid and with sodium hydroxide. The solutions were analyzed by evaporation of a sample to dryness and weighing the solid. Reagent grade chemicals were used in both these preparations.

Extraction Measurements.—As Blake, *et al.*,[9] have reported the rate of iron(III) extraction by DPA is much slower than is the rate of uranium(VI) extraction. Iron extraction by 0.1 *M* DPA in a slowly stirred system (40 ml. of each phase, unbroken interface) had a half time of *ca.* 16 hr. at 0.1 *M* $HClO_4$ and *ca.* 75 hr. at 0.5 *M* $HClO_4$. With similar solutions in a 120-ml. separatory funnel shaken at 120 strokes/min. half times of *ca.* 0.4 and 2 hr., respectively, were found. With 4 ml. of each phase in the rapidly shaken 20-ml. vials used in nearly all the measurements reported here, the corresponding half times were 0.1 and 0.5 hr.

The extractions were usually done with 4-ml. volumes of each phase in a 20-ml. screw-capped vial (with a polyethylene cone-type sealing liner), one vial for each sample. As many as 40 of these at a time were shaken (at 200 strokes/min. using an 8-in. shaker arm) in a 25 ± 0.02° thermostat. Duplicate samples were run in nearly all cases, one being shaken considerably longer than the other. Shaking times were 2–3 days, several times longer than was judged necessary for equilibrium. The solutions were separated using a small separatory funnel, then centrifuged and 1-ml. samples of each phase were introduced into small test-tubes for counting. Counting rates varied from 600 counts/min. (*ca.* twice the background) to 300,000 counts/min., counting times being sufficient for at least 10,000 counts. The usual precision of analysis was better than 1% relative error and material balances usually checked to within 2%. Equilibrations were run in which the tracer and the tracer-free iron were initially in the same phase, initially in different phases, and both initially in both phases. Regardless of the course of the extraction, the results were in satisfactory agreement, giving good evidence of equilibrium.

A portion of the extractions at higher iron concentrations involved larger solution volumes (up to 50 ml. of each phase) per sample, so that several other analyses could be made on the equilibrated phases. These included water analysis of the organic phase by Karl Fischer titration[12]; perchlorate analyses of the organic phase (by stripping with aqueous HCl and determining the perchlorate in the aqueous phase)[12] and acid analysis of the aqueous phase by potentiometric titration with standard base.

Isopiestic Measurements.—The apparatus and procedure used are the same as previously described.[6,8] Triphenylmethane was used as the reference solute in all the measurements. In general, the solutions were as dilute (*ca.* 0.01–0.02 *m* particle concentrations) as could be conveniently run. The outgassing procedure, as in the previous octane measurements,[8] involved freezing the solution samples to ensure adequate removal of air.

Results and Discussion

The DPA molarities given (*M* DPA or C_{DPA}) are total concentrations using the molecular weight of the monomer. The following symbols expressing DPA concentration also will be used

C_{HX}, total concn., as monomer, unreacted with Fe(III)

$C_{(HX)_2}$, $C_{(HX)_3}$, actual soln. concn. of dimer and trimer, resp.

All, of course, are organic phase concentrations. Additional concentration symbols to be used include

$C_{Fe(o)}$, $C_{Fe(a)}$, total iron(III) concn. in organic and aqueous phase, resp.

C_H, aqueous hydrogen ion concn.

The iron(III) extraction coefficient will be denoted by E_a^o ($= C_{Fe(o)}/C_{Fe(a)}$).

Low Iron Concentrations.—If the extraction reaction shown in equation 2 is the only one occurring to an appreciable extent at low iron levels ($C_{Fe(o)}/C_{DPA} < 0.1$) — and this will be borne out by the results — then the corresponding equilibrium quotient is

$$Q = \frac{C_{Fe(o)}C^3_H}{C_{Fe(a)}C^3_{(HX)_2}} = E_a^o C^3_H / C^3_{(HX)_2} \qquad (3)$$

If all the unreacted DPA is dimeric, then

(8) C. F. Baes, Jr., Report ORNL-2737, July (1959).

(9) C. A. Blake, K. B. Brown and C. F. Coleman, Report ORNL-1903, June (1955), p. 106. The DPA, obtained from the Virginia-Carolina Chemical Co., was purified by J. M. Schmitt of this Laboratory.

(10) Fe-59-P, obtained from the Isotopes Division of Oak Ridge National Laboratory.

(11) *Cf.* G. E. Moore and K. A. Kraus, *J. Am. Chem. Soc.*, **72**, 5792 (1950).

(12) These analyses were performed by the Analytical Chemistry Division of the Oak Ridge National Laboratory.

(13) I. M. Kolthoff and E. B. Sandell, "Textbook of Quantitative Inorganic Analysis," Rev. Ed., The Macmillan Co., New York, N. Y., 1948, p. 609.

TABLE I

EXTRACTION RESULTS AT LOW IRON(III) CONCENTRATIONS

Aqueous ionic strength 2.0 M, 25°

$C_{Fe(o)}$	C_H	E_a°	$E_a^\circ C^3_H$	$Q' \times 10^{-5}$ [a]	C_{HX} [b]	$\frac{C_{DPA} - C_{HX}}{C_{Fe(o)}}$
			0.0100 M DPA			
5.97×10^{-7}	0.4974	1.69	0.208	16.7		
4.15×10^{-6}	.4971	1.66	.204	16.4		
3.68×10^{-5}	.4971	1.60	.197	16.9		
7.07×10^{-4}	.3057	1.62	.0462	19.3	0.00583	5.9
8.92×10^{-4}	.3043	0.987	.0278	22.2	0.0048	5.8
			0.0250 M DPA			
1.58×10^{-4}	0.3070	79	2.27	13.1		
2.89×10^{-4}	.6189	9.0	2.12	13.5		
3.19×10^{-4}	.2277	155	1.83	11.9		
0.00125	.3069	32.7	0.95	14.0	0.0179	5.7
157	.2277	49	.578	9.18	148	6.5
163	.6172	2.64	.621	10.4	152	6.0
207	.3065	12.2	.351	8.99	123	6.1
240	.6127	1.15	.265	9.69	111	5.8
			0.100 M DEPA [c]			
0.00178	2.0304	8.2	68.8	7.15		
189	1.5404	17.8	65.1	6.97		
196	1.0494	54	62.4	6.77		
198	0.8044	116	60.4	6.58		
199	.5584	352	61.3	6.70		
200	.3134	1770	54.5	5.96		
342	.5006	343	43.0	6.85	0.0795	6.0
680	.5005	151	19.0	7.30	568	6.4
.01005	.5000	49	6.18	7.91	367	6.3

[a] Defined by equation 4. [b] The unreacted DPA concentration, obtained from the plot in Fig. 1 at the value of $E_a^\circ C^3_H$ listed in column 4. [c] The first six measurements in this series were obtained using 0.102 M DPA.

$$Q' = 8E_a^\circ C^3_H/(C_{DPA} - 6C_{Fe(o)})^3 \qquad (4)$$

This quotient, which will be evaluated from the measurements, is distinguished from the previous one by a prime to denote that it will differ from it if, as is suggested by the isopiestic results,[8] the DPA undergoes partial association beyond the dimer. In addition, Q' (and Q) will vary if the activity coefficients of the four species involved in equation 2 are not constant. In the present measurements the concentration of FeX_6H_3 does not exceed 0.01 M and the aqueous Fe^{+++} and H^+ ion concentrations are generally low compared to the 2 M ionic strength used, so that their activity coefficients are expected to remain nearly constant. Appreciable variation is expected only in the activity coefficients of the DPA species.

A portion of the extraction results at low iron levels are compared in Table I with the expression in equation 4. Referring to the first six measurements at 0.1 M DPA, the acidity varied from 0.3 to 2 M while $C_{Fe(o)}$ remained nearly constant with the result that $E_a^\circ C^3_H$ was constant within the accuracy of measurement. This verifies that E_a° is inversely proportional to the cube of the aqueous acidity. Referring to the first three measurements at 0.01 M DPA, it is seen that $E_a^\circ C^3_H$ remains constant as $C_{Fe(o)}$ varies from 6×10^{-7} to 4×10^{-5} M. This verifies that here the iron–DPA extraction complex is mononuclear in iron. However, the values of Q' listed in the table do not remain constant as $C_{Fe(o)}$ is increased further or, especially, as the DPA concentration level is changed.

The variation of Q' with the DPA concentration is reflected by the additional measurements in Fig. 1. In the range 0.004–0.1 M DPA, the slope of this plot of log $E_a^\circ C^3_H$ *vs.* log $[C_{DPA} - 6C_{Fe(o)}]$ is 2.65, rather than 3 as expected from equations 2–4. Values of the unreacted DPA concentration C_{HX} listed in Table I were read from this plot at corresponding values of $E_a^\circ C^3_H$. The difference $(C_{DPA} - C_{HX})$ corresponds to the DPA which has been consumed in extracting the iron, and so the ratio $(C_{DPA} - C_{HX})/C_{Fe(o)}$ listed in the last column of the table corresponds to the average mole ratio of DPA to iron in the extraction complexes formed. In all cases this ratio was found to be 6 within the accuracy of its determination. It should be noted that this ratio does not merely result from the assumption $C_{HX} = C_{DPA} - 6C_{Fe(o)}$ applied to the results in Fig. 1 since there the iron concentration level was relatively low $(C_{Fe(o)}/C_{DPA} < 0.01)$ so that the C_{HX} value obtained was relatively insensitive to the choice of complexing ratio. It appears, therefore, that the reaction in equation 2 is essentially correct in that it denotes the formation of FeX_6H_3 at low iron levels.

Accordingly, the wide variation in Q' is attributed to partial further association of DPA and/or variation in the activity coefficients of the DPA species in solution. If the following trimerization reaction is assumed

$$3(HX)_2 \rightleftarrows 2(HX)_3;\ Q_t = C^2_{(HX)_3}/C^3_{(HX)_2} \qquad (5)$$

then it can be shown that

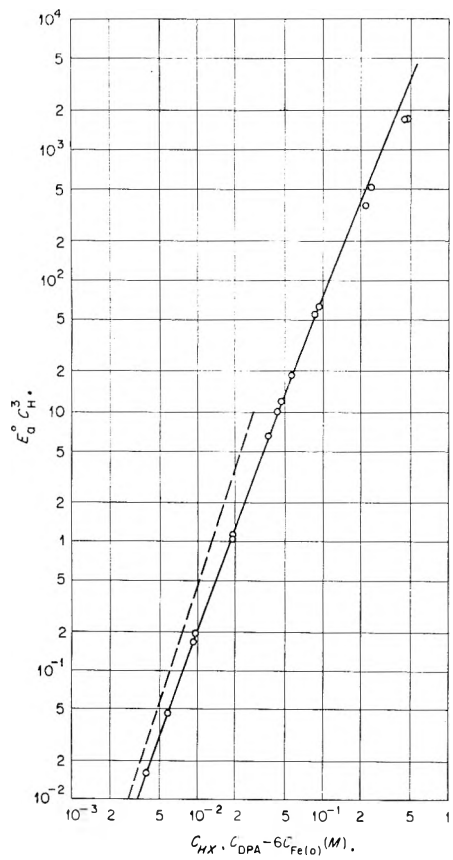

Fig. 1.—The dependence of iron(III) extraction on the DPA concentration at low iron levels. $C_{Fe(o)}/C_{DPA} < 0.01$, 2 M aqueous ionic strength, 25°. The solid curve was calculated from equation 7; the dashed line has a slope of 3.

$$(Q')^{1/3} = Q^{1/3} - \frac{3}{\sqrt{8}} \frac{Q_t^{1/3}}{Q^{1/6}} \sqrt{Q'C_{HX}} \qquad (6)$$

and so if all activity coefficients are constant $(Q')^{1/3}$ should be a linear function of $\sqrt{Q'C_{HX}}$. This relation is found to fit the results in Fig. 1, giving

$$(Q')^{1/3} = 152.4 - 0.2747 \sqrt{Q'C_{HX}} \qquad (7)$$

in the range 0–0.3 M DPA. The coefficients give

$$Q = 3.54 \times 10^6, Q_t = 10\ M^{-1}$$

The agreement of equation 7 with the results is indicated by the solid curve in Fig. 1.

This agreement, of course, does not mean that partial trimerization of DPA is the sole cause of the variation in Q'. While the assumption of constant activity coefficients for the DPA species is reasonable at the lower concentrations involved, some variation is to be expected as C_{DPA} approaches 0.3 M. In addition there is the possibility of further association. Without more direct evidence for this specific reaction (equation 5), the success of this interpretation should be considered no more than a good indication of the nature of DPA–octane non-ideal solution behavior. Accordingly, it is perhaps more useful to express the observed variation of Q' in terms of a practical activity coefficient $y_{(DPA)_2}$ for DPA which refers to an infinite dilution standard state of the dimer. Then $y_{(DPA)_2} = (Q'/Q)^{1/3}$ and from equation 7

$$y_{(DPA)_2} = 1 - 4.80 \sqrt{y^3_{(DPA)_2}(C_{HX}/2)} \qquad (8)$$

The isopiestic results for DPA in dry octane solutions have been compared with activity coefficient values given by this equation.[8] Assuming a unit activity coefficient for the reference solute in these measurements (triphenylmethane), the results gave

$$\log \gamma_{(DPA)_2} = -0.523 m^{1/3}_{(DPA)_2} + 0.420 m_{(DPA)_2}$$

in the range $m_{(DPA)_2}$ (the DPA molality as dimer) = 0.02–0.16. Solving equation 8 for $y_{(DPA)_2}$ as a function of the DPA molarity as dimer and converting to the molality scale gives

$$\log \gamma_{(DPA)_2} = -0.643 m^{1/3}_{(DPA)_2}$$

in the same concentration range. These two expressions lead to a 10% discrepancy in $\gamma_{(DPA)_2}$ at 0.02 m, which increases to a 35% discrepancy at 0.16 m; however, this agreement seems acceptable in view of the approximation that $\gamma_{TPM} = 1$ and since equation 8 refers to water-saturated octane solutions while the isopiestic measurements were made on dry octane solutions.

High Iron Concentrations.—Extraction results at iron:DPA ratios greater than 0.1 are presented in Fig. 2. $C_{Fe(o)}/C_{DPA}$ is plotted *vs.* $C_{Fe(o)}$ (normalized to an aqueous acidity of 1 M) at 0.1 M and 0.025 M DPA. As the equilibrium aqueous iron concentration is increased, the Fe:DPA mole ratio soon exceeds 0.167 (corresponding to FeX_6H_3), levels off at *ca.* 0.38, then rises sharply and again levels off at *ca.* 0.6. Thus, it appears that at least two additional complexes are formed as the iron concentration is increased. Since both these complexes contain more iron than corresponds to the complete replacement of all the acidic hydrogen of the extractant (Fe:DPA = 0.333), they must involve the anions ClO_4^- or OH^-, or both.

Results of perchlorate analyses of the organic phase are presented in the lower portion of Fig. 3. Beginning at an iron:DPA ratio of 0.167, the ClO_4:DPA ratio rises from near zero to 0.125 at iron:DPA = 0.375 and then remains constant within the scatter of the results. The simplest stoichiometries for the additional extraction complexes consistent with these analyses, the water analyses[14] also shown in Fig. 3, and the extraction results are

$$Fe_3X_8ClO_4 \cdot ca.\ 5H_2O;\ Fe_5X_8ClO_4(OH)_6 \cdot ca.\ 7H_2O$$

The isopiestic measurements are presented in the upper portion of Fig. 3 (open circles). The quantity plotted is the ratio of the iron concentration in the DPA solution to the triphenylmethane (TPM) concentration in the reference solution at isopiestic equilibrium. If ideal solution behavior is assumed at the relatively low concentrations involved (0.011–0.018 m TPM), then this ratio should be n, the average number of iron atoms per solute species in the DPA solutions. As ex-

(14) Water analyses were obtained by the usual Karl–Fischer procedure and also by a procedure in which salicylic acid was added to liberate as water any OH present in the sample and through complex formation to prevent possible interference caused by reduction of iron(III). Results by the two methods agreed below iron:DPA = 0.375. At higher iron levels the latter method gave the higher results, and these are shown in Fig. 3. That hydrolyzed iron is present in the more concentrated solutions is suggested also by a pronounced deepening in color of the octane solutions as iron:DPA is increased beyond 0.375.

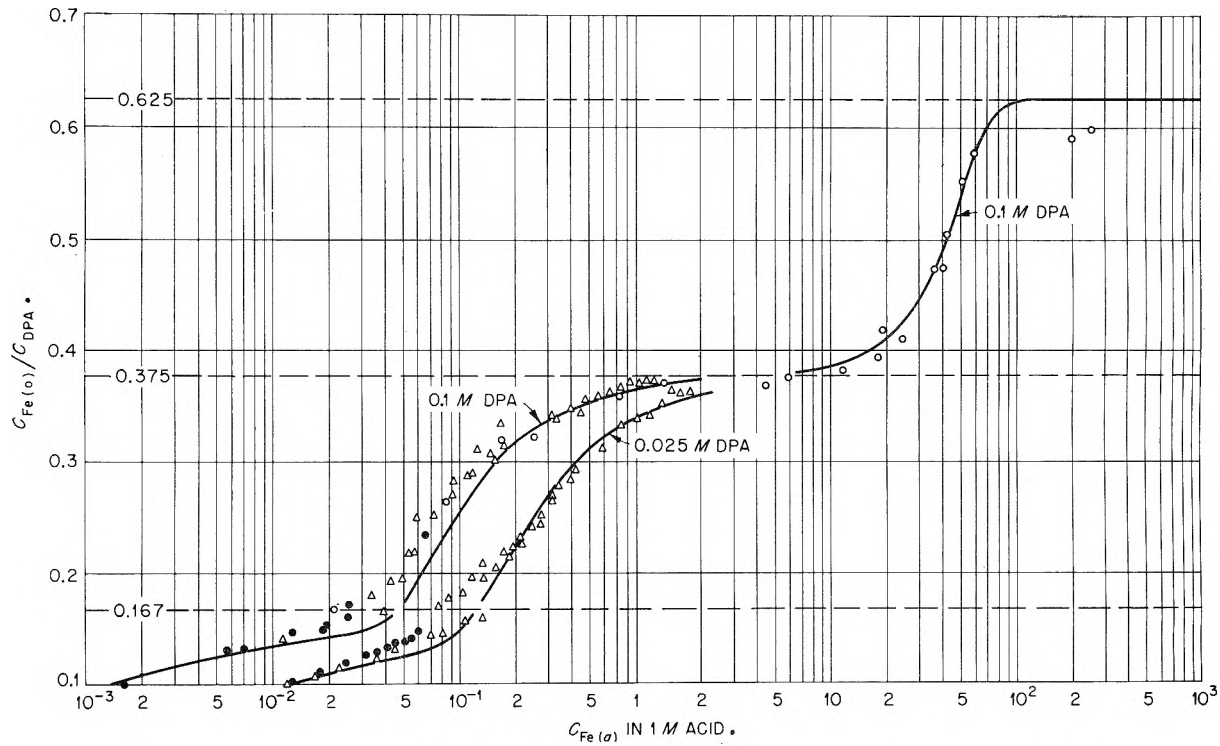

Fig. 2.—Iron(III) extraction isotherms at high iron concentrations. C_{DPA} = 0.1 M and 0.025 M, 2 M aqueous ionic strength, 25°C: ●, C_H = 0.5–0.6 M; △, C_H = 0.2–0.3 M; ○, C_H = 0.07–0.1 M. To normalize the results to a constant aqueous acidity (C_H = 1 M): $C_{Fe(o)}/C_{H_3}$ is plotted on the abscissa for $C_{Fe(o)}/C_{DPA}$ <0.167 and >0.375; in the range $C_{Fe(o)}/C_{DPA}$ = 0.167–0.375, $C_{Fe(o)}/C_H^{2.4}$ is plotted as the abscissa (*cf.* equations 9 and 10). The curves were calculated assuming equations 9 and 10 with the corresponding equilibrium quotients $Q_2 = 250\ M^{0.15}$ and $Q_3 = 1.2 \times 10^{-5}\ M^{4.75}$ (*cf.* footnote 16).

pected, n is 1 at iron:DPA = 0.167 and consistent with the proposed complex $Fe_5X_8ClO_4(OH)_6$, it approaches *ca.* 5 as iron:DPA approaches 0.625. The intermediate values, however, are seen to go through a maximum at iron:DPA = 0.375, with n ~12. This suggests the second extraction complex to be $[Fe_3X_5ClO_4\cdot hyd]_4$. The solid curve in the upper part of Fig. 3 shows the expected variation of n with composition on the simplifying assumption that the only organic solution species are FeX_6H_3 and $[Fe_3X_5ClO_4\cdot hyd]_4$ in the range iron:DPA = 0.167–0.375, and $[Fe_3X_5ClO_4\cdot hyd)_4$ and $Fe_5X_8ClO_4(OH)_6\cdot hyd$ in the range iron:DPA = 0.375–0.625. The agreement of this curve with the results is satisfactory considering the scatter of the points. It is by no means certain, however, that so large a species as $[Fe_3X_5ClO_4\cdot hyd]_4$ would behave ideally in solution; so the extent of association is considered fairly uncertain, *e.g.*, n may be as low as 9 or considerably greater than 12.

The viscosity measurements also shown in Fig. 3 reflect the association of the second complex showing a sharp maximum near iron:DPA = 0.375.

Returning now to the extraction results in Fig. 2, the equilibrium between the first and second extraction complexes may be written (neglecting hydration)

$$0.8FeX_6H_3(o) + Fe^{+++}(a) + 0.6ClO_4^-(a) \rightleftharpoons 0.15[Fe_3X_5ClO_4]_4(o) + 2.4H^+(a) \quad (9)$$

It is seen that for each mole of iron extracted from the aqueous phase, 2.4 moles of acid appear in the aqueous phase.[15] Accordingly, to normalize the extraction results at the various acidities used (0.07–0.6 M H^+) to the same acidity, the function $C_{Fe(o)}/C_H^{2.4}$ was plotted as the abscissa in the range $C_{Fe(o)}/C_{DPA}$ = 0.167–0.375. At the higher iron levels, the principal extraction reaction is written

$$0.25[Fe_3X_8ClO_4]_4(o) + 2Fe^{+++}(a) + 6H_2O(a) \rightleftharpoons Fe_5X_8ClO_4(OH)_6(o) + 6H^+(a) \quad (10)$$

As at low iron levels, 3 moles of acid appear in the aqueous phase per mole of iron extracted and so, in this range, $C_{Fe(o)}/C^3_H$ is plotted as the abscissa in Fig. 2.

The smooth curves shown in Fig. 2 were calculated from these two extraction reactions (eq. 9 and 10) using the equilibrium quotient values

$$Q_2 = \frac{C_{12}^{0.15}C_H^{2.4}}{C_1^{0.8}C_{Fe(a)}C_{ClO_4}^{0.6}} = 250\ M^{0.15}$$

$$Q_3 = \frac{C_5C^6_H}{C_{12}^{0.25}C^2_{Fe(a)}} = 1.2 \times 10^{-5}M^{4.75}$$

in which the concentrations of the first, second and third extraction complexes are denoted by C_1, C_{12} and C_5, respectively.[16] In the range $C_{Fe(o)}/$

(15) This acid yield is independent of the degree of association of $Fe_3X_8ClO_4$.

(16) In calculating the curves in Fig. 2: For the range $C_{Fe(o)}/C_{DPA}$ >0.375, it was assumed that the second and third extraction complexes were the only organic solution species. Then

$$C_{Fe(o)} = 12C_{12} + 5C_5;\ C_{DPA} = 32C_{12} + 8C_5$$

Solving for C_{12} and C_5

$$C_{12} = 0.125(0.375C_{DPA} - C_{Fe(o)})$$
$$C_5 = 0.5(C_{Fe(o)} - 0.375C_{DPA})$$

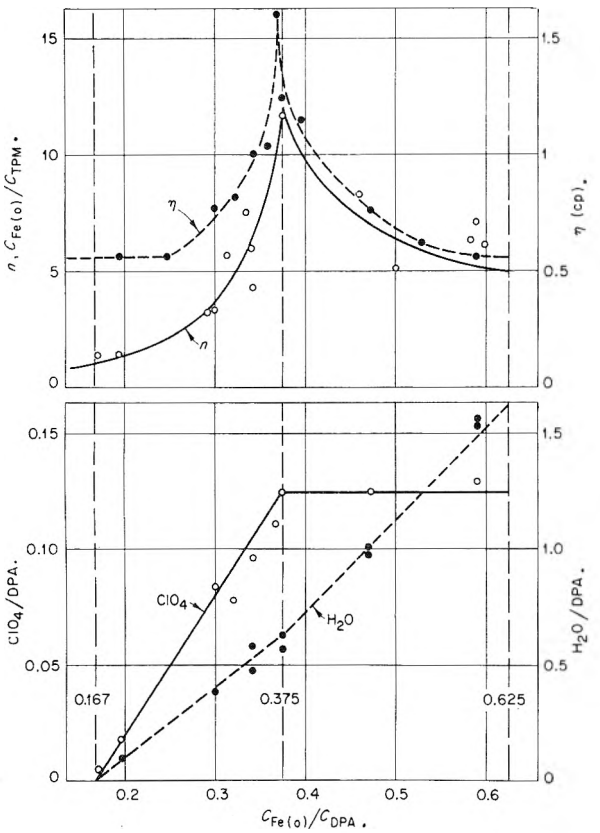

Fig. 3.—Results on octane solutions at high iron: DPA ratios. Here n is the average number of iron atoms per solute species (assuming ideal solution behavior) from isopiestic equilibrations with triphenylmethane–octane solutions (C_{TPM} = 0.011–0.018 m). These n values, as well as the ClO_4:DPA and H_2O:DPA mole ratios, are compared with curves calculated on the assumption that the only solute species are: FeX_6H_3 and $[Fe_3X_8ClO_4{\cdot}5H_2O]_4$ in the range $C_{Fe(o)}/C_{DPA}$ = 0.167–0.375; $[Fe_3X_8ClO_4{\cdot}5H_2O]_4$ and $Fe_5X_8ClO_4(OH)_6{\cdot}7H_2O$ in the range $C_{Fe(o)}/C_{DPA}$ = 0.375–0.625.

C_{DPA} = 0.375–0.625, the extraction results agree well enough with the behavior predicted from equation 10, with the exception of the two points at the highest values of $C_{Fe(o)}/C^3_H$. Their deviations are greater than the expected errors in determining $C_{Fe(o)}$, $C_{Fe(a)}$ and C_H, and more results at these high concentrations would be desired. However, measurements here are relatively difficult.[17] A limiting iron:DPA combining ratio of 0.6, which these two results tend to suggest, rather than the predicted value 0.625, may be ruled out since a stock solution was prepared which, by analysis, gave $C_{Fe(o)}/C_{DPA}$ = 0.629, in agreement within experimental error with the predicted value.

In the range $C_{Fe(o)}/C_{DPA}$ = 0.3–0.375, the results at both 0.1 and 0.25 M DPA agree with the behavior predicted from equation 9. At lower iron levels, the results at 0.1 M DPA show appreciable deviation, as do the 0.025 M DPA results at still lower iron levels. These deviations may result from the presence of less associated $Fe_3X_8ClO_4$ species, from the presence of a new species intermediate between FeX_6H_3 and $[Fe_3X_8ClO_4]_4$, or they may result simply because the assumption of ideal behavior of all the organic solution species which was made in calculating the curves is inadequate.

The over-all agreement between the extraction results and the calculated curves assuming $[Fe_3X_8ClO_4]_4$ as the second complex was distinctly better than that found if a much larger polymer of $Fe_3X_8ClO_4$ is assumed, or if a smaller one is assumed. Taken together, the extraction results, the viscosity results, the isopiestic results and the organic solution analyses provide a reasonably consistent body of evidence for the proposed extraction complexes.

Comparing the extraction behavior of iron(III) with that previously reported for uranium(VI),[6] at low metal concentrations both are consistent with the general reaction in equation 1. However, in the case of uranium, the (less extensive) data on DPA concentration dependence of extraction gave no evidence that DPA is partially trimeric in hexane.[18] At high metal concentrations, both uranium(VI) and iron(III) form polymerized metal–DPA complexes. While in the case of uranium it was possible to propose plausible structures for these complexes, in the present case none suggest themselves. The presence of perchlorate in the higher complexes of iron with DPA is new to the chemistry of this extractant in dilute acid systems. The possibility that other anions may be similarly involved in extractions of iron(III) and other trivalent cations by DPA should be considered in any future investigations. A significant conclusion to be drawn from the two investigations is that the chemistry involved in such solvent extraction systems is by no means simple, and, at least for the present, is unpredictable.

Acknowledgments.—It is a pleasure to thank W. E. Oxendine for valuable technical assistance, particularly in the numerous extraction measurements. The authors wish also to express their appreciation to J. A. Hill for his contribution to the study of the extraction rates.

Introducing these expressions into the quotient for Q_3, Q_3 was then estimated from the extraction results.

For $C_{Fe(o)}/C_{DPA} < 0.375$, it was assumed that

$$C_{Fe(o)} = C_1 + 12C_{12};\ C_{DPA} = C_{HX} + 6C_1 + 32C_{12}$$

wherein C_6 is neglected but the concentration of unreacted DPA, C_{HX} is included. Solving for C_1 and C_{12}

$$C_1 = 0.8[0.375(C_{DPA} - C_{HX}) - C_{Fe(o)}]$$
$$C_{12} = 0.15[C_{Fe(o)} - 0.167(C_{DPA} - C_{HX}]$$

To obtain an approximate value of Q_3, C_{HX} was at first neglected in these expressions for C_1 and C_{12}. With the resulting Q_3 value, it was then possible to estimate C_{HX} from the plot in Fig. 1 (which relates C_1 $C_{Fe(a)}$ and C_{HX}). With these C_{HX} values, a final estimate of Q_3 was then made from the extraction data in Fig. 2.

(17) Since the changes in acidity on extraction are comparable to the final value desired (which must be less than 0.1 M if $C_{Fe(a)}$ is not to exceed 0.1–0.2 M), the equilibrium acidity cannot be calculated with confidence from acid balance but instead must be determined by titration in the presence of a relatively large amount of iron.

(18) A small deviation of the uranium extraction results from the expected second power dependence on DPA concentration was in the opposite direction and was tentatively ascribed to partial dissociation of the dimer. In view of later work (ref. 5 and 7), this now seems unlikely.

THE CONSTITUTION OF CRYOLITE AND $NaF-AlF_3$ MELTS

BY W. B. FRANK AND L. M. FOSTER

Alcoa Research Laboratories, Aluminum Company of America, New Kensington, Pennsylvania

Received July 9, 1959

The composition of molten cryolite is considered from the standpoint of dissociation to logical products. Calculations employing experimental densities provide an excellent fit with the data for dissociation to NaF and $NaAlF_4$, with K = 0.09 at 1000°. Densities for Na_3AlF_6 and $NaAlF_4$ of 2.210 and 1.873 g./ml., and gram ion volumes for Na^+, F^-, AlF_4^- and AlF_6^{-3} of 5.7, 15.8, 61.6 and 77.9 are derived. Molten cryolite at 1000° has this composition by mole fraction: Na_3AlF_6, 0.384; NaF, 0.411; and $NaAlF_4$, 0.205. The heat of dissociation of cryolite is ΔH = 22 kcal./mole.

Introduction

When a sodium fluoride–aluminum fluoride mixture in the stoichiometric ratio of cryolite ($3NaF \cdot AlF_3$) is fused and solidified, the product is entirely cryolite by X-ray and petrographic examination. Phase diagrams of the $NaF-AlF_3$ system have been reported by Fedotieff and Iljinskii,[1] Puschin and Baskow,[2] Hardouin,[3] Lorentz, Jabs and Eitel,[4] and recently by Grjotheim.[5] Cryolite melts congruently. The compound maximum is broad, indicating partial dissociation into simpler species in the molten state. Grjotheim[5] calculated the liquidus curve in the vicinity of the cryolite composition according to the four schemes (sodium was assumed to be completely ionized in all cases)

$$2AlF_6^{-3} = Al_2F_{11}^{-5} + F^- \quad (1)$$

$$AlF_6^{-3} = AlF_5^{-2} + F^- \quad (2)$$

$$AlF_6^{-3} = AlF_4^- + 2F^- \quad (3)$$

$$AlF_6^{-3} = Al^{+3} + 6F^- \quad (4)$$

It was necessary in the calculation to assume the heat of dissociation to be zero so the dissociation constant would be independent of temperature. Also, ΔC_P was assumed to be zero and no dissociation was considered in the solid.

By trying various degrees of dissociation, arbitrarily chosen, for each scheme, and comparing the calculated with the observed curve, Grjotheim eliminated (1) and (2). Scheme 3 gave a somewhat better fit than (4), but he stated that the choice between these would have to be substantiated by other information, and suggested that both schemes may be operative simultaneously.[6] The best fit for scheme 3 was obtained with α = 0.3 and K = 0.06.

Some of the quantities employed in Grjotheim's calculations have since been revised. The heat of fusion of cryolite now has been reported as about 28 kcal./mole (*vs.* 20.85 used by Grjotheim) and the heat capacity of the liquid has been found to be higher than that of the solid.[7,8] Moreover, there is now evidence of partial dissociation in the solid.[9]

Grjotheim clearly recognized the sources of error in his method and particularly pointed out the difficulty in taking cognizance of non-ideal behavior at the melting point where all of the calculations were made.

The present work treats the composition of these melts from the standpoint of melt densities corresponding to various dissociation schemes. The calculations are no less arduous than Grjotheim's but involve fewer assumptions and provide more detailed information.

Experimental

Composition of $NaF-AlF_3$ Melts.—Several investigators[10-12] observed a maximum in the density curve of sodium fluoride–aluminum fluoride melts at approximately 33 weight % (20 mole %) aluminum fluoride. Vajna[13] found a similar maximum but at 37 weight % aluminum fluoride. While the absolute values of the densities vary, there is good agreement, with the exception of Vajna's results, as to the composition of the melt at maximum density. Calculations are presented here to explain this variation of density with composition in terms of an equilibrium between cryolite and logical dissociation products.

The method consists of the steps:

1. Three dissociation schemes are considered.

Scheme I. Dissociation to sodium fluoride and aluminum fluoride

$$Na_3AlF_6 = 3NaF + AlF_3$$

$$K_I = \frac{[a_{NaF}]^3[a_{AlF_3}]}{[a_{Na_3AlF_6}]} \quad (5)$$

Scheme II. Dissociation to sodium fluoride and chiolite

$$3Na_3AlF_6 = 4NaF + Na_5Al_3F_{14}$$

$$K_{II} = \frac{[a_{NaF}]^4[a_{Na_5Al_3F_{14}}]}{[a_{Na_3AlF_6}]^3} \quad (6)$$

Scheme III. Dissociation to sodium fluoride and sodium tetrafluoroaluminate

$$Na_3AlF_6 = 2NaF + NaAlF_4$$

$$K_{III} = \frac{[a_{NaF}]^2[a_{NaAlF_4}]}{[a_{Na_3AlF_6}]} \quad (7)$$

2. The composition of the melt is calculated for a series of arbitrarily chosen equilibrium constants K for each scheme

Let N = weighed-in mole fraction of NaF on a sodium fluoride–aluminum fluoride basis

n = no. of moles of undissociated cryolite at equilibrium

The expressions for the number of moles present at equilibrium for each scheme become the following.

(1) P. P. Fedotieff and W. P. Iljinskii, *Z. anorg. Chem.*, **80**, 121 (1913).

(2) N. Puschin and A. Baskow, *ibid.*, **81**, 347 (1913).

(3) M. Hardouin, *Publ. sci. et tech. ministere air (France)*, Paris 1933, p. 34 (see ref. 5, p. 10).

(4) R. Lorentz, A. Jabs and W. Eitel, *Z. anorg. Chem.*, **83**, 39 (1913).

(5) K. Grjotheim, *Kgl. Norske Videnskab Selskabs Skrifter*, No. 5 (1956).

(6) In a private communication, Grjotheim states that, based on similar calculations with other systems, scheme 3 is now much preferred.

(7) D. M. Alfright, Thesis, Carnegie Inst. of Tech., 1956.

(8) C. J. O'Brien and K. K. Kelley, *J. Am. Chem. Soc.*, **79**, 5616 (1957).

(9) Alcoa Research Labs., to be published.

(10) Z. F. Lundina, *Trans. All-Union Aluminum and Magnesium Inst.*, **13**, 5 (1936). (See *Disc. Faraday Soc.*, **1**, 311 (1947).)

(11) G. A. Abramov and P. A. Kozunov, *Trans. Leningrad Ind. Inst.*, **1**, 60 (1939).

(12) J. D. Edwards, C. S. Taylor, L. A. Cosgrove and A. S. Russell, *J. Electrochem. Soc.*, **100**, 508 (1953).

(13) A. Vajna, *Alluminio*, **19**, 541 (1950).

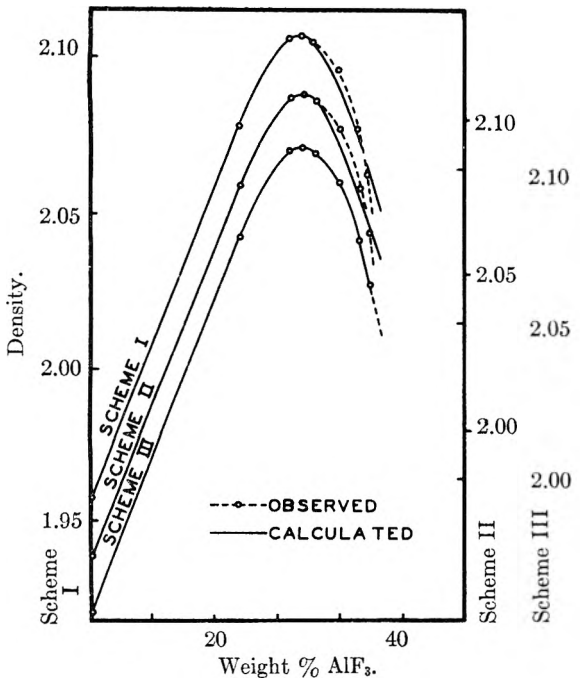

Fig. 1.—Densities of NaF–AlF_3 melts at 1000°.

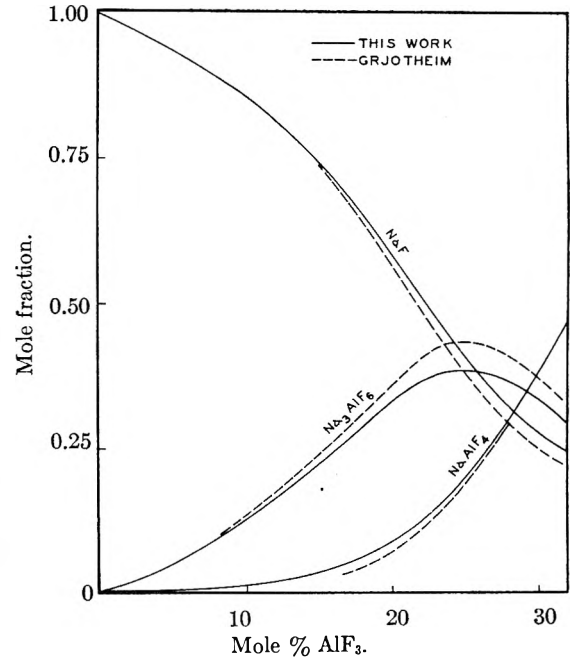

Fig. 2.—Composition of NaF–AlF_3 melts at 1000°.

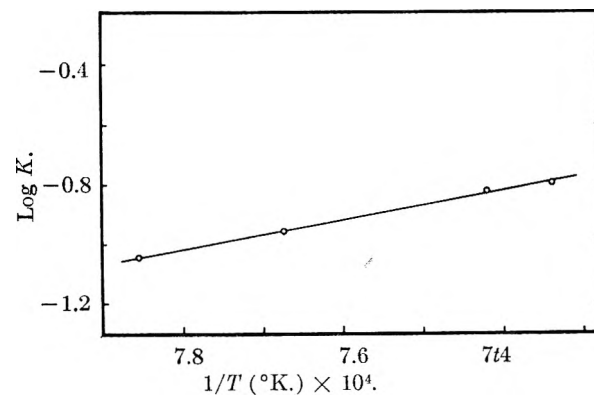

Fig. 3.—Dissociation constant of cryolite as a function of temperature.

Scheme I.

$$\begin{aligned}\text{Moles NaF} &= N - 3n\\ \text{Moles AlF}_3 &= 1 - N - n\\ \text{Moles Na}_3\text{AlF}_6 &= n\\ \text{Total Moles} &= 1 - 3n\end{aligned}$$

Scheme II.

$$\begin{aligned}\text{Moles NaF} &= \tfrac{1}{3}(8N - 5 - 4n)\\ \text{Moles 5NaF·3AlF}_3 &= \tfrac{1}{3}(1 - N - n)\\ \text{Moles Na}_3\text{AlF}_6 &= n\\ \text{Total Moles} &= \tfrac{1}{3}(7N - 4 - 2n)\end{aligned}$$

Scheme III.

$$\begin{aligned}\text{Moles NaF} &= 2N - 1 - 2n\\ \text{Moles NaAlF}_4 &= 1 - N - n\\ \text{Moles Na}_3\text{AlF}_6 &= n\\ \text{Total Moles} &= N - 2n\end{aligned}$$

Assuming that the activity of each component is equal to its mole fraction, the expressions for activities of the species for each scheme become

Scheme I.

$$\begin{aligned}[a_{\text{NaF}}] &= \frac{N - 3n}{1 - 3n}\\ [a_{\text{AlF}_3}] &= \frac{1 - N - n}{1 - 3n}\\ [a_{\text{Na}_3\text{AlF}_6}] &= \frac{n}{1 - 3n}\end{aligned}$$

Scheme II.

$$\begin{aligned}[a_{\text{NaF}}] &= \frac{8N - 5 - 4n}{7N - 4 - 2n}\\ [a_{5\text{NaF}\cdot 3\text{AlF}_3}] &= \frac{1 - N - n}{7N - 4 - 2n}\\ [a_{\text{Na}_3\text{AlF}_6}] &= \frac{3n}{7N - 4 - 2n}\end{aligned} \qquad (9)$$

Scheme III.

$$\begin{aligned}[a_{\text{NaF}}] &= \frac{2N - 1 - 2n}{N - 2n}\\ [a_{\text{NaAlF}_4}] &= \frac{1 - N - n}{N - 2n}\\ [a_{\text{Na}_3\text{AlF}_6}] &= \frac{n}{N - 2n}\end{aligned} \qquad (10)$$

Substituting into (5), (6) and (7), and simplifying

$$K_{\text{I}} = \frac{(N - 3n)^3(1 - N - n)}{n(1 - 3n)^3} \qquad (11)$$

$$K_{\text{II}} = \frac{(8N - 5 - 4n)^4(1 - N - n)}{27n^3(7N - 4 - 2n)^2} \qquad (12)$$

$$K_{\text{III}} = \frac{(2N - 1 - 2n)^2(1 - N - n)}{n(N - 2n)^2} \qquad (13)$$

The resulting fourth power, fifth power and cubic equations are solved for the moles of undissociated cryolite n at a number of different compositions for each selected equilibrium constant by the method of successive approximations. The activities are then calculated for each of the three components from (8), (9) and (10), and the compositions are expressed as weight % of each of the three components.

3. Series of melt densities are calculated for the series of compositions determined for each equilibrium constant by assigning a series of arbitrary but reasonable densities to

the second dissociation product (*i.e.*, AlF_3, $Na_5Al_3F_{14}$ or $NaAlF_4$) and to the undissociated cryolite. (The density of pure molten sodium fluoride is known from direct measurement.) If volumes are additive, the density of the melt is

$$d = \frac{100}{\frac{\text{wt. \% } Na_3AlF_6}{\text{density } Na_3AlF_6} + \frac{\text{wt. \% NaF}}{\text{density NaF}} + \frac{\text{wt. \% } AlF_3,\ Na_5Al_3F_{14} \text{ or } NaAlF_4}{\text{density } AlF_3,\ Na_5Al_3F_{14} \text{ or } NaAlF_4}} \quad (14)$$

4. The value of K and the densities of undissociated cryolite and the second dissociation product that give the best agreement with the experimental curve are chosen for each scheme.

5. The best fits for three dissociation schemes are compared to give the most probable composition of molten cryolite.

The experimental densities used were those of Edwards, *et al.*,[12] which were the most recent values.

It was found empirically that the value of the equilibrium constant determines the sharpness of the density maximum and the composition of the melt at maximum density. The density of the undissociated cryolite determines the value of the density maximum and, to a lesser degree, the composition of maximum density. The density of the second dissociation product determines the slope of the right branch of the curve and, to some extent, the composition of maximum density. Although it would be difficult to prove mathematically, values for these parameters that give the best fit with the measured densities appear to provide a unique solution to the problem.

The best fit to the experimental data for each scheme is shown for 1000° in Fig. 1. It is seen that in each case there is general conformity to the experimental curve, particularly on the sodium fluoride side of the maximum. There is no basis for discarding the data point on the right-hand branch that is missed in Schemes I and II, however, and in these cases it was impossible to adjust the parameters so as to give a better fit to the right-hand branch without greatly distorting other parts of the curve.

Almost perfect agreement with measured densities is obtained by dissociation into sodium fluoride and sodium tetrafluoroaluminate, $NaAlF_4$, (Scheme III), with an equilibrium constant of 0.090, and densities of undissociated molten cryolite and molten sodium tetrafluoroaluminate of 2.210 and 1.873 g./ml., respectively. (Edwards' density for sodium fluoride at 1000° was 1.957 g./ml.) This scheme is also the one favored by Grjotheim.

From the constant K for this dissociation it is possible to calculate the composition of the melt at other $NaF-AlF_3$ ratios. Figure 2 gives these calculated melt compositions, and those of Grjotheim, at 1000°, as a function of the weighed-in composition. The compositions are shown only to 35 mole % AlF_3. The proposed dissociation scheme does not apply to melts richer in AlF_3 than the $NaAlF_4$ composition, and probably would cease to apply somewhat before that. (The experimental density data were carried only to 29 mole % AlF_3.)

The Effect of Temperature on the Dissociation.—Edwards, *et al.*,[12] determined melt densities from approximately 950 to 1090°, where permitted by the liquid range. Their data were reported as empirical equations giving the density as a function of temperature at each composition. The procedure outlined in the preceding section was also employed to determine the dissociation constant at 1030, 1075 and 1090° according to dissociation Scheme III, which had provided the best fit to the experimental data at the lower temperature. An excellent fit of the calculated curves to the experimental data was likewise obtained at these temperatures. The dissociation constant K and α, the degree of dissociation calculated from

$$K = \frac{4\alpha^3}{(1-\alpha)(2\alpha+1)^2} \quad (15)$$

are given in Table I.

TABLE I

THE DISSOCIATION OF CRYOLITE AT DIFFERENT TEMPERATURES

Temp., °C.	K	α
1000	0.09	0.35
1030	.11	.38
1075	.15	.42
1090	.16	.43

From

$$\frac{d \ln K}{dT} = \frac{\Delta H}{RT^2} \quad (16)$$

ΔH, the heat of dissociation per mole of dissociating cryolite, was calculated. The plot of log K *versus* $1/T$ is shown in Fig. 3. There is no consistent deviation from a straight line, indicating that ΔH is insensitive to temperature over the range studied. A heat of dissociation of ΔH = 22 kcal./mole is calculated from the slope.

Molar Volumes.—The following molar volumes are calculated from the densities of the three species at 1000°: NaF = 21.5 ml./mole, $NaAlF_4$ = 67.3 ml./mole, Na_3AlF_6 = 95.0 ml./mole. If the ion volumes of Na^+ and F^- are taken to be proportional to the cube of their crystal radii (r_{Na^+} = 0.97 Å., r_{F^-} = 1.36 Å.), gram ion volumes of 5.7 ml./g. ion and 15.8 ml./g. ion are obtained for Na^+ and F^-, respectively. By subtracting the sodium volume from the volumes of the other two species, the gram ion volumes of the fluoroaluminate ions are: AlF_4^- = 61.6 ml./g. ion; AlF_6^{-3} = 77.9 ml./g. ion.

Discussion

Whereas exact agreement with experimental densities could be obtained only for Scheme III, fair agreement also was obtained for the other two schemes. The choice of Scheme III is supported by considerable other evidence, however. The work of Grjotheim has been mentioned already. Howard[14] identified $NaAlF_4$ in quenched vapor from molten cryolite. On reheating, the material disproportionates to chiolite and aluminum fluoride, but it can be retained at room temperature and some of its properties have been determined. The exist-

(14) E. H. Howard, *J. Am. Chem. Soc.*, **76**, 2041 (1954).

ence of a species in the vapor does not necessarily imply that the same species is a major component of the liquid. (From thermodynamic considerations, the same species must be present in the melt but the vapor pressure of the pure species may be high or its activity coefficient may be large relative to other species.) As will be shown in a subsequent paper, the concentration of $NaAlF_4$ in the vapor over molten cryolite is very high because of the high vapor pressure of $NaAlF_4$ relative to NaF and Na_3AlF_5. It will also be shown in this paper that the vapor composition of NaF–AlF_3 melts can be correlated with the melt compositions calculated here.

A final argument supporting the dissociation to $NaAlF_4$ is the reasonable change in coördination number of aluminum from 6, in AlF_6^{-3}, to 4, in AlF_4^-, at high temperatures.

There are, on the other hand, arguments against the other two dissociation schemes. Chiolite, $5NaF{\cdot}3AlF_3$ (Scheme II) is a lattice-type compound, and as such has parallels of equal or greater complexity in other solid systems. The existence of the very large $Al_3F_{14}^{-5}$ ion in solution is highly unlikely, however.

Aluminum fluoride cannot be passed off as an illogical component of melts, and, in fact, Scheme I is generally accepted in the older literature. Aluminum fluoride is volatile, however, and, if present as such, should appear in the vapor. Furthermore, the density that had to be assigned to AlF_3 (1.711 at 1000°) to give the best fit to the experimental curve seems much too low in view of its high density at room temperature compared to sodium fluoride and cryolite. (It should be pointed out that Scheme I cannot be distinguished from Grjotheim's fourth scheme—dissociation to Na^+, Al^{3+} and F^-—by density calculations alone, since the degree of ionization of the various species is not considered. However, transport experiments in cryolite–alumina melts[15] showed Al^{+3} to be essentially absent and Grjotheim's fourth scheme can be eliminated on that account.)

The assumption of additive volumes that was necessary for the calculations might be questioned. If the system were non-ideal in this respect, however, departure from ideality should be greater as the melting point is approached. Figure 4 shows the densities of undissociated cryolite and sodium tetrafluoroaluminate that provided the best fits to the experimental density curves at four temperatures. The curves are straight lines, showing constant expansion coefficients and are roughly parallel to the curve for sodium fluoride, which was experimentally determined. If there were a departure from additive volumes that was temperature dependent, it would be evident in these curves.

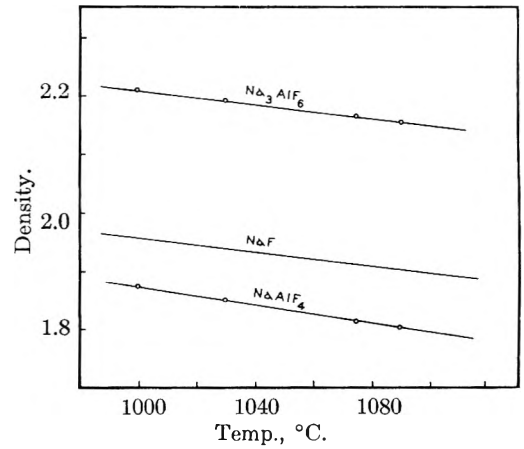

Fig. 4.—Densities of the components of molten cryolite (NaF experimental, $NaAlF_4$ and Na_3AlF_6 calculated at temperatures shown).

The whole concept of equality of mole fractions and activities is subject to question in ionic melts. This matter will be discussed further in the next paper, where it will be shown that in mixtures of ionic components with a common ion—sodium in the present case—the ion fraction product reduces to the simple mole fraction, as employed here.

The possibility of dimerization of the sodium fluoride from the dissociation of cryolite was not considered. This would involve a second equilibrium for the extent of dissociation to monomers, which would be concentration dependent. This could not be handled by the present method since there are not enough independent variables. The error that would result if dimerization were appreciable would come from the assumption that the density assigned to the sodium fluoride was independent of concentration. This matter cannot be resolved without independent evidence for the dimerization of alkali halides.

(15) W. B. Frank and L. M. Foster, This Journal, **61**, 1531 (1957).

THE CONFORMATION OF POLYMER MOLECULES. III. CELLULOSE TRICAPROATE[1]

BY W. R. KRIGBAUM AND L. H. SPERLING[2]

Department of Chemistry, Duke University, Durham, N. C.

Received July 20, 1959

Cellulose tricaproate exhibits the properties characteristic of inflexible chain polymers. The intrinsic viscosity $[\eta]$ decreases rapidly with temperature, and the ratio of the $[\eta]$ values in different solvents is independent of molecular weight. In thermodynamically good solvents the molecular expansion factor α remains near unity and is independent of molecular weight. Theta temperatures were determined for the tricaproate in dimethylformamide and in a dioxane–water mixed solvent. Light scattering measurements were performed upon six fractions spanning a thirty-fold $\langle M \rangle_w$ range. The Flory hydrodynamic parameter Φ' is still below its asymptotic limit for a degree of polymerization $\langle N \rangle_w = 2600$, and decreases at lower molecular weights. The same variation has been reported for cellulose trinitrate, and this is in accord with the recent theoretical treatment of Stockmayer and Albrecht. On the other hand, the $(\overline{s_0^2}/N)$ ratio for the tricaproate becomes larger as the molecular weight is decreased, which is the reverse of the variation predicted for non-gaussian chains by Benoit and Doty, and observed experimentally for cellulose trinitrate. Under theta conditions $[\eta] \sim M^{1/2}$, despite a considerable variation of both Φ' and $(\overline{s_0^2}/N)$ with molecular weight. Due to the cancellation of these opposing variations, the exponent a in the relation $[\eta] = K'M^a$ is only slightly larger than 0.5 for thermodynamically good solvents. This low value of the molecular weight exponent observed in good solvents is unique, since under these conditions $a = 0.7$ to 0.8 for flexible chain polymers and $a \sim 1.0$ for the lower cellulose esters. The $(\overline{s_0^2}/N)$ ratios observed in a good solvent, 1-chloronaphthalene, are smaller than those measured under theta conditions in dimethylformamide. This suggests that the unusual variation of $(\overline{s_0^2}/N)$ with molecular weight observed for the tricaproate is a skeletal effect. An examination of the solvent dependence of $[\eta]$ suggests that London dispersion forces, rather than dipole interactions, are responsible for the high barrier to rotation about the chain bonds which gives the cellulose derivatives their unique molecular properties. Thus the difference between the cellulosics and the more flexible molecules is one of degree, rather than kind.

The study of flexible chain polymers has led to a rather satisfactory understanding of the manner in which the molecular size and hydrodynamic properties of these polymers depend upon such factors as the molecular weight, temperature and solvent power. This behavior may be summarized briefly as follows. The unperturbed mean-square radius of gyration $\overline{s_0^2}$ is proportional to the molecular weight M. Thus, at a given temperature the $(\overline{s_0^2}/M)$ ratio is a property of the polymer examined, and is independent of the chemical nature of the particular theta solvent chosen. As the temperature is raised the $(\overline{s_0^2}/M)$ ratio decreases slowly, indicating a relatively small potential energy hindering rotation. In thermodynamically good solvents the average molecular dimensions are expanded by a factor $\alpha = (\overline{s^2}/\overline{s_0^2})^{1/2}$ which increases with molecular weight, at least over the range which is accessible to study.

The relation of Flory and Fox[3] adequately describes the behavior of the intrinsic viscosity for these polymers

$$[\eta] = \Phi' (\overline{s_0^2}/M)^{3/2} M^{1/2} \alpha^3 \qquad (1)$$

where Φ' is a constant. The equation implies that for viscosities measured under Flory theta conditions the $[\eta]_\Theta/M^{1/2}$ ratio should be independent of molecular weight. This predicted constancy has been verified[4] for polystyrene and polyisobutylene down to molecular weights of the order of 10,000.

For thermodynamically good solvents the treatment of Flory[5] predicts $\alpha \sim M^{0.1}$, so that according to equation 1 the exponent a in the empirical molecular weight relation

$$[\eta] = K'M^a \qquad (2)$$

should exhibit a maximum value of 0.8. Experience has shown that this rule also is generally obeyed.

In summary, one obtains the impression that the principal factors affecting the behavior of flexible chain polymers are well in hand, and that the objective of further refinements will be limited to improved quantitative agreement.

There is a second class of polymers, of which the cellulose derivatives are the best known examples, whose behavior is quite different from that outlined above. The $(\overline{s_0^2}/M)$ ratio for these polymers varies with molecular weight, and only approaches an asymptotic value for molecular weights of the order of 10^5–$10^{6.6}$.[6,7] In thermodynamically good solvents the molecular expansion factor α is only slightly larger than unity, and for many of these polymers is essentially independent of molecular weight.

The intrinsic viscosities of the cellulosics display large negative temperature coefficients,[8–9] reflecting the relatively high barrier to rotation about the chain bonds. For a fixed temperature, the ratio of the intrinsic viscosities in two different solvents appears to be practically independent of molecular weight, and does not correlate with the values of the second virial coefficient[9–10] as do those of the polymers having more flexible chains.

(1) For the preceding papers of this series see W. R. Krigbaum and D. K. Carpenter, THIS JOURNAL, **59**, 1166 (1955); **62**, 1586 (1958).

(2) Buckeye Cellulose Corporation, Memphis, Tenn.

(3) P. J. Flory and T. G. Fox, Jr., *J. Am. Chem. Soc.*, **73**, 1904 (1951).

(4) W. R. Krigbaum, L. Mandelkern and P. J. Flory, *J. Polymer Sci.*, **9**, 381 (1952).

(5) P. J. Flory, *J. Chem. Phys.*, **17**, 303 (1949).

(6) A. M. Holtzer, H. Benoit and P. Doty, THIS JOURNAL, **58**, 624 (1954).

(7) M. L. Hunt, S. Newman, H. A. Scheraga and P. J. Flory, *ibid.*, **60**, 1278 (1956).

(8) L. Mandelkern and P. J. Flory, *J. Am. Chem. Soc.*, **74**, 2517 (1952).

(9) P. J. Flory, O. K. Spurr, Jr., and D. K. Carpenter, *J. Polymer Sci.*, **27**, 231 (1958).

(10) W. R. Moore and J. Russell, *J. Colloid Sci.*, **8**, 243 (1953); **9**, 338 (1954).

Finally, for cellulose trinitrate the parameter Φ' in equation 1 has been found[7,11] to decrease quite markedly as the molecular weight is lowered.

From the foregoing it is clear that the essential difference between these two classes of polymers is the more inflexible molecular structure characteristic of the latter group. For these polymers the dependence of the intrinsic viscosity upon solvent power and temperature must reflect primarily variations of the unperturbed molecular dimensions. However, the origin of the forces responsible for this large hindrance potential, and the influence of the solvent upon this rotational barrier, require further elucidation.

The fact that many of the cellulose derivatives have extremely high melting points makes the direct measurement of their unperturbed dimensions very difficult, if not impossible. The only data obtained under theta conditions are those of Mandelkern and Flory for the tributyrate and tricaprylate esters.[8] Only in the latter case were they able to achieve theta conditions using a single liquid as the solvent, but unfortunately the intrinsic viscosity of this polymer does not have a large negative temperature coefficient, as do the butyrate and lower esters. We have therefore selected the tricaproate for investigation, hoping to obtain a polymer which could be studied conveniently under theta conditions, but which still retains the properties characteristic of the molecules with strongly hindered rotation. Theta temperatures were determined by osmotic pressure and precipitation temperature measurements. We then performed a study of the molecular dimensions and hydrodynamic behavior of a series of fractions, both under theta conditions and in thermodynamically good solvents.

Experimental

Samples.—Two batches of cellulose tricaproate having a total weight of 115 g. were prepared from purified cotton linters by the method of Malm, *et al.*[12] Analysis of these gave for the first C = 63.1% and H = 8.80%, and for the second C = 63.2% and H = 8.89%. These compare favorably with the theoretical triester composition, C = 63.1% and H = 8.76%. The two samples were individually subjected to two stages of fractionation by a rapid extraction process described elsewhere.[13] The dioxane–water system was employed, and the initial polymer concentration was 1% in each case. The $\langle M\rangle_w/\langle M\rangle_n$ ratio for the whole polymer was estimated from the cumulative curve to be about 4.5, while for most of the fractions this ratio fell in the range 1.1–1.6.

Viscosity.—Flow times were measured using a Ubbelohde viscometer. The solutions were filtered into the viscometer through a medium porosity sintered glass disc. Kinetic energy corrections were applied, but the effect of shear rate was not investigated.

Osmometry.—Stabin osmometers[14] were used with Type 300 regenerated cellulose mem ranes.[15] Static measurements were obtained and the difference in height of the liquid levels was read to 0.01 mm. by means of a cathetometer.

Light Scattering.—The light scattering apparatus has been described previously.[16] The solutions were clarified by filtration into the light scattering cell through ultrafine porosity sintered glass, followed by centrifugation in the cell at 55,000 *g* for 30–45 minutes according to the procedure described by Dandliker and Kraut.[17] Comparison of the scattering curves for these solutions with those clarified by filtration alone indicated the centrifugal procedure to be definitely superior.

A cross-sectional view of the temperature controlled cell holder is shown in Fig. 1. Outer glass cell A, which is filled with solvent, serves as a constant temperature bath. Magnetic stirrer I is turned by disc magnet J. The latter is cut in the form of a pulley, and is belt driven by a motor attached to base K. Cell A is wrapped with blackened asbestos paper, and carries two windings of resistance wire. One of these serves as a steady heater and the other as an intermittent heater controlled by a Sargent Model S Thermonetor. Brass top B allows the insertion of the thermistor probe and a copper–constantan thermocouple used to measure the cell temperature. Scattering cell E is positioned by the blackened brass plate C which fits over Teflon cap D, and by stand H. The entire assembly is positioned on the stage of the light scattering instrument by two perpendicular bars meeting the sides of stand K.

The turbidities reported are relative to a 0.50% toluene solution of the Cornell standard polystyrene, taking for the latter $\tau = 3.51 \times 10^{-3}$ cm.$^{-1}$ at 4358 Å. and 1.36×10^{-3} cm.$^{-1}$ at 5461 Å.[16,18-19] The reciprocal of the reduced intensity for the standard polystyrene solution was a linear function of $\sin^2(\theta/2)$ to within 1% from 45 to 125°, and corresponded to a dissymmetry z_{45}, of 1.18 ± 0.01 at 4358 Å. and 1.12 ± 0.01 at 5461 Å. Measurements of dn/dc were performed using a Brice–Phoenix differential refractometer calibrated with aqueous sucrose solutions, taking for the latter $dn/dc = 0.1436$ at 5461 Å.

Experimental Results

A. Determination of Theta Temperatures.—The two theta solvents investigated for cellulose tricaproate were dimethylformamide and a dioxane–water mixture (100 to 7 by volume).

The theta temperature for the single solvent was determined by osmotic pressure measurements performed upon fraction *D* at 30, 41.6 and 53.5°. The results appear plotted as π/c *vs.* c in Fig. 2. A membrane dissymmetry which developed during the course of these measurements introduced a fairly large uncertainty in the results obtained for the lowest concentration. The second virial coefficient A_2 may be expressed as

$$A_2 = (\bar{v}^2/V_1)\psi_1(1 - \Theta/T)\,F(X) \qquad (3)$$

where $\bar{v}$ and V_1 are the partial specific volume of the polymer and the molar volume of the solvent, respectively. Since A_2 vanishes at the theta temperature, from the plot of A_2 *vs.* t (°C.) shown in the insert to Fig. 2, we obtain $\Theta = 314 \pm 1$°K. After assignment of this value, the $\psi_1 F(X)$ products shown in column four of Table I were calculated. These are found to be essentially independent of temperature, and to lead to a value of the entropy parameter, ψ_1, of 0.10 ± 0.01. This behavior should be contrasted with the relatively large temperature dependence of $F(X)$ observed for polyisobutylene[20] and polystyrene[21] in the

(11) M. M. Huque, D. A. I. Goring and S. G. Mason, *Can. J. Chem.*, **36**, 952 (1958).

(12) C. J. Malm, J. W. Mench, D. L. Kendall and G. D. Hiatt, *Ind. Eng. Chem.*, **43**, 684 (1951).

(13) W. R. Krigbaum and A. M. Kotliar, *J. Polymer Sci.*, **32**, 323 (1958).

(14) J. V. Stabin and E. H. Immergut, *ibid.*, **14**, 209 (1954).

(15) Obtained from Sylvania Division, American Viscose Corporation, Fredericksburg, Va.

(16) D. K. Carpenter and W. R. Krigbaum, *J. Chem. Phys.*, **24**, 1041 (1956).

(17) W. B. Dandliker and J. Kraut, *J. Am. Chem. Soc.*, **78**, 2380 (1956).

(18) C. I. Carr, Jr., and B. H. Zimm, *J. Chem. Phys.*, **18**, 1624 (1950).

(19) A. Oth, J. Oth and V. Desreux, *J. Polymer Sci.*, **10**, 551 (1953).

(20) W. R. Krigbaum and P. J. Flory, *J. Am. Chem. Soc.*, **75**, 1775 (1953).

(21) W. R. Krigbaum, *ibid.*, **76**, 3738 (1954).

vicinity of the theta temperature. Since $F(X)$ is a function of $X = 2(\alpha^2 - 1)$, the observation that for cellulose tricaproate $F(X)$ is nearly independent of temperature near theta places this polymer in the inflexible chain category.

TABLE I

THERMODYNAMIC PARAMETERS FOR CELLULOSE TRICAPROATE DETERMINED OSMOTICALLY

A. Fraction D in dimethylformamide

t(°C.)	$10^{-5}\langle M\rangle_n$	$10^5 A_2$	$\psi_1 F(X)$
30.0	1.36	−5.8	0.103
41.6	1.31	0.5	...
53.5	1.29	6.5	0.107

B. Fraction E in dioxane–water (100:7)

t(°C.)	$10^5\langle M\rangle_n$	$10^5 A_2$ ($t = 0$)	$10^5 A_2$ ($t = \infty$)
37.1	(2.06)	−1.9	8.5
41.2	(2.06)	−0.94	17
49.4	(2.06)	3.7	46

The determination of the theta temperature for the dioxane–water system was performed both by osmometry and by precipitation temperature measurements. The osmotic measurements were complicated by partitioning of the mixed solvent across the membrane. This effect has been investigated theoretically,[22-26] but has not received much attention from the experimental point of view.

We may expect the observed osmotic pressure to increase with time, since the composition of the solvent in the solution compartment will become progressively richer in the thermodynamically good solvent. However, because we do not start at osmotic equilibrium there will be two processes going on simultaneously. It turns out that the normal approach to osmotic equilibrium by the gross transfer of solvent through the membrane is 5 to 15 times more rapid than the partitioning of the solvent.

As shown by the open circles in Fig. 3, if Δh is set to a high value there is initially a rapid decrease toward osmotic equilibrium, followed by a slow rise (due to exchange of solvent) which continues for several days. We let Δh_0 and Δh_∞ be the equilibrium differences in heights which would be observed at zero time (no solvent interchange) and at infinite time (after completion of interchange), and designate the non-equilibrium value observed at time t be Δh_t. Furthermore let $\delta h_t = \Delta h_\infty - \Delta h_t$ and $\delta h_0 = \Delta h_\infty - \Delta h_0$ (see Fig. 3). If we assume that the exchange of solvent follows the same first-order rate law as does the normal approach to equilibrium, then after a sufficient time

$$\log \delta h_t = \log \delta h_0 - k_1 t \qquad (4)$$

For each set of data a trial value of Δh_∞ was assumed and the corresponding δh_t values were plotted as log δh_t *vs.* t. This process then was repeated using a better approximation for Δh_∞ until a linear relation was obtained. From the intercept of this line, which is δh_0, and the assumed value of Δh_∞ one may calculate the value of Δh_0 which would have been observed if no solvent exchange had taken place. Some typical results obtained for the log δh_t *vs.* t plot are illustrated in Fig. 4. Our data show that δh_0 for a given solution increases quite rapidly with temperature, and that k_1 is, to a first approximation, a linear function of the polymer concentration. In this connection we note that since the volume of the solvent compartment is at least twenty times that of the solution cell, the composition on the solvent side can be assumed to be unaffected by the interchange.

Figure 5 shows the values of π/c obtained at three temperatures for fraction E in the dioxane–water mixed solvent. The filled circles correspond to values of Δh_0 (no interchange). For comparison, the open circles in Fig. 5 illustrate the behavior of π/c corresponding to Δh_∞ (complete exchange)

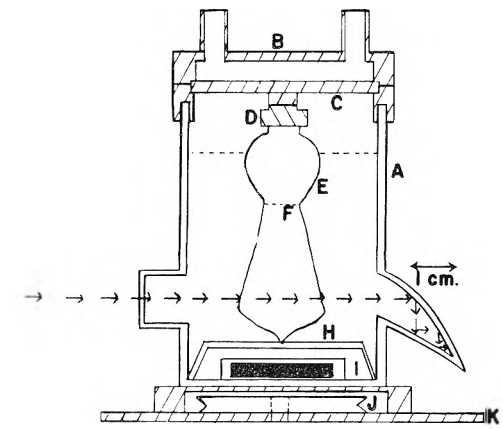

Fig. 1.—Diagram of the temperature controlled cell holder for light scattering (see text for discussion).

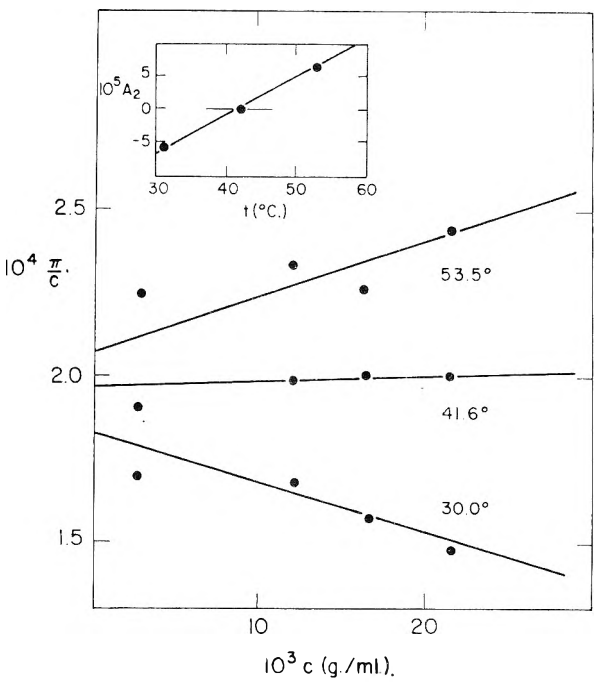

Fig. 2.—Osmotic data for cellulose tricaproate fraction D in dimethylformamide at three temperatures.

(22) G. Gee, *Trans. Faraday Soc.*, **40**, 463, 468 (1944).
(23) F. T. Wall, *J. Am. Chem. Soc.*, **66**, 447 (1944).
(24) R. L. Scott, *J. Chem. Phys.*, **17**, 268, 279 (1949).
(25) T. Kawai, *J. Chem. Soc. Japan*, **25**, 336, 341 (1952); **26**, 6 (1953).
(26) W. R. Krigbaum and D. K. Carpenter, *J. Polymer Sci.*, **14**, 241 (1954).

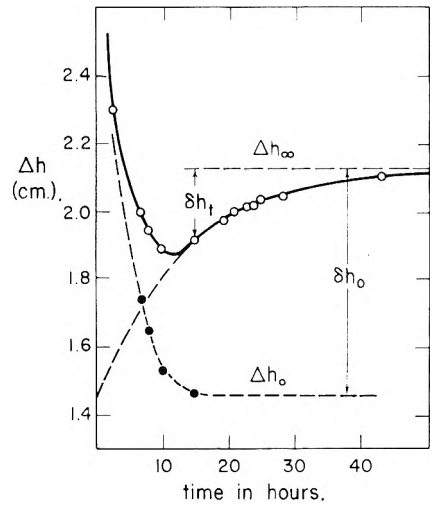

Fig. 3.—The variation of Δh with time for cellulose tricaproate in the dioxane–water mixed solvent as observed with solvent interchange (○) and as calculated for no interchange (●).

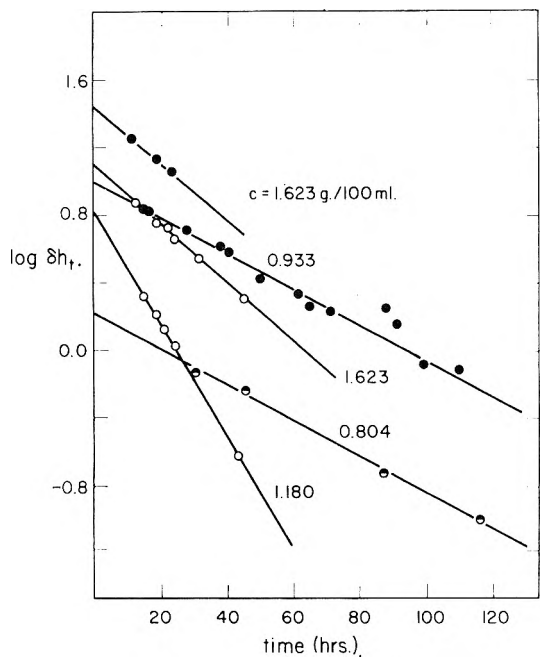

Fig. 4.—Plot of log δh_t *vs.* time used to eliminate the effect of solvent exchange for the osmotic data obtained at 49.4° (●), 41.2° (○) and 37.1° ( ).

at the two temperatures. Measurements also were conducted upon this same polymer fraction in dioxane at 35°, yielding $\langle M \rangle_n = 206{,}000$ and $A_2 = 7 \times 10^{-4}$. The lines in Fig. 5 were drawn so that the intercepts correspond to this molecular weight. The A_2 values obtained for the mixed solvent are shown in Part B of Table I. Upon plotting the A_2 values corresponding to zero time against temperature, as shown in the insert to Fig. 5, there is obtained $\Theta = 316 \pm 3$°K.

Precipitation temperature measurements were also performed for the same dioxane–water mixture. Solutions varying in concentration from 0.1 to 8% were prepared using two polymer fractions having $\langle M \rangle_n$ values of 206,000 and 743,000. These were sealed in small glass tubes and placed

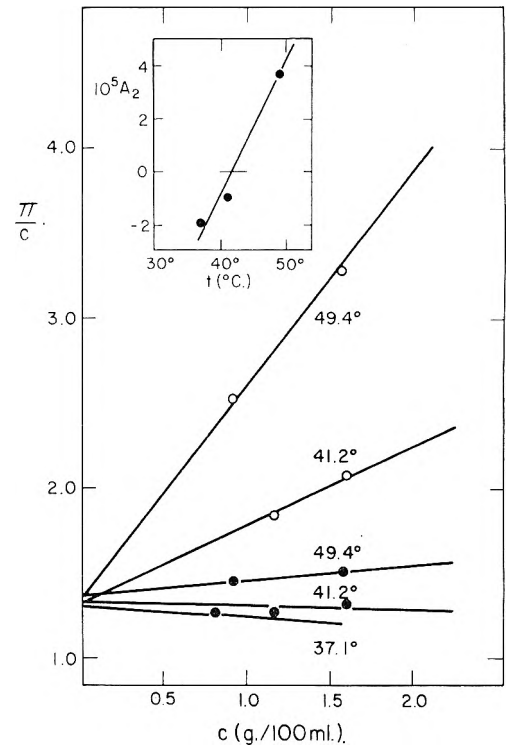

Fig. 5.—π/c *vs.* c for cellulose tricaproate fraction E in the dioxane–water mixed solvent if no interchange of solvent takes place (●) and after completion of the solvent exchange (○).

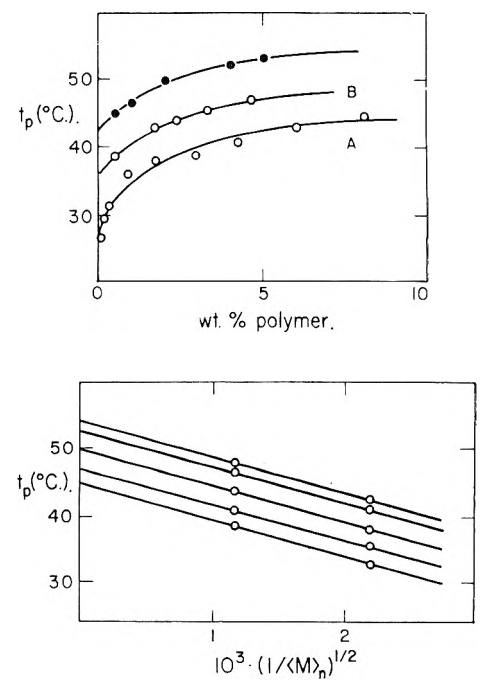

Fig. 6.—(Above) Precipitation temperatures for $\langle M \rangle_n = 2.06 \times 10^5$ (curve A) and 7.43×10^5 (curve B) measured in the dioxane–water mixed solvent. The filled circles represent precipitation temperatures extrapolated to $M = \infty$. (Below) Smoothed precipitation temperatures plotted against $(1/\langle M \rangle_n)^{1/2}$ for the concentrations (reading from top to bottom) 5, 4, 2, 1 and 0.5%.

in a water-bath. The temperature was raised until all the samples were dissolved completely, and then slowly lowered (10°/hr.). The temperature was recorded at which each sample became

sufficiently turbid to obscure the numbers on a thermometer held behind it. The bath then was warmed slowly and the temperatures at which the solutions became clear were recorded again. This process was repeated until reproducible results were obtained. Although it was rather difficult to distinguish the point at which phase separation occurred, the difference between the precipitation and solution temperatures was usually less than 2°.

We have treated the data according to the procedure of Mandelkern and Flory.[8] The precipitation temperatures observed for each molecular weight were plotted against concentration as shown in the upper part of Fig. 6. Smoothed values were read from these curves for several concentrations, and these were plotted against $(1/\langle M\rangle_n)^{1/2}$ as illustrated in the lower portion of Fig. 6. The intercepts, representing the precipitation temperature at each concentration for a polymer of infinite molecular weight, are indicated by the filled circles in the upper graph. These were extrapolated to zero concentration to obtain $\Theta = 316 \pm 2°K.$

Although the close agreement between the theta values determined by the two methods is partially fortuitous, we do feel that these measurements constitute a verification of the semi-empirical procedure of Mandelkern and Flory for the treatment of precipitation temperature data for ternary systems.

B. Determination of the Molecular Weight Heterogeneity.—A knowledge of the number-average molecular weight is required to characterize the heterogeneity of the polymer samples. This information is essential for the evaluation of the parameter Φ' appearing in equation 1. Newman, *et al.*,[27] have pointed out that for a heterogeneous polymer equation 1 becomes

$$[\eta] = \Phi' \langle(\bar{s}^2)^{3/2}\rangle_n/\langle M\rangle_n \qquad (5a)$$

whereas $\langle\bar{s}^2\rangle_z$ and $\langle M\rangle_w$ are the quantities actually measured. Thus, in terms of the experimental quantities

$$[\eta] = (\Phi'/q_\Phi)(\langle\bar{s}^2\rangle_z)^{3/2}/\langle M\rangle_w \qquad (5b)$$

where

$$q_\Phi = \frac{(\langle\bar{s}^2\rangle_z)^{3/2}\langle M\rangle_n}{\langle(\bar{s}^2)^{3/2}\rangle_n\langle M\rangle_w} \qquad (6)$$

the evaluation of the correction factor, q_Φ, has been discussed elsewhere.[7,27-29] Nevertheless, a few words emphasizing the important role played by polymer heterogeneity may be in order at this point. If one assumes a weight fraction distribution of the form

$$f(N) = (y^{h+1}/h!)\, N^h e^{-yN} \qquad (7)$$

and ignores the small variation of the expansion factor α with molecular weight, then the correction factor becomes[29]

$$q_\Phi = \frac{(h+2)^{3/2}\ \Gamma(h+2)}{(h+1)^2\ \Gamma(h+1.5)} \qquad (8a)$$

(27) S. Newman, W. R. Krigbaum, C. Laugier and P. J. Flory, *J. Polymer Sci.*, **14**, 451 (1954).

(28) A. R. Shultz, *J. Am. Chem. Soc.*, **76**, 3422 (1954).

(29) W. R. Krigbaum and D. K. Carpenter, THIS JOURNAL, **59**, 1166 (1955).

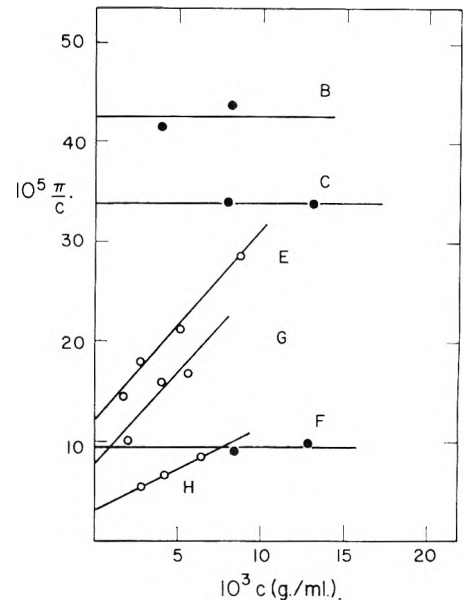

Fig. 7.—Osmotic pressure data for cellulose tricaproate fractions in DMF at 41° (●) and in dioxane at 35° (○).

This correction amounts to 60% of the experimental value when $\langle M\rangle_w/\langle M\rangle_n = 1.5$, and $q_\Phi = 1.95$ when $\langle M\rangle_w/\langle M\rangle_n = 2.0$. If reliable Φ' values are to be obtained, the need for accurate knowledge of the polydispersity becomes more essential as the $\langle M\rangle_w/\langle M\rangle_n$ ratio increases. This remark applies particularly to the cellulosics, which are quite difficult to fractionate effectively. There is another aspect of the q_Φ correction which warrants our attention. If one employs the Lansing–Kramer distribution in place of equation 7, then the appropriate correction is[27]

$$q_\Phi = (\langle M\rangle_w/\langle M\rangle_n)^{13/8} \qquad (8b)$$

Values calculated according to those two relations diverge rapidly as the $\langle M\rangle_w/\langle M\rangle_n$ ratio increases. Since the precise *form* of the molecular weight distribution is seldom (if ever) known, this introduces an uncertainty which can only be minimized by keeping the molecular weight distribution as narrow as possible. In the calculations which follow we have used the correction as given by equation 8a.

Figure 7 shows the results obtained by osmotic pressure measurements performed upon fractions B, C and F in the theta solvent, dimethylformamide at 41° (314°K.), and for fractions E, G and H in a thermodynamically good solvent, dioxane, at 35°. The determination of $\langle M\rangle_n$ for fraction D was discussed in Part A. These $\langle M\rangle_n$ and A_2 values are listed in columns three and seven of Table II. Columns four and five give $\langle M\rangle_w$ values determined by light scattering measurements (described below) using dimethylformamide and 1-chloronaphthalene as the solvents. The A_2 values observed using the latter solvent appear in column eight.

C. Light Scattering Measurements.—Molecular weights and dimensions were determined using three solvents: 1-chloronaphthalene at 24°, the dioxane–water mixture at 63°, and dimethylformamide at 41° (theta conditions).

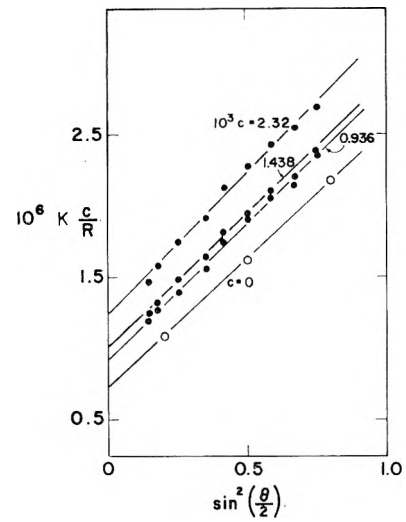

Fig. 8.—Angular dependence of the reciprocal scattering intensity for fraction H in 1-chloronaphthalene. Values extrapolated to infinite dilution are indicated by open circles.

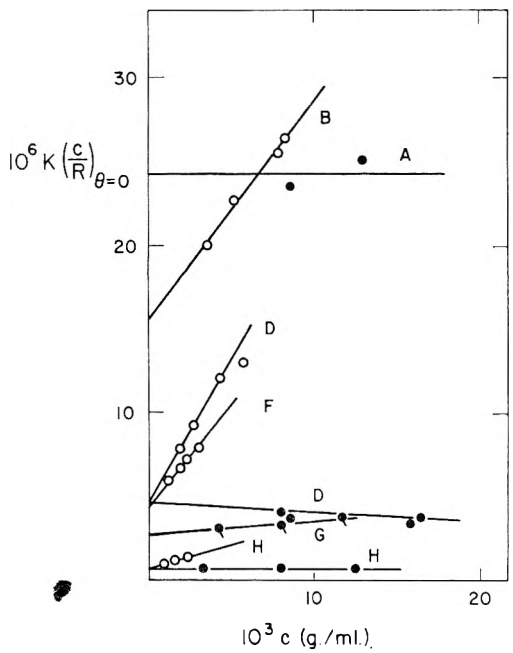

Fig. 9.—Reciprocal of the reduced scattering intensity at zero angle plotted against concentration for cellulose tricaproate in DMF at 41° (●) and in 1-chloronaphthalene at 24° (○).

TABLE II

MOLECULAR WEIGHT DATA FOR FRACTIONS OF CELLULOSE TRICAPROATE

Fraction	% of whole polymer	$\langle M\rangle_n$	$\langle M\rangle_w$ DMF	$\langle M\rangle_w$ 1-Cl-N	$\frac{\langle M\rangle_w}{\langle M\rangle_n}$	$10^4 A_2$ Dioxane	$10^4 A_2$ 1-Cl-N
A	4.2	.....	41,700	....	..	..	..
B	5.6	61,000	....	62,500	1.03	..	6.5
C	2.8	76,000	(98,400)[a]		(1.3)	..	..
D	19.6	132,000	208,000	212,000	1.61	..	8.6
E	14.4	206,000	(195,000)[a]		(~1.0)	7.0	..
F	12.1	275,000	....	236,000	(~1.0)	..	5.0
G	4.0	315,000	352,000	....	1.12	6.9	..
H	11.1	743,000	1,480,000	1,310,000	1.76	3.0	1.1

[a] Calculated from eq. 10a.

Most of the cellulose derivatives have refractive indices near that of the tricaproate, $n = 1.47$. The solvents which have been chosen for light scattering studies have had lower refractive indices, *e.g.*, acetone (1.36) and ethyl acetate (1.37). Past experience has shown that clarification of the solutions becomes progressively more difficult as the refractive index of the solvent is decreased. Water, which has an unusually low refractive index (1.33), is an outstanding case in point. This suggests that the dust particles responsible for the undesired scattering have a relatively high refractive index. This reasoning led us to choose 1-chloronaphthalene ($n = 1.63$) as a thermodynamically good solvent for light scattering measurements. We experienced no difficulty with the clarification of these solutions. The dn/dc value measured at 24° for the 5461 Å. wave length was 0.147.

We were unable to perform light scattering measurements at the theta temperature of the dioxane–water mixed solvent due to phase separation at the concentration level required to achieve sufficient excess scattering. As would be expected from Fig. 6, viscosity measurements could be carried out for solutions of much lower concentration at the theta temperature without difficulty. The light scattering measurements were therefore performed at 63°. The dn/dc value observed at this temperature was 0.104 for the 5461 Å. wave length.

Of the three solvents investigated, this mixed solvent had the lowest refractive index and was the most difficult to clarify. After our customary filtration and centrifugation procedure described in the Experimental Section, each solution was carefully transferred to another cell and centrifuged again for 30 minutes at 50,000 *g* before the measurements were performed. Dry weight analysis indicated that this procedure did not change the solution concentration by a measurable amount.

The refractive index of dimethylformamide is 1.43, and the dn/dc values measured at 5461 and 4358 Å. were 0.0478 and 0.0442, respectively.

The data were plotted as Kc/R *vs.* $\sin^2(\theta/2)$, where R is the reduced scattering intensity. This is illustrated in Fig. 8, in which the filled circles represent data obtained for three concentrations of fraction H dissolved in 1-chloronaphthalene. The intercepts represent the corresponding values at zero angle, and these must be plotted against concentration. Figure 9 shows the zero angle intercepts plotted against concentration for all of the fractions. The intercepts of these lines were used to evaluate the weight-average molecular weights, $\langle M\rangle_w$. In order to determine the *z*-average mean-square radii of gyration, $\langle s^2\rangle_z$, data for other angles were plotted in the same fashion as the zero angle data shown in Fig. 9, and the intercepts were plotted against $\sin^2(\theta/2)$ as illustrated by the open circles in Fig. 8. Then $\langle s^2\rangle_z$ was determined in the usual fashion from the (slope/intercept) ratio of this line. Since the concentration dependence was essentially linear, equivalent results could be obtained using the Zimm plot.[30] Figure 10 shows the data obtained under theta conditions for fraction H in dimethylformamide plotted in this way.

(30) P. Outer, C. I. Carr and B. H. Zimm, *J. Chem. Phys.*, **18**, 830 (1950).

The depolarization correction varied from 1.03 to 1.07 for these solvents. Fluorescence was observed at the 4358 Å. wave length during the measurements upon fractions A, D and H in dimethylformamide. The fluorescent intensity was measured and an appropriate correction was applied. The corrected $\langle M\rangle_w$ for fraction A differed by only 5% from the value determined at the green wave length, while the corrected value for fraction H was 13% higher than that measured in 1-chloronaphthalene.

The $\langle M\rangle_w$ values appear in columns four and five of Table II. The values listed for fractions A and D in dimethylformamide are those measured at the green wave length (where no fluorescence was observed). Column eight of Table II gives the values of the second virial coefficient A_2 calculated from the 1-chloronaphthalene data.

The weight-average and z-average degrees of polymerization, $\langle N\rangle_w$ and $\langle N\rangle_z$, appear in columns two and three of Table III, while column four gives the experimental $\langle\overline{s^2}\rangle_z$ values. The Φ' values listed in column five were calculated according to equations 5b and 6. The values of the intrinsic viscosity required for this calculation were taken from Table IV which appears in a later section. Comparison with the value $\Phi' = 3.2 \times 10^{22}$ characteristic of randomly coiling polymers shows that the Φ' value exhibited by a cellulose tricaproate having $\langle N\rangle_w = 2660$ has not yet reached this asymptotic value.

TABLE III

MOLECULAR SIZE AND HYDRODYNAMIC PARAMETERS

Fraction	$\langle N\rangle_w$	$\langle N\rangle_z$	$10^{12}\langle\overline{s^2}\rangle_z$ (cm.^{2})	$10^{-22}\Phi'$	α	$10^{16}\langle\overline{s_0^2}\rangle_z/\langle N\rangle_z$
	A. 1-Chloronaphthalene at 24°					
B	124	127	5.49	0.24	1.01	424
D	420	579	12.0	.87	1.09	175
F	466	532	9.49	1.03	1.05	162
H	2600	3710	51.5	1.40	1.05	126
	B. Dimethylformamide at 41°					
A	83	..	..	..	..	..
D	411	564	17.0	0.60	..	301
G	696	770	17.8	.62	..	231
H	2920	4400	65.5	1.47	..	149
	C. Dioxane–water (100:7) at 63°					
H	2600	3710	56.2	1.15	1.05	138

Holtzer, *et al.*,[6] concluded from their observations upon cellulose trinitrate in acetone that although Φ' may increase somewhat with $\langle N\rangle_w$, this variation is within their experimental uncertainty. On the other hand, Hunt, *et al.*,[7] reported that Φ' exhibits its asymptotic value for the trinitrate in ethyl acetate only when $\langle N\rangle_w > 2000$. Huque, *et al.*,[11] investigated a series of high molecular weight nitrate samples ($\langle N\rangle_w$ = 2200 to 8400) in both of the solvents mentioned above. Their data for ethyl acetate confirm the conclusion of Hunt and co-workers, but they report that for acetone Φ' is still increasing with $\langle N\rangle_w$ at the highest molecular weight investigated. For their three samples of highest molecular weight $\Phi' \cong 4 \times 10^{22}$, which exceeds the asymptotic value, 3.2×10^{22}. The heterogeneities of these samples were not measured; however, one might expect the distributions to be even broader than $\langle M\rangle_w/\langle M\rangle_n = 2.0$ as assumed by these authors, which would augment the reported Φ' values, thus further increasing the discrepancy.

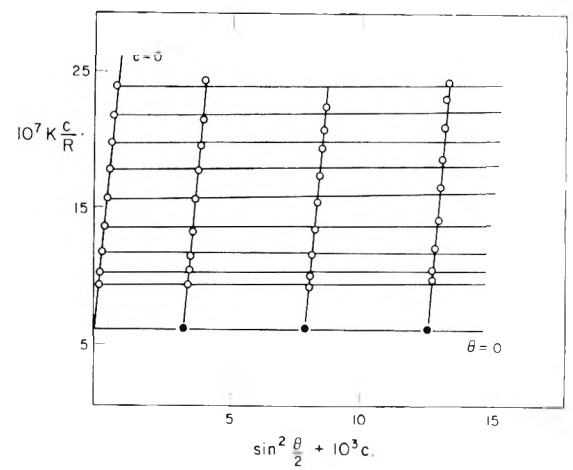

Fig. 10.—Zimm plot of the data for fraction H in dimethylformamide at the theta temperature.

A recent theoretical investigation by Stockmayer and Albrecht[31] has shown that the Flory parameter P appearing in the expression for the frictional constant depends to some extent upon the excluded volume. It seems quite likely that the same will be true of the parameter Φ'. Since this variation arises from the departure of the chain from gaussian form, one would expect inflexible chains, such as the cellulosics, to exhibit a similar behavior as the molecular weight is decreased.

Turning next to the molecular dimensions, we have calculated the values of the molecular expansion factor $\alpha = ([\eta]/[\eta]_\Theta)^{1/3}$ appearing in column six of Table III from the observed A_2, $\langle M\rangle_w$ and $[\eta]$ (Table IV below) through use of the relationship[32]

$$[\eta] - [\eta]_\Theta = 1.43 \times 10^{-25}\,\Phi'\,A_2\langle M\rangle_w \qquad (9)$$

The α-values for the tricaproate in thermodynamically good solvents are seen to be only slightly larger than unity and essentially independent of molecular weight. As mentioned previously, this behavior is exhibited by the trinitrate[6,7] and appears to be characteristic of inflexible molecules. The $\langle\overline{s_0^2}\rangle_z/\langle N\rangle_z$ ratios calculated through use of these α-values are listed in column seven of Table III, and appear plotted against $\langle N\rangle_w$ in Fig. 11. The number of repeating units in the chain was chosen as the independent variable in order to permit a more meaningful comparison with the published data for the trinitrate.[6,7,11]

We observe in Fig. 11 that for both polymers $(\overline{s_0^2}/N)$ approaches an asymptotic value at very high degrees of polymerization. For shorter chains the $(\overline{s_0^2}/N)$ ratio exhibits a marked solvent dependence. Since the tricaproate exhibits *smaller* dimensions in the thermodynamically good solvent, 1-chloronaphthalene, than in the theta solvent, di-

(31) W. H. Stockmayer and A. C. Albrecht, *J. Polymer Sci.*, **32**, 215 (1958).

(32) W. R. Krigbaum, *J. Polymer Sci.*, **18**, 315 (1955).

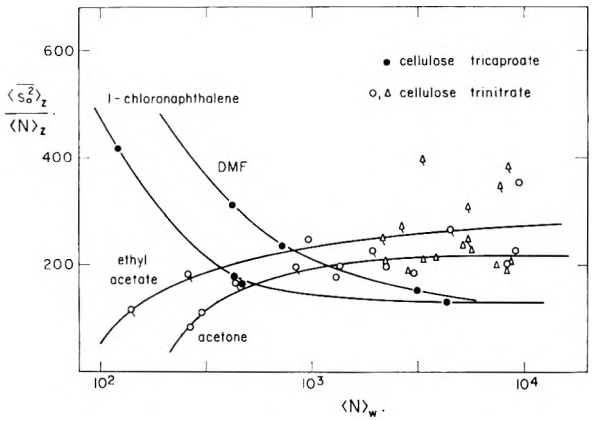

Fig. 11.—$\langle s_0^2 \rangle_z / \langle N \rangle_z$ plotted against $\langle N \rangle_w$ for cellulose tricaproate (filled circles) in dimethylformamide and 1-chloronaphthalene and for cellulose trinitrate in ethyl acetate (○)[7], (△)[11] and in acetone (○),[6] (△).[11]

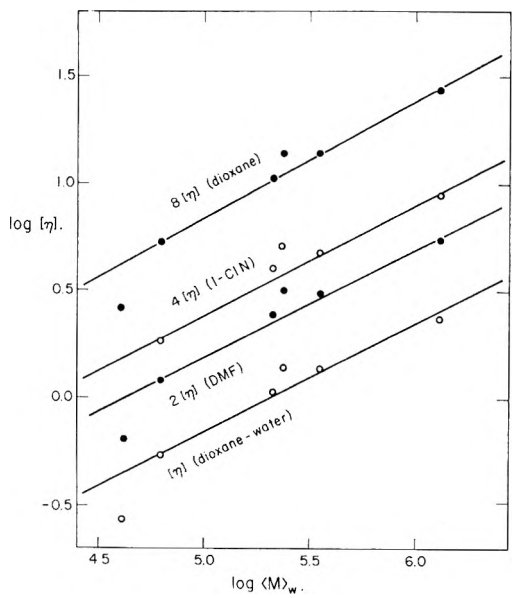

Fig. 12.—Molecular weight dependence of the intrinsic viscosity for cellulose tricaproate in dioxane at 35°, in 1-chloronaphthalene at 24°, in dimethylformamide at 41° and in the dioxane–water mixed solvent at 43°.

methylformamide, we can be certain that in this case the solvent dependence is strictly a skeletal effect.

For the trinitrate $(\overline{s_0^2}/N)$ approaches an asymptotic value at large N *from below*. This behavior has been interpreted in terms of Benoit and Doty's treatment of non-gaussian chains.[33] However, as shown in Fig. 12, the $(\overline{s_0^2}/N)$ ratios for the tricaproate in both solvents approach an asymptotic limit *from above*. The earliest work on cellulose acetate[34] and nitrate[35] also indicated an increase of $(\overline{s_0^2}/N)$ as N was diminished, but these results are of doubtful validity due to inadequate clarification of the solutions. Nevertheless, we believe that the decrease of this ratio observed for the tricaproate is real in view of its profound influence upon the molecular weight dependence of the intrinsic viscosity, as will be discussed below. If this be true, the treatment of non-gaussian chains developed by Benoit and Doty is not universally applicable to inflexible polymers. The most plausible explanation for the unexpected behavior exhibited by the tricaproate involves a shifting of the population in the various rotational states as the molecular weight is increased.

D. Intrinsic Viscosities.—Table IV lists the intrinsic viscosities measured in four solvents. These appear in Fig. 12 plotted against molecular weight using the conventional log-log scale. In order to separate the lines, the intrinsic viscosities shown for dimethylformamide, 1-chloronaphthalene and dioxane have been multiplied by the factors 2, 4 and 8, respectively. The relationships obtained are

$$[\eta] = 1.25 \times 10^{-3} (\langle M \rangle_w)^{0.67} \quad \text{(dioxane)} \quad (10a)$$
$$[\eta] = 1.70 \times 10^{-3} (\langle M \rangle_w)^{0.61} \quad \text{(1-chloronaphthalene)} \quad (10b)$$
$$[\eta]_\Theta = 2.45 \times 10^{-3} (\langle M \rangle_w)^{0.50} \quad \text{(dimethylformamide)} \quad (10c)$$
$$[\mu]_\Theta = 2.24 \times 10^{-3} (\langle M \rangle_w)^{0.50} \quad \text{(dioxane–water)} \quad (10d)$$

In fitting these points we have neglected the data for fraction A of lowest molecular weight, since these consistently fell below the lines representing the remainder of the data.

TABLE IV

INTRINSIC VISCOSITY DATA

Fraction	$\langle M \rangle_w$	[η] Dioxane 35°	[η] 1-Cl-N 24°	[η] DMF 41°	[η] Dioxane–water 43°
A	41,700	0.326	..	0.32	0.27
B	62,500	.66	0.46	.60	.539
C	(98,400)	.90	..	..	...
D	212,000	1.32	1.00	1.22	1.07
E	(195,000)	1.32	..	..	..
F	236,000	1.72	1.27	1.58	1.38
G	352,000	1.72	1.18	1.53	1.36
H	1,310,000	3.36	2.19	2.72	2.35

One immediately notices the unusually low values of the molecular weight exponent, a, in the good solvents, dioxane and 1-chloronaphthalene. We recall that the corresponding a values for flexible chain polymers fall in the range 0.7–0.8, while for cellulose trinitrate and triacetate a = 0.9–1.0. For an explanation of these differences we must consider the various factors in equation 1

$$[\eta] = \Phi'(\overline{s_0^2}/M)^{3/2} M^{1/2} \alpha^3 \quad (1)$$

As mentioned above, both Φ' and $(\overline{s_0^2}/M)$ are independent of molecular weight for flexible chain polymers, so that the molecular weight dependence resides in the $M^{1/2}\alpha^3$ product. For cellulose derivatives, on the other hand, α^3 is near unity at all molecular weights. In the case of the trinitrate both Φ' and $(\overline{s_0^2}/M)$ increase with molecular weight, resulting in a large molecular weight exponent, a. However, for the tricaproate the variations of these two quantities nearly cancel, so that the factor $M^{1/2}$ makes the principal contribution in this case.

We observe that for the tricaproate in the two theta solvents the exponent is 0.50, just as would be expected of a flexible chain polymer. However, both Φ' and $(\overline{s_0^2}/M)$ are varying with molecular

(33) H. Benoit and P. Doty, THIS JOURNAL, **57**, 958 (1953).
(34) R. S. Stein and P. Doty, *J. Am. Chem. Soc.*, **68**, 159 (1946).
(35) R. M. Badger and R. H. Blaker, THIS JOURNAL, **53**, 1056 (1949).

weight over the range of these measurements. If we assume that equations 10d and 10c can be extrapolated to higher molecular weights where Φ' would attain its asymptotic value, then from equation 1 we estimate $10^{16}(\overline{s_0^2}/N) = 85$–$95$. Reference to Fig. 13 shows that the latter is a reasonable asymptotic value for the DMF curve. From these values we obtain an effective bond length, $b = (\overline{r_0^2}/N)^{1/2}$, of 22–24 Å. and a limiting persistence length q as calculated according to the relation of Benoit and Doty,[22] of 50–55 Å. For comparison, the values for the trinitrate are $b = 35$ Å. and $q = 117$ Å. Thus, although the tricaproate is more extended at low degrees of polymerization, its dimensions in the asymptotic region are smaller than those of the trinitrate.

Flory, Spurr and Carpenter[9] have concluded that the large negative temperature coefficient of the intrinsic viscosity characteristic of cellulose derivatives must have its origin in skeletal effects, rather than in osmotic effects. This is illustrated quite clearly in Table V, where the viscosities for our fraction H of highest molecular weight as measured in the dioxane–water theta solvent are compared with those reported by Carpenter and Krigbaum[1] for a high molecular weight polystyrene in the theta solvent cyclohexane. In each case the temperature was varied over a range of approximately 20°. For polystyrene the intrinsic viscosity increases with temperature almost as rapidly as α^3, since the accompanying decrease in $(\overline{s_0^2}/M)$ is inconsequential. The A_2 value increases relatively slowly with temperature due to the concomitant decrease of the factor $F(X)$ appearing in equation 3. On the other hand the A_2 value for the tricaproate increases much more rapidly with temperature, since $F(X)$ remains near unity. However, in spite of this more rapid increase of solvent power, the skeletal effect predominates and $[\eta]$ falls off at higher temperatures due to the rapid reduction of $(\overline{s_0^2}/M)$.

TABLE V

TEMPERATURE DEPENDENCE OF $[\eta]$

Cellulose tricaproate, $\langle M\rangle_w$ = 1.31 × 10⁶, in dioxane–water (100:7)			Polystyrene, $\langle M\rangle_w$ = 3.20 × 10⁶, in cyclohexane		
t(°C.)	$10^4 A_2$	$[\eta]$	t(°C.)	$10^4 A_2$	$[\eta]$
43	0.0	2.35	35	0.00	1.29
51	0.4	2.20	45	.31	1.78
61	1.2	2.08	55	.54	2.10

Conclusions

We have seen that cellulose tricaproate qualifies as an inflexible chain polymer. Its unperturbed molecular dimensions decrease rapidly with temperature, and in thermodynamically good solvents the molecular expansion factor α is not much larger than unity and is independent of molecular weight. The departure of Φ' from its asymptotic value provides further evidence that the tricaproate chains are non-gaussian. However, the tricaproate does not obey the treatment of non-gaussian chains set forth by Benoit and Doty, since $(\overline{s_0^2}/N)$ increases as the molecular weight is decreased. This exceptional behavior may be explained if the hindrance potential heavily favors one rotational conformation, and if the population of bonds in the available rotational states becomes more randomly distributed as the molecular weight is increased.

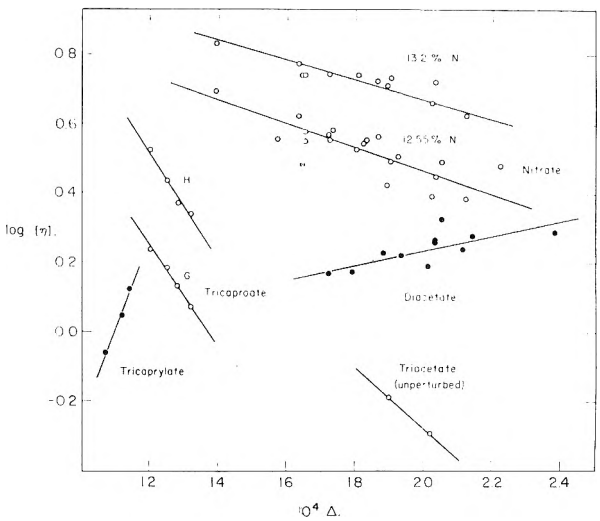

Fig. 13.—Correlation of the solvent dependence of the intrinsic viscosity for cellulose nitrates,[38] acetates,[10] tricaproate and tricaprylate[8] with the Δ parameter defined in the text.

We would like to obtain some information concerning the origin of the forces responsible for the high rotational barriers in these polymers. We have seen that the $(\overline{s_0^2}/N)$ ratios for both the trinitrate and the tricaproate exhibit a large solvent dependence if the molecular weight is below the asymptotic region. This is certainly a manifestation of a skeletal effect in the latter case, since the observed dimensions are smaller in a good solvent, 1-chloronaphthalene, than those measured under theta conditions in DMF. Turning to Table IV, the intrinsic viscosities listed for these two solvents fall in the same order. Furthermore, except for the $[\eta]$ value for fraction H in dioxane, the ratio of the intrinsic viscosities in any two of these solvents is independent of molecular weight, again suggesting that the solvent dependence is predominantly due to variations of the unperturbed dimensions. In view of these considerations we have examined the solvent dependence of the intrinsic viscosity more closely, hoping to obtain thereby some insight into the forces responsible for the rotational energy barrier.

Since the thermodynamic interactions are excluded from consideration, one might look for a correlation between the intrinsic viscosity and some physical constant characterizing the solvent. Let us assume that dipolar interactions are responsible for the skeletal effect. We should then expect some relationship between the intrinsic viscosity and the dielectric constant of the solvent. Onsager[36] has shown that if the dipole is imagined to lie in a spherical cavity of radius b, and to be surrounded by a continuous medium of dielectric constant ϵ, then in the medium the reaction field of the dipole is reduced by the factor f

$$f = \frac{1}{b^3}\frac{2\epsilon - 2}{2\epsilon + 1} \qquad (11)$$

(36) L. Onsager, *J. Am. Chem. Soc.*, **58**, 1486 (1936).

However, attempts by Moore and Russell[10] to relate the intrinsic viscosity of cellulose diacetate to the dielectric constant of the solvent met with no apparent success. Hence, the type of dispersion force first treated by London[37] appears to offer the only remaining possibility. In this case the time scale of the fluctuation is too short to permit orientation of a solvent dipole, so that one must consider instead the electron polarizability of the solvent. Thus, to modify equation 11 for application to an instantaneous dipole we replace ϵ by n^2, where n is the refractive index of the solvent. Before making use of this modified version of the equation, the magnitude of the poorly-defined cavity radius b must be assigned. We have arbitrarily equated this to the sum of the radii of a polymer segment and a solvent molecule. Since only a relative scale of values is desired, we have defined a parameter Δ as

$$\Delta = \frac{(n^2 - 1)/(2n^2 + 1)}{(V_1^{1/3} + V_p^{1/3})^3} \qquad (12)$$

where V_1 and V_p are the molar volumes of solvent and of a polymer segment, respectively. In order to test this relation we require viscosity data for a given polymer sample in a variety of solvents. Fortunately, Moore and Russell have obtained this type of data for cellulose acetate[10] and nitrate[38] samples having different degrees of substitution in a wide variety of polar solvents. Figure 13 shows log $[\eta]$ plotted as a function of Δ. The correlation is quite satisfactory, particularly in view of the wide variety and highly polar nature of these solvents. The dispersion forces become weaker as Δ increases, hence we expect a negative slope if skeletal effects predominate. This is the case for the tricaproate and for three nitrate esters (one not shown). However, the slope is positive for the tricaprylate data[8] when these are adjusted to a common temperature, and for the diacetate and triacetate (not shown) esters.[10] We believe that in these cases the chains are more flexible, at least under the conditions of these measurements, so that the opposing variation of the osmotic expansion overtakes the skeletal effect. This is indicated in Fig. 14 by the fact that the $[\eta]_\theta$ values as calculated by Flory, Spurr and Carpenter[9] for the triacetate exhibit the expected negative slope.

The assumption stated above implies that it should be possible to correlate *both* the skeletal and osmotic effects with the Δ parameter. In this connection it is interesting that Moore[38] found that for a given class of solvents (*e.g.*, ketones, formates, acetates, etc.) the intrinsic viscosity of cellulose nitrate could be correlated with the cohesive energy density (c.e.d.) of the solvent. Thus, he was able to express a skeletal effect in terms of a parameter which has been used for many years as a measure of the energy change on mixing. This suggests that the Δ parameter and c.e.d. are interrelated. We therefore plotted Δ values (assuming $V_p = 100$ cc.) for a number of liquids against their c.e.d. values. The points conformed reasonably well to a linear relationship, although some systematic deviations were apparent. In particular, the Δ values of the higher paraffins were somewhat low, those of the aromatics tended to be high, and that for CS_2 was considerably above the line. In general, however, the deviations were not large, so that we would anticipate about the same success in predicting energy changes from Δ values as that achieved using c.e.d.

In summary, dispersion forces, rather than dipole interactions, appear to be responsible for the high potential barrier to rotation in the cellulosics. Hence, the difference between these polymers and those having more flexible chains must be one of degree, rather than kind.

Acknowledgment.—This investigation was supported by the Allegany Ballistics Laboratory, an establishment owned by the United States Navy and operated by Hercules Powder Company, under Contract NOrd 10431. L. H. S. wishes to express his appreciation to the Tennessee Eastman Corp. for a fellowship during the final year of his graduate study.

(37) F. London, *Trans. Faraday Soc.*, **33**, 8 (1937).
(38) W. R. Moore, *J. Polymer Sci.*, **5**, 91 (1950); **7**, 175 (1951).

THE KINETICS OF THE REACTION BETWEEN URANIUM(IV) AND CERIUM(IV)[1]

BY F. B. BAKER, T. W. NEWTON AND MILTON KAHN

University of California, Los Alamos Scientific Laboratory, Los Alamos, New Mexico and the University of New Mexico, Albuquerque, New Mexico

Received July 20, 1959

The kinetics of the reaction between uranium(IV) and cerium(IV) was studied in perchloric acid–sodium perchlorate solutions at $\mu = 2$, over the perchloric acid concentration range 0.80 to 2.00 M. The rate for the principal reaction path was found to be proportional to both the $CeOH^{+3}$ and U^{+4} concentrations and inversely proportional to the hydrogen ion concentration. The thermodynamic quantities of activation in 2 M perchloric acid at 2.4° were found to be $\Delta H^{\ddagger} = 14.0 \pm 0.7$ kcal./mole, $\Delta S^{\ddagger} = 6.2 \pm 2.5$ e.u., and $\Delta F^{\ddagger} = 12.2 \pm 0.2$ kcal./mole. A potentiometric study of the hydrolysis of cerium(IV) in the aforementioned media indicates $CeOH^{+3}$ to be the predominant species in solution over the perchloric acid concentration range from 0.300 to 2.00 M.

Introduction

The kinetics of the oxidation of uranium(IV) by iron(III),[2] oxygen,[3] plutonium(VI)[4] and plutonium(IV)[5] have already been studied. The present investigation of the oxidation of uranium(IV) by cerium(IV) was undertaken to provide further kinetic information for comparison with that already available.

The rate was found to be first order with respect to both $CeOH^{+3}$ and U^{+4} and inversely proportional to the perchloric acid concentration. Potentiometric measurements indicate that the principal cerium(IV) species is $CeOH^{+3}$ in the acid concentration ranges studied.

Experimental

Reagents.—Stock solutions of cerium(IV) perchlorate were prepared by electrolytic oxidation[6] of cerium(III) perchlorate, which in turn was obtained by digestion of cerium(III) oxalate in fuming perchloric acid. Small amounts of oxalate were added cautiously to the fuming acid. In general about 90% of the cerium was present as cerium(IV). The cerium(IV) concentration was determined by titration with standardized ferrous sulfate; the total cerium concentration was determined by a standard spectrophotometric procedure.[7] The acid concentration of the cerium(IV) stock solution was determined by titration with standard base after removal of the total cerium as cerium(III) oxalate. Cerium(III) oxalate was prepared from ceric ammonium nitrate by reduction with hydrogen peroxide and subsequent precipitation with oxalic acid.

Uranium(IV) stock solutions were prepared by electrolytic reduction of uranyl perchlorate solutions, which were prepared by dissolving pure uranium oxide (U_3O_8) in fuming perchloric acid. Approximately 80% of the total uranium was reduced to uranium(IV). The uranium(IV) concentration was determined by titration with standard ceric sulfate. The total uranium concentration was determined by reduction with zinc amalgam, air oxidation (zinc reduction of U(VI) gives some U(III) which is oxidized to U(IV) by O_2 in 1 M sulfuric acid) and titration with standard ceric sulfate. The acid concentration was determined by removing the uranium with a cation-exchange (Amberlite IR 120) column in the acid form and titrating with standard base. The titrations were corrected for the hydrogen ion equivalent of the metal ions removed.

The perchloric acid used was prepared from concentrated acid which had been purified by boiling at atmospheric pressure and then again under reduced pressure.

Sodium perchlorate was prepared by neutralizing reagent grade sodium carbonate with perchloric acid, boiling out the carbon dioxide and crystallizing from water several times. Sodium perchlorate stock solutions were analyzed gravimetrically by drying aliquots at 150° to constant weight. Distilled water was redistilled from alkaline permanganate in an all Pyrex still.

Rate constants obtained from runs using sodium perchlorate which had been crystallized three times were the same within experimental error as those in which the twice-crystallized salt was used.

E.M.F. Measurements.—The hydrolysis of cerium(IV) was studied potentiometrically by measurement of the potential of the cerium(III)–cerium(IV) couple as a function of perchloric acid concentration employing a procedure very similar to those reported elsewhere.[8,9]

The total cerium concentration in all reaction mixtures was 3.51×10^{-3} M. The cerium(IV)–cerium(III) ratios were varied by addition of hydrogen peroxide. Sodium perchlorate was used to maintain the ionic strength at 2.0. The concentration of cerium(IV) in the reaction mixture was determined spectrophotometrically[7] and was found to be constant within the experimental error during the potential measurements.

Measurement of Reaction Rates.—The reaction rates were determined by following the change in concentration of cerium(IV) with time spectrophotometrically. In order to make observations on the cerium(IV) concentration within a sufficiently short time after mixing, the following procedure was adopted. Appropriate amounts of reagents, including the uranium(IV), were pipetted into a plugged, thermostated funnel which led directly into a thermostated (±0.1°) 10-cm. absorption cell. The cerium(IV) solution was added subsequently by means of a modified hypodermic syringe with constant stirring. After about 4 seconds, when mixing was complete, the plug was removed to allow the mixed solution to drain into the absorption cell. It was possible to take the first reading within 10 seconds of zero time. The cerium(IV) concentration was determined from its absorbance at 2900 Å., where the molar absorptivity is about 2000 M^{-1} cm.$^{-1}$. The absorbance as a function of time was read from the recorder chart of a Cary Recording Spectrophotometer, Model 14, which moved at a speed of eight inches per minute. Initial cerium(IV) concentrations were determined spectrophotometrically as in the procedure used in the e.m.f. measurements.

Results and Discussion

Hydrolysis of Cerium(IV).—Sherrill, King and Spooner[9] found in their potentiometric study of the cerium(III)–cerium(IV) couple in perchloric acid (0.202 to 2.38 M) at 25° that the hydrolysis of cerium(IV) could be represented by the equations

$$K_1 = \frac{[CeOH^{+3}][H^+]}{[Ce^{+4}]} \qquad (1)$$

(1) This work was done under the auspices of the U. S. Atomic Energy Commission at the Los Alamos Scientific Laboratory under the Advanced Study Program with the University of New Mexico and is based on a thesis to be submitted by F. B. Baker in partial fulfillment of the requirements for the degree of Doctor of Philosophy in the Graduate School of the University of New Mexico.

(2) R. H. Betts, *Can. J. Chem.*, **33**, 1780 (1955).

(3) J. Halpern and J. G. Smith, *ibid.*, **34**, 1419 (1956).

(4) T. W. Newton, THIS JOURNAL, **62**, 943 (1958).

(5) T. W. Newton, *ibid.*, **63**, 1493 (1959).

(6) G. F. Smith, G. Frank and A. E. Kott, *Ind. Eng. Chem., Anal. Ed.*, **12**, 268 (1940).

(7) A. I. Medalia and B. J. Byrne, *Anal. Chem.*, **23**, 453 (1951).

(8) S. W. Rabideau, *J. Am. Chem. Soc.*, **79**, 3675 (1957).

(9) M. S. Sherrill, C. B. King and R. C. Spooner, *ibid.*, **65**, 170 (1943).

and

$$K_2 = \frac{[Ce(OH)_2^{+2}][H^+]}{[CeOH^{+3}]} \quad (2)$$

where the brackets indicate concentrations in moles per liter. Sherrill, *et al.*, found the hydrolysis represented by equation 1 to be essentially complete and the hydrolysis quotient for the second step to be 0.6.

Because the study referred to above was carried out only at 25° and varying ionic strength, it was necessary to extend the study of hydrolysis of cerium(IV) as a function of temperature and at constant ionic strength in order to interpret the kinetic data.

The formal potential E_f for the cerium(III)-cerium(IV) couple is related to the hydrolysis quotients K_1 and K_2 by the expression

$$E_f = E^{0\prime} = \frac{RT}{F} \ln \left(1 + \frac{K_1}{[H^+]} + \frac{K_1K_2}{[H^+]^2}\right) \quad (3)$$

where the constant $E^{0\prime}$ involves the standard potential and the activity coefficients. For the case where $K_1 >> [H^+]$, equation 3 becomes

$$E_f = \left(E^{0\prime} - \frac{RT}{F} \ln K_1\right) - \frac{RT}{F} \ln \left(\frac{[H^+] + K_2}{[H^+]^2}\right) \quad (4)$$

The formal potentials were extrapolated to zero cerium(IV) concentration to correct for polymerization.[10,11] At the highest cerium(IV) concentration it was estimated from the data given by King and Pandow[10] that at least 90% of the cerium(IV) was monomer.

Values of the formal potentials calculated using equations 3 or 4 and limiting K_1, K_2 pairs are compared with the experimental formal potentials in Table I. The choice of the limits for K_1, K_2 pairs is based on an experimental error of 0.4 mv.

Although the values for K_1 and K_2 given in Table I are quite uncertain they are sufficiently precise for the analysis of the kinetic data and suggest that in 2 *M* perchloric acid the first hydrolysis step is at least 85% complete at 25°; at 1.6° this hydrolysis step is at least 70% complete but not more than 90% complete. Considering the relatively small value of K_2 at both temperatures it is concluded that the predominant species in 2 *M* perchloric acid is $CeOH^{+3}$, in agreement with Sherrill, *et al.*

Stoichiometry.—The stoichiometry of the reaction 2Ce(IV) + U(IV) = 2Ce(III) + U(VI) was checked by adding an excess of cerium(IV) to uranium(IV) under experimental conditions similar to those used in the rate runs. The amount of cerium(IV) reduced in excess of that equivalent to the uranium(IV) and was small (< 2%) and attributed to a trace of oxidizable impurity present in the stock solutions.

Rate Law.—The rate of oxidation of uranium(IV) by cerium(IV) was investigated at 2.4° in the perchloric acid concentration range from 0.800 to 2.00 molar and an ionic strength of 2.00; the initial cerium(IV) and uranium(IV) concentrations ranged from 4.2 to 6.0 × 10^{-5} *M* and 2.6 to 8.8 × 10^{-5} *M*, respectively. The linearity of the plots described below suggested that the rate of reaction was first order with respect to both cerium(IV) and uranium(IV). Where the concentration of uranium(IV) in moles per liter was considerably larger than one-half of the cerium(IV) concentration, plots of log[U(IV)]/[Ce(IV)] *versus* time yielded straight lines up to the point where the reactions were about 80% complete. For rate runs where the concentration of uranium(IV) was close to one-half that of cerium(IV), straight lines were obtained from plots of the reciprocal of the average concentrations *versus* time; the average concentration is defined as (2[U(IV)] + [Ce(IV)])/2 at time *t*. The second-order rate constant *k'* at a particular hydrogen ion concentration is defined by the equation

$$-d[Ce(IV)]/dt = 2k'[U(IV)][Ce(IV)]$$

The constancy of the second-order rate constant *k'* at a hydrogen ion concentration of 2.00 *M* is shown in Table II. Similar experiments were done at other hydrogen ion concentrations, and the results are summarized in Table III.

(10) E. L. King and M. L. Pandow, *J. Am. Chem. Soc.*, **74**, 1966 (1952).

(11) L. Heidt and M. Smith, *ibid.*, **70**, 2476 (1948).

TABLE I

HYDROLYSIS OF CERIUM(IV) IN PERCHLORIC ACID SOLUTIONS AT μ = 2.00 FORMAL POTENTIALS OBTAINED FROM THE DATA COMPARED WITH THOSE CALCULATED, FOR VARIOUS VALUES OF K_1 AND K_2

25°

$[H^+]$, *M*	Exp., E_f	Calculated: Best values,[a] E_f	Upper limit, K_1[b] E_f	Lower limit, K_1[c] E_f
2.000	1.7275	1.7278	1.7271	1.7268
1.000	1.7083	1.7083	1.7079	1.7088
0.500	1.6876	1.6874	1.6875	1.6879
0.300	1.6706	1.6706	1.6713	1.6704
$\Sigma d(mv.)^2$		0.1	1.0	0.9

1.6°

$[H^+]$, *M*	Exp., E_f	Best values,[d] E_f	Upper limit, K_1,[e] E_f	Lower limit, K_1,[f] E_f
2.000	1.7207	1.7210	1.7214	1.7210
1.000	1.7061	1.7062	1.7059	1.7068
0.500	1.6899	1.6895	1.6892	1.6897
0.300	1.6759	1.6758	1.6761	1.6752
$\Sigma d(mv.)^2$		0.3	1.1	1.1

[a] $K_1 >> [H^+]$, K_2 = 0.15 and $(E^{0\prime} - (RT/F) \ln K_1)$ = 1.7119. [b] $K_1 >> [H^+]$, K_2 = 0.12 and $(E^{0\prime} - (RT/F) \ln K_1)$ = 1.7108. [c] K_1 = 10, K_2 = 0.22 and $E^{0\prime}$ = 1.7750. [d] K_1 = 8, K_2 = 0.08, $E^{0\prime}$ = 1.7598. [e] K_1 = 14, K_2 = 0.05, $E^{0\prime}$ = 1.7711. [f] K_1 = 5, K_2 = 0.14, $E^{0\prime}$ = 1.7518.

TABLE II

VALUES OF THE RATE CONSTANT *k'* IN 2.00 *M* PERCHLORIC ACID AT 2.4° AND μ = 2.00

Run	$[U(IV)]_0$, $M \times 10^5$	$[Ce(IV)]_0$, $M \times 10^5$	*k'*, M^{-1} sec.$^{-1}$
1	6.06	5.05	464
2	3.50	4.25	455
3	7.08	4.28	472
4	8.83	4.27	447
5	8.02	6.01	483
6	2.62	5.06	462
7	2.62	5.06	458

Because the rate was found to be proportional to the reciprocal of the hydrogen ion concentration

TABLE III

VALUES OF THE RATE CONSTANTS k' AND k_1 IN PERCHLORIC ACID SODIUM PERCHLORATE SOLUTIONS AT 2.4° AND $\mu = 2$

$[H^+]$, M	No. determ.[a]	Av. obsd. k', M^{-1} sec.$^{-1}$	k_1, sec.$^{-1}$	Calcd. k', M^{-1} sec.$^{-1}$
2.00	7	460	1190	480
1.25	7	810	1240	820
1.00	5	1030	1240	1040
0.80	5	1380	1320	1310

[a] The mean deviation from the average k' was in the range from 2 to 2.5% and the maximum deviation ranged from 2 to 4.3%.

the following rate law is proposed, which is written in terms of the predominant species in solution

$$-\frac{d[Ce(IV)]}{dt} = 2k_1\frac{[U^{+4}][CeOH^{+3}]}{[H^+]} \quad (5)$$

Inasmuch that the hydrolysis of U^{+4} is negligible[12,2] in the acid concentration range studied $[U^{+4}] = [U(IV)]$. From equations 1 and 2

$$[CeOH^{+3}] = [Ce(IV)][H^+]/([H^+]^2/K_1 + [H^+] + K_2) \quad (6)$$

The dependence of k' on the hydrogen ion concentration obtained from equations 5 and 6, is given by the expression

$$k' = \frac{k_1}{[H^+]^2/K_1 + [H^+] + K_2} \quad (7)$$

The values of k_1 given in the fourth column of Table III were calculated using equation 7. The small increase in k_1 with decreasing hydrogen ion concentration (see Table III) can be explained by assuming a lack of constancy of the pertinent activity coefficients or by postulating an additional path which would not contribute significantly to the over-all reaction rate. Because the systematic variation in k_1 was almost within the estimated probable error of k_1 it was decided to eliminate this minor path from further consideration.

The values of k' given in the last column of Table III which were calculated using the average of k_1, 1250 ± 150 sec.$^{-1}$, are in satisfactory agreement with the experimental values of k' indicating that the rate law given by equation 5 is satisfactory.

Mechanism.—The rate law (equation 5) for the rate-determining reaction shows that the formation of the activated complex from the principal species in solution can be represented by the net process[13]

$$CeOH^{+3} + U^{+4} + H_2O = [\text{activated complex}]^{+6} + H^+ \quad (8)$$

This rate-determining reaction is probably

$$U(IV) + Ce(IV) \longrightarrow U(V) + Ce(III) \quad (9)$$

followed by the fast reaction

$$U(V) + Ce(IV) \longrightarrow U(VI) + Ce(III) \quad (10)$$

An alternative to reaction 9 is

$$U(V) + U(V) \longrightarrow U(VI) + U(IV) \quad (11)$$

On the basis of published rate constants[14,15] it can be shown that reaction 11 cannot contribute significantly to the experimentally established rate law.

It is of interest to compare the net activation process (equation 8) with that of the analogous reaction between plutonium(IV) and uranium(IV)[5]

$$Pu^{+4} + U^{+4} + 2H_2O = [\text{activated complex}]^{+6} + 2H^+$$

Although cerium(IV) is principally $CeOH^{+3}$ and plutonium(IV) principally Pu^{+4} in acid solution the activated complexes are formally the same for both reactions.

Temperature Dependence.—The rate of reaction has been studied over the temperature range from 2.4 to 15.6° at a perchloric acid concentration of 2.00 M. The results are summarized in Table IV; values of k_1 were calculated from the experimentally determined values of k' using equation 7 and the appropriate values of K_1 and K_2. Because K_1 was evaluated only at one temperature, the values given for K_1 in the last column of Table IV were estimated by assuming (from consideration of the relative ionic radii of Pu^{+4}, Ce^{+4} and U^{+4}) that the entropy of hydrolysis is 24 ± 6 e.u., for the reaction $Ce^{+4} + H_2O = CeOH^{+3} + H^+$, which is within the range of the entropies of hydrolysis for the analogous hydrolytic reactions of Pu^{+4} and U^{+4}.[3,8,12] The values of K_2 were obtained by interpolation on a log K_2 *versus* $1/T$ plot using the data given in Table I.

TABLE IV

TEMPERATURE DEPENDENCE FOR THE RATE OF REACTION AT 2.00 M PERCHLORIC ACID CONCENTRATION

Temp., °C.	k', M^{-1} sec.$^{-1}$	k_1, sec.$^{-1}$	K_1, M	K_2, M
2.4	460 ± 9[a]	1190	8	0.08
8.0	810 ± 20	2030	10	.10
15.6	1670 ± 40	4050	14	.14

[a] These uncertainties are the average deviation from the mean.

The constants log A and E_a in the Arrhenius equation were obtained by a method of least squares and are 14.6588 and 14.6 kcal./mole, respectively; values of the rate constants calculated using these values of log A and E_a agree with the average values tabulated in the second column of Table IV within 1%. The values of the entropy, heat and free energy of activation were calculated[16] for the net activation process (equation 8) and are $\Delta S^\ddagger = 6.2 \pm 2.5$ e.u., $\Delta H^\ddagger = 14.0 \pm 0.7$ kcal./mole and $\Delta F^\ddagger = 12.2 \pm 0.2$ kcal./mole. These values pertain to the reaction in 2.00 M perchloric acid at 2.4°. The uncertainties were estimated by combining the probable error of the rate constants and the uncertainty of the hydrolysis quotients K_1 and K_2.

Effect of Sulfate.—Several runs were made at 2.4° and 2 M perchloric acid with added sodium sulfate. The sulfate concentration was varied from 0.0010 to 0.10 M. The rates in this range increased with increasing sulfate concentration and were immeasurably faster than in pure 2 M per-

(12) K. A. Kraus and F. Nelson, *J. Am. Chem. Soc.*, **72**, 3901 (1950).

(13) T. W. Newton and S. W. Rabideau, *J. Phys. Chem.*, **63**, 365 (1959).

(14) D. M. H. Kern and E. F. Orlemann, *J. Am. Chem. Soc.*, **71**, 2102 (1949).

(15) H. Imai, *Bull. Chem. Soc. Japan*, **30**, 873 (1957).

(16) S. Glasstone, K. Laidler and H. Eyring, "The Theory of Rate Processes," McGraw-Hill Book Co., New York, N. Y., 1941, pp. 195–199.

chloric acid. However, in 1.1 M sulfuric acid in which the sulfate concentration was estimated to be 0.45 M, the rate was measurable and only 1.3 times as fast as the rate under comparable conditions of 1.5 M perchloric acid at $\mu = 2$.

These results suggest that the effect of sulfate is similar to that found in the neptunium(IV)–neptunium(VI) reaction which has been extensively studied.[17]

Acknowledgments.—The authors gratefully acknowledge many helpful discussions with Professor G. Scatchard primarily concerning the hydrolysis of cerium(IV). They also acknowledge discussions with Dr. C E. Holley, Jr., and especially with Dr. J. F. Lemons, under whose general direction this work was done.

(17) J. C. Sullivan, D. Cohen and J. C. Hindman, *J. Am. Chem. Soc.*, **79**, 4029 (1957).

THE THERMODYNAMIC PROPERTIES OF THE SYSTEM: HYDROCHLORIC ACID, POTASSIUM CHLORIDE AND WATER FROM 0 TO 40°

BY HERBERT S. HARNED

Contribution No. 1530 from the Department of Chemistry of Yale University, New Haven, Connecticut

Received July 27, 1959

Parameters of equations which permit the calculation of the activity coefficients of both electrolytic components and the activity of water in the system, hydrochloric acid, potassium chloride and water from 0 to 40°, have been obtained. The magnitude and sign of the excess heat of mixing as a function of temperature has been estimated.

In an earlier communication, a thorough investigation of the thermodynamic properties of the system hydrochloric acid, sodium chloride and water from 0 to 50° has been recorded.[1] The present contribution contains a similar calculation for aqueous solutions containing hydrochloric acid and potassium chloride.

The calculations are based on the equations

$$\log \gamma_1 = \log \gamma_{1(0)} - \alpha_{12(0)} m_2 - \beta_{12} m_2^2 \qquad (1)$$

$$\log \gamma_2 = \log \gamma_{2(0)} - \alpha_{21(0)} m_1 - \beta_{21} m_1^2 \qquad (2)$$

to be applied at constant total molalities $m = m_1 + m_2$. In these equations γ_1, m_1 and γ_2, m_2 represent the activity coefficients and molalities of the acid and the salt in their mixtures, respectively, $\gamma_{1(0)}$ is the activity coefficient of the acid of molality m in water and $\gamma_{2(0)}$, the activity coefficient of the salt in water at molality m. The quantities $\alpha_{12(0)}$, $\alpha_{21(0)}$, β_{12} and β_{21} are the empirical coefficients of the linear and quadratic terms.

Calculations of the Parameters of Equations 1 and 2.—The coefficient $\alpha_{12(0)}$ was obtained by reconsideration of the electromotive force data of Harned and Hamer[2] and Harned and Gancy[3] for the activity coefficient of the acid, γ_1, in the mixtures. The activity coefficients, $\gamma_{1(0)}$, of the acid in water were obtained from the data of Harned and Ehlers[4] as tabulated by Harned and Owen.[5] The values of log $\gamma_{1(0)}$ and $\alpha_{12(0)}$ from 0 to 40° at 5° intervals are given in Table I for the system at total molalities 1, 2 and 3. Since all the experimental evidence indicates that log γ_1 varies linearly with the acid or salt concentration at constant total molality, it is assumed that β_{12} equal zero.

The parameter $\alpha_{21} = \alpha_{21(0)} + \beta_{21} m_1$ was computed by the method of MacKay.[6] Values of log $\gamma_{2(0)}$ required for this calculation were obtained from the data of Harned and Cook[7] and are recorded in the third column of Table I.

TABLE I

DATA FOR COMPUTING THE ACTIVITY COEFFICIENTS OF HYDROCHLORIC ACID, γ_1, AND POTASSIUM CHLORIDE, γ_2, IN SOLUTIONS OF 1, 2 AND 3 m TOTAL MOLALITIES

t	log $\gamma_{1(0)}$	log $\gamma_{2(0)}$	$\alpha_{12(0)}$	$\alpha_{21(0)}$
		$\beta_{21} = -0.006$		
		$m = m_1 + m_2 = 1$		
0	$\bar{1}.9253$	$\bar{1}.7694$	0.0670	−0.0740
5	$\bar{1}.9224$	$\bar{1}.7745$	.0650	− .0714
10	$\bar{1}.9188$	$\bar{1}.7767$	.0625	− .0681
15	$\bar{1}.9153$	$\bar{1}.7188$	.0605	− .0655
20	$\bar{1}.9118$	$\bar{1}.7810$	.0585	− .0629
25	$\bar{1}.9079$	$\bar{1}.7824$	.0558	− .0602
30	$\bar{1}.9041$	$\bar{1}.7810$	.0540	− .0586
35	$\bar{1}.8999$	$\bar{1}.7810$	.0520	− .0568
40	$\bar{1}.8957$	$\bar{1}.7803$	.0500	− .0560
		$m = m_1 + m_2 = 2$		
0	0.0326	$\bar{1}.7380$	0.0680	−0.0640
5	.0286	$\bar{1}.7435$	.0665	− .0615
10	.0224	$\bar{1}.7497$	.0645	− .0585
15	.0166	$\bar{1}.7543$	.0625	− .0555
20	.0103	$\bar{1}.7582$	.0605	− .0535
25	.0039	$\bar{1}.7604$	.0590	− .0514
30	$\bar{1}.9967$	$\bar{1}.7619$	.0570	− .0485
35	$\bar{1}.9894$	$\bar{1}.7627$	.0550	− .0470
40	$\bar{1}.9824$	$\bar{1}.7619$	.0530	− .0465
		$m_1 + m_2 + 3$	$\beta_{21} = -0.005$	
0	0.1620	$\bar{1}.7319$	0.0690	−0.0595
5	.1544	$\bar{1}.7396$	.0680	− .0575
10	.1464	$\bar{1}.7451$	.0660	− .0545
15	.1377	$\bar{1}.7497$	.0650	− .0510
20	.1287	$\bar{1}.7526$	.0640	− .0485
25	.1192	$\bar{1}.7566$	.0630	− .0440

(1) H. S. Harned, *J. Phys. Chem.*, **63**, 1299 (1959).

(2) H. S. Harned and W. J. Hamer, *J. Am. Chem. Soc.*, **55**, 2194 (1933).

(3) H. S. Harned and A. B. Gancy, *ibid.*, **62**, 627 (1958).

(4) H. S. Harned and R. W. Ehlers, *ibid.*, **55**, 2179 (1933).

(5) H. S. Harned and B. B. Owen, "The Physical Chemistry of Electrolytic Solutions," 3rd Ed., Reinhold Publ. Corp., New York, N. Y., 1958, p. 716.

(6) H. A. C. MacKay, *Trans. Faraday Soc.*, **51**, 903 (1955). See also ref. 5, p. 628, 629.

(7) H. S. Harned and M. A. Cook, *J. Am. Chem. Soc.*, **59**, 1920 (1937). See also ref. 5, p. 727.

The method of evaluation of $\alpha_{21(0)}$ and β_{21} is shown in Fig. 1 in which $-\alpha_{21}$ is plotted against m_1. The solid graphs in the figure are straight lines with a slope of -0.006 which is taken to be the value of β_{21} at all temperatures. This result is quite consistent over the temperature range from 10 to 40°. On the other hand, the results at 0 and 5° are less consistent as shown by the dashed lines. This discrepancy may be due to experimental errors which are more likely to occur at these lower temperatures. However, the results at m_1 equals 1 and 1.5 agree closely with the assumed straight lines. Values of $\alpha_{21(0)}$, obtained from these graphs, are given in Table I.

It was shown in the earlier communication[1] that thermodynamics imposes two restrictions on the use of the quadratic equations 1 and 2. The first requirement is that at a given temperature $(\beta_{12} - \beta_{21})$ is not a function of the total molality m. Since in present instance β_{12} is zero, β_{21} must also be independent of m. Thermodynamics also requires that, at constant temperature, $(\alpha_{12(0)} + \alpha_{21(0)}) + 2m\beta_{21}$ must be constant.[8] In Table II, values of this latter quantity at 1, 2 and 3 total molalities are recorded. It is clear from the data in this table that the required constancy occurs at 1 and 2 total molalities over the entire temperature range. At 25°, a similar constancy occurs at 1, 2 and 3 total molalities. At temperatures from 20 to 0°, the results at 3 total molality indicate an increasing departure from constancy. Our calculations indicate that as the total concentration increases above $2m$, β_{21} increases and has a value of -0.005 at $3m$.

TABLE II

$(\alpha_{12(0)} + \alpha_{21(0)}) + 2m\beta_{21}$ AT 1, 2 AND 3 TOTAL MOLALITIES
$\beta_{21} = -0.006$

t	$m = 1$	$m = 2$	$m = 3$
0	−0.0190	−0.0200	−0.0265
5	− .0184	− .0190	− .0255
10	− .0176	− .0180	− .0245
15	− .0170	− .0170	− .0220
20	− .0164	− .0170	− .0205
25	− .0164	− .0164	− .0170
30	− .0166	− .0155	.....
35	− .0168	− .0160	.....
40	− .0180	− .0175	.....

The Excess Heat of Mixing.—The estimation of the excess heat of mixing, ΔH_M^E, will be restricted to the case where both electrolytic components are at the same concentration. Thus when $m_1 = m_2$

$$\Delta H_M^E = 2.303RT^2 m_1 m_2 \frac{d[(\alpha_{12(0)} + \alpha_{21(0)}) + 2\beta_{21}m_2]}{dT} \quad (3)$$

an equation derived in the earlier communication.[1] Values of $(\alpha_{12(0)} + \alpha_{21(0)})$ and $(\alpha_{12(0)} + \alpha_{21(0)} + 2\beta_{21}m_2)$ are given in Table III and graphs of the

(8) In the earlier contribution (Ref. 1) equations (16), (17) and (18) are in error. The term $2m\ d(\beta_{12} + \beta_{21})/dm$ should be $m\ d(\beta_{12} + \beta_{21})/dm$. As a result equation (18) should read $(\alpha_{12(0)} + \alpha_{21(0)}) + m(\beta_{12} + \beta_{21}) + \int_0^m (\beta_{12} + \beta_{21})\,dm$ = constant. This reduces to equation (18) if $(\beta_{12} + \beta_{21})$ is not a function of m. In the present case, since β_{12} is zero and thermodynamics requires the constancy of $(\beta_{12} - \beta_{21})$, β_{21} is not a function of m and $(\alpha_{12(0)} + \alpha_{21(0)}) + 2m\beta_{21}$ is independent of m. Table II in the previous contribution is correct.

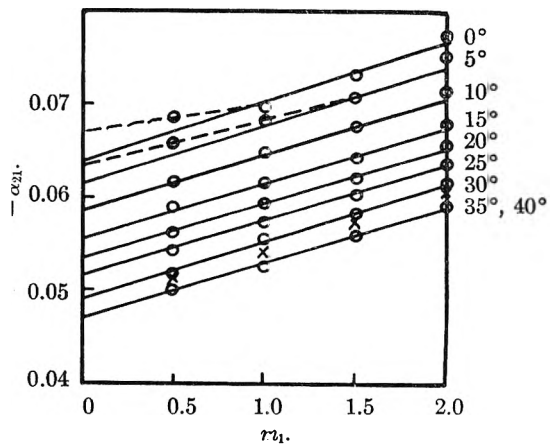

Fig. 1.—$-\alpha_{21}$ *versus* m_1.

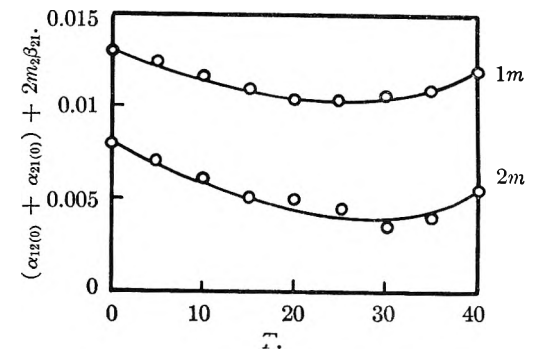

Fig. 2.—$(\alpha_{12(0)} + \alpha_{21(0)}) + 2m_2\beta_{21}$ *versus* T at 1 and 2 total concentrations.

latter quantity at 1 and 2 total molalities are shown in Fig. 2. The nature of these curves indicates that the excess heat of mixing will be positive below 25° and negative at the higher temperatures. At 1 m total molality, Young, Wu and Krawitz[8] obtain −3 cal. for the excess heat of mixing per mole of solute at 25°.

TABLE III

$(\alpha_{12(0)} + \alpha_{21(0)})$ AND $(\alpha_{12(0)} + \alpha_{21(0)}) + 2m_2\beta_{21}$ WHEN $m_1 = m_2$ AT 1 AND 2 m TOTAL MOLALITIES

	$m = 1$		$m = 2$	
t	$(\alpha_{12(0)} + \alpha_{21(0)})$	$(\alpha_{12(0)} + \alpha_{21(0)}) + 2\beta_{21}$	$(\alpha_{12(0)} + \alpha_{21(0)})$	$(\alpha_{12(0)} + \alpha_{21(0)}) + 2\beta_{21}$
0	−0.0070	−0.013(	+0.0040	−0.0080
5	− .0064	− .012(	.0050	− .0070
10	− .0056	− .011(	.0060	− .0060
15	− .0050	− .011(	.0070	− .0050
20	− .0044	− .010(	.0070	− .0050
25	− .0044	− .010(	.0076	− .0044
30	− .0046	− .0106	.0085	− .0035
35	− .0048	− .0108	.0080	− .0040
40	− .0060	− .0120	.0065	− .0055

Osmotic Coefficients.—The osmotic coefficients of mixtures ϕ and subsequently the activity a_w, of the third component, water, may be computed by the equations

$$\phi - \phi_{2(0)} = \frac{2.303m}{2}\left[(\alpha_{12(0)} - \alpha_{21(0)})\frac{m_1^2}{m^2} - 2\alpha_{21(0)}\frac{m_1}{m} + 2m(\beta_{12} - \beta_{21})\frac{m_1^2}{m^2} - \frac{4}{3}m(\beta_{12} - \beta_{21})\frac{m_1^3}{m^3}\right] \quad (4)$$

(8) T. F. Young, Y. C. Wu and A. A. Krawitz, *Trans. Faraday Soc.*, **24**, 37 (1958).

and

$$\phi - \phi_{1(0)} = \frac{2.303m}{2}\left[(\alpha_{21(0)} + \alpha_{12(0)})\frac{m_2^2}{m_1^2} - 2\alpha_{12}\frac{m_2}{m} + 2m(\beta_{21} - \beta_{12})\frac{m_2^2}{m^2} - \frac{4}{3}m(\beta_{21} - \beta_{12})\frac{m_2^3}{m^3}\right] \quad (5)$$

and

$$\ln a_w = -\frac{2m\phi}{55.51} \quad (6)$$

Values of the osmotic coefficients of the acid $\phi_{1(0)}$ and potassium chloride, $\phi_{2(0)}$, required for this calculation are given at suitable temperatures in Table IV.

TABLE IV

OSMOTIC COEFFICIENTS OF HYDROCHLORIC ACID, $\phi_{1(0)}$, AND POTASSIUM CHLORIDE, $\phi_{2(0)}$

m	0°	10°	20°	25°	30°	40°
1	1.055	1.049	1.043	1.040	1.036	1.030
2	1.216	1.206	1.197	1.189	1.183	1.170
3	1.394	1.374	1.357	1.348	...	...
			$\phi_{2(0)}$			
1	0.879	0.888	0.894	0.896	0.897	0.898
2	.880	.897	.908	.912	.914	.919
3	.910	.923	.933	.937	.939	.943

Summary

(1) By means of equations 1 and 2 and the data in Table I, the activity coefficients of hydrochloric acid and potassium chloride may be calculated precisely in their mixtures in water at 1, 2 and 3 total molalities and from 0 to 40°.

(2) By equations 4, 5 and 6, the osmotic coefficients and the activity of water in these mixtures may be computed.

(3) Our estimate of the excess heat of mixing per mole of solute is in reasonable agreement with the calorimetric data.

(4) The special value of the present contribution resides in indicating the behavior of the system over a wide range of concentration and of temperature.

This contribution was supported in part by The Atomic Energy Commission under Contract AT-(30–1)1375.

INTERACTIONS IN AQUEOUS SOLUTIONS. I. CALCULATION OF THE TURBIDITY OF SUCROSE SOLUTIONS AND CALIBRATION OF LIGHT SCATTERING PHOTOMETERS

BY D. STIGTER

Contribution from the Western Regional Research Laboratory,[1] 800 Buchanan Street, Albany 10, California

Received July 29, 1959

The thermodynamic part of the light scattering equation for two-component systems is connected with the osmotic coefficient and the solution density in a closed expression. Also the reciprocal turbidity is expanded in powers of the volume concentration of the solute. The coefficients in this expansion are given up to that of the fourth power of the concentration. Calculations for aqueous sucrose solutions at 25° are based on literature data on the osmotic coefficient and the solution density. The results are compared with turbidity data by Maron and Lou.[4] Data are tabulated for concentrations up to 0.7 g. of sucrose per cc. of solution.

Introduction

Recently Hill[2] has given a treatment of two-component solutions in which various thermodynamic functions are expanded in powers of the weight concentration of the solute. The results have been applied to the light scattering of two-component systems.[3] In the following, this light scattering expansion is extended by deriving the coefficients of the next three higher powers of the volume concentration of the solute. The resulting expression is used to evaluate the turbidity of aqueous sucrose solutions at 25°. In order to investigate the convergence of the expansion, the turbidity is derived also from a closed expression. In both cases the relevant thermodynamic information is obtained from literature data on the osmotic coefficient and on the density of sucrose solutions. The object is to provide data for the (absolute) turbidity of sucrose solutions over a large concentration range which may be utilized for the calibration of light scattering photometers.

Maron and Lou[4] have calculated the turbidity of sucrose solutions with the help of osmotic pressure data. Their results have been used by Princen and Mysels[5] for calibration purposes. However, Hill[3] has shown that the thermodynamic information obtained from osmotic pressure is not identical with that involved in light scattering. This invalidates the exactness of Maron and Lou's procedure.

Theoretical

The general light scattering equation[6–8] specialized for two-component systems may be written as

$$\tau = \frac{32\pi^3 kT}{3\lambda^4}\frac{m_2\nu^2(\partial\nu/\partial m_2)^2_{p,T}}{\rho_2(\partial\mu_2/\partial m_2)_{p,T}} \quad (1)$$

τ is the turbidity due to concentration fluctuations for isotropic particles small compared with the

(1) A laboratory of the Western Utilization Research and Development Division, Agricultural Research Service, U. S. Department of Agriculture.

(2) T. L. Hill, *J. Am. Chem. Soc.*, **79**, 4885 (1957).

(3) T. L. Hill, *J. Chem. Phys.*, **30**, 93 (1959).

(4) S. H. Maron and R. L. H. Lou, *J. Phys. Chem.*, **59**, 231 (1955).

(5) L. H. Princen and K. J. Mysels, Office of Naval Research, Contract Nonr-274(00). Project NR 356-254, 11th Technical Report, Sept. 1958. L. H. Princen, Thesis, Utrecht, 1959.

(6) H. C. Brinkman and J. J. Hermans, *J. Chem. Phys.*, **17**, 574 (1949).

(7) J. G. Kirkwood and R. J. Goldberg, *ibid.*, **18**, 54 (1950).

(8) W. H. Stockmayer, *ibid.*, **18**, 58 (1950).

wave length of light λ; ν is the refractive index of the solution; μ_2 is the chemical potential of the solute per molecule; m_2 is the solute concentration in moles per mole of solvent; ρ_2 is the solute concentration in number of molecules per unit volume of solution.

Hill[2,3] introduces a set of expansions which is thermodynamically self-consistent.

$$\frac{\mu_2(p,T,m_2)}{kT} = \frac{\mu_2^0(p,T)}{kT} + \ln m_2 + \sum_{n\geq 2} \frac{n}{n-1} C_n(p,T) m_2^{n-1} \quad (2)$$

$$\frac{m_2}{\rho_2} = v_1 + m_2\bar{v}_2^0 + kT \sum_{n\geq 2} \frac{1}{n-1} \left(\frac{\partial C_n}{\partial p}\right)_T m_2^n \quad (3)$$

v_1 is the molecular volume of the solvent; $\bar{v}_2^0$ is the partial molecular volume of the solute at infinite dilution. The chemical potential of the solvent[2] may also be expressed in terms of the coefficients $C_n(p,T)$

$$\frac{\mu_1(p,T,m_2)}{kT} = \frac{\mu_1^0(p,T)}{kT} - m_2 - \sum_{n\geq 2} C_n(p,T) m_2^n \quad (4)$$

At present it is convenient to connect the C_n's with the (practical) osmotic coefficient[9] of the solvent which is defined by

$$\phi(p,T,m_2) = \frac{1}{m_2}\left[\frac{\mu_1^0(p,T)}{kT} - \frac{\mu_1(p,T,m_2)}{kT}\right] \quad (5)$$

The comparison of eq. 4 and 5 yields

$$\phi(p,T,m_2) = 1 + \sum_{n\geq 2} C_n(p,T) m_2^{n-1} \quad (6)$$

With eq. 2 and 6 and observing that

$$\left(\frac{\partial \nu}{\partial m_2}\right)_{p,T} = \left(\frac{\partial \nu}{\partial \rho_2}\right)_{p,T}\left(\frac{\partial \rho_2}{\partial m_2}\right)_{p,T} \quad (7)$$

eq. 1 is converted into

$$\frac{32\pi^3}{3\lambda^4}\nu^2\left(\frac{\partial \nu}{\partial \rho_2}\right)^2_{p,T}\frac{\rho_2}{\tau} = \frac{\rho_2^2}{m_2^2}\frac{\Phi + m_2(\partial\phi/\partial m_2)_{p,T}}{(\partial\rho_2/\partial m_2)^2_{p,T}} \quad (8)$$

Information on the solution density suffices to connect ρ_2 and m_2 and obtain $(\partial\rho_2/\partial m_2)_{p,T}$. Thus the right-hand side of eq. 8, containing the thermodynamic quantities involved in light scattering, can be evaluated from the osmotic coefficient and the solution density.

An alternative expression is obtained when the right-hand side of eq. 8 is expanded in powers of the concentration with the help of eq. 3 and 6. Using the dimensionless volume concentration $\rho_2 v_1$ (the number of moles of solute, ρ_2/N_0, per volume $N_0 v_1$ of solution), eq. 8 becomes

$$\frac{32\pi^3}{3\lambda^4}\nu^2\left(\frac{\partial \nu}{\partial \rho_2}\right)^2_{p,T}\frac{\rho_2}{\tau} = \sum_{n\geq 1} T_n(\rho_2 v_1)^{n-1} \quad (9)$$

$T_1 = 1$; $T_2 = 2C_2 + 2(\bar{v}_2^0/v_1)$;

$T_3 = 3C_3 + 6C_2(\bar{v}_2^0/v_1) + 3(\bar{v}_2^0/v_1)^2 + (4kT/v_1)(\partial C_2/\partial p)_T$;

$T_4 = 4C_4 + 12C_3(\bar{v}_2^0/v_1) + 12C_2(\bar{v}_2^0/v_1)^2 + 4(\bar{v}_2^0/v_1)^3 + (3kT/v_1)(\partial C_3/\partial p)_T + 10C_2(kT/v_1)(\partial C_2/\partial p)_T + 15(\bar{v}_2^0/v_1)(kT/v_1)(\partial C_2/\partial p)_T$;

$T_5 = 5C_5 + 20C_4(\bar{v}_2^0/v_1) + 30C_3(\bar{v}_2^0/v_1)^2 + 20C_2(\bar{v}_2^0/v_1)^3 + 5(\bar{v}_2^0/v_1)^4 + (8kT/v_1)(\partial C_4/\partial p)_T + 7C_2(kT/v_1) \times (\partial C_3/\partial p)_T + 15(\bar{v}_2^0/v_1)(kT/v_1)(\partial C_3/\partial p)_T + 18C_3(kT/v_1)(\partial C_2/\partial p)_T + 50C_2(\bar{v}_2^0/v_1)(kT/v_1)(\partial C_2/\partial p)_T + 16(kT/v_1)^2(\partial C_2/\partial p)^2_T + 40(\bar{v}_2^0/v_1)^2(kT/v_1)(\partial C_2/\partial p)_T$

(9) H. S. Harned and B. B. Owen, "The Physical Chemistry of Electrolytic Solutions," Reinhold Publ. Corp., New York, N. Y., 1943, p. 12.

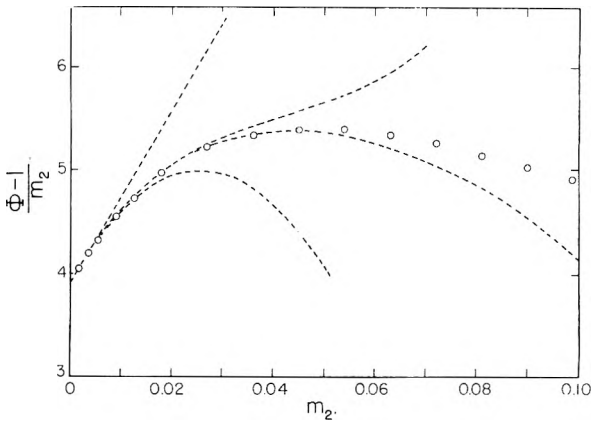

Fig. 1.—Osmotic coefficient of aqueous sucrose solutions at 25°: open circles, ref. 9; dashed curves, eq. 13 with successive terms.

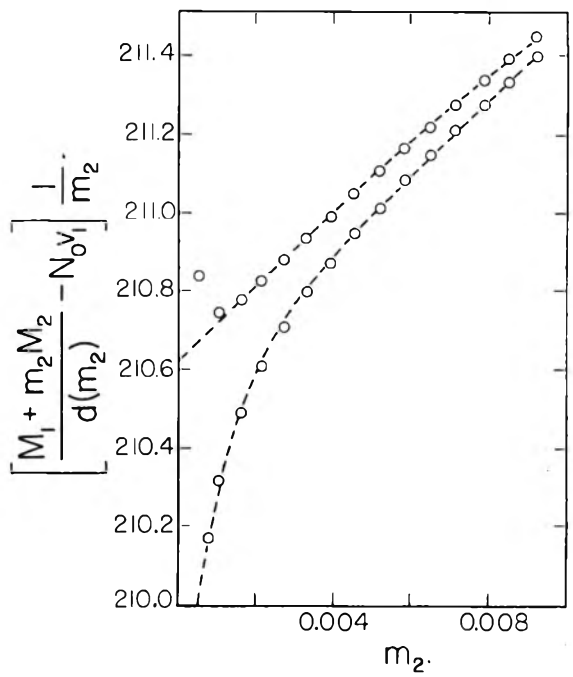

Fig. 2.—Test of data on density[10] of aqueous sucrose solutions at 20° with eq. 12: lower curve, density of water from ref. 10; upper curve, density of water adjusted.

The coefficients C_n occurring in the T_n's may be obtained from the osmotic coefficient by means of eq. 6. The quantities v_1, $\bar{v}_2^0$ and $(\partial C_n/\partial p)_T$ are connected with the solution density by the following reasoning.

A unit volume of solution contains ρ_2 solute molecules and $\rho_1 = \rho_2/m_2$ solvent molecules, or $\rho_2 M_2/N_0$ grams of solute and $\rho_2 M_1/m_2 N_0$ grams of solvent. M_2/N_0 and M_1/N_0 are the weights of a solute and a solvent molecule, respectively, measured in grams. Hence the solution density, expressed in grams per unit volume, is

$$d(p,T,m_2) = \rho_2 M_2/N_0 + \rho_2 M_1/m_2 N_0 \quad (10)$$

This gives on rearrangement

$$N_0 m_2/\rho_2 = (M_1 + m_2 M_2)/d(p,T,m_2) \quad (11)$$

and comparison with eq. 3 shows that

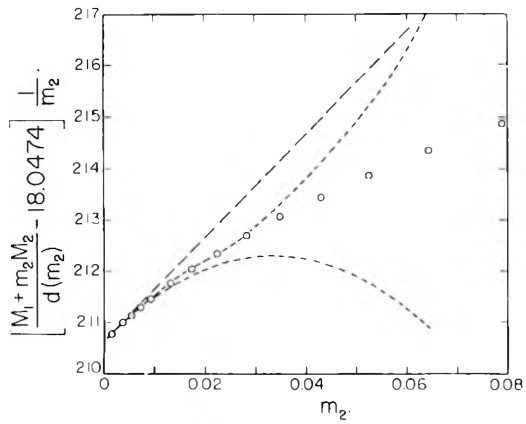

Fig. 3.—Test of data on density of aqueous sucrose solutions at 20° with eq. 14: open circles, ref. 10 with adjusted density of water; dashed curves, eq. 14 with successive terms.

$$\frac{M_1 + m_2M_2}{d(p,T,m_2)} = N_0v_1 + N_0\bar{v}_2{}^0m_2 + RT \sum_{n\geq 2} \frac{1}{n-1}\left(\frac{\partial C_n}{\partial p}\right)_T m_2{}^n \quad (12)$$

Light Scattering of Sucrose Solutions

Values of the osmotic coefficient of aqueous sucrose solutions at 25° and 1 atm. pressure were taken from a table by Harned and Owen (ref. 9, p. 289). In Fig. 1 $(\phi - 1)/m_2$ is plotted *versus* m_2. Extrapolation to $m_2 = 0$ gives $C_2 = 3.92$. Further deviation plots give successive coefficients C_n and the series 6 for ϕ becomes, at 1 atm. and 25°,

$$\phi = 1 + 3.92m_2 + 83.8m_2{}^2 - 1620m_2{}^3 + 12800m_2{}^4 \ldots \quad (13)$$

The dashed curves in Fig. 1 take into account successive terms of this expansion.

Extensive tables of the density of aqueous sucrose solutions at 20° and 1 atm. pressure are available in the literature.[10] The molar volume $N_0v_1(p,T)$ in expansion 12 is equal to $M_1/d(p,T,0)$, where $d(p,T,0)$ is the density of the pure solvent. In Fig. 2 the function $[\{(M_1 + m_2M_2)/d(m_2)\} - N_0v_1]/m_2$ is plotted *versus* m_2 for aqueous sucrose solutions at 20° and 1 atm. The lower curve is based on the recorded[10] density of water $d = 0.998234$ at 20° which gives $N_0v_1 = 18.04787$ cc./mole. Following eq. 12 the curve extrapolates to $N_0\bar{v}_2{}^0$ for $m_2 = 0$. The strong initial curvature is unexpected and may show that the density of water, employed in the computation, is inconsistent with the remaining density data. Linear extrapolation becomes possible when the value for the density of water is increased slightly. The upper curve in Fig. 2 has been computed with $d = 0.998262$ for the density of water at 20°. Using this value three coefficients $(RT/n-1)(\partial C_n/\partial p)_T$ in expansion 12 were evaluated from successive deviation plots. The result is, at 1 atm. and 20°

$$(M_1 + m_2M_2)/d(m_2) = 18.0474\,(1 + 11.670m_2 + 5.60m_2{}^2 - 83m_2{}^3 + 1330m_2{}^4 \ldots) \quad (14)$$

In Fig. 3 the function $[\{(M_1+m_2M_2)/d(m_2)\} - 18.0474]/m_2$ is compared with the expansion. The dashed curves take into account successive terms of the series.

The coefficients in series 12 are expected to be temperature-dependent. The density of aqueous sucrose solutions at 25° is 0.1% to 0.2% lower than at 20° (ref. 10, p. 648). At present, the density data at 20° will be used without corrections in the right-hand side of eq. 8 and 9. The resulting error, when the results are used at 25°, is expected to be of the order of 0.1%.

We are now in a position to evaluate the coefficients in eq. 9 up to T_5 by means of the information in eq. 13, 14, 6 and 12.

For computational purposes the refractive index of the solution for p and T constant is expanded in powers of the concentration

$$\nu = \nu_1 + a_1(\rho_2v_1) + a_2(\rho_2v_1)^2 + \ldots \quad (15)$$

The result for eq. 9 is

$$H^*\frac{\rho_2v_1}{\tau} = 1 + 31.18(\rho_2v_1) + 957(\rho_2v_1)^2 + 18800(\rho_2v_1)^3 + 272000(\rho_2v_1)^4 + \ldots \quad (16)$$

and eq. 8 becomes

$$H^*\frac{\rho_2v_1}{\tau} = \frac{\rho_2{}^2}{m_2{}^2}\frac{\phi + n_2\,(\partial\phi/\partial m_2)_{p,T}}{(\partial\rho_2/\partial m_2)^2{}_{p,T}} \quad (17)$$

with

$$H^* = HS = \frac{32\pi^3}{3\lambda^4}v_1\left[\frac{\partial\nu}{\partial(\rho_2v_1)}\right]^2_{p,T} \quad (18)$$

The concentration independent part of H^* is

$$H = \frac{32\pi^3}{3\lambda^4}v_1\nu_1{}^2a_1{}^2 \quad (19)$$

Expansion 15 yields

$$S = \left[1 + \frac{a_1}{\nu_1}(\rho_2v_1) + \frac{a_2}{\nu_1}(\rho_2v_1)^2 + \ldots\right]^2 \times \left[1 + 2\frac{a_2}{a_1}(\rho_2v_1)\ldots\right]^2 \quad (20)$$

Inserting the constants and the refractive index data reported by Maron and Lou,[4] eq. 18 becomes for $\lambda = 4358$ Å.

$$H^* = 0.03714[1 + 2.054(\rho_2v_1) - 0.71(\rho_2v_1)^2\ldots]^2 \times [1 - 0.69(\rho_2v_1)\ldots]^2 \quad (21)$$

and for $\lambda = 5461$ Å.

$$H^* = 0.01449[1 + 2.032(\rho_2v_1) - 0.67(\rho_2v_1)^2\ldots]^2 \times [1 - 0.66(\rho_2v_1)\ldots] \quad (22)$$

Equations 21 and 22 are used to evaluate $H^*\rho_2v_1/\tau$ for the turbidity data of Maron and Lou.[4] The recorded turbidity data are corrected for depolarization effects according to the data and the procedure employed by Maron and Lou.[4] In Fig. 4 the results are compared with curves derived from the right-hand side of eq. 16 and 17. In eq. 17 ϕ and $(\partial\phi/\partial m_2)_{p,T}$ were obtained by interpolation from the reported[9] data for ϕ and a table of $\Delta\phi/\Delta m_2$ derived from these data. The factors m_2/ρ_2 and $(\partial m_2/\partial\rho_2)_{p,T}$ in eq. 17 were evaluated from the concentration table for sucrose solutions at 20° (ref. 10, p. 632) and from the relevant values of $\Delta\rho_2/\Delta m_2$. For not too high concentrations, we have also employed the rapidly converging series derived from eq. 3

$$\frac{m_2}{\rho_2}\left(\frac{\partial\rho_2}{\partial m_2}\right)_{p,T} = \frac{\rho_2v_1}{m_2}\left[1 - \frac{kT}{v_1}\sum_{n\geq 2}\left(\frac{\partial C_n}{\partial p}\right)_T m_2{}^n\right] \quad (23)$$

(10) F. J. Bates, *et al.*, "Polarimetry, Saccharimetry and the Sugars," Circular C440 of the Natl. Bur. of Standards, U. S. Govt. Printing Office, Washington, 1942, p. 626.

In view of eq. 12 and 14 the series in brackets in eq. 23 is

$$1 - 5.60m_2^2 + 166m_2^3 - 3990m_2^4 \ldots \quad (24)$$

Figure 4 shows that at least one more term in series 16 would be required to cover the concentration range under study. For concentrations smaller than $\rho_2 v_1 = 0.02$ the results obtained from eq. 16 and 17 differ by no more than the computational error of about 0.1% which corresponds with the accuracy of the data on ϕ (ref. 9, p. 289).

The experimental points at the highest concentration are, respectively, 9.2 and 14.5% higher than the theoretical value from eq. 17 (solid curve). For the remaining points the per cent. difference with the solid curve is plotted in Fig. 5. The average differences are −1.7% and 2.9% for λ = 4368 and 5461 Å., respectively, indicated by the dashed lines in Fig. 5. The average deviations of the points from these lines are 1.0% and 1.8%, respectively.

Discussion

The statistical thermodynamical part of the light scattering theory must be considered straightforward and exact. Accepting the data on the osmotic coefficient and solution density, the values of $H^*\rho_2 v_1/\tau$ calculated with eq. 17—and with eq. 16 at sufficiently low sucrose concentrations—are accurate to about 0.1%. The discrepancies in Figs. 4 and 5, therefore, must be due to errors in the optical data. It seems likely that inaccurate calibration of the light scattering photometer and errors in the depolarization correction cause the systematic errors[11] of −1.7% for λ = 4368 Å. and 2.9% for λ = 5461 Å.

It is noted in Fig. 4 that at a few concentrations there is some correlation between the random errors at both wave lengths. This may indicate significant errors in the concentration determinations.

It should be mentioned that various approximations of the factor $\nu^2(\partial\nu/\partial\rho_2)^2_{p,T}$ of the light scattering equation are encountered in the literature.[4,12] For the present data on sucrose the concentration-dependent part of $\nu^2(\partial\nu/\partial\rho_2)^2_{p,T}$, the series S in eq. 20, changes for both wave lengths about 6% in the concentration range under study. This change is (nearly) proportional with the sucrose concentration. Hence a change in the refractive index factor, for instance the omission of S in eq. 18 for H^*, would add a significant trend to the points in Fig. 5.

No explanation is given for the very large discrepancy at the highest sucrose concentration in Fig. 4. More experiments on sucrose solutions are desirable. In particular the correction for depolarization requires further attention.

As an aid in the calibration of light scattering photometers, some data are listed in Table I. The volume concentrations have been converted with the help of the data at 25° (ref. 10, p. 626 and 648). $H^*\rho_2 v_1/\tau$ has been evaluated by means of eq. 16 and 17.

We now discuss some light scattering equations which frequently are employed in the literature.

(11) W. Kraut and W. B. Dandliker, *J. Polymer Sci.*, **18**, 563 (1955).
(12) See, *e.g.*, G. Oster, *Chem. Revs.*, **43**, 323, 354 (1948).

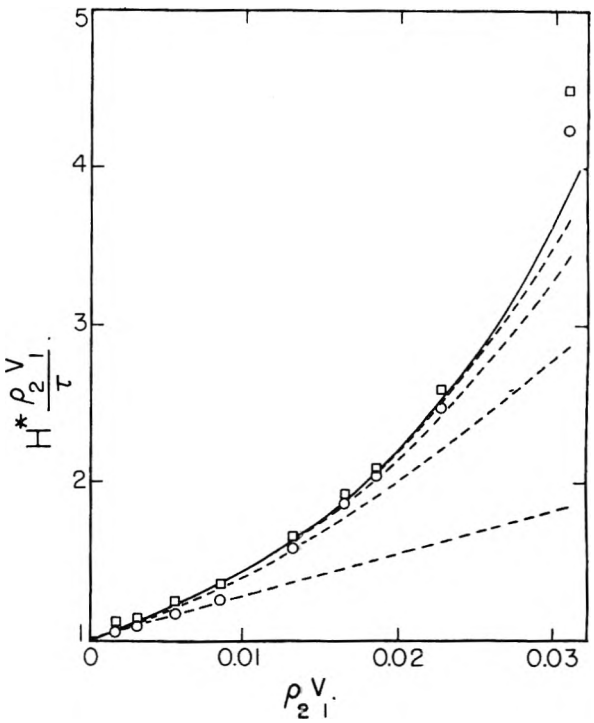

Fig. 4.—Light scattering by aqueous sucrose solutions at 25°: full curve, eq. 17; dashed curves, eq. 16 with successive terms; □, 4358 Å., Maron and Lou[4]; ○, 5461 Å., Maron and Lou.[4]

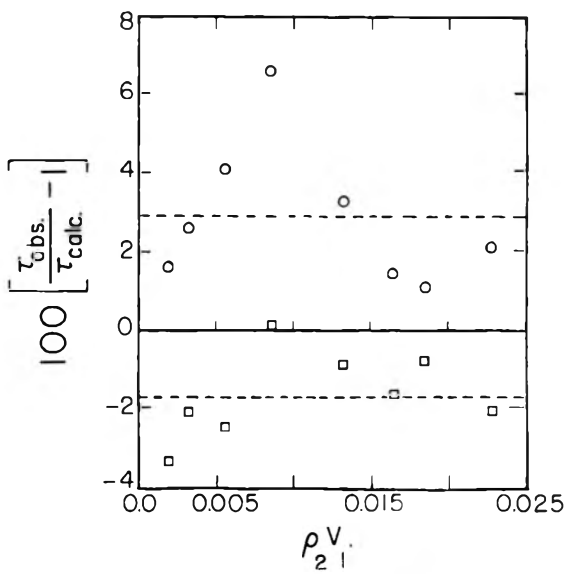

Fig. 5.—Equation 17 compared with data by Maron and Lou[4]: □, 4358 Å.; ○, 5461 Å.

Following Debye[13] the turbidity of a solution can be connected with the osmotic pressure. Hill[3] has given an exact treatment of this connection. A few remarks may be added here. Hill[2] introduces the osmotic pressure in the expansion

$$\frac{1}{kT}\int_{p-\pi}^{p} v_1(p',T)\mathrm{d}p' = m_2 + \sum_{n\geq 2} C_n(p,T)m_2^n \quad (25)$$

If the pure solvent is incompressible this eq. becomes[2]

(13) P. Debye, *J. Appl. Phys.*, **15**, 338 (1944).

TABLE I

LIGHT SCATTERING DATA FOR AQUEOUS SUCROSE SOLUTIONS AT 25° FROM EQ. 17

Sucrose concn. G./cc. soln.	Sucrose concn. G./g. water	$\rho_2 v_1$	$\frac{H^* \rho_2 v_1}{\tau}$
0.05	0.05176	0.002640	1.090
.10	.10690	.005279	1.194
.15	.16583	.007919	1.317
.20	.2290	.010558	1.462
.25	.2968	.013198	1.634
.30	.3698	.015837	1.832
.35	.4488	.018477	2.064
.40	.5344	.021116	2.335
.45	.6276	.02376	2.652
.50	.7293	.02640	3.031
.55	.8410	.02903	3.48
.60	.9641	.03167	4.01
.65	1.1006	.03431	4.64
.70	1.2530	.03695	5.40

$$\left(\frac{\pi v_1}{kT}\right)_{p,T} = m_2 + \sum_{n\geq 2} C_n(p,T) m_2^n \qquad (26)$$

In view of eq. 2 and 26, eq. 1 can be converted into

$$\frac{32\pi^3 kT}{3\lambda^4}\nu^2\left(\frac{\partial \nu}{\partial \rho_2}\right)^2 \frac{\rho_2}{\tau} = \left(\frac{\partial \pi}{\partial \rho_2}\right)_{p,T} \frac{\rho_2^2 v_1}{m_2^2} \Big/ \left(\frac{\partial \rho_2}{\partial m_2}\right)_{p,T} \qquad (27)$$

It is noted that: (1) eq. 27 is exact only when the solvent is incompressible. Application to aqueous solutions introduces only a negligible error on this account; (2) the concentration factor $(\rho_2^2 v_1/m_2^2)/(\partial\rho_2/\partial m_2)_{p,T}$ in eq. 27 usually is omitted. Following eq. 23 and eq. 3 this omission is justified when the partial volume of the solute is essentially independent of the concentration; (3) the main difficulty in eq. 27 is that the osmotic pressure (as it appears in eq. 25) should be measured at a constant pressure of the solution. It is customary, however, to measure π at constant pressure, $p-\pi$, of the solvent and approximate in eq. 27

$$\frac{1}{kT}\left(\frac{\partial \pi}{\partial \rho_2}\right)_{p,T} \approx \frac{1}{kT}\left(\frac{\partial \pi}{\partial \rho_2}\right)_{p-\pi,T} = 1 + \sum_{n\geq 2} n B_n(p-\pi,T)\rho_2^{n-1} \qquad (28)$$

where the B_n's are the osmotic pressure virial coefficients. The comparison with Hill's expressions[3] shows that eq. 28 is correct if the dependence of the B_n's on the pressure is negligible and if there is no solute solvent interaction except for a volume effect of the solute. Presumably B_n depends on pressure sensibly only through the compressibility which renders the relevant changes of the B_n's negligible. However, solute–solvent interaction like solvation or hydrogen bonding may introduce (in B_2) terms of the order of the molecular volume of the solute. Such terms are comparable with B_2 in the case of uncharged particles[14] but probably insignificant when dealing, *e.g.*, with highly charged protein molecules.

Another light scattering equation encountered in the literature may be written as

$$\frac{32\pi^3}{3\lambda^4}\nu^2\left(\frac{\partial \nu}{\partial \rho_2}\right)^2 \frac{\rho_2}{\tau} = \rho_2\left(\frac{\partial \mu_2/kT}{\partial \rho_2}\right)_{p,T} \qquad (29)$$

With eq. 2 and 3, one may expand the right-hand side of this equation

$$\rho_2\left(\frac{\partial \mu_2/kT}{\partial \rho_2}\right)_{p,T} = 1 + \left(2c_2 + \frac{\bar{v}_2^0}{v_1}\right)\rho_2 v_1 \ldots \qquad (30)$$

The comparison with eq. 9 shows a difference of $\bar{v}_2^0/v_1$, with T_2. Again, for uncharged particles this may be of the order of magnitude of T_2 while for highly charged colloids the difference between eq. 29 and eq. 1 is insignificant.

Acknowledgment.—It is a pleasure to thank Mr. Y. Tomimatsu for very useful discussions and for checking the derivations.

(14) D. Stigter, THIS JOURNAL, **64**, 118 (1960).

INTERACTIONS IN AQUEOUS SOLUTIONS. II. OSMOTIC PRESSURE AND OSMOTIC COEFFICIENT OF SUCROSE AND GLUCOSE SOLUTIONS

BY D. STIGTER

Contribution from the Western Regional Research Laboratory,[1] 800 Buchanan Street, Albany 10, California

Received July 29, 1959

The second and third osmotic pressure virial coefficients are discussed for spheres and ellipsoids with London–van der Waals attraction. Osmotic data on aqueous solutions of sucrose and glucose are interpreted in terms of virial coefficients. The results show definite attraction between sucrose–sucrose, sucrose–water and glucose–glucose molecules. It is concluded that London–van der Waals forces alone do not explain the data. It is probable that hydrogen bonding occurs.

Introduction

In recent years considerable advances have been made in establishing formal connections between thermodynamic properties of solutions and molecular properties on the basis of rigorous statistical mechanical considerations.[2–5] The application of these results to a real system requires the introduction of a (necessarily approximate) mathematical model of the system. In many cases the mathematical treatment of a physically adequate model is prohibitively difficult. The present paper deals with solutions of simple, uncharged molecules (two-component systems). An attempt is made to evaluate the intermolecular interaction on the basis of a simple model. In particular the interpretation of the osmotic pressure of the solution

(1) A laboratory of the Western Utilization Research and Development Division, Agricultural Research Service, U. S. Department of Agriculture.

(2) W. G. McMillan and J. E. Mayer, *J. Chem. Phys.*, **13**, 276 (1945).

(3) T. L. Hill, "Statistical Mechanics," McGraw-Hill Book Co., New York, N. Y., 1956, Ch. 6, 8.

(4) T. L. Hill, *J. Am. Chem. Soc.*, **79**, 4885 (1957).

(5) T. L. Hill, *J. Chem. Phys.*, **30**, 93 (1959).

and of the osmotic coefficient of the solvent is discussed.

Let us consider an osmotic system in which a solvent (component 1) is present on both sides of the membrane and a solute (component 2) on one side only. The solute concentration is ρ_2 molecules per unit volume of solution. The temperature T and the chemical potential of the solvent μ_1 are uniform throughout the system. The pressures in the solvent and in the solution compartment are p_0 and $p_0+\pi$, respectively.

The osmotic pressure π may be expanded in powers of the solute concentration ρ_2

$$\pi/kT = \rho_2 + B_2(p_0,T)\rho_2^2 + B_3(p_0,T)\rho_2^3 \ldots . \quad (1)$$

The linear term in this expansion represents van't Hoff's law, the higher terms account for the "non-ideality" of the solution. Following McMillan and Mayer,[2,3] the virial coefficients B_2, B_3...in eq. 1 depend on cluster integrals as in the virial expansion of the pressure of imperfect gases.

$B_2(p_0,T)$ is related to the potential of average force $W_{12}(p_0,T)$ between two solute molecules in positions $\mathbf{r}_1$ and $\mathbf{r}_2$, respectively, in the situation of infinite dilution (pure solvent)

$$B_2 = -\frac{1}{2V}\int_V\int_V (e^{-W_{12}/kT} - 1)\mathrm{d}\mathbf{r}_1\mathrm{d}\mathbf{r}_2 \quad (2)$$

where V is the volume of the system.

$B_3(p_0,T)$ is related to the interaction between three solute molecules, also for $\rho_2 = 0$. In cases where this interaction is pairwise additive, we have

$$B_3 = -\frac{1}{3V}\int_V\int_V\int_V (e^{-W_{12}/kT} - 1)(e^{-W_{23}/kT} - 1)(e^{-W_{13}/kT} - 1)\,\mathrm{d}\mathbf{r}_1\mathrm{d}\mathbf{r}_2\mathrm{d}\mathbf{r}_3 \quad (3)$$

In eq. 1 the volume concentration ρ_2 is employed. In the following an expansion of π in powers of the weight concentration, m_2 moles of solute per mole of solvent, will be required. ρ_2 in eq. 1 refers to the pressure $p_0 + \pi$ in the solution compartment. Firstly this quantity $\rho_2(m_2,p_0+\pi,T)$ is converted into $\rho_2(m_2,p_0,T)$ by means of the compressibility of the solution

$$\kappa(m_2,p,T) = -\left(\frac{\partial \ln V}{\partial p}\right)_{T,m_2} \quad (4)$$

Since ρ_2 is inversely proportional to the volume V of the solution

$$\kappa(m_2,p,T) = (\partial \ln \rho_2/\partial p)_{T,m_2} \quad (5)$$

Neglecting terms of order κ^2 and the pressure dependence of κ one obtains from eq. 5

$$\rho_2(p_0 + \pi) = (1 + \kappa\pi)\rho_2(p_0) \quad T \text{ constant} \quad (6)$$

and, using eq. 1 for π

$$\rho_2(p_0 + \pi) = \rho_2(p_0) + \kappa kT\rho_2^2(p_0) + \kappa kTB_2\rho_2^3(p_0) + \ldots \quad T \text{ constant} \quad (7)$$

The relation between $\rho_2(p_0)$ and m_2 is [4,5]

$$\rho_2(p_0) = m_2/v_1 - \bar{v}_2^0(m_2/v_1)^2 + \{\bar{v}_2^{\bar{2}0} - kTv_1(\partial C_2/\partial p)_T\}(m_2/v_1)^3 \ldots \quad T \text{ constant}, p_0 \quad (8)$$

v_1 is the molecular volume of the (pure) solvent at p_0,T and $\bar{v}_2^0$ is the partial molecular volume of the solute at $p_0,T,m_2 = 0$. With eq. 8 and 9, and the expansion

$$\kappa(m_2) = \kappa_0 + lm_2 + \ldots \quad T \text{ constant} \quad (9)$$

eq. 7 now becomes

$$\rho_2(p_0 + \pi) = m_2/v_1 + (\kappa_0 kT - \bar{v}_2^0)(m_2/v_1)^2 + \{\kappa_0 kTB_2 - 2\kappa_0 kT\bar{v}_2^0 + \bar{v}_2^{\bar{2}0} - kTv_1(\partial C_2/\partial p)_T + lv_1kT\}(m_2/v_1)^3 \ldots \quad T \text{ constant} \quad (10)$$

Substitution of eq. 10 into 1 yields the desired result

$$\pi/RT = m_2/N_0v_1 + A_2(m_2/N_0v_1)^2 + A_3(m_2/N_0v_1)^3 \ldots . \quad (11)$$

with

$$A_2 = N_0B_2 - N_0\bar{v}_2^0 + \kappa_0 RT$$

$$A_3 = N_0^2B_3 - 2N_0^2B_2\bar{v}_2^0 + N_0^2\bar{v}_2^{\bar{2}0} - RTN_0v_1(\partial C_2/\partial P)_T + 3N_0B_2\kappa_0 RT - 2\kappa_0 RTN_0\bar{v}_2^0 + lRTN_0v_1$$

N_0 is Avogadro's number; m_2/N_0v_1 is the solute concentration in moles per unit volume of solvent.

We now turn to the osmotic coefficient which measures the excess chemical potential of the solvent (at constant pressure and temperature) due to the presence of the solute.

An expression for the (practical) osmotic coefficient is[6]

$$\phi(p,T,m_2) = 1 + C_2(p,T)m_2 + C_3(p,T)m_2^2 + \ldots . \quad (12)$$

The connection between the coefficients in eq. 12 and 1 has been discussed by Hill,[5] who finds

$$2C_2(p,T)v_1 = 2B_2(p,T) - \bar{v}_2^0(p,T) + b_{11}(p,T) \quad (13)$$

and a more elaborate expression for C_3 which is not required here.

The term $b_{11}(p,T)$ in eq. 13 depends on the potential of average force $W_{12}'(p,T)$ between one solute molecule and one solvent molecule in positions $\mathbf{r}_1$ and $\mathbf{r}_2$, respectively, for $m_2 = 0$ (pure solvent)

$$b_{11} = \frac{1}{V}\int_V\int_V (e^{-W_{12}'/kT} - 1)\mathrm{d}\mathbf{r}_1,\mathrm{d}\mathbf{r}_2 \quad (14)$$

With eq. 11 B_2 and B_3 may be evaluated from osmotic pressure data since the remaining terms in A_2 and A_3 are easily obtained from density[6] and compressibility data. Then eq. 13 may be used to find b_{11}.

In summary it can be stated that in two component systems osmotic pressure data give information on solute–solute interaction, while additional data on the osmotic coefficient (or on light scattering[6]) also give information on solute–solvent interaction. It should be realized that experiments only give some kind of average of the potential functions W and W' through eq. 2, 3 and 14. It is obvious that a large number of potential functions can be constructed which fit the limited amount of experimental evidence. This number of functions, however, is reduced to a reasonable choice if the underlying model is to be acceptable from a physical point of view.

Review of Model Calculations

For the ideal case of no interaction between particles whose dimensions may be neglected W and W' vanish everywhere. Hence, according to eq. 2, 3 and 14, B_2, B_3 and b_{11} all equal zero. Also the higher virial coefficients vanish (compare ref. 3).

For solute spheres of volume v_2, large compared

(6) D. Stigter, THIS JOURNAL, **64**, 114 (1960).

with the size of the spherical solvent molecules, 2, 3 and 14 may be converted into[7]

$$B_2 = -12v_2 \int_0^\infty (e^{-W_x/kT} - 1)x^2 dx \quad (15)$$

$$B_3 = -96v_2^2 \int_0^\infty (e^{-W_x/kT} - 1)x dx \int_0^\infty (e^{-W_y/kT} - 1)y\, dy \int_{|x-y|}^{x+y} (e^{-W_z/kT} - 1)z\, dz \quad (16)$$

$$b_{11} = +24v_2 \int_0^\infty (e^{-W_x'/kT} - 1)x^2\, dx \quad (17)$$

where x, y and z are the distances between the centers of the relevant molecules expressed in units of the diameter of the solute sphere.

For rigid, non-interacting molecules the potentials of interaction are

$$W_x = \infty \quad \text{for } x \leq 1 \qquad = 0 \quad x > 1 \quad (18)$$

with analogous expressions for W_y and W_z. In addition, in eq. 17

$$W_x' = \infty \quad \text{for } x \leq \tfrac{1}{2}(1 + d_1/d_2) \qquad = 0 \quad x > \tfrac{1}{2}(1 + d_1/d_2) \quad (19)$$

d_1 and d_2 are the diameters of the solvent and the solute spheres, respectively. For potentials 18 and 19 the virial coefficients are (compare ref. 7)

$$B_2 = 4v_2,\ B_3 = 10v_2^2 \text{ and } b_{11} = -v_2(1 + d_1/d_2)^3 \quad (20)$$

In the theory of imperfect gases, Keesom[8,9] has introduced the model of rigid, attracting spherical molecules with an interaction potential of the general form

$$W_x = \infty \quad \text{for } x \leq 1 \qquad = -W_0/x^m \quad x > 1 \quad (21)$$

where W_0 is the (positive) value of the attraction potential between two spheres in contact. Deviations from ideal behavior of a number of monatomic gases are rather well explained by this potential with $m = 6$ (compare ref. 9, p. 291 ff.). Such interaction has also been discussed theoretically and is generally referred to as London–van der Waals interaction. It plays an important role in discussions of the stability of colloidal suspensions,[10] of properties of smaller molecules and crystal structure.[11] The knowledge of London–van der Waals forces, experimentally as well as theoretically, is far from satisfactory. For this reason it is interesting to investigate the Keesom model in connection with the present systems.

For the second virial coefficient,[8,9] one obtains from eq. 15 and 21, for $m>3$

$$B_2 = 4v_2 \left\{1 - 3 \sum_{\tau=1}^{\infty} \frac{1}{\tau!(\tau m - 3)} \left(\frac{W_0}{kT}\right)^\tau\right\} \quad (22)$$

Special values of m give

$$B_2 = 4v_2 \{1 - (3/2)W_0/kT - (3/14)(W_0/kT)^2 - (1/24)(W_0/kT)^3 \ldots\} \quad m = 5 \quad (23)$$

$$B_2 = 4v_2 \{1 - W_0/kT - (1/6)(W_0/kT)^2 - (1/30)(W_0/kT)^3 \ldots\} \quad m = 6 \quad (24)$$

To evaluate W_0 from B_2 the reverted series are convenient

$$W_0/kT = 0.6667(1 - B_2/4v_2) - 0.06349(1 - B_2/4v_2)^2 + 0.003863(1 - B_2/4v_2)^3 \ldots \quad m = 5 \quad (25)$$

$$W_0/kT = (1 - B_2/4v_2) - (1/6)(1 - B_2/4v_2)^2 + (1/45)(1 - B_2/4v_2)^3 \ldots \quad m = 6 \quad (26)$$

In treating the third virial coefficient the method of Hill[7] is employed and B_3 is expanded in powers of W_0/kT.

$$B_3 = R_0 + R_1(W_0/kT) + R_2(W_0/kT)^2 + R_3(W_0/kT)^3 + \ldots \quad (27)$$

The leading term in this expansion obviously represents the result for non-interacting hard spheres, quoted earlier, $R_0 = 10v_2^2$.[3] Inserting proper integration limits,[7] we obtain with eq. 16 and 21

$$R_1 = -288v_2^2 \int_1^2 \frac{dx}{x^{m-1}} \int_{x-1}^1 y\, dy \int_{x-y}^1 z\, dz \quad (28)$$

$$R_2 = -144v_2^2 \int_1^2 \frac{dx}{x^{2m-1}} \int_{x-1}^1 y\, dy \int_{x-y}^1 z\, dz + 576v_2^2 \int_1^\infty \frac{dx}{x^{m-1}} \int_x^{x+1} \frac{dy}{y^{m-1}} \int_{y-x}^1 z dz \quad (29)$$

$$R_3 = -48v_2^2 \int_1^2 \frac{dx}{x^{3m-1}} \int_{x-1}^1 y dy \int_{x-y}^1 z dz + 288v_2^2 \int_1^\infty \frac{dx}{x^{2m-1}} \int_x^{x+1} \frac{dy}{y^{m-1}} \int_{y-x}^1 z dz + 288v_2^2 \int_1^2 \frac{dx}{x^{2m-1}} \int_1^x \frac{dy}{y^{m-1}} \int_{x-y}^1 z dz + 288v_2^2 \int_2^\infty \frac{dx}{x^{2m-1}} \int_{x-1}^x \frac{dy}{y^{m-1}} \int_{x-y}^1 z dz - 192v_2^2 \int_1^\infty \frac{dx}{x^{m-1}} \int_x^{x+1} \frac{dy}{y^{m-1}} \int_1^{x+y} \frac{dz}{z^{m-1}} - 192v_2^2 \int_1^\infty \frac{dx}{x^{m-1}} \int_{x+1}^\infty \frac{dy}{y^{m-1}} \int_{y-x}^{x+y} \frac{dz}{z^{m-1}} \quad (30)$$

The integrations in eq. 28 and 29 were carried out for $m = 5$ and 6. The results are, respectively

$$B_3 = 10v_2^2[1 - 1.2000(W_0/kT) + 0.8088(W_0/kT)^2 + \ldots] \quad m = 5 \quad (31)$$

$$B_3 = 10v_2^2[1 - 1.0318(W_0/kT) + 0.4578(W_0/kT)^2 + \ldots] \quad m = 6 \quad (32)$$

The Keesom potential may be used also to treat solute–solvent interaction. Instead of eq. 19 we have

$$W_x' = \infty \quad \text{for } x \leq (1 + d_1/d_2)/2 \qquad = -W_0'(2x)^{-m}(1 + d_1/d_2)^m \text{ for } x > (1 + d_1/d_2)/2 \quad (33)$$

W_0' is the (positive) value of the attractive potential between a solute and a solvent sphere in contact. Inserting this potential in eq. 17 one obtains

$$b_{11} = -v_2(1 + d_1/d_2)^3 \left\{1 - 3 \sum_{\tau=1}^{\infty} \frac{1}{\tau!(\tau m - 3)} \left(\frac{W_0'}{kT}\right)^\tau\right\} \quad (34)$$

Comparison of this result with eq. 22 shows that in expansion 23–26 W_0' may be substituted for W_0 and $-b_{11}/(1 + d_1/d_2)^3$ for $B_2/4$.

Thus far we have discussed spherical molecules only. Calculations for non-spherical particles are

(7) Compare T. L. Hill, *Faraday Soc. Disc.*, **21**, 31 (1956).

(8) W. H. Keesom, *Comm. Phys. Lab. Leiden*, Suppl., **24B**, 32 (1912).

(9) R. H. Fowler and E. A. Guggenheim, "Statistical Thermodynamics," University Press, Cambridge, England, 1939, p. 289.

(10) E. J. W. Verwey and J. Th. G. Overbeek, "Theory of the Stability of Lyophobic Colloids," Elsevier Publ. Co., Amsterdam, 1948.

(11) See, *e.g.*, H. Mark and A. V. Tobolsky, "Physical Chemistry of High Polymer Systems," Interscience Publishers, Inc., New York, N. Y., 1950, Ch. IV and V.

more difficult. Isihara has evaluated the second virial coefficient for non-interacting, rigid ellipsoids[12] and for non-interacting, rigid, dumbbell-shaped particles.[13] His results may be written as

$$B_2 = f \times 4v_2 \qquad (35)$$

where again v_2 denotes the particle volume. The correction factor f equals unity for a sphere and increases when the particle becomes more asymmetrical.

In view of eq. 20 and 35 the third virial coefficient, for small departures from spherical shape, should be close to

$$B_3 = f^2 \times 10v_2^2 \qquad (36)$$

b_{11} is estimated for the ellipsoidal solute particle and a (much smaller) solvent sphere. The volume of an elongated rotation ellipsoid with long axis $2a$ and short axis $2b$ is $v_2 = (4\pi/3)ab^2$. When d_1 again denotes the diameter of the solvent sphere, eq. 14 yields approximately for rigid, non-interacting bodies (compare eq. 20)

$$b_{11} = -v_2(1 + d_1/2a)(1 + d_1/2b)^2 \qquad (37)$$

The next case is that of non-spherical *attracting* solute particles. To evaluate the attraction effects, the particles are replaced by spheres of the same volume, v_2, and, as before, a Keesom type of attraction potential is assumed. For particles which are not too asymmetrical, this substitution should lead to fair approximations for the interaction coefficients which may be obtained by appropriate conversions of eq. 22–26, 31, 32 and 34, by means of eq. 35–37. For example, in eq. 25 and 26, v_2 is replaced by fv_2, etc.

Derivation of Interaction Coefficients from Experimental Data

Extensive data have been reported on the osmotic pressure of aqueous sucrose and glucose solutions.[14–17] Some of the results are shown in Fig. 1–6. In Fig. 1 the quantity $\pi N_0 v_1/RTm_2$ is plotted *versus* $m_2/N_0 v_1$ for aqueous sucrose solutions at 25° as derived from Morse's data.[15] It is observed that the original data (unfilled points) do not extrapolate to unity for $m_2 = 0$ as required by eq. 11. Moreover, the apparent curvature at low concentrations is unexpected. This anomaly, already visible in the original presentation,[15] could not be explained satisfactorily by Morse. The anomaly disappears when the recorded osmotic pressures are reduced by a small, constant amount Δ (filled points). The data for sucrose at 30°, plotted in Fig. 2, show a similar trend, although less pronounced.

It appears that the experimental procedure[15] might well justify the present correction method. In the osmotic cells, porous clay membranes were employed in which copper ferrocyanide had been precipitated. In order to repair possible leaks in the (washed) membranes during an osmotic pressure run, 0.005 mole of $CuSO_4$ and 0.002 mole of $K_4[Fe(CN)_6]$ per kg. water was added to the solvent and the solution compartment, respectively (ref. 15, p. 86). Since the salt ions presumably did not pass through the membrane, it might be that an (osmotic) activity difference of the salt across the membrane contributed significantly to the recorded osmotic pressures. No results of blank runs were reported (compare ref. 15, p. 90). It is stated, however, that in the later experiments, presumably at the higher temperatures for sucrose and for the glucose runs (see below), the salt concentrations were reduced tenfold and other alterations were made (ref. 15, p. 88). This might explain the difference between the Δ value at 25° for sucrose and at 30°. Of course, the data might also be biased by calibration errors.

In addition to the correction Δ for π, we have

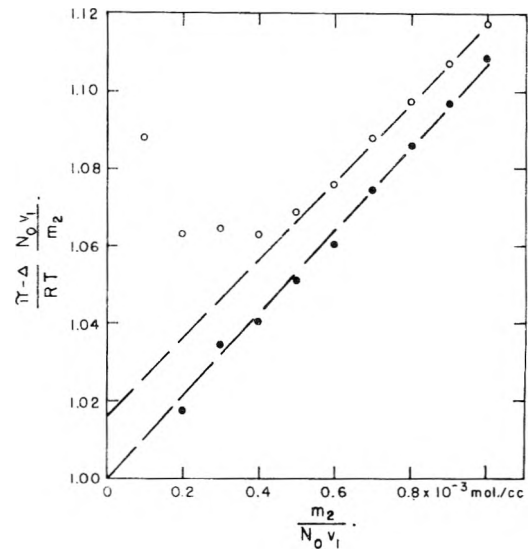

Fig. 1.—Osmotic pressure of aqueous sucrose solutions at 25° by Morse[15]: ○, uncorrected (Δ = 0); ●, corrected (Δ = 0.22 atm.)

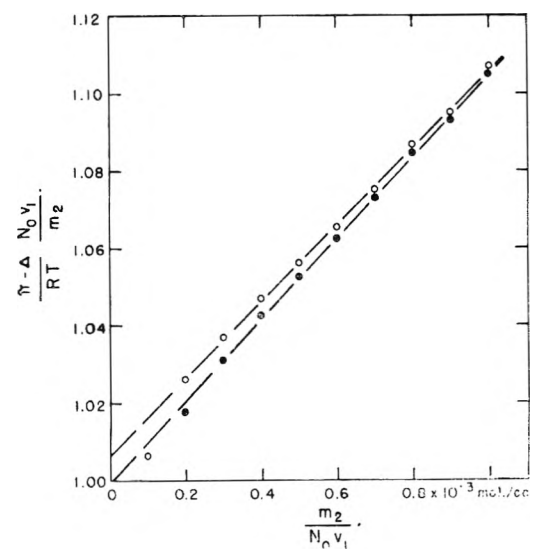

Fig. 2.—Osmotic pressure of aqueous sucrose solutions at 30° by Morse[15]: ○, uncorrected (Δ = 0); ●, corrected (Δ = 0.044 atm.).

(12) A. Isihara, *J. Chem. Phys.*, **18**, 1446 (1950).
(13) A. Isihara, *ibid.*, **19**, 397 (1951).
(14) Earl of Berkeley and E. G. J. Hartley, *Phil. Trans. Roy. Soc., (London)*, **A206**, 481 (1906).
(15) H. N. Morse, *Publ. Carnegie Inst. Washington*, No. 198 (1914).
(16) J. C. W. Frazer and R. T. Myrick, *J. Am. Chem. Soc.*, **38**, 1907 (1916).
(17) P. Lotz and J. C. W. Fraser, *ibid.*, **43**, 2501 (1921).

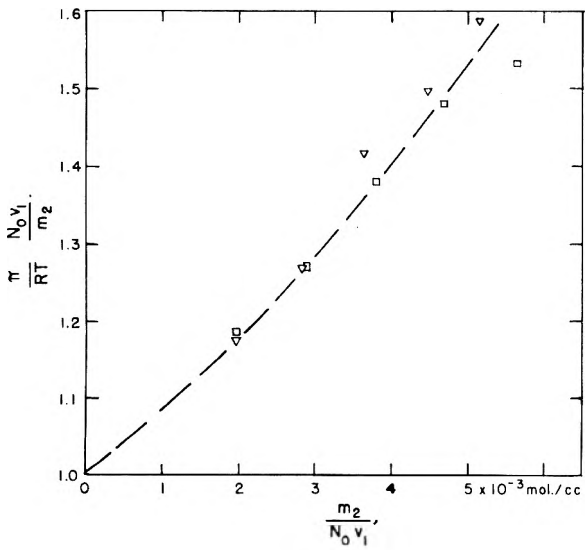

Fig. 3.—Osmotic pressure of aqueous sucrose solutions at 30°: □, Frazer and Myrick[16]; ▽, Lotz and Frazer.[17]

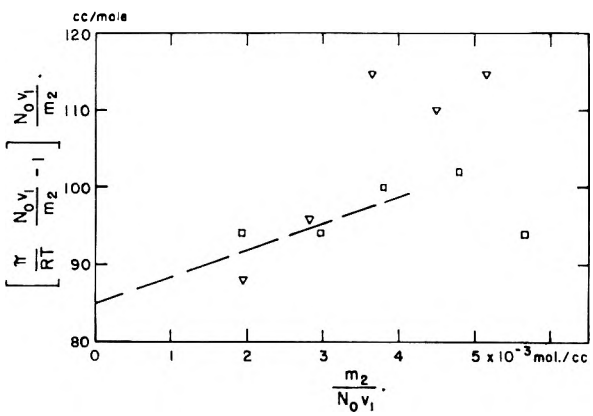

Fig. 4.—Osmotic pressure of aqueous sucrose solutions at 30°: □, Frazer and Myrick[16]; ▽, Lotz and Frazer.[17]

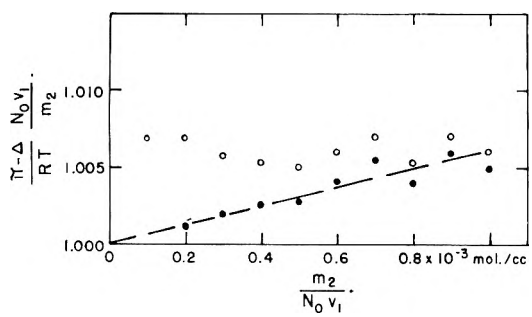

Fig. 5.—Osmotic pressure of aqueous glucose solutions at 30° by Morse[15]: ○, uncorrected (△ = 0); ●, corrected (Δ = 0.028 atm.).

recalculated the concentrations with oxygen = 16 as the molecular weight basis and used the value $R = 82.07$ cc. atm. per °C. per mole for the gas constant. The original molar concentrations were based on H = 1 and the value $R = 81.50$ (ref. 15, p. 116).

Figure 3 shows data on sucrose at 30° at higher concentrations, each point being the average of several measurements. Although the spread in the experimental points is considerable, a slight curvature is apparent. This is somewhat clearer

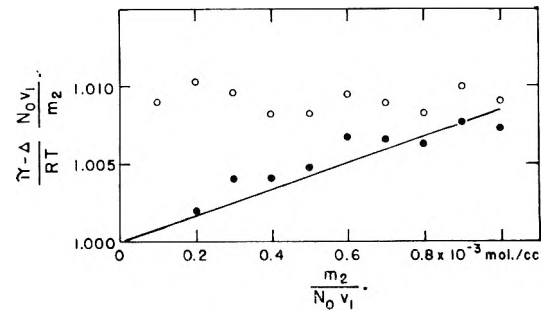

Fig. 6.—Osmotic pressure of aqueous glucose solutions at 40° by Morse[15]: ○, uncorrected (△ = 0); ●, corrected (Δ = 0.042 atm.).

from the (slope of the) deviation plot in Fig. 4. Figures 5 and 6 present data on glucose at 30 and 40°, respectively.

These values of A_2 and A_3 are estimated from the relevant figures.

Fig. 1 A_2 = 105 cc./mole for sucrose at 25°
Fig. 2 A_2 = 105 cc./mole for sucrose at 30°
Fig. 4 A_2 = 85 cc./mole for sucrose at 30°
A_3 = 4000 (cc./mole)² for sucrose at 30°
Fig. 5 A_2 = 6 cc./mole for glucose at 30°
Fig. 6 A_2 = 8 cc./mole for glucose at 40°

On the basis of these results, we assume for sucrose at 25° $A_2 = 95$ cc./mole and $A_3 = 4000$ (cc./mole)²; for glucose at 25° $A_2 = 5$ cc./mole. It is difficult to estimate the possible errors of these values. Fortunately, it will appear that a large error in A_2 or A_3 corresponds to a much smaller relative error in B_2 and B_3, respectively.

In Table I the various terms occurring in eq. 11 are listed. The values of $N_0\bar{v}_2^0$, N_0v_1, and $RTN_0v_1 \times (\partial C_2/\partial P)_T$ are taken from a previous paper.[6] Compressibility data[18] for aqueous sucrose solutions at 0 and 30° give at 25° approximately for eq. 9

$$\kappa = 4.6 \times 10^{-5} - 0.5 \times 10^{-3} m_2$$

TABLE I

CALCULATION OF B_2 AND B_3 FOR SUCROSE IN WATER AT 25°

A_2 = 95 cc./mole	A_3 = 4 × 10³ (cc./mole)²
$N_0\bar{v}_2^0$ = 211.0 cc./mole	$2N_0^2B_2\bar{v}_2^0$ = 128.7 × 10³ (cc./mole)²
$-\kappa_0 RT$ = −1.1 cc./mole	$-N_0^2\bar{v}_2^{02}$ = −44.5 × 10³ (cc./mole)²
N_0B_2 = 305 cc./mole	$RTN_0v_1\left(\frac{\partial C_2}{\partial p}\right)_T$ = 0.0 × 10³ (cc./mole)²
	$-3N_0B_2\kappa_0RT$ = −1.0 × 10⁰ (cc./mole)²
	$2\kappa_0RTN_0\bar{v}_2^0$ = 0.5 × 10³ (cc./mole)²
	$-lRTN_0v_1$ = 0.2 × 10³ (cc./mole)²
	$N_0^2B_3$ = 88 × 10³ (cc./mole)²

It is seen that the compressibility terms in Table I are insignificant as expected for aqueous solutions.

We now apply eq. 13 to calculate the coefficient of the sucrose–water interaction. From the osmotic coefficient it was found previously[6] $2C_2N_0v_1 = 141.7$ cc./mole for sucrose in water at 25°. Hence eq. 13 yields $N_0b_{11} = -257$ cc./mole.

For glucose the data on solution density[19] lead to $N_0\bar{v}_2^0 = 112.0$ cc./mole at 20°. At 25° we take $N_0\bar{v}_2^0 = 112$ cc./mole. Neglecting the compressibility term eq. 11 yields $N_0B_2 = 117$ cc./mole.

(18) Earl of Berkeley, E. G. J. Hartley and C. V. Burton, *Phil. Trans. Roy. Soc. (London)*, **A218**, 295 (1919).

(19) F. J. Bates, *et al.*, Polarimetry, Saccharimetry and the Sugars, Circular C 440 of the National Bureau of Standards, U. S. Government Printing Office, Washington 1942, p. 652.

Discussion

In choosing molecular models for sucrose and glucose recourse is taken to data on crystallographic parameters, on the partial molecular volume and on the rate of diffusion. A sucrose molecule may be represented approximately by an elongated rotation ellipsoid with axial ratio 2:1. A glucose molecule is roughly spherical.[20] Setting the molecular volume equal to $\bar{v}_2^0$ one may calculate the diffusion coefficient with the relation[21]

$$D = \frac{kT}{6\pi\eta a\sqrt{3}} \ln \frac{1 + 0.5\sqrt{3}}{1 - 0.5\sqrt{3}} \qquad (38)$$

for the sucrose molecule with long axis $2a = 2(3\bar{v}_2^0/\pi)^{1/3}$ and with

$$D = \frac{kT}{6\pi\eta a} \qquad (39)$$

for the glucose sphere with radius $a = (3\bar{v}_2^0/4\pi)^{1/3}$.

The results for diffusion in water at 25° obtained from eq. 38 and 39 with the values of $\bar{v}_2^0$ from the foregoing section are given in Table II and compared with experimental data.[22]

TABLE II

	$10^6 \times D$ cm.²/sec. from $\bar{v}_2^0$	exp.	Ratio
Sucrose	5.324	5.209	1.022
Glucose	6.864	6.728	1.020

The diffusion experiments were carried out at solute concentrations of about 0.8 wt. %, but it is stated that the concentration dependence of the rate of diffusion is very slight.[22] The explanation of the differences of about 2% in Table II is probably that the actual molecules are not exactly spheroidal and that the surface of the molecules is not smooth (as assumed in the calculations) but uneven with side groups projecting somewhat into the water. One might account for such a fine structure by raising the values of $\bar{v}_2^0$ some 6 or 7% in the evaluation of B_2 and B_3. However, we rather use the experimental data on $\bar{v}_2^0$ and consider the differences derived from Table II as a measure of the uncertainty of the results.

The experimental values of the various interaction coefficients derived in the preceding section are collected in Table III. Also shown are the results for rigid, non-interacting molecules calculated from eq. 35–37 with $f = 1$ for glucose and $f = 1.13$ for sucrose.[12] In the evaluation of N_0b_{11} the water molecules have been considered as spheres with diameter $d_1 = \sqrt[3]{6v_1/\pi}$.

In all cases a large discrepancy is noted which is far beyond any error in experiment or calculation. The differences indicate attractive interaction between sucrose–sucrose, sucrose–water and glucose–glucose molecules.

The differences between the experimental and the theoretical values in Table III are tested with the interaction potentials of eq. 21 and 33. The attractive potentials between two molecules in contact are presented in Table IV for two choices of the distance dependence of the potential. Furthermore, using the result for W_0 as obtained from N_0B_2, the third virial coefficient of sucrose is given for the model under study.

TABLE III

COMPARISON OF EXPERIMENTAL INTERACTION COEFFICIENTS WITH RESULTS FOR RIGID NON-INTERACTING MOLECULES

	Exp.	Theor.	
Sucrose N_0B_2	305	954	cc./mole
$N_0^2B_3$	88×10^3	568×10^3	(cc./mole)²
N_0b_{11}	−257	−655	cc./mole
Glucose N_0B_2	117	448	cc./mole

TABLE IV

INTERACTION POTENTIALS FOR KEESOM TYPE OF INTERACTION

Sucrose–sucrose		
W_0 from N_0B_2	$N_0^2B_3$ from W_0	
$0.43kT$	405×10^3 (cc./mole)²	$m = 5$
$0.61kT$	363×10^3 (cc./mole)²	$m = 6$
Glucose–glucose	Sucrose–water	
W_0 from N_0B_2	W_0' from N_0b_{11}	
$0.46kT$	$0.38kT$	$m = 5$
$0.66kT$	$0.55kT$	$m = 6$

It is interesting to compare the values of the interaction potential in the various cases. If the assumed type of interaction potential were correct one would expect that W_0 depends on the size of the interacting molecules. Thus the attraction between two glucose molecules in contact should be weaker than that between two sucrose molecules in contact. In addition, W_0' for the sucrose–water interaction should be considerably smaller. Finally, the values of $N_0^2B_3$ in Table IV are much larger than the experimental value 88×10^3 (cc./mole)² in Table I.

It seems that these inconsistencies cannot be removed by introducing refinements in the model such as the fine structure of the interacting molecules or the addition of a very short-range repulsive component to the Keesom potential to replace the rigid molecules (Lennard-Jones potential). It is likely that a major component of the attraction potential is short-range and localized such as in hydrogen bonding.

A very crude estimate of the effect of hydrogen bonding on the over-all interaction may be obtained as follows. The potential energy of hydrogen bonds is known to be of the order of $8kT$ at room temperature (4–5 kcal. per mole). Let us, therefore, assume that at the surface of the sucrose molecule is a square well potential of depth $W_1' = 8kT$ and width w (in three perpendicular directions) for trapping a water molecule. The relevant contribution to N_0b_{11} in eq. 14 would be

$$N_0 \int_0^w \int_0^w \int_0^w (e^{+8} - 1)dxdydz \text{ cc./mole}$$

A value of +398 cc./mole for this integral (see Table III) gives $w = 0.6$ Å.

When a hydrogen bond is formed between sucrose and water, one should also account for the cleavage of a hydrogen bond between two water molecules.[23] This will increase the value $w = 0.6$ Å. estimated above. Still, this length probably remains of the

(20) A. J. C. Wilson, ed., "Structure Reports II," Oosthoek, Utrecht, 1957, p. 624.

(21) R. Gans, *Sitz. Ber. Akad. München*, 191 (1911).

(22) L. G. Longsworth, *J. Am. Chem. Soc.*, **75**, 5705 (1953).

(23) Thanks are due to Professor Terrell L. Hill and to Dr. S. N. Timasheff for drawing attention to this point.

order of the amplitude of atomic vibrations and shows the difference in Table III may well be explained by the presence of a small number of hydrogen bonding sites at the surface of the sucrose molecule. The same holds for the interaction between glucose and between sucrose molecules.

Of course, any detailed (quantum mechanical) treatment of hydrogen bonding should account for the known structure and for the orientation of the interacting molecules. A useful first approximation might be a parabolic potential well (harmonic oscillator), the curvature being estimated from spectral data. Such a treatment is not undertaken at present.

In terms of the Keesom potential hydrogen bonding would correspond to a very steep attractive potential distance curve (apart from orientation effects). This means a large value of m, say, 12 or 20. It is noted in Table IV that a sufficiently large value of m would bring $N_0^2B_3$, as calculated from N_0B_2, in line with the low experimental value. This conclusion however, is only partly valid. The present computations of B_3, with the Keesom potential, are based on the assumption that the attractive forces (between three molecules) are additive. This is certainly not true for attraction originating from hydrogen bonding in which case pair interaction saturates the relevant bonding sites. This saturation effect should be taken into account and B_3 should be evaluated with a (quantum) statistical mechanical expression which is more general than eq. 3.

It is noted in passing also that the London–van der Waals dispersion forces ($m = 6$) are not strictly additive. As shown in recent discussions of the behavior of imperfect gases[24-27] slight deviations may occur for very small distances between the interacting molecules. This phenomenon is not expected to change the above arguments in a qualitative sense.

The values of the interaction potentials in Table IV should be considered as (estimates of) the upper limit of the London–van der Waals attraction between the relevant molecules in aqueous solutions. For a number of gases the comparison of the boiling temperature and the Lennard–Jones potential between pairs of molecules (see ref. 9, p. 285) reveals that, at not too low pressures, condensation occurs when the minimum of the pair interaction potential becomes of the order of $-{}^3/_2\ kT$. On this basis alone the present values of W_0 in Table IV for (water soluble) glucose and sucrose cannot be rejected. Also the role of London–van der Waals forces in phenomena like the aggregation of (much larger) protein molecules cannot be settled on the basis of the present results. Study of solutions of simpler molecules which cannot form localized bonds or a theoretical treatment of hydrogen bonding as indicated above would help in separating the various types of interaction and their influence on stability phenomena.

(24) P. Rosen, *J. Chem. Phys.*, **21**, 1007 (1953).
(25) B. M. Axilrod, *ibid.*, **19**, 719 (1951).
(26) L. Jansen, Thesis, Leiden, 1955; *J. Chem. Phys.*, **22**, 1701 (1954).
(27) T. Kihara, *Rev. Mod. Phys.*, **27**, 412 (1955); *J. Phys. Soc., Japan*, **11**, 1045, 1050 (1956).

SCAVENGER STUDIES IN THE γ-RADIOLYSIS OF HYDROCARBON GASES AT VERY LOW CONVERSIONS

BY R. A. BACK[1]

The Physical Chemistry Laboratory, McGill University, Montreal, Canada

Received July 31, 1959

Experiments at very low conversions, using ethylene or propylene as scavengers for hydrogen atoms, indicate that about two-thirds of the hydrogen produced in the γ-radiolysis of ethane, propane, *n*-butane and *n*-pentane, in the gas phase, arises from hydrogen atoms. This is considerably higher than indicated from previous studies at higher conversions, and it is suggested that unsaturates produced in the radiolysis acted as internal scavengers in the latter systems, thus reducing the apparent yield of "radical" hydrogen. Kinetic evidence is presented indicating that the unsaturates used as scavengers in the present work removed hydrogen atoms by a simple addition reaction and did not interfere in other stages of the radiolysis.

Introduction

In a recent study of the radiolysis of saturated hydrocarbon gases, at very low conversions, behavior considerably different from that previously reported at much higher conversions was observed.[2] *G*-values for hydrogen were roughly double the earlier values, and unsaturates, previously reported only in traces, were found to be major reaction products. Further, yields of both hydrogen and unsaturates were observed to decrease considerably with increasing time of irradiation. It was concluded from these observations that as the unsaturates produced in the radiolysis accumulated, they began to act as "internal" scavengers for hydrogen atoms, being themselves consumed in the process, leading eventually to a constant, much-reduced yield of hydrogen, and a very low steady-state concentration of unsaturates, as observed in the earlier work done at high conversions. A very similar behavior has been demonstrated in the mercury-photosensitized decompositions of a number of saturated hydrocarbons.[3-6]

(1) Division of Pure Chemistry, National Research Council, Ottawa, Canada. National Research Council of Canada postdoctorate fellow at McGill University.
(2) R. A. Back and N. Miller, *Trans. Faraday Soc.*, **55**, 911 (1959).
(3) R. A. Back, *ibid.*, **54**, 512 (1958).
(4) R. A. Back, *Can. J. Chem.*, in press.
(5) P. W. Beck, D. V. Kniebes and H. E. Gunning, *J. Chem. Phys.*, **22**, 672 (1954).
(6) R. Cvetanovic, to be published. Reported in part at the 1958 Annual Meeting of the Royal Society of Canada at Edmonton.

A simple corollary of this mechanism is that scavenger experiments done at high conversions should lead to low values for the "radical" yields of various products, especially hydrogen, because of the "internal" scavenger already present. Thus experiments done at very low conversions should measure true initial radical yields considerably higher than those previously reported. This paper reports the results of such experiments.

Experimental

Hydrocarbon gases were irradiated in a cylindrical Pyrex vessel of about 570-ml. volume which could be inserted in a reproducible position in the collimator of a Co^{60} therapy unit of about 1000 curies.[7] The irradiations were of about 3 hours duration.

Hydrocarbons used were all Phillips Research-grade gases. Ethane was subjected to special treatment to remove small amounts of methane and ethylene which were found to be present.[4] Other gases were purified and degassed as previously described.[2] The irradiation vessel was thoroughly baked out under high vacuum before use and was carefully evacuated to remove non-condensible gases before sealing

After irradiation, the vessel was attached through a break-seal to an analysis system essentially similar to that used previously.[2] Gases were removed by a mercury diffusion pump backed by a Toepler pump, through a suitable train of traps including two at −210°. Hydrogen was the only product measured, and was separated from methane by diffusion through a palladium thimble at 300°.

In the scavenger experiments, the pure hydrocarbons were at 800 mm. pressure, except *n*-pentane, which was at 400 mm. Ethylene was the scavenger used throughout, while propylene was used in some experiments with propane. In the experiments with added scavenger, the pressure of the original hydrocarbon was adjusted to maintain constant electron density independent of composition of the gas. All results were corrected for radioactive decay of the γ-source, assuming a hydrogen yield proportional to dose. No absolute dosimetry was attempted. In all the experiments, the conversion, defined as $(2 \times H_2)$/hydrocarbon, was less than 0.003%.

Results

In Fig. 1 is shown the hydrogen yield from the radiolysis of propane as a function of propane pressure. The shape of this plot provides some information about the nature of the radiation absorbed in the system. A simple calculation shows that direct absorption of γ-rays could account for only about 1% of the observed decomposition, so presumably the effective radiation consisted of secondary electrons ejected from the walls of the vessel. If G_{H_2} for propane is reasonably independent of pressure, so that the hydrogen yield measures approximately the energy absorbed, the nearly linear curve, slightly concave upwards, indicates a relatively high average energy for the secondary electrons. (The curve in Fig. 1 may be compared with the initial portion of the hydrogen yield *vs.* pressure plot found in the α-radiolysis of pentane[2]). Thus the absorption of energy in the present study must have been almost homogeneous, with most of the secondary electrons completely traversing the reaction vessel with only a small fractional loss of energy.

In Fig. 2, the hydrogen yield from the radiolysis of propane–propylene mixtures is plotted against the mole per cent. propylene. Under the experimental conditions of constant electron density,

(7) The author is indebted to the Jewish General Hospital of Montreal for very kindly providing the Co^{60} therapy unit used in these experiments.

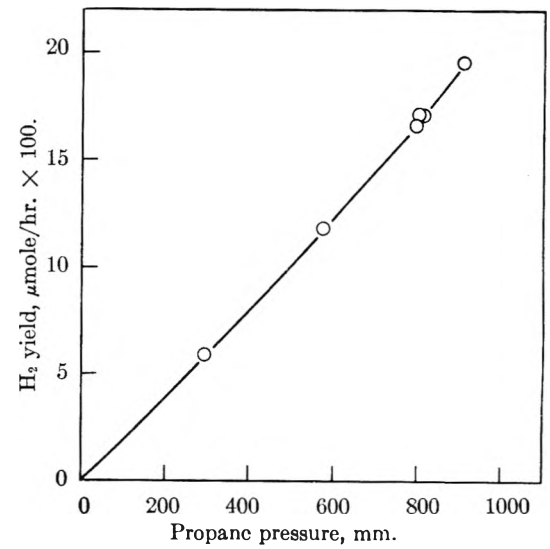

Fig. 1.—Hydrogen yield from the γ-radiolysis of propane as a function of propane pressure.

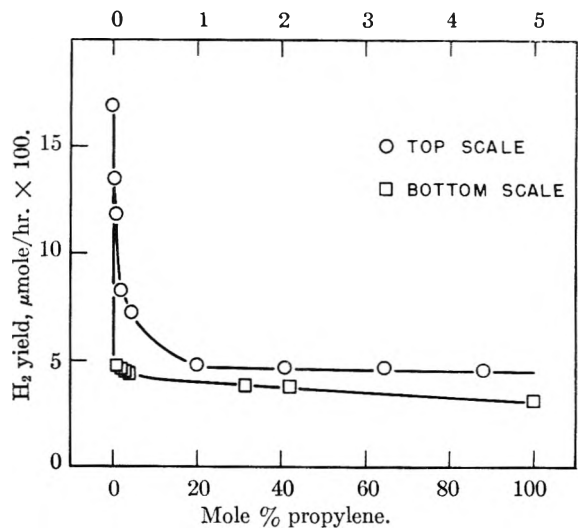

Fig. 2.—Hydrogen yield from propane–propylene mixtures.

and thus approximately constant energy input, the linear extrapolation of the lower curve back to the pure-propane axis should give as intercept the yield of "molecular" hydrogen (hydrogen not arising from hydrogen atoms) from pure propane. The "radical" hydrogen (that formed from hydrogen atoms) is of course given by the difference between the total and the molecular yields. In Table I are shown molecular, radical and total

TABLE I

HYDROGEN YIELDS FROM γ-RADIOLYSIS OF HYDROCARBONS

Pressure, mm., 25°	Hydrocarbon	—Hydrogen yield, μmoles/hr.[a]— Total	Radical	Molecular	% radical	Molecular H_2, calcd. from mass spectra
852	Ethylene	0.032	...	0.032	0	
870	Propylene	.031	...	.031	0	
800	Ethane	.236	0.148	.088	63	0.089
800	Propane	.169	.126	.043	75	.043
800	*n*-Butane	.114	.073	.041	64	.036
400	*n*-Pentane	.181	.121	.060	67	.047

[a] Corrected for differences in the energy absorbed, taking propane at 800 mm. as a standard.

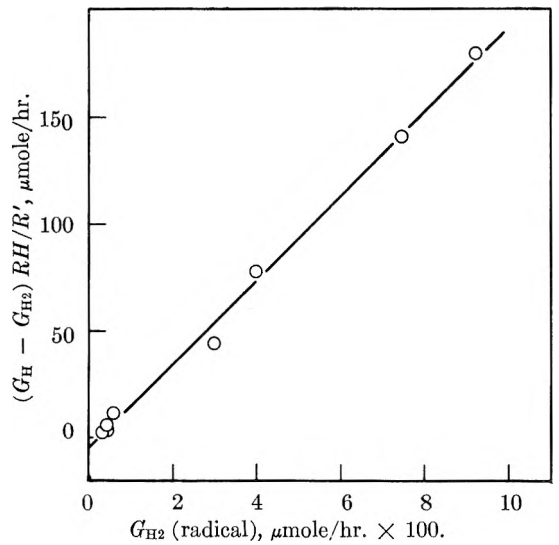

Fig. 3.—A plot of equation 2 for propane–propylene mixtures.

hydrogen yields from the radiolyses of ethane, propane, *n*-butane and *n*-pentane, obtained in a similar fashion, using ethylene as scavenger, and of ethylene and propylene. These values have all been corrected for differences in stopping power, taking propane at 800 mm. as a standard. The stopping power was assumed to be proportional to electron density, with a dependence of energy absorbed on electron density similar to that shown by propane (Fig. 1), assuming G_{H_2} for propane to be independent of pressure. Thus the values in Table I are yields per unit energy absorbed, or relative *G*-values.

Discussion

As anticipated, the per cent. radical hydrogen found in these experiments was considerably higher than that indicated from previous studies done at higher conversions.[8-11] By considering the radical hydrogen alone, the results may be treated in a way entirely analogous to that used for the mercury-photosensitized decompositions.[3,4] The pertinent reactions are

$$RH \xrightarrow{\text{rate} = G_H} H + \text{other products} \quad (1)$$

$$\xrightarrow{\text{rate} = G_{R'}} R' + \text{other products} \quad (2)$$

$$H + RH \xrightarrow{k_3} H_2 + \dot{R} \quad (3)$$

$$H + R' \xrightarrow{k_6} \dot{R} \quad (6)$$

$$H + R' \xrightarrow{k_7} H_2 + \dot{R}' \quad (7)$$

where RH is an alkane, R′ is any unsaturate, $\dot{R}$ is any alkyl radical and $\dot{R}'$ is an unsaturated radical resulting from the abstraction of a hydrogen atom from the α-position of an unsaturate. G_H includes all modes of formation of hydrogen atoms, while $G_{R'}$ includes all modes of formation of unsaturates, both primary processes and secondary ones such as the disproportionation of alkyl radicals. The reactions are numbered to correspond with similar ones in the mercury-photosensitized system.[3,4]

From this mechanism, we may derive the equation

$$G_{H_2}(\text{radical}) = \frac{G_H(k_3[RH] + k_7[R'])}{k_3[RH] + (k_6 + k_7)[R']} \quad (1)$$

G_{H_2} (radical) will equal G_H initially, will decrease as R' accumulates in the system, and will become constant if $[R']$ achieves a steady-state value before appreciable depletion of RH has occurred. In the mercury-photosensitized decomposition of ethane, this steady state was achieved after about 0.05% conversion with an estimated ethylene concentration of one part in 80,000.[4] In the radiolysis system, one would expect the steady state to be reached at about the same conversion. Thus Dorfman,[8] for example, found 34% radical hydrogen from the radiolysis of ethane, with a minimum conversion of 0.3%, almost certainly in the steady-state region. The 63% radical hydrogen, measured at 0.003% conversion in the present study, is probably close to the true initial value. Again, one may compare the value of 75% radical hydrogen from propane at 0.003% conversion with the value of 58% measured by Yang and Manno, using NO scavenger at higher conversions.[12]

Equation 1 may be re-written as

$$[G_H - G_{H_2}(\text{radical})]\,[RH]/[R'] = A\,[G_{H_2}(\text{radical})] - B(G_H) \quad (2)$$

where $A = (k_6 + k_7)/k_3$, and $B = k_1/k_3$. G_H is given simply by G_{H_2} (radical) in the absence of unsaturate, and, since relative *G*-values may be used, the data for the propane–propylene mixtures (Fig. 2), up to 5% propylene, were plotted according to this equation in Fig. 3, making proper allowance for the slight decrease of G_H and G_{H_2} (molecular) with increasing propylene content. A good straight line was obtained, and from the slope and intercept, one obtains $k_6/k_3 = 1940$ and $k_7/k_3 = 32$. These values may be compared with values of 1300–1500 and 50–80 found for the same two ratios in the mercury-photosensitized decomposition of propane.[4] The difference in the values of k_7/k_3 is of no significance, as the inaccuracy of the intercept is obvious. The agreement between the values of k_6/k_3 may be regarded as excellent, considering the combined errors of the two determinations. This agreement, and the linearity of the plot in Fig. 3, constitute impressive evidence that the propylene in the radiolysis system was acting as a simple chemical scavenger for hydrogen atoms and did not interfere in other stages of the radiolysis mechanism. Using ethylene as a scavenger, almost exactly the same yield of radical hydrogen was obtained as with propylene, and it is probably safe to conclude that this technique does indeed measure the hydrogen arising from hydrogen atoms in these systems. The linearity of the data in Fig. 2 for propylene content greater than 5% also indicates that there was no

(8) L. M. Dorfman, THIS JOURNAL, **62**, 29 (1958).

(9) H. A. Dewhurst, *ibid.*, **62**, 15 (1958).

(10) W. H. T. Davison, "Reactions of Free Radicals in the Gas Phase," Special Publication No. 9, The Chemical Society, London, 1957, p. 151.

(11) L. H. Gevantman and R. R. Williams, THIS JOURNAL, **56**, 569 (1952).

(12) K. Yang and P. J. Manno, *J. Am. Chem. Soc.*, **81**, 3507 (1959).

abnormal "interaction" between propylene and propane in the radiolysis system, as the yields of molecular hydrogen from the two components appear to be purely additive.

The hydrogen yields shown in Table I superficially show no particular trends. Molecular yields from the unsaturates are appreciably lower than from the alkanes, but of the same order of magnitude. The molecular hydrogen from the alkanes most probably comes from ionic processes, and it is interesting to compare the observed relative molecular yields with those which may be calculated from mass-spectrometer cracking patterns.[13] The latter are included in Table I and are seen to follow the trend of the observed values fairly well. The calculation considered only ionization processes, as indicated in the mass spectra, and took no account of molecular hydrogen which might arise by subsequent neutralization or ion–molecule reactions.

It was concluded from a previous study that less than half of the radical hydrogen from the radiolysis of alkanes came from ionic processes,[2] and the high yields of radical hydrogen indicated in the present results lead to the same conclusion. It was further calculated[2] that from 60 to 80% of the hydrogen from the α-radiolysis of *n*-pentane arose from hydrogen atoms, which compares favorably with the 67% now found experimentally with γ-rays. A major source of hydrogen atoms is almost certainly a simple excitation process

$$RH \rightsquigarrow RH^* \longrightarrow \dot{R} + H \qquad (8)$$

similar to that observed in the photolysis of the alkanes.[14,15] Ionic processes leading to atomic hydrogen include ionization-cracking reactions, as observed in mass spectra, and ion-molecule reactions, followed by neutralization

$$RH^+ + RH \longrightarrow RH_2^+ + \dot{R} \qquad (9)$$

$$RH_2^+ + e^- \longrightarrow RH + H \qquad (10)$$

The reaction

$$RH_2^+ + e^- \longrightarrow \dot{R} + H_2 \qquad (11)$$

which gives rise to molecular hydrogen is a likely alternative to reaction 10, although the agreement between observed yields of molecular hydrogen and those predicted from ionization-cracking alone suggests that reaction 11 is perhaps not important.

Finally, the present results emphasize again the need to work at extremely low conversions if one hopes to study the basic processes of radiolysis. Particularly in any system in which unsaturates are formed in the early stages, conversions even as low as 0.1% may completely obscure the initial processes, and unfortunately almost all previous studies of the radiolysis of the alkanes in the gas phase suffer from this fault. The present investigation has been concerned only with the effect on hydrogen yield, but almost certainly all other products formed from free radicals may be affected in a similar way. It should be noted that unsaturates are produced in large yields as primary radiolysis products[2] as well as by the disproportionation reactions that are their sole mode of synthesis in the mercury-photosensitized decompositions,[3,4] so that their effects in the radiolysis systems are probably much larger. The obvious need to remove even minute traces of unsaturated impurities from the original hydrocarbon should also be noted.

(13) American Petroleum Institute, Research Project 44.
(14) W. E. Groth and G. Scharfe, *Z. physik. Chem.*, **2**, 142 (1954).
(15) M. H. J. Wijnen, *J. Chem. Phys.*, **24**, 851 (1956).

MULTICOMPARTMENT PERMSELECTIVE MEMBRANE CELLS FOR THE PREPARATION OF ACIDS AND BASES

BY LIONEL M. RAFF, FRANK A. IDDINGS AND GEORGE W. MURPHY

University of Oklahoma, Norman, Oklahoma

Received August 3, 1959

Acids and bases can be generated from salts in electrochemical cells containing many compartments separated by permselective membranes. In the ideal case, this "reverse neutralization" yields products in the ratio of two, three or more equivalents of both acid and base per faraday (depending on the cell structure), which are free from contaminating electrolytes. One equivalent is produced at the electrodes by the customary oxidation–reduction processes, but the others are formed without appreciable over-voltage effects by forced dissociation of water in particular compartments. Two cells have been constructed and studied experimentally. The current efficiency for the formation of sodium hydroxide and sulfuric acid from one molar sodium sulfate was studied in the case of cell I, which contained seven compartments, and yields in the limit two equivalents each of acid and base per faraday. Similar studies were made on the formation of sodium hydroxide and hydrochloric acid from one molar sodium chloride in cell II, which contained fifteen compartments, yielding in the limit four equivalents each of acid and base per faraday. Current efficiencies are reported as a function of degree of conversion and a theoretical analysis of the power requirement is presented. It is shown that most of the power is expended as an I^2R drop in the highly resistive water compartments.

Introduction

In recent years synthetic ion-exchange (permselective) membranes have been applied to a variety of problems,[1] notably the electrodialytic deionization of saline waters.[2] A new membrane application is described herein which results in the forced dissociation of water and hence the formation of acid and base. In the ideal case, this

(1) K. S. Spiegler, *J. Electrochem. Soc.*, **100**, 303C (1953).

(2) "Proceedings of the 1957 Symposium on Saline Water Conversion," National Academy of Sciences-National Research Council, Publication 568, 179 (1958).

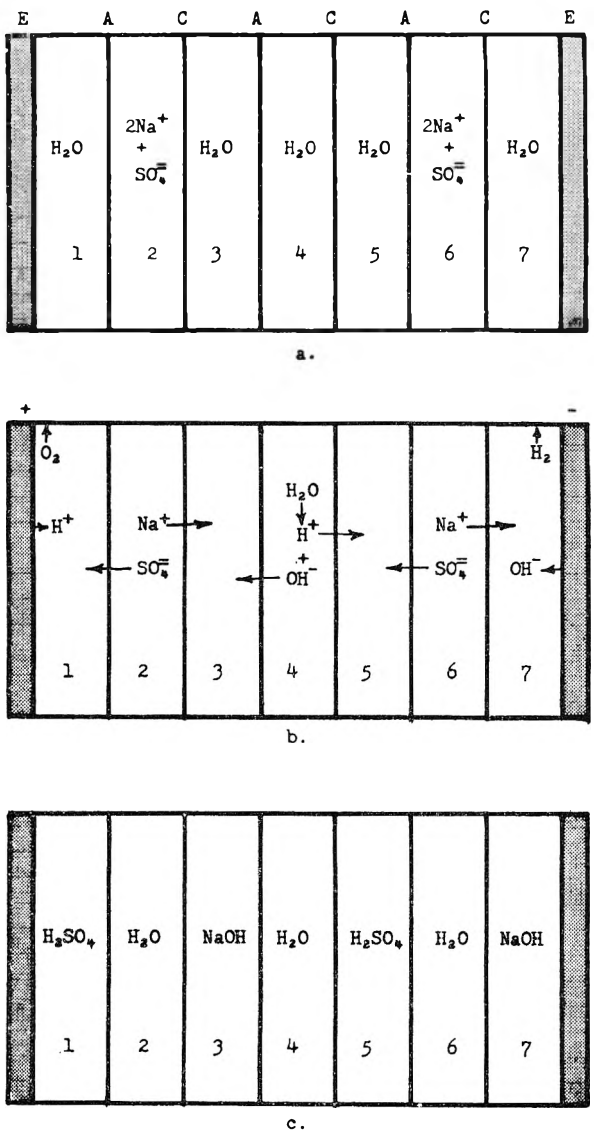

Fig. 1.—Cell I, schematic cross-section, illustrating principle: A, anion-permeable membrane; C, cation-permeable membrane; E, electrode; a, initial state; b, showing ion movement after applying potential difference to electrodes; c, final state after passage of sufficient current to exhaust salt from compartments 2 and 6.

"reverse neutralization" yields products in the ratio of two, three or more equivalents of both acid and base per faraday, depending on the electrolytic cell structure, which are free from contaminating electrolytes. Furthermore, except for the one equivalent of acid and base formed at the electrodes there are no overvoltage effects to compare with those of ordinary electrolytic cells.

It has been known for many years that unwanted *p*H changes occur in membrane cells designed for electrodialysis, especially when the current density is high. The theory of this effect has been developed by Manegold and Kalauch,[3] but it has not been suggested heretofore that membrane cells can be designed and operated for the efficient production of acid and base rather than for salt removal.

(3) E. Manegold and K. Kalauch, *Kolloid Z.*, **86**, 313 (1939).

Figure 1 shows the cross section of a seven-compartment electrolytic cell, hereafter referred to as cell I, formed from six membranes and two electrodes. Three each of cation- and anion-selective membranes are arranged alternately, with the former type adjacent to a cathode and the latter to an anode of inert material. Compartments 1, 3, 4, 5 and 7 contain pure water initially, while 2 and 6 are filled with a sodium sulfate or other salt. Passage of current through the cell results in the ionic movement and electrode processes shown in Fig. 1b. The key compartment is 4. To support the current, hydrogen ion must pass from 4 to 5 and hydroxyl ion from 4 to 3, but this can continue to take place only through forced dissociation of the water in 4. After sufficient current has passed to exhaust the salt from 2 and 6, the contents of the different compartments are as represented in Fig. 1c, with two equivalents each of acid and base having been produced per faraday.

The above discussion is based on perfectly selective membranes. Imperfections in available membranes will result in lower current efficiency for acid and base in the appropriate compartments and the formation of acid in compartments where it would be otherwise unexpected. It will be seen later that some acid was actually found experimentally in compartments 2 and 6. This is due to the fact that the anion-permeable membranes employed are inferior in permselectivity to the corresponding cation-permeable membranes. Referring to Fig. 1b, the imperfect anion-permeable membrane will permit some hydrogen ion to pass from 1 to 2, and the imperfect cation-permeable membrane will permit some hydroxyl ion to pass from 3 to 2. Because the cation-permeable membrane is a more effective screen for hydroxyl ions than the anion-permeable membrane for hydrogen ions, compartment 2 will become acidic. The same consideration applies to compartment 6.

The following cell configuration, hereafter referred to as cell II, yields, with ideal membranes, four equivalents of acid and base per faraday

	E C A C A.....C A C E
Compartment	1 2 3 4(thin)..... 13 14 15
Initial state	H_2O salt H_2O H_2O ..... H_2O salt H_2O
Final state	base H_2O acid H_2O ..... base H_2O acid

Omission of two repeating units of four compartments each identical with the first four compartments is indicated by the dotted lines. Symbols are as in the legend to Fig. 1. The extension to any number of equivalents per faraday will be evident.

Theoretical Analysis of Energy Efficiency.—In the three-compartment cell E–H_2O–C–Na_2SO_4–A–H_2O–E (initial state), basically the same as one previously reported[4] the function of the membranes is to keep the acid formed at the anode and the base formed at the cathode free from contaminating electrolyte; otherwise, this is no different from a conventional electrolytic cell without membranes and is subject to the same overvoltage effects at the

(4) Rohm and Haas Co., "Amberplex Ion-Permeable Membranes," Bull. 8-11, Philadelphia, 1952.

electrodes. In the seven-compartment cell of Fig. 1, an additional equivalent of acid and base is produced by the dissociation of water in the center compartment. Because no oxidation–reduction electrode reactions are involved, it is a reasonable supposition that overvoltage effects due to formation of this extra equivalent will be very small, if they are present at all. It is of interest to compare the energy efficiency for production of this extra equivalent with that for the first equivalent of acid and base produced at the electrodes.

Let E' be the voltage drop across the seven-compartment cell and E'' the drop across the three-compartment cell left after removal of compartments 3, 4 and 5 with their respective membranes, each measured after passage of the same current for the same length of time. After incomplete electrolysis, $E^0 = E'' - E'$ is the voltage across the compartments and membranes which have been removed, with the configuration $Na_2SO_4(2)$–C–NaOH(3)–A–$H_2O(4)$–C–$H_2SO_4(5)$–A–$Na_2SO_4(6)$. E^0 is made up of five parts

$$E^0 = IR_3 + IR_4 + IR_5 + e + v \qquad (1)$$

where R_3, R_4 and R_5 are the resistances of respective compartments of the cell, e is the back reversible e.m.f., and v is the irreversible voltage drop at the membranes. All except v can be calculated to a reasonable approximation. Since E^0 is measurable, v can then be determined.

The over-all process for discharge of one faraday (assuming ideal membranes) is

$$(Na^+)_3 + (OH^-)_3 + (H^+)_5 + {}^1/_2(SO_4^=)_5 = (Na^+)_2 + (OH^-)_4 + (H^+)_4 + {}^1/_2(SO_4^=)_6$$

and the free energy change is

$$\Delta F = -RT \ln \frac{(Na^+)_2(OH^-)_4(H^+)_4(SO_4^=)_6{}^{1/2}}{(Na^+)_3(OH^-)_3(H^+)_5(SO_4^=)_5{}^{1/2}} \qquad (2)$$

$$= -RT \ln \frac{K_w(Na^+)_2(SO_4^=)_6{}^{1/2}}{(Na^+)_3(OH^-)_3(H^+)_5(SO_4^=)_5{}^{1/2}}$$

The symbols in parentheses refer to activities, which will be approximated by concentrations, and the subscripts refer to compartments; K_w is the ion product constant of water.

Thus the back e.m.f. is given by

$$e = \frac{RT}{F} \ln \frac{K_w(Na^+)_2(SO_4^=)_6{}^{1/2}}{(Na^+)_3(OH^-)_3(H^+)_5(SO_4^=)_5{}^{1/2}} \qquad (3)$$

Experimental

In addition to the seven-compartment (I) and fifteen-compartment (II) cells, a five-compartment cell obtained by elimination of the two extreme membranes and compartments from cell I has been studied experimentally. This cell served to validate the principle, but as current efficiency in the catholyte and anolyte chambers was poor, it was soon abandoned in favor of cell I.

Experiments with both cells I and II were designed to obtain the gross electrolyte transport that occurs in the several compartments. No attempt was made to evaluate the magnitude of electroösmosis, for the reliability of such determination is limited by uncertain compartment geometry due to membrane swelling and buckling.

Cell I. (**Fig. 2**).—All membranes were Amberplex, manufactured by Rohm and Haas Co. They were held between frames 4″ long, 1.5″ wide (not including six bolting ears) and 1/4″ thick. The exposed membranes measured 1.03″ × 3.625″. The two end frames were monel and the seven interior ones were Lucite. Electrodes were sheets of smooth platinum attached to the faces of the monel frames. Small tubulations were fitted to the top and bottom of each

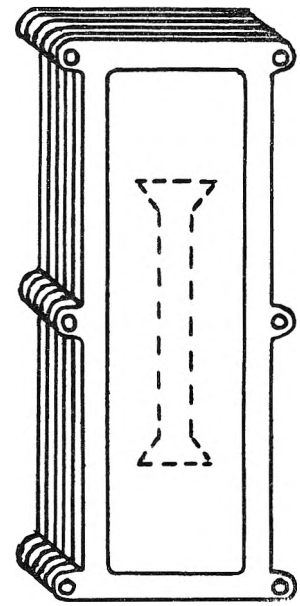

Fig. 2.—Cell I, external view. Dotted line, Lucite membrane spacer. Exposed membrane area defined by interior rectangle, less area of spacer (when used).

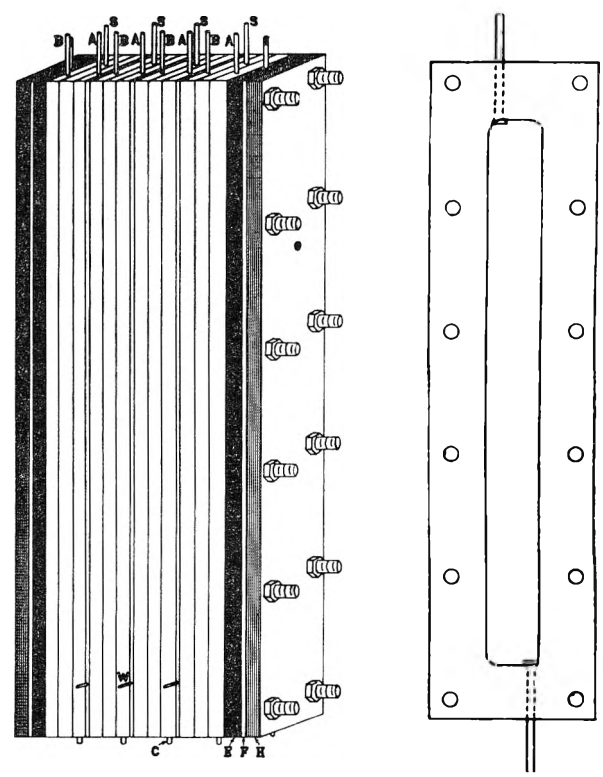

Fig. 3.—Cell II: a, external view. Upper exit tubes: B, base; A, acid; S, salt. Lower tubes, C, all salt inlet. W, water inlet for thin compartments. E, electrodes; F, insulating spacer; H, brass plate. b, Polyethylene spacer for membranes of cell II.

frame to allow solution entry and exit. The unit was held together by compression in a vise with insulated jaws.

Current was supplied from a 110-volt d.c. generator through a voltage divider. During an experiment the current was kept steady by manual adjustment.

Sodium sulfate solutions of accurately known concentrations were made up by weight. Acid and base concentrations were determined by titration.

For investigation of the voltage drop in the center com-

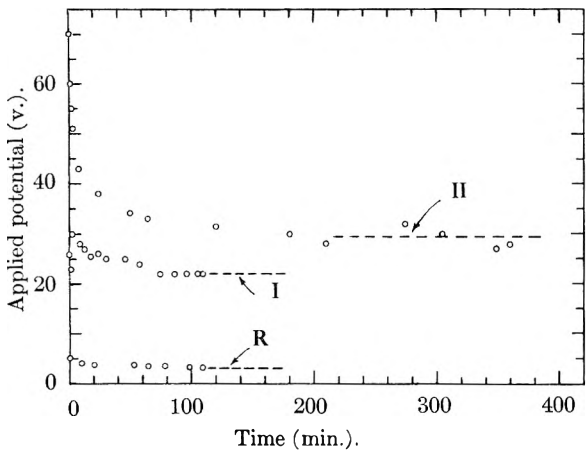

Fig. 4.—Attainment of limiting voltage at constant current for three cells. I, cell I, lim. 22.0 volts; II, cell II, lim. 29.5 volts; R, reduced cell, lim. 3.5 volts.

partment and the irreversible effects at the membranes, some modification of the cell was necessary. Owing to the strong tendency of the membranes to swell and buckle and thus change the geometry of the compartment, the calculation of resistance from a measured specific resistance is not very exact. In order to minimize this effect, narrow quarter-inch thick internal Lucite spacers were inserted centrally between the membranes of each compartment (Fig. 2). These spacers were held in place by the pressure of the vise and served to maintain a constant spacing between membranes over most of their area.

With cell I set up as before, a constant current of 50 ma. was maintained, and a record was kept of the voltage at various time intervals. At the conclusion of the experiment, the concentrations of acid and base in compartments 1, 2, 3, 5, 6 and 7 were determined. The conductivity of the liquid from compartment 4 was determined.

Following these measurements, the center section of cell I, consisting of compartments 3, 4 and 5 with their respective four membranes, was removed. The remaining three-compartment cell, hereafter referred to as the reduced cell, was then filled with salt solution in the center compartment and distilled water in the outer compartments. Current was passed for the same length of time as in the previous experiment with cell I and the voltages were again recorded as a function of time.

Cell II. (**Fig. 3**).—Membranes were Nalfilm-1 (cation permeable) and Nalfilm-2 (anion permeable) obtained from National Aluminate Co. The frames of outside dimensions 3″ × 12″ were machined from polyethylene stock. Two thicknesses were used, $^1/_4$″ for compartments 1, 2, 3, 5, 6, 7, 9, 10, 11, 13, 14, 15 and $^1/_{16}$″ for compartments 4, 8, 12. The compartments in which water is electrolyzed were thinner so that the over-all voltage drop would be smaller. One-fourth inch sheet graphite electrodes were used. The exposed membranes and electrodes were 1″ × 10″. Stainless steel tubulations were fitted to the top and bottom of the polyethylene frames. The whole set of membranes was compressed between heavy brass plates, with the aid of twelve $^1/_4$″ brass screws.

The experimental approach for static runs was similar to that of cell I. The inert graphite anode permitted generation of chlorine from sodium chloride solutions, which was the starting material for all experiments. However, the chlorine rapidly attacked the stainless steel tubes and bleached the adjacent membrane (the electrical properties of the membrane appeared to be unaffected). Consequently, for most experiments, a depolarizing solution of 1 *N* sodium sulfite was substituted for water in the anode compartment. For others Na_2SO_4 instead of NaCl was used in compartment 14 and water was retained in the anode compartment.

Cell II was designed with steady-state flow experiments in mind, and for this purpose the inlet (bottom) and exit (top) tubes were connected to appropriate manifolds. No flow experiments are reported here.

Results of Experiments

Yields of acid or base produced in different compartments and the corresponding normalities at various times are given in Tables I and II for typical sets of experiments with the two cells. In Table II the current efficiency averaged over all compartments is also presented. The steady decrease in efficiency during a run is characteristic of both cells.

The maximum at 609 minutes in acid content of compartment 6, Table I, undoubtedly is due to the steady depletion of sodium ion in that compartment. Sodium ion is the predominant ion transported into compartment 7 when its concentration is high, but as its concentration falls, a progressively greater amount of transport is taken over by hydrogen. At low sodium ion concentrations, a point is ultimately reached when the hydrogen ion can be transported from compartment 6 to 7 through the cation-selective membrane faster than it can be transported in from compartment 5 to 6 through the imperfect anion-selective membrane.

The maxima in acid concentration of compartment 5 and in base of compartment 3, and corresponding maxima in compartments of cell II are partly due to a natural phenomenon appearing after prolonged electrolysis at constant current. Consider the ideally constituted cell I after electrolysis of Fig 1c. Further current can be passed through the cell only by electrolytic dissociation of the water contained in compartments 2 and 6, as well as 4. A leveling off of concentration would be expected in the ideal case. In practice, imperfection of the membrane between 4 and 5 permits loss of sulfate ion and hence net loss of acid from compartment 5.

The progress of voltage with time required to maintain a constant current is illustrated in Fig. 4 for cells I (50 ma.) and II (150 ma.) and the reduced cell (50 ma.). Cell II shows a much more pronounced voltage decrease, as would be expected from the addition of four extra water compartments which become good conductors as the electrolysis proceeds. A rough comparison of the final voltages of these two cells and the reduced cell shows that about 18.5 volts is required to obtain the extra equivalent of acid and base with cell I; the three extra equivalents of acid and base obtained with cell II demand 8.7 volts each. Of course this is due primarily to the lowered resistance of the three thin water compartments. Because of uncertain compartment geometry and water conductivity, a close correspondence of voltage drops in water compartments of the two cells is not to be expected.

Analysis of the final voltages for cell I and the reduced cell permits a rough calculation of overvoltage effects at the membranes in the following manner: The drop across the center section of cell I is 22.0 − 3.5 = 18.5 volts. Substituting the concentrations from Table II into equation 2, we find e = 2.04 volts. Because R_4 is much larger than R_2 or R_5, the first and third terms to the right of equation 1 can be dropped. The specific conductivity of the water in compartment 4 was found to be 9.20×10^{-5} ohm^{-1}cm.$^{-1}$, and the

TABLE I

TYPICAL RESULTS OBTAINED WITH CELL I[a]

Time, min.	Farad. × 10^{-3}	Meq. of acid or base produced in compartment no. 1(H^+)	2(H^+)	3(OH^-)	5(H^+)	6(H^+)	7(OH^-)
69	2.14	1.38	0.38	0.95	1.11	0.37	1.33
70	2.18	1.32	.30	1.20	0.81	0.19	1.76
116	3.60	2.35	.78	2.66	1.91	0.73	3.18
160	4.97	2.73	.88	...	1.75	0.58	3.07
402	12.5	6.50	2.88	8.44	5.41	1.61	9.71
609	18.9	8.68	3.64	10.45	7.58	1.77	11.37
841	26.1	10.54	3.85	10.29	7.46	0.60	11.70
874	27.2	10.29	3.42	9.19	8.08	0.29	9.15
1179	36.6	11.20	3.42	8.42	6.44	0.00	12.60
		Normality of acid or base					
69	..	0.1095	0.0233	0.1171	0.0877	0.0143	0.1500
160	..	.247	.0695	.191	.136	.0466	0.236
841	..	.857	.294	.644	.470	.0624	1.079
874	..	.860	.240	.727	.847	....	1.436
1179	..	.895	.230	.655	.352	.00	0.908

[a] Initial concentration of sodium sulfate in compartments 2 and 6, 1.256 *N*. No acid or base was ever found in compartment 4. Current constant at 50 ma. Data are from nine experiments with no sampling except after electrolysis for the reported time.

TABLE II

TYPICAL RESULTS OBTAINED WITH CELL II[a]

Time, min.	Farad. × 10^{-3}	Milliequivalents of H^+ or OH^- formed: 1 OH^-	5 OH^-	9 OH^-	13 OH^-	3 H^+	7 H^+	11 H^+	15 H^+	H^+, comb. salt soln. 2,5,8,11	Approx. *N*, H^+ or OH^-	% current effic.
115	10.74	8.98	8.96	...	6.56	7.70	...	6.18	6.54	3.70	0.2	83.2
160	14.92	12.79	12.80	12.62	13.04	12.36	12.08	12.25	9.68	4.83	.3	85.7
290	27.07	21.16	23.30	22.90	17.98	19.34	14.55	20.48	12.34	7.01	.66	84.7
360	33.60	25.44	25.79	25.89	27.65	21.62	22.88	23.44	20.18	8.20	.7	76.5
480	44.79	30.51	31.52	30.54	33.70	24.05	28.00	29.05	24.82	18.80	.8	68.2
600	56.57	33.74	35.75	29.27	34.36	29.36	27.92	29.38	35.38	20.58	.9	59.7
720	67.20	40.98	39.88	36.70	39.84	34.85	26.10	33.04	36.42	25.15	1.0	59.3
785	72.20	37.80	39.30	30.48	41.42	34.70	33.60	27.60	34.50	22.70	1.0	54.4
960	88.55	40.40	41.60	22.80	46.10	26.25	23.63	23.28	40.00	23.26	1.1	47.0

[a] Initial concentration of NaCl in compartments 2, 6 and 10, and of Na_2SO_4 in compartment 14, 2 *N*. Current constant at 150 ma.

IR_4 drop computed from this value and the known area of exposed membrane (corrected for spacer area of 0.485 in.^{2}) was calculated to be 16.5 volts. Hence, by equation 2

$$v = E - e - IR_4 = 18.5 - 2.0 - 16.5 = 0.0$$

This result is admittedly only an approximation. The acid present in compartments 2 and 4 has been ignored. It has been assumed that the concentration of sulfate ion in compartment 6 at time t is its original concentration minus the amount of sulfuric acid produced in compartment 5, and a similar assumption has been made in calculating the amount of sodium ion present in compartment 2 at time t. The activities have been replaced by concentrations in equation 3. However, the calculation does serve to point out that the main source of energy dissipation is the IR drop present in compartment 4.

THE REDUCTION OF HIGH SURFACE AREA URANIUM TRIOXIDE[1]

By R. E. DeMarco and M. G. Mendel

Chemical Department, National Lead Co. of Ohio, Cincinnati 31, Ohio

Received August 13, 1959

The hydrogen reduction of high surface area, X-ray amorphous, UO_3 was studied at temperatures of 300 to 400° and at hydrogen partial pressures of $^1/_4$ to 1 atm. The reduction was found to consist of two consecutive steps associated with the reactions: $UO_3 + H_2 \rightarrow UO_{2.66}$ and $UO_{2.66} + H_2 \rightarrow UO_2$. The linear weight loss–reaction time curves indicated that both reactions are primarily controlled by adsorption of hydrogen on the product oxide surface. Activation energies of 27 and 39 kcal./mole were calculated for the reduction of UO_3 and of $UO_{2.66}$.

Introduction

The mechanism involved in the reduction of UO_3 to UO_2 has not been firmly established. Except for Tanford, *et al.*,[2] who assumed prior thermal decomposition to U_3O_8, the reduction has been considered a continuous one-step reaction. Orrich[3] and Kuhlman[4] assumed that UO_3 was reduced to UO_2 by a one-step, first-order reaction. DeHollander[5] employed zero-order kinetics in his investigation of the reduction reaction. Moore and Maness[6] used phase boundary kinetics for interpreting their data on the reduction of large spherical UO_3 particles.

Notz and Mendel[7] have obtained data on the reduction of γ-UO_3 to UO_2 which indicate that one, two or three steps may be involved in the over-all chemical reaction. They found that time required for 95% reduction was a direct function of the UO_3 surface area and that the total surface area of the sample was unchanged throughout the reduction.

The divergent postulations of these authors can be reconciled when the effects of the physical properties (*e.g.*, surface area, tap density) of the starting, intermediate and/or product uranium oxides on the observed reduction rate are considered.

In order to minimize the effect of these secondary variables on the reduction reaction, a high surface area, low tap density UO_3 was employed in this study. Under these conditions, the experimentally determined reaction rate should more closely approximate the true reduction kinetics and secondary diffusional effects should be minimized.

Materials.—The UO_3 used in this study was prepared by the thermal decomposition at 300 to 400° in a flowing helium atmosphere of −100 mesh uranium peroxide dihydrate.

Anal. Calcd. for $UO_4 \cdot 2H_2O$: uranium, 70.41; peroxy oxygen, 9.46. Found: uranium, 70.20 ± 0.07; peroxy oxygen, 9.44 ± 0.11.

An oxygen-to-uranium ratio of 3.05 ± 0.03 was determined by ignition of this thermally produced uranium trioxide to U_3O_8. X-Ray powder diffraction patterns of UO_3 prepared by thermal decomposition of $UO_2 \cdot 2H_2O$ indicate a very low order crystallinity.

The following physical properties of the uranium trioxide starting material were determined: nitrogen surface area = 26.3 $m.^2/g.^{-1}$; mean agglomerate size = 2 μ; tap density = 1.6 g. $cc.^{-1}$.

Equipment and Procedure.—Uranium peroxide dihydrate samples, 2.000 ± 0.002 g., were evenly distributed on the surface of a circular, 2.25 inch diameter, platinum reaction pan. The sample and pan were then suspended from a constant load, 0 to 100 mg. optical range, balance in the reaction chamber which had previously been brought to the desired reduction temperature. Decomposition of the peroxide to uranium trioxide was allowed to proceed for 30 minutes in a helium atmosphere flowing at one l./min. (S.T.P.) before hydrogen was admitted. Weight loss–reaction time curves were obtained for the decomposition and hydrogen reduction reactions to permit rate constant calculation.

The reduction chamber consisted of a 4-inch diameter closed quartz tube with a clamp on the lid. This chamber was heated by a 2500-watt, vertically mounted, split tube furnace. The reduction temperature was measured by a chromel–alumel thermocouple and controlled by a West (Model J.S.) stepless controller.

Hydrogen and helium gas flow rates to the reaction chamber were measured by calibrated glass rotameters.

Results and Conclusions

Typical curves for the hydrogen reduction of UO_3 to UO_2 in the 300 to 400° temperature range investigated are shown in Fig. 1. These experimental curves show that the reduction of UO_3 to UO_2 consists of two consecutive chemical reactions. The first step is the reduction of the starting uranium trioxide to an intermediate non-stoichiometric compound $UO_{2.56 \pm 0.03}$. The second step is the reduction of this intermediate oxide to the uranium dioxide product.

Table I

Reduction Rate as a Function of Temperature

Reductn. temp. (°C.)	Reductn. rate at 1 atm. H_2: $UO_{3.05} \rightarrow UO_{2.56}$ (mg. $min.^{-1}$ $m.^{-2}$)	Reductn. rate at 1 atm. H_2: $UO_{2.56} \rightarrow UO_{2.02}$ (mg. $min.^{-1}$ $m.^{-2}$)
305 ± 2	0.75×10^{-2}	.....
323 ± 2	1.73×10^{-2}	.....
349 ± 2	3.28×10^{-2}	0.34×10^{-2}
371 ± 2	8.88×10^{-2}	1.25×10^{-2}
391 ± 2	17.5×10^{-2}	3.23×10^{-2}
402 ± 2	22.8×10^{-2}	4.85×10^{-2}
410 ± 2	24.9×10^{-2}	6.01×10^{-2}
419 ± 2	33.5×10^{-2}	7.93×10^{-2}

The linearity of the reduction curves of Fig. 1 and the previously determined surface area dependence[7] of the reaction indicate that phase boundary or nucleation and growth kinetics are not rate controlling. These data are most suitably

(1) This paper is based on work performed for the Atomic Energy Commission by the National Lead Company of Ohio at Cincinnati, Ohio.

(2) C. Tanford, R. L. Tichenor and C. E. Larson, "Uranium Oxides, The Reduction of UO_3," U.S.A.E.C. Report No. AECD-3961, 1945.

(3) N. C. Orrich, "Hydrogen Reduction Rates of Uranium Trioxides as Obtained with a Thermobalance," U.S.E.A.C. Report No. K-1081, 1953 (Confidential).

(4) C. W. Kuhlman, "Reduction of Uranium Trioxide with Hydrogen–Nitrogen Mixtures," U.S.A.E.C. Report No. MCW-215, 1945.

(5) W. R. DeHollander, "A Kinetic Study of the Reduction of Uranium Oxides with Hydrogen," U.S.A.E.C. Report No. HW-46685, 1956.

(6) R. H. Moore and R. F. Maness, "Reduction of UO_3 to UO_2 with Hydrogen," U.S.A.E.C. Report No. HW-38321, 1955 (Confidential).

(7) K. J. Notz, Jr., and M. G. Mendel, *J. Inorg. & Nuclear Chem.*, (to be published).

explained by reactions which are primarily controlled by the hydrogen adsorption rate on the surface of the product oxide. The initial deviation from linearity noted in the reduction of UO_3 to $UO_{2.56}$ may be attributed to the time required for formation of an external product ($UO_{2.56}$) shell.

Rate data for both reduction steps as a function of temperature and hydrogen partial pressure are given in Tables I and II, respectively. In reduction rate calculations, the 26.3 m.^{2}/g. surface area of the starting UO_3 was considered to equal the total area of the partially reduced sample[7] at time "t". Attempts to study the reaction at higher temperatures resulted in curves unnecessarily complicated by the presence of simultaneous reaction.

An activation energy of 26.6 ± 1.0 kcal./mole and an exponential hydrogen pressure dependence of 0.62 ± 0.03 were calculated, from this data, for the reduction of UO_3 to $UO_{2.56}$. The reduction of $UO_{2.56}$ to UO_2 was similarly found to have an activation energy of 39.1 ± 1.0 kcal./mole and an 0.43 ± 0.03 exponential hydrogen pressure dependence.

TABLE II

REDUCTION RATE AS A FUNCTION OF H_2 PARTIAL PRESSURE

H_2 partial pressure (atm.)	Reduction rate at 402 ± 2°: $UO_{3.05} \rightarrow UO_{2.56}$ (mg. min.$^{-1}$ m.$^{-2}$)	$UO_{2.56} \rightarrow UO_{2.02}$ (mg. min.$^{-1}$ m.$^{-2}$)
1.00	22.8×10^{-2}	4.85×10^{-2}
0.80	17.8×10^{-2}	3.99×10^{-2}
.60	16.4×10^{-2}	3.90×10^{-2}
.50	14.8×10^{-2}	3.69×10^{-2}
.40	13.4×10^{-2}	3.28×10^{-2}
.33	12.0×10^{-2}	3.12×10^{-2}
.25	8.72×10^{-2}	2.53×10^{-2}

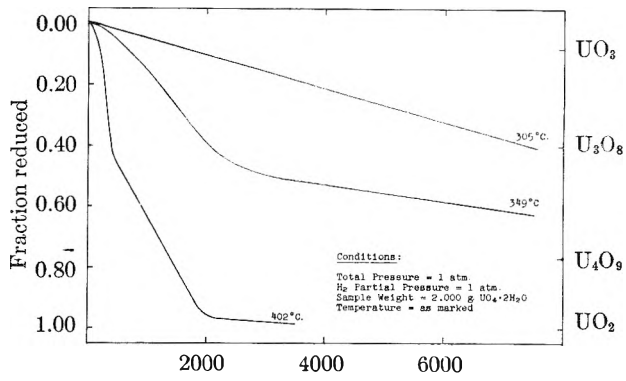

Fig. 1.—Hydrogen reduction of UO_3 to UO_2.

Acknowledgments.—The helpful discussions with personnel of the Technical Division, which contributed to successful completion of this study, are gratefully acknowledged. The authors wish to express appreciation to Dr. H. R. Hoekstra, of Argonne National Laboratories, for his review of and helpful suggestions in the preparation of this paper.

THE SOLUBILITY OF SILVER SULFATE IN ELECTROLYTE SOLUTIONS. PART 6. HEATS AND ENTROPIES OF SOLUTION *vs.* TEMPERATURE. SPECIES PRESENT IN HNO_3 AND H_2SO_4 MEDIA[1]

BY R. W. STOUGHTON AND M. H. LIETZKE

Contribution from the Chemistry Division, Oak Ridge National Laboratory, Oak Ridge, Tenn.

Received August 13, 1959

The concentrations of the various species present in 0.1, 0.5, 1.0 *m* solutions of H_2SO_4 and of HNO_3 saturated with respect to Ag_2SO_4 are discussed as a function of temperature. The values of the solubility product, of the enthalpy and entropy of solution, and of the standard partial molal entropy of the solute Ag_2SO_4 are given *vs.* temperature to 200°.

Introduction

The previous papers in this series describe the solubility of Ag_2SO_4 in KNO_3,[2] K_2SO_4,[3] H_2SO_4,[4] HNO_3[5] and $MgSO_4$[6] solutions. In all cases the data show good agreement with solubilities calculated on the basis of the solubility of Ag_2SO_4 in pure water and on the assumption that the activity coefficient of Ag_2SO_4 can be expressed as a single parameter Debye–Hückel expression. The single parameter was found to be essentially independent of temperature to about 200°, although it did show some variation with concentration of supporting electrolyte in certain cases. In the cases not involving acid media complete dissociation was assumed for both Ag_2SO_4 and the supporting electrolyte. In the cases involving acidic media the incomplete dissociation of HSO_4^- and HNO_3 were taken into account. The values of the acid constants (see ref. 4, 5 and 6 for the equations relating the acid constants with the temperature. These equations are based on Raman data in the range 0 to 60°; however, they give values in agreement with those obtained[7] from conductivity measurements of A. A. Noyes and co-workers up to 306°.) for these species *vs.* temperature were obtained from T. F. Young,[7] while the variation of the

(1) This paper is based upon work performed for the United States Atomic Energy Commission at the Oak Ridge National Laboratory operated by Union Carbide Corporation.

(2) M. H. Lietzke and R. W. Stoughton, THIS JOURNAL, **63**, 1183 (1959).

(3) M. H. Lietzke and R. W. Stoughton, *ibid.*, **63**, 1186 (1959).

(4) M. H. Lietzke and R. W. Stoughton, *ibid.*, **63**, 1188 (1959).

(5) M. H. Lietzke and R. W. Stoughton, *ibid.*, **63**, 1190 (1959).

(6) M. H. Lietzke and R. W. Stoughton, *ibid.*, **63**, 1984 (1959).

(7) T. F. Young, private communication; also T. F. Young, L. F. Maranville and H. M. Smith, "The Structure of Electroytic Solutions," Edited by W. J. Hamer, John Wiley and Sons, Inc., New York, N. Y., 1959, Chapter 6, pp. 35–63.

TABLE I

EQUATIONS FOR THE SOLUBILITY OF Ag_2SO_4 *vs.* TEMPERATURE

$$s = a + b(t - 25) + c(t - 25)^2 + d(t - 25)^3$$

Medium	*a*	*b*	*c*	*d*
0.1 *m* H_2SO_4	2.92×10^{-2}	7.1776×10^{-4}	-1.3662×10^{-6}	-1.5068×10^{-9}
0.5 *m* H_2SO_4	3.32×10^{-2}	3.9347×10^{-4}	1.2470×10^{-5}	-3.0062×10^{-8}
1.0 *m* H_2SO_4	3.47×10^{-2}	1.8596×10^{-4}	1.7047×10^{-5}	-2.2684×10^{-8}
0.1 *m* HNO_3	4.28×10^{-2}	7.0255×10^{-4}	-2.4271×10^{-6}	3.4621×10^{-9}
0.5 *m* HNO_3	7.86×10^{-2}	9.4984×10^{-4}	9.7508×10^{-6}	-2.9565×10^{-8}
1.0 *m* HNO_3	1.08×10^{-1}	1.6819×10^{-3}	5.5406×10^{-6}	5.7552×10^{-9}

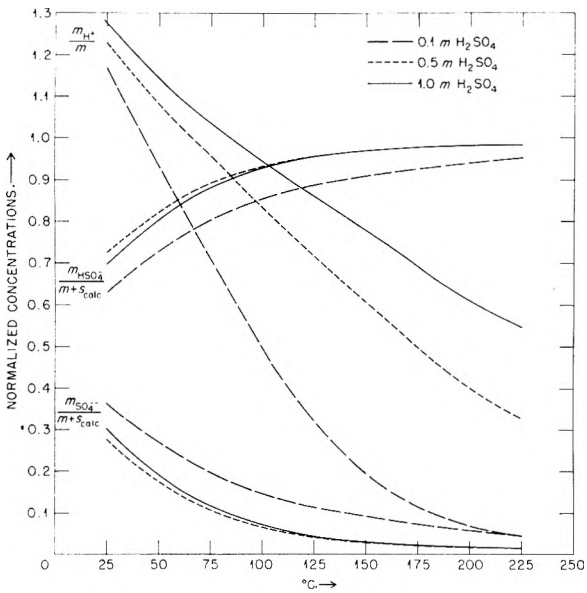

Fig. 1.—Normalized concentrations *vs.* temperature in 0.1, 0.5 and 1.0 *m* H_2SO_4 media.

acid quotients with ionic strength were assumed to be given by single parameter Debye–Hückel equations.[4,5] A high speed digital computer was used in all cases in determining the best values for the various Debye–Hückel parameters and in calculating the concentrations of the various species in the acidic media. The purpose of this paper is to present the concentrations of species present in the HNO_3 and H_2SO_4 media and the heats and entropies of solution of silver sulfate *vs.* temperature.

Calculations and Discussion

Species in H_2SO_4 Solutions.—In the H_2SO_4 solutions the calculated solubilities[4] were determined by considering the equilibria

$$Ag_2SO_4 = 2Ag^+ + SO_4^{--} \qquad (1)$$

and

$$HSO_4^- = H^+ + SO_4^{--} \qquad (2)$$

and the solubilities were calculated by determining the concentrations of all species present and the ionic strength by successive approximation. The experimental solubility s_0 for Ag_2SO_4 in pure water may be represented as a function of centigrade temperature *t* by using equation 3 or 3a; while the solubility in 0.1, 0.5 and 1.0 *m* H_2SO_4 is given by the cubic equations whose coefficients are shown in Table I.

$$s_0 = 1.7260 \times 10^{-2} + 4.3344 \times 10^{-4}t - 1.6898 \times 10^{-6}t^2 \qquad (3)$$

$$= 1.65535 \times 10^{-2} + 4.45825 \times 10^{-4}t - 1.76083 \times 10^{-6}t^2 + 1.54066 \times 10^{-10}t^3 \qquad (3a)$$

The equations in Table I fit the experimental data to within about 2% to 225°. Either equation 3 or 3a shows agreement to within about 2% to 250°. All the equations indicated in Table I were determined from the experimental data by the method of least squares. In Fig. 1 is shown a plot of the calculated normalized concentrations: $m_{HSO_4^-}/(m + s_{calc})$ the fraction of total sulfate in the form HSO_4^-; $m_{SO_4^{--}}/(m + s_{calc})$ the fraction of total sulfate in the form of SO_4^{--}; and m_{H^+}/m, the ratio of H^+ to the molality of H_2SO_4. Here *m* is the molality of H_2SO_4 and s_{calc} is the calculated molal solubility of Ag_2SO_4 (which is close to the observed value). A plot of these relative or normalized concentrations is easier to read than one showing the actual concentrations themselves. Using the equations whose parameters are given in Table I and the curves in Fig. 1, the concentrations of any assumed species in 0.1, 0.5 or 1.0 *m* H_2SO_4 may be calculated.

As expected from the decrease in HSO_4^- acid constant with temperature, the concentrations of H^+ and SO_4^{--} decrease, and that of HSO_4^- increases with increasing temperature in all cases.

Species in HNO_3 Solutions.—In HNO_3 solutions an additional equilibrium over those shown in expressions 1 and 2 must be taken into account

$$HNO_3 = H^+ + NO_3^- \qquad (4)$$

The concentrations of all species present were calculated on the basis of the equilibria 1, 2 and 4. The solubilities in 0.1, 0.5 and 1.0 *m* HNO_3 may be represented as a function of temperature by using the coefficients in Table I. In Fig. 2 are shown the calculated relative concentrations $m_{HSO_4^-}/s_{calc}$, the fraction of total sulfate in the form of HSO_4^-; $m_{SO_4^{--}}/s_{calc}$, the fraction of total sulfate in the form of SO_4^{--}; and m_{H^+}/m, the ratio of H^+ to total nitric acid, all as a function of temperature for 0.1, 0.5 or 1.0 *m* HNO_3. The ionic concentrations of HSO_4^-, SO_4^{--} and H^+ can be obtained as in the previous case by using Table I and values read from the curve in Fig. 2.

As expected, the concentrations of H^+ and SO_4^{--} show a general decrease and that of HSO_4^- an increase with increasing temperature. Table II shows the calculated per cent. of HNO_3 undissociated *vs.* molality *m* and temperature. The concentration of NO_3^- is nearly equal to the molality *m* of HNO_3, being lower by about 6% in the worst case (*i.e.*, 200° and *m* = 1.0); the actual values may be obtained from the percentages of undissociated HNO_3 shown in Table II.

Heats and Entropies of Solution.—At each 25° interval from 25 to 200°, values of log K_s (the molality solubility product) for each of the five

TABLE II

PERCENTAGES OF HNO_3 UNDISSOCIATED *vs.* MOLALITY AND TEMPERATURE

m_{HNO_3}	t(°C.) 25	50	100	150	200
0.1	0.14	0.18	0.23	0.25	0.25
0.5	0.44	0.64	1.37	2.30	3.02
1.0	0.63	1.00	2.20	4.01	5.78

media studied were plotted against the square root of the ionic strength. In Fig. 3 the plots for 25, 100 and 200° are shown. It can be seen that the curves deviate from the Debye-Hückel limiting law at the higher temperatures in a manner similar to that at room temperature, except that all the curves are steeper at the higher temperatures, as expected from the increase in slope shown by the limiting law. In the case of each supporting electrolyte, and at each 25° interval, the value of log K_s^0 (the activity product) was calculated by using the Debye-Hückel expression and the value of the single parameter showing best fit at the lowest concentration of the supporting electrolyte studied.[2-6] At 25°, data do not exist for the K_2SO_4 media. Values of log K_s^0 at 25° were averaged for HNO_3, H_2SO_4 and $MgSO_4$ media. At all other temperatures values obtained for K_2SO_4 media were included in the average. Since the KNO_3 data were the most difficult to obtain experimentally[2] and hence felt to be the least reliable, the corresponding log K_s^0 values were not included in the averaging.

The extrapolated values of log K_s^0 in H_2SO_4, HNO_3 and $MgSO_4$ media were all within ±0.006 of a log unit of the average −4.835 at 25°. The log K_s^0 for the KNO_3 was higher in algebraic value by 0.103 of a log unit. Both of these deviations increased steadily with temperature so that at 200° the maximum deviation of the values for K_2SO_4, H_2SO_4, HNO_3 and $MgSO_4$ media from the average was within ±0.030 of a log unit; the log K_s^0 value for KNO_3 was algebraically 0.195 of a log unit higher. The average log K_s^0 (excluding the KNO_3 values) was fitted between 25 and 200° to the following quadratic equation by the method of least squares.

$$T \log K_s^0 = -3008.01 + 12.0635T - 0.0228473T^2 \quad (5)$$

Using the usual thermodynamic equation

$$\left(\frac{\partial \frac{\Delta F^0}{T}}{\partial T}\right)_P = -\frac{\Delta H^0}{T^2} \quad (6)$$

and the equation

$$\Delta F^0 = -RT \ln K_s^0 \quad (7)$$

the enthalpy change when one mole of solid Ag_2SO_4 dissolves into the standard solution becomes

$$\Delta H^0 = 2.30259RT^2 \left(\frac{\partial \log K_s^0}{\partial T}\right)_P \quad (8)$$

where R is the molal gas constant; T is the absolute temperature and the term in parentheses may be obtained by taking the derivative of equation 5.

The corresponding enthalpy change when one mole of solid Ag_2SO_4 dissolves into the (nearly) saturated solution in water becomes[8]

(8) I. M. Klotz, "Chemical Thermodynamics," Prentice-Hall, New York, N. Y., 1950, p. 333.

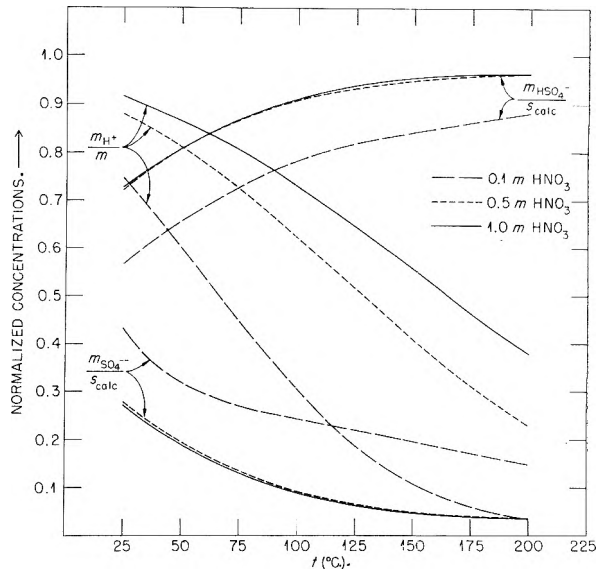

Fig. 2.—Normalized concentrations *vs.* temperature in 0.1, 0.5 and 1.0 *m* HNO_3 media.

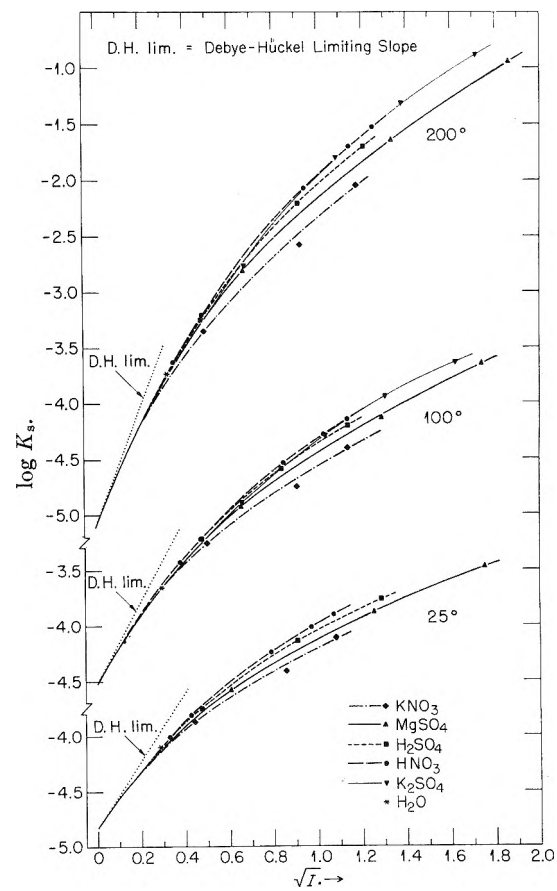

Fig. 3.—Log K_s *vs.* square root of ionic strength at 25, 100 and 200° in various electrolyte media.

$$\Delta H_{sat} = \nu RT^2 \left(\frac{\partial s_0}{\partial T}\right)_{sat} \left[\left(\frac{\partial \ln \gamma_\pm}{\partial s_0}\right)_T + \left(\frac{1}{s_0}\right)_{sat}\right] \quad (9)$$

Here ν is the assumed number of solute species per mole of Ag_2SO_4 dissolved (3 in this case), s_0 is the solubility of Ag_2SO_4 in water and $\gamma\pm$ is the mean ionic activity coefficient of Ag_2SO_4. As seen in the previous papers[2-6] ln $\gamma\pm$ in the absence of a sup-

porting electrolyte may be expressed as a one-parameter Debye–Hückel equation

$$\ln \gamma_{\pm} = -\frac{2s_T\sqrt{3s_0}}{1 + A_s\sqrt{3s_0}} \qquad (10)$$

where s_T is the limiting Debye–Hückel slope for a univalent ion at any temperature. The best value for A_s appears to be about 0.70 for the desired conditions.

On taking the derivative of (10)

$$\left(\frac{\partial \ln \gamma_{\pm}}{\partial s_0}\right)_T = \frac{-3s_T}{1 + A_s\sqrt{3s_0}}\left[\frac{1}{\sqrt{3s_0}} - \frac{A_s}{1 + A_s\sqrt{3s_0}}\right] \qquad (11)$$

where the value of s_0 between 25 and 200° is given to within about ±2% by either equation 3 or 3a.

Using equations 9, 11 and 3, or 3a, values of ΔH_{sat} may be determined; equation 3a was used in obtaining the values given in Table III.

The standard entropy change when solid Ag_2SO_4 dissolves into the standard solution may be calculated using equations 7 and 8 since

$$T\,\Delta S^0 = \Delta H^0 - \Delta F^0 \qquad (12)$$

The entropy change when the solid dissolves into the (nearly) saturated solutions ΔS_{sat} is equal to $\Delta H_{sat}/T$ since $\Delta F_{sat} = 0$.

The standard partial molal entropy of Ag_2SO_4 $\bar{S}^0$ may be determined by adding to ΔS^0 at any temperature the entropy of the solid Ag_2SO_4 S_s^0. The latter was calculated as a function of temperature using the 25° value 47.9 ± 0.2 e.u. and the equation for the heat capacity *vs.* temperature both given in Kelley's compilation[9]

$$S_s^0 = 47.9 + 23.1 \ln \frac{T}{298.16} + 0.0279(T - 298.16)$$

The values calculated for the various thermodynamic functions *vs.* temperature are given in Table III. The values given have not been corrected to one atmosphere pressure although the corrections should be relatively small. Using the three density values for dilute Ag_2SO_4 solutions at 15 and 25° given in the International Critical Tables an average apparent molal volume of about 30 ml. was obtained. On the assumption that this value is equal to the partial molal volume at infinite dilution and at 200° an estimate can be made for correcting (from the highest pressure of 15 atmospheres water vapor) to one atmosphere to get the ΔF^0 value. This estimation indicates a correction of only about 10 cal. in 10,000. The corrections in the other quantities should also be small.

The value of 40.8 e.u. for $\bar{S}^0$ at 25° may be compared with 39.44 e.u. obtained by adding up the ionic entropies (of 2 Ag^+ and SO_4^{--}) using Latimer's Tables.[10] The 32.4 e.u. at 100° is close to a value of about 33 ± 1 e.u. estimated by Cobble[11] from his 100° compilation of ionic entropies.

(9) K. K. Kelley, Bulletin 476, U. S. Dept. of the Interior, Bureau of Mines, U. S. Government Printing Office, Washington, D. C., 1949.

TABLE III

VALUES OF THERMODYNAMIC FUNCTIONS FOR Ag_2SO_4 *vs.* TEMPERATURE

(ΔH values are in kcal.; entropy values are in e.u.)

t	log K_s^0	ΔH^0	ΔH_{sat}	ΔS^0	ΔS_{sat}	$\bar{S}^0$
25	−4.835	4.47	5.49	− 7.14	18.40	40.8
50	−4.622	2.85	3.60	−12.37	11.13	38.1
75	−4.538	1.09	2.34	−17.60	6.71	35.3
100	−4.531	−0.79	1.26	−22.82	3.38	32.4
125	−4.591	−2.81	0.17	−28.05	0.44	29.3
150	−4.705	−4.96	−1.07	−33.28	− 2.52	26.2
175	−4.877	−7.23	−2.65	−38.50	− 5.92	23.0
200	−5.113	−9.64	−4.93	−43.73	−10.42	19.7

The value of log K_s^0 is negative and changes relatively little with temperature; hence the value of $\overline{\Delta F^0}$ is always positive and increases approximately proportionally with T. Both ΔH^0 and ΔS^0 decrease with temperature, both showing relatively large negative values at 200°. Since the entropies of both pure water[9,12] and the solid S_s^0 increase with temperature, the behavior of ΔS^0 indicates that the presence of the solute increases the amount of "structure" shown by the solvent at any temperature and that this effect is much greater the higher the temperature. The fact that the partial molal entropy $\bar{S}^0$ decreases appreciably with temperature indicates that the solute may be producing even more structure in the solution at the higher temperatures than exists at 25°. It is interesting to note that the sum $\bar{S}^0$ plus the entropy of two moles of water[10,12] is nearly constant (74.3 ± 0.3 e.u.) from 25 to 100° and that the sum $\bar{S}^0$ plus the entropy of three moles of water is nearly constant (95.7 ± 0.7 e.u.) from 100 to 200°.

According to the work of R. J. Raridon and K. A. Kraus[13] the ΔH^0 for solution of AgCl is nearly constant from room temperature to about 200°. This indicates that ΔC_p^0 is nearly zero in this range and hence that ΔS^0 for solution of AgCl changes little with temperature. It would thus appear that the sulfate ion is largely responsible for the decrease in the ΔS^0 for Ag_2SO_4 with temperature.

Acknowledgments.—The authors wish to thank Drs. G. Scatchard, K. A. Kraus and J. W. Cobble for interesting discussions concerning this work.

(10) W. M. Latimer, "Oxidation Potentials," Second Edition, Prentice–Hall, New York, N. Y., 1952, pp. 72 and 190.

(11) J. W. Cobble, private communication.

(12) N. S. Osborne, H. F. Stimson and E. F. Fiock, *J. Research Natl. Bur. Standards*, **5**, 411 (1930); N. S. Osborne, H. F. Stimson and D. C. Ginnings, *ibid.*, **18**, 389 (1937).

(13) R. J. Raridon, Ph.D. Thesis, Vanderbilt University, (January 1959).

A BALANCED ISOPIESTIC APPARATUS. APPLICATION TO $CeCd_{\sim 6}$ SOLID SOLUTION SYSTEMS[1,2]

BY GUY R. B. ELLIOTT AND JOE F. LEMONS

Contribution from the University of California, Los Alamos Scientific Laboratory, Los Alamos, New Mexico

Received August 25, 1959

An apparatus is described for determining the vapor pressure of a volatile component in solution in non-volatile components over a range of compositions and temperatures. By coupling an analytical balance with an isopiestic equilibrator operating in a temperature gradient and suspended in a freely pivoting position, it is possible to measure the solution composition and deduce the vapor pressure of the volatile component from a knowledge of the vapor pressure of the pure component as a function of temperature. By changing the temperature in small increments it is possible also to change solution compositions in small increments and to measure the variation of thermodynamic activity with these very small changes of composition. The vapor pressure is reported for cadmium over solid solutions of cerium and cadmium of various compositions in the region $CeCd_{\sim 6}$ at 847 and 912°K. At 847°K. measurements of eight compositions between the phase region limits of approximately $CeCd_{6.093}$ and $CeCd_{5.967}$ show that the cadmium vapor pressure changes gradually with composition across the phase. At 912°K. the phase limits are approximately $CeCd_{6.118}$ and $CeCd_{5.971}$; measurements at nineteen compositions within this range show a trend in cadmium vapor pressure similar to that observed at 847°K. Uncertainty in assignment of exact compositions rests principally on starting material impurities rather than on uncertainties of the method. Some possible models to explain the change in cadmium activity with composition in solid $CeCd_{\sim 6}$ are discussed. A very good fit to the experimental data is achieved with a model which assumes perfect solution in a $CeCd_6$ lattice of cadmium atoms in defect sites and of cadmium atoms surrounding cerium holes. Heats and entropies of reactions between standard states representing species within the phase are calculated. As operated the balance readily detected a shift of one part in three million of the suspended weight.

Introduction

A program has been undertaken to study factors influencing the solubility of metals in each other. For this work a method was sought for measuring metal activities which would allow accurate and unambiguous calculation from relatively simple measurements on a large number of compositions. These requirements were met by an isopiestic apparatus, operating with a volatile and a non-volatile metal, suspended in a furnace arrangement and attached to a balance. The furnaces provide suitable temperature gradients and the balance records changes in weight resulting from the distillation of the volatile metal; thus it is possible to calculate alloy compositions at different stages of distillation.

The principle of coupling a balance with an isopiestic equilibrator has been tested by Seith and Krauss[3] who, however, did not achieve highly sensitive balance performance. As demonstrated by Hargreaves,[4] the dew-point approach was more successful and much of the later isopiestic work followed this procedure. Recently, Herasymenko,[5] Trumbore[6] and Rosenthal and co-workers[7] have very successfully equilibrated a pure volatile metal with an alloy of that metal at a higher temperature.

In this study cerium was chosen as the non-volatile metal. It is planned that alloys of several lanthanide and actinide elements will be studied in the hope that their great similarity will permit the isolation of some of the factors involved in metal solubility.

Zinc was considered for the volatile metal because it had been shown to dissolve actinides into regular solution (log solubility is a constant times the reciprocal temperature).[8] However, cadmium was chosen because its volatility is higher than that of zinc. It was found that solutions of cerium in cadmium were nearly perfect in a limited region tested.

The compound $CeCd_6$ has been identified and X-rayed but its structure was not worked out.[9]

Theory

For an isolated system under isothermal conditions the components of a solution will be in dynamic equilibrium with the vapor and each possible gaseous species will exhibit a partial pressure characteristic of the solution at that temperature. If one component of the solution is appreciably volatile while the other components, or possible compounds, are negligibly volatile the vapor will consist of essentially pure volatile component. If a portion of the container in contact with such a pure gas phase is maintained at a lower temperature, the volatile component will distil from the solution and condense on the wall. The process will continue until the vapor pressure decrease of the volatile component due to alloying compensates for the vapor pressure decrease due to cooling, both relative to the pure volatile component at the higher temperature. (A limitation is discussed below.) If one knows the solution and pure volatile component temperatures, the alloy composition, and from independent measurements the vapor pressure of the pure volatile component as a function of temperature, then he can calculate the vapor pressure and closely approximate the thermodynamic activity of the volatile component in the alloy. For a particular solution temperature and a particular temperature for the condensed volatile species a specific alloy will always be formed.

The design of the present equipment avoids the

(1) This work was performed under the auspices of the Atomic Energy Commission.

(2) Presented in part at the 134th National Meeting of the American Chemical Society, Chicago, 1958.

(3) W. Seith and W. Krauss, *Z. Elektrochem.*, **44**, 98 (1938).

(4) R. Hargreaves, *J. Inst. Metals*, **64**, 115 (1939).

(5) P. Herasymenko, *Acta Met.*, **4**, 1 (1956).

(6) F. A. Trumbore, "Method for the Determination of Vapor Pressures over Liquidus and Solidus Alloys. Vapor Pressure of Arsenic over Germanium-Arsenic Alloys," 128th National Meeting of the American Chemical Society, Minneapolis, Minn., 1955.

(7) F. D. Rosenthal, G. J. Mills and F. J. Dunkerly, *Trans. AIME*, 153 (April 1958).

(8) G. R. B. Elliott, H. M. Feder, R. U. Sweezer, unpublished data.

(9) A. Iandelli and R. Ferro, *Gazz. chim. ital.*, **84**, 463 (1954).

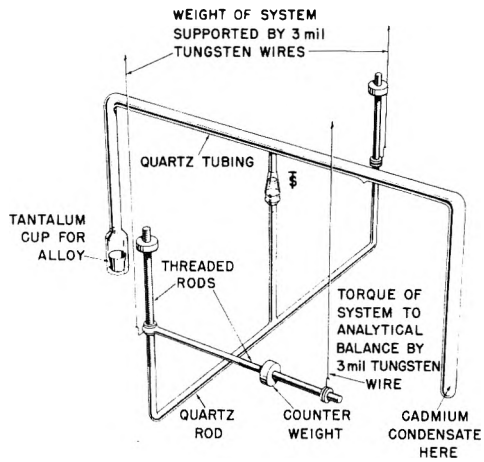

Fig. 1.—The suspension system used to measure the cerium–cadmium alloy composition after cadmium evaporation and condensation had taken place.

problem of a gas pressure difference resulting from the temperature difference. As has been pointed out,[10] if the pressure is too low or if a capillary tube in a temperature gradient connects the alloy and cadmium regions, a pressure difference may exist due to thermal transpiration. The pressure nonuniformity may exist under such conditions because then the viscous flow of the gas due to a pressure difference may not override the thermal transpiration which reflects the different velocities of the gas at the two temperatures.

The problem of thermal transpiration is discussed by Dushman[11] who presents experimental data[12] on hydrogen. Kennard[13] presents theoretical equations for calculation of the pressure difference. An extrapolation of the hydrogen data with estimated corrections for the different properties of cadmium gas makes it appear unquestionable that at pressures providing a practical mass transfer rate necessary for the measurements the pressure difference between the alloy and cadmium regions will be insignificant.

Experimental

Apparatus.—The apparatus consists of three main parts: an isopiestic equilibrator, a suspension and balance system and an arrangement of furnaces with their regulating equipment. The first two parts are indicated schematically in Fig. 1 and are described below.

Isopiestic Equilibrator.—The isopiestic equilibrator is an evacuated and sealed quartz tube consisting of two vertical legs joined at their tops to a horizontal section. Projecting down from the center of the horizontal section is a closed standard taper joint which serves only as a mechanical connector with which to attach the equilibrator to the suspension and balance system. Since quartz is not attacked by cadmium under the experimental conditions, one vertical leg is an adequate container for condensed cadmium; however, it is necessary to contain the cerium in a tantalum cup in the other leg of the quartz tube.

The following tube sizes are commonly used for the equilibrator: cadmium leg, 10 mm. o.d.; horizontal tube and part of alloy leg, 12 mm. o.d.; region of tantalum cup for alloy, 16 mm. o.d. (dimpled to make the cup fit more closely). The legs are 22 cm. long and the horizontal bar 45 cm. The tantalum cup is 25 mm. long by 13.5 mm. diameter. These tube and cup diameters represent a practical compromise with respect to preserving a reasonable volume for cadmium and alloy with fairly rapid vapor transfer, minimizing air bouyancy complications and concentrating the alloy and cadmium in slim columns of short length at a given lever arm distance from a fulcrum. The lengths are convenient for furnace construction.

The quartz equilibrator and tantalum crucible, *in situ*, are outgassed by flaming to red heat and evacuating through a side arm. The vacuum is broken with argon and the equilibrator is disconnected from the vacuum system to allow clean and accurately weighed cerium ($\sim$ 0.88 g.) and cadmium ($\sim$ 4.6 g.) to be introduced through the arm. Finally the equilibrator is evacuated and the arm sealed off (the remaining tip shows on Fig. 1).

A final feature not shown in Fig. 1 is the incorporation of small cups centered above each leg of the equilibrator into which weights may be placed to facilitate calibration of the equipment.

Suspension and Balance System.—The suspension system (Fig. 1), the principal parts of which are mounted in a plane perpendicular to the equilibrator, is constructed of 8 mm. quartz rod terminating in threaded (6–32) brass rods attached with epoxy resin. The horizontal rod is 70 cm. long and the combination vertical arms are 25 cm. long. Hooks fastened by adjustable nuts to the vertical rods are in turn attached to two 3-mil tungsten support wires rigidly attached to vibration damped supports. A horizontal rod parallel to the plane of the equilibrator holds a third hook which is attached to a 3-mil tungsten wire suspended from an analytical balance arm by the balance stirrup. Each of the three threaded rods supports a threaded adjustable counterweight.

The balance is the chain adjustable, magnetic damped type modified by drilling a hole through the base to accommodate the support wire. The balance is vibration damped and positioned so that the plane of the balance arm and the support wire is parallel to the plane of the two fixed support wires.

The support rod hooks and counterweights must be adjusted so that the center of mass of the suspension-equilibrator system lies on a line joining the wire-hook contact points on the vertical threaded rods. The counterweight of the horizontal threaded rod is used to balance the system. All supports must be adjusted so that the three support wires are nearly parallel; otherwise the balance may be too unstable or too insensitive to permit final sensitivity adjustment at the balance sensitivity bob. In any case the balance must be used as a null instrument, since a variable system sensitivity as the balance swings is inherent in this type of suspension.

Furnaces and their Regulation.—Three different temperature regions have to be controlled during a run: First, the alloy must be maintained at some temperature around 900°K.; second, the cadmium condensation leg must be maintained a few tenths to fifty or so degrees lower; finally, all other portions of the equilibrator must be at least a few degrees hotter than the cadmium leg. Rapid variation of the temperature should be minimized at the ends of the equilibrator legs; however, some drift can be tolerated if the temperature difference between the legs remains nearly constant or if the drift is slow enough for maintenance of essential equilibrium between alloy and pure cadmium in the equilibrator.

The above requirements suggested smoothing temperatures with a large capacity heat sink. Around each leg of the equilibrator there is a series of three copper pipes and discs making nesting cups with about a half centimeter air space between. The outer pipes are 15 cm. o.d. and 25 cm. long; the inner-most pipes are 5 cm. i.d. and 15 cm. long; the discs are 2.5 cm. thick. Since the copper is a much better conductor than the air space, each inner ring is of more uniform temperature than the one outside it, and the inner hot zone is of uniform temperature throughout. Furthermore, the high heat capacity of the copper smooths temperature fluctuations caused by controller drift in the heating element circuit.

Heat is supplied to the outer copper pipes by commercial resistance heaters which have relatively non-inductive coil windings. These heaters are roughly regulated by variable autotransformers, and the fine control is provided by elec-

(10) L. Brewer, private communication.

(11) S. Dushman, "Scientific Foundations of Vacuum Technique," Section 1–12, John Wiley and Sons, Inc., New York, N. Y., 1949.

(12) F. C. Tompkins and D. W. Wheeler, *Trans. Faraday Soc.*, **29**, 1248 (1933).

(13) E. H. Kennard, "Kinetic Theory of Gases," Sections 39, 186 and 187, McGraw-Hill Book Co., New York, N. Y., 1938.

tronic controllers regulating, on-off, about 15% of the power. The controllers are operated from several dry cells connected in parallel to reduce drift.

A third commercial element which is controlled only by a variable autotransformer maintains the bulk of the equilibrator at a temperature hotter than the legs.

The signal to the electronic controllers is from platinum–platinum 10% rhodium thermocouples placed between a heater and its copper block; each thermocouple is protected to within one centimeter of its tip from a.c. pickup by a grounded shield. Further pickup protection is provided by a filtering circuit through a 50 microfarad condenser to ground. Finally, the outer copper blocks are also grounded.

Two types of control thermocouple signal are used: The potential of the thermocouple for the alloy leg is fed as a direct signal, the junction in the controller being temperature compensated. The cadmium leg temperature is controlled by a differential couple with the reference junction buried in the furnace insulation at a steady temperature region reflecting the alloy temperature.

In measuring the actual alloy and cadmium temperatures, a precise knowledge of the temperature difference is more important than a precise knowledge of the absolute temperature because the alloy activity varies rapidly with composition but slowly with alloy temperature. The platinum–platinum 10% rhodium thermocouples are read on a Rubicon Type B potentiometer to 1 microvolt for absolute temperature and to about 0.2 microvolt for differential temperatures. The couples are within grounded shields where they are in the region of a.c. heaters and are themselves grounded at one potentiometer pole. Junctions of copper lead wires to thermocouples are electrically insulated from the ice-bath in which they are immersed.

A single wiring arrangement allows measurement of absolute or differential temperatures through three external lead wires. The differential portion of the couple is made from adjacent sections of the same spool of wire to ensure highly accurate temperature difference readings. Absolute temperatures are known to $\pm 1°$ from checks of the spoolwire against N.B.S. standards.

The furnace insulation is ordinary low temperature (1250°) firebrick except where more strength is required; then the harder intermediate temperature (1450°) brick is used. The furnace is designed to minimize convection by having the temperature gradient from the bottom to the top of the furnace and by having all openings in the insulation near the bottom so that the hot gasses are trapped by the closely packed insulation at the top of the furnace. (Essential elimination of convection is necessary both for temperature regulation and for smooth balance operation.)

Over-all dimensions of the firebrick insulation are 75 cm. wide, 90 cm. high, 110 cm. long. In this large mass channels are cut to accommodate the furnaces and the equilibrator-suspension system. The alloy and cadmium regions are separated from the hotter horizontal region of the equilibrator by insulating brick discs with small clearance holes to just pass the moving legs of the equilibrator.

Around the whole apparatus is placed a sealed cover to eliminate room breezes.

Materials.—Reagent grade cadmium was distilled, the first and last fractions being discarded. The purest cerium available from the Ames Laboratory, U. S. Atomic Energy Commission was provided through the courtesy of Dr. F. H. Spedding. Chemical analysis of the cerium showed: oxygen, 0.24–0.20%; nitrogen, 80 p.p.m.; tantalum, 340 p.p.m. Spectroscopic analysis showed no detectable impurities except: magnesium, 0.03%; calcium, 0.05%. The tantalum cups were produced by Mallory–Schwarzkopf Metals, Inc. of Austria and distributed by the Rembar Company, Dobbs Ferry, N. Y.; such crucibles show negligible attack after a run.

General Operation.—Preliminary direct calibration of the system is accomplished at room temperature by weighing a known load over one leg and then over the other leg of the equilibrator. However, a more accurate system calibration is obtained by observing directly the apparent change in weight resulting from the distillation of a known weight of cadmium. This is accomplished by first establishing the precise temperature conditions for obtaining a specific alloy composition. From preliminary observations on the system using the direct calibration a composition is selected such that only a very small amount of cadmium is moved from the alloy under the selected temperature conditions. Thus, even though the primary calibration is crude, the alloy composition can be established with precision. A second equilibrator containing a much larger amount of cadmium relative to cerium is then subjected to the same temperature conditions, and from the known transfer of cadmium when equilibrium has been established, the apparent change in weight can be evaluated and a calibration factor determined.

Apparent starting weight for the balance is originally obtained with the furnaces hot and with the temperature difference small enough so that cadmium cannot condense. In this way bouyancy and thermal expansion corrections are minimized. Original alloy composition is known from the weights of the cerium and cadmium charged.

The following key data are recorded (as well as corollary data on furnace control and time): (a) weight on balance to bring it to null position, (b) alloy furnace thermocouple reading, (c) differential thermocouple reading indicating the temperature difference between alloy and cadmium. These data may be combined with a calibration factor and a known apparent original weight to give the alloy composition corresponding to the measured alloy and cadmium temperatures.

Limits of a phase region, *e.g.*, $CeCd_{\sim 6}$, are determined by a dynamic process because it proves quite common that a given phase will supersaturate with respect to some of its components and will not easily nucleate to the thermodynamically more stable adjacent phases. In this procedure use is made of a mixture of adjacent phases prepared by temporarily adjusting the temperature differential so that the alloy is sufficiently enriched, or impoverished, with respect to cadmium to "force" the nucleation of the second phase. Such an alloy mixture in an equilibrator will gain weight if the cadmium temperature is high enough for the cadmium richer phase to be stable; correspondingly, it will lose weight if the cadmium temperature is too low for the richer phase to be stable; at a precisely correct temperature no tendency will exist for cadmium transfer to take place. This cadmium temperature at which the two phases coexist in equilibrium is also the temperature corresponding to the limit of the single phase region, and the pertinent composition can be established from a plot of alloy composition at a given temperature *versus* condensed cadmium temperature.

In practice, with this equipment it is not possible to attain a specific temperature with adequate precision or to maintain a temperature for a sufficient length of time to establish it as corresponding to a two phase region; therefore it is necessary to determine the equilibrium temperature by a dynamic, nonequilibrium process. The cadmium temperature at which vapor equilibrium exists with the alloy is established by starting with a two phase alloy composition from which cadmium is being continuously distilled as a result of the cadmium temperature being below the equilibrium value. The cadmium temperature is then allowed to drift slowly upward through the equilibrium value; as the temperature of the cadmium passes through the equilibrium value, cadmium begins to distil back into the alloy as a result of the cadmium-rich phase having been stabilized. The balance records such a change in the direction of distillation, and the equilibrium temperature is observed. The equilibrium temperature is also checked for conditions suitable to a downward drift in cadmium temperature, and the equilibrium temperatures are found to agree by the two approaches within 0.1°.

Performance.—The balance is stable while the furnaces are hot if the magnetic dampers are used. Sensitivity is ordinarily set at 0.2 mg., or one fourth the sensitivity normally used for an analytical balance; since movement of cadmium in the equilibrator results in removal of weight from one side and deposition on the other, the effective balance sensitivity is twice as great and the movement of 0.1 mg. of cadmium can be measured. (If large amounts of cadmium are moved during a run, the center of mass of the equilibrator suspension system may rise or fall and change the balance system sensitivity.) The balance arrest is normally only partially released so that balance movement is limited to ± 3 small divisions. Ordinarily the balance is not arrested during a run; however, arresting and subsequent release will not change a balance reading more than 0.1 mg.

Temperature drift because of changing controller or ambient conditions is a major source of difficulty. During the summer months the problem is worse as the laboratory

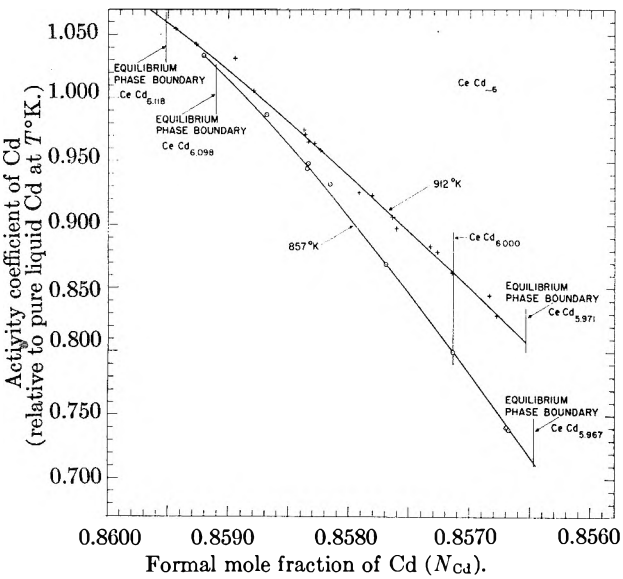

Fig. 2.—The variation of cadmium activity coefficient across the $CeCd_6$ phase.

switches from day-time cooling to night-time heating. Under such conditions the furnace temperatures will vary over roughly a degree range during a 24-hour period; the temperature difference is somewhat more stable varying in roughly a 0.3° range. The major difference between the 847°K. and the 912°K. readings reported under Results is that the former were taken most often at about 4 A.M. when there had been a long period of steady temperature (±0.03° in differential temperature) while the latter were taken at random periods after at least 8 hr. equilibration.

It appeared not to matter whether equilibrium was approached from a cadmium-rich or cadmium-lean alloy; the points of Fig. 2 represent roughly equal numbers of readings from each side scattered randomly throughout the series. This randomness was achieved deliberately in the larger changes of composition but unintentionally in the small changes of composition due to fluctuations in system temperature. Data were considered to represent an equilibrium measurement if the balance weight remained constant for a period of several hours while temperature conditions remained static.

In general, equilibrium was attained in less than 8 hr. if only a few milligrams of cadmium had to diffuse through the solid. On the other hand, it often requires a week to convert from one cerium–cadmium solid solution region to another.

Metallographic and X-ray crystallographic analyses also confirmed the fact that equilibrium could be established between the whole alloy specimen and the pure cadmium. A $CeCd_{6.00}$ specimen was prepared by gas phase reaction from the components and in the reactor tube which had been used for most of the vapor pressure measurements. The specimen showed only a single clean phase at 500× magnification. Lower magnification showed pipes and fractures in the specimen which were undoubtedly important to the rapid attainment of equilibrium observed. Presumably the pipes and fractures resulted from volume changes as one cerium–cadmium compound was converted to another.

The X-ray crystallographic studies were carried out on a composition $CeCd_{4.34}$ (actually the $CeCd_{\sim 4.5}$ phase) and showed the same crystal structure in a thin skull as in the bulk material in an alloy prepared by equilibration with pure cadmium at a lower temperature.

Results

The data are summarized in Table I. The cadmium activities are based on pure liquid at 847°K. or 912°K. as the standard states using the standard free energy equation of Kelley[14] for vaporization of liquid cadmium to obtain the pertinent vapor pressure data. The recorded activity is the ratio of the vapor pressure of the pure cadmium phase at the specified temperature to the corresponding vapor pressure of pure cadmium at the temperature of the alloy. The activity coefficient is obtained by dividing the activity by the mole fraction.

Rather than to plot the curve of activity of the cadmium *versus* mole fraction, we have chosen to plot the slope of that curve, namely the cadmium activity coefficient, against mole fraction. This latter type of plot may indicate a slight curvature which would be difficult to find in the former. The data are plotted in Fig. 2, and the curves are calculated as described later.

The measurements were taken with the alloy temperatures varying by no more than ±1.5°; the condensed cadmium temperatures ranged from 7.4 to 28.1° lower than the thermodynamically stable alloy for the approximately 847°K. measurements and 6.3 to 23.8° lower for the 912°K. alloy. The size of the circles and pluses in Fig. 2 corresponds to an uncertainty of ± 0.1°K. in the temperature difference between the alloy and the cadmium plus an uncertainty of ± 0.15 mg. in the weight change of the alloy because of cadmium condensation in the cooler leg.

It must be emphasized that we do not know the actual cadmium mole fractions corresponding to a given activity coefficient to as high an accuracy as the five significant figures plotted might indicate; these figures are carried only to show accurate *relative* values resulting from the measurement of small composition changes. Actually, uncertainties in the amount of impurities in the starting compositions and uncertainties in corrections to be applied for known impurities could change the fourth figure of the mole fractions by as much as 3 units.

Discussion

At both temperatures the cadmium activity coefficient relative to pure liquid cadmium varies continuously and smoothly with composition. This smooth variation of activity coefficient extends beyond the equilibrium phase limit as may be noted in one point on Fig. 2; several other such metastable superheated or undercooled equilibrium values were measured in preliminary work which cannot be precisely correlated with these later measurements.

Apparently no steric or bonding limits determine the phase boundaries; rather, the phase limits appear to be determined by competition between the possible phases for the cadmium atoms.

The phase region is narrow, varying by only 0.3% in cadmium mole fraction, and would probably be called a compound rather than a solid solution by those who make such distinction. The variation of activity with composition clearly has little relationship to the formal mole fraction since a 0.3% increase in cadmium mole fraction increases by over 40% the activity coefficient relative to pure liquid at 847°K.

Although it is admittedly difficult to establish

(14) K. K. Kelley, Contributions to the Data on Theoretical Metallurgy. III. The Free Energies of Vaporization and Vapor Pressures of Inorganic Substances. U. S. Bureau of Mines Bulletin 383 (1935). $\Delta F^0_{Cd(l) \rightarrow Cd(g)} = 26{,}110 + 4.97\ T \log T - 40.15T$.

TABLE I

TEMPERATURE–ACTIVITY COEFFICIENT DATA FOR $CeCd_{\sim 6}$ SOLID SOLUTION REGION

T_1[a]	$T_1 - T_2$[a]	Cd transferred[b]	Mole fraction of Cd[c]	Activity of Cd	Activity coefficient of Cd	Exptl. minus calcd. mole fraction
574.0	0.00	0.0000	0.87025			
573.9	26.00	.5135	.85668	0.63285[d]	0.73872	−0.00001
573.9	25.85	.5126	.85670	.63457	.74071	− .00002
574.1	21.56	.4980	.85714	.68572	.80001	.00000
574.3	16.88	.4792	.85770	.74553	.86922	− .00001
572.7	12.90	.4634	.85816	.79987	.93208	+ .00007
574.9	11.89	.4574	.85834	.81419	.94856	+ .00004
574.4	12.15	.4571	.85835	.81048	.94423	+ .00001
574.0	9.60	.4454	.85869	.84746	.98692	+ .00005
573.7	6.92	.4275	.85921	.88789	1.03338	.00000
					Av.	+ .00001
639.0	22.87	.5102	.85678	.70958	0.82819	− .00002
638.9	21.62	.5081	.85684	.72333	.84418	+ .00010
639.0	20.19	.4976	.85715	.73937	.86259	− .00001
639.5	18.93	.4938	.85727	.75372	.87921	+ .00006
638.9	18.62	.4915	.85733	.75745	.88350	+ .00005
639.9	17.58	.4821	.85761	.76946	.89721	− .00008
639.7	16.91	.4810	.85764	.77733	.90636	− .00001
639.9	15.67	.4755	.85781	.79212	.92342	+ .00002
639.4	15.49	.4718	.85792	.79422	.92575	− .00006
639.6	13.16	.4607	.85824	.82266	.95854	.00000
640.3	12.75	.4591	.85829	.82769	.96435	+ .00001
639.9	12.65	.4573	.85834	.82894	.96575	− .00002
639.8	12.26	.4564	.85837	.83387	.97146	+ .00002
639.3	12.26	.4564	.85837	.83387	.97146	+ .00002
639.7	12.02	.4559	.85838	.83686	.97493	+ .00005
639.3	9.93	.4416	.85880	.86351	1.00548	.00000
639.3	8.19	.4365	.85895	.86623	1.03176	+ .00019
639.3	7.44	.4254	.85927	.89614	1.04291	+ .00001
639.8	6.67	.4197	.85944	.90635	1.05458	.00000
					Av.	+ .00002

[a] T_1 is alloy temperature; T_2 is pure cadmium temperature. [b] Balance weight change times balance factor, 0.4757. [c] 0.8563 g. of Ce initially present. Correcting for 0.30% inert impurities (mostly oxide) gives 6.093×10^{-3} moles Ce. 4.6074 g. of Cd initially present (assumed pure). [d] The activity is known to four figures, but the fifth figure was used in calculations.

microscopic characteristics from macroscopic measurements, there seemed to be merit in examining various solid solution models to see if a model could be found which was both reasonable and consistent with the observed activity measurements. It may be noted (Fig. 2) that within experimental error the measurements at both temperatures of the activity coefficient–composition relationship lie on curves of decreasing radius of curvature as the cadmium concentration increases. No change of behavior occurs as the curve passes through the stoichiometric composition. The shape of the curves both at the ends and at the stoichiometric composition precludes the use of several of the more obvious simple models which might be considered to explain the data.

Further checking of the validity of an assumed model can be made thermodynamically by examining the interconsistency and magnitudes of the heats and entropies which can be derived from the mathematical formulation of the model.

It must be emphasized that we recognize there may be other models than the one selected in this paper which offer an equally satisfactory explanation for the observed data.

Models Considered.—Possibly the most obvious model one might consider would be a simple Henry's Law solution of excess cadmium in a parent lattice.[15] One might, as a first approximation, neglect the effect of cadmium in the parent lattice on the cadmium activity and assume the cadmium activity was proportional to the mole fraction of the excess cadmium. A variation of the activity coefficient of the excess cadmium could then account for the observed curvature.

This model is unsatisfactory in that the same change in cadmium activity would not be expected on removing a cadmium atom from a stoichiometric lattice as from adding an excess cadmium to the lattice. To avoid a discontinuity in the change of activity with composition near the stoichiometric parent compound, it would be necessary to choose a parent lattice not in the composition range of the experiments. Considering the narrow phase region, it would seem most unsatisfactory to choose a parent lattice other than $CeCd_6$.

A second obvious approach would be to consider

(15) That dilute solution laws may be applied to solid solutions has been demonstrated both theoretically and experimentally (a) C. D. Thurmond, THIS JOURNAL, **57**, 827 (1953), (b) C. D. Thurmond and J. D. Struthers, *ibid.*, **57**, 831 (1953).

the equilibria which must exist between the various types of lattice imperfections and the perfect lattice sites. In such a model the cadmium activity might be proportional to the mole fraction of a specific type of imperfection, *e.g.*, a "misplaced" cadmium atom. Shifting the composition from stoichiometric $CeCd_6$ by the addition or removal of cadmium atoms might be essentially equivalent to adding or removing some "misplaced" cadmium atoms; the attempted change of concentration of this species would result in a general shift of the various equilibria and the activity coefficient of the cadmium might vary smoothly through the parent composition.

This second model in its simplest form, namely that the activity is proportional to the mole fraction of "misplaced" cadmium atoms and that these "misplaced" atoms are involved significantly in only one equilibrium, may be used to approximate to a few parts in ten thousand the cadmium mole fraction corresponding to a specific activity coefficient. However, the model leads to a slightly reversed curvature from that obtained with the experimental data.

If it is assumed that the "misplaced" cadmium atoms can enter into another significant equilibrium in which six of the "misplaced" atoms can combine to reduce the concentration of "misplaced" atoms, then a curve can be calculated which reproduces the experimental points within a few parts in one hundred thousand in the observed mole fraction corresponding to a specific activity coefficient. This is within the apparent scatter of the data. Data showing the difference between experimentally observed and calculated values for the formal mole fraction of cadmium, N_{Cd}, are given in Table I. The calculated values are based on the equation

$$N_{Cd} = \frac{a^6K_IK_{II}K_{III}^6 + 5K_I - 4aK_IK_{III} + 6aK_{III} - 5a^2K_{III}^2}{-a^7K_{II}K_{III}^7 + 6K_I - 5aK_IK_{III} + 7aK_{III} - 6a^2K_{III}^2}$$

where N_{Cd} is the formal mole fraction of cadmium; a is the corresponding activity; and the K's represent equilibrium quotients which have values as follows: at 847°K. $K_I = 0.0162000$, $K_{II} = 800.000$, $K_{III} = 0.157810$; at 912°K. $K_I = 0.0425000$, $K_{II} = 75.0000$, $K_{III} = 0.221240$. The elements of the equation will be developed in the following section.

Although the choice of specifically six "misplaced" cadmium atoms reacting together was based on chemical or structural rather than mathematical reasoning, it seems necessary to assume a rather large power mathematical dependence on the non-stoichiometric excess cadmium concentration to account for the observed decreasing radii of curvature in Fig. 2. (Assigning the curvature to a change in the activity coefficient of the excess cadmium atoms is not satisfying because one would expect the activity coefficient to stay constant or rise rather than to drop as the most readily available sites were filled first during the departure of the alloy from stoichiometric $CeCd_6$.)

The possibility of interaction of several "misplaced" atoms to form clusters limits the type of defect these "misplaced" atoms can represent. They probably could not represent the atoms around a cerium or cadmium hole since six such atoms could hardly react further together. Neither could they represent crystal surface atoms for then the crystal size would influence the activity. They could represent either cadmium atoms in interstitial positions or in cerium holes or some other defect not considered. We choose to speak of interstitial cadmium atoms from entropy considerations which will be developed later. Also it seems plausible that the sixth power shift of the curves in Fig. 2 represents the agglomeration of six cadmium atoms to form a cerium hole while extending the basic lattice.

In more common terms the model is thought of as primarily Frenkel cadmium defects in the equilibrium stoichiometric lattice. Also present are smaller numbers of Shottky cerium defects. The terminology is not applicable with non-stoichiometric lattices.

Some theoretical[16] and experimental[17] treatments of intraphase equilibria have been presented. The problem of solute molecules being able either to enter interstitial positions or to extend the basic lattice has been treated with regard to dissolving copper in germanium.[18]

Assumptions for Calculation of Curves through the Experimental Data.—In order to calculate the curves of Figure 2 assignments of possible species and associated equilibria were made as follows:

First, it was assumed that the basic structure, $CeCd_6$, was in equilibrium with imperfect sites containing cadmium holes resulting from the loss of one cadmium atom (designated $CeCd_5$) and with interstitial (or otherwise especially reactive) cadmium atoms, Cd*. This equilibrium may be expressed in the usual form

$$K_I = \frac{(\mathfrak{N}_{CeCd_5})(\mathfrak{N}_{Cd^*})}{\mathfrak{N}_{CeCd_6}} \qquad \begin{aligned} K_{I\ 847°K} &= 0.0162 \pm 0.005 \\ K_{I\ 912°K} &= 0.0425 \pm 0.012 \end{aligned}$$

The exact meaning of the mole fraction $\mathfrak{N}$ and the basis for the assignment of the values of the equilibrium constants K_I are discussed later; activity coefficients of the species are taken as unity.

Second, an equilibrium was assumed in which the interstitial cadmium atoms react to form clusters of cadmium, Cd_6, which extend the basic lattice while creating cerium vacancies.

$$K_{II} = \frac{\mathfrak{N}_{Cd_6}}{(\mathfrak{N}_{Cd^*})^6} \qquad \begin{aligned} K_{II\ 847°K} &= 800 \pm 30 \\ K_{II\ 912°K} &= 75 \pm ? \end{aligned}$$

Finally, it was assumed that the observed cadmium activity was proportional to the concentration of interstitial cadmium atoms.

$$K_{III} = \frac{\mathfrak{N}_{Cd^*}}{a_{Cd}} \qquad \begin{aligned} K_{III\ 847°K} &= 0.15781 \\ K_{III\ 912°K} &= 0.22124 \end{aligned}$$

In this paper some of the symbols for mole fraction are carried in script to indicate that an unusual "mole fraction" is implied. As is custom-

(16) For example, see (a) C. Wagner, "Thermodynamics of Alloys," Addison-Wesley, Boston, Mass., 1952, p. 54; and (b) F. A. Kroger and H. J. Vink, "Solid State Physics," Vol. 3, Editors F. Seitz and D. Turnbull, Academic Press, New York, N. Y., 1956, p. 329.

(17) H. Reiss, C. S. Fuller and F. J. Morin, *The Bell System Tech. J.*, XXXV, 535 (1956) and M. W. Davies and F. D. Richardson, *Trans. Faraday Soc.*, **55**, 604 (1959).

(18) (a) F. Van der Maesen and J. A. Brenkman, *J. Electrochem. Soc.*, **102**, 229 (1955); (b) F. C. Frank and D. Turnbull, *Phys. Rev.*, **104**, 617 (1956).

ary the "mole fraction" is the ratio of "moles" of the substance in question to the total "moles" present. But the total moles present are considered to be made up of the sum of the moles of perfect $CeCd_6$ sites, the moles of $CeCd_5$ sites, the moles of interstitial cadmium atoms and the moles of cadmium clusters (or Cd_6 sites in which a cerium atom is missing).

Method of Obtaining Curves and their Numerical Values.—The curves of Fig. 2 were established by testing different combinations of K values as defined in the preceding section until a fit to the data was obtained. The slope of the curve is determined primarily by K_I. As mentioned earlier the application of K_{II} can eliminate the sag of the curve obtained from K_I and K_{III} alone and can create a bulge with decreasing radius of curvature at higher cadmium mole fractions. Changing K_{III} will move the curve up or down almost bodily with only minor changes in slope and curvature. The uncertainties associated with the K values were established by a rather liberal estimate of what values of K might be considered to fit the data obtained.

TABLE II

COROLLARY THERMODYNAMICS DERIVED FROM THE SELECTED EQUILIBRIUM CONSTANTS

	Primary reactions assumed	Heat contents and entropies $\Delta H_{880°K.}$ kcal./mole	$\Delta S_{880°K.}$, cal./deg. mole
I	Formation of Cd holes and interstitials in $CeCd_6$ lattice[a]		
	$CeCd_6 = CeCd_6 + Cd^*$	22.5	18.4
II	Formation of Ce holes from interstitial cadmium atoms[a]		
	$6Cd^* = Cd_6$	−55.3	−52.1
	Corollary reactions implied		
III	Creation of Ce and Cd holes in lattice[a]		
	$6CeCd_6 = 6CeCd_5 + Cd_6$		
	(Based on I and II)	79.9	58.6
IV	Cd removed from $CeCd_6$ and placed at surface[b]		
	lattice = lattice + $CeCd_6$		
	(Apportioned from III assuming Cd hole has R ln 6 more entropy and 4 kcal. less heat of formation that Ce hole)	10.8	8.9
	(Recommended value)[c]	9 ± 2.5	9 ± 2
V	Ce removed from $CeCd_6$ and placed at surface[b]		
	lattice = lattice + Cd_6		
	(As in IV)	14.8	5.3
	(Recommended value)[c]	13 ± 2.5	55 ± 2
VI	Cd from $CeCd_6$ surface placed in interstitial position[b]		
	lattice = lattice + Cd*		
	(Based on I and IV)	11.7	9.6
	(Recommended value)	13 ± 2.5	9.5 ± 2
VII	Cd from $CeCd_6$ surface placed in gas[b]		
	lattice = lattice + Cd(g)		
	(Estd. from Cd data[19] and assuming Cd is bound by 0.7 kcal. more and has 6/7 R ln 7/6 more entropy in $CeCd_6$)	26.0	25.2
VIII	Cadmium interstitial to gas[a]		
	$Cd^* = Cd(g)$		
	(Based on VI and VII)	14.3	15.6
	(Based on $\mathfrak{N}_{Cd^*}$ and VII)	11.2	
	(Based on $\mathfrak{N}_{Cd^*}$ and obsd. Cd pressure)	10.3	
	(Based on estimate of crystal vol. available to interstitial and neglecting other interactions)	(14 to 17)	
	(Recommended value)[c]	12 ± 2.5	15.5 ± 2

[a] All gaseous species at hypothetical 1 atmosphere, all condensed phase species at hypothetical mole fraction of 1. [b] Infinite surface, holes or interstitials at hypothetical mole fraction of 1. [c] The recommended values are intermediate between the extreme values calculated by various paths as in reaction VIII. The uncertainties have no formal mathematical basis but are believed to include the true value for the process indicated.

Corollary Conclusions Based on the Assumed Model.—The equilibrium constants imply an intraphase thermodynamics. Four reference states for the cadmium have been chosen with perfect solution being assumed throughout: first, the hypothetical pure $CeCd_6$; second and third, solute standard states corresponding to infinite dilution for interstitial cadmium atoms and for cadmium clusters surrounding cerium holes; fourth, the gaseous standard state of unit activity at one atmosphere pressure. In Table II various postulated reactions are described, and calculated values are given for the heat content and entropy values associated with them as derived from the equilibrium constants. (See "Assumptions for calculation of curves.")

For reaction I in which both a hole and a cadmium interstitial are formed, a heat of 22.5 kcal./mole and an entropy of 18.4 cal./deg. mole were found. These values are probably within a kilocalorie and an entropy unit of the true values, assuming the model is correct. For the agglomeration of six interstitial cadmium atoms to one cerium hole (reaction II) a heat and entropy of −55.3 kcal./mole and −52.1 cal./deg.-mole were found; these values are perhaps within three or four kilocalories or entropy units of the correct values.

The following heats and entropies associated with forming a mole of the species in an infinite lattice are consistent with the data and other estimated values and appear reasonable: cadmium hole, about 9 kcal. and 9 e.u.; cadmium interstitial, about 13 kcal. and 9.5 e.u.; cerium holes, about 13 kcal. and 5.5 e.u. It can be seen in Table II how these values were deduced. The interconsistency of the experimental and estimated data is shown by the fairly good agreement resulting from the calculation of the heat of vaporization of interstitial cadmium atoms by four different paths.

Comparison of the Conclusions with Other Work.—We know of no other work against which the conclusions from the assumptions can be directly checked. However, various aspects can be compared with situations in other systems which seem to be similar.

Number of Lattice Imperfections.—The number of holes implied, approximately 2.0 and 3.4% of the atoms, respectively, at 847 and 912°K. (Table III) is large but is comparable with extrapolated values from other work. For example with 30% zinc in silver a heat of formation of vacancies of about 11.8 kcal./mole has been reported.[20] The mole fraction of vacancies formed at 673°K. but estimated to be "frozen in" at 573°K. is reported to be

(19) L. Brewer, "National Nuclear Energy Series IV-19B, Chemistry and Metallurgy of Miscellaneous Materials: Thermodynamics," Editor, L. L. Quill, McGraw-Hill Book Co., New York, N. Y., 1950.

(20) A. S. Nowick and R. J. Sladek, *Acta Met.*, **1**, 131 (1953).

5×10^{-4}. This value may be extrapolated to 912°K. to yield an anticipated 2.5% vacancies. (However, these removed atoms apparently went to extend the lattice rather than to interstitial sites as presumably did the cadmium atoms.)

TABLE III

EXAMPLES OF THE NUMBERS OF DEFECTS IN THE $CeCd_{\sim 6}$ LATTICE AS DERIVED FROM POSTULATED EQUILIBRIA

Composition	Temp., °K. Alloy	Temp., °K. Cadmium	Mole fraction: Interstitial atoms	Mole fraction: Cerium holes	% dislocated atoms
$CeCd_{6.000}$	847	825.4	$\mathfrak{N}_{Cd^*} = 0.10821$	$\mathfrak{N}_{Cd_6} = 0.00128$	1.96
	912	891.7	.16357	.00144	3.37
$CeCd_{6.101}$	847	840.7	.14005	.00603	
	912	903.7	.19718	.00441	

The likelihood that an appreciable number of interstitial atoms is present may be inferred from the rapid attainment of gas–solid equilibrium experimentally observed in the cerium–cadmium system. Such rapid diffusion would accompany the low activation energy for motion of an interstitial.[21]

Neither the high temperature structure of $CeCd_6$ nor its detailed low temperature structure plus expansion with temperature have been worked out. It would be of interest to know this information to see how much room is available for interstitial atoms. Earlier work[9] which identified the compound did not establish its structure. (This work did establish the structures of $CeCd_2$ and $CeCd_{11}$.)

Recently Mr. F. H. Ellinger of this Laboratory has indexed an X-ray diffraction powder pattern of $CeCd_{6.00}$ which we had prepared by gas phase reaction. The compound has a primitive cubic unit cell with $a = 15.783 \pm 0.001$ Å. Based on the volume of the cubes surrounding an elemental cerium or an elemental cadmium atom, Mr. Ellinger finds room for 24.10 $CeCd_6$ formula units in the $CeCd_6$ unit cell; similar calculations based on $CeCd_2$ and $CeCd_{11}$ yield 24.18 formula units per unit cell. The presence of 24 $CeCd_6$ units per unit cell seems probable with an X-ray density of 8.255 grams per cubic centimeter.[22] The most one can say about interstitials is that there appears to be extra room in the crystal even at room temperature.

Thermodynamic Quantities.—There is no work on closely related systems with which the heats and entropies may be checked. However, in some cases other systems have given similar results. The heat of formation of a hole in 30% zinc–70% silver is 11.8 kcal./mole[20]; we find about 9 kcal. for a cadmium hole and about 13 kcal. for a cerium hole. By comparison with hole mechanism self-diffusion in sodium, the heat of activation for cadmium self-diffusion has been estimated as 25.3 kcal./mole.[23,24] Measurements indicate that the values are 18.2 or 19.1 kcal.[25] depending on whether diffusion is parallel or perpendicular to the hexagonal axis. The fair agreement with the prediction and the analogy with the zinc diffusion pointed out by the authors[25] suggests that cadmium diffusion is truly by a hole mechanism. Since the heat of formation of a hole is normally one third to two thirds of its heat of activation for diffusion one would predict 6 to 13 kcal. for the heat of formation of a hole in cadmium and a little more for a cadmium hole in $CeCd_{\sim 6}$ where we find about 9 kcal./mole.

Osipov calculates a quantity "q" which he considers to be the activation energy for sites of "local melting." The calculations involve the heat of fusion of the element, its absolute entropy and its melting temperature. For cadmium the value is 6.112 kcal./mole.[26] He is able to calculate values for other metals which reproduce the measured values reported to be the heats of formation of vacancies as determined by techniques used for our reported values in the previous paragraph. He feels that neither technique *necessarily* yields the heat of formation of a vacancy.[27]

The heats of formation for interstitial atoms have been calculated in the range at least from over 100 kcal./mole for a copper interstitial[28] to less than 3 kcal. for sodium crowdions.[29] It is of interest to note that Huntington[25] did not consider 18 or 19 kcal. for the energy of activation for cadmium diffusion to be out of the range of feasibility for an interstitial mechanism. Our value for the heat of formation of a cadmium interstitial in $CeCd_{\sim 6}$ is about 13 kcal.; normally the heat of formation of an interstitial is only slightly less than the heat of activation for diffusion so the two evaluations are in the same general range.

An entropy of 3 to 10 cal./deg. mole for the formation of holes in 30% zinc–70% silver may be calculated from reported data[20] assuming that the holes were "frozen-in" between the equilibrium temperature and 200 degrees lower. We find about 9 e.u. for the cadmium hole and about 5.5 e.u. for the cerium hole. The entropy of formation of a defect seems unlikely to be larger than the entropy of activation for diffusion by that process. Activation entropies for vacancy diffusion in eight cubic metals have been calculated with results in the range of 6 to 15 e.u.[30] Entropies of activation for sodium diffusion have been reported as 7.3 e.u. by a vacancy mechanism and 10.9 e.u. by an interstitial mechanism.[31] Our value for the entropy of formation of a cadmium interstitial is about 9.5 e.u.

Acknowledgments.—The authors much appreciate their very stimulating discussions with other members of the Los Alamos Scientific Laboratory staff, particularly those with Drs. T. W. Newton and C. E. Holley. They also are very grateful to Professors Leo Brewer of the University of California and Norman Nachtrieb of the University of

(21) See discussion of interstitial mobility, *e.g.*, "Vacancies and Other Point Defects in Metals and Alloys," Paper 1781 by A. H. Cottrell, The Institute of Metals, London, 1958, p. 7.

(22) F. H. Ellinger, private communication.

(23) N. H. Nachtrieb, "The Effects of High Pressure on the Rates of Atom Movements in Crystals," ASTIA document No. 86594 (April 30, 1956).

(24) N. H. Nachtrieb and G. S. Handler, *Acta Met.*, **2**, 797 (1954).

(25) E. S. Wajda, G. A. Shirn and H. B. Huntington, *ibid.*, **3**, 39 (1955).

(26) K. A. Osipov, *Doklady Akad. Nauk, USSR*, **121**, 637 (1958).

(27) K. A. Osipov, *ibid.*, **121**, 855 (1958).

(28) H. B. Huntington, *Phys. Rev.*, **91**, 1097 (1953).

(29) H. Paneth, *ibid.*, **80**, 708 (1950).

(30) A. D. LeClaire, *Acta Met.*, **1**, 442 (1953).

(31) N. H. Nachtrieb, E. Catalano and J. A. Weil, *J. Chem. Phys.*, **20**, 1185 (1952).

Chicago who examined an earlier version of this manuscript and offered very important suggestions for its improvement. Mr. Fred Hutchison was of much assistance in helping to design modifications of balances while the weighing technique was being developed. Mr. J. T. Simmons specially modified some of our controllers to yield closer temperature control.

THE DISSOCIATION PRESSURE OF RUTHENIUM TRICHLORIDE[1]

BY W. E. BELL, M. C. GARRISON AND ULRICH MERTEN

John Jay Hopkins Laboratory for Pure and Applied Science, General Atomic Division of General Dynamics Corporation, San Diego, California

Received August 28, 1959

The dissociation pressure of $RuCl_3$ was measured over the range 650 to 839°. From the slope of the log P *versus* $1/T$ line and an estimated ΔC_p of 4.5 cal./mole °K., $\Delta H^0_{1020°K.} = -57.2 \pm 1.0$ kcal./mole and $\Delta H^0_{298} = -60.5 \pm 2.0$ kcal./mole for $Ru(s) + 3/2Cl_2(g) = RuCl_3(s)$. S^0_{298}, $RuCl_3(s)$ is calculated to be 30.5 e.u., and the dissociation pressure is calculated to be 1 atm. at 853°. No other ruthenium chlorides appear to exist as stable condensed phases in the temperature range investigated under chlorine pressures up to 1 atm.

Introduction

The dissociation pressure of $RuCl_3$ has been determined over the temperature range 650 to 839° by a static and a dynamic method. This work was undertaken because previously reported dissociation pressure data for $RuCl_3$ appeared inadequate. Wohler and Balz[2] reported data over the range 450 to 752°; however, their data on a plot of log P_{Cl_2} *versus* $1/T$ are scattered and show considerable curvature. Remy and Kohn[3] reported data over a small temperature range—689 to 841°. Their data are somewhat scattered and do not agree with the data of Wohler and Balz.

Experimental

Static Method.—The apparatus for the static method consisted essentially of a dead-end reaction tube connected through a small sulfuric acid manometer to a chlorine supply and mercury manometer. Pulverized ruthenium sponge was placed in the reaction tube and brought to about 700° under vacuum. Chlorine gas was introduced to 1 atm. pressure. (During evacuation and introduction of chlorine, the sulfuric acid manometer was pivoted to take the acid into a side arm.) When the reaction tube reached temperature and when 20 to 50% of the metal had been converted to $RuCl_3$, as indicated by a decrease in chlorine pressure, dissociation pressures were measured by balancing the external chlorine pressure with the pressure in the reaction tube. The sulfuric acid manometer indicated when the external and internal pressures were equal. Absorption and evolution of chlorine were observed, respectively, when the external pressure was 1 to 2 mm. above and below the internal pressure. Several measurements were made at each temperature and averaged. The dissociation pressure was taken to be the reading on the mercury manometer, corrected for the pressure across the sulfuric acid manometer and for the pressure of the ruthenium-containing vapor species.[4] In all cases, the gaseous chloride contribution was less than 10% of the observed dissociation pressure.

Dynamic Method.—Dissociation pressures were measured dynamically by the transpiration method. Ruthenium metal was placed in the reaction tube and heated under vacuum to about 700°. Chlorine was then admitted into the system to form $RuCl_3$. At temperature, argon was allowed to flow through the reaction tube at a rate of about 2 to 4 ml. STP (Cl_2 + A)/min.; this was shown by flow-rate studies to be low enough to assure equilibrium conditions in the reaction tube. According to calculations[5] made with an argon–chlorine interdiffusion coefficient estimated by methods outlined by Reid and Sherwood,[6] diffusion effects are negligible in this experiment at flow rates greater than ~ 0.4 cm.^{3} STP/min. The effluent chlorine gas was collected in KI solution and was determined volumetrically, using standard thiosulfate solution. The argon was collected in inverted volumetric flasks, with the sample collectors being changed after each 25 or 50 ml. argon throughput. The chlorine partial pressure was calculated from the quantities of argon and chlorine collected.

Figure 1 shows typical behavior for the chlorine partial pressure as a function of argon throughput. The chlorine partial pressure decreased until the dissociation pressure was reached; at this point a plateau was obtained. After decomposition of the $RuCl_3$, the chlorine partial pressure again decreased. The plateaus obtained were not quite horizontal, probably as a result of a small temperature gradient in the reaction tube. The dissociation pressure at each temperature was taken to be the average of the values on the plateau.

Materials.—Pulverized ruthenium sponge (99.995% purity, Johnson Matthey) was employed. The chlorine gas (99.85% min. purity, Matheson Co.) flowed through a sulfuric acid bubbler and P_2O_5 powder before it entered the reaction tube. The argon gas (99.998% min. purity, Matheson Co.) flowed through P_2O_5, hot copper gauze and a sulfuric acid bubbler.

General.—The stopcocks were lubricated with Kel-F grease. The corrosive action of chlorine gas on the mercury manometer was retarded by a layer of sulfuric acid on top of the mercury. The reaction tubes were Vycor.

Auxiliary heaters were added at each end of the tube furnace employed to minimize temperature gradients in the furnace. The main winding of the furnace was controlled by a Weston–Putmo time-proportioning controller, and the auxiliary heaters were separately controlled by two West type-J controllers. With this arrangement the temperature of the reaction tube was steady to within ±0.5°. Temperatures were measured with one Pt, Pt–10% Rh and with four chromel–alumel thermocouples in conjunction with a Rubicon potentiometer. These measurement thermocouples were located at intervals in a tube mounted alongside the reaction tube. The thermocouples were calibrated against a standard Pt, Pt–10% Rh thermocouple certified by the National Bureau of Standards.

Results

The dissociation pressure data are summarized in Table I, and estimated uncertainties for the pressure values are given. Temperatures are believed to be accurate to ±2°. The data give a straight-line relationship between log P and $1/T$

(1) This work was supported in part by the U. S. Atomic Energy Commission under Contract AT(04-3)164.

(2) L. Wohler and P. Balz, *Z. anorg. allgem. Chem.*, **137**, 411 (1924).

(3) H. Remy and M. Kohn, *ibid.*, **137**, 365 (1924).

(4) W. E. Bell, M. C. Garrison and U. Merten, to be published.

(5) U. Merten, *ibid.*, **63**, 443 (1959).

(6) R. C. Reid and T. K. Sherwood, "The Properties of Liquids and Gases," McGraw–Hill Book Co., Inc., New York, N. Y., 1958, pp. 266–277.

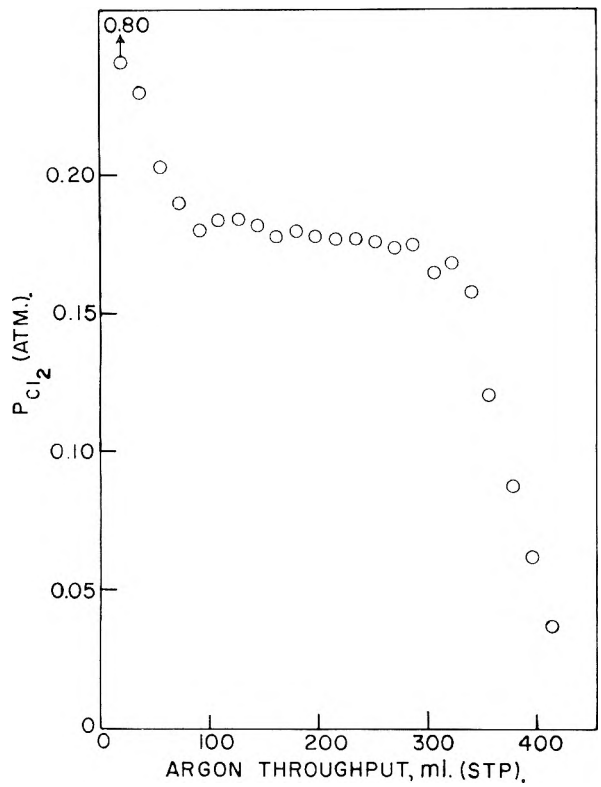

Fig. 1.—Chlorine partial pressure as a function of argon throughput at 750°.

within experimental error. From the slope of this line, we calculate at the mean temperature of the measurements (1020°K.)

$$\Delta H^0_{1020} = -57.2 \pm 1.0 \text{ kcal./mole}$$

and from this

$$\Delta S^0_{1020} = \frac{\Delta H^0}{T} - 3/2\ R \ln P = -50.9 \pm 1.0 \text{ e.u.}$$

for the reaction

$$\text{Ru(s)} + 3/2\text{Cl}_2\text{(g)} = \text{RuCl}_3\text{(s)} \qquad (1)$$

The dissociation pressure is calculated to be 1 atm. at 853°.

Table I

Chlorine Pressures in Equilibrium with $RuCl_3$(s) and Ru(s) at Various Temperatures

Method	T (°C.)	P_{Cl_2} (atm.)
Dynamic	650	0.023 ± 0.001
Static	661	.032 ± .001
Static	691	.057 ± .002
Dynamic	700	.069 ± .002
Static	722	.112 ± .004
Static	748	.172 ± .007
Static	748	.182 ± .007
Dynamic	750	.178 ± .004
Static	779	.308 ± .010
Dynamic	800	.442 ± .008
Static	820	.615 ± .015
Static	839	.801 ± .020

Crystals taken from the reaction tube after quenching showed a chlorine content, as determined gravimetrically by hydrogen reduction, within 1% of the theoretical value for $RuCl_3$. In the transpiration experiments at 750 and 800°, where the decomposition reaction was carried to completion, only one pressure plateau was observed. This suggests that $RuCl_3$ is the only stable, solid chloride of ruthenium in the temperature range and pressure range investigated; this indication was confirmed by X-ray diffraction examination of samples that contained less than 3 moles of Cl per mole of Ru and which were annealed for several hours at 700° and quenched. These samples showed only diffraction lines for Ru (metal) and $RuCl_3$. In agreement with the results of Stroganov and Ovchinnikov,[7] we found the black form of $RuCl_3$ to be isomorphous with the violet form of $CrCl_3$.

Discussion

From a rough rule given by Kubaschewski and Evans,[8] we estimate that ΔC_p for reaction 1 is about 4.5 cal./mole °K., and assuming it to be constant over the range 298 to 1020°K., we calculate

$$\Delta H^0_{298} = -60.5 \pm 2.0 \text{ kcal./mole}$$
$$\Delta S^0_{298} = -56.4 \pm 2.0 \text{ e.u.}$$
$$\log P_{Cl_2} = -\frac{9005}{T} - 1.510 \log T + 12.61$$

The uncertainties given for ΔH^0_{298} and ΔS^0_{298} are based on an estimated uncertainty of ±1.0 cal./mole °K. for ΔC_p and on the experimental uncertainties given previously for ΔH^0_{1020} and ΔS^0_{1020}.

Combining ΔS^0_{298} with standard entropies, S^0_{298} (Ru) = 6.9 ± 0.5 e.u. and $S^0_{298}(Cl_2)$ = 53.3 ± 0.02 e.u., given by Kelley,[9] we obtain S^0_{298} $RuCl_3$(s) = 30.5 ± 2.5 e.u. This may be compared with the value 38.0 ± 5.0 e.u. estimated by Brewer, *et al.*,[10] and with the value 33.2 e.u. estimated by Latimer's rules.[11]

The $RuCl_3$ present in the hot zone of the reaction tube was in all cases the black form; however, both the black and the brown forms described by Hill and Beamish[12] were observed in the condenser. As was previously mentioned, the black form of $RuCl_3$ is isomorphous with the violet form of $CrCl_3$, and it is interesting to note that Doerner[13] found the standard entropy for $CrCl_3$ to be 31.0 e.u., a value almost identical with the standard entropy for $RuCl_3$ found in this work.

The results of Remy and Kohn,[3] after correction for the ruthenium–chloride vapor contribution,[4] agree fairly well with our results. The results of Wohler and Balz[2] on a plot of log P_{Cl_2} *versus* $1/T$ show considerable curvature even after correction is made for the vapor contribution and are not in agreement with the present work.

Acknowledgments.—The authors are indebted to Dr. L. J. Dykstra and Mr. J. M. Dixon for performing the X-ray analyses.

(7) E. V. Stroganov and K. V. Ovchinnikov, *Vestnik Leningrad Univ.*, **12**, No. 22, Ser. Fiz. i Khim., No. 4, 152 (1957).

(8) O. Kubaschewski and E. L. Evans, "Metallurgical Thermochemistry," 3d ed., Pergamon Press, New York, N. Y., 1958, p. 187.

(9) K. K. Kelley, Bull. U. S. Bur. Mines, No. 477, 1950.

(10) L. Brewer, *et al.*, in "The Chemistry and Metallurgy of Miscellaneous Materials: Thermodynamics," National Nuclear Energy Series, Div. IV, Vol. 19B, McGraw–Hill Book Co., Inc., New York, N. Y., 1950, pp. 76–192.

(11) W. M. Latimer, *J. Am. Chem. Soc.*, **73**, 1480 (1951).

(12) M. A. Hill and F. E. Beamish, *ibid.*, **72**, 4855 (1950).

(13) H. A. Doerner, Bur. of M. Tech., Paper 577, 1937.

THE ADSORPTION OF HYDROXYL IONS FROM AQUEOUS SOLUTION ON THE SURFACE OF AMORPHOUS SILICA

BY W. M. HESTON, JR., R. K. ILER AND G. W. SEARS, JR.

Contribution from Industrial and Biochemicals Department, E. I. du Pont de Nemours & Co., Inc., Experimental Station, Wilmington, Delaware

Received September 10, 1959

The number of hydroxyl ions adsorbed per unit area of surface of amorphous silica from a solution of sodium hydroxide increases with *p*H and also with the concentration of sodium ions in solution within the concentration ranges studied. It is shown that the adsorption of hydroxyl ions per unit of surface area is essentially independent of the specific surface area of the silica. The total adsorption capacity of the surface of silica for hydroxyl ions has never been previously measured, because it is not possible to saturate the surface of silica with hydroxyl ions in a solution of sodium hydroxide alone due to the dissolution of silica above about *p*H 10.7. However, in a strong solution of sodium chloride, the adsorption of alkali continues to *p*H 12 without dissolution of silica, and the surface can be saturated. Thus, for the first time it has been possible to demonstrate that the adsorption capacity is about 3.5 hydroxyl ions per square millimicron.

While it is known that the surface of amorphous silica in water is negatively charged in neutral and alkaline aqueous solutions, the relation between charge per unit area and *p*H was not studied quantitatively, until Bolt[1] measured the relationship between charge density, electrolyte concentration and *p*H. However, there still remains the question as to whether the adsorption of hydroxyl ions per unit area of surface varies with specific surface area or particle size in the absence of salt. Furthermore, the maximum adsorption capacity of the surface for alkali has not been determined.

In this paper, further data are combined with that of Bolt to present an over-all picture of the adsorption of hydroxyl ions on the surface of silica, independent of particle size and expressed as the fraction of the maximum possible number of OH^- ions which can be adsorbed per unit of surface area.

Bolt[1] measured the effect of Na^+ ion concentration on adsorption of OH^- ions by changing the alkalinity and the salt (NaCl) content of a sol and measuring the *p*H. However, in sols relatively free of salt, containing only NaOH as the added electrolyte, it is more difficult to relate OH^- ion adsorption to total Na^+ ion concentration. In the present work, it was possible to study this relationship by adding NaOH to salt-free sols of different particle sizes and concentrations and show that the adsorption of OH^- ions was affected by the concentration of Na^+ counterions in the same way as when these were present as NaCl.

Extending a method developed by Sears,[2] in which the adsorption of OH^- ions was measured in a concentrated solution of sodium chloride, it was found possible to measure the maximum adsorption capacity of the silica surface for OH^- ions. With this figure, all the adsorption data can be expressed as the fraction of the adsorption sites occupied by OH^- ions.

Experimental

Preparation of Silica.—Sol A (10 mμ particles) was prepared by passing a dilute solution of sodium silicate containing 3% SiO_2 and having an SiO_2:Na_2O ratio of 3.25:1.0 through the hydrogen form of an ion-exchange resin ("Nalcite" HCR), adding alkali to adjust the ratio to 90:1, and concentrating the sol by evaporation at 100° until the silica concentration was 13.0%.[3]

Sol B (20 mμ particles) was prepared by a process differing from that for Sol A, in that in the evaporation process only one-tenth of the alkali-stabilized dilute sol was placed in the evaporator and the remainder was added slowly as evaporation proceeded, so that the volume of sol in the evaporator increased to somewhat less than twofold its original volume.[4] These sols were characterized by methods already described[5] and deionized by passage through a mixture of anion- and cation-exchange resins.[6] They were diluted to yield samples which were alkalized by adding different quantities of 4.78 *N* NaOH. The water and alkali solutions were maintained free from CO_2. These samples were stored in stoppered polythene bottles.

To determine the specific surface area of the silica in Sols A and B, a sample of each of the deionized materials was concentrated by evaporation of water at 60° until a gel formed, the hydrogel was broken up and washed with acetone and dried at 140° under moderate vacuum. The surface area was determined by nitrogen adsorption. The silica of Sol A had a specific surface area of 318 sq. meters per gram; that of Sol B, 149 sq. meters per gram.

The *p*H of the diluted and alkalized samples was measured within one hour after preparation. Subsequent *p*H measurements were made after one week, but in many cases the value had dropped. In the samples containing least silica and most alkali, it was calculated that a considerable portion of the silica particles could have passed into solution as sodium silicate. Only the *p*H data on freshly alkalized sols were employed in this study. Even here, it is to be expected that minor contamination with sodium silicate occurred in the more alkaline samples. The *p*H measurements were made with alkali-resistant, Type E-2 glass electrodes at 25°, using a Beckman Model G *p*H meter.

The data reported here must be considered to be only approximately correct because of the complications in measuring *p*H in colloid systems. As shown by Bolt,[1] the potentiometric measurements in concentrated sols involving a concentrated KCl junction (*e.g.*, *p*H measurement) should be corrected for junction potentials of unknown magnitude. This junction potential arises as a result of the unequal diffusion of K and Cl ions in a colloid system, which contains regions of high electric potential; the corresponding difference in *p*H between a sol and its dialysate is referred to in the literature as the suspension effect. The magnitude of this junction potential is determined by the nature of the colloid, the sol concentration, and the concentration of neutral electrolyte in the system, and approaches zero for infinite dilution of the sol. However, our *p*H data, uncorrected for the suspension effect, are reproducible and therefore significant for the purposes of this investigation.

Calculations

In Table I, the composition of the sol samples is indicated by the data in the first five columns. The equivalents of hydroxyl ions adsorbed on the silica surface per liter of water (a_s), is obtained by

(1) G. H. Bolt, THIS JOURNAL, **61**, 1166 (1957).

(2) G. W. Sears, Jr., *Anal. Chem.*, **28**, 1981 (1956).

(3) P. G. Bird, U. S. Patent 2,244,325 (National Aluminate Co., 1941).

(4) M. F. Bechtold and O. E. Snyder, U. S. Patent 2,574,902 (E. I. du Pont de Nemours & Co., Inc., 1951).

(5) G. B. Alexander and R. K. Iler, THIS JOURNAL, **57**, 932 (1953).

(6) J. M. Rule, U. S. Patent 2,577,485 (E. I. du Pont de Nemours & Co., Inc., 1951).

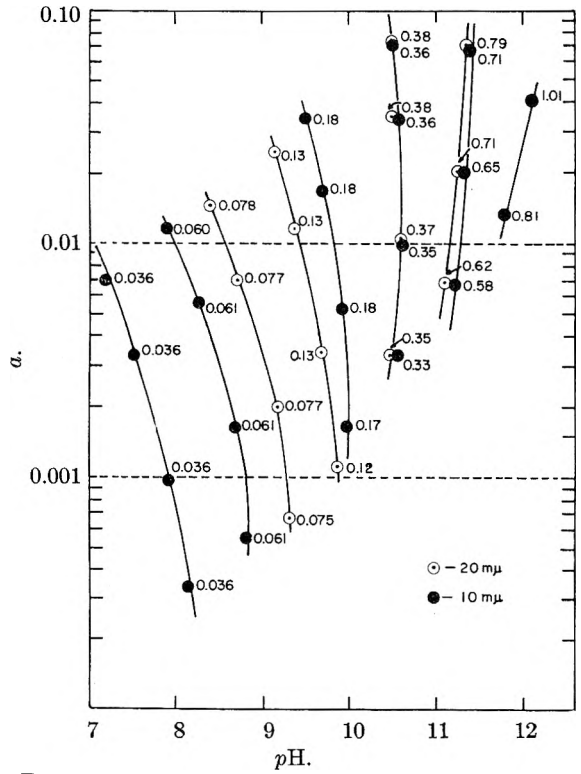

Fig. 1.—Relation between alkali concentration a and pH at nearly constant f. Each line represents a series of dilutions of a given sol. Figures indicate values of f.

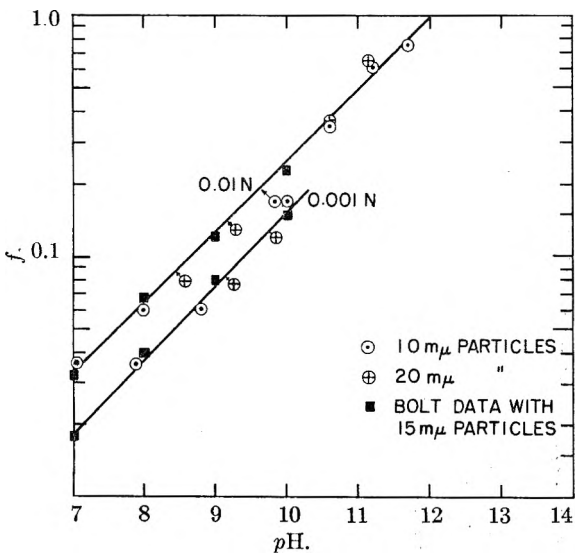

Fig. 2.—Relation between f and pH at constant sodium ion concentration, based on values interpolated from Fig. 1.

subtracting the concentration of free OH^- ions (h), estimated from pH, from (a), the total amount of base in the system.

The concentration of base (a) is expressed as equivalents per liter of water (more precisely, water and electrolytes, excluding colloid) in the system. The volume of water (W) per 100 ml. of sol is expressed by the empirical formula

$$W = 100 - 0.438C$$

where C is the concentration of silica in grams per 100 ml.

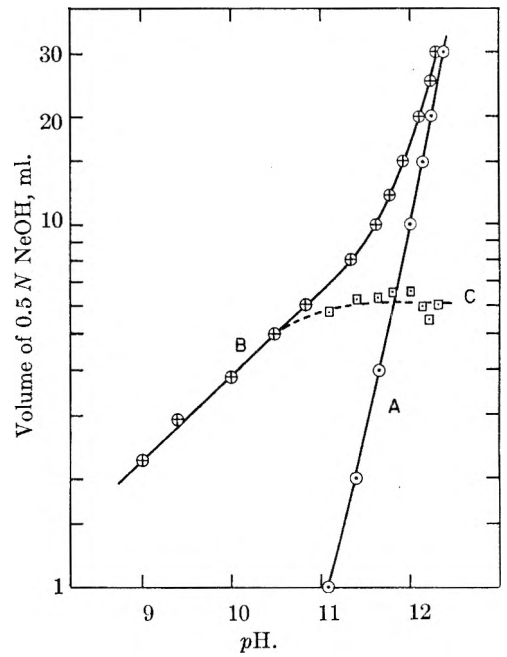

Fig. 3.—Titration of the surface of silica in a concentrated salt solution: line A, titration of NaCl solution, 30 g./150 ml.; line B, titration of silica sol in NaCl solution—1.5 g. SiO_2, 342 m.²/g., and 30 g. NaCl/150 ml.; line C, difference between line B and A.

The initial silica surface (S) expressed as square meters per liter of water in the system, is calculated from

$$S = \frac{10^3 CA}{W}$$

where A is the specific surface area of the silica in m.²/g.

The fraction of surface sites occupied by adsorbed OH^- ions (f) is calculated on the basis that there are 3.5 sites per square millimicron, or 0.58×10^{-5} equivalents per square meter. Whence

$$f = \frac{a_s}{0.58 \times 10^{-5} S} = 1.72 \times 10^5 \frac{a_s}{S} = 172 \times \frac{W}{C} \times \frac{a_s}{A}$$

In Fig. 1, the log of the concentration of Na^+ ions in the system, equivalent to a, is plotted against pH for each series of sols. The figures shown near the points indicate the values of f at these points. It is possible then to interpolate values of f and pH where the sodium ion concentrations are 0.001 and 0.01 normal, respectively. These interpolated values are plotted in Fig. 2. Also in Fig. 2, Bolt's[1] data have been recalculated and plotted, taking into account that one coulomb corresponds to 6.28×10^{18} electronic charges or adsorbed OH^- ions. Thus, 1 microcoulomb per sq. cm. corresponds to 0.0628 hydroxyl ions per square millimicron.

Maximum Adsorption Capacity of the Surface.—By titrating a sample of silica having a specific surface of 342 square meters per gram, in a 20% solution of NaCl, dissolution of the silica at high pH was inhibited. By subtracting a blank for the NaCl solution alone, the number of OH^- ions adsorbed in the pH range 10.5–12.0 was calculated to approach a constant at 3.5 ± 0.3 OH^- ions per square millimicron, as shown in Fig. 3. The pH did not change on standing for half an hour, even

TABLE I

Part.[a] diam., mμ	(C) g. SiO_2/100 ml. sol	(R) Molar ratio SiO_2:Na_2O	(a) Total equiv. NaOH/l. of H_2O × 10^3	Init. pH	(h) Equiv. OH^-/l. of H_2O × 10^3	(a_s) Equiv. adsbd. OH^-/l. of H_2O × 10^3	f
10	10	500	7.0	7.21	Negl.	7.0	0.036
10	5	500	3.4	7.56	Negl.	3.4	.036
10	1.5	500	1.0	7.94	Negl.	1.0	.036
10	0.5	500	0.334	8.18	Negl.	0.33	.036
10	10	300	11.64	7.91	Negl.	11.64	.060
10	5	300	5.68	8.29	Negl.	5.68	.061
10	1.5	300	1.68	8.70	Negl.	1.68	.061
10	0.5	300	0.56	8.83	Negl.	0.56	.061
10	10	100	35.0	9.50	0.03	35	.18
10	5	100	17.06	9.71	.05	17.0	.18
10	1.5	100	5.24	9.96	.09	5.15	.18
10	0.5	100	1.66	10.00	.1	1.56	.17
10	10	50	69.8	10.50	.32	69.5	.36
10	5	50	34.2	10.58	.39	33.8	.36
10	1.5	50	10.1	10.62	.42	9.7	.35
10	0.5	50	3.34	10.54	.35	3.0	.33
10	10	25	140.0	11.43	2.7	137	.71
10	5	25	68.2	11.40	2.5	65.7	.71
10	1.5	25	20.1	11.33	2.15	18.0	.65
10	0.5	25	6.67	11.12	1.3	5.37	.58
10	10	12.5	279	12.40	25	254	1.32
10	5	12.5	136.0	12.35	22.5	113.5	1.21
10	1.5	12.5	40.3	13.10	12.5	27.8	1.01
10	0.5	12.5	13.5	11.79	6.1	7.4	0.81
20	20	500	14.7	8.42	0.003	14.7	.078
20	10	500	7.0	8.72	.005	7.0	.077
20	3	500	2.03	9.19	.015	2.01	.077
20	1	500	0.67	9.34	.022	0.65	.075
20	20	300	24.4	9.14	.014	24.4	.13
20	10	300	11.6	9.37	.023	11.6	.13
20	3	300	3.38	9.70	.05	3.33	.13
20	1	300	1.11	9.87	.075	1.03	.12
20	20	100	73.2	10.49	.31	72.9	.38
20	10	100	35.0	10.50	.32	34.7	.38
20	3	100	10.2	10.63	.43	9.8	.37
20	1	100	3.35	10.50	.32	3.0	.35
20	20	50	146.5	11.24	1.75	144	.76
20	10	50	70.0	11.36	2.3	67.7	.79
20	3	50	20.3	11.25	1.8	18.5	.71
20	1	50	6.7	11.10	1.25	5.4	.62

[a] 10 mμ: A = 318 m.²/g.; 20 mμ: A = 149 m.²/g.

at *p*H 12, indicating that the silica was not dissolving.

The saturation value of the surface is estimated from the fact that 1.5 g. of silica having a specific surface of 342 m.²/g. was saturated (line C, Fig. 3) by about 6 ± 0.5 ml. of 0.5 *N* NaOH solution

$$OH^- \text{ per sq. m}\mu = \frac{6.0 \times 10^{-3} \times 0.5 \times 6 \times 10^{23}}{1.5 \times 342 \times 10^{18}} = 3.5 \pm 0.3$$

Discussion

It is of interest, in Fig. 2, that the values for the 10 mμ and the 20 mμ particles are in essential agreement, showing that, if all other conditions are equal, the fraction of the surface sites occupied by OH^- ions, or the charge density, is the same on particles of different sizes even in salt-free sols.

Bolt's data were obtained in the presence of added NaCl, while ours were not, yet there is substantial agreement. Moreover, Bolt found essentially the same relation between charge density and *p*H for sols containing 3, 10 and 30% silica. It is therefore concluded that within the *p*H range of 7 to 10.5 and with silica particles of colloidal size, the number of OH^- ions adsorbed per unit surface at a given *p*H and Na^+ ion concentration is relatively independent of the concentration of silica, the particle size, and the source of the sodium ions. In other words, the adsorption of OH^- ions at a given *p*H depends chiefly on the concentration of the sodium ions; this is true even when the only sodium present is the sodium hydroxide added as base for stabilization. Obviously this will not hold for extremely dilute sols or at very high cation concentrations but is evidently true for the range studied.

It has been previously estimated that there are about four sites for OH^- ion adsorption per square

millimicron.[7] The figure 3.5 ± 0.3 is the first directly determined value, and is probably more dependable. The fact that silica is not depolymerized at *p*H 12 in strong salt solution suggests that Na^+ ions are held very close to the OH^- ions, forming an impermeable barrier to prevent the underlying silica from dissolving.

(7) R. K. Iler, "The Colloid Chemistry of Silica and Silicates," Cornell University Press, Ithaca, N. Y., 1955, p. 248.

At the highest *p*H values, calculated *f* values are somewhat greater than unity. This may be explained by the fact that at such high alkalinity, silica reacts rapidly with the alkali, causing the measured *p*H to be somewhat low, and the calculated a_s to be correspondingly too high. This effect is observed only in the salt-free systems, since the rate of silica dissolution at high *p*H in the presence of high salt concentration is very slow.

SURFACE ACTIVITY OF FLUORINATED ORGANIC COMPOUNDS AT ORGANIC LIQUID–AIR INTERFACES. PART II. SURFACE TENSION–CONCENTRATION CURVES, ADSORPTION ISOTHERMS AND FORCE–AREA ISOTHERMS FOR PARTIALLY FLUORINATED CARBOXYLIC ESTERS[1]

BY N. LYNN JARVIS AND W. A. ZISMAN

U. S. Naval Research Laboratory, Washington 25, D. C.

Received September 11, 1959

This investigation was undertaken to study the ability of a series of partially fluorinated carboxylic esters to depress the surface tension of a group of pure organic liquids. The surface activity of these solutes in the different solvents was shown to vary with the hydrocarbon content, fluorocarbon content, and the number and position of associating groups in the solute. The balance between these organophilic and organophobic groups in the solute molecules which gave maximum surface tension depression varied with the surface tension of the solvent and the solubility of the solute in it. In this report surface tension *vs.* concentration curves, adsorption *vs.* concentration isotherms, and graphs of monolayer film pressure *vs.* area per molecule of adsorbed solute are given for each fluorochemical in the various organic solvents. Theoretical calculations from these data give the extent of adsorption and explain the orientation and packing of the molecules adsorbed at the interface of liquid and air. A discussion is given of the effect of the organophobic and organophilic constituents of the solute molecules on the extent of adsorption and on the tendency to associate with the various solvents.

Introduction

In Part I of this investigation[2] we demonstrated that a large group of compounds can be rapidly screened for surface activity in an organic liquid on the basis of their initial spreading coefficients on the given liquid substrate. Ellison and Zisman[3] have shown that a number of partially fluorinated compounds, having positive initial spreading coefficients, are highly adsorptive at many organic liquid–air interfaces. The degree of adsorption, as well as the spreading coefficient, was shown to depend upon the ratio of organophobic to organophilic constituents in the solute molecule with respect to the organic substrate used.

Fluorocarbon radicals or groups are preferred organophobic constituents of solutes which are designed to be surface active agents in organic liquids because of their effectiveness in lowering the surface energy[4–7] and their decreased solubility in most liquids. The more highly associating hydrocarbon groups are especially suitable as the organophilic group or radical for such surface active solutes. Carboxylic ester, ether, silicate, sulfonate, phosphate or other polar groups can be used to connect chemically the fluorocarbon and hydrocarbon groups in the surface active agent and they may function either as organophobic or organophilic groups depending upon the nature of the substrate. In a partially fluorinated solute, therefore, the organophobic/organophilic ratio may be altered by varying the fluorocarbon content, hydrocarbon content and the nature, number and position of the polar groups. One complicating factor, however, is that the surface activity of the solute will vary with its solubility and with the surface tension of the organic solvent, so that one would not expect any single fluorinated solute to be equally efficient in depressing the surface tension of all organic liquids.

This report is concerned with the ability of various partially fluorinated compounds to depress the surface tensions of a group of organic liquids having a wide range of surface tensions. By applying the Gibbs adsorption equation to the resulting surface tension *vs.* concentration data, the surface excess of the solute has been calculated. In most cases monolayer adsorption has been deduced, and hence it is possible to give the isotherms of film pressure (F) *vs.* the area per adsorbed molecule (A) at 20°.

Materials and Methods Used

The compounds used as surface active agents were highly purified partially fluorinated esters of mono-, di- and tricarboxylic acids with various fluorine to hydrogen ratios, all of which were synthesized for this investigation by J. G. O'Rear and co-workers in this Laboratory.[8] These com-

(1) Presented at the Annual Meeting of the Colloid Division, American Chemical Society, Atlantic City, New Jersey, September 14, 1959.

(2) N. L. Jarvis and W. A. Zisman, THIS JOURNAL, **63**, 727 (1959).

(3) (a) A. H. Ellison and W. A. Zisman, *ibid.*, **60**, 416 (1956); (b) **63**, 1121 (1959).

(4) H. M. Scholberg, R. A. Guenthner and R. I. Coon, *ibid.*, **57**, 923 (1953).

(5) G. H. Rohrback and G. H. Cady, *J. Am. Chem. Soc.*, **71**, 1938 (1949).

(6) R. H. Haszeldine and F. Smith, *J. Chem. Soc.*, 602 (1951).

(7) H. W. Fox and W. A. Zisman, *J. Colloid Sci.*, **5**, 514 (1950).

(8) P. D. Faurote, C. M. Henderson, C. M. Murphy, J. G. O'Rear and H. Ravner, *Ind. Eng. Chem.*, **48**, No. 3, 445 (1956).

pounds, with selected physical constants, are listed in Table I.

TABLE I

PHYSICAL CONSTANTS OF PARTIALLY FLUORINATED CARBOXYLIC ESTERS AT 20°

Ester	Mol. wt.	F/H[a]	Surface tension (dynes/cm.)	Density (g./ml.)
Bis-(ϕ'-butyl) 3-methylglutarate	511.1	1.17	20.7	1.504
Bis-(ϕ'-hexyl) 3-methylglutarate	711.1	1.83	19.7	1.610
Bis-(ϕ'-octyl) 3-methylglutarate	911.2	2.50	19.5	1.689
Bis-(ψ'-heptyl) 3-methylglutarate	774.3	1.71	25.6	1.648
Hexyl ϕ-butyrate	298.2	0.53	19.2	1.231
1,2,3-Trimethylolpropane tris-(ϕ-butyrate)	722.3	1.91	21.2	1.614

[a] F/H is ratio of number of fluorine atoms to number of hydrogen atoms per molecule.

Surface tensions given in Table I were determined by Ellison and Zisman.[3b] Surface active impurities present in the fluorocompounds were removed by slowly percolating each sample through an adsorption column packed with activated alumina and "Florisil" just prior to being used in these experiments.

The system of nomenclature adopted by O'Rear, *et al.*,[8] for partially fluorinated compounds was used in Table I. The abbreviations are

$F(CF_2)_nCOOH$	ϕ-acid
$H(CF_2)_nCOOH$	ψ-acid
$F(CF_2)_nCH_2OH$	ϕ'-alcohol
$H(CF_2)_nCH_2OH$	ψ'-alcohol

The nomenclature is extended to derivatives of these compounds. Also, the 3-methylglutarate derivatives will be abbreviated 3-MEG, and 1,2,3-Trimethylolpropane as 1,2,3-TMP.

Seven organic liquids with graded surface tensions and different chemical compositions were used as solvents. These liquids and their surface tensions at 20° are: hexadecane (27.4 dynes/cm.), mineral oil (29.9 dynes/cm.), bis-(2-ethylhexyl) sebacate (31.0 dynes/cm.), nitromethane (36.2 dynes/cm.), Alkazene 42, or 1,2-dibromoethylbenzene, (38.2 dynes/cm.), tricresyl phosphate (40.4 dynes/cm.) and propylene carbonate (41.1 dynes/cm.). Sources of liquids, methods of purification, and essential physical constants have been reported in Part I.[2] Hexadecane, mineral oil and Alkazene 42 were selected as representative non-associating solvents, and the remaining solvents represent associating liquids.

Solutions in each organic liquid were prepared by delivering specified amounts of the fluoro-chemical from a microburet and bringing the solution up to volume with the organic solvent. Then the solution was warmed slightly to ensure complete solution and allowed to stand at least 24 hours, with intermittent shaking, before surface tension measurements were made. All solutions of partially fluorinated solutes in propylene carbonate, nitromethane, tricresyl phosphate and bis-(2-ethylhexyl) sebacate were found to completely wet a clean, polished, platinum foil. Only when solutions in Alkazene 42, mineral oil and hexadecane approached saturation did they exhibit an appreciable contact angle. Surface tensions of those solutions which gave contact angles on platinum approaching zero were determined with a Cenco- du Nuoy interfacial tensiometer using a ring of 6.008 cm. circumference and the correction tables of Harkins and Jordan.[9] Surface tensions of the remaining solutions were measured with the Cassel modification of the maximum bubble pressure method,[10,11] which is independent of the contact angle. The accuracy of the measurements with each method was ± 0.1 dyne/cm. All measurements were made at 20 ± 0.4°.

Results

I. Surface Tension–Concentration Curves.—The surface activity of each partially fluorinated solute in the various organic solvents is given by the surface tension *vs.* concentration isotherms of Fig. 1. Concentrations up to 0.08 mole/l. were reported. As expected, the initial slope of each curve varied greatly with the solvent and fluorocarbon solute used. The initial slope of each curve and the minimum surface tension attained by each solution in the concentration ranges studied are both indications of the organophobic/organophilic ratios in the solute molecules with respect to the solvent, and are measures of their surface activity.

Gibb's adsorption equation in its simplest form is

$$\Gamma = -\frac{c}{RT}\left(\frac{\partial\gamma}{\partial c}\right) \qquad \text{(i)}$$

where Γ is the "surface excess" of solute, c the solution concentration, and γ the solution surface tension. From this relation it follows that the initial slope $(\partial\gamma/\partial c)_{\text{initial}}$ of each curve (see Table II) is proportional to the initial value of Γ/c, or the initial adsorption per mole of solute. Table II reveals that the less soluble the surface active agent, or the greater the F/H ratio of a given class of esters, the greater the initial value of $(\partial\gamma/\partial c)$, and hence the greater the corresponding value of Γ/c. This is demonstrated by the behavior of the ϕ'-derivatives of 3-MEG in propylene carbonate, where the magnitude of the initial slopes increase from 610 to 87,400 as the F/H ratios increase from 1.17 to 2.50. Bis-(ψ'-heptyl) 3-MEG, however, with an F/H ratio of 1.71, has an initial slope in the same solvent of 370, considerably less than that of bis-(ϕ'-hexyl) 3-MEG with a similar F/H ratio. It is believed that the terminal hydrogen of the ψ'-compound is associating with the propylene carbonate, thus increasing its solubility.

As was expected, the ester group is strongly organophilic in propylene carbonate. 1,2,3-TMP tris-(ϕ-butyrate) has a slightly larger F/H ratio than bis-(ϕ'-hexyl) 3-MEG but has a smaller initial slope; this shows that the additional carboxyl group increased the solubility. Nitromethane and bis-(2-ethylhexyl) sebacate showed the same general behavior as propylene carbonate toward the partially fluorinated carboxylic esters. Note that each of these solvents has polar oxygen groups which are accessible for association with the polar groups of the surface active agents.

The fluoroesters behaved quite differently when dissolved in one of the non-associating solvents, tending to give larger values of $(\partial\gamma/\partial c)_{\text{initial}}$ than associating solvents with corresponding surface tensions. Compared to other diesters, bis-(ψ'-heptyl) 3-MEG gave a larger increase in $(\partial\gamma/\partial c)_{\text{initial}}$, indicating that the terminal hydrogen has little interaction with these solvents. It appears that the carboxyl groups of all solutes have little or no association with these liquids. Note that 1,2,3-TMP tris-(ϕ-butyrate) has a considerably larger initial slope in Alkazene 42 than bis-(ϕ'-hexyl) 3-MEG, although both have nearly equal F/H ratios.

(9) W. D. Harkins and H. F. Jordan, *J. Am. Chem. Soc.*, **52**, 1751 (1930).

(10) H. M. Cassel, U. S. Patent 2,448,768 (Sept. 7, 1948).

(11) N. L. Jarvis and W. A. Zisman, NRL Report 5306, May 6, 1959. To be published.

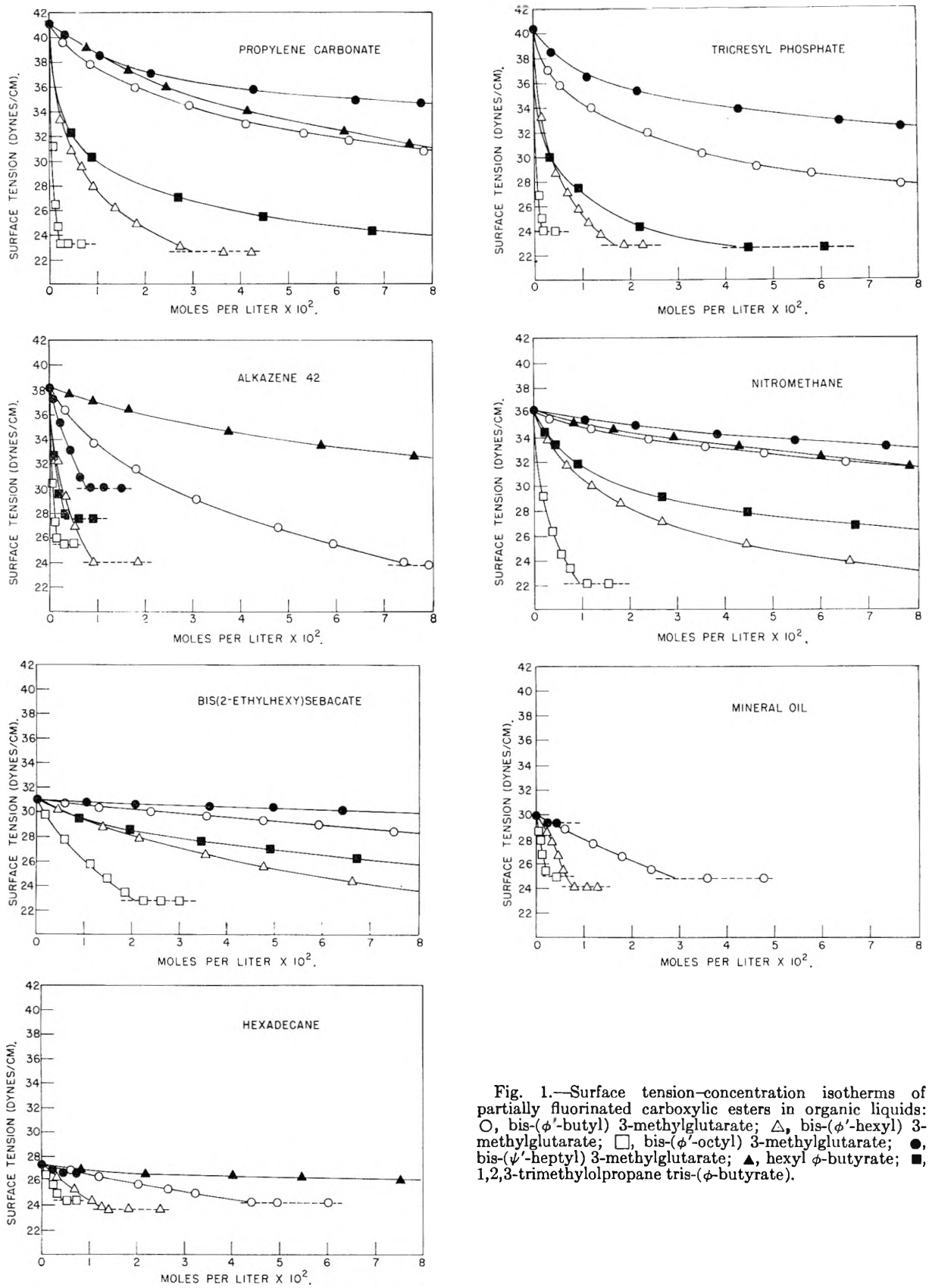

Fig. 1.—Surface tension–concentration isotherms of partially fluorinated carboxylic esters in organic liquids: ○, bis-(ϕ'-butyl) 3-methylglutarate; △, bis-(ϕ'-hexyl) 3-methylglutarate; □, bis-(ϕ'-octyl) 3-methylglutarate; ●, bis-(ψ'-heptyl) 3-methylglutarate; ▲, hexyl ϕ-butyrate; ■, 1,2,3-trimethylolpropane tris-(ϕ-butyrate).

All of the fluorochemicals studied were somewhat less soluble in tricresyl phosphate than in the other oxygen containing substrates, possibly because the cresyl groups of the solvent molecules sterically hinder association of the polar group of the surface active agent with the polar phosphate group.

TABLE II

EFFECT OF SOLVENT AND SOLUTE COMPOSITION ON INITIAL SLOPE OF SURFACE TENSION *vs.* CONCENTRATION CURVES (AT 20°)

Surface active solute	F/H	Solute surface tension (dynes/cm.)	Initial slope × 10^2						
			Hexadecane	Mineral oil	Bis-(2-ethylhexyl) sebacate	Nitromethane	Alkazene 42	Tricresyl phosphate	Propylene carbonate
Hexyl ϕ-butyrate	0.53	19.2	0.8	..	0.7	0.5	1.6	...	3.0
Bis-(ϕ'-octyl) 3-methylglutarate	2.50	19.5	9.0	22.5	7.4	75.9	328.0	816.0	874.0
Bis-(ϕ'-hexyl) 3-methylglutarate	1.83	19.7	3.3	9.8	1.9	9.5	54.1	190.5	80.0
Bis-(ϕ'-butyl) 3-methylglutarate	1.17	20.7	1.1	1.9	0.5	1.2	8.7	19.1	6.1
1,2,3-Trimethylolpropane tris-(ϕ-butyrate)	1.91	21.2	..	11.0	2.2	8.7	134.0	108.0	61.3
Bis-(ψ'-heptyl) 3-methylglutarate	1.71	25.6	2.3	3.8	0.3	0.5	14.2	7.7	3.7

Table II shows that $(\partial\gamma/\partial c)_{initial}$ generally tends to increase as the surface tension of the solvent increases. Ellison and Zisman[3b] made a similar observation of solutions of ψ'-nonyl butyrate in a series of solvents and found their data fit the equation

$$-(\partial\gamma/\partial c)_{initial} = \alpha e^{\beta(\gamma solvent - \gamma solute)} \quad (ii)$$
$$= \alpha e^{\beta(\Delta\gamma)}$$

Hence, a plot of log $(-\partial\gamma/\partial c)_{initial}$ *vs.* $\Delta\gamma$ was a straight line. Figure 2 is such a plot for solutions of bis-(ϕ'-butyl)3-MEG in each of the solvents studied by us. Graphical points for Alkazene 42, tricresyl phosphate, mineral oil and hexadecane fall on line (1) of Fig. 2, whereas those for the more highly associating solvents, propylene carbonate, nitromethane and bis-(2-ethylhexyl) sebacate, fall on line (2). This indicates equation (ii) must be modified to account explicitly for differences in behavior of these fluorinated solutes in associating and non-associating solvents.

To examine the subject further, a plot of log $(-\partial\gamma/\partial c)_{initial}$ *vs.* $\Delta\gamma$ was made for bis-(ϕ'-octyl) 3-MEG, which is much less soluble in each substrate than bis-(ϕ'-butyl) 3-MEG. Inasmuch as the solubilities are an indication of the relative degree of association, approximate solubilities of these two homologous solutes are given in Table III. The solubility was estimated from the surface tension *vs.* concentration curves in Fig. 1, the solubility limit being the concentration at which the extrapolated surface tension *vs.* concentration curve intersected a horizontal line representing the surface tension of the saturated solution. Table III reveals that the solubility of bis-(ϕ'-butyl) 3-MEG in the non-associating solvents is about an order of magnitude lower than in the associating solvents. It is also seen that bis-(ϕ'-octyl) 3-MEG has fairly low solubility in all the solvents studied, hence the lines corresponding to the associating and non-associating solvents in Fig. 2 are much closer together.

TABLE III

SOLUBILITY OF BIS-(ϕ'-BUTYL) AND BIS-(ϕ'-OCTYL) 3-MEG IN VARIOUS SOLVENTS AT 20°

Solvent	Surface tension (dynes/cm.)	Solubility, moles/l. of Bis-(ϕ'-butyl) 3-methylglutarate	Solubility, moles/l. of Bis-(ϕ'-octyl) 3-methylglutarate
Propylene carbonate	41.1	>0.300	0.0020
Tricresyl phosphate	40.4	$\cong$ .200	.0014
Nitromethane	36.2	> .300	.0094
Bis-(2-ethylhexyl) sebacate	31.0	> .300	.0208
Alkazene 42	38.2	.076	.0014
Mineral oil	29.9	.029	.0026
Hexadecane	27.4	.044	.0042

It is evident from Fig. 2, that the values of α and β for a given solute are not the same for the associating solvents as for the non-associating solvents. Values of these constants for each solute in Fig. 2 are given in Table IV. Note α and β are less for the more soluble solute.

TABLE IV

CONSTANTS α AND β FOR BIS-(ϕ'-BUTYL) 3-MEG AND BIS-(ϕ'-OCTYL) 3-MEG DETERMINED FROM FIG. 2

Solute	In associating solvents		In non-associating solvents	
	α	β	α	β
Bis-(ϕ'-butyl) 3-MEG	1.59	0.291	25.71	0.208
Bis-(ϕ'-octyl) 3-MEG	3.98	0.462	60.26	0.343

Although the initial slope of a surface tension *vs.* concentration curve and the maximum or limiting surface tension depression at high concentrations are both related to the organophobic/organophilic ratio of the solute, a large initial slope does not necessarily imply a large maximum surface tension depression. As the organophobic portion of the molecule becomes larger, the initial slope and the maximum surface tension depression obtainable within the concentration limits shown in Fig. 1 will both increase. Eventually a point will be reached beyond which any further increase in the organophobic/organophilic ratio will cause the solubility to decrease rapidly, with a subsequent increase in the initial slope, and a decrease in the maximum extent to which the surface tension may be lowered. In other words, even though a solute may cause a large initial slope in a surface tension *vs.* concentration isotherm, it may be too insoluble to bring about a large surface tension depression.

When the solute is a liquid, the difference between the surface tensions of the pure substrate and pure solute represents the maximum possible surface tension lowering $\Delta\gamma_{max}$, and 100 $(\Delta\gamma/\Delta\gamma_{max})$ may be termed the "efficiency" of the surface active agent in that solvent. Values of the "efficiency" of each solute in the various solvents are reported in Table V. All efficiencies are calculated for saturated solutions or for concentrations of 0.1 mole/liter, whichever is the lower concentration. Efficiencies as high as 92% and as low as 0% were obtained with 1,2,3-TMP tris-(ϕ-butyrate), showing the necessity of a proper solubility balance; if the solubility is too low or too high, the surface active efficiency as defined here is decreased.

Also it is seen that 1,2,3-TMP tris-(ϕ-butyrate) is much more effective as a surface active agent in

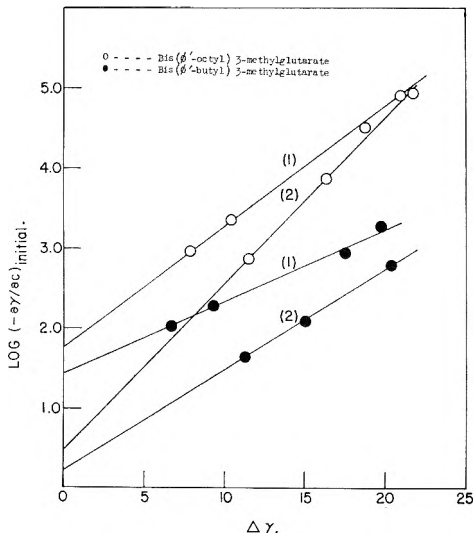

Fig. 2.—Plot of log $(-\partial\gamma/\gamma c)$ initial *vs.* $\Delta\gamma$ [(1) non-associating solvents and (2) associating solvents].

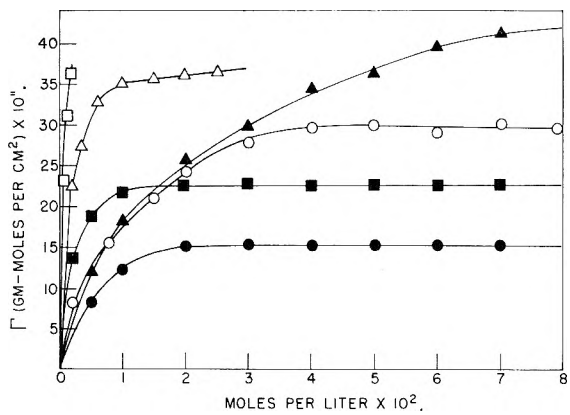

Fig. 3.—Surface excess of partially fluorinated carboxylic esters in propylene carbonate: ○, bis-(ϕ'-butyl) 3-methylglutarate; △, bis-(ϕ'-hexyl) 3-methylglutarate; □, bis-(ϕ'-octyl) 3-methylglutarate; ●, bis-(ψ'-heptyl) 3-methylglutarate; ▲, hexyl ϕ-butyrate; ■, 1,2,3-trimethylolpropane tris-(ϕ-butyrate).

propylene carbonate or tricresyl phosphate than either bis-(ϕ'-hexyl) 3-MEG or bis-(ϕ'-octyl) 3-MEG, yet the latter two solutes have approximately the same or greater F/H ratios and considerably higher initial values of $(\partial\gamma/\partial c)$. The greater surface active efficiency of 1,2,3-TMP tris-(ϕ-butyrate) is a result of the greater solubility of the fluorinated triester than either fluorinated diester. For a similar reason bis-(ϕ'-hexyl) 3-MEG is a more effective surface active agent in propylene carbonate and tricresyl phosphate than the less soluble bis-(ϕ'-octyl) 3-MEG.

The additional carboxyl group in 1,2,3-TMP tris-(ϕ-butyrate) increases its solubility in nitromethane and bis-(2-ethylhexyl) sebacate over bis-(ϕ'-hexyl) or bis-(ϕ'-octyl) 3-MEG, decreasing its efficiency considerably below these methylglutarates. Hexyl ϕ-butyrate, bis-(ϕ'-butyl) 3-MEG and bis-(ψ'-heptyl) 3-MEG are also much less efficient in these associating solvents than the other three fluoroesters, primarily due to their greater solubility.

Efficiencies of the partially fluorinated esters as surface active agents will be quite different in the non-associating substrates, Alkazene 42, mineral oil and *n*-hexadecane, than they were in the polar liquids. In these solvents the carboxyl group will tend to be organophobic as illustrated by 1,2,3-TMP tris-(ϕ-butyrate), which is considerably less soluble and less efficient than a diester with a corresponding F/H ratio. In hydrocarbon solvents bis(ϕ'-butyl) 3-MEG and bis-(ϕ'-hexyl) 3-MEG were the most efficient surface active agents; however, the minimum surface tension value observed was not as great as that obtained with an appropriate associating solvent. It is possible to obtain more efficient surface active fluoroesters for non-associating liquids using a monoester with an appropriate organophobic/organophilic balance as reported by Ellison and Zisman.[3a]

II. Adsorption Isotherms.—From the surface tension *vs.* concentration curves in Fig. 1, Γ, the surface excess of solute molecules adsorbed at each interface was calculated using the Gibbs equation in the form of equation i. Rigorously, equation i should be expressed in terms of activities rather than concentrations; however, because only dilute solutions were used, concentration was assumed to be a good approximation of the activity in calculating the surface excess. It was also found, using the adsorption equation ii of Guggenheim[12] that there is very little error inherent in ignoring the effect of

$$-\frac{1}{RT}\frac{\partial\gamma}{\partial x} = \frac{\Gamma_2}{x} - \frac{\Gamma_1}{1-x} \qquad \text{(ii)}$$

competitive adsorption of the solvent molecules with the dilute concentrations used.

The calculated adsorption isotherms shown in Fig. 3 for each of the partially fluorinated esters dissolved in propylene carbonate are typical of those obtained in the other organic solvents. Differences in the initial slope and the minimum of the Γ *vs.* concentration curve are evidently the result of variations in solubility and differences in orientation of the adsorbed molecules in the interface. It was observed in Fig. 1 that the more soluble bis-(ϕ'-hexyl) 3-MEG gave a great surface tension depression in propylene carbonate than bis-(ϕ'-octyl) 3-MEG, although the latter has a greater F/H ratio and a lower surface tension. This can be explained by the adsorption isotherms of Fig. 3. Each adsorption isotherm gave the same limiting value of Γ, indicating that at saturation each solution will have the same number (36.8×10^{-11} mole/cm.^{2}) of solute molecules in excess in the interface. This number does not include, however, those solute molecules which would be present in the surface layer due to a uniform distribution of the bulk phase at saturation; this amounts to 1.05×10^{-11} mole/cm.^{2} for the more soluble compound, bis-(ϕ'-hexyl) 3-MEG, and only 0.16×10^{-11} mole/cm.^{2} for bis-(ϕ'-octyl) 3-MEG. Thus the total concentration of solute in the surface phase is greater for the more soluble compound, giving its saturated solution a lower surface tension.

Once the first plateau in the adsorption isotherm has been reached, there is no further increase in Γ over the concentration range studied. There is found a slight decrease in two curves which may be due to neglect of solvent adsorption. As the con-

(12) E. A. Guggenheim, "Thermodynamics," Interscience Publishers, Inc., New York, N. Y., 1950, p. 217.

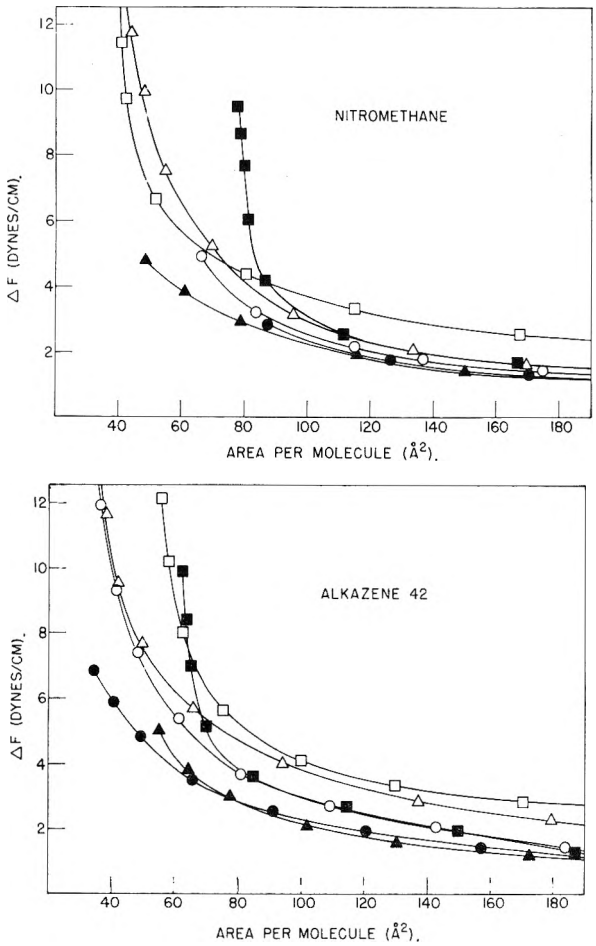

Fig. 4.—Force–area isotherms of partially fluorinated carboxylic esters in (a) nitromethane and (b) Alkazene 42: ○, bis-(ϕ'-butyl) 3-methylglutarate; △, bis-(ϕ'-hexyl) 3-methylglutarate; □, bis-(ϕ'-octyl) 3-methylglutarate; ●, bis-(ψ'-heptyl) 3-methylglutarate; ▲, hexyl ϕ-butyrate; ■, 1,2,3-trimethylolpropane tris (ϕ-butyrate).

centration of the bulk solution increases further, however, more solute molecules will be added to the interface and further decreases in surface tension are obtained. Thus compounds such as bis-(ϕ'-hexyl) 3-MEG or 1,2,3-TMP tris-(ϕ-butyrate), which contain sufficient fluorine to cause a rapid initial rise in the adsorption isotherm and have organophilic groups that gives them appreciable solubility in propylene carbonate, will ultimately reach a lower surface tension than ones having a very steep isotherm but lower solubility.

The largest value of Γ attainable by each of the solutes will be determined by the size and orientation of the fluoroester molecules in the interface. The greater the area occupied by each molecule in the surface, the lower the maximum possible value of Γ.

III. Force–Area Isotherms.—In order to study more extensively the orientation of the adsorbed partially fluorinated esters at each organic liquid–air interface, force–area isotherms were computed for the fluoroesters in each substrate by assuming that the solute molecules adsorb as a unimolecular film, each molecule of which occupied an area A, and by substituting the film pressure F for the total surface tension lowering. Results are given for the

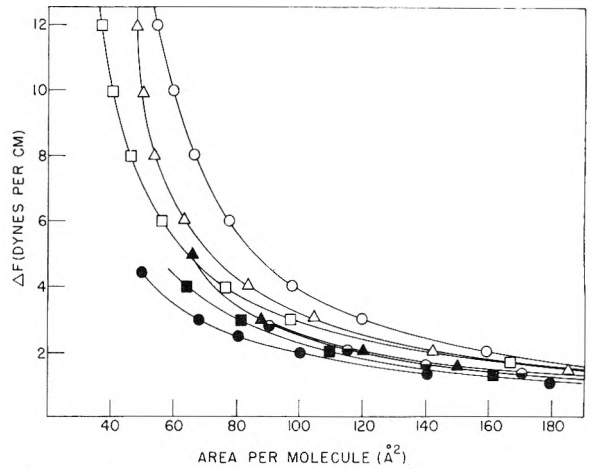

Fig. 5.—Force–area isotherm of bis-(ϕ'-butyl) 3-methylglutarate in each organic solvent: ○, tricresyl phosphate: △, propylene carbonate; □, Alkazene 42; ●, mineral oil; ▲, nitromethane; ■, bis-(2-ethylhexyl) sebacate; ◒, hexadecane.

fluoroesters in Alkazene 42 and nitromethane in Fig. 4, and for bis-(ϕ'-butyl) 3-MEG in each of the solvents studied in Fig. 5. These F *vs.* A curves are typical of the remaining isotherms which are not reported. The minimum value of A in each case (see Table VI) varied with the structure of the compound and the organophobic/organophilic balance of the solute with respect to the substrate. Where the fluoroester was quite soluble in the organic substrate, no minimum value of A was attained in the concentration ranges studied. Also, if the solubility was very low, the closest possible packing of the monolayer was not attainable.

Arrington and Patterson[13] have reported that the limiting area/molecule of the higher ψ-alkanoic compounds $H(CF_2)_{10}CH_2OH$ and $H(CF_2)_{12}COOH$, when spread as insoluble monolayers on water, was approximately 29 Å.^{2}. This is slightly larger than the cross-sectional area of 24.5 Å.^{2} determined from the Stuart–Briegleb ball models. In this investigation hexyl ϕ-butyrate, when adsorbed at the interface of propylene carbonate and air, occupied 35.2 Å.^{2} per molecule at a solution concentration of 0.3 mole per liter. This value approaches the limiting area/molecule for a fluorinated paraffin chain on water. Therefore, this compound adsorbs as a monolayer at the free surface of propylene carbonate, with the organophobic fluorocarbon group oriented away from the liquid substrate, probably with its axis tilted somewhat from vertical. A limiting value of A close to that of a vertically oriented ϕ-alkane chain could not be reached, possibly because of the high solubility.

Studies of the fluoroesters of dicarboxylic acids having low solubilities in Alkazene 42 and mineral oil resulted in minimum values of A of 34.2 to 38.5 Å.^{2}, approximately the same as that of hexyl ϕ-butyrate in propylene carbonate, even though there was a methyl side chain on each dicarboxylic acid. Assuming these compounds each adsorb as a monomolecular film, it must be postulated that at low values of A each adsorbs with only

(13) C. H. Arrington and G. D. Patterson, THIS JOURNAL, **57**, 247 (1953).

TABLE V

EFFICIENCY OF SURFACE ACTIVE SOLUTE IN EACH ORGANIC SOLVENT

Surface active solute	F/H	Surface tension (dynes/cm.) 20°	Efficiency of solute in each solvent (%) Hexadecane	Mineral oil	Bis-(2-ethylhexyl) sebacate	Nitromethane	Alkazene 42	Tricresyl phosphate	Propylene carbonate
Hexyl ϕ-butyrate	0.53	19.2	17.1[a]	..	..	31.3[a]	32.8[a]	..	51.8[a]
Bis-(ϕ'-octyl) 3-methylglutarate	2.50	19.5	37.9	47.1	70.4	83.4	68.0	68.3	75.9
Bis-(ϕ'-hexyl) 3-methylglutarate	1.83	19.7	49.1	55.8	72.6[a]	84.5[a]	76.2	84.4	85.5
Bis-(ϕ'-butyl) 3-methylglutarate	1.17	20.7	46.3	54.3	31.1[a]	32.5[a]	82.3	68.0[a]	54.0[a]
1,2,3-Trimethylolpropane tris-(ϕ-butyrate)	1.91	21.2	0.0	9.2	59.3[a]	67.2[a]	62.9	92.7	89.4[a]
Bis-(ψ'-heptyl) 3-methylglutarate	1.71	25.6	38.9	11.6	22.2[a]	29.4[a]	64.3	58.8[a]	44.8[a]

[a] Efficiency of solution of 0.1 mole/liter rather than of a saturated solution.

TABLE VI

MINIMUM AREA/MOLECULE OBTAINED FROM FORCE–AREA ISOTHERMS AT 20°

Surface active solute	Minimum area, A_0, (Å.²/molecule) in each solvent: Hexadecane	Mineral oil	Bis-(2-ethylhexyl)-sebacate	Nitromethane	Alkazene 42	Tricresyl phosphate	Propylene carbonate
Bis-(ϕ'-butyl) 3-methylglutarate	86.9	38.5	69.5[a]	64.8[a]	34.8	48.4[a]	49.9[a]
Bis-(ϕ'-hexyl) 3-methylglutarate	82.8	34.5	42.6	40.8	35.4	43.0	44.3
Bis-(ϕ'-octyl) 3-methylglutarate	86.9	37.0	44.2	40.6	56.0[b]	41.0	44.0
Bis-(ψ'-heptyl) 3-methylglutarate	417.0[b]	600.0[b]	184.0[a]	82.5[a]	34.2	80.0[a]	92.8[a]
Hexyl ϕ-butyrate	269.0[a]	....	....	48.8[a]	61.0[a]	...	35.2
1,2,3-Trimethylolpropane tris-(ϕ-butyrate)	....	321[b]	68.5	76.4	62.2	63.0	65.9

[a] Too soluble to approach limiting area/molecule over concentration range investigated. [b] Too insoluble to form close-packed monolayer.

one fluorocarbon chain oriented away from the surface, the other remaining essentially in the substrate. The same diesters adsorb with limiting areas/molecule of 41 to 44 Å.² in propylene carbonate, nitromethane and bis-(2-ethylhexyl) sebacate, the liquids studied in which they are most soluble. In addition, these diesters give lower minimum surface tensions in these associating substrates, indicating greater concentrations of fluorine in those interfaces where they apparently occupy greater areas/molecules. When adsorbed from solution in hexadecane, these diesters had minimum areas of 83–86 Å.²/molecule, with about the same solution surface tension as in Alkazene 42 and mineral oil.

It appears that these fluorinated diesters at high concentrations adsorb from all of the organic solvents studied, except hexadecane, with one fluorocarbon chain essentially exposed to the air and the other immersed in the organic substrate. In the non-associating liquids, Alkazene 42 and mineral oil, there is little tendency for the carboxyl groups to interact with the solvent, and the molecular axis may orient in a somewhat vertical position with the carboxyl groups having as little contact as possible with the liquid. The molecules may be in a slightly staggered or tilted position, however, to allow maximum interaction between the hydrocarbon groups and the substrate. In hexadecane the large area/molecule indicates the fluorocarbon groups in the diesters are not in closest packing, and it is possible the fluorocarbon groups are both oriented toward the air.

In the highly associating solvents, the diesters must orient in a somewhat similar manner to Alkazene 42 and mineral oil but with the carboxyl groups strongly interacting with the substrate liquid. This interaction between the carboxyl groups and the polar substrates apparently increases the tilt of the adsorbed monolayer molecules away from vertical, increasing the area/molecule and decreasing the minimum surface tension obtained by removing the carboxyl groups more completely from the interface.

The tricarboxylic ester 1,2,3-TMP tris-(ϕ-butyrate) gives a minimum area/molecule of around 65 Å.² in all the substrate liquids in which it forms a saturated solution in the concentration range studied. This area, approximately equivalent to the cross sectional area of two fluorocarbon chains, indicates that the compound adsorbs at the organic liquid–air interface with two fluorocarbon chains directed away from the interface and one remaining in the solution. From the low minimum surface tension value obtained, it is apparent the fluorine atoms in this surface are more closely packed than in the other fluoroesters.

Discussion

It has been shown that small amounts of a suitable fluorine-containing solute, often less than 1% by weight or 0.01 mole/liter, is able to reduce the surface tension of organic solvents up to 50%. The extent to which the free energy of an organic liquid surface will be decreased is a function of the particular fluorochemical used as the solute, for a given compound cannot be expected to have the same surface active efficiency in all solvents. Resulting from such adsorption, the free surface of the solution will have a high fluorine content, and one would expect large changes in some of the physical and chemical properties of the interface.

The fluoroesters investigated adsorbed primarily as unimolecular films at the surface of each organic solvent, the adsorbed molecules being in a gaseous or otherwise expanded state, with 1,2,3-TMP tris-(ϕ-butyrate) appearing to be more condensed

at high concentration than the other compounds reported. Larger surface tension depressions are obtained the higher the surface tension of the solvent. Solvents having roughly the same order of solubility for the surface active agent, or the same tendency to associate with it, will behave similarly so that a straight line is obtained when log $(-\partial\gamma/\partial c)_{\text{initial}}$ is plotted against $\Delta\gamma$, the difference in surface tensions of solvent and solute. It is apparent that the general features of the surface activity of fluorinated solutes in aqueous solutions are logical extension of the present discussion, with the solvent being more highly associated. In this case also, the fluorochemicals must be designed to have proper balance between soluble and insoluble groups to be highly adsorptive at the liquid–air interface.

SURFACE ACTIVITY OF FLUORINATED ORGANIC COMPOUNDS AT ORGANIC LIQUID–AIR INTERFACES. PART III. EQUATION OF STATE OF ADSORBED MONOLAYERS AND WORK OF ADSORPTION OF A FLUOROCARBON GROUP[1]

BY N. LYNN JARVIS AND W. A. ZISMAN

U. S. Naval Research Laboratory, Washington 25, D. C.

Received September 11, 1959

Previous investigations have demonstrated that a wide variety of partially fluorinated carboxylic esters are capable of adsorbing as unimolecular films at the interfaces between various organic liquids and air and also that these films are usually in a gaseous or otherwise expanded state. The present study has shown that isotherms of film pressure (F) *vs.* area (A) per adsorbed molecule of solute, at large values of A, obey the simple equation of state $(F + F_0)(A - A_0) = kT$. However, as the film pressures increase, the deviation from this equation increases. The two-dimensional analog of the van der Waals equation $(F + a/A^2)(A - A_0) = kT$, which includes a more definitive correction factor for the intermolecular attraction between neighboring molecules in the film, was in good agreement with the experimental data even at very low areas per molecule. The constants "a" and A_0 of the second equation were calculated for the F *vs.* A isotherms of each solute in the various solvents, and the relation of these constants to the organophobic–organophilic balance in the solute molecules and to the association of solute and solvent molecules is discussed. In addition, the work of adsorption, $\Delta\lambda$, of $-CF_2-$ groups at each organic liquid–air interface was calculated. The plot of $\Delta\lambda$ *vs.* solvent surface tension was a straight line, which extrapolated fairly well to the value for $-CF_2-$ groups adsorbed at the water–air interface, as determined from surface tension *vs.* concentration isotherms given in the literature for fluorinated solutes in water.

Introduction

In part II of this investigation[2] we showed from a study of a group of partially fluorinated carboxylic esters that when there is an appropriate balance between the organophobic and organophilic constituents of the molecules the ester is able to serve as a surface active solute and considerably depress the surface tension of various organic solvents. From the resulting surface tension *vs.* concentration curves, it was possible to calculate adsorption isotherms and F *vs.* A isotherms. Analysis of these data resulted in the conclusion that the more surface active fluoroester solutes adsorbed as unimolecular films at several organic liquid–air interfaces. The orientation and packing of the adsorbed solute molecules depended not only upon their molecular structure but also upon their solubility and the extent to which they associated with the molecules of the organic solvent.

The shape of the F *vs.* A isotherms in Part II as well as the minimum areas per adsorbed solute molecule reveal that the monolayer is neither in closest possible packing nor condensed. It is, therefore, of interest to determine from the data of Part II: (a) whether the adsorbed molecules are in a gaseous or otherwise expanded state and (b) which form of the equation of state best fits the experimental F *vs.* A curves.

Fluorochemical solutes used in this study were bis-(ϕ'-butyl) 3-methylglutarate, bis-(ϕ'-hexyl) 3, methylglutarate, bis-(ϕ'-octyl) 3-methylglutarate-bis-(ψ'-heptyl) 3-methylglutarate, hexyl ϕ-butyrate and 1,2,3-trimethylolpropane tris-(ϕ-butyrate). The method of purification of the compounds and selected physical constants are given in Part II. In this study 3-methylglutarate will be abbreviated 3-MEG and 1,2,3-trimethylolpropane as 1,2,3-TMP. The organic solvents propylene carbonate, tricresyl phosphate, Alkazene 42 or 1,2-dibromoethylbenzene, nitromethane, bis-(2-ethylhexyl) sebacate, mineral oil and hexadecane were also described in Part II of this investigation. All experiments were carried out at 20°.

Results

Equation of State of Adsorbed Monolayers.—The F *vs.* A isotherms of Part II are similar in general configuration to many reported for hydrocarbon derivatives adsorbed at oil–water interfaces[3,4] which were in the gaseous or otherwise expanded states. In the liquid-expanded and gaseous states, the F *vs.* A isotherms for many non-ionized, polar, surface-active agents having hydrocarbon hydrophobic "tails" are described by the well-known Langmuir equation[5]

$$(F + F_0)(A - A_0) = kT \qquad \text{(i)}$$

In this expression T is the absolute temperature, k

(1) Presented at the Annual Meeting of the Division of Colloid Chemistry, American Chemical Society, September 14, 1959.

(2) N. L. Jarvis and W. A. Zisman, THIS JOURNAL, **64**, 150 (1960).

(3) (a) N. Pilpel, *J. Colloid Sci.*, **11**, 51 (1956); (b) A. E. Alexander and T. Teorell, *Trans. Faraday Soc.*, **35**, 727 (1939).

(4) E. Hutchinson, *J. Colloid Sci.*, **3**, 219 (1948).

(5) I. Langmuir, *J. Chem. Phys.*, **1**, 756 (1933).

the Boltzmann constant, A_0 the limiting area per molecule of the adsorbed film and F_0 a corrective term necessitated by the forces of attraction (or intermolecular cohesion) between neighboring adsorbed solute molecules. Some analytical similarity in behavior between monolayers of fluoroesters at the free surface of organic liquids and of uncharged hydrocarbon derivatives at oil–water interfaces is to be expected because of the low values of F_0 operative between perfluoro groups in the former case and the weak forces of attraction in the later case which result from the existence of mixed films of the hydrocarbon portions of the polar molecules with the solvent molecules in the oil phase.[3,4,6]

Using a modification of equation i, in which kT was replaced by a different constant C, which was determined for each isotherm, Pilpel[3a] found that for films of certain alcohols and ketones, adsorbed at the benzene–water interface, the values of F_0 were between 0.4 and 2.3. The results of similar calculations for expanded films of bis-(ϕ'-butyl) 3-MEG in propylene carbonate and tricresyl phosphate are given in Table I. From the resulting values of F_0 of 0.05 and 0.06, it is evident that the correction for intermolecular cohesion between these fluorocarbon molecules is an order of magnitude less than between the polar hydrocarbon compounds reported. Equation i, however, fits the experimental data for the fluoroesters only when the monolayers are quite expanded. As each film becomes more condensed and the cohesive forces between solute molecules become more appreciable, deviations from equation i become larger.

A much better fit to our experimental F *vs.* A curves at values of A less than 150 Å.^{2} is obtained using the two-dimensional analog of the van der Waals equation of state for gases first used by Langmuir[7]

$$(F + a/A^2)(A - A_0) = kT \qquad \text{(ii)}$$

Hedge[8] has recently shown that equation ii can be obtained from the general equation of state for gaseous monolayers derived by Phillips and Rideal.[9] In the case of neutral uncharged molecules their term E_v for the energy of cohesion between adsorbed molecules can be equated to $a/$Å^2. Thus the stronger the cohesive forces between adsorbed molecules at a given value of A, the larger "a" will be. Accordingly, we can assume that E_v will be greatest at closest packing and that it will decrease inversely as the fourth power of the average distance between the adsorbed molecules. Obviously the molecules of the monolayer will have fewer points of contact as the film expands thus diminishing the effect of the "short range" cohesive forces. The term E_v in equation ii will also be influenced by the dilution effect of any solvent molecules which are able to adsorb as the result of association with solute molecules to form a mixed film.

The value of "a" can be expected to remain constant over a given range of film pressures only if the adsorbed molecules maintain the same orientation with respect to each other and the solvent. As the monolayer expands, the closely packed solute molecules can begin to assume different orientations, and the points of contact or of nearest approach between neighboring molecules may be altered. This change in orientation may also affect the extent of interaction or association between solvent and solute molecules, which could also cause the value of "a" to vary with the film pressure. In the last column of Table I will be found the values of "a" for bis-(ϕ'-butyl) 3-MEG in propylene carbonate. It will be seen that as A increases to 145 Å.^{2}, "a" begins to increase significantly. Similar increases in "a" begins to increase significantly. Similar increases in "a" at large areas per molecule were computed from most of the F *vs.* A isotherms. Such variations in "a" do not cause significant deviations of the experimental data from the curve of equation ii because at such large values of A the term a/A^2 becomes quite small.

The constants "a" and A_0 in equation ii were determined for each F *vs.* A isotherm reported. By first assuming a reasonable value for A_0 and then substituting experimentally determined values of F and A from a given isotherm into equation ii, a series of values for "a" were calculated. This procedure was repeated assuming different values for the limiting area, A_0, from 20 to 50 Å.^{2}. The best values of A_0 were those leading to the series of values for "a" which showed the least variation with F. The third and fourth columns of Table I show how F_0 from equation i and "a" from equation ii vary with F when A_0 is assumed to be 31×10^{-16} cm.^{2}. This was the best choice of A_0 as "a" has a nearly constant value of 2.7×10^{-28} over a wide range of A.

Figure 1 shows graphically that equation ii is in much better agreement with the experimental force–area isotherms than equation i. Hedge has shown that equation ii describes the F *vs.* A isotherm of lecithin monolayers at the air–water interface much better than equation i.

TABLE I

VARIATION OF "a" AND F_0 WITH AREA PER MOLECULE (A) FOR A MONOLAYER OF BIS-(ϕ'-BUTYL) 3-MEG ADSORBED AT THE INTERFACE OF PROPYLENE CARBONATE AND AIR

(Based on $A_0 = 31 \times 10^{16}$ cm^2.)

Film pressure F (dynes/cm.)	Area per solute molecule $A \times 10^{16}$ (cm.^{2})	Calcd. constants F_0 and "a" from Eq. i F_0 (dynes/cm.)	Calcd. constants F_0 and "a" from Eq. ii "a" $\times 10^{28}$ (dyne-cm.^{2})
2	145.0	1.5	3.2
3	104.3	2.5	2.7
4	84.6	3.5	2.5
5	71.8	4.9	2.5
6	62.6	6.8	2.6
7	56.5	8.7	2.9
8	53.5	9.9	2.9
10	51.1	10.2	2.6
12	49.0	10.4	2.7

Assuming the term a/A^2 is the correct expression for the energy of cohesion between these uncharged, adsorbed, solute molecules, "a" would be expected to decrease with increasing fluorination of the solute

(6) W. A. Zisman, *J. Chem. Phys.*, **9**, 534, 729, 789 (1941).
(7) I. Langmuir, *J. Am. Chem. Soc.*, **54**, 2798 (1932).
(8) D. G. Hedge, *J. Colloid Sci.*, **12**, 417 (1957).
(9) N. J. Phillips and E. K. Rideal, *Proc. Roy. Soc. (London)*, 232 (1955).

and to increase with addition of associating groups such as carboxyl. This is shown to be true in Table II where "a" and A_0 are given for each of the partially fluorinated esters dissolved in Alkazene 42 and nitromethane. In both solvents as the F/H ratio increases in going from bis-(ϕ'-butyl) 3-MEG, to bis-(ϕ'-hexyl) 3-MEG and bis-(ϕ'-octyl) 3-MEG, the value of "a" decreases regularly. The plot of "a" *vs.* F/H shows that "a" decreases rectilinearly as F/H rises for each of these solutes. The large values of "a" for 1,2,3-TMP tris-(ϕ-butyrate) and bis-(ψ'-heptyl) 3-MEG are due to the presence of additional associating groups, an added carboxyl group and the terminal highly polar $-CF_2H$ group, respectively. Values of A_0 range from 22 to 36 Å.^{2} for all solutes except 1,2,3-TMP tris-(ϕ-butyrate) and bis-(ψ'-heptyl 3-MEG dissolved in nitromethane, and 1,2,3-TMP tris-(ϕ-butyrate) dissolved in Alkazene 42. Such variations in A_0, however, cause little change in the values calculated for "a."

TABLE II

VALUES OF CONSTANTS "a" AND A_0 FOR FLUOROESTERS ADSORBED FROM SOLUTIONS IN ALKAZENE 42 AND NITROMETHANE

Surface active solute	Atomic ratio fluorine/ hydrogen	Solvent: Alkazene 42 $A_0 \times 10^{16}$ (cm.^{2})	Alkazene 42 "a" $\times 10^{28}$ (dyne-cm.^{3})	Nitromethane $A_0 \times 10^{16}$ (cm.^{2})	Nitromethane "a" $\times 10^{28}$ (dyne-cm.^{3})
Bis-(ϕ'-octyl) 3-MEG	2.50	28	1.3	22	1.2
1,2,3-TMP tris-(ϕ-butyrate)	1.91	42	4.5	49	4.9
Bis-(ϕ'-hexyl) 3-MEG	1.83	25	2.0	31	2.8
Bis-(ψ'-heptyl) 3-MEG	1.71	25	3.2	42	4.9
Bis-(ϕ'-butyl) 3-MEG	1.17	27	2.8	36	3.8
Hexyl ϕ-butyrate	0.53	33	4.0	35	4.2

Values of "a" and A_0 calculated from the F *vs.* A isotherms of bis-(ϕ'-butyl) 3-MEG in each of the solvents are given in Table III. The values of A_0 and "a" are seen to be a function of the organic solvent used, A_0 varying from 27 to 36 Å.^{2}. It is apparent that "a" increases with decreasing surface tension and increases with increasing solubility.

TABLE III

CONSTANTS "a" AND A_0 OF EQUATION ii FOR BIS-(ϕ'-BUTYL) 3-MEG ADSORBED FROM VARIOUS ORGANIC LIQUIDS

Organic solvent	Solvent surface tension at 20°	$A_0 \times 10^{16}$ (cm.^{2})	"a" $\times 10^{28}$ (dyne-cm.^{3})
Propylene carbonate	41.1	31	2.7
Tricresyl phosphate	40.4	31	1.7
Alkazene 42	38.2	27	2.8
Nitromethane	36.2	36	3.8
Bis-(2-ethylhexyl) sebacate	31.0	34	4.0
Mineral oil	29.9	32	4.0
Hexadecane	27.4	30	3.8

That these adsorbed monolayers are in the gaseous state at low film pressures is also evident from a graph of FA/kT *vs.* F, using the method of

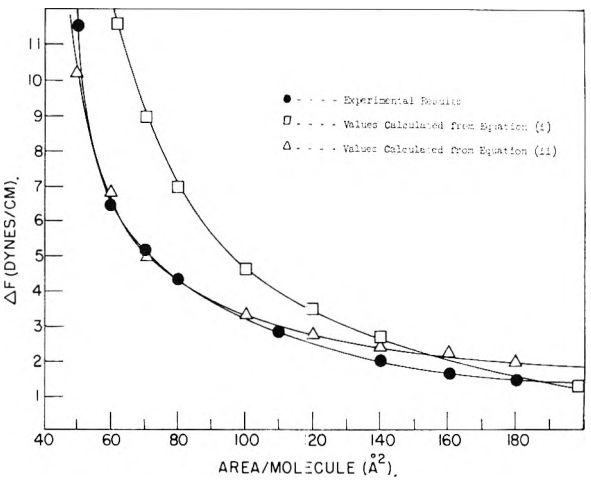

Fig. 1.—Force–area isotherms of bis-(ϕ'-butyl) 3-methylglutarate adsorbed at propylene carbonate–air interface.

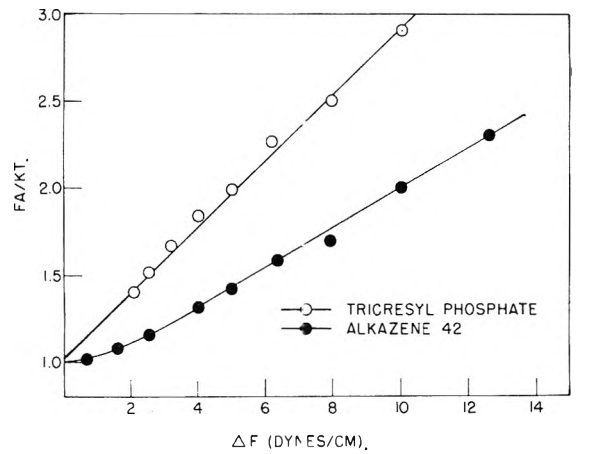

Fig. 2.—FA/kT *vs.* F for bis-(ϕ'-butyl) 3-methylglutarate adsorbed at alkazene 42–air and propylene carbonate–air interfaces.

Schofield and Rideal.[10] Results for bis-(ϕ'-butyl) 3-MEG in tricresyl phosphate plot as a straight line in Fig. 2 with an intercept of 1.0 at $F = 0$. When the solvent is Alkazene 42, the plot deviates from linearity by curving at $F = 3$ dynes/cm, and approaching $FA/RT = 1$ asymptotically as F approaches zero. The slope of these lines at high film pressures is greater the higher the surface tension of the organic substrate.

Work of Adsorption.—Differences in the reversible work of adsorption ($\lambda_1 - \lambda_2$) of two homologous fluoroesters having concentrations c_1 and c_2, respectively, and differing only in the number of $-CF_2-$ groups can be estimated for their adsorption at the interface of air with an organic liquid by the method of calculation used by Langmuir[11] in discussing adsorption of fatty acids at the air–water interface. Thus, if c_1 and c_2 are small, it follows from the same theoretical argument that

$$\lambda_1 - \lambda_2 = RT \ln \left(\frac{\Gamma_1}{c_1} \Big/ \frac{\Gamma_2}{c_2} \right) \qquad \text{(iii)}$$

Values of $\lambda_1 - \lambda_2 = \Delta\lambda$ were determined for the (ϕ'-butyl) and (ϕ'-hexyl) as well as for the (ϕ'-

(10) R. K. Schofield and E. K. Rideal, *Proc. Roy. Soc.* (*London*), 232 (1925).

(11) I. Langmuir, *J. Am. Chem. Soc.*, **39**, 1848 (1917).

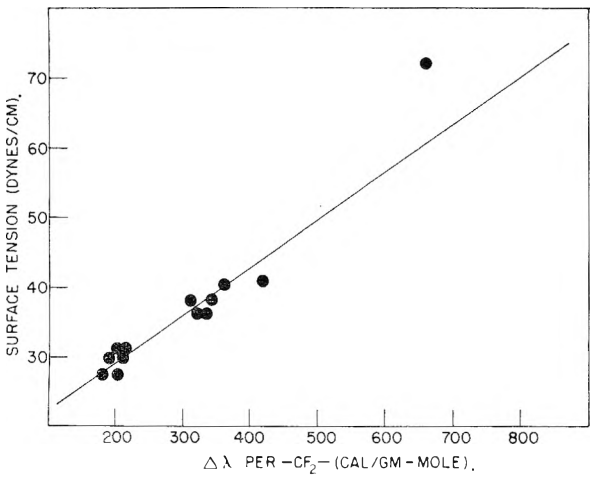

Fig. 3.—Work of adsorption per $-CF_2-$ group *vs.* surface tension of organic solvent.

hexyl) and (ϕ'-octyl) diesters of 3-MEG adsorbed at the surface of each organic liquid. Concentrations used corresponded to values of A of at least 150 Å.^{2} so that it was reasonable to assume each solute molecule adsorbed at the interface with both fluorocarbon chains lying essentially parallel to the surface. It is further assumed that all $-CF_2-$ groups occupy equivalent positions with respect to the structure of the surface layer. Since the solutes are diesters, each pair of successive homologs differ by four $-CF_2-$ groups per molecule. Therefore values of $\Delta\lambda$ calculated for each pair from equation iii were divided by four to give the reversible work per $-CF_2-$ group. Results of the calculations are given in Table IV.

As expected, the reversible work of adsorption per $-CF_2-$ group decreased with the surface tension of the organic liquid as shown in Figure 3. A value of $\Delta\lambda$ for adsorption of $-CF_2-$ groups at the water–air interface can be calculated from the concentration *vs.* surface tension of ϕ-octanoic and ϕ-decanoic acids dissolved in water at 25° reported by Bernett and Zisman.[12] The value of $\Delta\lambda$ in water was approximately 650 cal./g.-mole for solutions of less than 0.002 mole/liter, corresponding to an area per molecule greater than 150 Å.^{2}. This calculation was made by applying the Gibbs adsorption equation in the form

$$\Gamma = -\frac{c}{RT}\left(\frac{\partial\gamma}{\partial c}\right) \qquad \text{(iv)}$$

using concentration instead of activity and assuming no interaction between solute molecules. As calculated here, $\Delta\lambda$ per $-CF_2-$ group on water is somewhat less than the value of approximately 850 cal./g.-mole obtained by extrapolating the straight line of Fig. 3 to the surface tension of water. This difference may be due to errors in calculating the adsorption excess arising from the assumption of no interaction between solute molecules. Langmuir found the average increase in $\Delta\lambda$ per CH_2 group at the interface of water and air to be about 625 cal. per g.-mole.

TABLE IV

REVERSIBLE WORK OF ADSORPTION PER $-CF_2-$ GROUP FOR PARTIALLY FLUORINATED (ϕ-ALKYL) 3-MEG DIESTERS ADSORBED AT INTERFACE OF ORGANIC LIQUID WITH AIR

Organic solvent	Solvent surface tension (dynes/cm.)	Reversible work per $-CF_2-$ group (cal./g.-mole) From butyl and hexyl derivatives	Reversible work per $-CF_2-$ group (cal./g.-mole) From hexyl and octyl derivatives
Propylene carbonate	41.1	420	420
Tricresyl phosphate	40.4	360	360
Alkazene 42	38.2	340	310
Nitromethane	36.2	330	320
Bis-(2-ethylhexyl) sebacate	31.0	210	200
Mineral oil	29.9	210	190
Hexadecane	27.4	180	200

(12) M. K. Bernett and W. A. Zisman, THIS JOURNAL, **63**, 1911 (1959).

NOTES

THE TEMPERATURE COEFFICIENT OF RESISTANCE OF Pd–H ALLOYS[1]

BY ROBERT J. FALLON AND GILBERT W. CASTELLAN

Contribution from the Department of Chemistry, The Catholic University of America, Washington 17, D. C.

Received February 13, 1959

Fisher in 1906[2] and Kruger and Gehm in 1933[3] studied the relationship between the hydrogen content and relative resistance of palladium wires, and obtained essentially the same results, even though their studies were made at different temperatures. Fisher worked at 18° and Kruger and Gehm worked at 0°. Sieverts and Danz,[4] in 1937, measured the resistance of a palladium wire at 20° after cathodic charging with hydrogen and obtained a curve slightly different from that obtained by Fisher and Kruger and Gehm.

The hydrogen content as a function of relative resistance of a 15 mil palladium wire was determined at 49.3° in connection with some other work.[5] The wire was placed in a Teflon cell which contained hydrogen stirred 2 N H_2SO_4. The wire occluded hydrogen and the resistance was measured with a Mueller thermometer bridge that could be read to ± 0.0001 Ω. The hydrogen content of the wire was determined by a procedure suggested by the work of Lewis and Ubbelohde.[6] The wire was broken from the leads and placed

(1) From a dissertation submitted by Robert J. Fallon to the Faculty of the Graduate School of Arts and Sciences of the Catholic University of America in partial fulfillment of the requirements of the degree of Doctor of Philosophy.

(2) F. Fisher, *Ann. Physik*, **20**, 503 (1906).

(3) F. Kruger and G. Gehm, *ibid.*, **16**, 174 (1933).

(4) A. Sieverts and W. Danz, *Z. physik. Chem.*, **B38**, 46 (1937).

(5) R. J. Fallon and G. W. Castellan, THIS JOURNAL, **64**, 4 (1960).

(6) F. A. Lewis and A. R. Ubbelohde, *J. Chem. Soc.*, 1710 (1954).

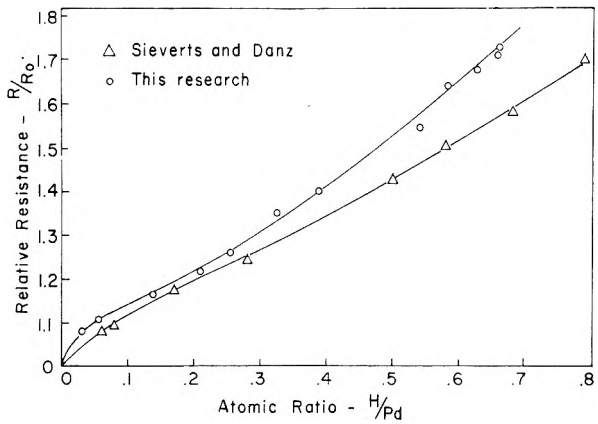

Fig. 1.—Dependence of relative resistance on hydrogen content of palladium wire at two different temperatures.

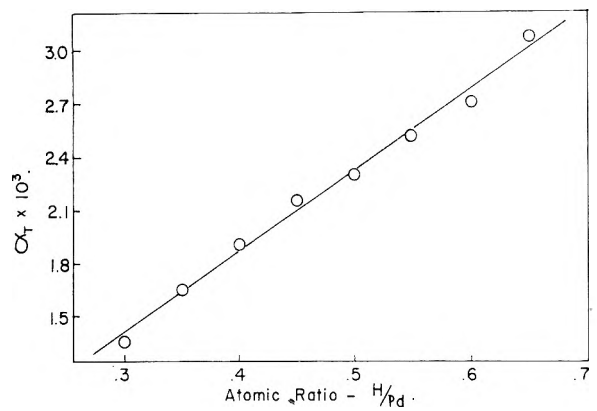

Fig. 2.—Temperature coefficient of resistance of palladium *vs.* hydrogen content.

in a 250-ml. erlenmeyer flask which contained a measured amount of standardized ceric ammonium sulfate in a 1 *N* sulfuric acid solution. The flask was placed in a shaker and further amounts of ceric solution were added until the yellow color persisted for at least 12 hr. The solution then was titrated with ferrous ammonium sulfate using one drop of 0.025 *M* ferroin as indicator. A Gilmont ultramicroburet which could be read to 0.001 ml. was used in this titration. Two blanks were run simultaneously to give a check on the concentration of the ferrous solution which decreased slightly on standing.

The values obtained by Sieverts and Danz at 20° and the values obtained here at 49.3° were plotted as shown in Fig. 1. From these plots the values of the temperature coefficient of resistance (α_T) were calculated and are plotted in Fig. 2. The equation of the line in Fig. 2 is

$$\alpha_T = 0.038(10^{-3}) + 4.58(10^{-3})(\mathrm{H/Pd})$$

MIE THEORY OF LIGHT SCATTERING—LIMITATIONS ON ACCURACY OF APPROXIMATE METHODS OF COMPUTATION

By Richard D. Murley

Research Department, British Titan Products Company Limited, 10 Stratton Street, London W.1, England

Received July 3, 1959

The scattering of light by small particles is of considerable technological importance, particularly to manufacturers of pigments. The calculation of the scattering properties of colloidal spheres is extremely tedious using the rigorous theory of Mie[1] and any approximate methods simplifying this work are of real value.

The total incident flux scattered by a spherical particle radius r is $\pi r^2 Q$, where Q is the scattering coefficient. Q is a function of n and x, where n is the refractive index of the particle relative to the surrounding medium and $x = 2\pi r/\lambda$ (λ is the wave length of the incident light in the surrounding medium). An approximate method for determining Q with an accuracy of $\pm 3\%$ is given by Penndorf[2] and this has been compared with values of Q calculated by the complete formula of Mie for $n = 1.831$. Both sets of results are given in Fig. 1,

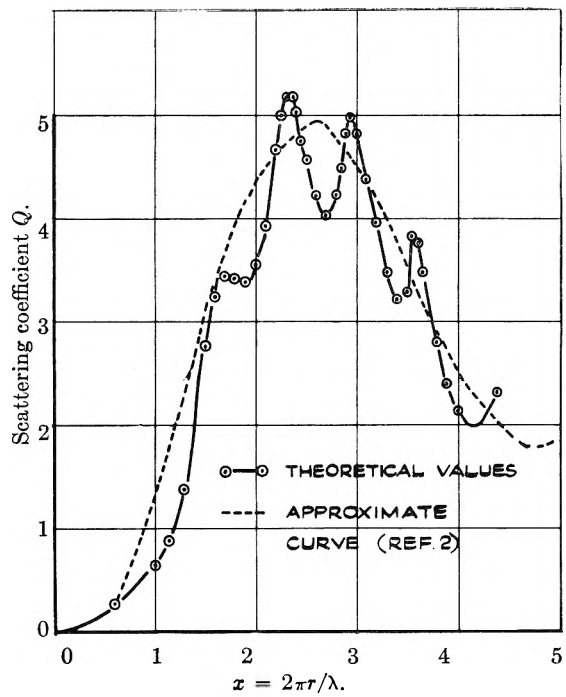

Fig. 1.—Plot of scattering coefficient Q against x for refractive index $n = 1.831$.

and there is seen to be considerable discrepancy between the approximate and full calculations. This difference is due to the ripple structure which is present in the true curve and which has been removed by the approximation. A minimum in the ripples occurs at the first maximum of the approximation for this value of n, and it is seen from the figure that in general the ripple structure has become of considerable importance.

In view of this result it appears that the use of approximate methods such as the one described must be limited to $n \leqslant 1.6$, where the accuracy is more rigorously established. The results of using approximate methods of calculation for systems with a narrow particle size distribution, and mean diameter lying in the range of the first maximum of the scattering function Q, could be extremely misleading for higher values of n. For this type of system the accuracy given by the approximate method does not approach 2–3% in the given example.

(1) G. Mie, *Ann. Physik*, [4] **25**, 377 (1908).
(2) R. B. Penndorf, This Journal, **62**, 1537 (1958).

The author wishes to thank the directors of British Titan Products Company Limited for permission to publish this note.

ROLE OF MULTIPLE BONDING IN ELECTRON TRANSFER REACTIONS

By E. R. Nightingale, Jr.[1]

Department of Chemistry, University of Pittsburgh, Pittsburgh 13, Pennsylvania

Received July 13, 1959

Factors which influence the rate and mechanism of oxidation–reduction reactions warrant consideration because the nature of the electron transfer process is so inadequately understood. One such factor whose role has not been previously assessed is that of bond order and the effect of resonance shortening. The only series of compounds for which sufficient data are available to permit interpretation appears to be that of the oxygenated halogenates, ClO_3^-, ClO_4^-, BrO_3^-, IO_3^- and IO_4^-. The present note concerns the effect of multiple bonding on the rate of the electron transfer process and correlates the character of the X–O bond with the reactivity of the halogenates both in homogeneous solution and for electrode reactions.

Experimentally, it is observed that the order of decreasing chemical reactivity $IO_3^- > BrO_3^- > ClO_3^-$, ClO_4^- parallels the shortening of the X–O bond from that expected for the single covalent bond distance. The effect of this bond shortening upon the rate or mechanism of the electron transfer process is, of course, subject to the same limitations as the previous interpretations of bond shortening[2-5] since the nature of multiple bonding is not well understood. The classical treatment of Pauling[6] relates bond shortening to the amount of double-bond character. However, this explanation is not satisfactory for heteropolar bonds because it fails to account for the shortening of the covalent bond distance and the increase in the bond energy caused by the partial ionic character of the bond. Furthermore, in species such as PO_4^{-3} and SiO_4^{-4}, the shortening is sufficient to predict complete double bonding and thus place a formal negative charge on the central atom which is contrary to the charge distribution predicted from electronegativities.

Recently, Pauling[7] has revised the original interpretation of bond shortening to account for the partial ionic character and partial π-bond character of heteropolar bonds. This treatment alleviates the objection of formal negative charge on the more electropositive central atom and retains the Pauling electroneutrality principle[8] that the electronic charge on each atom within a stable molecule is close to zero and in no case greater than $\pm 1\epsilon$.

Table I compares the interatomic distance and multiple bond character of the X–O bonds in a series of oxygenated halogenates. With the exception of the periodate ion, the per cent. of π-bond character calculated considering partial ionic character and bond moment neutralization[7] agrees well with the double bond character calculated using the older Pauling relation[6]; the calculated bond distances also agree rather closely with the experimental values. It seems probable that the failure of the periodate values to correspond more closely results from the failure of both theories to account adequately for the interaction between elements from the different periods with appreciably different electronegativities. Ninety per cent. double-bond character for periodate is too large because it fails to allow for the bond shortening due to the partial ionic character. Similarly, 25% π-bond character for periodate appears too small and suggests that the decrease in bond moment neutralization with periodic row number[7] is too large, at least for atoms with coördination number of four. If the excess shortening of the I–O bond is all attributed to partial π-bonding, the π-bond character of the I–O bond in periodate is calculated as approximately 55%.

Table I

Interatomic Distance and Multiple Bond Character of X–O Bonds in Oxygenated Halogenates

	IO_3^-	BrO_3^-	ClO_3^-	ClO_4^-	IO_4^-
Pauling single covalent bond length,[a] Å.	1.99	1.80	1.65	1.65	1.99
Experimental bond length, Å.	1.83[b]	1.68[c]	1.48[d]	1.48[e]	1.79[f]
Per cent. double-bond character[g]	20	35	60	60	90
Schomaker–Stevenson single covalent bond length,[g] Å.	1.97	1.82	1.68	1.68	1.97
Calcd. bond length,[h] Å.	1.87	1.68	1.50	1.50	1.86
Per cent. π-bond character[h]	21	37	54	63	25

[a] Calcd. from ref. 6. [b] $NaIO_3$. [c] $KBrO_3$. [d] $NaClO_3$. [e] $NaClO_4$. [f] $NaIO_4$. [g] Calcd. from ref. 2. [h] Calcd. from ref. 7.

Utilizing the partial π-bond concept, the decrease in chemical reactivity (*vide infra*) which accompanies the increasing π-bond character may be explained by the fact that increased π-bonding utilizes the oxygen p-orbitals and makes them less available for intermolecular bonding. Using this principle, the behavior of the iodate ion in aqueous solution recently has been attributed to lack of appreciable double-bond character.[9] Conductance and viscosity data indicate that the iodate ion is appreciably hydrated whereas the BrO_3^-, ClO_3^-, ClO_4^- and IO_4^- ions are less extensively hydrated because of the increase in bond order. Double-bonding localizes the negative charge on the central halogen atom thereby rendering the charge less accessible for (presumably hydrogen) bonding with the solvent molecules.

While extensive rate data are not available to permit a quantitative correlation between bond order and reactivity, several significant comparisons may be made. Halperin and Taube[10] have studied the transfer of oxygen in the reaction of halogenates

(1) On leave from the University of Nebraska, Lincoln 8, Nebraska.

(2) V. Schomaker and D. P. Stevenson, *J. Am. Chem. Soc.*, **63**, 37 (1941).

(3) A. F. Wells, *J. Chem. Soc.*, 55 (1949).

(4) M. Huggins, *J. Am. Chem. Soc.*, **75**, 4126 (1953).

(5) M. G. Brown, *Trans. Faraday Soc.*, **55**, 694 (1959).

(6) L. Pauling, "The Nature of the Chemical Bond," Cornell University Press, 2nd Ed., Ithaca, N. Y., 1948.

(7) L. Pauling, This Journal, **56**, 361 (1952).

(8) L. Pauling, *J. Chem. Soc.*, 1461 (1948).

(9) E. R. Nightingale, Jr., and R. F. Benck, This Journal, **63**, 1777 (1959).

(10) J. Halperin and H. Taube, *J. Am. Chem. Soc.*, **74**, 375 (1952).

with sulfite. In acid medium, the reaction of iodate and bromate with sulfite is very rapid[11] whereas the reaction of chlorate, which possesses a considerably larger bond order, proceeds at a measurable velocity.[12] The exchange of oxygen between iodate and water is immeasurably rapid, while both bromate and chlorate exchange with half-times of the order of many hours.[10] Halperin and Taube suggest that the difference between the oxygen lability of iodate and of bromate and chlorate may lie in the tendency for iodine to assume coördination numbers greater than 3 or 4, but there is no evidence for the existence of a stable para-iodate or similarly hydrated species in aqueous solution. However, the ability to expand the coördination sphere is related to the absence of appreciable multiple bond character and the availability of the d-orbitals, and the role of bond hybridization cannot adequately be evaluated without further exchange data, particularly for perchlorate and periodate.

Further information is available from a study of the electrode processes. In *p*H 0 medium, the half-wave potentials for the reduction of IO_4^-, IO_3^- and BrO_3^- at the dropping mercury electrode (d.m.e.) are + 0.38,[13] + 0.06,[14] and − 0.11[14] v. *vs.* s.c.e., respectively. Chlorate and perchlorate are not reduced at the d.m.e. Measuring the overpotential as the difference between the standard electrode potential and the half-wave potential, the overpotentials for the reduction of IO_4^-, IO_3^- and BrO_3^- are 1.2, 0.7 and 1.3 v., respectively. The overpotential for a slow (irreversible) reaction is related, though not in a simple manner, to the rate of the electrode reaction, and we estimate the relative rates of reduction as $IO_3^- > BrO_3^- \geq IO_4^-$. Assuming the bond hybridization to be invariant, the effect of the number of coördinating atoms may be illustrated by comparing, for example, the iodate and periodate ions. For the completely σ-bonded structure, the formal charge on the iodine atom is more positive in periodate than in iodate. However, the greater π-bonding in periodate reduces more effectively this formal charge and leaves the iodine atom less electropositive than in iodate. The iodate ion is therefore more reactive because of the more electrophilic iodine atom and the greater availability of the oxygen *p*-orbitals. Recently, Gierst[15] has measured the rates of reduction of iodate and bromate in alkaline medium at 25° at a mercury electrode. For a rate constant of 10^{-3} cm./sec., the potentials for the iodate and bromate reduction are − 1.05 and − 1.45 v. *vs.* s.c.e., respectively, corresponding to overpotentials of about 1.06 and 1.81 v.[16] The values for αn_α are 0.96 for iodate and 0.65 for bromate,[15] where α is the transfer coefficient. Assuming that the number n_α of electrons transferred in the rate determining step is two in each case, the values for the transfer coefficient of 0.48 for iodate and 0.32 for bromate are congruous with the increase in the bond order for these species. The fact that chlorate cannot be reduced at the mercury electrode suggests that the transfer coefficient is sufficiently small to preclude an appreciable reaction rate prior to the hydrogen evolution.

Acknowledgment.—Stimulating discussions with Dr. D. H. McDaniel are gratefully acknowledged.

(11) A. Schwicker, *Chem. Zentr.*, **15**, 845 (1891).

(12) A. C. Nixon and K. B. Krauskopf, *J. Am. Chem. Soc.*, **54**, 4606 (1932).

(13) P. Souchay, *Anal. Chim. Acta*, **2**, 17 (1948).

(14) I. M. Kolthoff and E. F. Orleman, *J. Am. Chem. Soc.*, **64**, 1044, 1970 (1942).

(15) L. Gierst, private communication.

(16) From these data, the reaction rates may be calculated for any arbitrary value of overpotential. For instance, the ratio of the rate of reduction of iodate to that of bromate is approximately 10^3 at a constant overpotential of 1.4 v.

THE INTERMOLECULAR FORCE CONSTANTS OF RADON

BY GEORGE A. MILLER

Contribution from the Chemistry Department, Georgia Institute of Technology, Atlanta, Georgia

Received July 9, 1959

In a recent article, Srivastava and Saxena[1] have calculated the Lennard-Jones(6–12) potential parameters of radon. Their method involves a correlation of the thermal diffusion of mixtures of rare gases with a function of their molecular weights. The values they have obtained, $\sigma = 4.48$ A. and $\epsilon/k = 484$°K., lead to an unusually high dispersion energy of 2.16×10^{-57} erg cm.^{6}. It is the purpose of this paper to estimate the potential parameters by other means.

First, the polarizability of radon will be estimated using the known polarizabilities of the other rare gas atoms as a guide. Pauling's formula[2] for atomic polarizability (α) is given by

$$\alpha = \frac{3}{8} a^3 \Sigma \left(\frac{n_i}{Z - S_i(\alpha)} \right)^4 (5n_i^2 + 7) \qquad (1)$$

where $a = 0.528$ Å., n_i is the principal quantum number of the ith electron, Z is the atomic number, $S_i(\alpha)$ is the screening constant and $(Z - S_i(\alpha))$ the effective nuclear charge acting on the ith electron, and the summation is over all electrons in the atom. Actually, the polarizability may be accurately considered to arise from the outer two shells only. In the case of the rare gases, the contribution from the next-to-outer shell is always small and can be estimated from the polarizability of ions iso-electronic to the rare gas core. Table I gives the polarizability of the outer two shells of the rare gases along with the associated screening constants calculated from equation 1. The s-, p- and d-subshells are coalesced to give an averaged screening constant. The $5s^2p^6d^{10}$ contribution in radon has been obtained from the polarizability of the mercuric ion.[3]

The calculated screening constants associated with the outer shell are broken down into a consistent (but not unique) scheme of individual screening contributions in Table II. The arrangement is similar to that of Slater.[4] A contribution to the total screening effect on an outer electron from an s^2p^6 shell is made by the other electrons in that shell

(1) B. N. Srivastava and S. C. Saxena, *Physica*, **22**, 253 (1956).

(2) L. Pauling, *Proc. Roy. Soc. (London)*, **A114**, 181 (1927); L. Pauling and J. Sherman, *Z. Krist.*, **81**, 1 (1932).

(3) Landolt-Bornstein, "Zahlenwerte und Funktionen," Springer-Verlag, Berlin, 1950–1951.

(4) J. C. Slater, *Phys. Rev.*, **36**, 57 (1930).

TABLE I

POLARIZABILITY SCREENING CONSTANTS

Atom	α (A.^{3}) (see ref. 3)	Outer shell	α	$S(\alpha)$	Second shell	α	$S(\alpha)$
He	0.211	$1s^2$	0.211	0.415	...	...	...
Ne	0.398	$2s^2p^6$	0.398	5.31	$1s^2$	0.00016	0.40
A	1.63	$3s^2p^6$	1.62	12.17	$2s^2p^6$	.0074	5.30
Kr	2.48	$4s^2p^6$	2.42	28.00	$3s^2p^6d^{10}$	.0595	19.68
Xe	4.01	$5s^2p^6$	3.81	44.10	$4s^2p^6d^{10}$	.197	35.64
Rn	...	$6s^2p^6$	...	...	$5s^2p^6d^{10}$	.280	62.69

plus those in the inner shells. The total screening constant is thus a sum of terms from Table II. This scheme leads to a screening constant of 73.4 for the $6s^2p^6$ shell of radon, an effective nuclear charge of 12.6 and a total polarizability of 4.50 Å.^{3}

TABLE II

THE CONTRIBUTION PER ELECTRON TO THE SCREENING OF AN s^2p^6 TYPE ELECTRON

Principal shell	Type of shell s^2	s^2p^6	d^{10}	f^{14}
Outer	...	0.527	...	...
Second	0.810	0.810	0.783	0.783
Third	1.00	1.00	0.810	0.810
Fourth	1.00	1.00	1.00	1.00

Screening constants are known to vary with the type of property being calculated. Pauling has shown[2] that it is possible to estimate these variations. Thus if $S(\alpha)$ is the polarizability screening constant and $S(E)$ the energy screening constant of a valence electron, then, in terms of effective nuclear charge

$$Z - S(\alpha) = {}^1/_2\{3(Z - S(E)) - 1\} \qquad (2)$$

$$Z - S(E) = n\left(\frac{E}{13.53}\right)^{1/2}$$

where E is the ionization potential in electron-volts. Since the ionization potential of radon is known,[3] it is possible to calculate the polarizability of the $6s^2p^6$ shell with the help of the above equations. However, ionization refers to the removal of an outer p-electron whereas the values of $S(\alpha)$ in Table I refer to the average effect in an outer s^2p^6 shell. For this reason, and due to the approximate nature of equation 2, a more satisfactory result may be obtained by plotting $(Z - S(\alpha))$ from Table I against the same quantity calculated from E, for all the rare gases. Table III gives the results of such a comparison. The extrapolated value of the effective nuclear charge for the $6s^2p^6$ shell of radon yields a total polarizability of 5.86 Å.^{3}.

TABLE III

THE EFFECTIVE NUCLEAR CHARGE FOR THE OUTER SHELL FROM IONIZATION POTENTIALS

Atom	E (see ref. 3)	$Z - S(E)$	$Z - S(\alpha)$ From E	$Z - S(\alpha)$ From Table I
He	24.56	1.36	1.54	1.59
Ne	21.56	2.53	3.30	4.69
A	15.76	3.24	4.36	5.83
Kr	14.0	4.07	5.61	8.00
Xe	12.13	4.74	6.61	9.90
Rn	10.75	5.35	7.53	11.8 (extrap.)

The dispersion energy between two atoms obeying the Lennard-Jones (6–12) potential is given by $4\epsilon\sigma^6$. The polarizability of the second electronic shell of the rare gas atoms is always small in comparison with that of the outer shell. Therefore, it is reasonable to make use of the approximation[6] that the dispersion energy is proportional to $N^{1/2}\alpha^{3/2}$, where N is the number of electrons in the outer shell. This relationship is treated empirically by plotting log $4\epsilon\sigma^6$ against log $N\alpha^3$ for the rare gases. The two derived polarizabilities of radon (4.50 and 5.86 Å.^{3}) give extrapolated values of 6.61×10^{-58} and 11.0×10^{-58} erg cm.^{6}, respectively, for the dispersion energy of radon.

As a further test, use is made of the empirical relation[6] that n/r plotted against $Z^{1/2}$ gives a straight line of small positive slope for the rare gases, where r is the "covalent" radius. The attempt then is made to replace r with other parameters of atomic size: first the Bohr radius, second the parameter $\sigma/2$. The Bohr radius of the outer electronic shell is calculated from the size screening constant $S(s)$ by the equation

$$R = n^2a/(Z - S(s))$$

where, following the method of Pauling[2]

$$Z - S(s) = {}^1/_3\{4(Z - S(\alpha)) - 1\}$$

The values of n/R are found to be almost independent of Z for the heavier atoms and support that value of α obtained from the ionization potential of radon. A similar plot of $2n/\sigma$ against $Z^{1/2}$ yields a slightly curved line which extrapolates to a value of $\sigma = 4.36$ Å. for radon. If $R = 1.23$ is taken as the favorable value for radon, a plot of $\sigma/2$ against R extrapolates to a value of $\sigma = 4.34$ Å. for radon. These calculations are summarized in Table IV.

TABLE IV

VARIOUS SIZE PARAMETERS OF THE RARE GASES

Atom	$Z - S(\alpha)$	$Z - S(s)$	R	n/R	σ^c	$2n/\sigma$
He	1.585	1.78	0.296	3.27	2.60	0.77
Ne	4.69	5.92	.357	5.60	2.78	1.44
A	5.83	7.44	.639	4.70	3.41	1.76
Kr	8.00	10.33	.818	4.89	3.61	2.22
Xe	9.90	12.87	1.025	4.88	4.04	2.49
Rn	11.8[a]	15.4	1.23	4.86	(4.34)	
	12.6[b]	16.5	1.15	5.21	...	(2.75)

[a] From Table III. [b] From Table II. [c] See ref. 8.

From the melting, boiling and critical points (T_m, T_b, T_c) it is possible to estimate ϵ/k. Table V summarizes this relationship for the rare gases. A rounded value of $\epsilon/k = 290°$K. is chosen for radon from the data.

Two values of the dispersion energy of radon may be obtained independently from the above calcula-

(5) J. C. Slater and J. G. Kirkwood, *Phys. Rev.*, **37**, 682 (1931).
(6) R. T. Sanderson, *J. Inorg. & Nuclear Chem.*, **7**, 288 (1958).

TABLE V

Atom	ϵ/k[a]	T_m	T_b	T_c	ϵ/kT_m	ϵ/kT_b	ϵ/kT_c
Ne	35.5	26.5	27.3	44.5	1.34	1.30	0.78
A	123	84.0	87.5	151	1.46	1.41	0.815
Kr	178	117	120	210	1.52	1.48	0.85
Xe	221	161	166	290	1.37	1.33	0.76
Rn	...	202[b]	211[b]	377[c]	...	...	...

[a] See ref. 8. [b] R. W. Gray and W. Ramsay, *J. Chem. Soc.*, 95, 1073 (1909). [c] G. Woolsey, *J. Am. Chem. Soc.*, 59, 1577 (1937).

tions. From the value $\alpha = 5.86$ Å.^{3}, a value of 11.0×10^{-58} erg cm.^{6} already was obtained. Accepting the derived Lennard-Jones (6–12) potential parameters to be $\sigma = 4.35$ Å. and $\epsilon/k = 290$°K., a value of 10.8×10^{-58} erg cm.^{6} is obtained.

The results of this paper may be compared with the diffusion experiments of Hirst and Harrison.[7] The first approximation formula[8] for the diffusion coefficient of a binary mixture of gases is given by

$$D_{12} = 0.002628 \frac{[T^3(M_1 + M_2)/2M_1M_2]^{1/2}}{P\sigma_{12}^2 \Omega_{12}^{(1,1)*}} \quad (3)$$

where the symbols have the usual meaning (ref. 8). The diffusion coefficients calculated from equation 3 and the usual combination rules $\sigma_{12} = {}^1/_2(\sigma_1 + \sigma_2)$, $\epsilon_{12} = \sqrt{\epsilon_1\epsilon_2}$ do not agree with the experimental results, as is shown in Table VI. In fact no consistent set of parameters (σ, ϵ/k) can be found for radon which will reproduce the data satisfactorily. Therefore, these data cannot be used to improve the estimate made here of the potential parameters of radon.

TABLE VI

THE DIFFUSION COEFFICIENTS (cm.^{2} sec.$^{-1}$) FOR RADON IN FOUR DIFFERENT GASES AT 1 ATM. AND 15°

Binary mixture	Exptl.	Calcd.
Rn–H_2[a]	0.476	0.514
Rn–He[b]	.351	.465
Rn–Ne	.217	.172
Rn–A	.092	.086

[a] For hydrogen, $\sigma = 2.92$, $\epsilon/k = 31.3$ (ref. 8); [b] For helium, $\sigma = 2.60$, $\epsilon/k = 8.1$ (ref. 8).

(7) W. Hirst and G. E. Harrison, *Proc. Roy. Soc.* (*London*), **A169**, 573 (1938).

(8) J. O. Hirschfelder, C. F. Curtiss and R. B. Bird, "Molecular Theory of Gases and Liquids," John Wiley and Sons, Inc., New York, N. Y., 1954.

PREPARATION AND STRUCTURE DETERMINATION OF SOME NEW CUBIC AND TETRAGONALLY-DISTORTED PEROVSKITES

BY LOTHAR H. BRIXNER

Contribution from the Pigments Department, E. I. du Pont de Nemours & Co., Inc., Wilmington, Delaware

Received July 15, 1959

The perovskite structure and compounds crystallizing in this crystallographic type have been the subject of a great number of publications, dating back to Goldschmidt's[1] investigations on the theoretical requirements and relationships for this structure. More recently, Roth[2] gave a rather comprehensive summary and classification of perovskite-type compounds. In this paper, Roth discusses the $A^{II}B^{IV}O_3$ and the $A^{III}B^{III}O_3$ type on the basis of ionic radii of the constituent ions. All reported compounds consist of two oxide components, except for some solid solutions as in the $BaTiO_3/BaZrO_3$ system. Perovskites with substitutions in the A-sites of the type $La_{0.5}Ba_{0.5}MnO_3$ have been reported by Waugh[3]; and those with substitutions in the B-sites, of the type $LaZr_{0.5}Mg_{0.5}O_3$, have been reported by Rabenau.[4] A very recent publication by Galasso, Katz and Ward[5] describes B-site substitutions of the type $A^{II}(B_x^{II}B_y^{III}B_z^{V})O_3$, where A^{II} = Ba, Sr; B^{II} = Sr, Ca, Zn, Fe, Co, Ni; B^{III} = Co, Fe; and B^{V} = Ta or Nb. Scholder and Brixner[6] prepared perovskites with tetravalent molybdenum such as $BaMoO_3$, but no perovskites containing hexavalent molybdenum or tungsten have been reported. The $(NH_4)_3[FeF_6]$-type structure of Ba_3WO_6, as reported by Steward and Rooksby,[7] is, however, closely related to the perovskite structure. If these hexavalent ions are to be incorporated in the perovskite structure with a bivalent A-ion, 50 mole % of another bivalent ion of proper size must also be introduced in order to restore electroneutrality. This results in a compound such as $BaMo_{0.5}Ni_{0.5}O_3$, whose lattice parameter of 4.0225 Å. is almost identical with that of the cubic modification of $BaTiO_3$ (4.0121 Å.).

While in the titanate system the barium compound is tetragonally distorted at room temperature and the strontium compound is truly cubic at room temperature, the opposite is true for the new, substituted compounds. The compound $SrMO_{0.5}Ni_{0.5}O_3$ is tetragonally distorted with a c/a of 1.006, although Goldschmidt's tolerance factor of 0.88 should allow a true perovskite structure. All structural determinations were based on X-ray powder diffraction data. The absence of superstructure lines indicates a random distribution of the substituting ions.

Experimental

The starting materials used (all oxides, except for $SrCO_3$ and $BaCO_3$) were of best available purity and the components were weighed according to stoichiometry to the nearest milligram. Mixing was done by milling under acetone in a mechanical agate ball mill. The filtered and dried mixture usually was prefired at 1000° in a platinum dish until the theoretical CO_2-loss was observed. The reaction mixture then was ball-milled again (this time dry) and pressed into a 1-inch diameter pellet at 20,000 p.s.i. This pellet finally was fired for 4–6 hours between 1200 and 1400°. The reactions were carried out in air, except when there was a possibility of oxidation, as for instance in the case of $SrCr_{0.5}Nb_{0.5}O_3$ (the mixture would tend to form $SrCrO_4$ in air). For these compounds, all components were used in oxide form. Barium and strontium oxides were prepared from their corresponding carbonates by decomposition at 1200° under vacuum. When a vacuum of better than 10^{-5} mm. was achieved, the reaction was considered complete. The mixtures with the alkaline earth oxides were pressed directly at 40,000 p.s.i. into ${}^1/_2$-inch diameter pellets and fired at 1400° under argon

(1) V. M. Goldschmidt, *Skrifter Norske Videnskaps-Akad. Oslo I. Mat. Naturv, Kl.*, No. 2 (1926).

(2) R. S. Roth, *J. Research Natl. Bureau Standards*, **58**, 75 (1957).

(3) J. S. Waugh, *Mass. Inst. Technol. Progress Report*, No. XXIII, 54 (1958).

(4) A. Rabenau, *Z. anorg. allgem. Chem.*, **288**, 221 (1956).

(5) F. Galasso, L. Katz and R. Ward, *J. Am. Chem. Soc.*, **81**, 820 (1959).

(6) R. Scholder and L. Brixner, *Z. Naturforsch.*, **10b**, 178 (1955).

(7) S. G. Steward and H. P. Rooksby, *Acta Cryst.*, **4**, 503 (1951).

TABLE I

LATTICE PARAMETERS AND DENSITIES OF THE PREPARED COMPOUNDS

No.	Composition	a_0, Å.	c_0, Å.	c/a	Color	X-Ray density, g./cc.	Pycnometric density, g./cc.
1	$BaMo_{0.5}Co_{0.5}O_3$	4.0429	...	...	Black	6.60	6.49
2	$BaMo_{0.5}Ni_{0.5}O_3$	4.0225	...	...	Olive	6.70	6.54
3	$BaW_{0.5}Co_{0.5}O_3$	4.050	...	...	Black	7.67	7.51
4	$BaW_{0.5}Ni_{0.5}O_3$	4.0326	...	...	Light green	7.76	7.60
5	$SrMo_{0.5}Ni_{0.5}O_3$	3.9237	3.9474	1.006	Tan	5.82	5.81
6	$SrMo_{0.5}Co_{0.5}O_3$	3.9367	3.9764	1.01	Black	5.74	5.48
7	$SrW_{0.5}Co_{0.5}O_3$	3.9502	3.9746	1.006	Dark brown	6.46	6.39
8	$SrW_{0.5}Ni_{0.5}O_3$	3.9310	3.9592	1.007	Light green	6.97	6.90
9	$SrCr_{0.5}Nb_{0.5}O_3$	3.9421	...	...	Light green	5.64	5.62
10	$SrGa_{0.5}Nb_{0.5}O_3$	3.9477	...	...	White	5.85	5.78
11	$BaIn_{0.5}Nb_{0.5}O_3$	4.1454	...	...	White	6.74	6.74
12	$SrIn_{0.5}Nb_{0.5}O_3$	4.0569	...	...	White	5.95	5.85

purified over hot Ti–Zr alloy shavings. The reaction product was also reground, pressed and refired.

Analysis.—All compounds were analyzed for at least one metal component; most for two or all three.

Anal. Calcd. for $BaMo_{0.5}Co_{0.5}O_3$: Ba, 52.27; Mo, 18.25; Co, 11.21. Found: Ba, 52.60; Mo, 18.07; Co, 10.98.

Calcd. for $BaMo_{0.5}Ni_{0.5}O_3$: Ba, 52.29; Mo, 18.26; Ni, 11.17. Found: Ba, 51.97; Mo, 18.76; Ni, 10.93.

Calcd. for $BaW_{0.5}Co_{0.5}O_3$: Ba, 44.77; W, 29.99; Co, 9.60. Found: Ba, 43.64; W, 30.05; Co, 9.71.

Calcd. for $BaW_{0.5}Ni_{0.5}O_3$: B, 44.79; W, 29.99; Ni, 9.56. Found: Ba, 44.12; W, 28.88; Ni, 9.93.

Calcd. for $SrMo_{0.5}Ni_{0.5}O_3$: Sr, 41.15; Mo, 22.53; Ni, 13.78. Found: Sr, 41.40; Mo, 23.07; Ni, 13.82.

Calcd. for $SrMo_{0.5}Co_{0.5}O_3$: Mo, 22.51; Co, 13.83. Found: Mo, 22.67; Co, 13.71.

Calcd. for $SrW_{0.5}Co_{0.5}O_3$: W, 35.77; Co, 11.46. Found: W, 34.93; Co, 11.41.

Calcd. for $SrW_{0.5}Ni_{0.5}O_3$: W, 35.79; Ni, 11.42. Found: W, 34.86; Ni, 11.09.

Calcd. for $SrCr_{0.5}Nb_{0.5}O_3$: Cr, 12.50; Nb, 22.32. Found: Cr, 11.98; Nb, 21.73.

Calcd. for $SrGa_{0.5}Nb_{0.5}O_3$: Nb, 21.41. Found: Nb, 20.78.

Calcd. for $BaIn_{0.5}Nb_{0.5}O_3$: Nb, 16.06. Found: Nb, 16.12.

Calcd. for $SrIn_{0.5}Nb_{0.5}O_3$: Nb, 19.40. Found: Nb, 18.97.

X-Ray Study.—The parameters of all cubic compounds were determined on the basis of powder diffraction patterns obtained in a 114.6 mm. Philips camera at 24.5°. The samples were sealed in 0.2 mm. Lindemann glass capillaries and exposed to copper K α radiation (λ 1.5418 Å.) for 3 to 5 hours. The readings were taken visually at constant temperature with a Hilger and Watts film measuring rule with 0.05 mm. vernier divisions. All films were corrected for film shrinkage and a_0 was obtained by extrapolation *vs.* $\frac{1}{2}(\cos\theta/\sin\theta) + (\cos^2\theta/\theta)$ according to Nelson and Riley.[8] The parameters can be considered accurate to ±0.0005 Å.

The tetragonal compounds containing nickel also were X-rayed with copper K α radiation with a Norelco diffractometer at 26°. A chart speed of $\frac{1}{2}$" per minute at a goniometer speed of $\frac{1}{8}$° per minute was selected. Tungsten powder was used as an internal standard. Cobalt K α radiation was used for the compounds containing cobalt. The 411 (330), 420, 332, 422 lines of the compound $SrMo_{0.5}Ni_{0.5}O_3$ were step-scanned at 0.02° steps for accurate parameter determination. The parameters of the compounds investigated so far are summarized in Table I.

Density.—The densities were determined on powdered specimens of −200 mesh. The samples were weighed into a 5-ml. pycnometer and CCl_4 was distilled onto the sample under vacuum.

Acknowledgment.—The author is indebted to Messrs. Keith R. Babcock and Anthony F. Matera for their assistance in the X-ray work.

(8) J. B. Nelson and D. P. Riley, *Proc. Phys. Soc. (London)*, **57**, 160 (1945).

A SEMIEMPIRICAL METHOD FOR DETERMINING BOND DISSOCIATION ENERGIES AND THE RESONANCE ENERGIES OF FREE RADICALS

BY CHEVES WALLING

Contribution from the Department of Chemistry, Columbia University New York, N. Y.

Received July 15, 1959

The difference between the bond dissociation energies $D(CH_3\text{–}H)$ and $D(R\text{–}H)$ is commonly taken as the resonance energy of the free radical R·, and is an important quantity in discussing the energetics (and often rates) of free radical processes.[1] Unfortunately, methods of determining $D(R\text{–}H)$ either directly or *via* thermochemical cycles become extremely difficult when R is a complex group and many values which would be useful in free radical chemistry are unavailable.

Evans[2] and Evans, Gergely and Seaman,[3] using arguments based on potential energy surfaces, have proposed that, in radical addition reactions to olefins, changes in heat of reaction (ΔH) and activation energy (E_a) may be related to resonance energies of the attacking radical (R_A), the olefin (R_M) and the radical formed on addition (R_F) *via* eq. (1)

$$\alpha\Delta H = \Delta E_a = \alpha(R_a + R_M - R_F) \qquad (1)$$

Subsequent extensive work on radical additions, notably in copolymerization reactions, has shown that (1) is certainly not generally applicable. Steric and polar effects (which are not taken into account) often have quite as large effects on the rates and activation energies of radical reactions as the resonance factors considered above. Nevertheless, in the case of a terminal olefin $CH_2{=}CR_2$ reacting with a non-polar and not easily polarizable radical, (1) might be a valid approximation and provide a basis for estimating R_F and $D(R\text{–}H)$ in cases where adequate data are available.

Szwarc and his students recently have published extensive data on the relative reactivities of olefins toward methyl radicals. Szwarc's results appear in the form of k_2/k_1 ratios, the ratio of reactivities of

(1) C. Walling, "Free Radicals in Solution," John Wiley and Sons Inc., New York, N. Y., 1957, Chapter 2.

(2) M. G. Evans, *Disc. Faraday Soc.*, **2**, 271 (1947).

(3) M. G. Evans, J. Gergely and E. C. Seaman, *J. Polymer Sci.*, **3**, 866 (1948).

olefins relative to isooctane toward methyl radicals, usually (and in the cases used here) in solution at 65°. From (1) and the relation stated earlier

$$R_F = D(\text{CH–H}) - D(\text{R–H}) \qquad (2)$$

we may write

$$\log k_2/k_1 = A + B[R_M + D(\text{R–H})] \qquad (3)$$

where $B = -\alpha/2.303RT$ and A is a constant providing methyl radical additions to different olefins have the same pre-exponential factors. Szwarc's data indicate that the latter is an adequately valid assumption in these systems. From (3), the linearity of a plot of $\log k_2/k_1$ *vs.* $R_M + D(\text{R–H})$ for a number of olefins should provide a test of the validity of Evans' hypothesis. Pertinent data are given in Table I. Values of $D(\text{R–H})$ are taken from a recent summary by the writer,[4] with the assumption that $D(CH_3CH_2CR_2\text{–H}) = D(CH_3CR_2\text{–H})$ which appears to be true within the present accuracy of bond dissociation energies. Values of R_M have been calculated as the difference in heats of hydrogenation of the olefins and of ethylene using Wheland's summary[5] of the measurements by Kistiakowsky and co-workers.

TABLE I

ENERGY AND RATE PARAMETERS OF OLEFINS

Olefin	k_2/k_1 (65°)	R_M (kcal./mole)	D(R–H) (kcal./mole)
Ethylene[a]	34.1[6]	0	98
Propylene	22[11]	1.7	94
Isobutylene	36[7]	4.4	90
Styrene	792[8]	4.2	77.5[c]
Butadiene[a]	2000[9]	3.3[b]	78
Vinyl acetate	34[10]	0.7	...
Ethyl vinyl ether	8[10]	6.1	...
Methyl methacrylate	1420[10]	4.2	...

[a] k_2/k_1 divided by 2 before plotting in Fig. 1. [b] Taken as the difference in heats of hydrogenation of butadiene and *trans*-2-butene subtracted from that of ethylene. [c] Taken as the same as D(Benzyl-H).

The data of Table I are plotted in Fig. 1, and are certainly consistent with a linear relation toward $R_M + D(\text{R–H})$ within the present experimental uncertainty in bond dissociation values (circles are drawn with radii corresponding to ±0.5 kcal., uncertainties are at least double this). While points cluster badly at either end of the scale, which makes the test less critical than might be desired, it should be pointed out that the results on methyl radicals are perhaps the first set providing reliable data on olefins possessing a wide enough range of reactivities for any convincing test of the Evans relationship.

(4) Ref. (1), p. 50.

(5) G. W. Wheland, "Resonance in Organic Chemistry," John Wiley and Sons, Inc., New York, N. Y., 1955, pp. 78–85. While there has been considerable discussion as to whether the differences are strictly interpretable in terms of resonance energy, they still seem to be the ones needed in this calculation.

(6) R. P. Buckley and M. Szwarc, *J. Am. Chem. Soc.*, **78**, 5696 (1956).

(7) R. P. Buckley, F. Leavitt and M. Szwarc, *ibid.*, **78**, 5557 (1956).

(8) F. Leavitt, M. Levy, M. Szwarc and V. Stannett, *ibid.*, **77**, 5493 (1955).

(9) A. Rajbenbach and M. Szwarc, *ibid.*, **79**, 6343 (1957).

(10) M. Szwarc, *J. Polymer Sci.*, **16**, 367 (1955).

(11) R. P. Buckley and M. Szwarc, *Proc. Roy. Soc.* (*London*), **A240**, 396 (1957).

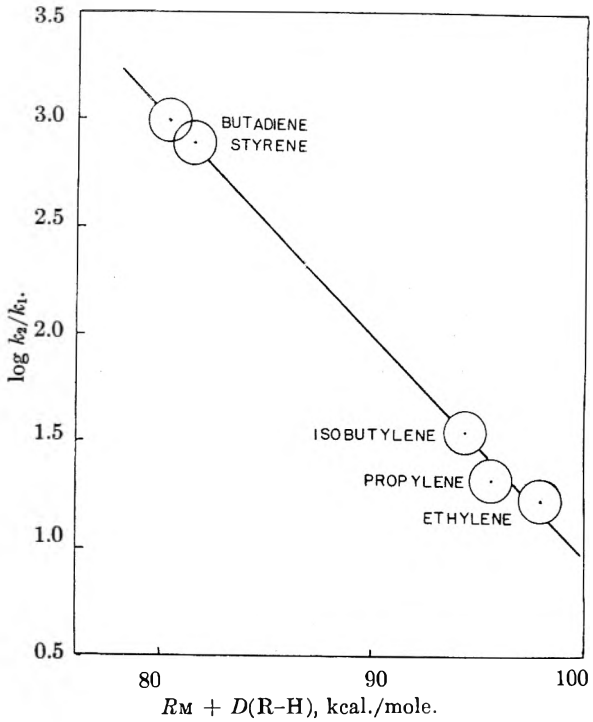

Fig. 1.—Energy–rate relationship in the addition of methyl radicals to terminal olefins.

The line in Fig. 3 fits the equation

$$\log k_2/k_1 = 11.36 - 0.104[R_M + D(\text{R–H})] \qquad (4)$$

and its slope corresponds to a value of $\alpha = 0.16$, significantly less than to 0.4 proposed by Evans[3] from theoretical considerations.

Equation 4, in turn, may be used to predict bond dissociation energies and resonance stabilizations for additional radicals where data on appropriate olefins are available. This has been done for the 1-acetoxyethyl, 1-ethoxyethyl and 2-carbomethoxyisopropyl radicals in Table II, using data on vinyl acetate, ethyl vinyl ether, and methyl methacrylate from Table I, and taking $D(CH_3\text{–H}) = 102$ kcal.

TABLE II

CALCULATED VALUES OF R_F AND D(R–H) (IN KCAL./MOLE TO NEAREST KCAL.)

Radical	R_F	D(R–H)
$CH_3\underset{\displaystyle OC_2H_5}{\overset{\displaystyle OCOCH_3}{CH}}\cdot$	8	94
$CH_3\underset{\displaystyle COOCH_3}{\overset{\displaystyle OC_2H_5}{CH}}\cdot$	8	94
$(CH_3)_2\underset{\displaystyle COOCH_3}{C}\cdot$	27	75

From Table II, the effects of an acetoxy or alkoxy group on resonance stabilization are equal and comparable to a methyl group since D(isopropyl–H) is also 94 kcal. The result with ethyl vinyl ether resolves a puzzling discrepancy. In a number of radical reactions (autoxidation, halogenation and chain transfer) α-hydrogens of saturated ethers are readily abstracted. On the other hand, vinyl ethers appear notably unreactive when compared with vinyl acetate or allyl derivatives in copoly-

merization.[12] From Tables I and II, we see that, although the α-alkoxy radical enjoys considerable resonance stabilization, addition reactions to vinyl ethers must overcome the large resonance stabilization of the olefin (R_M = 6.1 kcal.).

Finally our calculations indicate a resonance stabilization of the carbonyl conjugated radical from methyl methacrylate actually larger than that of benzyl and allylic radicals, although the difference may not be beyond the uncertainty of the method. If so, the order of resonance stabilization $\cdot C(C{=}O) < \phi{-}C\cdot$, $\cdot C{-}C{=}C$ deduced from copolymerization data[12] needs to be reversed.

It would be of interest to extend the calculations of Table II to additional systems. A number of values of k_2/k_1 are available, but needed are additional values of R_M, either from heats of hydrogenation or precise heats of formation or combustion.

(12) F. R. Mayo and C. Walling, *Chem. Revs.*, **46**, 191 (1950).

SODIUM OZONIDE[1]

BY I. J. SOLOMON AND A. J. KACMAREK

Chemistry Research Division, Armour Research Foundation of Illinois Institute of Technology, Technology Center, Chicago 16, Illinois

Received July 16, 1959

The ozonides of the heavier alkali metals, including KO_3, RbO_3 and CsO_3, have been prepared and characterized.[2-4] These compounds are prepared by the reaction of the respective dry, powdered hydroxide with gaseous ozone. The ozonide then is isolated by extraction with liquid ammonia. Sodium ozonide has also been reported.[3-5] However reports on its preparation, stability and solubility are contradictory. Whaley and Kleinberg[3] stated that sodium ozonide prepared at room temperature is insoluble in liquid ammonia and stable at room temperature. McLachlan, Symons and Townsend[5] confirmed these observations. On the other hand, Nikolskii, Bagdassaryan and Kazarnovskii[4] ozonized sodium hydroxide at temperatures between −50 and −60°, and produced an ozonide which is soluble in liquid ammonia but which is reported to be considerably less stable than the sodium ozonide prepared at room temperature.

McLachlan, *et al.*, obtained a single peak at 440 mμ by a diffuse reflectance measurement on the solid bed of sodium hydroxide after ozonization. They also reported a single peak at 435 mμ for the potassium salt in ammonia solution. We have found that the visible spectra of ammonia and dimethylformamide solutions of the alkali ozonides are relatively independent of the cation, and consist of a characteristic six-pointed structure with a maximum at 450 mμ. The spectra of various ozonides obtained in our laboratories with ammonia as the solvent are shown in Fig. 1. Since these spectra are quite intense, even for dilute solutions, we believed that they could be used to resolve the reported discrepancies in the properties of sodium ozonide.

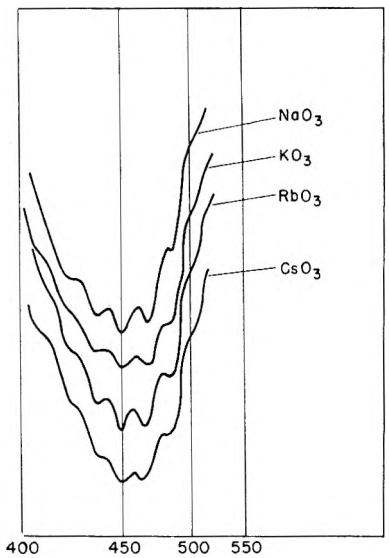

Fig. 1.—Visible spectra of ozonide compounds in liquid ammonia.

Therefore, we carried out several experiments in which a bed of sodium hydroxide was ozonized and extracted at various temperatures. Ozonization and extraction with liquid ammonia at −60° produced a red solution which exhibited the characteristic spectrum; but if the bed was allowed to warm to room temperature for 20 minutes and then extracted, no soluble material was found. Ozonization at 25° produced a transitory red color in the reaction bed which quickly faded to yellow when the flow of ozone was stopped. However, after ozonization was stopped, if the ozone–oxygen mixture was pumped out quickly and the bed immediately quenched at −196°, subsequent extraction produced an ozonide solution; but if two or more minutes elapsed after the flow of ozone was stopped, quenching and extraction did not yield any ozonide.

In another experiment sodium hydroxide was ozonized at −60° and then extracted six times with liquid ammonia. After the second extraction no soluble material was noted. Diffuse reflectance measurements of the insoluble solid showed the characteristic ozonide spectra.

Thus it appears that a soluble sodium ozonide is formed easily at −60° and is stable at that temperature. It is also formed at 25°, but it is unstable under these conditions and quickly decomposes. Further evidence for these conclusions was obtained when two samples of sodium ozonide were prepared at −60° and the amount of oxygen evolved was observed as the samples were warmed to room temperature. After oxygen evolution had ceased, the samples were hydrolyzed to determine the amount of sodium superoxide present, since it was assumed that sodium ozonide decomposes with the same stoichiometry as potassium ozonide, eq.

(1) This research was supported in part by the United States Air Force under Contract No. AF 49(638)-618 monitored by the Air Force Office of Scientific Research of the Air Research and Development Command. Spectral data by Ralph Hites of this Foundation.

(2) I. A. Kazarnovskii, G. P. Nikolskii and T. A. Ableteova, *Doklady Akad. Nauk, S.S.S.R.*, **64**, 69 (1949).

(3) T. P. Whaley and J. Kleinberg, *J. Am. Chem. Soc.*, **73**, 79 (1951).

(4) G. P. Nikolskii, Z. A. Bagdassaryan and I. A. Kazarnovskii, *Doklady Akad. Nauk, S.S.S.R.*, **77**, 69 (1951).

(5) A. O. McLachlan, M. C. R. Symons and M. G. Townsend, *J. Chem. Soc.*, 952 (1959).

1 and 2, and thus the amount of oxygen formed during hydrolysis should be the same as the amount formed during thermal decomposition.

$$2NaO_3 \longrightarrow 2NaO_2 + O_2 \quad (1)$$
$$2NaO_2 + 2H_2O \longrightarrow 2NaOH + H_2O_2 + O_2 \quad (2)$$

The values found were 6.1 and 5.9 cc. during hydrolysis, compared to 2.0 and 2.5 cc. during decomposition of the ozonized sample. This indicates that considerable amounts of the superoxide are also formed at −60°, although the results can also be attributed to the presence of some unextracted ozonide.

We have confirmed the fact that diffuse reflectance measurements on the sodium ozonide formed at 25° show a broad peak at approximately 450 mμ, although no ozonide can be extracted. We also have found that the decomposed bed from the preparation at −60° gives the same absorption. One possible explanation for this and the results of McLachlan, *et al.*, is that a small amount of sodium ozonide is trapped in the sodium hydroxide and thus stabilized toward thermal decomposition. Since sodium hydroxide is not soluble in liquid ammonia, the trapped material would not be extracted. Another possibility is that sodium ozonide exists in two forms, one being soluble in liquid ammonia and unstable at room temperature, and the other being insoluble and stable. However, it does not appear that the ozonides formed at the two different temperatures are chemically different, since their spectra are identical.

The idea of two crystalline structures of ozonides is not unfounded, in that we have observed that potassium ozonide may exist in two forms. Zhdanov and Zvonkova[6] have found potassium ozonide to have the tetragonal potassium bifluoride lattice of potassium azide. However, we have found that potassium ozonide may also exist in the monoclinic potassium nitrite structure. These results have also been predicted by Smith.[7] Currently, we are investigating all of these possibilities.

(6) G. S. Zhdanov and Z. V. Zvonkova, *Zhur. Fiz. Khim.*, **25**, 100 (1951).

(7) P. Smith, THIS JOURNAL, **60**, 1471 (1956).

SPHERULITE GROWTH RATES IN POLYETHYLENE CROSSLINKED WITH HIGH ENERGY ELECTRONS

BY FRASER P. PRICE

Contribution from the Research Laboratory of the General Electric Company, Schenectady, New York

Received July 20, 1959

It is known that when polyethylene is crosslinked by ionizing radiation at temperatures above the crystal melting point, the equilibrium degree of crystallinity below the melting point is reduced.[1] Also the size and perfection of the crystallites comprising this crystallinity is reduced.[2] In view of these facts it is worth inquiring about the effects of irradiation upon the growth of spherulites. This note reports the results of some studies of the growth rates of spherulites growing from crosslinked melts. Since a photographic technique, which relied upon the birefringence of the growing spherulite, was used and since there is a persistence of birefringence in the melts of polyethylene irradiated when crystalline,[3,4] this study is only concerned with spherulite growth from melts of polyethylene that was irradiated when molten.

Experimental

The polyethylene was Marlex 50 obtained from the Phillips Petroleum Co., Bartlesville, Oklahoma. Pressed sheets about 1 mil thick supported on microscope cover slips were irradiated at 150° in an atmosphere of nitrogen with 800 KV peak electrons. The electrons were supplied by a G.E. resonant transformer type electron generator.

Spherulite growth rates were measured using the polarizing microscope and photographic techniques. A special hot stage consisting of two insulated brass blocks was constructed. These blocks were mounted side by side about one quarter inch apart and were heated electrically. One block, the melting block, was held at some temperature T_1 above the melting temperature to ±1° by adjusting the heat input to the requisite value. The other block, the growing block, was held at some temperature T_2 below the melting point to ±0.1° by a thermocouple controlled relay system which actuated the heater. The growing block had a small hole bored through it to permit the use of transmitted light. In order to minimize temperature variations from stray air currents, a small brass cup with an appropriately placed glass-covered viewing hole was inverted over the specimen when observations were being made. The temperature of the growing block was determined by a thermocouple located in the block close to the central hole. Benzoic acid, U.S. Bur. of Std. calorimetric grade, was used to calibrate the thermocouple.

The procedure in making a run was as follows: place 1 *mil* sample between cover slips on the melting block at T_1; after 10 min. place brass cup, which was at T_2, over specimen and slide it over the hole in the growing block; focus microscope and take photomicrographs at appropriate intervals. Kodak Plus X film was used in a Leica camera fitted to the microscope with a Mikas photomicrographic adapter. The negatives were projected on a screen and the diameters of selected spherulites were determined as functions of time. Plots of diameter *versus* time were good straight lines.

The growing block also was used to determine crystal melting points. In these determinations the temperature was raised at 0.1°/min. and the temperature at which the last observable crystals disappeared was taken as the melting point.

Results and Discussion

The results of this study are presented in Table I. The data show that growth rates can be determined to ±5% (*cf.* runs at 100 MR, T_2 = 100.0°). It can also be seen that changing T_1 does not alter the growth rate (*cf.* runs at no dose, T_2 = 122.5–122.9°). As has been determined for other polymers[4] the growth rate is determined primarily by the growth temperature T_2. Each set of data at a particular dose shows that there is a temperature range in which the growth rate is extremely sensitive to temperature. This effect has been observed in other polymers by other investigators[5,6] and has been attributed to an enhanced nucleation rate immediately ahead of the advancing spherulite boundary.

The results given in the table show that as the dose is increased the temperature at which compar-

(1) A. Charlesby and L. Callaghan, *J. Phys. Chem. Solids*, **4**, 306 (1958).

(2) L. Mandelkern, D. E. Roberts, J. C. Halpin and F. P. Price, *J. Am. Chem. Soc.*, **82**, in press (1960).

(3) C. F. Hammer, W. W. Brandt and W. L. Peticolas, *J. Polymer Sci.*, **24**, 291 (1957).

(4) F. P. Price, *J. Am. Chem. Soc.*, **74**, 311 (1952).

(5) P. J. Flory and A. D. McIntyre, *J. Polymer Sci.*, **18**, 592 (1955).

(6) F. P. Price in "Growth and Perfection of Crystals," John Wiley and Sons, New York, N. Y., 1958, p. 533.

TABLE I

SPHERULITE GROWTH RATES IN IRRADIATED POLYETHYLENE

T_1 (°C.)	T_2 (°C.)	Diametral growth rate (mm./min. × 10^2)
	Dose = 0 MR.	
191	120.7	1.34
192	122.9	1.24
193	125.1	0.218
196	127.0	0.013
168	122.4	1.06
153	122.5	1.21
	Dose = 20 MR.	
195	114.0	1.21
195	116.4	2.59
195	118.6	0.51
	Dose = 40 MR.	
195	113.1	3.5
195	113.8	2.7
195	114.6	2.6
195	115.8	0.79
195	117.0	.54
195	117.8	.028
	Dose = 100 MR.	
195	100.0	.87
195	100.0	.74
195	101.8	.39
195	104.0	.095

able growth rates are observed is decreased. Melting points of 133, 128, 121 and 113° were determined for specimens receiving respectively doses of 0, 20, 40 and 100 MR. The melting point given here for the unirradiated polymer is lower than the usually accepted one (137.5° determined dilatometrically) presumably because of the rapid heating rate. In spite of the difference the melting point depression per unit of radiation is probably correct.[2] The dominant effect of ionizing radiation on molten polyethylene is the introduction of intermolecular crosslinks. These crosslinks result in decreased size and increased imperfection of the crystallites which form from the melt on cooling.[2] The net result is a decrease in the equilibrium value of both the crystal melting point and the degree of crystallinity. The spherulites that develop from such a cross-linked melt are thus forming in a medium of extremely high macroscopic viscosity and are composed of crystals of lowered melting point. If the growth of the spherulite were controlled by diffusion of material to the spherulite-melt boundary, then the increase in viscosity with dose would be expected to inhibit growth markedly. On the other hand, if the spherulite growth were controlled by a nucleation process, then it is to be expected that the growth rate would depend only on the supercooling below the crystal melting point. The data in the table indicate that comparable growth rates occur at equal degrees of supercooling, regardless of the dose. Thus, even though considerable disruption of the crystallites results from the radiation and even though the spherulites are developing in a crosslinked matrix, the predominant effect of that radiation on the spherulite growth rates seems to be due largely to the suppression of the crystal melting point. As noted above this is consistent with the concept of nucleation control of spherulite growth.

SURFACE TENSION, INTERMOLECULAR DISTANCE AND INTERMOLECULAR ASSOCIATION ENERGY OF PURE NON-POLAR LIQUIDS[1]

BY RALPH G. STEINHARDT, JR.

Department of Chemistry, Hollins College, Virginia

Received July 23, 1959

An approximate linear relation between molar refraction R and the parachor P has been established empirically,[2-6] which may be expressed as

$$R = k'P + C \quad (1)$$

in which k' and C are empirical constants. As C is small compared with $k'P$, it usually may be neglected without serious error.[5] Thus, (1) may be written approximately

$$R = k_1P \quad (2)$$

in which k_1 is the slope of the least-squares line of regression forced statistically through the origin. The parachor may be expressed in the usual approximate form[7]

$$P = V_m\gamma^{1/4} \quad (3)$$

in which V_m is the molar volume and γ is the surface tension. The Clausius–Mosotti equation for molar refraction of visible light in non-polar liquids may be expressed as

$$R = \frac{4}{3}\pi N\alpha_E \quad (4)$$

in which N is Avogadro's number and α_E is the electron polarizability. Substituting (3) and (4) in (2) yields

$$\frac{4}{3}\pi N\alpha_E = k_1V_m\gamma^{1/4} \quad (5)$$

To obtain an equation that yields γ as a function of molecular characteristics only, it is useful to employ an expression for V_m in terms of the average distance d between molecular centers in a liquid. Define V_{mol} as the effective volume per molecule. Confining attention to a pure non-polar liquid composed of spherical (or quasi-spherical) molecules, and thereby assuming spherical configuration of V_{mol}

$$V_{mol} = \frac{4}{3}\pi(d/2)^3 \quad (6)$$

and, therefore

$$V_m = k_2NV_{mol} = k_2\frac{4}{3}\pi N(d/2)^3 \quad (7)$$

in which k_2 is a constant the value of which depends only upon the structure of the liquid. By

(1) Presented before the Division of Physical Chemistry at the 135th Meeting of the American Chemical Society, April 5-10, 1959.

(2) W. Herz, *Z. anorg. Chem.*, **159**, 316 (1927).

(3) M. M. Samygin, *J. Phys. Chem. (USSR)*, **10**, 455 (1937).

(4) F. W. Lima, *Anais Assoc. Quim. Brasil*, **6**, 185 (1947).

(5) E. R. Suarez, *Anales real soc. Espan. Fis. y Quim. (Madrid)*, **48B**, 548 (1952).

(6) A. M. Talati, *J. Ind. Chem. Soc.*, **30**, 583 (1953).

(7) S. Sugden, *J. Chem. Soc.*, **125**, 32 (1924).

substitution of (7) in (5), division by $(4/3)\pi N$, and solution for γ

$$\gamma = (\alpha_E/d^3)^4 k_3 \qquad (8)$$

in which $k_3 = (8/k_1k_2)^4$. From (8) it is clear that the temperature-dependency of γ for liquids of the considered type is due solely to the temperature-dependency of d. It is known that α_E is temperature-invariant,[8] and k_3 is temperature-invariant since k_1 is known empirically to be independent of temperature and k_2 (which is structure-sensitive only) cannot be expected in this case to be a function of temperature.

London's approximation for the dispersion energy E_{dis} of a system containing molecules of one kind only may be stated[9]

$$E_{dis} = -\frac{3}{4}\frac{\alpha_E^2}{d^6} h\nu_0 \qquad (9)$$

if it is assumed that $\alpha_E = \alpha$, the total polarizability. In (9), ν_0 is the frequency of a London oscillator and h is Planck's constant. Using (8) and (9)

$$E_{dis} = -\frac{3}{4}\frac{\gamma^{1/2}}{k_3^{1/2}} h\nu_0 \qquad (10)$$

As $h\nu_0$ may be replaced by the molecular ionization potential without serious error,[10] and as molecular ionization potentials are approximately the same for most organic molecules,[11] (10) may be written

$$E_{dis} = k_4\gamma^{1/2} \qquad (11)$$

for such liquids, in which $k_4 = -(3/4)h\nu_0 k_3^{-1/2}$. As this discussion is limited to non-polar liquids, the total molar intermolecular association energy $E_a = NE_{dis}$ and

$$k_5 = \frac{E_a}{\gamma^{1/2}} \qquad (12)$$

is obtained for pure non-polar organic liquids composed of spherical molecules. In (12), $k_5 = Nk_4$. If the development of (12) is valid, the value of k_5 will have the following characteristics:

1. It will be of the same order of magnitude for all non-polar organic liquids composed of spherical or quasi-spherical molecules.
2. For a liquid composed of aspherical non-polar organic molecules it will in general be different from the k_5 value of a similar liquid composed of spherical or quasi-spherical molecules, and the magnitude of the difference will increase as the aspheric characteristic increases.
3. It will be temperature-invariant for non-polar liquids.

To test k_5 for these characteristics, the molar internal latent heat of vaporization is considered to be equal to the molar intermolecular association energy

$$E_a = \Delta H_v - RT \qquad (13)$$

in which ΔH_v is the total molar latent heat of vaporization at absolute temperature T and R is the ideal gas constant. Using (13), the Clausius–Clapeyron equation

$$\frac{dp}{dT} = \frac{\Delta H_v p}{RT^2} \qquad (14)$$

the differentiated form of the Antoine equation

$$\frac{dp}{dT} = \frac{(\log_e 10)pB}{(T + C)^2} \qquad (15)$$

and appropriate values of surface tension[12,13] and Antoine constants,[14] k_5 may be evaluated as a function of temperature for various compounds. In (14) and (15), p is the vapor pressure at absolute temperature T and B and C are Antoine constants, which depend empirically upon the compound only.

Values of k_5 for five representative non-polar liquids composed of quasi-spherical organic molecules are given in Table I. It is apparent that the prediction of constancy of k_5 with respect to spherical molecules is valid. It is to be noted that the value of k_5 does not depend upon the chemical nature, polarizability, or molecular weight of the molecule.

TABLE I

Compound	k_5 (20°)
CCl_4	1.44
C_6H_6	1.43
Cyclohexane	1.48
Cyclohexene	1.49
Cyclopentane	1.37

The prediction of progressive deviation of k_5 with increasing asphericity is validated by the data given in Table II.

TABLE II

Compound	k_5 (20°)
n-Pentane	1.51
n-Hexane	1.66
n-Heptane	1.84
n-Octane	2.02
n-Nonane	2.22

That k_5 is almost but not strictly temperature-invariant is indicated by the data in Table III, in which values of $\Delta k_5/\Delta T$ are given over temperature ranges from 40 to 85°.

TABLE III

Compound	$\Delta k_5/\Delta T$	Compound	$\Delta k_5/\Delta T$
CCl_4	0.0014	*n*-Pentane	0.0027
C_6H_6	.0012	*n*-Hexane	.0026
Cyclohexane	.0014	*n*-Heptane	.0007
Cyclohexene	.0013	*n*-Octane	.0018
Cyclopentane	.0033	*n*-Nonane	.0015

Acknowledgments.—The author wishes to thank the National Science Foundation for the award of a Science Faculty Fellowship under the provisions of which much of this work was carried out and Miss Lesley Williams for performing most of the computations. Thanks are due also to Dr. Luther Brice of Virginia Polytechnic Institute and to Dr. B. Widom and Dr. S. H. Bauer of Cornell University for many helpful discussions.

(8) R. Schmidt, *Physik. Z.*, **39**, 574 (1938).

(9) F. London, *Z. physik. Chem.*, **B11**, 222 (1930).

(10) Y. K. Syrkin and M. E. Dyatkina, "Structure of Molecules and the Chemical Bond," translated and revised by M. A. Partridge and D. O. Jordan, Interscience Publishers, Inc., New York, N. Y., 1950, p. 265.

(11) T. M. Sugden, A. D. Walsh and W. C. Price, *Nature*, **148**, 372 (1941).

(12) Landolt–Börnstein, "Zahlenwerte und Funktionen," Springer, Berlin, 6te Auflage, 1956, II Band, 3 Teil, Ss. 421–30.

(13) T. Alty and G. F. Clark, *Can. J. Research*, **10**, 129 (1934).

(14) N. A. Lange, "Handbook of Chemistry," Handbook Publishers, Inc., Sandusky, Ohio, 9th edition, 1956, pp. 1424–38.

A THERMOANALYTICAL STUDY OF THE RECIPROCAL SYSTEM $2KNO_3 + BaCl_2 \rightleftarrows 2KCl + Ba(NO_3)_2$

By Virginia D. Hogan and Saul Gordon

Pyrotechnics Chemical Research Laboratory, Picatinny Arsenal, Dover, New Jersey

Received July 27, 1959

A thermoanalytical study of the binary oxidant system potassium perchlorate–barium nitrate[1] revealed varied and interesting thermal effects which suggested an evaluation of the high temperature phenomena characteristic of the stoichiometric potassium chloride–barium nitrate and barium chloride–potassium nitrate systems. Investigation of these systems utilizing the techniques of differential thermal analysis and thermogravimetry shows the fusion of a eutectic mixture of barium nitrate and potassium chloride at 300° and a solid state metathetical reaction between potassium nitrate and barium chloride at approximately 250°. The potassium chloride and barium nitrate formed by the latter reaction are the stable salt pair in this reciprocal system.

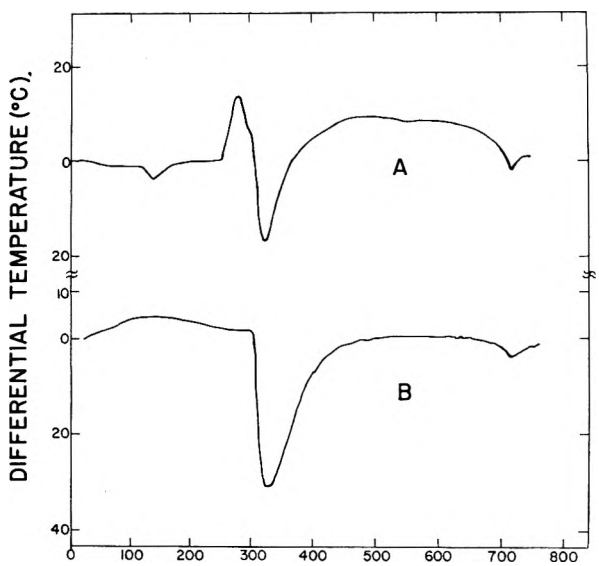

Fig. 1.—DTA curves for 2:1 mole ratio of (A) KNO_3–$BaCl_2$ and (B) KCl-$Ba(NO_3)_2$, obtained at a heating rate of 15° per minute.

Reagents.—Barium nitrate, Analytical Reagent (Mallinckrodt Chemical Works), potassium nitrate, potassium chloride, barium chloride, analytical reagent (Fisher Scientific Company) were used.

Instrumentation and Procedures.—The differential thermal analysis and thermogravimetric analysis apparatus employed have been described previously.[2] Three to five gram samples were taken for the differential thermal analyses and an equal volume of alumina served as the reference material. On the differential thermal analysis curves, the temperature difference between the sample and reference materials is plotted as a function of sample temperature. The furnace was programmed for a linear heating rate of 15° per minute. Three hundred and fifty mg. samples were used for all thermogravimetric analysis with a full-scale range for changes in weight of 200 mg. The furnace was programmed for a linear heating rate of 10° per minute. The compositions studied were 2:1 mole ratio potassium chloride–barium nitrate (36–64% by weight) and 2:1 mole ratio potassium nitrate–barium chloride (49–51% by weight). Ten grams of each composition was prepared and samples for individual determinations were taken from the bulk supply. The samples containing barium chloride were dried at 190°.

Results and Discussion

Barium and potassium chlorides do not show any thermal reactions or weight losses up to 750°. Barium nitrate melts at 600° and decomposes endothermically at 700°.[1] Potassium nitrate undergoes endothermic crystalline transition from the rhombic to the trigonal lattice at 128°, melts at 334° and begins to decompose endothermically at 750°.[3] As shown in Fig. 1 the potassium chloride–barium nitrate mixture exhibits partial melting at 370°. It is completely liquid at 460° and begins to decompose at 700°. The potassium nitrate–barium chloride system exhibits the endothermic crystalline transition of potassium nitrate at 128°, then a well defined "sugar loaf" exothermic peak which begins at 255°. This exotherm is followed by an endothermic peak of similar shape which begins at 300°, as evidenced by the change in slope, before the system has recovered from the effects of the exothermic reaction. Partial melting is observed at 330° just after the peak of the endotherm. The sample is completely molten and clear at 500° and begins to bubble rapidly at 550°. Brown fumes signifying decomposition of nitrate ion are observed at 700°. The thermogravimetric curves previously reported for these systems are equivalent and confirm these observations.[1]

The low temperature endotherm at 300° displayed by the potassium chloride–barium nitrate system results from the fusion of a eutectic mixture of the two salts. The reciprocal system potassium nitrate–barium chloride exhibits a pair of thermal bands, *viz.*, an exotherm at 250° and an endotherm at 300° which can be explained as the result of an exothermal metathetical reaction and subsequent eutectic fusion of the products. For the reaction $BaCl_2 + 2KNO_3 \rightarrow Ba(NO_3)_2 + 2KCl$, ΔF at 255° is −1.5 kcal./mole and ΔH at 255° is −8.2 kcal./mole, showing that it is both thermodynamically spontaneous and exothermal. The reaction postulated was experimentally confirmed by heating a finely ground mixture of 2 to 1 mole ratio potassium nitrate–barium chloride in a muffle furnace for 3.5 hr. at 270°. No visible melting was observed, although the sample sintered. X-Ray diffraction analysis of the previously heated sample revealed that it consisted of only barium nitrate and potassium chloride, the stable salt pair in this reciprocal system.

The thermoanalytical data suggest that this reaction occurs in the solid state. Potassium nitrate crystals are trigonal and potassium chloride, barium chloride and barium nitrate crystals are cubic at 255°. In addition the crystal radii of K^+ and Ba^{++} are almost identical, 1.33 and 1.35 Å., respectively.[4] These properties are indicative of a

(1) V. Hogan and S. Gordon, This Journal, **62**, 1433 (1958).

(2) V. Hogan, S. Gordon and C. Campbell, *Anal. Chem.*, **29**, 306 (1957).

(3) V. Hogan and S. Gordon, This Journal, **63**, 93 (1959).

(4) L. Pauling, "The Nature of the Chemical Bond," Cornell Univ. Press, Ithaca, New York, 1944, pp. 343–350.

simple lattice structure and spatial symmetry that should facilitate the ionic mobility necessary to effect a solid state metathetical reaction.[3] However, the rapid rate of the reaction as measured by the time interval between the initial point and the maximum point of the exothermal band on the DTA curve, Fig. 1, may not be consistent with the diffusion rates associated with volume diffusion of ions in solid state crystals at these temperatures. This time interval is approximately one minute for a nominal sample weight of two grams. As an alternative, the reaction mechanism may involve micromelting of the salts at the crystalline interfaces with subsequent rapid recrystallization of the insoluble stable salt pair. This is consistent with both the gross sintering effect observed and the abrupt onset of the exothermal reaction at 255°. This latter explanation may also apply to the previously reported exothermal solid state reaction between barium perchlorate and potassium nitrate.[3]

SURFACE CONDUCTANCE OF SUSPENDED PARTICLES

By Norman Street

Department of Mining and Metallurgical Engineering, University of Illinois, Urbana, Illinois

Received July 24, 1959

With suspensions it is possible to use an approach to the measurement of surface conductivity very similar to that used on porous plugs. This involves the assumption that the double layer ions can be redistributed throughout the interparticulate liquid without altering the conductance of the porous plug or suspension; in fact of course the average electric field is different at the surface and in the bulk solution. However, the equations available for the calculation of surface conductivity from measured zeta potentials also implicitly involve the same assumption. Thus for a porous plug[1]

$$\lambda_s = (A/S)\Delta K$$

where

λ_s = surface conductivity
A/S = hydraulic radius
ΔK = difference between the bulk conductivity of the electrolyte soln. and the apparent conductivity when present in the pores of the plug

For a suspension there is an additional conductance caused by the movement of the charged suspended particles themselves under the influence of the imposed field. We can write the suspension conductivity as

$$K_s = NQU + K/F$$

where

N = number of particles per cc.
Q = particle charge
U = particle mobility under unit field
K = apparent conductivity of interparticulate soln.
F = formation factor (*i.e.*, $F = K/K_s$ when $Q = 0$, $\lambda_s = 0$)

However

$$K = k(1 + \lambda_s S/kA)$$

when k is the bulk value of the solution conductivity, and so

$$K_s = NQU + k/F + \lambda_s S/FA \qquad (1)$$

When the particles are large the contribution from the moving particles is very small[2] and equation 1 reduces to the equation used by Street[3] for the determination of the surface conductivity of clay particles

$$\lambda_s = (FK_s - k)(A/S)$$

As pointed out by Henry[2] we cannot readily measure surface conductivity from suspension measurements since the particle charge calculated from mobility is dependent on surface conductivity, hence the calculation is made by a series of approximations.

However, it is possible to avoid this, if we put $N = \rho/V$, and since $S/A = S_w/(1 - \rho) = \rho\beta/(1 - \rho)$ where

ρ = volume concn. of the particles
V = volume of one particle
S_w = surface area of solid per cc. of suspension
β = surface area of solid per cc. of solid

then

$$K_s = QU\rho/V + k/F + \rho\lambda_s\beta/F(1 - \rho)$$

and

$$f(K_s) = \frac{K_s - k/F}{\rho} = QU/V + \lambda_s\beta/F(1 - \rho)$$

and so it follows that

$$\tau = \mathrm{d}/\mathrm{d}\rho\,[f(K_s)] = -\frac{\lambda_s\beta\,[(1 - \rho)\mathrm{d}F/\mathrm{d}\rho - F]}{F^2(1 - \rho)^2} \qquad (2)$$

F can be put equal to $(x+\rho)/x(1 - \rho)$, (Fricke[4]) and here x is a function of particle shape and conductivity and in fact corrects for the change of field in the interparticulate solution resulting from the removal of excess ions from a surface and their redistribution through the solution. Then

$$\tau = -\frac{x\lambda_s\beta}{(x + \rho)^2} \qquad (3)$$

and for spherical particles $x = 2$ and so when a is the particle radius

$$\tau = -\frac{2\lambda_s\beta}{(2 + \rho)^2} = -\frac{6\lambda_s\rho}{a(2 + \rho)^2}$$

Experimental

An approximate check of equation 3 was made using a Ca kaolinite[3] for which $\beta = 44.6 \times 10^4$ and the axial ratio was 8 (incorrectly reported as 12 by Street [3]); with this axial ratio $x = 0.6$ for particles of zero conductivity. The conductivity measurements were made at 50 cycles per second, *i.e.*, below the frequency at which the electrophoresis effect disappears.[5]

Results and Discussion

Table I gives λ_s calculated from the slopes of the curves and λ_s calculated from zeta potential = 30 millivolts.[6]

TABLE I

k	λ_s(measd.)	λ_s(calcd.)
5.3×10^{-5}	1×10^{-9}	0.53×10^{-9}
3.15×10^{-5}	0.4×10^{-9}	0.41×10^{-9}

Actually x depends on the conductivity (ap-

(1) N. Street, This Journal, **62**, 889 (1958).
(2) D. C. Henry, *Trans. Faraday Soc.*, **44**, 1021 (1948).
(3) N. Street, *Australian J. Chem.*, **9**, 333 (1956).
(4) H. Fricke, *Phys. Rev.*, **24**, 575 (1924).
(5) Th. Svedberg and H. Anderson, *Kolloid Z.*, **24**, 156 (1919).
(6) N. Street and A. S. Buchanan, *Australian J. Chem.*, **9**, 540 (1956).

parent) of the particles as well as their geometry, except when they are spherical, and so it will be higher than the 0.6 given here for zero conductivity. Nevertheless these very limited measurements at least show the correct order of magnitude and indicate that it will be useful to carry out careful experiments using spherical particles. Calculation of zeta potentials from such measurements may provide useful checks on double layer theory.

HYDROTHERMAL REACTIONS IN THE Na_2O–GeO_2–H_2O SYSTEM. II. INFRARED STUDIES OF GERMANIUM DIOXIDE[1]

BY ELWOOD R. SHAW, JAMES F. CORWIN AND HARRY V. KNORR[2]

Contribution from the Department of Chemistry, Antioch College, Yellow Springs, Ohio

Received July 31, 1959

During the investigation of the hydrothermal reactions of germanium dioxide[3] variations which depended on the conditions of the reaction were noted in the indices of refraction and infrared patterns of inversion products which according to X-ray analyses consisted of the hexagonal form. Studies of these products have indicated that the reaction GeO_2 (amorphous, $N = 1.607$) → GeO_2 (hexagonal, $N_0 = 1.697$, $N_E = 1.724$) proceeds through intermediate states which contain varying amounts of difficultly removed water and/or quantities of a finely divided low index form. The fibrous variety of these intermediates has been described previously as a "chalcedony-like variety of germania."[4]

The crystal structure of germanium dioxide from aqueous solution with or without subsequent ignition was found by Goldschmidt[5] to be trigonal. Crystals formed by heating the tetragonal form of germanium dioxide at 1100° for two hours and also by heating fused germanium dioxide for four hours at 1080° were studied by Laubengayer and Morton[6] and found to belong to the hexagonal system. Comparisons of X-ray patterns of the hydrolyzed oxide with those of the above preparations by fusion also were made and only one crystalline form was indicated. The presence of heat stable $H_2Ge_5O_{11}$ was ruled out by Brauer and Renner[7] on the basis that on ignition the X-ray pattern of the hexagonal form was the same throughout and no fixed water content was found.

The infrared pattern for the hexagonal form of germanium dioxide has been reported in the literature with principal bands in the 2 to 15 μ region reported at 10.34, 11.31 and 13.90 μ.[8]

(1) This research was supported by the United States Air Force through the Air Force Office of Scientific Research of the Air Research and Development Command, under Contract No. AF 18(600)1490. Reproduction in whole or in part is permitted for any purpose of the United States Government.

(2) Kettering Foundation, Yellow Springs, Ohio.

(3) E. R. Shaw, J. F. Corwin and J. W. Edwards, *J. Am. Chem. Soc.*, **80**, 1536 (1958).

(4) J. W. White, E. R. Shaw and J. F. Corwin, *Am. Mineralogist*, **43**, 580 (1958).

(5) V. Goldschmidt, *Naturwissenshaften*, **14**, 295 (1926).

(6) A. W. Laubengayer and D. S. Morton, *J. Am. Chem. Soc.*, **54**, 2303 (1932).

(7) G. Brauer and H. Renner, *Z. anorg. allgem. Chem.*, **278**, 108 (1955).

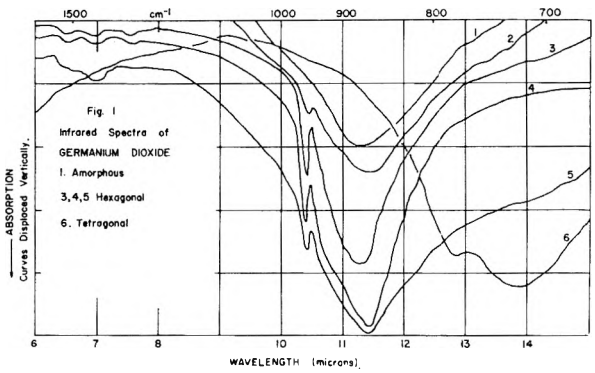

Fig. 1.—Infrared patterns of germanium dioxide: (1) freshly fused glass; (2) commercial sample of glass after standing 1 year; (3) glass heated in water for 1 day at 90–100°; (4) commercial sample, 99.99% pure, A. D. Mackay Co.; (5) hydrothermal preparation from glass, 200° for 3 hours; (6) hydrothermal preparation from glass, 400° for 3 days.

Recently, the spectra of the three forms of germanium dioxide have been reported with bands at: amorphous 11.17 μ; hexagonal 10.38 μ, 11.30μ; tetragonal 13.89 μ.[9]

Experimental

All samples were examined from 2 to 15 μ with a Perkin–Elmer Model 21 infrared spectrophotometer equipped with a sodium chloride prism. The samples were ground alone to the desired particle size either in an agate mortar or in a Wig-L-Bug Amalgamator[10] following which samples in the order of 3 mg. were then reground in the amalgamator for about two minutes with one gram of reagent grade potassium chloride. The mixed samples were pressed into a transparent plate at 40,000 p.s.i. in a vacuum press.

Germanium dioxide samples were obtained commercially or prepared hydrothermally as described earlier.[3] Water introduced into the sample during grinding with potassium chloride and indicated by weak but sharp bands at 2.95 and 6.10 μ was removed for water determination experiments by drying the pressed plate in a desiccator. Otherwise these bands were not objectionable since the band height was relatively constant in the humidity controlled analysis room. All samples were predried at 110° prior to any type of water determination.

Results and Discussion

The spectra for germanium dioxide are shown in Fig. 1 and the band locations shown in Table I. Bands due to absorbed water which could be removed by drying the pellet at 110° were not included. The precision of determining the location of the broad bands and their reproduction depended on the symmetry of the band at its maximum. In all cases, with a properly prepared sample, it was between 0.02–0.05 μ. The sharp band at 10.43 μ did not vary over ±0.01 μ regardless of the preparation and appeared whenever a small quantity of the soluble form was present in a form other than in a solid solution.

The devitrification of amorphous GeO_2 proceeds slowly in air (pattern 2), much more rapidly in hot water (pattern 3) and very rapidly under hydrothermal conditions (pattern 5). After short runs of the latter two methods, the birefringent product exhibits variable indices of refraction

(8) L. D'Or, M. Haccuria and R. Machirous, *Compt. rend. congr. intern. chim. ind. 27e Congr., Brussels, 1954, Ind. chim. belge*, **20**, 150 (1955).

(9) E. R. Lippincott, A. V. Valkenburg, C. E. Weir and E. N. Bunting, *J. Research Natl. Bur. Standards*, **61**, 61 (1958).

(10) Crescent Dental Manufacturing Co., Chicago, Illinois.

TABLE I

INFRARED BANDS IN THE SPECTRA OF GERMANIUM DIOXIDE

	Pattern and sample	Indices of refraction N_O	N_E	Bands (μ)[a]								
	Amorphous											
1.	Freshly fused	1.607										11.25b, s
2.	Devitrified in air	[b]	[b]						10.44w			11.40b, s
	Hexagonal											
	Hydrolysis in water at 90–100°											
	Dried at 110°	1.66–1.67	1.67–1.69	2.95w	6.1w	6.5w	7.0w	7.6w	10.22s	10.9sh		11.35b, s
3.	Dried at 400°	1.67–1.69	1.68–1.70			6.5w	6.9w	7.5w	10.43s	11.1sh		11.35b, s
	Dried at 1050°	1.68–1.69	1.69–1.70			6.5w	6.9w	7.5w	10.43	11.05sh		11.35b, s
	Hydrolysis, HCl + $Na_4Ge_9O_{20}$	1.63–1.64	1.64–1.65						10.42s			11.44b, s
4.	Commercial A. D. Mackay Co.	1.64–1.66[c]				6.5w	7.0w	7.6w	10.43s	11.25sh		11.47b, s
	Commercial Eagle Picher Co.	1.64–1.66[c]				6.5w	7.0w	7.6w	10.42s	11.0sh		11.45b, s
5.	Hydrothermal 200° for 3 hr.	1.697	1.724						10.44s			11.45b, s
	Tetragonal											
6.	Hydrothermal 400° for 3 days	1.9	2.1							12.9b, s		13.9b, s

[a] sh—shoulder; s—strong; w—weak; b—broad. [b] Surface layer is hexagonal with same indices as hydrolysed variety. [c] Very fine powder, treatment uncertain, probably hydrolysed from $GeCl_4$.

which rise as the reaction proceeds, as does the broad band of the spectra, until the characteristic rhombohedrons of the hexagonal form appear. The rhombohedrons have the appearance of forming only after solution and redeposition from solution, while the lower index material described above appears to be the result of an *in situ* type inversion. The cubical habit of the hexagonal form prepared hydrothermally is of interest since it displays diagonal extinction in contrast to that observed for the same habit by Laubengayer and Morton.[6] The difference in indices of refraction of the products of the two preparations has been previously pointed out.[3,4]

It is presumable that under hydrothermal conditions water penetrates the amorphous structure and aids in the formation of centers where inversion takes place. The resulting crystallites are small and variably oriented so that under crossed nicols a rotating black cross is observed in the clear birefringent crystals rather than complete extinction. As shown by the loss of 0.9% weight and non-appearance of the weak broad bands near 3 and 6 μ after drying the sample at 400° absorbed water detectable by infrared methods has been removed. Ignition at 1000° caused a total loss of weight of 1.3% but the indices were raised to only between 1.68–1.70 and the broad band of the spectra was not moved perceptibly from 11.35 μ.

The presence of other crystalline forms has been disproven by X-ray analyses[4–6] and the presence of a low index compound with water has been ruled out.[7] The extremely small and randomly oriented crystallites of the "hydrolysed form" could contribute to the low index of refraction of this form, whether prepared from the enneagermanate, tetrachloride or inverted from the amorphous form. The presence of the amorphous form as a minor part of a mixture does not appreciably affect the infrared pattern of the hexagonal form other than in the possible formation of a shoulder on the broad band and also the presence of a small amount would not be detected by X-ray analysis.

As only the products of the incomplete inversions to single crystals exhibit, in addition to the low index of refraction, an anomalous location of the broad band at 11.35 μ, it is presumable that the band location is varied by the presence of small centers of incompletely inverted glass. Thus, it is evident that to be reproducible, the infrared patterns of inorganic compounds prepared by inversion must be based on well crystallized samples.

THE COMPOSITION AND ENTHALPY OF DISSOCIATED WATER VAPOR

BY P. J. FRIEL AND R. C. GOETZ

General Electric Company, Missile and Space Vehicle Department, Philadelphia 4, Pennsylvania

Received July 28, 1959

We have calculated the enthalpy and composition of dissociated water vapor to 5000°K. for total pressures between 0.001 and 10 atmospheres assuming the gas mixture to be in chemical equilibrium. In this temperature range the following reactions occur

$$H_2O = {}^1/_2H_2 + OH \quad (1)$$

$$H_2O = {}^1/_2O_2 + H_2 \quad (2)$$

$${}^1/_2H_2 = H \quad (3)$$

$${}^1/_2O_2 = O \quad (4)$$

The equilibrium constants for reactions 1 to 4 are

$$K_1 = \frac{X_{OH}\, X_{H_2}{}^{1/2}}{X_{H_2O}}\, p_t{}^{1/2} \quad (5)$$

$$K_2 = \frac{X_{H_2}\, X_{O_2}{}^{1/2}}{X_{H_2O}}\, p_t{}^{1/2} \quad (6)$$

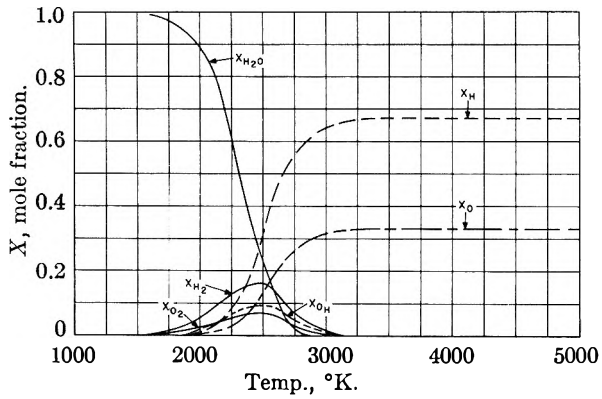

Fig. 1.—The composition of dissociated water vapor from 1600 to 5000°K.; total pressure 0.001 atm.

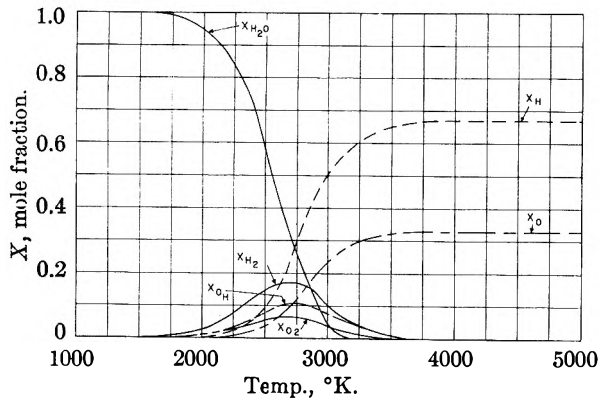

Fig. 2.—The composition of dissociated water vapor from 1600 to 5000°K.; total pressure 0.01 atm.

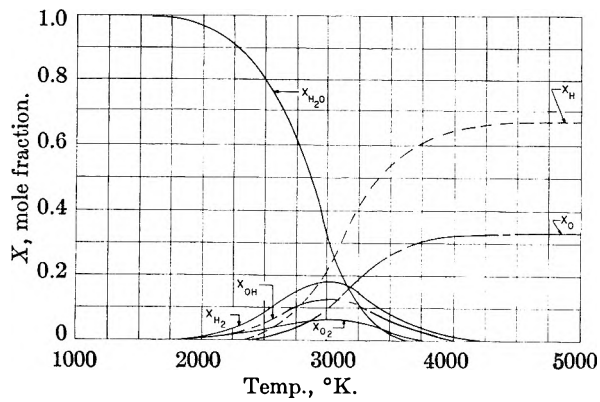

Fig. 3.—The composition of dissociated water vapor from 1600 to 5000°K.; total pressure 0.1 atm.

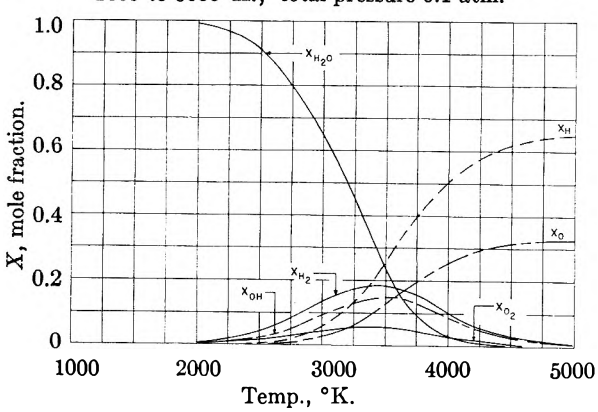

Fig. 4.—The composition of dissociated water vapor from 2000 to 5000°K.; total pressure 1 atm.

$$K_3 = \frac{X_H}{X_{H^{1/2}}}\, p_t^{1/2} \qquad (7)$$

$$K_4 = \frac{X_O}{X_{O_2}^{1/2}}\, p_t^{1/2} \qquad (8)$$

Where X is the mole fraction of the various species and p_t is the total pressure of the gas mixture. There are six composition variables in the system. Therefore, in order to determine the gas composition at any temperature and pressure (starting with one mole of undissociated water vapor) two additional equations are required in addition to the four shown above and they are

$$\sum_i X_i = 1 \qquad (9)$$

i.e., the sum of the mole fractions of all components must equal one and

$$\frac{2X_{H_2O} + 2X_{H_2} + X_{OH} + X_H}{X_{H_2O} + 2X_{O_2} + X_{OH} + X_C} \qquad (10)$$

i.e., the hydrogen–oxygen ratio must always equal two. Values of the equilibrium constants in equations 5 to 8 at various temperatures are available in the literature.[1-4] Consequently, the composition of the gas can be determined at each temperature for various total pressures by solving equations 5 to 10 simultaneously. This system of equations has been solved by an iterative technique on the Burroughs E101 Digital Computer. The results are shown in Figs. 1 to 5 in which the mole fraction of each component is plotted as a function of temperature for total pressures equal to 0.001, 0.01, 0.1, 1 and 10 atmospheres. Shown in Fig. 6 is a plot of Z, the total number of moles of gas formed by the dissociation of one mole of water vapor as a function of temperature for the various pressures.

The enthalpy of the gas mixture was determined simply by calculating the energy required to form a gas of the various compositions shown in Fig. 1 to 5 at room temperature (298.1°K.) and adding to this the energy required to heat a gas of this composition from room temperature to the temperature under consideration, *i.e.*

$$H = \Delta H_{298} + \sum_i n_i(H_{iT} - H_{i298}) \qquad (11)$$

where ΔH_{298} is the heat of the reaction

$$(1 - n_{H_2O})H_2O = n_OO + n_HH + n_{O_2}O_2 + n_{H_2}H_2 + n_{OH}OH \qquad (12)$$

and n_i is the number of moles of i in the mixture (i = H_2O, O, H, etc.) H_{iT} is the enthalpy content of species i at temperature T while H_{i298} is the enthalpy content of i at 298.1°K. Also

$$\Delta H_{298} = \sum_{i \neq H_2O} n_i H_{fi} - (1 - n_{H_2O})H_{fH_2O} \qquad (13)$$

where the first term refers to the heat of formation of the products of (12) at 298.1°K. (i = O, H, etc.) and H_{fH_2O} is the heat of formation of water vapor. Values of the heats of formation of the various species at 298.1°K. and their enthalpy contents at

(1) V. N. Huff and C. S. Calvert, *Natl. Advisory Comm. Aeronaut., Tech. Notes*, 1653 (1948).

(2) H. W. Wooley, *ibid.*, 3270 (1955).

(3) V. N. Huff, *et al.*, *Natl. Advisory Comm. Aeronaut., Rept.*, 1037 (1951).

(4) F. D. Rossini, *et al.*, Natl. Bur. Standards (U. S.), Circ. 461, 1947.

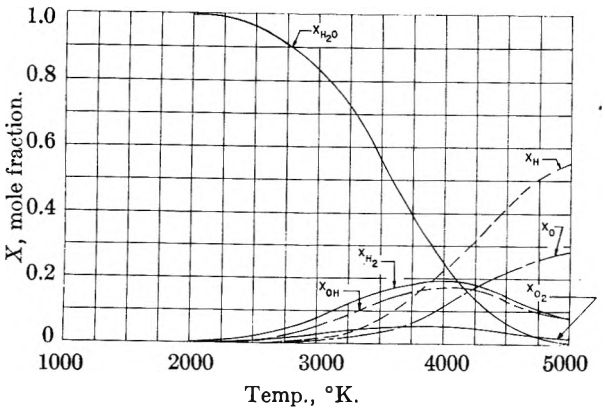

Fig. 5.—The composition of dissociated water vapor from 2000 to 5000°K.; total pressure 10 atm.

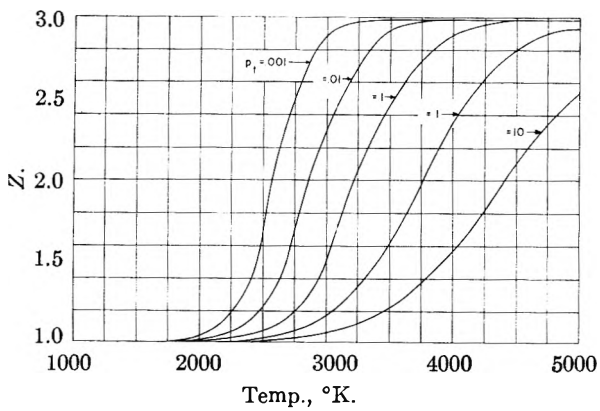

Fig. 6.—The total number of moles of gas (Z) formed by the dissociation of water vapor.

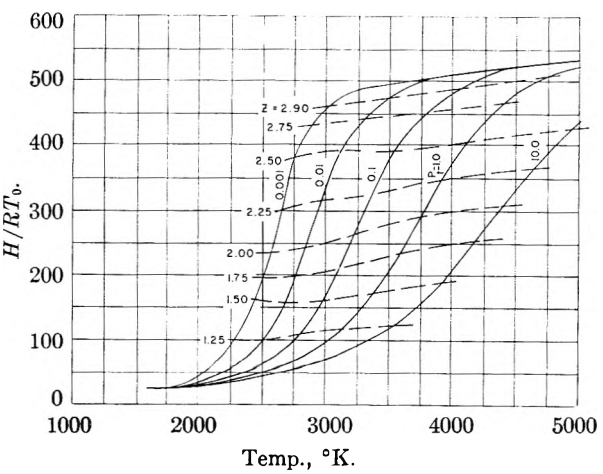

Fig. 7.—The enthapy of dissociated water vapor.

various temperatures are also available.[3-6] The results of the enthalpy calculations are shown in Fig. 7 in which values of H/RT_0 (R = gas constant, T_0 = 273.16°K.) are plotted as a function of temperature for various pressures. Values of H/RT_0 for constant values of Z are also indicated.

(5) F. D. Rossini, *et al.*, ref. 4, Circ. 500, 1952.
(6) J. Hilsenrath, *et al.*, ref. 4, Circ. 564, 1955.

NON-ADDITIVE POLAROGRAPHIC WAVES IN THE ANODIC OXIDATION OF IODIDE

BY ALVIN L. BEILBY[1] AND A. L. CRITTENDEN

Department of Chemistry, University of Washington, Seattle, Washington

Received August 6, 1959

Cases of failure of polarographic waves to be additive have been discussed by Miller and Orlemann[2] and more recently by Anson and Lingane[3] and by Auerbach.[4] In these cases, one of the products of the electrode reaction diffuses from the electrode and reacts with incoming reducible species to form a reducible species having a different diffusion coefficient.

Kolthoff and Jordan[5] have observed two waves in the anodic oxidation of iodide in chloride medium at rotating platinum electrodes; the first corresponding to oxidation to iodine, the second to oxidation to iodine monochloride. The second step was found to be lower than the first step when the electrode was rotated but of equal height when the electrode was stationary. The explanation given was that iodine is formed very rapidly but that its subsequent oxidation to iodine chloride is slow enough to permit some iodine to escape from the electrode. A similar lowering of the second step was observed by Morgan[6] at stationary electrodes. It appears that the lowering of the second wave can be explained adequately, at least for stationary electrodes, by the reaction of iodine chloride with incoming iodide to form slower-diffusing iodine. A numerical calculation of the magnitudes of the two waves expected as a result of these ideas has been made. It has been assumed that, for the second step, both iodine and iodide are oxidized immediately to iodine monochloride at the electrode and that the concentrations of iodine and iodide are zero at the electrode surface. It is assumed that the three species, together with chloride, are in equilibrium except at the electrode surface. The initial solution contains only iodide and chloride. It is further assumed that the concentration of chloride is sufficiently large that its concentration may be regarded as constant throughout. Linear diffusion is assumed.

Experimental

The electrical charge transferred during a fixed period of electrolysis from a fixed time (t_1) after application of cell potential to a second fixed time (t_2) at constant potential was measured using previously described equipment.[7] The microelectrode was in the form of a square plate forged on the end of a platinum wire and sealed into the end of a vertically-mounted glass tube. Such an electrode should be more nearly planar than a cylindrical wire. Also it has been shown that diffusion to cylindrical electrodes is essentially linear under the conditions used.[7] Measurements were made at 25.0°.

(1) Based on the Ph.D. thesis of Alvin L. Beilby, 1958. Standard Oil Company of California Fellow, 1957–1958.
(2) S. L. Miller and E. F. Orlemann, *J. Am. Chem. Soc.*, **75**, 2001 (1953).
(3) F. C. Anson and J. J. Lingane, *ibid.*, **79**, 1015 (1957).
(4) C. Auerbach, *Anal. Chem.*, **30**, 1723 (1958).
(5) I. M. Kolthoff and J. Jordan, *J. Am. Chem. Soc.*, **75**, 1571 (1953).
(6) E. Morgan, Thesis, University of Washington, 1956.
(7) G. L. Booman, E. Morgan and A. L. Crittenden, *J. Am. Chem. Soc.*, **78**, 5533 (1956).

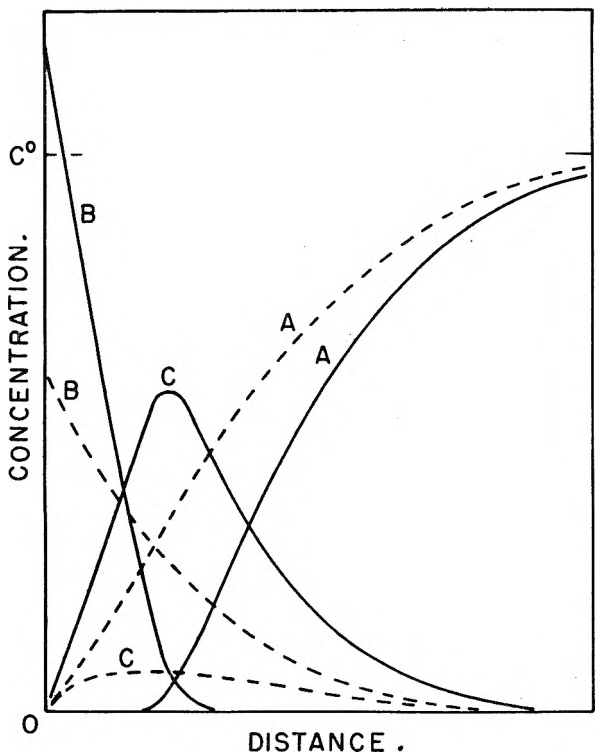

Fig. 1.—Concentration gradients near the electrode surface: solid lines, oxidation of iodide in hydrochloric acid, $K' = 10^{-3}$; dashed lines, oxidation of iodide in sulfuric acid, $K' = 1.4$. Both scales are arbitrary.

Numerical Calculations.—The diffusion processes can be described by the equations

$$\frac{\partial C_A}{\partial t} = D_A \frac{\partial^2 C_A}{\partial x^2} + R(x, t) \quad (1)$$

$$\frac{\partial C_B}{\partial t} = D_B \frac{\partial^2 C_B}{\partial x^2} + R(x, t) \quad (2)$$

$$\frac{\partial C_C}{\partial t} = D_C \frac{\partial^2 C_C}{\partial x^2} - R(x, t) \quad (3)$$

where the subscripts A, B and C refer to iodide, iodine chloride and iodine, respectively, and $R(x,t)$ represents change in the quantity of material in the volume increment because of chemical equilibrium. At the electrode surface

$$D_A\left(\frac{\partial C_A}{\partial x}\right)_{x=0} + D_B\left(\frac{\partial C_B}{\partial x}\right)_{x=0} + 2D_C\left(\frac{\partial C_C}{\partial x}\right)_{x=0} = 0 \quad (4)$$

The equilibrium can be written: $K = C_A C_B / C_C C_D$ or $K' = K(C_D)$ where C_D is the concentration of chloride (assumed to be constant). The initial conditions are $C_A(x,0) = C^0$, $C_B(x,0) = 0$, $C_C(x,0) = 0$. Also $C_A(0,t) = 0$, $C_C(0,t) = 0$.

A finite difference method[8] has been applied to obtain solutions for the above equations using an International Business Machines Type 650 digital computer. Three networks of values of the three concentrations at various times (nk) and distances (mh) are obtained. Concentration gradients for the three species computed for two values of K' are shown in Fig. 1. The quantity of iodine chloride produced may be computed from the area under its curve. At the end of calculation of each row of points corresponding to a particular time, the area is computed by the summation

$$\text{Area } B = h[{}^1/_2 C_B(0, t) + \sum_{i=1}^{m} C_B(ih, t)] = h\Sigma_B \quad (5)$$

Since neither the time or volume increments, h and k, need be specified, but only the ratio $r = D_C k/h^2$, at constant time ($t = nk$)

$$\text{Area } B = (D_C t/rn)^{1/2}\Sigma_B \quad (6)$$

where n is the number of rows computed. The constancy of the quantity $\Sigma_B/n^{1/2}$ with increasing n serves as a test for the convergence of the computations, similar tests being used for the other species. In addition, conservation of mass requires that the ratio $\Sigma_A/\Sigma_B + 2\Sigma_C$ be unity.

The total charge transferred should be proportional to area B plus area C, or to area A minus area C. If no reaction between iodide and iodine chloride were to occur, the charge could be calculated by[7]

$$Q = 2nFAC^0(Dt/\pi)^{1/2} \quad (7)$$

or by numerical methods similar to but simpler than that used for the case with reaction. Results of such calculations are shown as checks in the first two rows of Table I. In both the simple case, and the case with reaction, the areas for iodine chloride, B, converged less rapidly than did the other areas, thus it is advisable to take the charge as proportional to area A minus area C.

TABLE I

RATIOS OF AREAS FOR VARIOUS VALUES OF K'

K'	$\frac{\Sigma_A - \Sigma_C}{\Sigma_{A(no.rx.)}}$	$\frac{\Sigma_A}{\Sigma_B + 2\Sigma_C}$
No reaction (numerical)	...	0.972
No reaction (analytical)	...	1
1×10^3	1.003	0.924
1×10^2	1.001	.918
1×10^1	0.993	.915
1	.958	.935
1×10^{-1}	.914	.948
1×10^{-2}	.891	.953
1×10^{-3}	.887	.948

$D_A = 2 \times 10^{-5}$, $D_B = 1 \times 10^{-5}$, $D_C = 1 \times 10^{-5}$, $nk = 25k$, $r = 0.100$

Results and Discussion

In all calculations made, the initial concentration of iodide (C^0) was taken as unity. The value of K' must be calculated with C_D expressed in such units as to make C_A^0 unity. Therefore, to the extent that results vary with K', linearity between bulk concentration and wave height is not to be expected.

Table I shows results computed[9] for various values of K'. Deviations from unity of data in column three may be taken as measures of the convergence of the calculations. The principal discrepancy arises from slow convergence of the area B. Column 2 gives the ratio of charge transferred with reaction to the charge expected if no interaction

(8) W. E. Milne, "Numerical Solution of Differential Equations," John Wiley and Sons, Inc., New York, N. Y., 1953, Chap. 8.

(9) Computations in Tables I and III were carried out only to a few iterations in order to demonstrate the effects involved. Computations for cases investigated experimentally were carried out to a sufficient number of iterations to obtain convergence to three significant figures, usually about seventy rows ($nk = 70$) being required.

were to occur. It is seen that the magnitude of K' affects the results only in a limited range. At values of 10^2 or greater results are essentially the same as without reaction. With values of K' less than about 10^{-3}, little change occurs; the reaction between iodide and iodine chloride can be considered to go to completion.

The effect of various values of diffusion coefficients can be seen for the case of complete reaction in Table II. Although the diffusion coefficients D_A and D_C affect results significantly, little effect is found by changing D_B.

It is interesting to note that if the values of D_A and D_C are the same, the charge transferred is the same as that expected in the absence of reaction. The same result may be obtained by adding equations 1 and 3 and making the substitution $C_Y = C_A + C_C$. Also, the charge transferred is proportional to the flux of species A plus the flux of species C at the electrode surface. Thus, the same equations and boundary values are obtained as those applying to the simple case without reaction, and the charge transferred is the same. If the diffusion coefficient of the iodine formed by reaction is greater than that of the incoming iodide, a higher than normal charge is to be expected, and *vice versa*.

TABLE II

EFFECT OF DIFFUSION COEFFICIENTS ON WAVE HEIGHT

$D_A \times 10^5$	$D_B \times 10^5$	$D_C \times 10^5$	$\frac{\Sigma_A - \Sigma_C}{\Sigma_A \text{ (no.rx.)}}$
1	1	0.5	0.885
1	1	1	1.000
0.5	1	1	1.143
0.5	2	1	1.138
2	1	2	1.000
2	2	1	0.885
2	1	1	.887
2	0.5	1	.889

$K' = 1 \times 10^{-3}$, $nk = 25k$

Oxidation of Iodide in Hydrochloric Acid.—The oxidation of iodide was studied in 0.25 M hydrochloric acid solution. For a bulk concentration of iodide of 0.001 M, the equilibrium constant K' was taken as 1.9×10^{-6}, based on the data of Latimer,[10] a value small enough to allow the reaction to be considered to go to completion. The diffusion coefficient of iodide was taken as 1.99×10^{-5} cm.^{2} sec.$^{-1}$ for reasons discussed below. The diffusion coefficient of iodine chloride is uncertain but was taken as equal to that of iodine, for which a value of 1.11×10^{-5} cm.^{2} sec.$^{-1}$ was taken.[5] Using these values, the ratio of charge transferred with reaction to charge expected in absence of reaction was computed to be 0.899. The two wave heights were measured at +0.60 and +0.85 volt *versus* S.C.E., correcting for small residual charges. Without reaction, the second wave should be twice the height of the first. In Table III are shown values of the ratio of total height of the second wave to twice the height of the first. The results agree well with the calculated value, indicating that the interaction of iodide and iodine chloride is sufficient to explain the lowering of the second wave.

The Interaction of Iodide and Iodine.—The height of the wave observed in the oxidation of iodide to iodine should be affected in a manner similar to the case described above through the formation of triiodide ion from iodine liberated at the electrode surface. The equilibrium constant K' has a value of 1.4 for millimolar iodide solutions,[11] thus the effect should be much smaller than that due to iodine chloride. The ratio of charge with reaction to charge without reaction was computed to be 0.983 for millimolar iodide solutions and should be slightly different for different iodide concentrations. The experimental verification of this ratio is difficult. However, the wave height for the oxidation of iodide to iodine in 0.125 M sulfuric acid was found to be slightly lower than the first wave in 0.25 M hydrochloric acid. In sulfuric acid, triiodide is presumably formed; but in hydrochloric acid, complexing of iodine with chloride probably occurs at the concentrations used. The ratio of the charges in the two acids varied from 0.977 to 0.990, with a mean value of 0.987. The difference appears to be greater than that due to viscosity alone. Diffusion coefficients for iodide in various concentrations of sulfuric acid were calculated from diffusion charges using equation 7. If interaction between iodide and iodine is not considered, the value of the diffusion coefficient of iodide obtained by extrapolation to infinite dilution is too low. However, if the factor for interaction is applied, the value of 2.05×10^{-5} cm.^{2} sec.$^{-1}$ previously reported for infinite dilution[12] is obtained. The diffusion coefficient for iodide in 0.125 M sulfuric acid solution which would be observed if no interaction occurred was calculated to be 1.99×10^{-5} cm.^{2} sec.$^{-1}$. The same result was obtained for iodide in 0.25 M hydrochloric acid solution by application of equation 7 to the first wave in the oxidation of iodide.

TABLE III

OXIDATION OF IODIDE IN HYDROCHLORIC ACID

Electrolysis time $t_1 - t_2$ (sec.)	Concn., mmoles	$\frac{\text{Height—2nd wave}}{2 \times \text{height 1st wave}}$
0.5–0.6	0.500	0.899
2.0–2.4	.500	.899
4.0–4.8	.500	.889
0.1–0.2	1.000	.893
1.0–1.2	1.000	.890
4.0–4.8	1.000	.888
0.5–0.6	1.500	.881
2.0–2.4	1.500	.880
4.0–4.8	1.500	.890

(10) W. M. Latimer, "Oxidation Potentials," 2nd Ed., Prentice-Hall Inc., New York, N. Y., 1952, pp. 54, 63.

(11) J. J. Lingane, "Electroanalytical Chemistry," Interscience Publishers, Inc., New York, N. Y., 1953, p. 116.

(12) H. S. Harned and B. B. Owen, "The Physical Chemisty for Electrolytic Solutions," 2nd Ed., Reinhold Publ. Corp., New York, N. Y., 1950, p. 172.

PERCHLORATE FORMATION CONSTANTS FOR SOME WEAK BASES IN ACETIC ACID

BY TAKERU HIGUCHI AND KENNETH A. CONNORS

Contribution from the School of Pharmacy, University of Wisconsin, Madison, Wisconsin

Received August 6, 1959

The relative basicity of a compound B in a given solvent is conveniently measured by the extent of

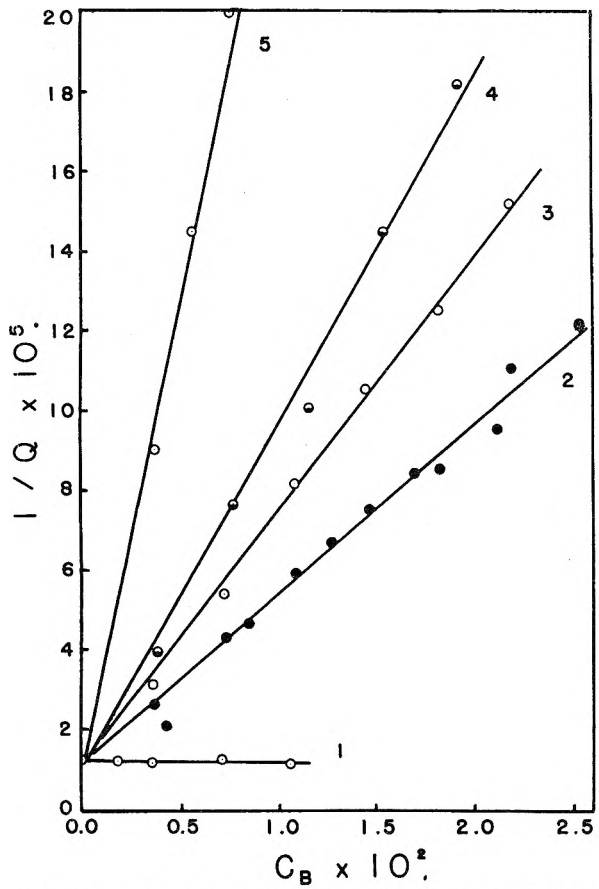

Fig. 1.—Application of equation 4 to some weak bases (*p*-naphtholbenzein indicator): 1, phenobarbital; 2, salicylamide; 3, benzamide; 4, acetanilide; 5, acetophenetidin.

its reaction with a reference acid HA to give a salt BHA. The quantitative measure of the extent of reaction is the salt formation constant K_f^{BHA} defined by equation 1

$$K_f^{BHA} = C_{BHA}/C_B C_{HA} \qquad (1)$$

In acetic acid solutions dissociation is slight and activities are replaced by concentrations; the quantities in equation 1 represent undissociated species. (The symbolism used follows that of Kolthoff and Bruckenstein.)[1]

Experimental evaluation of salt formation constants is facilitated with the use of indicators. Because acetic acid cannot easily be made completely anhydrous the effect of the weak base water upon the indicator equilibrium must be considered. The neutralization reactions to form the salts of the indicator and of water are characterized by the constants K_f^{IHA} and K_f^{WHA}, respectively. Consideration of these competing equilibria leads to the expression

$$1/Q = K_f^{WHA} C_{H_2O}/K_f^{IHA} + 1/K_f^{IHA} \qquad (2)$$

where Q, the apparent indicator constant, is given by

$$Q = (I_a/I_b)V/N(X - R) \qquad (3)$$

Q is found by a photometric titration method. I_a/I_b is the experimentally observed indicator ratio (identical with the ratio C_{IHA}/C_I for the weakly basic indicators considered here), V is the total volume of titration solution, N is the normality of the titrant acid, X is the volume (in ml.) of titrant added at any point and R is the volume of titrant equivalent to acid bound as indicator salt. For the indicators Nile blue A and malachite green, $R = V(A_b - A)/Na_b$, where A = absorbance, A_b = absorbance when the indicator is completely converted to the basic form and a_b is the molar absorptivity of the basic form. For Sudan III and *p*-naphtholbenzein, $R = VA/Na_a$, where a_a is the molar absorptivity of the acidic form. These differences arise because of the nature of the absorption spectra of the indicators.[2,3]

Q is evaluated through titration of an acetic acid solution of the indicator with the acid HA. Values of the absorbance are recorded at several values of X; from the absorbance the quantities I_a/I_b and R can be calculated. A plot of I_a/I_b *vs.* $(X - R)$ then yields a straight line, from the slope of which Q is determined by equation 3.

According to equation 2 the quantity $1/Q$ should be linear with the molar concentration of water. This relationship has been observed. The value of K_f^{WHA} is found to be 38 ± 8 from these plots.[4]

In a similar development the more complicated system consisting of an indicator I, a very weak base B, and water gives Equation 4

$$1/Q = K_f^{BHA} C_B/K_f^{IHA} + (1 + K_f^{WHA} C_{H_2O})/K_f^{IHA} \qquad (4)$$

In order for equation 4 to hold the condition $(K_f^{WHA} C_{H_2O}) << (K_f^{BHA} C_B)$ must be satisfied, Q is evaluated as before, this time as a function of C_B with C_{H_2O} held constant. Since K_f^{IHA} is known through equation 2, K_f^{BHA} can be found.

Experimental

Apparatus.—Bausch and Lomb Spectronic 20 colorimeter; 2 ml. microburet graduated to 0.01 ml.; circulation apparatus for photometric titration.[5]

Indicators: Sudan III, recrystallized from 1:1 benzene–absolute ethanol; m.p. 203°. *p*-Naphtholbenzein, recrystallized from glacial acetic acid; m.p. 236–241°. Nile blue A and malachite green, used directly.

Acetic Acid: dried by refluxing with boron triacetate and distilling from an all-glass apparatus 6, analyzed by visual Karl Fischer titration of an aliquot in an equimolar quantity of pyridine.

Bases: phenobarbital, recrystallized from 50% ethanol, m.p. 172–174°; salicylamide, recrystallized from water, m.p. 138–139°; acetanilide, recrystallized from water, m.p. 112–113.5°; acetophenetidin, recrystallized from water, m.p. 133–135°. Benzamide, prepared by shaking benzoyl chloride with aqueous ammonia. The precipitate was recrystallized three times from water; m.p. 127°.

The titrations were performed with a previously described titration unit.[3,5] Perchloric acid was the titrant acid in all cases, being 0.1 N for Sudan III titrations and 0.008 N for the other indicators. Values of absorbance were recorded in the range $0 < I_a/I_b < 2$. The indicator ratio is calculated with the usual equation[7]; the evaluation was made in this work by means of nomographs constructed for the purpose.[8]

(1) I. M. Kolthoff and S. Bruckenstein, *J. Am. Chem. Soc.*, **78**, 1 (1956).

(2) T. Higuchi, J. A. Feldman and C. R. Rehm, *Anal. Chem.*, **28**, 1120 (1956).

(3) T. Higuchi and K. A. Connors, *Anal. Chem.*, in press.

(4) An expression which is equivalent to equation 2 has been published by S. Bruckenstein and I. M. Kolthoff, *J. Am. Chem. Soc.*, **79**, 5915 (1957); these authors find $K_f^{WHA} = 39$.

(5) C. R. Rehm, J. I. Bodin, K. A. Connors and T. Higuchi, *Anal. Chem.*, **31**, 483 (1959).

(6) W. C Eichelberger and V. K. LaMer, *J. Am. Chem. Soc.*, **55**, 3633 (1933).

(7) C. Rehm and T. Higuchi, *Anal. Chem.*, **29**, 367 (1957).

Discussion

Figure 1 illustrates the application of equation 4 to several weak bases; the indicator was *p*-naphtholbenzein. Another point, lying off the graph, falls on line 5. The linear relationship appears to hold for these data, all of which were obtained in acetic acid solutions 0.018 *M* with respect to water. Phenobarbital shows no basic properties in this system.

Table I lists the perchlorate formation constants for all of the indicators and weak bases as determined by the methods outlined here. The table also includes some values for stronger bases (acetamide, urea, 2,6-dimethyl-α-pyrone, thiourea and caffeine) which were evaluated *via* the exchange constants ($K_{ex} = K_f^{IHA}/K_f^{BHA}$) of these bases as determined by the so-called modified type II photometric titration.[3] The uncertainties given are based upon an assigned uncertainty of 0.05×10^5 in the value for *p*-naphtholbenzein and upon the relative precision of the exchange constants, about 5%. The accuracy of the constants for the weaker bases is a rough estimate only. Because of the graphical treatment of data, a quantitative evaluation of the errors is difficult.

TABLE I

PERCHLORATE FORMATION CONSTANTS FOR SOME BASES AND INDICATORS IN ACETIC ACID

Compound	$K_f^{BHClO_4}$
Salicylamide	$4.8 \pm 0.4 \times 10^2$
Benzamide	$7.1 \pm .5 \times 10^2$
Acetanilide	$9.2 \pm .5 \times 10^2$
Acetophenetidin	$3.2 \pm .6 \times 10^3$
Acetamide	$1.1 \pm .2 \times 10^4$
Urea	$8.5 \pm .7 \times 10^4$
Dimethylpyrone	$1.4 \pm .3 \times 10^5$
Thiourea	$1.5 \pm .2 \times 10^5$
Caffeine	$2.4 \pm .5 \times 10^5$
Sudan III	$9.1 \pm .5 \times 10^2$
Nile Blue A	$3.9 \pm .6 \times 10^4$
p-Naphtholbenzein	$1.1 \pm .05 \times 10^5$
Malachite Green	$1.8 \pm .2 \times 10^5$

The constant for acetophenetidin was found by the method given here and also by the modified type II technique; agreement was within the uncertainty given in Table I.

Constants such as those in Table I are rapidly evaluated; the use of photometric titrations for the determination of Q promotes the simplicity of the operation. Such salt formation constants permit convenient and quantitative examination of such very weakly basic compounds as amides; the correlation of amide basicity with other amide reactions or with structure is presently limited by the few reliable values of amide basicities available. The data of Table I suggest that the base strength of unsubstituted amides may be compared usefully with the acid strength of the corresponding acids; nearly the same effects are operative in both cases.

Thiourea seems to be a stronger base than urea according to the perchlorate formation constants; this is contrary to the situation in water or methanol.[9] This reversal may be due to a very specific solvation effect or to the dependence of the salt formation constant on the dissociation constants of the acid HA and the salt BHA.[10]

In some preliminary experiments the effect of benzene on salt formation in acetic acid has been studied. The system was *p*-naphtholbenzein–water; equation 2 was employed. The ratio K_f^{WHA} (*i.e.*, the slope of the $1/Q$ *vs.* C_{H_2O} plot) increases linearly with decreasing dielectric constant over the benzene mole fraction range 0.000 to 0.491 (the dielectric constant changes from 6.20 to 2.83 in this range).[11] The data are not sufficiently accurate to obtain reliable values of the individual constants. This increase in perchlorate formation constant may be the result of increased extent of formation of higher ionic aggregates.

(8) K. A. Connors, Ph.D. Thesis, University of Wisconsin, 1959.
(9) R. G. Pearson and J. Tucker, *J. Am. Chem. Soc.*, **71**, 749 (1949).
(10) T. Higuchi and C. R. Rehm, *Anal. Chem.*, **27**, 408 (1955).
(11) C. P. Smyth and H. E. Rogers, *J. Am. Chem. Soc.*, **52**, 1824 (1930).

NOTE ON THE MOLECULAR WEIGHT DEPENDENCE OF BLENDING EFFECTS ON THE STRESS–RELAXATION BEHAVIOR IN POLYVINYL ACETATE FILM

BY KAZUHIKO NINOMIYA[1] AND MICHITARO SAKAMOTO

Physical Chemistry Laboratory, Department of Fisheries, Kyoto University, Maizuru, Japan

Received August 7, 1959

Recently it was shown experimentally for polyvinyl acetate[2] and polyisobutylene[3] that in the rubbery region the relaxation modulus of a blend consisting of two fractionated components could quantitatively be represented in terms of those of the components by

$$E_{bl}(t) = w_1 E_1(t/\lambda_1) + w_2 E_2(t/\lambda_2) \qquad (1)$$
$$w_1 + w_2 = 1$$

Here $E_{bl}(t)$ and $E_i(t)$ represent, respectively, the relaxation moduli of the blend and its i-th component ($i = 1, 2$), and w_i is the weight fraction of the i-th component. The constant λ_i was expected to be equal to the ratio of the number-average molecular weight, $\bar{M}_{nbl}$, of the blend to that of the i-th component, $\bar{M}_{ni}$,[2] *i.e.*

$$\lambda_i = \bar{M}_{nbl}/\bar{M}_{ni} \qquad (2)$$

However, no experimental data for $\bar{M}_n$ were available for the polymers to test the validity of equation 2. Recently osmotic measurements for the polyvinyl acetate specimens used in the previous work[2] were carried out to determine the values of $\bar{M}_n$ for those. The present note is essentially concerned with tests of validity of equation 2 made with these experimental data for $\bar{M}_n$.

Experimental

Samples used for osmotic pressure measurements were FVI, FVII, FIX, FX, FXI and FXIII (for their details, see Table I in ref. 2, and also Table I in ref. 4). The measurements were made in acetone solutions of those samples at 26.0°, by the Schulz–Wagner type osmometers[5]

(1) The Japan Synthetic Rubber Co. Ltd., Yokkaichi Plant, Yokkaichi, Japan.
(2) K. Ninomiya, *J. Colloid Sci.*, **14**, 49 (1959).
(3) H. Leaderman and K. Ninomiya, in preparation for publication.
(4) K. Ninomiya and H. Fujita, *J. Colloid Sci.*, **12**, 204 (1957).

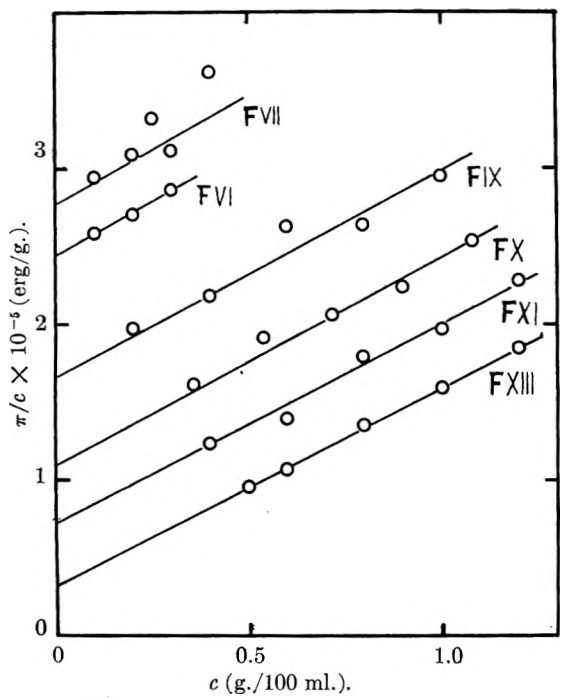

Fig. 1.—Plots of π/c *vs.* c for six polyvinyl acetate fractions in acetone at 26.0°.

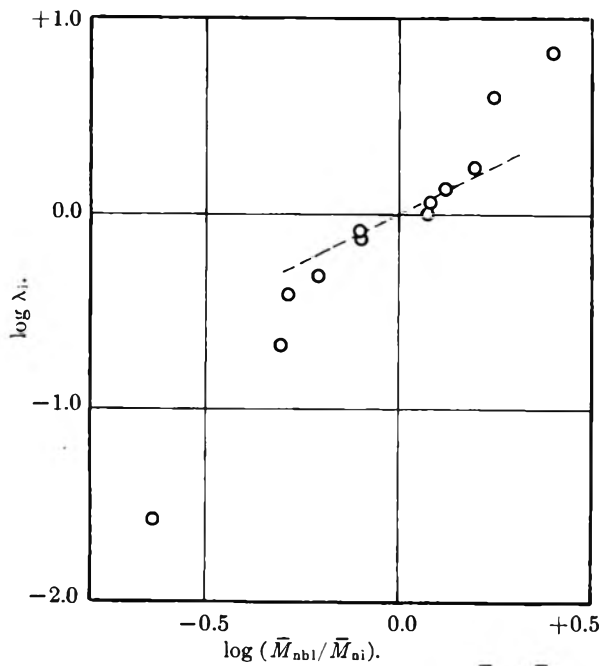

Fig. 2.—Doubly logarithmic plots of λ_i *vs.* $\bar{M}_{nbl}/\bar{M}_{ni}$ for six polyvinyl acetate blends; dashed line indicates the relation of equation 2.

fitted with semi-permeable membranes of du Pont Cellophane 600[6]; the conditioning of the membrane was made in 30% aqueous solution of sodium hydroxide.

Results and Discussion

Figure 1 shows the usual plots of π/c *vs.* c for the six polyvinyl acetate fractions. The value of $\bar{M}_n$ for each fraction, determined from its intercept on the ordinate, is given in Table I, together with the second virial coefficient A_2. The values of $\bar{M}_n$ for six blends, A, C, D, F, G and H (for their designations, see Table I in ref. 2) were calculated from the values of $\bar{M}_n$ for the fractions and their weight compositions in respective blends, and are given in Table I. The value of $\bar{M}_{nbl}/\bar{M}_{ni}$ was calculated for each of the six blends and was plotted against the value of the corresponding λ_i on a log-log graph in Fig. 2. It is apparent from Fig. 2 that equation 2 only approximates the tangent at the coördinate origin and that the plots deviate progressively from the predicted relation as the ratio $\bar{M}_{nbl}/\bar{M}_{ni}$ is more apart from unity. It was found that the data can be represented well by

$$\log \lambda_i = \{1 + \mu [(\bar{M}_{n2}/\bar{M}_{n1}) - 1]\} \log (\bar{M}_{nbl}/\bar{M}_{ni}) \quad (3)$$

for

$$\bar{M}_{n2} > \bar{M}_{n1}$$

where μ is a constant. The value of μ for this case was 0.25. Table II compares the observed values of log λ_i with those calculated in terms of equation 3, where $\mu = 0.25$. As seen in Table II, both the observed and calculated values of log λ_i agree fairly well with one another for each blend. It is of interest to observe that λ_i can be expressed in terms of an equation which contains only number-average molecular weights for both blend and its components.

The authors wish to thank Professor H. Fujita of Kyoto University for showing interest in this work.

TABLE I

NUMBER-AVERAGE MOLECULAR WEIGHTS, $\bar{M}_n$, OF POLYVINYL ACETATE FRACTIONS AND BLENDS. SECOND VIRIAL COEFFICIENT, A_2 (ml.^{3} mole g.$^{-2}$) OF FRACTIONS IN ACETONE AT 26.0°

Fraction	FVI	FVII	FIX	FX	FXI	FXIII
$\bar{M}_n \times 10^{-5}$	1.0	0.90	1.5	2.3	3.5	7.6
$A_2 \times 10^4$	5.6	5.6	5.4	5.4	5.2	5.1
Blend	A	C	D	F	G	H
$\bar{M}_n \times 10^{-5}$	3.8	1.8	1.2	1.4	1.2	2.8

TABLE II

COMPARISON OF VALUES OF LOG λ_i OBSERVED AND CALCULATED

Blend		A	C	D	F	G	H
logλ_1	obsd.	+0.83	+0.60	+0.00	+0.24	+0.13	+0.06
	calc.	+ .80	+ .66	+ .09	+ .28	+ .17	+ .09
logλ_2	obsd.	− .68	−1.58	− .13	− .32	− .42	− .09
	calc.	− .62	−1.68	− .11	− .29	− .40	− .11

(5) F. Daniels, *et al.*, "Experimental Physical Chemistry," Fifth Edition, McGraw-Hill Book Co., New York, N. Y., 1956, p. 218.

(6) This was furnished from the University of Wisconsin through the kindness of Professor John D. Ferry.

POLARIZABILITIES IN BORON-CONTAINING BONDS AND OCTETS

BY HANS WEIDMANN AND HOWARD K. ZIMMERMAN, JR.

Department of Chemistry, Agricultural and Mechanical College of Texas, College Station, Texas

Received August 10, 1959

A recent paper by Christopher and Tully[1] presents octet refractivities for B:Ö:C and B:C̈l: structural elements, as well as bond refractivities for B:C when the carbon is either aliphatic or aromatic. This work was based entirely upon refrac-

(1) P. M. Christopher and T. J. Tully, *J. Am. Chem. Soc.*, **80**, 6516 (1958).

tion data cited in a review paper by Lappert[2] which covered the literature to the end of 1955 and considered results there reported on 69 compounds containing boron. Lappert's paper contains but a fraction of the data now known in this subject. Nevertheless, the relatively large measure of discordance among the atomic refractivities given for boron in the literature[3-5] emphasizes the need stated by Christopher and Tully, for an analysis of refractivity data which reflects the status of electronic structures. Aside from their work, the only recorded information of this sort of which we are aware is a "B–O bond refractivity"[6] of 1.67.

Since it is desirable that bond and octet refractivities for use in future investigations should be based on a greater proportion of the available modern data than is the case for those derived by Christopher and Tully, we have reexamined the question employing data appearing through 1958. Thus a wider statistical sample is available upon which conclusions may rest. The methods of calculation were similar to those used by Christopher and Tully, but the values of Vogel[7] and of Warrick[8] were adopted for the "known" structural refractivities. The results are shown in Table I.

These results may be considered in three ways: (1) their relation to the less broadly based results by Christopher and Tully, (2) the possible influence of structural variations in determining their values and (3) their reliability and utility as guides for further research.

The present study impressively confirms the results of Christopher and Tully for the B:$\ddot{\text{O}}$:C_{alkyl} and B:$\ddot{\text{Cl}}$: octets. On the other hand, our results differ significantly from theirs for the B:C bond refractivities, both aliphatic and aromatic. In the alkyl series, independent corroboration of our value,[9] as well as our relatively low value for the mean deviation, suggests that the value 1.92 to 1.93 is to be preferred. In the aromatic series, we think both results must be regarded as only approximately valid.

Structural considerations probably preclude the existence of a reproducible value for the B:C_{aryl} refractivity as a consequence of the relative mobility of the π-electrons in an aromatic system. For example, the results of Torssell[10] strongly suggest the presence of resonance contributions in the B:C_{aryl} bond. A similar rationalization probably applies to our result for the B:$\ddot{\text{O}}$:C_{aryl} octet, which is both very rough and based upon an undesirably small statistical sample. It may also be that a non-bonding electron-pair type of resonance phenomenon[11] is responsible for the relatively wide statistical variation found for the B:$\ddot{\text{O}}$:B octet. However, this is not easy to reconcile with the result for B:$\ddot{\text{O}}$:Si, where one would expect both the reduced electronegativity of Si (compared to C), together with the possibility of d-orbital availability, to lead to a larger polarizability than is observed. Dispersion studies to examine this question would be interesting.

The increasing polarizability of the octet C:$\ddot{\text{X}}$: (X = halogen) with decreasing electronegativity of X is marked and quite in line with expectations. (A value for B:$\ddot{\text{Br}}$: of 7.5 ± 2.0 obtained from two compounds is exceedingly unreliable, but tends in the same direction.) The virtual identity of the B:$\ddot{\text{F}}$: octet and B:C_{alkyl} bond refractivities suggests that the non-bonding electrons of the fluorine atom play little if any part in polarizability. The similarity of the B:N bond refractivity to both these former values lends a degree of credibility to a view that the polarizability of boron bonds is primarily a property of the boron atom, although such a conclusion is obviously oversimplified.

If this idea has any truth to it, one should expect to find no significant variations in the B:$\ddot{\text{O}}$:C_{alkyl} octet refractivity as a result of variations in the nature of the alkyl substituents. Indeed, Christopher and Tully failed to find any such variations. However, among the wider sample used in the present instance, 21 compounds occurred for which Taft alkyl polar substituent parameters[12] could be computed. Of these 21 substances, fourteen gave a fair correlation between octet refractivity and substituent parameter. This hint is suggestive of a possible polar perturbation of polarizability, but it is not yet convincing. The variations, if present, are so small that measurements of a very high order of precision will be necessary to establish their effects quantitatively.

With respect to the reliability and utility of the results given, we have seen already that the bond and octet refractivities in which aromatic structures are represented are not highly reproducible from one substance to another. Thus, until a better quantitative description of the electron dynamics of such systems than is now available may appear, little precise significance may be attached to these parameters. On the other hand, the statistical reliability of most of the remaining parameters seems fairly good. Although the experimental determination of refractivity is often complicated by the sensitivity of many boron compounds toward atmospheric moisture and oxygen, errors from these causes are usually large enough to be quite obvious. It is believed that most such errors have been limited in the present study by selection of the data. The possible disturbing ef-

(2) M. F. Lappert, *Chem. Revs.*, **56**, 959 (1956).

(3) K. Torsell, *Acta Chem. Scand.*, **8**, 1779 (1954), gives a range of 3.07 to 5.27 for the atomic refractivity of boron in a variety of organoboron compounds.

(4) M. F. Lappert, *J. Chem. Soc.*, 1768 (1956), cites 2.65 for the atomic refractivity of boron in orthoborates.

(5) M. F. Lappert, *ibid.*, 2790 (1958), cites R_B = 2.20 in metaborates.

(6) P. A. McCusker and T. Ostdick, *J. Am. Chem. Soc.*, **80**, 1103 (1958).

(7) A. I. Vogel, "Practical Organic Chemistry," 3rd ed., Longmans, Green & Co., New York, N. Y., 1957, pp. 1035–1036.

(8) E. L. Warrick, *J. Am. Chem. Soc.*, **68**, 2455 (1946).

(9) G. F. Hennion, P. A. McCusker and J. V. Marra, *ibid.*, **80**, 3481 (1958).

(10) K. Torssell, *Svensk Kem. Tidskr.*, **69**, 34 (1957).

(11) T. Nash, *J. Appl. Chem. (London)*, **6**, 300 (1956).

(12) R. W. Taft, *J. Am. Chem. Soc.*, **75**, 4231 (1953).

fects of alternative structures in computing the results have been minimized by attempting to calculate refractivities for the alternative possibilities in doubtful cases, and by eliminating cases in which significant ambiguities appeared.

TABLE I

SUMMARY OF BOND AND OCTET REFRACTIVITIES

Structure	No. of cpds.	No. of struct. iterations	Ref.	Structural refractivity This work	Ref. 1
B:O:C_{alkyl}	52	171	1,2,13–19	3.10± 0.14	3.14± 0.14
B:O:C_{aryl}	4	9	13,15,25, 27	2.68± 0.30	
B:O:B	12	36	5,33	3.48± 0.26	
B:O:Si	10	28	6,38,39	3.34± 0.14	
B:Cl:	22	31	1,4,14,16, 19,20	6.79± 0.16	6.79± 0.21
B:F:	6	11	2,24,32,34	1.91± 0.12	
B:C_{alkyl}	16	37	1,9,21,22, 24,31, 36,37	1.92± 0.10	1.75± 0 19
B:C_{aryl}	47	61	1,3,24–28, 32,34,35	2.01± 0.23	2.96± 0.23
B:N	3	8	30	1.85± 0.05	

(13) H. Steinberg and D. L. Hunter, *Ind. Eng. Chem.*, **49**, 174 (1957).
(14) W. Gerrard and M. F. Lappert, *J. Chem. Soc.*, 3084 (1955).
(15) J. A. Blau, W. Gerrard and M. F. Lappert, *ibid.*, 4116 (1957).
(16) E. W. Abel, J. D. Edwards, W. Gerrard and M. F. Lappert, *ibid.*, 501 (1957).
(17) M. J. Frazer, W. Gerrard and M. F. Lappert, *ibid.*, 739 (1957).
(18) W. Gerrard, M. F. Lappert and H. B. Silver, *ibid.*, 3285 (1956).
(19) W. Gerrard, M. F. Lappert and H. B. Silver, *ibid.*, 1647 (1957).
(20) J. D. Edwards, W. Gerrard and M. F. Lappert, *ibid.*, 1670 (1955).
(21) R. Köster, *Ann.*, **618**, 31 (1958).
(22) W. Gerrard, M. F. Lappert and R. Shafferman, *J. Chem. Soc.*, 3828 (1957).
(23) W. Gerrard, M. F. Lappert and R. Shafferman, *ibid.*, 3648 (1958).
(24) P. B. Brindley, W. Gerrard and M. F. Lappert, *ibid.*, 824 (1956).
(25) S. H. Dandegaonker, W. Gerrard and M. F. Lappert, *ibid.*, 2872 (1957).
(26) P. B. Brindley, W. Gerrard and M. F. Lappert, *ibid.*, 1540 (1956).
(27) E. W. Abel, W. Gerrard and M. F. Lappert, *ibid.*, 112 (1957).
(28) E. W. Abel, W. Gerrard and M. F. Lappert, *ibid.*, 3833 (1957).
(29) E. W. Abel, W. Gerrard and M. F. Lappert, *ibid.*, 5051 (1957).
(30) W. Gerrard, M. F. Lappert and C. A. Pearce, *ibid.*, 381 (1957).
(31) G. F. Hennion, P. A. McCusker, E. C. Ashby and A. J. Rutkowski, *J. Am. Chem. Soc.*, **79**, 5190 (1957).
(32) C. Curran, P. A. McCusker and H. S. Makowski, *ibid.*, **79**, 5188 (1957).
(33) P. A. McCusker, E. C. Ashby and H. S. Makowski, *ibid.*, **79**, 5179 (1957).
(34) P. A. McCusker and H. S. Makowski, *ibid.*, **79**, 5185 (1957).
(35) E. W. Abel, S. H. Dandegaonker, W. Gerrard and M. F. Lappert, *J. Chem. Soc.*, 4697 (1956).
(36) P. A. McCusker, E. C. Ashby and H. S. Makowski, *J. Am. Chem. Soc.*, **79**, 5182 (1957).
(37) G. F. Hennion, P. A. McCusker and J. V. Marra, *ibid.*, **81**, 1768 (1959).
(38) M. G. Voronkov and V. N. Zgonnik, *J. Gen. Chem. U.S.S.R.*, **27**, 1550 (1957).
(39) B. N. Dolgov, Yu. I. Khudobin and N. P. Kharitonov, *Doklady Akad. Nauk S.S.S.R.*, **122**, 607 (1958).

INTERACTIONS IN THE BINARY LIQUID SYSTEM N,N-DIMETHYLACETAMIDE–WATER: VISCOSITY AND DENSITY

BY RAYMOND C. PETERSEN

Research Laboratories, Sprague Electric Company, North Adams Massachusetts

Received August 11, 1959

Plots of viscosity *versus* composition for binary liquid mixtures normally are not linear whether the composition be expressed in units of mole fraction, weight fraction or volume fraction. Beyond this lack of linearity, many binary liquid systems are known for which the viscosity goes through a minimum, while another, less well-known, class of mixtures exhibits a viscosity maximum, an example of this class being water–dioxane.[1] An especially striking example of this class, due to the exceptional magnitude of its maximum, is found in mixtures of water with N,N-dimethylacetamide (DMA). In this system, the maximum viscosity is about 4.4 times the viscosity of water, while the viscosity of DMA is just slightly higher than that of water (all measured at room temperature). Measurements were made of viscosities and, of necessity, densities of several mixtures of DMA with water at a temperature of 24.05°.

Experimental

Materials.—Eastman Kodak Co. white label DMA was used without further purification. This material was compared by vapor fractometry with three samples of itself containing known added amounts of water (from 0.5 to 1.5%) and was found to contain 0.63 ± 0.04% water by weight. No other impurities were revealed by the vapor fractometer. Water used was ordinary laboratory distilled water. Mixtures were prepared by weight and compositions determined assuming the DMA to contain 0.63% water. The DMA used throughout this series of measurements all came from one bottle. Weights were calibrated against an N.B.S.-calibrated set of weights.

Temperatures.—Temperature was measured by a thermometer which had been compared with an N.B.S.-calibrated thermometer and was maintained at 24.05° in an oil thermostat bath. Temperature generally varied less than 0.05° from this.

Viscosity.—Viscosities were measured in a single Ostwald-Fenske size 100 viscometer. Samples were measured into the viscometer using a 10-ml. pipet, the liquid having been filtered through glass wool in the process of filling the pipet to remove dust particles. Poiseuille's equation, with the kinetic energy correction included,[2] was used to calculate viscosities. Pure water was used as the reference liquid, its viscosity at 24.05° being taken as 0.9101 centipoise.[3] Efflux time ranged from 1.2 to 5.4 minutes.

Density.—Density was measured in a Reischauer specific gravity bottle having a capacity of about 25 cc. Water was again used as the calibrating liquid, the density of water at 24.05° being taken as 0.99728 g./cc.[4] The apparent precision of measurement was about 0.01%.

Temperature Dependence of Viscosity.—Viscosities of several of the mixtures also were measured at 26.55° and the fractional change in viscosity per degree, $d \ln \eta/dT$, was computed. Values for mixtures not measured were estimated from a plot of $d \ln \eta/dT$ *vs.* composition. These values are subject to considerable error, but they may be

(1) J. A. Geddes, *J. Am. Chem. Soc.*, **55**, 4832 (1933).
(2) M. R. Cannon and M. R. Fenske, *Ind. Eng. Chem., Anal. Ed.*, **10**, 297 (1938).
(3) Obtained by interpolation from the relative values of Bingham and Jackson combined with the absolute value at 20° by Swindells, Coe and Godfrey. Data given in "Handbook of Chemistry and Physics," 38th ed., Chemical Rubber Publishing Co., Cleveland, Ohio, 1956, pp. 2028, 2030.
(4) Obtained by interpolation from data given in ref. 3, p. 1989.

used to convert viscosities at 24.05° to other temperatures in the vicinity of room temperature, the estimated additional error being about 0.05% for each degree removed from 24.05°.

Results

Table I lists efflux times, densities, viscosities and d ln η/dT of several mixtures of DMA and water. Each viscosity is the median of several different measurements. The average magnitude of the percentage deviation for all measurements from their respective medians was 0.067%.

TABLE I

Water (mole fract.)	Density (g./cc.)	Viscosity (cp.)	$-\frac{d \ln \eta}{dt} \times 100$ (%/°C.)
0.0298	0.9408	1.005	1.58
.0519	.9420	1.037	1.61
.0694	.9429	1.062	1.64
.0926	.9444	1.105	1.68
.2763	.9565	1.564	2.11
.4360	.9694	2.300	2.58
.5550	.9804	3.112	3.06
.6259	.9867	3.615	3.38
.6897	.9925	3.957	3.58
.7347	.9955	4.029	3.64
.7737	.9981	3.926	3.61
.8015	.9990	3.741	3.55
.8783	.9994	2.782	3.32
.9515	.9969	1.599	2.97
1.0000	.9973	0.910	2.24

The solutions were stored in screw-cap bottles and, as a test of stability, efflux times were remeasured for some of the solutions after storage periods ranging from 41 to 52 days. In each case, the time increased slightly, the increases ranging from 0.05% in the best case to 0.46% in the worst. In light of the very great dependence of viscosity on composition, these changes must be considered negligible.

The density of pure DMA, obtained by extrapolation, is 0.9392 g./cc.[5] while its viscosity is 0.961 centipoise.[6]

Discussion

The theory of viscosity of binary liquid mixtures is not well developed. Various treatments have been developed for ideal mixtures,[7] but in general no agreement is to be expected in cases where one component is associated or where association exists between the two components.

In the case of the DMA–water system, water is associated through hydrogen bonding, while DMA is generally considered to be unassociated. The viscosity maximum must be attributed either to compound formation or to a higher degree of association than exists in either water or DMA alone. Association can, of course, be considered to be a specific type of compound formation.

Geddes,[1] in discussing the dioxane–water system, states that when fluidity ($1/\eta$) is plotted *versus* weight per cent., the composition at which the fluidity deviates most from a straight line connecting the fluidities of the pure components is the composition of a compound formed between these components. This is justified only in cases where some very simple considerations are applicable. Some conditions under which this may be true are discussed by Bingham and Brown.[8] In Geddes' case the fact is emphasized that this point of maximum deviation occurs at a molar ratio (water: dioxane) of exactly 5:1, although no measurements were made between ratios of 3.9:1 and 6.4:1. In the DMA–water system this point of greatest deviation occurs at a water:DMA molar ratio of about 2.7:1, but no conclusions are to be drawn from this fact.

The qualitative explanation for a greater degree of association in mixtures of water–DMA than in water alone is straightforward. The carbonyl bond is highly polar. In resonance terminology, it has a high percentage of ionic character,[9] the oxygen being strongly negative, and stronger hydrogen bonds are formed between water and carbonyl oxygens than between water molecules. In the case of DMA, this effect is strengthened by the nitrogen atom, the resonance form II being perhaps fully as significant as form I.[9]

I II

The importance of structures similar to II in the case of mono-N-substituted amides has been discussed by Gutowsky and Holm[10] among others.

Certain implications of this explanation are clear. It predicts, for example, that similar, but less pronounced, behavior will be found in mixtures of simple ketones with water. In the case of mono-N-substituted amides mixed with water, the maximum in the viscosity–composition curve will be shifted toward the amide end and may become only a fairly broad, nearly flat region, due to the very strong hydrogen bonding in the amide itself.

(5) Using the temperature dependence of density of DMA obtained by J. R. Ruhoff and E. E. Reid, *J. Am. Chem. Soc.*, **59**, 401 (1937), this value is equivalent to 0.9430 g./cc. at 20°. Ruhoff and Reid report values at 20° (their own and two earlier ones) of 0.9413, 0.9405 and 0.9434 g./cc. Considering the possible great effect of certain impurities, this agreement is highly satisfactory.

(6) G. R. Lester, T. A. Grover and P. G. Sears, THIS JOURNAL, **60**, 1076 (1956), report the value 0.919 cp. for DMA at 25°. This is equivalent to about 0.932 cp. at 24.05°. Better agreement would be desirable, but again the strong dependence of viscosity on purity can explain the discrepancy.

(7) For example see S. Glasstone, K. J. Laidler and H. Eyring, "The Theory of Rate Processes," 1st ed., McGraw-Hill Book Co., Inc., New York, N. Y., 1941, pp. 514–516.

(8) E. C. Bingham and D. F. Brown, *J. Rheol.*, **3**, 95 (1932).

(9) L. Pauling, "The Nature of the Chemical Bond," 2nd ed., Cornell Univ. Press, Ithaca, N. Y., 1948, pp. 75, 131, 133, 207.

(10) H. S. Gutowsky and C. H. Holm, *J. Chem. Phys.*, **25**, 1228 (1956).

INTERACTIONS OF SERUM ALBUMIN AND SYNTHETIC POLYELECTROLYTES IN VARIOUS BUFFER SYSTEMS

BY HAJIME NOGUCHI

Physics Department, Aichi-Gakugei University, Okazaki, Japan

Received August 14, 1959

In the previous paper,[1] we reported experimental results on the interaction of albumin with polymers

(1) H. Noguchi, *Biochim. et Biophys. Acta*, **22**, 459 (1956).

TABLE I

COMPLEX FORMATION BETWEEN ALBUMIN AND POLYANION AT *p*H 5.2 AND 3°

Buffer	0.2 *M* buff.	0.1 *M* buff.—0.01 *M* salt			0.1 *M* buff.—0.1 *M* salt		
Salt	None	NaCl	KCl	KBr	NaCl	KCl	KBr
SCMC	Not formed	Formed	Formed	Formed	Not formed	Not formed	Not formed
(Complex $u \times 10^5$)		(−7.0)	(−6.9)	(−6.9)			
DS-1	Formed	Formed	Formed	Formed	Formed		
(Complex $u \times 10^5$)	(−6.1)	(−7.0)	(−5.3)	−(5.9)	(−6.3)		

TABLE II

MOBILITIES ($u \times 10^5$) OF ALBUMIN OF THE CONCENTRATION OF 0.53% AND POLYANION OF 0.25% IN VARIOUS ACETATE BUFFERS AT 0°

Buffer		0.1 *M* buff.—0.1 *M* salt				0.1 *M* buff.—0.01 *M* salt			0.2 *M* buff.
	Salt	None	NaCl	KCl	KBr	NaCl	KCl	KBr	None
*p*H 5.6	Albumin	− 2.7	− 3.3	− 3.6	−3.7	− 3.0	− 3.1		
*p*H 5.2	Albumin	− 1.9	− 2.2	− 2.3	−2.5	− 2.0	− 2.0	− 2.2	− 1.6
*p*H 5.2	SCMC	−11.0	−10.6	−11.6	−9.6	−10.0	−11.5	−11.4	−10.9
*p*H 5.2	DS-1	−16.8	−14.8			−15.0	−15.2	−15.7	

in the alkaline side of the isoelectric point of albumin. According to our findings, electric charges are necessary for polymers to form a soluble complex with albumin. In that work[1] we had paid no attention to the effect of buffer composition on the interaction, but in the course of successive experiments we found that the composition of buffer solutions had an influence on the interaction. In order to clarify the mechanism of the interaction of albumin with polyelectrolytes, we have investigated the soluble complex formation between them in various buffer systems.

Materials and Method

Human serum albumin was prepared by Cohn's method and found to be pure electrophoretically. Its isoelectric point was 4.7 in 0.1 *M* acetate buffer.

Sodium carboxymethyl cellulose (SCMC) was obtained from Hercules Powder Co. The molecular weight was 70,000 and the degree of substitution was 0.77.

Purified sodium dextran sulfate (DS) was kindly supplied by Dr. Sasaki of Nagoya University School of Medicine.[2] Two kinds were used for the present experiment: DS-1: molecular weight 32,000; degree of esterification 1.45 and DS-2: molecular weight 270,000; degree of esterification 2.04.

Solutions of albumin, polyelectrolytes and their mixtures were examined by Tiselius electrophoretic apparatus and the formation of the soluble complex was confirmed from the electrophoretic pattern.[1]

Results

(1) Interaction in Acetate Buffer Containing Neutral Salts.—In Table I are shown the results of electrophoresis on the mixture of albumin and polyelectrolytes, whose concentrations are 0.68 and 0.25%, respectively, in 0.1 *M* acetate buffer containing various concentrations of sodium chloride, potassium chloride and potassium bromide, and in 0.2 *M* acetate buffer. The results at *p*H 5.6 are similar to those at *p*H 5.2. From this table we can conclude that the soluble complex formation between albumin and SCMC is disturbed by increase in concentration of salts or buffer. On the other hand, DS has a stronger affinity to albumin than SCMC and added salts have no influence on the soluble complex formation between DS and albumin.

As given in Table II, the mobility of polyelectrolytes is hardly changed by addition of salts or increase in buffer concentration, while the mobility of albumin is slightly increased (negatively) with increasing concentration of salts and decreased with increasing buffer concentration. There is found a difference in the effect on the mobility among various kind of salts. The increase of the mobility by salts may be due to the adsorption of anions on albumin.[3,4] When DS is added to the buffer containing 0.1 *M* KCl and KBr, there appear flocculent white precipitates.[5]

By comparing Table I with Table II, however, we can see that independently of the degree and the direction of the change in mobility, the increase in the concentrations of salts and buffers always has the effect of breaking the soluble complex between albumin and SCMC. It was also confirmed by viscosity measurements that the molecular shape of SCMC and DS is not changed by addition of salts or acetate buffer to 0.1 *M* acetate buffer. At such high concentrations of small ions, the long-range electrostatic interaction between ionized groups is sufficiently suppressed. From these results it is allowable to say that the complex formation between albumin and SCMC is brought about by the short-range electrostatic interaction between ionized groups on them, as suggested in the previous paper,[1] and that small ions break the complex by screening this interaction. On the other hand, DS probably has another specific interaction with albumin molecule besides the simple electrostatic interaction. Although the SCMC has a lower degree of substitution than DS, this difference is not the cause of the difference in affinities to albumin because it was found that the degree of esterification of DS had no influence on the ability of complex formation in the range from 0.6 to 2.0.

(2) Interaction in Other Buffer Systems.—In addition to the acetate buffer, these three buffers having *p*H 5.6 were employed: (a) 0.1 *M* succinic acid–0.1 *M* sodium borate buffer of Kolthoff–Vleeschhouwer, (b) 0.1 *M* monopotassium

(2) S. Sasaki and H. Noguchi, *J. Gen. Physiol.*, **43**, 1 (1959).

(3) L. G. Longsworth and C. F. Jacobsen, THIS JOURNAL, **53**, 126 (1949).

(4) B. S. Schlessinger, *ibid*, **62**, 916 (1958).

(5) S. Sasaki (personal communication) has observed qualitatively in the process on the preparation of DS that potassium salt of DS is less soluble compared with the sodium salt.

citrate–0.1 N sodium hydroxide buffer of Kolthoff–Vleeschhouwer and (c) 0.1 M potassium biphthalate –0.1 N sodium hydroxide buffer of Clark–Lubs. According to our results, SCMC can form a soluble complex with albumin only in the acetate buffer, while DS can form the complex in all buffer systems except in potassium biphthalate–sodium hydroxide buffer, the ionic strength of which is 0.18. The mobilities of albumin, DS, and the complex of them measured in solutions mixed at various concentrations are given in Table III. When the concentration of DS is between 0.125 and 0.25%, we could observe only one pattern in all buffer systems; the mobility of this single peak was intermediate between those characteristic of albumin and DS, corresponding to that of the soluble complex. As seen in the table, the mobility of the soluble complex in solutions containing free albumin and no free DS differs considerably from the mobility in solutions containing free DS and no free albumin. This result may arise from the differences in the viscosity of solutions and in the proportion of albumin and DS in the complex.

TABLE III

COMPLEX OF SERUM ALBUMIN AND DS-2 AT pH 5.6 AND 0°

Buffer	Ionic str.	Albumin concn. (%)	DS-2 concn. (%)	Albumin $u \times 10^5$	Complex $u \times 10^5$	DS-2 $u \times 10^5$
Acetic acid–sodium acetate	0.10	0.83	0.40		−10.4	−16.8
		.83	.0625	−2.8	− 4.2	
Succinic acid–sodium borate	.23	.83	.375		− 9.9	−15.6
		.83	.0625	−3.8	− 5.1	
Monopotassium citrate–NaOH	.24	.83	.40		− 9.4	−15.1
		.83	.0625	−4.3	− 5.9	

At present, we cannot separate the specific effect of buffer anions due to binding on albumin from their non-specific effect due to screening. At least apparently, however, we can arrange various anions in the order of the affinity to albumin: acetic ion, SCMC, succinic ion and citrate ion, DS, biphthalate ion.

Discussion

Thus, we found that the composition of buffer has a considerable influence on the formation of soluble complex between polyanions and albumin, particularly through the specific interaction between small anions and albumin. The order of affinity of various small anions and polyanions is determined. Special attention must be paid to the difference between DS and SCMC. This means that the $-SO_3$ groups on polyanions have a stronger affinity to albumin than $-COO^-$ groups. A similar phenomenon was found in the interaction between fibrinogen and these polyanions as reported in the previous paper.[2] There we assumed that $-SO_3^-$ groups have a stronger tendency to make hydrogen bonds with amino groups on protein than $-COO^-$ groups. A similar situation is expected in the present case.

Acknowledgments.—I am very deeply indebted to Prof. Inoue for measuring the molecular weights of polyelectrolytes by the osmotic pressure method. It is a great pleasure to acknowledge the advice and discussion of Prof. Oosawa and Dr. Imai of Nagoya University.

THE ENRICHMENT OF LITHIUM ISOTOPES BY ION-EXCHANGE CHROMATOGRAPHY.[1] II. THE INFLUENCE OF TEMPERATURE ON THE SEPARATION FACTOR

BY D. A. LEE

Chemistry Division, Oak Ridge National Laboratory, Oak Ridge, Tennessee

Received September 16, 1959

Equilibrium constants for isotopic exchange reactions generally decrease with increasing temperature.[2] The manner in which the equilibrium constant of a reaction depends on temperature is readily deducible from thermodynamics. The van't Hoff reaction isochor defines the temperature coefficient of ln K_c

$$\left[\frac{\partial \ln K_c}{\partial T}\right] = \frac{\Delta H^0}{RT^2}$$

Assuming that ΔH^0 is independent of the temperature or that it varies only very slowly with the temperature, the equation may be integrated between two temperatures. This integration is valid if the temperature range is not large. ΔH^0 therefore can be determined from the slope of the line obtained by plotting log K_c against $1/T$. The heat of isotopic exchange is naturally quite small. Glueckauf,[3] using the data of Betts, Harris and Stevenson[4] for Na^{24} and Na^{22} separation by ion exchange, has calculated the heat of isotopic exchange to be 0.4 cal./mole.

The effect of temperature on the equilibrium constant (α) for the reaction

$$^6Li(H_2O)_x^+ + {}^7Li(H_2O)_y^+R^- \rightleftharpoons {}^7Li\,(H_2O)_x^+ + {}^6Li(H_2O)_y^+\,R^-$$

where $x > y$, and R^- are the exchange sites on the resin, was measured in a series of isotopic separation experiments performed at several temperatures between 3 and 59°. The method used in these experiments was described in the previous paper.[5]

TABLE I

SUMMARY OF EXPERIMENTS TO DETERMINE THE EFFECT OF TEMPERATURE ON α

Temp., °C.	Flow rate 10^{-3}, cm./sec.	Plates	$\frac{(Li^6/Li^7)res.}{(Li^6/Li^7)aq.}$ (α)
3	1.13	1400	1.0033
20	1.42	2000	1.0031
40.5	1.92	1900	1.0028
59	2.02	1700	1.0026

Experimental

One column was used in these experiments. Constant temperature water (± 0.3°) was circulated in a jacket around the resin column. The resin was analytical grade sulfonated polystyrene–divinylbenzene Dowex X-16 ground to 200-400 mesh. The resin column dimensions were 19 mm. i.d. and 1080 mm. long. The resin was washed thoroughly with 0.25 N HCl before adding 1 ml. of 8.75 N LiCl as the lithium band to the top of the column. The eluent in each experiment was 0.25 N HCl. The temperatures at which the experiments were made were 3, 20, 40.5 and 59°. The analyses were made as described previously.[5]

(1) This paper is based on work performed for the U. S. Atomic Energy Commission by Union Carbide Corporation.

(2) H. C. Urey, *J. Chem. Soc.*, 562 (1947).

(3) E. Glueckauf, *Trans. Faraday Soc.*, **54**, 1203 (1958).

(4) R. H. Betts, W. E. Harris and M. D. Stevenson, *Can. J. Chem.*, **34**, 65 (1956).

(5) D. A. Lee and G. M. Begun, *J. Am. Chem. Soc.*, **81**, 2332 (1959).

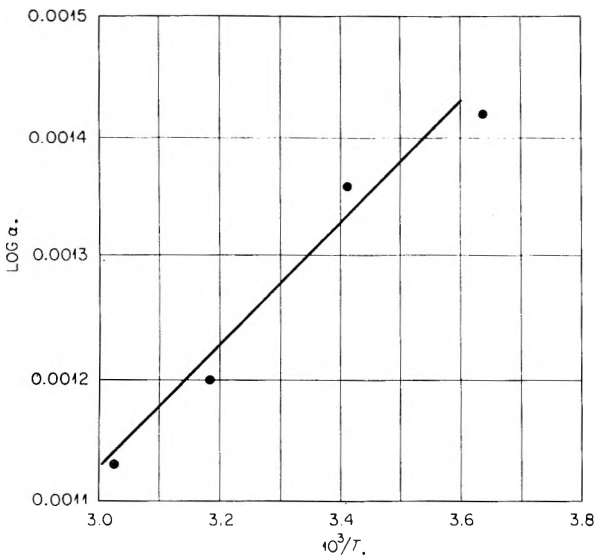

Fig. 1.—The log of α as a function of $10^3/T$.

Results and Discussion

The results of these experiments are summarized in Table I. The uncertainty in the isotopic equilibrium constants is estimated to be less than one digit in the last decimal place shown. As expected, the data show an inverse dependence upon temperature.

By plotting log α *vs.* $1/T$, a straight line was obtained, as shown in Fig. 1. The heat of exchange calculated from the slope of this line was 2.26 cal./mole and $-\Delta S$ was 1.81×10^{-3} cal./mole degree at 25°. These results are slightly higher than those given by Glueckauf[3] for the Na^{22}–Na^{24} exchange, and doubtless reflect the greater mass difference ratio ($\Delta M/M$) which exists between the isotopes of lithium as compared to Na^{22} and Na^{24}.

USE OF GLASS ELECTRODES TO MEASURE ACIDITIES IN DEUTERIUM OXIDE[1,2]

BY PAUL K. GLASOE[3] AND F. A. LONG

Department of Chemistry, Cornell University, Ithaca, New York

Received August 26, 1959

Recent studies have shown that a conventional glass electrode apparatus can be used to give fairly precise values of acidity in aqueous solutions, particularly when only relative values of the acidity are needed.[4,5] One situation where it would be helpful to have additional data on relative acidities is for solutions of weak acids and bases in the solvents D_2O and H_2O. We have therefore investigated the applicability of the glass electrode to measurement of acidity in D_2O solutions. A general study is already available on some of the properties of glass electrodes in D_2O,[6] but it does not give much consideration to the measurement of acidity in D_2O with ordinary electrodes. We have recently learned that this latter problem was considered some time ago by Hart, and by R. B. Fischer and R. A. Potter but the results are available only in special publications.[7,8]

Experimental

All measurements were made with a Beckman Model G *p*H meter at 25°. The Beckman No. 39166 (old No. 19166) glass electrode and saturated calomel electrode combination was used for all measurements, unless otherwise noted. The *p*H meter was standardized with conventional buffer mixtures chosen to be close to the range of the *p*H measurements. Reagent grade chemicals were used without further purification. Formic acid was redistilled and maleic acid, aniline hydrochloride and pyridinium perchlorate were recrystallized. The D_2O was 99.5 atom % deuterium. Solutions of NaOD were made by passing water vapor over sodium. Other solutions in D_2O were made by dissolving the anhydrous hydrogen compound (except for hydrochloric acid where a concentrated aqueous solution was diluted). For the low concentrations studied, this did not change the deuterium content by a significant amount. All concentrations are in moles (or equivalents) per liter.

Results and Discussion

Glass Electrode Measurements in Solutions of Strong Acids.—Solutions of roughly 0.01 *M* hydrochloric acid in H_2O and in D_2O were prepared by dilution and the exact concentration of acid was determined by titration with standard base. The averages of several *p*H meter readings with the standard electrode combination are given under (a) of Table I. For solutions of comparable acidity

TABLE I

GLASS ELECTRODES IN SOLUTIONS OF HYDROCHLORIC ACID IN H_2O AND IN D_2O

Solutions are 0.00976 *M* HCl in H_2O and 0.00983 *M* DCl in D_2O; *p*H meter standarized with *p*H 4.00 phthalate buffer

		Av. rdgs. H_2O soln.	Av. rdgs. D_2O soln.	Difference
(a)	Standard glass electrode—Beckmann No. 39166; 39168 calomel	2.08	1.69	0.40
(b)	Beckmann 1190-80 glass electrode; 1170 calomel	2.08	1.69	.39
(c)	Beckmann type E glass electrode; 1170 calomel	2.02	1.62	.40
(d)	"Synthetic" 1190-80 glass electrode; 1170 calomel	2.13	1.73	.40

the *p*H meter reading in D_2O solution is 0.40 *p*H unit lower than in H_2O solution. To determine whether this difference was characteristic only of this particular electrode system, these same solutions were measured using various glass electrode–calomel electrode combinations. The results are given in (b), (c) and (d) of Table I. It is apparent that the difference is constant for the different electrodes, within the error of reading the meter. The "synthetic 1190–80" electrode in (d), Table I, is an ordinary Beckman 1190–80 electrode from which the internal solution was poured out and replaced with a solution of 0.100 *M* HCl in H_2O. The

(1) Supported in part by a grant from the Atomic Energy Commission.

(2) Presented at the 136th meeting of the American Chemical Society, Atlantic City, September, 1959.

(3) National Science Foundation Science Faculty Fellow at Cornell University, 1958–1959.

(4) E. Grunwald, *J. Am. Chem. Soc.*, **73**, 4934 (1951).

(5) A. L. Bacarella, E. Grunwald, H. F. Marshall and E. L. Purlee, THIS JOURNAL, **62**, 856 (1958).

(6) D. Hubbard and G. W. Cleek, *J. Research Natl. Bur. Standards*, **49**, 267 (1952).

(7) R. G. Hart, Nat. Res. Council, Canada, CRE 423, June 1949.

(8) R. B. Fischer and R. A. Potter, A.E.C. document NODC-715, Sept. 12, 1945.

TABLE II

MEASUREMENTS WITH GLASS ELECTRODE FOR STRONG BASES IN H_2O AND IN D_2O

	Base	Acidity: $-\log C_{H^+}$	Acidity: $-\log C_{D^+}$	Δ calcd.	pH Reading: In H_2O	pH Reading: In D_2O	Δ exp.	ΔpD: (Δcalcd. − Δexp.)
(a)	NaOH NaOD	12.00	12.86	0.86	11.83	12.21	0.38	0.48
(b)	NaOH NaOD	12.00	12.86	.86	12.00[a]	12.47[a]	.47	.39
(c)	$Ba(OH)_2$ $Ba(OD)_2$	12.46	13.29	.83	12.38	12.82	.44	.39
(d)	$Ca(OH)_2$ $Ca(OD)_2$	12.28	13.14	.86	12.22	12.67	.45	.41

[a] Measurements made with type E (low sodium ion error) electrode.

actual potential of this electrode was markedly different from a normal 1190–80 electrode but even so the difference for the two solvents remains at 0.40 *p*H unit.[9]

These measurements indicate that the difference of 0.40 *p*H meter unit is not dependent on the particular type of glass electrode and that the *p*D of a solution in D_2O can be determined by use of the equation

$$p\mathrm{D} = p\mathrm{H\ meter\ reading} + 0.40 \qquad (1)$$

where the "*p*H meter reading" is obtained with an apparatus standardized to read *p*H in H_2O solutions. For convenience, we shall refer to the difference, *p*D minus *p*H meter reading, in this case 0.40, as Δ*p*D.[10]

Fisher and Potter[7] made studies of a glass electrode system using buffer solutions in D_2O and concluded that an equation like 1 could be used to give *p*D. However, they proposed a numerical constant of 0.25 rather than 0.40. Hart[8] did a similar study with solutions of hydrochloric acid in the two solvents and also with phosphate buffers (*p*H of from 5 to 7). He found values for the constant of equation 1 which range from 0.40 to 0.47. Hart also gave further consideration to the Fisher and Potter results and noted difficulties in the latters' work, both in the extrapolations and in the calculation of ionic strength. We conclude that the value of 0.40 for the constant of equation 1 agrees within experimental error with all of the earlier results.

Glass Electrode Measurements in Solutions of Strong Bases.—*p*H meter readings using the standard electrodes were made on solutions of 0.001009 *M* NaOH in H_2O and 0.001104 *M* NaOD in D_2O. The resulting average values are given under (a) in Table II. Calculation of the value of $-\log C_{D^+}$ or $-\log C_{H^+}$ for solutions of known concentration of hydroxide ion involves the ion product of water. This was taken to be 0.15×10^{-14} and 1.01×10^{-14} for D_2O and H_2O, respectively.[11]

The value of Δ*p*D of 0.48 for the sodium hydroxide solutions is significantly higher than that obtained for acid solutions. However, it is well known that the sodium ion error of the standard glass electrode depends on the *p*H at a fixed concentration of sodium ion. From the Beckman chart of sodium ion error it is found that for 0.01 *M* sodium ion at 25° the correction is 0.13 *p*H unit at *p*H 12.80 and 0.05 unit at *p*H 12.00. The value of Δ*p*D taking this into account is 0.48–0.08 = 0.40 *p*H unit, the same as the value for acid solutions. In agreement with this, a Δ*p*D value of 0.39 (Table IIb) was found for these same solutions with the Beckman type E electrode which has a negligible sodium ion error at these concentrations. Further confirmation of the similarity of Δ*p*D in acid and in base solutions is given by the results obtained with solutions of approximately 0.029 *N* barium hydroxide and 0.02 *N* calcium oxide in H_2O and D_2O (Table II, (c) and (d). These solutions would be expected to show an insignificant cation effect at these low concentrations. In both cases the Δ*p*D is 0.40 *p*H unit, within experimental error.

K_H/K_D Ratios for Some Weak Acids and Bases.—To determine whether the correction term 0.40 is applicable in the *p*H range between the extremes of strong acids and strong bases, the pK_a values for some weak acids were determined in H_2O and in D_2O using the glass electrode to measure *p*H and *p*D. For every acid, values of pK_H' or pK_D' (where K' is the concentration equilibrium constant) were calculated from the *p*H or *p*D value and the molar ratio of acid and conjugate base for each of several buffer ratios. Values of $\Delta pK'$, defined as $pK_D' - pK_H'$ were always calculated from pK_D' and pK_H' values for solutions of equal ionic strength. In most measurements the ionic strength was less than 0.10. Values of pK_H or pK_D were calculated from pK' using the activity coefficient expression

$$-\log f\pm = \frac{0.509\sqrt{I}}{1 + \sqrt{I}}$$

where I is ionic strength for molar concentrations. It made no difference, within experimental error, whether the K_H/K_D ratio was calculated from the average of the $\Delta pK'$ or the ΔpK values.

Table III summarizes the values of K_H/K_D obtained for a variety of weak acids. In general the agreement between the K_H/K_D ratios from glass electrode studies and from other methods of measurement is quite satisfactory, and it seems safe to conclude that the factor of 0.40 for Δ*p*D is applicable to measurements at intermediate acidities.

(9) In view of the frequent recommendation that a glass electrode should be equilibrated in water for several hours before use, it is worth noting that when a glass electrode was transferred from a water solution to a D_2O solution (or *vice versa*) the "*p*H" difference of 0.40 appeared to be established as rapidly as measurements could be made.

(10) As is well known, the definition of *p*H is somewhat fuzzy. One can assume that the definition of *p*D is equally so. Our implicit definition of *p*D is that it "means the same thing for solutions in pure D_2O that *p*H does for H_2O."

(11) R. W. Kingerley and V. K. LaMer, *J. Am. Chem. Soc.*, **63**, 3256 (1941).

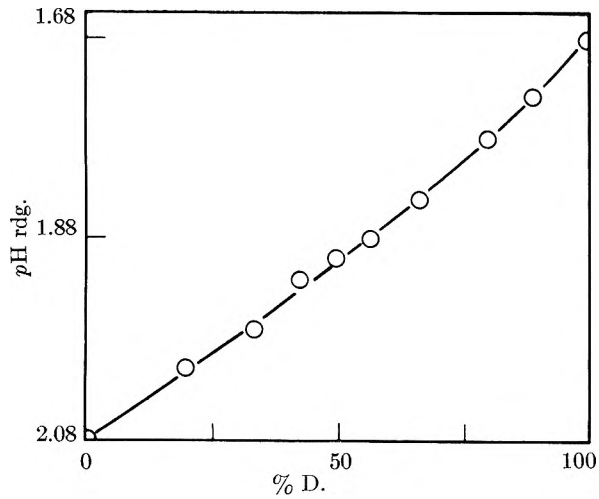

Fig. 1.—Dependence of pH meter reading for 0.01 M hydrochloric acid on atom per cent. deuterium of the aqueous solvent. Meter standardized to read pH for H_2O solutions.

TABLE III

K_D/K_H FROM MEASUREMENTS OF pH AND pD WITH GLASS ELECTRODE

Acid	pK^H	pK^D	ΔpK^a	K^H/K^D	K^H/K^D other
Acetic	4.73	5.25	0.52	3.3	3.33[12]
Formic	3.75	4.20	.45	2.8	2.5[13]; 2.7[14]
Aniline·HCl	4.55	5.13	.58	3.8	3.1[13]
Maleic, pK_1	1.98	2.53	.55	3.6	4.2[15]
Maleic, pK_2	6.28	6.61	.33	2.1	2.4[15]
Phosphoric, pK_1	2.11	2.31	.20	1.6	1.6[13]
Carbonic, pK_2	10.33	10.96	.63	4.3	4.4[16]
m-Nitroaniline·HCl	2.48	2.96	.48	3.0	3.8[17]

[a] Values of $\Delta pK'$, calculated from measurements of similar ionic strengths are the same, within experimental error.

Dependence of ΔpD on Deuterium Content of Solution.—Varying quantities of 0.010 M HCl in H_2O and 0.010 M DCl in D_2O were mixed to form a series of solutions of the same acid concentration but with different deuterium content. The "pH's" of these solutions were measured with the standard glass electrode. As Fig. 1 shows the reading of the pH meter is very nearly a linear function of the atom per cent. deuterium.

Source of Potential Difference Giving Rise to ΔpD.—The correction term ΔpD could arise from a change of potential in D_2O compared to H_2O for either or both the glass electrode and the calomel electrode. In an exploratory experiment on this point, after the pH meter was standardized with the standard electrodes, the calomel electrode was replaced by one containing a saturated solution of potassium chloride in D_2O. There was no significant change in the meter reading. It thus appears that the potential change is due solely to the glass electrode.

(12) S. Korman and V. K. LaMer, *J. Am. Chem. Soc.*, **58**, 1396 (1936).

(13) G. Schwarzenbach, *Z. Elektrochem.*, **44**, 46 (1938).

(14) J. C. Hornel and J. A. V. Butler, *J. Chem. Soc.*, 1361 (1936).

(15) G. Dahlgren and F. A. Long, *J. Am. Chem. Soc.*, **82**, in press (1960).

(16) J. Curry and Z. 7. Hugus, *ibid.*, **66**, 653 (1944). This reference lists 3.95 but recalculation for molar concentrations leads to the value 4.4 (J. Curry, private communication).

(17) E. Hogfeldt and J. Bigeleisen, *J. Am. Chem. Soc.*, **82**, 15 (1960).

THE NATURE OF THE S–O BOND IN DISULFUR MONOXIDE

BY P. A. GIGUÈRE

Department of Chemistry, Laval University, Québec, Canada

Received October 14, 1959

Recently Meschi and Myers[1] have reported the detailed microwave spectrum and molecular structure of disulfur monoxide, S_2O. Mass spectrometric and other measurements[2] had previously led them to positive identification of that unstable compound, which at one time[3] was mistaken for dimeric sulfur monoxide, $(SO)_2$. From analysis of the spectra they found for the molecule a bent S–S–O structure with the following parameters: S–S distance, 1.884 Å.; S–O, 1.465 Å.; S–S–O angle, 118 ± 0.5°. The authors also concluded: "the S–O bond is probably fairly close to a single bond." However, this view is not supported by the existing data. A single covalent S–O bond should be appreciably longer than the above, namely, 1.70 Å., from the sum of the covalent radii of the S and O atoms.[4] (The revised values corrected for partial ionic character of the bond[5] lead to nearly the same bond length, 1.69 Å.) The distance 1.51 Å. quoted by Meschi and Myers for the single S–O bond is in fact the interatomic distance in the tetrahedral SO_4^{--} ion where considerable double bond character is expected.

As for the double-bond radii of the atoms, their "normal" values are much more uncertain that those of the single bonds. At any rate the S–O bonds in SO_2, 1.432 Å., are definitely shorter than the sum of the Pauling's double-bond radii, 1.49 Å. The explanation for this has been given by Moffitt[6] who analyzed the electronic structure of various sulfoxides and sulfones by means of his self-consistent LCAO method and showed that in these molecules the S–O bonds are largely double, with the 3d orbitals of sulfur contributing appreciably to the π-bonding. The resulting hybrid bond is stronger than one involving a pure p- or d-bonding orbital of sulfur. Obviously, such is the case for disulfur monoxide where the central S atom can use its 3d orbital in hybridization (form I) rather than forming so-called coördinate bonds with large formal charge separation as in the canonical forms II and III

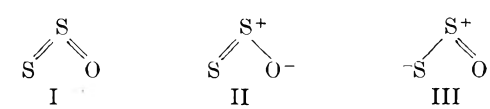

From the known vibrational frequencies of the S_2O molecule[7] the force constant for the S–O bond may be estimated roughly at 9.3×10^5 dynes cm.$^{-1}$

(1) D. J Meschi and R. J. Myers, *J. Mol. Spectroscopy*, **3**, 405 (1959).

(2) D. J. Meschi and R. J. Myers, *J. Am. Chem. Soc.*, **78**, 6220 (1956).

(3) For a review see P. W. Schenk, *Chem. Z.*, **67**, 273 (1943).

(4) L. Pauling, "The Nature of the Chemical Bond," Cornell University Press, Ithaca, N. Y., 1945.

(5) V. Schomaker and D. P. Stevenson, *J. Am. Chem. Soc.*, **63**, 37 (1941).

(6) W. Moffitt, *Proc. Roy. Soc. (London)*, **A200**, 409 (1950).

(7) A. V. Jones, *J. Chem. Phys.*, **18**, 1263 (1950).

which, according to the correlation of Moffitt, corresponds to a π-bond order of about 0.8 as compared with 0.93 for the bonds in SO_2. Therefore, it appears that the S–O bond in disulfur monoxide is best described as essentially double, although slightly less so than those in SO_2. Needless to say this minor point detracts in no way from the significance of Meschi and Myers' contribution.

COMMUNICATION TO THE EDITOR

THE VOLUME OF DIMERIC BISMUTH MONOHALIDE DISSOLVED IN MOLTEN BISMUTH TRIHALIDE

Sir:

A seemingly strong argument was presented[1] recently against the assumption[2] that Bi_2X_2 is an important species in solutions of bismuth metal in molten bismuth trihalides. Extremely small, even strongly negative, and concentration-dependent apparent molar volumes were reported which, in fact, are erroneous due to the use in the calculation of wrong values for the molar volume of the solution, $\bar{V}$. This volume, $\bar{V}$, had been calculated (in the case of chloride) from

$$\bar{V} = \frac{x_{Bi}M_{Bi} + x_{BiCl_3}M_{BiCl_3}}{\rho} = \frac{209x_{Bi} + 315.4\,(1 - x_{Bi})}{\rho}$$

where x is the mole fraction, M the molecular weight, and ρ the density of the solution in g. cm.$^{-3}$. This is the expression appropriate for the solute species Bi. Actually, the molar volume of the solution depends on the species postulated. In order to arrive at the value of the apparent molar volume of the species Bi_2Cl_2

$$\phi_{Bi_2Cl_2} = \frac{\bar{V} - (1 - x_{Bi_2Cl_2})\bar{V}_{BiCl_3}}{x_{Bi_2Cl_2}}$$

where

$$x_{Bi_2Cl_2} = \frac{3x_{Bi}}{4 - 3x_{Bi}}$$

the $\bar{V}$ must be calculated from

$$\bar{V} = \frac{x_{Bi_2Cl_2}M_{Bi_2Cl_2} + (1 - x_{Bi_2Cl_2})M_{BiCl_3}}{\rho} = \frac{489x_{Bi_2Cl_2} + 315.4\,(1 - x_{Bi_2Cl_2})}{\rho}$$

If this is done, one obtains from the same experimental data[1,3] for all three Bi–BiX_3 systems quite reasonable values of $\phi_{Bi_2X_2}$ almost independent of concentration and not much smaller than $\bar{V}_{BiX_3}$. For instance, for mole fractions $x_{Bi_2X_2}$ of 0.039 and 0.177 (x_{Bi} of 0.05 and 0.20), the values are

	Chloride 250°	Bromide 250°	Iodide 420°
$\phi_{Bi_2X_2}$	72, 72	74, 79	83, 92
$\bar{V}_{BiX_3}$	81.6	96.5	128

These calculations were made for Bi_2X_2 as the only solute species, although there is evidence[2] for an additional species, Bi_2. While the calculation of apparent molar volumes practically never can distinguish among various species, it is certain from the above calculations that the density measurements do not refute the assumption of Bi_2X_2.

CHEMISTRY DIVISION
OAK RIDGE NATIONAL LABORATORY — M. A. BREDIG
OAK RIDGE, TENNESSEE — H. A. LEVY
STANFORD RESEARCH INSTITUTE — F. J. KENESHEA
MENLO PARK, CALIFORNIA — DANIEL CUBICCIOTTI

RECEIVED NOVEMBER 25, 1959

(1) F. J. Keneshea, Jr., and D. Cubicciotti, *J. Phys. Chem.*, **63**, 1472 (1959).

(2) M. A. Bredig, *J. Phys. Chem.*, **63**, 978 (1959).

(3) F. J. Keneshea, Jr., and D. Cubicciotti, *J. Phys. Chem.*, **62**, 843 (1958), and **63**, 1112 (1959).